

UNIVERSITY OF CALIFORNIA, SAN DIEGO  
SCRIPPS INSTITUTION OF OCEANOGRAPHY  
VISIBILITY LABORATORY  
SAN DIEGO, CALIFORNIA 92152

**UNDERWATER LIGHTING BY SUBMERGED LASERS  
and Incandescent Sources**

S. Q. Duntley

DISTRIBUTION OF THIS DOCUMENT IS UNLIMITED

REPRODUCTION IN WHOLE OR IN PART IS PERMITTED  
FOR ANY PURPOSE OF THE UNITED STATES GOVERNMENT

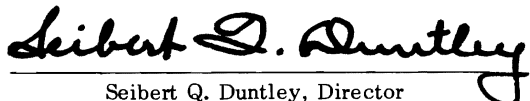
SIO Ref. 71-1


June 1971

Supported By  
U. S. Office of Naval Research  
Contract N00014-69-A-0200-6013  
Final Report

Approved:

Approved for Distribution:

  
Seibert Q. Duntley, Director  
Visibility Laboratory

  
William A. Nierenberg, Director  
Scripps Institution of Oceanography

## ABSTRACT

	Page
UNDERWATER LIGHTING BY SUBMERGED LASERS	
- - - was measured at virtually all distances on-axis and off-axis in seven kinds of water,	7-16 to 7-31
- - - is represented by an equation for engineering use,	7-33
- - - is predicted in other kinds of water,	7-36
- - - is predicted at any wavelength.	7-37
UNDERWATER LIGHTING BY SUBMERGED INCANDESCENT SOURCES	
- - - was measured at virtually all distances	
on-axis,	4-24 to 4-35
off-axis,	6-19
from a spherical lamp,	4-28
from a plane diffuser,	2-2
with polarization.	5-13
UNDERWATER LIGHTING FOR PHOTOGRAPHY	
- - - is illustrated	
at short ranges,	3-14
at long ranges,	3-15
by measurements,	3-8
by equations.	3-5
OPTICAL PROPERTIES OF WATER	
- - - are identified and defined in Appendix A,	
- - - have been measured by new techniques for	
attenuation,	2-8
scattering,	2-18
absorption.	2-20

# CONTENTS

ABSTRACT	iii
1. INTRODUCTION	1- 1
1.1 A Decade of Research	1- 1
1.2 Origin of the Research	1- 1
1.3 Guidelines	1- 2
1.4 Origin of the Field Station at Diamond Island	1- 2
1.5 The First Decade (1948 – 1958)	1- 4
1.6 The Second Era (1959 – 1966)	1- 4
1.7 Simulation of Ocean Conditions	1- 4
2. OPTICAL PROPERTIES OF WATER	2- 1
2.1 Exploration of Fundamentals	2- 1
2.2 Early Measurements of Underwater Lighting by Submerged Lamps	2- 1
2.3 Disappearance of Receding Submerged Lamps	2- 2
2.4 Measurement of the Volume Attenuation Coefficient	2- 3
2.5 Measurement of the Volume Scattering Function	2-14
2.6 Measurement of the Volume Absorption Coefficient	2-20
2.7 Measurement of Apparent Radiance Distribution	2-27
3. UNDERWATER LIGHTING FOR PHOTOGRAPHY	3- 1
3.1 Introduction	3- 1
3.2 Refractive Deterioration of Imagery	3- 1
3.3 The Optical Nature of Natural Waters	3- 4
3.4 Apparent Contrast of Illuminated Underwater Objects	3- 4
3.5 Measurements of Apparent Contrast	3- 6
3.6 Polarized Underwater Lighting	3- 8
3.7 Maximum Range of Underwater Imagery	3-10
3.8 Long Range Underwater Photography	3-12
3.9 Exposure Requirements	3-16
3.10 Silhouette Photography	3-17

4.	EXPERIMENTS WITH COLLIMATED LAMPS	4- 1
4.1	Simulation of Underwater Lasers	4- 1
4.2	The First Underwater Tower and Track	4- 4
4.3	The Second Underwater Tower and Track	4- 8
4.4	Irradiance On-Axis	4-24
5.	EXPERIMENTS WITH THE FIRST UNDERWATER LASER	5- 1
5.1	Introduction	5- 1
5.2	Characteristics of the Laser	5- 1
5.3	Mounting the Underwater Laser	5- 2
5.4	Divergence of the Underwater Laser	5- 8
5.5	Polarization of Light from the Underwater Laser	5-11
5.6	Measurements of Irradiance On-Axis	5-13
6.	LASER LIGHT IN LAKE WATER	6- 1
6.1	Introduction and Summary	6- 1
6.2	Studies of Irradiance On-Axis	6- 1
6.3	Radiance Distributions	6-16
6.4	Receiver Field of View	6-17
6.5	Diameter of the Receiver Aperture	6-18
6.6	Studies of Irradiance Off-Axis	6-20
7.	LASER LIGHT IN SIMULATED OCEAN WATER	7- 1
7.1	Introduction and Summary	7- 1
7.2	Survey of Sites for a Laser Experiment in the Ocean	7- 2
7.3	The Laboratory Tank	7- 3
7.4	Simulation of Natural Waters	7- 8
7.5	Installation and Use of the Laser	7-12
7.6	Studies of Irradiance Off-Axis	7-16
7.7	Irradiance Off-Axis in Clear Ocean Water	7-18
7.8	Off-Axis Irradiance in Other Waters	7-23
7.9	An Equation for Engineering Use	7-32
7.10	Special Uses of the Equation	7-36
8.	DESIRABLE FURTHER WORK	7-38
9.	ACKNOWLEDGEMENTS	9- 1

## APPENDICES

### APPENDIX A

“Light in the Sea,” J. Opt. Soc. Am. **53**, No. 2, February 1963.

### APPENDIX B

“Bibliography of Reports Describing Related Experiments 1948 – 1958.”

### APPENDIX C

“Field Test of a System for Predicting Visibility by Swimmers from Measurements of the Clarity of Natural Waters,” SIO Ref. No. 59-39, June 1959.

### APPENDIX D

“Reduction of Contrast by Atmospheric Boil,” J. Opt. Soc. Am. **53**, No. 3, March 1963.

### APPENDIX E

“Mala Wharf,” an excerpt from the log of the search for an ocean site for an underwater laser experiment.

### APPENDIX F

“Image Transmission by the Troposphere I,” J. Opt. Soc. Am. **47**, No. 6, June 1957.

### APPENDIX G

“Measurements of the Transmission of Light from an Underwater Point Source,” Report No. 5-11, October 1960.

### APPENDIX H

“Measurements of the Transmission of Light from an Underwater Source Having Variable Beam-Spread,” SIO Ref. 60-57, November 1960.

# 1. INTRODUCTION

## 1.1 A DECADE OF RESEARCH

This final report under contract N00014-69-A-0200-6013 presents the results of a ten-year program of research on underwater lighting by submerged light sources, including lasers. It covers the decade from 1961 through 1970 and is part of a continuing research program in hydrologic optics that has been carried out by the author and some of his colleagues since 1944.\* Many of the experiments were performed at a field station at Diamond Island in Lake Winnepesaukee, New Hampshire. The account which follows begins with brief descriptions of the origins of the research and of the field station.

## 1.2 ORIGIN OF THE RESEARCH PROGRAM

Recommendations in 1947-48 by an ad hoc Working Group of the present National Research Council Committee on Vision that research in hydrologic optics under Navy sponsorship should be initiated by the author resulted in the establishment of the Visibility Laboratory and the field station at Diamond Island. An uninterrupted succession of Navy contracts from 1948 to the present have been responsible for most of the Laboratory's in-water research. Other agencies have also participated including the National Science Foundation, the National Aeronautics and Space Administration, and the Departments of Commerce, Interior, and Transportation.

The chairman of the 1947 Working Group was Dr. Edward O. Hulburt, then Superintendent of the Optics Division of the Naval Research Laboratory, and its members included the author of this report. The task of the Group was to develop means for predicting by calculation the visibility of shallowly submerged objects.

After a considerable study during 1947, the Working Group concluded that new fundamental knowledge was needed concerning (1) the optical effects of water waves, (2) the manner in which submerged objects are illuminated by daylight, (3) the directional reflectance of submerged surfaces, and (4) image transmission by ocean water. It recommended, therefore, that research on these topics should be sponsored by the Navy. The Group also searched for a suitable principal investigator. It was found that, except for the author of this report, none of the scientists who had previously conducted optical research in the ocean were available. Accordingly he was urged by his fellow members on the Working Group to undertake the needed studies. The required research began in the summer of 1948 under an ONR contract.

---

\* Duntley, S. Q. (1946) VISIBILITY STUDIES AND SOME APPLICATIONS IN THE FIELD OF CAMOUFLAGE, Summary Tech. Rept. Div. 16, NRDC (Columbia Univ. Press, New York), Vol. 2, pp 210-212, available from DDC as AD 221102.

### 1.3 GUIDELINES

Several guidelines for the new experiments were developed by the Working Group and particularly by Dr. Hulburt. He advised that the costs and difficulties of conducting the experiments from aircraft at sea would be so great that the probability of eventual success would be low. He believed that the investigation would fall short of its goals unless an inexpensive and favorable outdoor working environment could be found. Dr. Hulburt recommended: (1) that the experiments should be initiated in a fresh-water lake, where many ocean complications would not be encountered; (2) that no aircraft be used, but that a structure be erected from the bottom of the lake to support the "aerial" observer and his measuring equipment; (3) that the site be reasonably isolated from public intrusion. Dr. Hulburt expected that the magnitudes of the the optical properties of lake water would differ from those of corresponding quantities in the oceans but that the significant optical *principles* would be identical. He recommended that the research be shifted to the ocean only after the principles were understood and the experimental techniques perfected. The Working Group unanimously endorsed these wise recommendations and the author proceeded with them as guidelines.

### 1.4 ORIGIN OF THE FIELD STATION AT DIAMOND ISLAND

A suitable site for the experiments was selected about two hours drive from the author's laboratory at M.I.T. It is located in Lake Winnepesaukee, New Hampshire at Diamond Island. As shown by the maps in Fig. 1-1, the island lies about one mile off the south shore of this large lake. In 1947 it was inhabited only by its owner, Frederick C. Spooner (M.I.T. '19) of Lincoln, Massachusetts. Roughly oval, it is three-eighths of a mile long, three-sixteenths of a mile wide, and comprises about 35 acres of mixed forest.

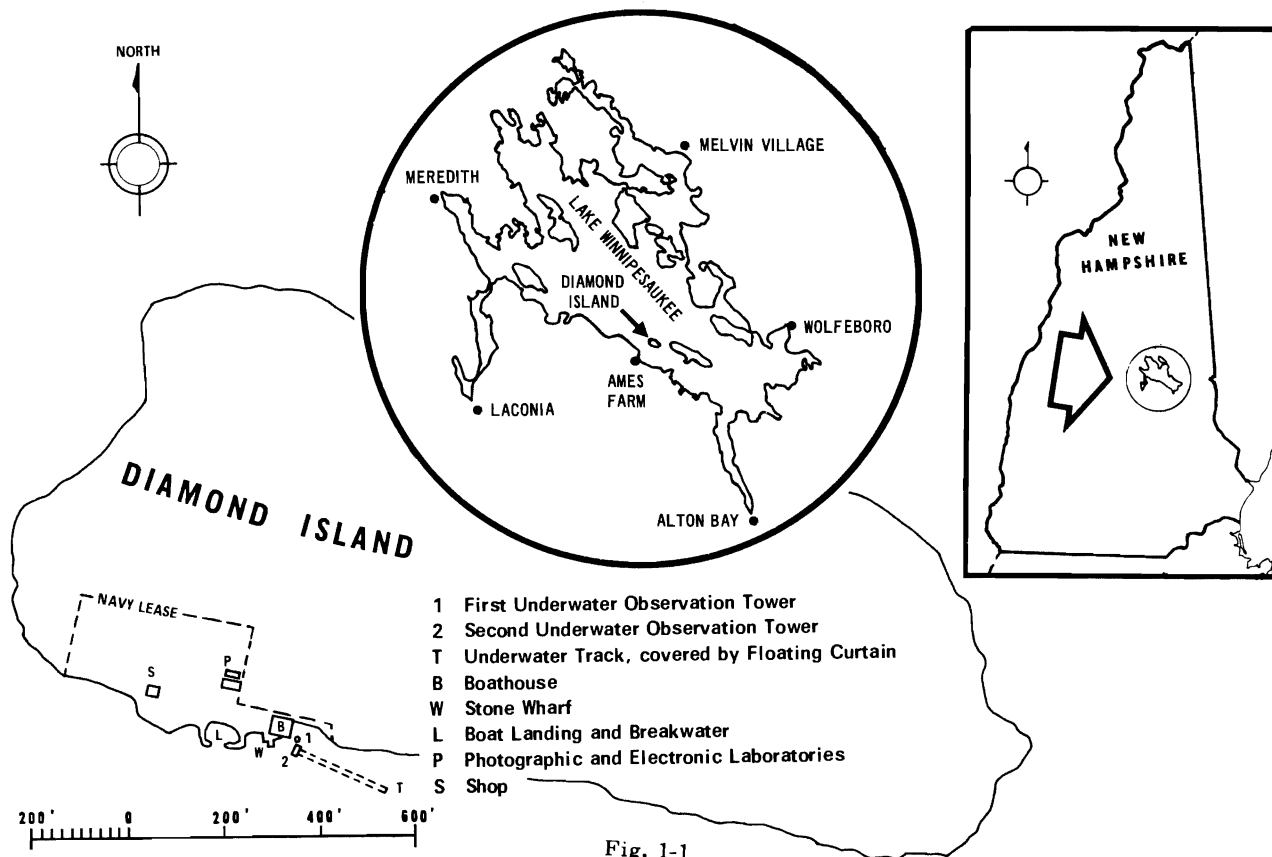


Fig. 1-1

Figure 1-2 shows oblique aerial photographs of the island as seen from the south. It is hilly, the highest ground being about a hundred feet above lake level. A location excellent for all aspects of the work existed on the south shore of the island. (See Fig. 1-2.) Arrangements were made among the Office of Naval Research, its contractor (the Massachusetts Institute of Technology), and the owner of Diamond Island (F. C. Spooner) for the establishment of a field station where the desired research could be conducted. Later, in 1952, the author moved the Visibility Laboratory from M.I.T. to the Scripps Institution of Oceanography of the University of California in San Diego, and custody of the field station shifted to that institution.

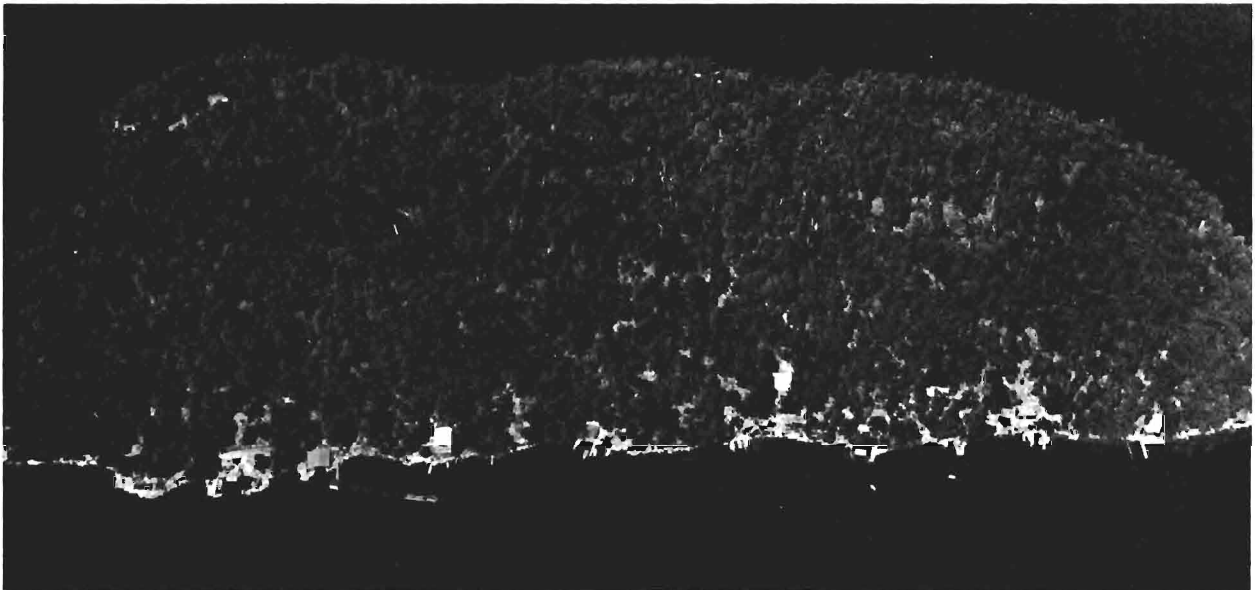
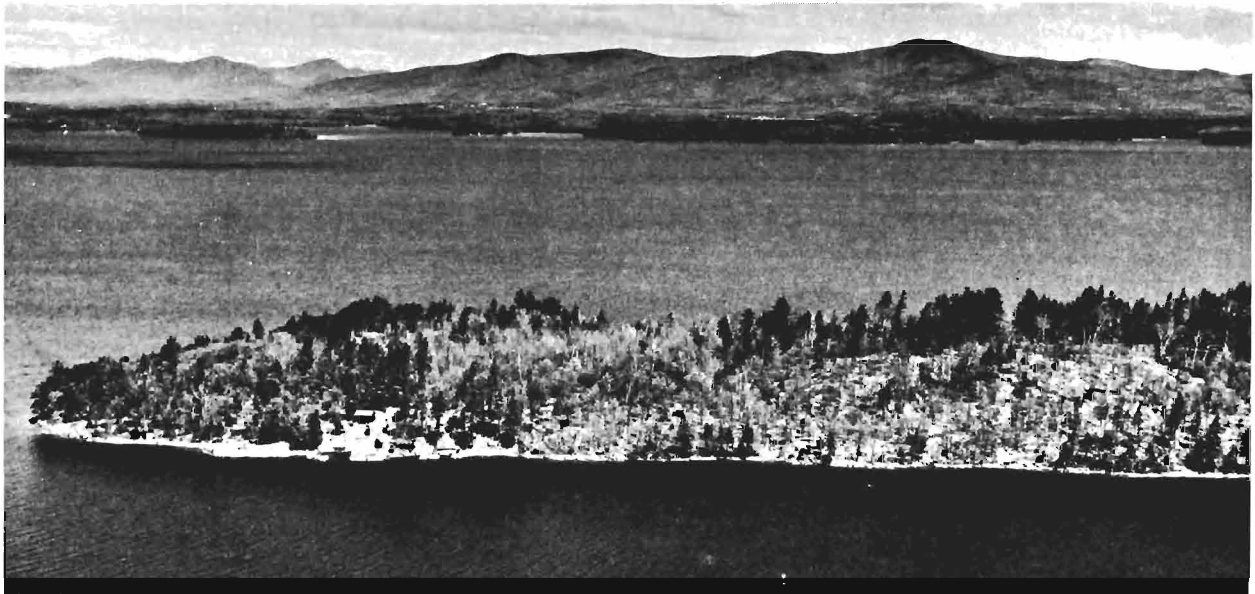


Fig. 1-2. Diamond Island, Lake Winnepesaukee, New Hampshire



The research at Diamond Island by the author and his colleagues began in 1948 and continued throughout successive summers until 1966. Subsequently, the U.S. Navy Underwater Sound Laboratory Center, New London, Connecticut acquired the facility and, in 1969, began experiments in underwater optics and acoustics there.

## **1.5 THE FIRST DECADE (1948 – 1958)**

The Visibility Laboratory experiments at Diamond Island comprise two distinct eras. The first decade was devoted to the original problem of the Working Group, which might be called "the daylight case" because all of the light was provided by the sun and the sky. Scant attention was given to objects illuminated by submerged artificial light sources.

Sunlight and skylight penetrate the water to illuminate any submerged object and, because of scattering within the water lower its apparent contrast. (See Appendix A, pages 225 to 233.) Optical effects of several kinds occur at the water surface and are complicated by the water wave structure. All of these phenomena were studied at Diamond Island under the entire gamut of lighting conditions, weather conditions, and directions of view. Many ancillary problems were also investigated. A full account of the research at Diamond Island in the first decade would, as a single document, make a report larger than this one. The results are spread, however, among many Visibility Laboratory reports and publications. Still other papers, chiefly by the author's colleagues, describe related experiments that they performed at sea. A bibliography of these writings is in Appendix B of this report.

## **1.6 THE SECOND ERA (1959 – 1966)**

The second era of research at the Diamond Island field station was concerned with underwater lighting from submerged artificial sources. Initially, lighting produced by submerged conventional sources was studied in the interest of underwater photography, television and direct viewing from submersibles or by swimmers. Experiments of this kind began in 1958 and dominated the program in 1959 and 1960. By 1961 interest had centered on the probable advent of underwater lasers capable of producing blue-green light either continuously or at very high peak power and short pulse duration. Actually no underwater laser source was available until 1964, but in anticipation of it experiments were conducted in 1961 and 1962 with an incandescent underwater projector which produced beams of light similar in diameter and collimation to those expected from underwater lasers. Experiments with underwater lasers were made at Diamond Island in 1964, 1965, and 1966.

## **1.7 SIMULATION OF OCEAN CONDITIONS**

Transfer of the laser experiments from the lake to the ocean was initiated in 1967. A site survey was made, but funds could not be found for so expensive a research undertaking. ONR funded, however, a program of simulated ocean laser experiments that were eventually conducted at model scale in a special laboratory tank. Preparations for this work proceeded throughout 1968, 1969, and early 1970. Financial supplementation was provided by the U.S. Naval Air Development Center, the U.S. Naval Ordnance Laboratory, the Department of Commerce, and Sea Grant College Program of the National Science Foundation. Extensive data on the propagation of laser beams through simulated ocean waters of many kinds were achieved during 1970.

This report covers all of the experiments on underwater artificial lighting made during the ten-year lifetime of Contract N00014-69-A-0200-6013, 1961-1970, including both the research at Diamond Island (1961-1966) and that in the ocean simulation tank. Many of the experimental and theoretical studies which preceded Contract N00014-69-A-0200-6013 were essential predecessors to it, and some of the initial experiments under it were preliminary to the subsequent work with submerged lasers. The relevant preliminary experiments are summarized in the section which follows.

## 2. OPTICAL PROPERTIES OF WATER

### 2.1 EXPLORATION OF FUNDAMENTALS

The first decade of research at Diamond Island (1948–1958), although dedicated to the daylight case, served to explore many of the fundamentals of hydrologic optics and thereby to lay the foundation for all of the research described in this report. One product of the first winter of contract N00014-69-A-0200-6013 was the writing of a paper entitled "Light in the Sea" which provides a comprehensive overview of these fundamentals. It also interprets the experiments with submerged incandescent lamps which were performed at Diamond Island during the summers of 1959, 1960, and 1961. A reprint of "Light in the Sea" has been included as Appendix A of this report, partly because it is a product of the contract but principally because it provides definitions of the concepts, the terminology, and the notation used throughout this report. It also includes essential descriptions of some of the apparatus used throughout contract N00014-69-A-0200-6013 and it presents the results of experiments with a highly collimated underwater light source that were performed at Diamond Island during the first summer of the contract. Numerous references to paragraphs, equations, and figures in "Light in the Sea" will be made throughout this report. The terminology and symbols it defines will be used but not defined again here. The concepts it develops will be referenced by page number, but the development will not be repeated. In short, it is assumed that readers will familiarize themselves with the contents of "Light in the Sea" (Appendix A).

This report also contains several other appendices drawn from previous reports or from papers which have evolved in the course of the long program. These appendices have been included to supplement and shorten this report.

### 2.2 EARLY MEASUREMENTS OF UNDERWATER LIGHTING BY SUBMERGED LAMPS

Although a few experiments during the first decade at Diamond Island employed submerged incandescent lamps for various purposes, the first extensive measurements of the underwater artificial lighting were performed in the summers of 1959 and 1960. The results are described in two reports which are included here as Appendices G and H. The principal results of the 1959–60 studies are also summarized briefly on pages 221, 222, and 223 of Appendix A. An interesting addition to one of these experiments was made in 1962 under contract N00014-69-A-0200-6013, as described in the following section.

## 2.3 DISAPPEARANCE OF RECEDING SUBMERGED LAMPS

A phenomenon having important implications to underwater imagery and the performance of underwater laser systems is described on page 221 of Appendix A, as follows: “. . . a receding, uniform, spherical lamp appears to be surrounded by a glow of scattered light which becomes proportionately more prominent as lamp distance is increased, until at some range, often 18 to 20 attenuation lengths, the lamp image can no longer be discerned and only the glow is visible.” Thus, any object becomes obscured by its own scattered light, even in otherwise unlighted water. Figure 15 on page 222 of Appendix A illustrates part of this phenomenon by means of curves showing the angular distribution of apparent radiance of a uniform spherical incandescent frosted lamp at a series of increasing distances up to 9.6 attenuation lengths. Because the apparent angular diameter of the lamp decreased from 38.4 milliradians to 6.7 milliradians in this experiment, interpretation of the curves is not simple. The experiment was repeated, therefore, in 1962 with the angular diameter of the source maintained constant at 10 milliradians.

Figure 2-1 shows how the 1962 experiment was configured. It was not possible to obtain a series of spherical lamps having a range of diameters suitable for such an experiment, but it was easy to achieve a corresponding result using a plane circular diffuse emitter. As depicted in Fig. 2-1, the same 1000-watt spherical underwater lamp used to produce Fig. 15 in Appendix A was housed in a water-filled, rectangular metal box one end of which was closed by a sheet of diffusing plastic. Several sheet metal caps were made to cover this end of the box. In the center of the first of these a circular aperture was cut one-half foot in diameter. Similar metal caps containing holes respectively one-fourth, one-eighth, and one-sixteenth foot in diameter were also made. The diffusely emitting plane source, masked to a diameter of one-half foot by means of the appropriate metal cap, was placed 50 feet in front of the image in water of the entrance pupil of the telephotometer. This image was 1.75 feet behind the water-glass surface of the observation window. The angular distribution of apparent radiance thus produced was measured by means of the same automatic scanning, photoelectric, telephotometer used to obtain the data in Fig. 15 of Appendix A. A photograph of this equipment and a description of it is given in Section 2.7 of this report. As in

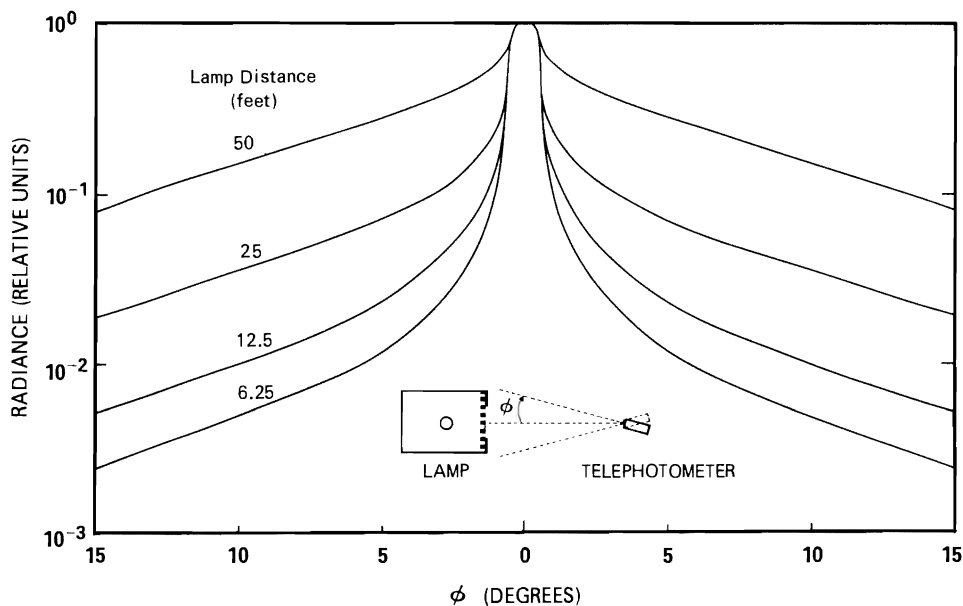


Fig. 2-1. Angular distributions of apparent radiance produced by plane circular, diffuse, submerged sources 10 milliradians in angular diameter.

the case of Fig. 15 of Appendix A, the telephotometer had a circular acceptance cone 0.25 degrees in angular diameter (in air) and had its spectral response limited by a Wratten 61 filter. Thus, a submerged circular plane source 10 milliradians in angular diameter was scanned with a 0.59 milliradian acceptance cone.

The lamp was then moved 25 feet closer to the telephotometer and the diameter of the plane emitting surface was reduced to a diameter of 1/4 foot, so that the apparent angular diameter of the source remained 10 milliradians. The new angular distribution of apparent radiance was then recorded. In this way a family of four radiance distribution measurements were made at lamp distances of 50, 25, 12.5, and 6.25 feet respectively but with the diameter of the plane emitting source correspondingly reduced (1/2 ft., 1/4 ft., 1/8 ft., 1/16 ft.) so that the source always subtended the same angle (10 milliradians) as seen from the telephotometer.

The resulting data are shown in Fig. 2-1. In each case the apparent radiance of the diffusely emitting plane surface has been normalized to unity in order to display the shape of the curves most simply. If desired, relative values of the apparent radiance of the diffusing disk can be easily calculated from the respective true water path lengths (48.25, 23.25, 10.75, and 4.50 feet) and the prevailing attenuation length (4.62 ft/ln) since the reduction of its apparent radiance with distance depends only on the attenuation coefficient  $\alpha$ , as illustrated by Fig. 14 on page 221 of Appendix A. The radiance distributions in Fig. 2-1 illustrate quantitatively the way in which the square-shouldered image of the circular disk disappears into its own scattered light with increasing lamp distance. By visual inspection, the spherical source could not be discerned at a lamp distance of 75 feet (16.2 attenuation lengths), although the water was bright with the scattered radiance from the lamp.

The limiting range at which a distant submerged lamp disappears in its own glow can be increased only slightly by providing more lamp power. A more powerful lamp produces a brighter glow which changes the adaptive state of the eye, thereby lowering its contrast threshold and enabling the lamp to be moved to a slightly greater distance before the apparent contrast between the lamp and the glow surrounding it is reduced to the new threshold value. It is futile to seek a substantial increase in the distance at which the outline of a self-luminous, submerged object is discernible simply by using a giant lamp. Replacement of the one kilowatt lamp with a 5 kilowatt bulb would have produced a brighter field of view from the observing port but would have increased only slightly the limiting distance at which the shape of the lamp could be seen.

## 2.4 MEASUREMENT OF THE VOLUME ATTENUATION COEFFICIENT

All of the sections to follow in this report make extensive use of a measurable optical property of water called the *spectral volume attenuation coefficient*. It relates to the image-transmitting properties of water and to the transmission of small diameter collimated beams of light, as well as to various other phenomena. A remarkable variety of different kinds of measurements yield identical values of this water property. This suggests that a basic property of water is being measured, since no unique experimental procedure is required. The spectral volume attenuation coefficient will be denoted in this report by the Greek letter alpha ( $\alpha$ ).\*

---

\* For reasons of convenience (see p. 216 of Appendix A), the reciprocal of alpha ( $1/\alpha$ ) appears much more often throughout this report than does alpha itself. Reciprocal alpha ( $1/\alpha$ ) is called attenuation length; in that distance through optically uniform water there is attenuation by a factor of  $1/e = 0.3679$ .

## WHAT IS ALPHA?

Several formal definitions of the spectral volume attenuation coefficient appear in the scientific literature. Some of the definitions are stated in words; others employ the language of mathematics. Most writers use a mixture of both. Three definitions of alpha given by the author in previous writings are quoted later in this section, but first it is important to note that every formal definition represents a model of nature. The very fact that many quite different models have been defined illustrates that attenuation has multiple aspects. It suggests that, actually, several different forms of spectral volume attenuation coefficient are possible, each for use in some particular circumstance. Amazingly, however, numerical values of alpha for natural waters are alike by nearly all reasonable techniques within the precision and accuracy of conventional, high quality radiometric measurements – photoelectric, photographic, or visual.

A succession of engineers and scientists have constructed apparatus intended to fulfill as closely as practicable the requirements implied by one or another of the definitions. Each builder points out that his design seeks to approximate some definition. Nearly each user becomes concerned about whether the instrument he is using measures alpha properly for his particular application. No one seems sure and this is a perpetual source of concern to the entire user community. It also disturbs some theoreticians, who seek to build models into useful mathematical structures of great complexity. The quandaries become more serious and more perplexing when the question is asked, "Do the optical processes of nature obey my model of alpha?" This question is rarely resolved to anyone's satisfaction, chiefly because it is more appropriate to ask "Do my alpha data adequately describe the pertinent observable effects?" The latter question can usually be answered by an emphatic "yes," because a bewildering variety of methods for measuring attenuation give the same numerical result within the accuracy and precision ordinarily achieved. Within that limit there is a unique, easily measurable, widely useful, numerical property of natural waters that can be called "alpha."

The spectral volume attenuation coefficient is the cornerstone of this report. The paragraphs which follow describe many experimental techniques and devices by means of which this universal water property can be measured. All of them, when properly executed, yield the same numerical value. Theoretical relations for the use of alpha appear throughout this report and its appendices. Many, many others can be found in the literature. Formal definitions of alpha will be postponed until this observable property of natural waters has been introduced by descriptions of means for its measurement and by examples of its use. This is a practical approach to what has sometimes seemed to be an illusive concept lying at the very foundation of hydrologic optics. It is hoped that the paragraphs which follow will show that there exists a real, unambiguous, useful descriptor of the monochromatic optical properties of natural waters which is easily measurable by any one of many different techniques and is directly useful in unifying the propagation of light and images through natural waters. Once this practical concept has been accepted, it is easy to place reliance on measurements and to use data and equations alike for deeper understanding and useful accomplishments.

## TECHNIQUES FOR MEASURING ATTENUATION

No attempt will be made to catalogue *all* available techniques for measuring the spectral volume attenuation coefficient alpha ( $\alpha$ ). There are dozens, and new methods or variants on old ones can easily be invented. It is, however, important to consider several significant and quite different types of measurements which, in all cases, yield the same numerical result. This will be done in the paragraphs which follow.

*Contrast Reduction.* The initial research at Diamond Island (1948) concerned the *visibility* of submerged objects, i.e., the limiting distance at which an underwater observer could visually detect a submerged object. Analogous experiments in air had already been made in the atmosphere as early as 1923 by Kochmeider in Germany and later by many others, including the author. The apparent contrast of objects viewed along horizontal atmospheric paths of sight against an apparent background of cloud-free horizon sky had been found to diminish exponentially with distance. An attenuation coefficient  $\alpha$  was assigned to this phenomenon. Underwater photographic telephotometry of objects along horizontal submerged paths of sight disclosed that the simple exponential form of contrast reduction equation also holds in daylight water.\* The first data on the volume attenuation coefficient of water at Diamond Island were, therefore, calculated from photographic telephotometry of submerged objects. Immediate use of this information, combined with laboratory visual thresholds, successfully predicted the ranges at which underwater observers could detect specific objects. The value of volume attenuation coefficient measured in this way was, therefore, the desired descriptor of water for studies of the visibility of submerged objects. Measurements of  $\alpha$  by any other technique had to be validated against underwater daylight telephotometry. Several years elapsed before serious efforts were made to devise other means for making attenuation measurements, because research interest was centered on exploring the laws of contrast transmission by various paths of sight through water and through the water surface.

*Transmissometer.* Experiments at sea and, later, Diamond Island research with artificial lights at night required an instrument for measuring alpha. Rudimentary light beam transmissometers had been used by others. The first such device seen by the author (1944) consisted of a wooden yardstick with a flashlight taped to one end and a waterproofed photoelectric photographic exposure meter taped to the other; it is not a recommended transmissometer. A succession of steadily improving Visibility Laboratory designs produced a truly excellent transmissometer (see Fig. 2-2) which was used at Diamond Island in 1958 for research described in Appendix C. These experiments used laboratory psychophysical visual detection threshold techniques underwater for the first time. They showed, in a very careful series of measurements,

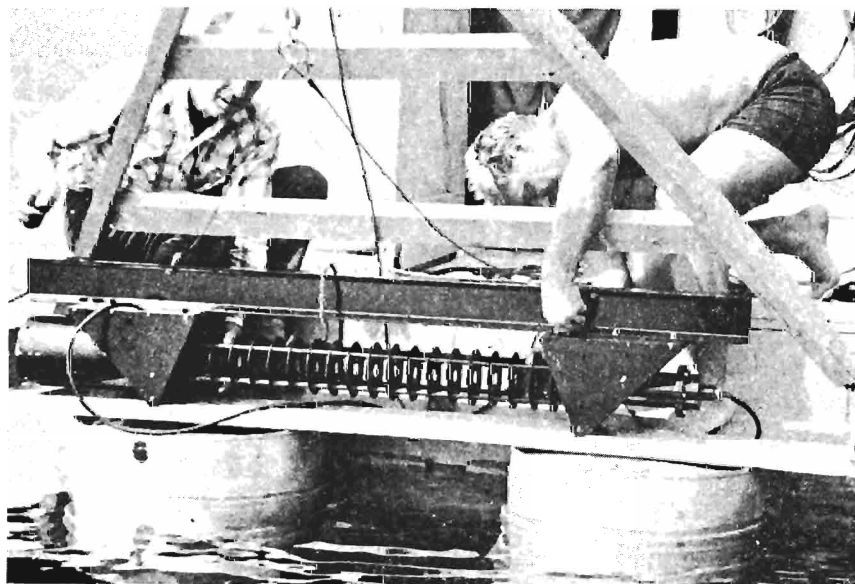


Fig. 2-2

Submersible photoelectric transmissometer in use at Diamond Island. Both light source and receiver were collimated. Personnel: John Foster (kneeling) and John E. Tyler.

\* Along horizontal paths of sight only.

that identical values of volume attenuation coefficient, valid for use in numerical predictions of the limiting visual detection ranges of small submerged objects, were produced both by daylight telephotometry and by the submersible transmissometer shown in Fig. 2-2.

*Alpha from Visual Threshold Range.* The underwater psychophysical experiments described in Appendix C show that laboratory visual threshold data are applicable to valid numerical predictions of visual threshold distances. Such laboratory thresholds show that black-suited swimmers *having no areas of higher reflectance* will, when deployed horizontally, lose sight of each other at a separation of 4 attenuation lengths when there is ample daylight. Thus, two swimmers can determine reciprocal alpha ( $1/\alpha$ ) simply by separating horizontally while connected by a measuring line. One fourth of their mutual disappearance range equals  $1/\alpha$ . No equipment other than a knotted, measured line is needed. Water clarity was measured in this way throughout the ocean research site survey described in Section 7 of this report.

*Alpha at High Collimation.* The completion in 1962 of the second underwater tower and track at Diamond Island, with precision remote pointing controls for the collimated incandescent underwater projector (see Sec. 4.3), enabled the volume attenuation coefficient to be measured with highly collimated beams of light over easily changed lengths of path. When used with the 2-watt concentrated-arc source and full 2-inch beam diameter the divergence of the projector was 0.175 milliradians (0.6 minutes of arc) measured at 1/30 power points. Any beam diameter down to 1/20 inch was available, with increased beam spread due to diffraction. When, for example, the projector using the 2-watt source was stopped down to a beam diameter of 0.1 inch, the beam divergence was 0.6 milliradians (2 minutes of arc) at 1/30 power points. These and various intermediate beam diameters were tried at lamp distances from 1 to 20 feet.

Several types of receivers were tested; one was the Visibility Laboratory Mark IV photoelectric telephotometer shown in Fig. 2-3. This superb instrument could be used with entrance pupil diameters from 35 mm to 1 mm and fields of view from 2 degrees to 0.1 minute of arc. Many combinations were tried on the underwater track. By varying the length of the water path and making a semilogarithmic plot of flux received vs. lamp distance, absolute values of alpha could be found from the slope of the resulting straight line without requiring an air reading. These trials were also repeated with identical facilities in the laboratory tank described in Section 7 of this report. In fact, such experiments are sometimes used as a student laboratory exercise in one of the author's courses. The values of attenuation coefficient are remarkably unaffected by beam and receiver geometry as long as (1) stray light is effectively eliminated and (2) the ratio of beam diameter to length of the water path is small. It is not necessary to have high collimation at both the light source and the receiver, although stray light is easier to suppress when some practical modicum of collimation is provided for both source and receiver. Beam divergence and receiver field of view of the order of 1 degree seems to be a good choice for fixed path transmissometers using an air measurement to establish the  $\alpha = 0$  reading. Their data agrees with that produced by daylight telephotometry, visual threshold range, and by several other techniques for measuring alpha which are described in paragraphs that follow. Higher collimation does not result in an appreciably different value of the volume attenuation coefficient.

*Alpha from Measurements of Irradiance On Axis.* The curves in Section 4.4 show several combinations of beam diameters, beam divergences, and path segments for which the alpha-slope is followed when the receiver is an irradiance collector. Many ways of measuring alpha are suggested by these curves. In most practical circumstances, however, they are not attractive options from the standpoint of convenience.



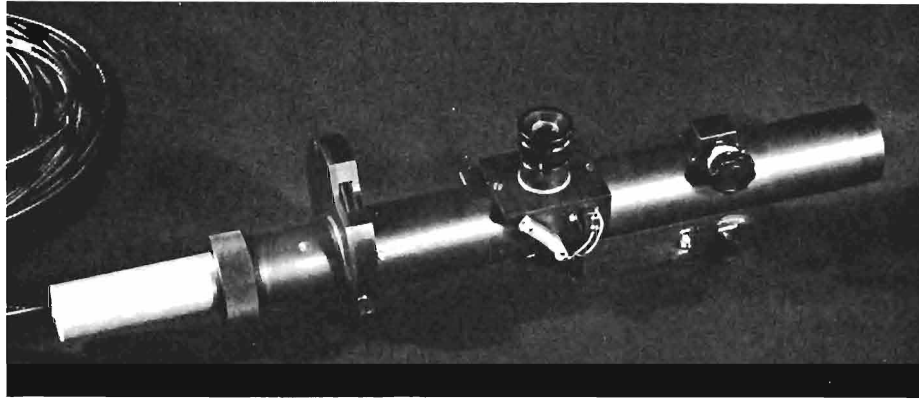


Fig. 2-3. Visibility Laboratory Mark IV photoelectric telephotometer.

*Alpha from Telephotometry of an Extended, Diffuse Source.* The most convenient way of measuring alpha at night with the underwater tower and track at Diamond Island made use of the Mark IV telephotometer and an extended, diffuse source of light at variable distance in the water. The method evolved from the experiment diagramed in Fig. 2-1. Telephotometer measurements of the apparent radiance of the center of the diffusely emitting surface produced a straight line on a semilogarithmic plot of apparent radiance vs. lamp distance. The numerical slope of this line agreed exactly with alpha measured by the transmissometer and other techniques described above. In this case all of the collimation was provided by the excellent telescopic optical system of the Mark IV telephotometer.

In practice the diffusely emitting surface was that of a special inside-coated 1000-watt diving lamp made for the author by the Large Lamp Department of the General Electric Company, Nela Park, Ohio through the courtesy of Dr. Sylvester K. Guth. These lamps have served many special research purposes throughout nearly 10 years. Fig. 4-9 shows one of the production type 1M/G25 G.E. 1000 watt clear diving lamps in place on the first underwater cart. Clear lamps were not used in measuring alpha. A corresponding mounting was provided on the second underwater cart. The Mark IV telephotometer was used with a 1/4 degree field of view. A standardized technique was adopted in which the apparent radiance of the bulb was measured at lamp distances of 8, 16, 24, and 32 feet. The results were plotted on special graph paper having a nomographic scale on which  $\alpha$  and  $1/\alpha$  could be read. Fig. 2-4 is an example of a typical determination of alpha by this technique. The volume attenuation coefficients were measured in this way throughout all of the experiments described in Sections 4, 5, and 6.

*Alpha for Laser Light.* Light from a continuous laser, like the argon-ion laser used in the laboratory tank, is easy to use for measuring the volume attenuation coefficient. Several of the foregoing techniques are applicable. For example, the method described in the preceding paragraph can be used by letting the laser beam strike a table tennis ball. This becomes a uniform diffusely emitting source suitable for telephotometry at selected distances. A more convenient method, illustrated by Fig. 2-5, was used, however, in taking the data given in Section 7. Light from the laser after passing through a water path of suitable length entered the measurement window and passed through an opaque stop having a clearance hole about 1 cm in diameter. The beam then traversed approximately 1 meter of air before entering an integrating sphere through a 1 cm clearance hole. The path length in water was varied by moving the cart, and the resulting photoelectric data were plotted in a manner similar to Fig. 2-4. This method was also used at

Diamond Island to measure alpha with light from the RCA underwater pulsed laser. This measurement was not made regularly because it was much more time consuming than telephotometry of the 1000 watt incandescent lamp. The value of alpha obtained with light from the RCA laser was identical with that found by means of incandescent light and the Wratten No. 61 filter.

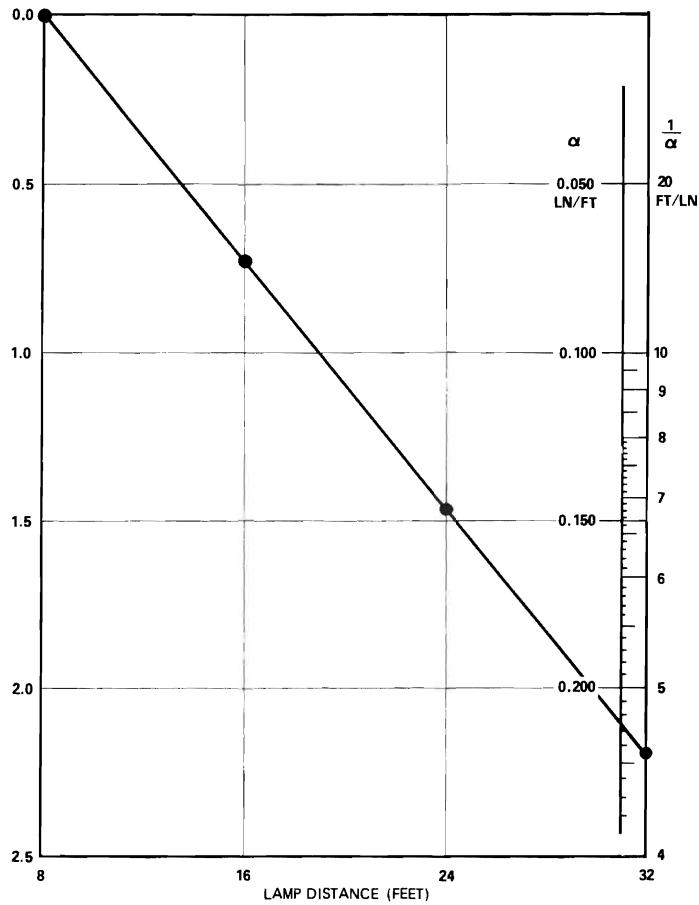


Fig. 2-4. Semilogarithmic plot of the relative apparent radiance of an extended, diffusely emitting, submerged source at 8, 16, 24, and 32 feet from the Mark IV telephotometer. Attenuation length and alpha are indicated by the intersection of the data line with a vertical nomographic scale. The 24-foot measured water path corresponded to about 5 attenuation lengths at Diamond Island.

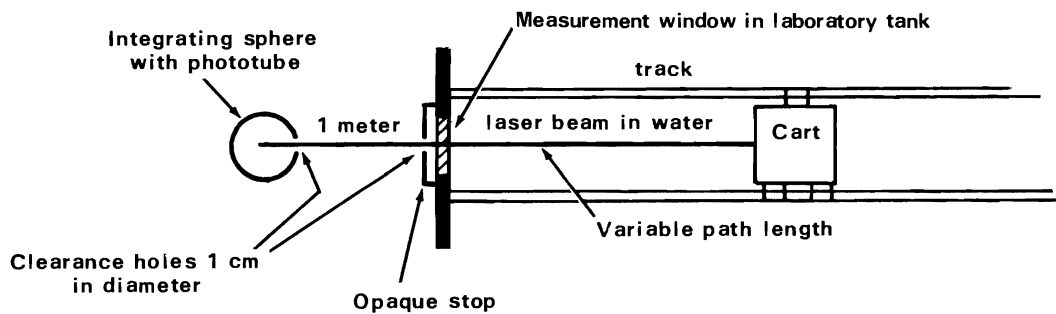


Fig. 2-5. Schematic plan view of technique for measuring volume attenuation coefficient ( $\alpha$ ) in the laboratory tank with light from the argon-ion laser (see Section 7).

## DEFINITIONS OF VOLUME ATTENUATION COEFFICIENT

A measurable optical property of natural waters that has been called the spectral volume attenuation coefficient has been introduced in terms of experiments, but formal definitions have been postponed for reasons given early in Section 2.4 (See p. 2-4). All of the several formal definitions appearing in the literature lead to conceptual uncertainties on the part of engineers concerned with specific applications. This is chiefly because the definitions tend either to ignore, or to be ambiguous with respect to, light which experiences scattering but at so small an angle that it still reaches the detector. The amount of such light may not be negligible, due to the intense scattering produced by all natural waters at very small forward angles. Practical systems differ with respect to the way they collect forward-scattered light. A theory-based statement like that on p. 216 of Appendix A which relates  $\alpha$  to "residual radiant power reaching a distance  $r$  without having been deviated by any scattering process" is less sensitive to the dilemma than are definitions which identify the attenuation coefficient with "residual image-forming light received by the detector" or which specify that light must be scattered sufficiently "to fall outside the summative diameter of the detector mosaic" to be counted as attenuated flux. The latter statements seem to imply that  $\alpha$  must be different for each application, depending not only upon the summative diameter of the detector mosaic but also upon more subtle details, including the phase delays, if any, in the scattered light.

No instrument for measuring  $\alpha$  can match all user applications. Perhaps it can match none exactly. Is the matter hopeless? Not at all. The experimental finding that identical numerical values are produced by a wide variety of quite different methods for measuring the volume attenuation coefficient indicates that inherent compensations are present which, within the precision and accuracy of conventional good radiometric techniques, suffice to produce a stable numerical optical property of natural waters that has widespread applicability to practical problems. For example, in a "lashed-together" comparison at the U.S. Navy's Morris Dam Test Facility in March 1970 identical values of  $\alpha$ , within instrumental precision, were measured in low clarity waters ( $\alpha = 2.4$  to  $\alpha = 3.4$  ln/m) with the excellent doubly collimated transmissometer described by R. W. Austin and T. J. Petzold,\* having an effective receiver field of view substantially less than 1-degree, and with the splendid doubly-collimated transmissometer described by G. Sorenson and R. C. Honey,\* which discriminates against light which has been scattered more than 1/6-degree from the beam axis.

Many comparisons of beam transmittance measurements using various geometries were made on the underwater optical benches at Diamond Island and in the laboratory ocean-simulation tank at Scripps Institution of Oceanography. These experiments included some with water paths several meters long and with very highly collimated source and receiver fields ( $> 0.2$  mr). Only in extreme cases were  $\alpha$  measurements sensitive to high transmissometer collimation. Existing instruments, such as those referenced above, as well as the many other techniques for  $\alpha$  measurement described earlier in this section, produce effectively identical measures of an attenuation coefficient which is applicable to naked-eye visibility by swimmers, to normal underwater photography and television, and to most other applications.

Specially measured attenuation coefficients may be needed for unusual imaging systems having very high resolution, but each such case needs to be studied individually using valid data on very small-angle scattering for the specific type of water in which the equipment is to be used. The latter requirement stems from the variability of scattering at very small forward angles depending upon the concentration of

\* See S.P.I.E. Underwater Photo-optical Instrument Application Seminar Proceedings p. 115-116 and p. 133-137, February 1968.

particles having diameters of 100 micrometers or more. In high resolution imagery, effects due to thermal inhomogeneities and salinity gradients in the water must also be considered.

#### SPECTRORADIOMETRIC MEASUREMENTS OF THE VOLUME ATTENUATION COEFFICIENT

Nearly all of the experiments made at Diamond Island were in a single spectral region, because only "monochromatic" effects were being studied. Most of the Visibility Laboratory's measurements of spectral effects in water have been made at sea. The spectral band used at Diamond Island was selected with care; it is defined by the Wratten No. 61 filter. (See Appendix G, Fig. 2.)

The criteria originally considered when the Wratten No. 61 green filter was selected (1949) included the following:

- (a) Absorption should be at or near minimum.
- (b) Absorption should be nonselective or nearly so.
- (c) Spectral band-width should be as large as possible in the interest of maximizing photoelectric sensitivity for long-range measurements.
- (d) The reflection function of the water (see p. 233 of Appendix A) should be independent of depth.
- (e) The effective spectral band pass established by the filter should not be appreciably narrowed by the action of the water at long path lengths.

The Wratten No. 61 filter seemed to fulfil these requirements best at Diamond Island on the basis of inferences from the results of tests with many band-pass and high-pass filters.

It was a happy coincidence that when the RCA laser appeared at Diamond Island fifteen years later that the wavelength of the light it emitted (530 nanometers) corresponded closely to the peak transmission of the Wratten No. 61 filter already in use at the field station. When, however, the initial measurements of irradiance on-axis at long range seemed to show that laser light propagated differently than did incandescent light (a tentative conclusion shown later to be untrue) the possibility that the effective band-pass established by the filter for incandescent light was narrowed by the action of the water at long path lengths arose once more. It was felt that a better exploration of this possibility than was accomplished in 1949 could and should be made.

The author's colleague, John E. Tyler, was asked to bring his new double-grating, recording, photoelectric submersible, two channel spectroradiometer to Diamond Island for the purpose of measuring the spectral volume attenuation coefficient with 10 nanometer resolution throughout the visible spectrum. From such data the effect of long water paths on spectral band-pass can be calculated.

In Fig. 2-6 workmen are preparing to hand Tyler's spectroradiometer to divers, who will mount it on the lake bottom. Tyler and Fred Pinkham, supervisor of the field station, supervise. In Fig. 2-7 Tyler operates the remote controls and annotates the recorder record as the spectral volume attenuation coefficient of lake water is measured from 400 nm to 700 nm with 10 nm monochromator band pass. The resulting data are given in Table 2.1, and are plotted as curve D in Fig. 2-8.

The transmittance of a Wratten No. 61 filter is also tabulated as a column in Table 2.1. The attenuation coefficient for the band-pass of the Wratten No. 61 filter and for a nonselective source-receiver combination were calculated for the first meter of path, the second meter of path, the third meter of path, and

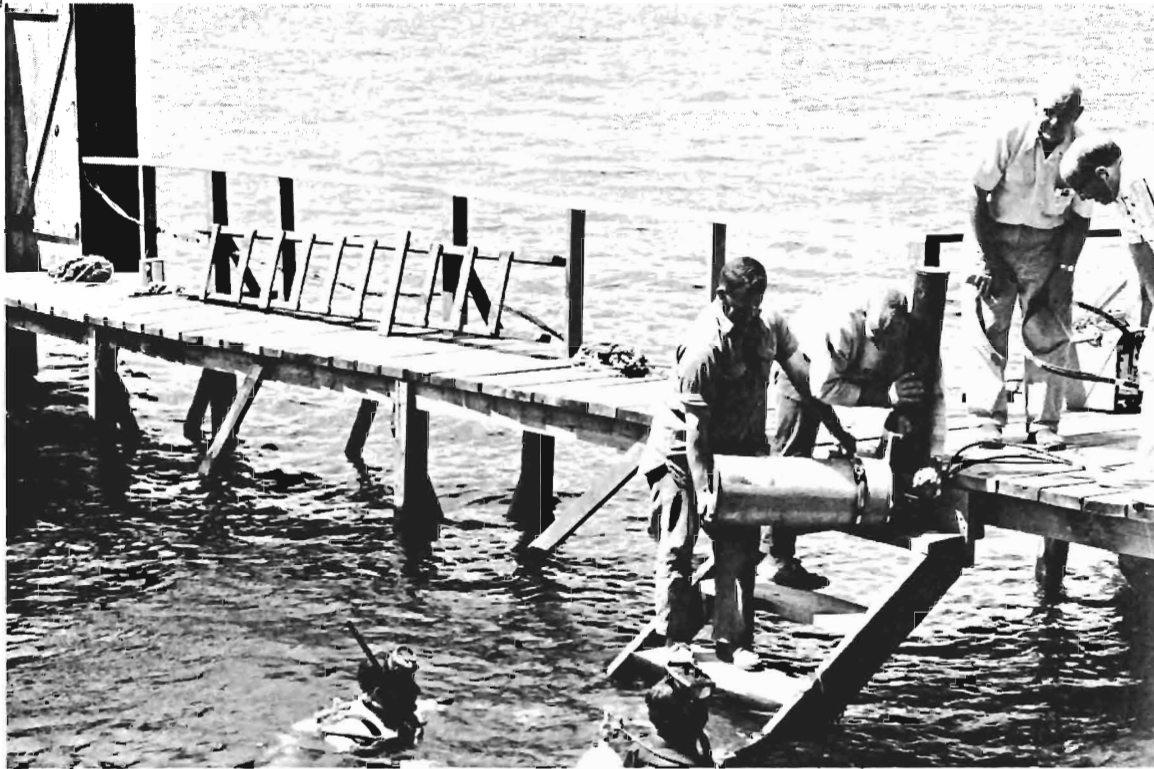


Fig. 2-6. Visibility Laboratory submergible double-grating, recording, photoelectric spectroradiometer being placed underwater to make spectral measurements of alpha.

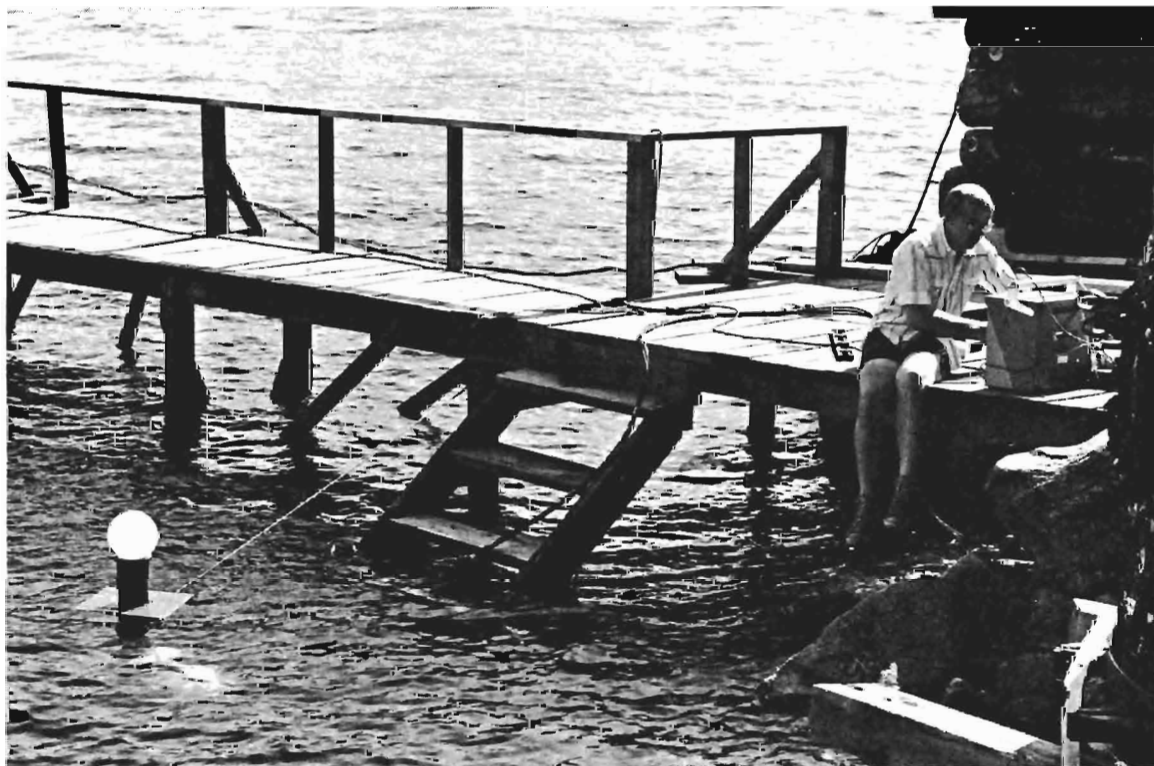


Fig. 2-7. Spectral volume attenuation coefficients being measured by John E. Tyler at Diamond Island.

TABLE 2.1

Wavelength (millimicrons)	Attenuation* Coefficient (relative values)	Transmittance* per unit of path length	Transmittance of Wratten No. 61 Filter
400	.870	0.419	
410	.798	0.450	
420	.750	0.472	
430	.685	0.504	
440	.615	0.541	
450	.575	0.563	
460	.548	0.578	
470	.522	0.593	
480	.500	0.606	.0033
490	.480	0.619	.0400
500	.462	0.630	.1660
510	.445	0.641	.3230
520	.430	0.650	.4000
530	.420	0.657	.3960
540	.414	0.661	.3450
550	.410	0.664	.2630
560	.408	0.665	.1730
570	.414	0.661	.0970
580	.428	0.652	.0440
590	.473	0.623	.0166
600	.575	0.563	.0038
610	.608	0.544	
620	.627	0.534	
630	.642	0.526	
640	.655	0.519	
650	.670	0.512	
660	.684	0.504	
670	.698	0.498	
680	.718	0.488	
690	.780	0.458	
700	.875	0.417	

---

\* The attenuation coefficients in this table are expressed in relative units. The water at Diamond Island has an attenuation length of about 1.5 meters/ln at 530 nm. Relative values of spectral transmittance lead to the conclusions drawn from these data.

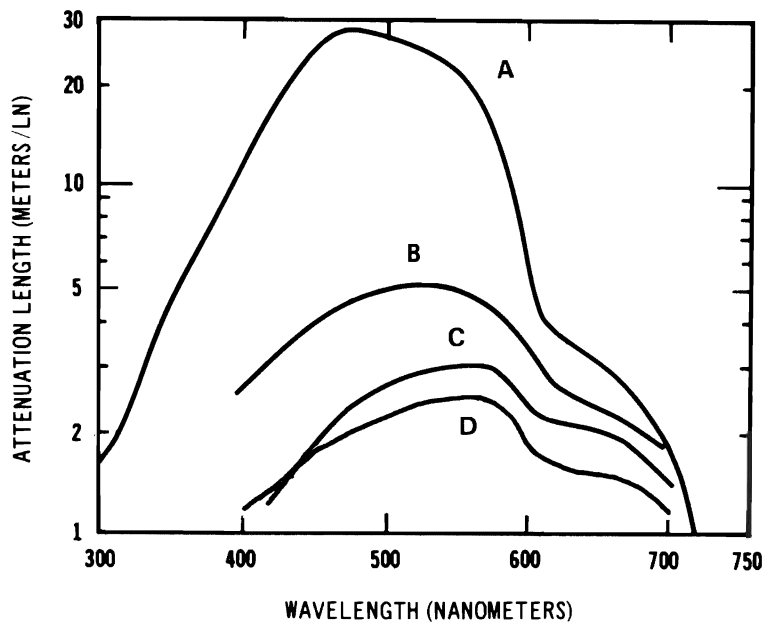


Fig. 2-8

Spectral attenuation length ( $1/\alpha$ ) vs wavelength for (A) distilled water, (B) Coastal water, (C) Chesapeake Bay, (D) Diamond Island. Data sources: A, B, C: E. O. Hulbert, *J. Opt. Soc. Am.* **35**, 698 (1945); D: Section 2.4 of this report using relative units. At Diamond Island the attenuation length for 530 nm is about 1.5 meters/ln.

so on. The result of this type of calculation out to 30 meters is shown in Fig. 2-9A. This demonstrates that the attenuation coefficient for the first meter of water is about 2 percent greater than the attenuation coefficient for monochromatic light of wavelength 530m $\mu$  and that this 2 percent effect gradually diminishes essentially to zero at a lamp distance of approximately 30 meters, or about 12.6 attenuation lengths for laser light. The calculations have been continued to lamp distances of 60 meters. The trend of the curve continues and at a lamp distance of 25 attenuation lengths the attenuation coefficient has become approximately 2 percent less than that for the laser beam. Additional interpretation is provided by Fig. 2-9B, in which an equivalent volume attenuation coefficient ( $\alpha'$ ) for the entire underwater path is plotted for path lengths (lamp distances) from 1 to 60 meters; this was calculated by equating the integrated beam transmittance for each path length to  $\exp[-\alpha' r]$  and solving for  $\alpha'$ . Figure 2-9 shows that the equivalent volume attenuation coefficient gradually approaches the spectral volume attenuation coefficient (0.420 ln/m) for 530 nm as the length of the path increases. For a 60 meter path the agreement is within 0.2 percent. It should be noted that the effect of lake water on the spectral band-pass of the Wratten No. 61 filter is small. No correction is required in the position of the plotted points in Fig. 6-1.

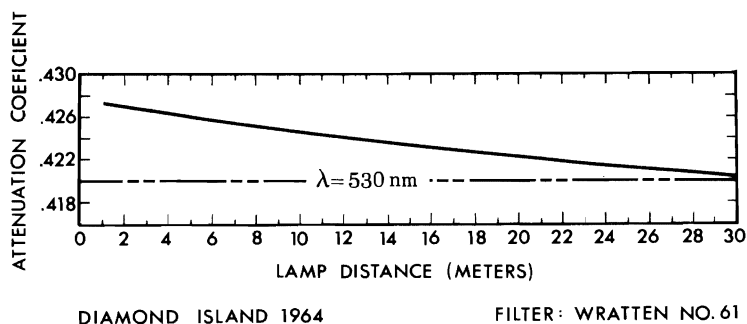


Fig. 2-9A. Illustrating the (small) change in attenuation coefficient with position along the underwater path.

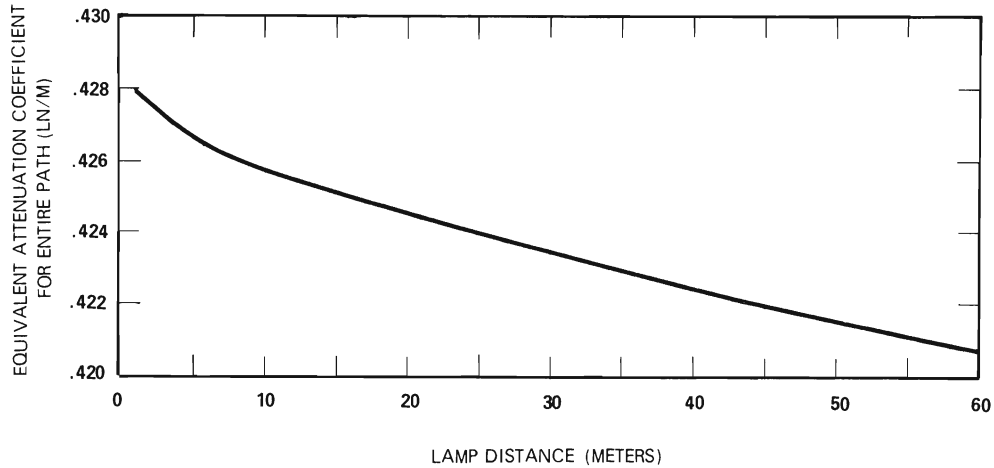


Fig. 2-9B. Illustrating the (small) change in equivalent attenuation coefficient with path length.

## 2.5 MEASUREMENT OF THE VOLUME SCATTERING FUNCTION

Measurements of the volume scattering function were made from 1950 until 1966. Most of them employed apparatus that was attached to a floating hollow box having a room with underwater windows. Technically a *caisson*, this floating instrument platform was known to Laboratory personnel as the *barge*. It is shown in Fig. 2-10 moored near the outer end of the underwater track. Both sides of the barge had

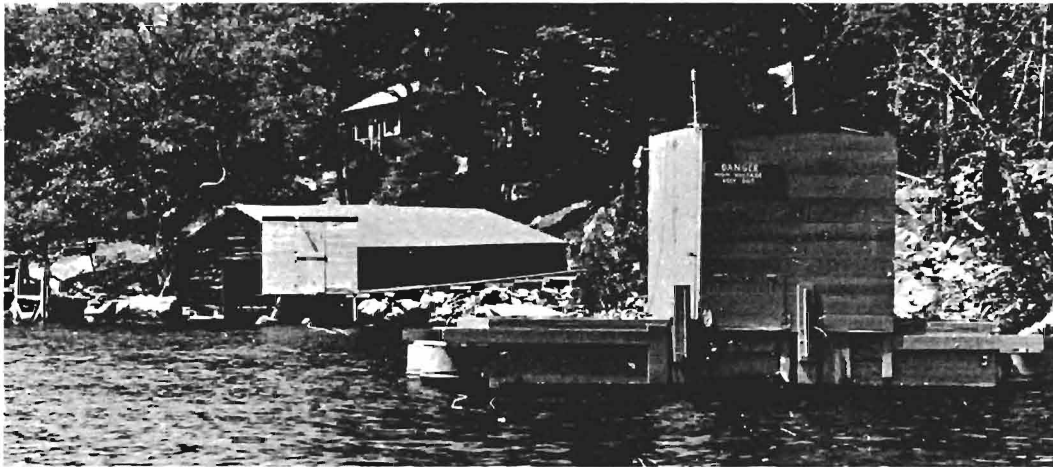


Fig. 2-10. Floating instrument platform (barge) moored near the outer end of the underwater track at Diamond Island. The laboratory building can be seen on the wooded slope beyond the boat house.

centrally located, circular underwater windows with their centers 2.5 feet below the water surface. These windows can be seen in Figs. 2-11 through 2-14, which show the caisson out of water on a marine railway at a local boat yard, where it was built from a Visibility Laboratory design in 1948.

Figures 2-11 through 2-14 show the scattering meter attached to the barge. In the position shown, the incandescent projector sends a beam of light outward above an I-beam and into a light-trap. The trap consists of a hollow tube which terminates in a black-glass mirror set at 45 degrees to the vertical. A re-



movable cap above the mirror permits easy focusing and beam alignment. The scattering volume is located directly above the pivot at the center of the I-beam. The Mark IV telephotometer, shown in Fig. 2-3, is used inside the barge. Its optical axis passes through the center of the underwater window and directly above the pivot. The telephotometer was focused so that its field stop was conjugated to the scattering volume. A circular field of view 1.0 degree in angular diameter was frequently used. Between the projector and the scattering volume is a rectangular *Waldram stop* having a rectangular aperture 1 inch high and 0.75 inches wide. This stop pivots about an off-center point on the I-beam and is maintained parallel to the axis of the telephotometer by means of a blackened tension line. Thus, it maintains the scattering volume constant at all scattering angles.

The telephotometer would measure the volume scattering function at a large scattering angle, say 140 degrees, if used in the position shown in Figs. 2-11 through 2-14. The I-beam is carried by a circular turntable equipped with detents at 5 degree intervals. In use, a swimmer turns the I-beam through 5 degree increments of angle as directed by the experimenter through an underwater loudspeaker. Measurements can be made at scattering angles from 5 to 165 degrees. At scattering angles of 5 and 10 degrees the light trap is removed and replaced by metal baffle plates put in place by the swimmer. Polarizers are sometimes used on the projector and on the telephotometer.

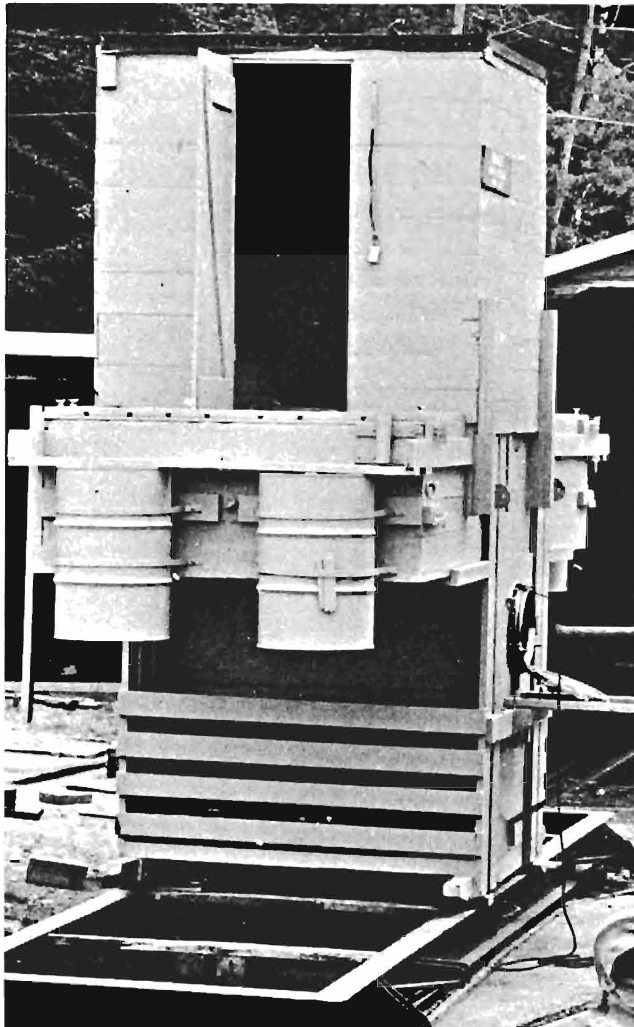


Fig. 2-11

Research barge out of water on a marine railway. Scattering meter attaches to the barge outside the circular underwater window on the right.

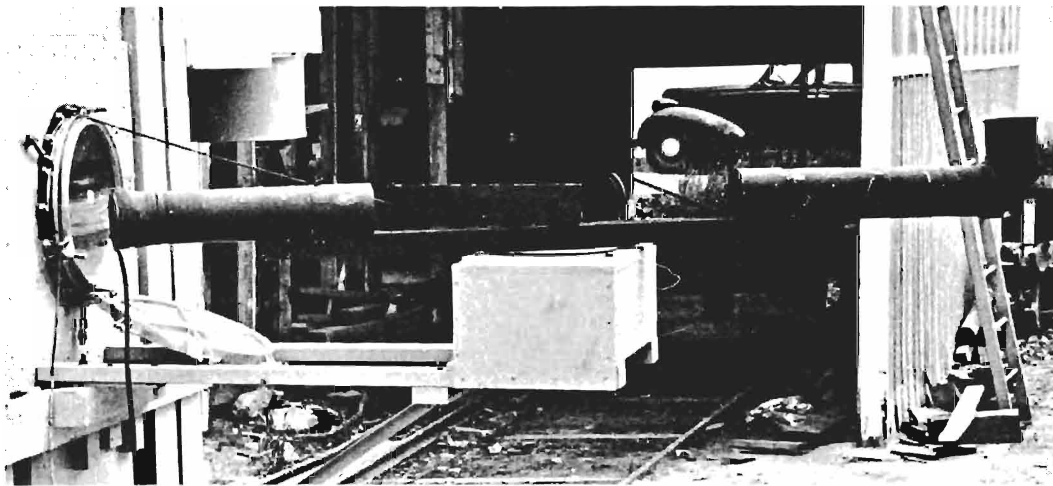


Fig. 2-12. Scattering meter attached to research barge.

Fig. 2-13.  
Scattering meter attached to  
research barge.

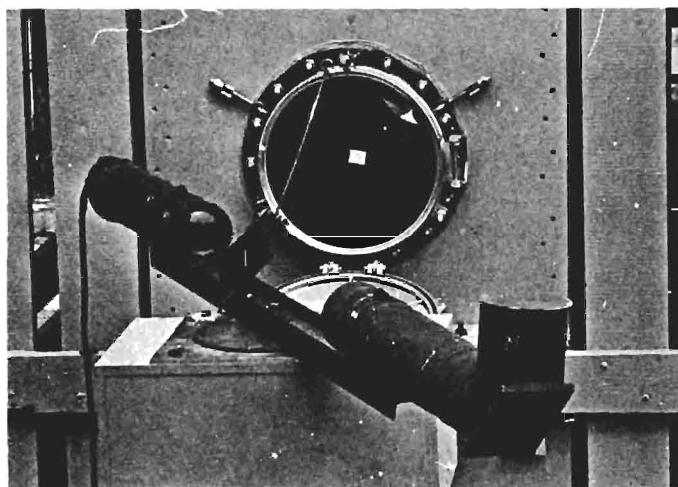
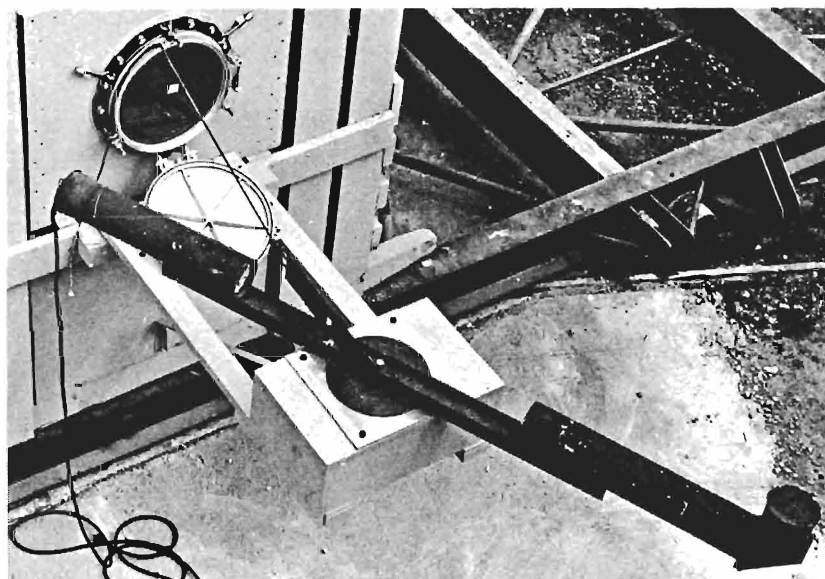


Fig. 2-14.  
Scattering meter attached to research barge.

*Calibration of the Scattering Meter.* The scattering meter was calibrated by mounting a black-glass mirror directly above the pivot point of the I-beam (i.e., at the center of the scattering volume) so that the light beam was reflected directly into the telephotometer inside the barge. Both the entrance pupil and the field stop of the telephotometer were larger than the light beam. Thus, the telephotometer measured the total power in the beam it received. The reflectance of the black-glass mirror was calculated from refractive index data by means of Fresnel's equation. These data together with geometrical measurements permitted the scattering meter to be calibrated in absolute units.

*Elimination of Stray Light.* A serious amount of stray light is caused by multipath (glow) effects in the water when the volume scattering function is measured at small angles. This must be minimized and data corrections determined for all values of the volume scattering function below 45 degrees. Minimization can be achieved by placing blackened metal plates in appropriate locations before each datum is taken. The experimenter, looking out through the window of the barge, can see the glow of multiply scattered light in the water and direct his swimmer-assistant in the best placing of the baffles. Erroneous readings cannot be avoided by this means alone, especially at scattering angles of 5, 10, and 15 degrees. Here stray light may equal or exceed that from the scattering volume. A simple correction to the data can, however, be generated as follows: After each datum has been taken, the swimmer-assistant holds a small, black, opaque piece of metal attached to a long wand-like handle in the path of the light from the projector just before it reaches the Waldram stop. No light then reaches the scattering volume; the residual reading of the telephotometer is a measure of the stray light. This value must be subtracted from the original (total) datum. Unless this correction is made, very serious distortions of the volume scattering function at small scattering angles will result.

*Measurements at the Underwater Tower.* The second underwater tower was equipped with windows on each side in addition to the one above the track. In mid-1964 the scattering meter described in the preceding paragraphs was removed from the barge and installed on the underwater tower, outside the window nearest shore. This location is directly beneath the door and footbridge shown in Fig. 2-6. All details of the measurement remained the same.

*Measurements with the Laser.* During an absence of the author from the field station in August 1965 several experiments were made by visiting scientists from the US Naval Ordnance Test Station, China, Lake, California. In one of these, the projector, Waldram stop, and light trap were removed from the I-beam of the scattering meter and the RCA underwater laser was mounted in place of the projector. The shape of volume scattering function curves thus produced appeared to have distortions typical of the effects of stray light at small scattering angles. This observation impelled the author to repeat the experiment during the following summer (1966). Stray light corrections were generated by catching the laser beam in a tiny black metal cup just before it reached the scattering volume. After these corrections were applied, the 1966 curves showed none of the distortions exhibited by the 1965 data.

For comparison, volume scattering function measurements were made with the scattering meter in its regular configuration (as in Figs. 2-11 through 2-14) on the same night in 1966 on which the laser data were obtained. The result is shown by the dashed line in Fig. 2-15. On this occasion a small-angle coaxial scattering meter of the type shown in Fig. 8 on p. 218 of Appendix A was used to measure the volume scattering function at 0.5 degrees; see Fig. 2-15. This instrument is shown in Fig. 2-16. It was designed and constructed by the Visibility Laboratory for the US Naval Air Development Center, and was first used extensively at sea by Dr. Robert Morrison, then of N.A.D.C.

The laser data are shown by diamonds in Fig. 2-15. At the larger scattering angles they parallel the incandescent curve but are slightly higher. Between 30 and 40 degrees the laser data make an unexplained decrease by a factor of about 2 and then parallel the incandescent curve again. There is no certain explanation of this anomaly in the laser data. It went unnoticed until after data reduction a day or two later. There was no opportunity to repeat the experiment. It may be speculated that some change occurred in the built-in photoelectric monitor system of the laser or in one of the oscilloscopes. Some operator error may have been made, or the oscilloscope pictures (i.e., the data points) may have been labeled incorrectly with respect to the scattering angle. The author believes that if it had been possible within the constraints of time and funds to have devoted another night to repeating the laser scattering experiment, the laser points would have formed a continuous, smooth curve parallel to and slightly above the nonpolarized incandescent curve at all scattering angles.

A reason for the small vertical displacement between the laser data and the incandescent points was sought. It was known that the laser light was polarized whereas the incandescent beam was not. A test of this effect was performed by replacing the projector of the scattering meter with the collimated underwater incandescent projector used for the experiments described in Section 3 of this report. The aperture of the projector was stopped down to a diameter of 3/16 inches as a rough match of the size of the laser

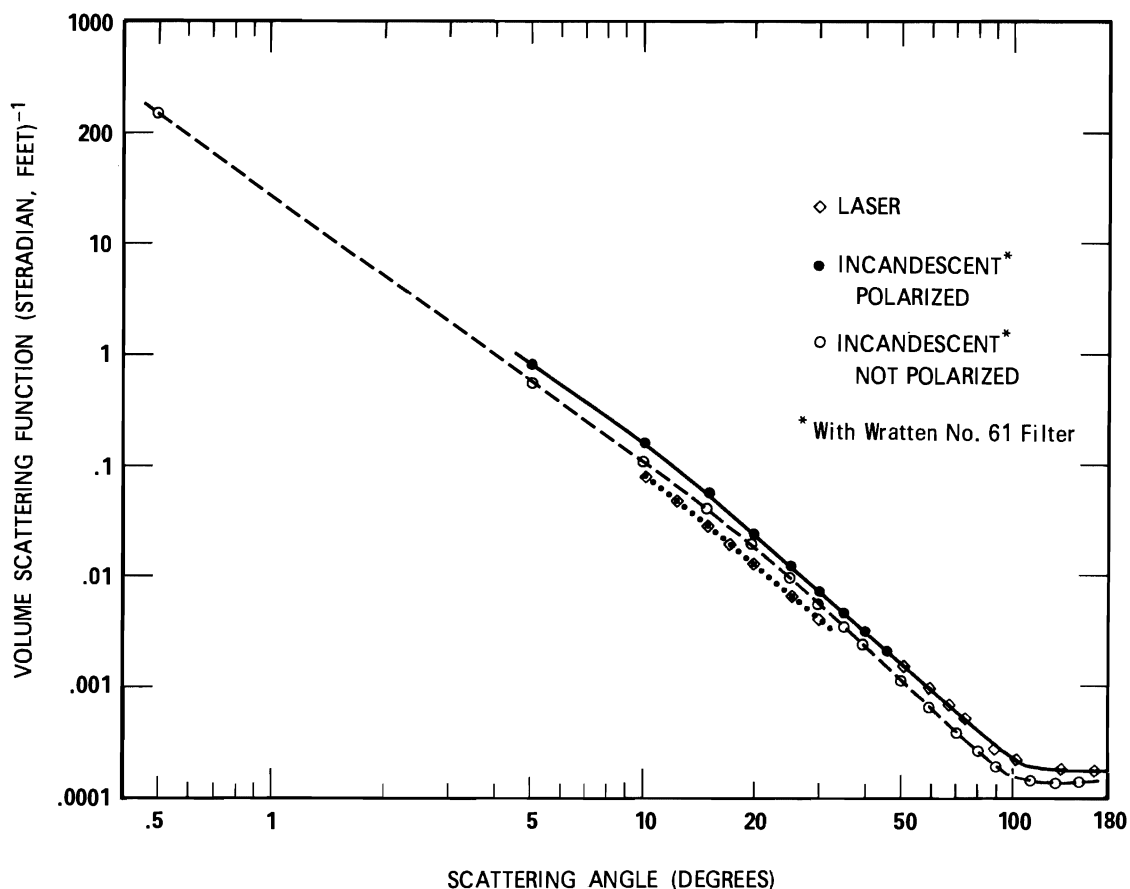


Fig. 2-15. Volume scattering function measurements at Diamond Island.

beam. The beam spread of 3.3 milliradians was used in order to further approximate the geometry of the laser beam. A linear polarizer was added to the projector and oriented to match the plane of polarization with that of the laser. The Waldram stop and the light trap were removed, just as in the case of the laser experiment. A full curve of the volume scattering function was run on a night when the measured attenuation length of the lake water closely matched that of the occasion when the laser data had been taken. The resulting data matched the position of the laser (diamond) points in Fig. 2-15 from 165 to 40 degrees so closely that any random differences were within the diamonds. Below 40 degrees the polarized incandescent data are shown by solid circles; they form a smooth continuation of the data at larger scattering angles. The solid curve in Fig. 2-15 represents the polarized incandescent data and the laser data as well between 40 and 165 degrees; the author believes that it also represents the volume scattering function for laser light at the smaller scattering angles. If so, laser light and similarly polarized incandescent light have identical volume scattering functions between scattering angles of 5 and 165 degrees.

*Form of the Volume Scattering Function.* The log-log plot of the volume scattering function vs. scattering angle in Fig. 2-15 is nearly a straight line from 0.5 to 70 degrees. The slope varies from  $-2.4$  to  $-2.9$ . At some small scattering angle the slope must diminish, perhaps to zero, in order to avoid an impossibly large total volume scattering coefficient. There is some earlier evidence from the small-angle scattering meter in Fig. 2-16 that diminution of the slope is seen at 0.25 degrees. If significant "roll-off" has begun at that angle, diffraction considerations would make it appear that the lake contains many low-index scatterers having effective diameters of 100 micrometers or more.



Fig. 2-16. Small angle *in situ* scattering meter similar in design to the coaxial scattering meter diagramed in Fig. 8 on p. 218 of Appendix A.

## 2.6 MEASUREMENT OF THE VOLUME ABSORPTION COEFFICIENT

The spreading of laser beams in water\* depends upon the ratio of the spectral volume attenuation coefficient ( $\alpha$ ) to the spectral volume absorption coefficient ( $a$ ), as shown in Section 7. Equipment capable of making *in situ* measurements of absorption in natural waters is rare,\*\* although a conventional irradiance meter can be used in the manner described on p. 233 of Appendix A to measure the net inward flow ( $dP/dv$ ) of monochromatic radiant power to any element of volume ( $dv$ ) in the daylight sea. That flow equals the product of the volume absorption coefficient ( $a$ ) and the scalar irradiance ( $h$ ), defined later in this section.†

At Diamond Island, measurements of the absorption coefficient ( $a$ ) were needed at night. This was accomplished with available submerged light sources by means of a technique based upon the divergence theorem described in the following paragraphs. The same method was later adapted for use in the ocean simulation laboratory tank (See Section 7), where all of the pertinent optical properties of the water were measured *in situ* with laser light.

Other methods for measuring the absorption coefficient *in situ* involve inescapable, inherent approximations, often of uncertain magnitude. The divergence theorem, however, is a rigorously exact principle, so that any experimental approximations are at the option of the experimenter and are sources of error only if corrections are not applied to the data.

### THE DIVERGENCE RELATION

The rigorous, fundamental principle governing absorption of light in water may be written‡

$$\nabla \cdot \bar{H} = ah, \quad (2-1)$$

where  $\bar{H}$  is the *spectral vector irradiance*, having components  $\bar{H}_x$ ,  $\bar{H}_y$ , and  $\bar{H}_z$ . For example,  $\bar{H}_x = H_x(+)-H_x(-)$ , where  $H_x(+)$  is the spectral power per unit of area flowing across the plane  $x = \text{constant}$  in the direction of increasing  $x$  and  $H_x(-)$  is the corresponding spectral power density on the same plane in the direction of decreasing  $x$ . The symbol  $h$  denotes *spectral scalar irradiance*, and  $a$  is the spectral volume absorption coefficient.

---

\* Also, the resolution of underwater imagery.

\*\* Sorenson, G. and Honey, R. C. "Instrumentation for Measuring the Visibility Limiting Characteristics of Sea Water" S.P.I.E. Underwater Photo-Optical Instrument Applications Seminar Proceedings p. 115, February 1968.

† Also defined on p. 399 and p. 400 in Vol. 1, Chapter 8, Section 4 of THE SEA, M. N. Hill, General Editor, Interscience Publishers, John Wiley & Sons, N. Y. 1962.

‡ Gershun, A. THE LIGHT FIELD, Svetovoe pole, Moscow 1936, see p. 102 of English translation in Journal of Mathematics and Physics 18, 51 (1939).

Preisendorfer, R. W., "The Divergence of the Light Field in Optical Media" SIO Ref. 58-41 (July 1957) PB 153 900, AD 247 620.

Preisendorfer, R. W., "Simple Formulas for the Volume Absorption Coefficient in Asymptotic Light Fields" SIO Ref. 58-79 (November 1958) PB 153 996, AD 212 742.

## SCALAR IRRADIANCE

Spectral scalar irradiance  $h(p)$  is the total monochromatic radiant power arriving at any specified point  $p$  from all directions  $\theta, \phi$  about the point. It can be calculated from the spectral radiance distribution  $N(p, \theta, \phi)$  about  $p$  by equation

$$h(p) = \int_{4\pi} N(p, \theta, \phi) d\Omega . \quad (2-2)$$

Scalar irradiance does not concern the directional nature of the light field; only the *total* power arriving from all directions is specified. It is related, by the velocity of light in the medium, to the volume density of spectral radiant energy.

## TECHNIQUE OF ABSORPTION MEASUREMENT

Convenience was served at Diamond Island, and in the laboratory tank as well, by using a 1-dimensional flow of light. Since daylight was not available, a spherical (effectively plane) light field was produced by a distant uniform spherical lamp. This was a special inside-frosted 1000 watt incandescent diving lamp made for the author by the General Electric Company as a modification of the commercial G.E. 25M-1 lamp. Alternatively, the spherical lamp was a table tennis ball lighted from the rear by a laser beam. The divergence relation (Eq. 2-1) then becomes

$$\frac{d\bar{H}(r)}{-dr} = a h(r) , \quad (2-3)$$

where  $r$  is the distance of the photometer from the lamp.

Instrumentation at the underwater tower, as well as in the laboratory tank, was simplified by measuring only the light moving away from the lamp (i.e., toward the photometer in the tower), thereby neglecting the return flux. This approximation was an excellent one, partly because the return flux was only 1 or 2 percent of the outgoing flux but also because both  $\bar{H}(r)$  and  $h(r)$  are affected nearly equally. Thus, a first-order correction for this small experimental approximation is provided automatically by the nature of Eq. 2-3. Analytically, the single-flow approximation can be represented as follows:

The integral  $\int_{4\pi} N(p, \theta, \phi) d\Omega$  can be subdivided into any desired number of parts. Thus, in the case of the spherically symmetric light field surrounding a uniform point source in uniform water, where the net flow of radiant power is radially outward,  $h(r) = h(r,+) + h(r,-)$ ; here

$$h(r,+) = \int_{\substack{\text{inner} \\ \text{hemisphere}}} N(r, \theta, \phi) d\Omega \quad (\text{outward flux}),$$

and

$$h(r,-) = \int_{\substack{\text{outer} \\ \text{hemisphere}}} N(r, \theta, \phi) d\Omega \quad (\text{return flux}).$$

At Diamond Island, and in most clear natural waters, integration of radiance distribution data shows that outward component of scalar irradiance  $h(p,+)$  comprises almost 99 percent of the total; thus,  $h(p,+)\gg h(p,-)$ . An equivalent statement holds for the corresponding outward and return components of irradiance. Thus,

$$H(r,+)=\int_{\text{inner hemisphere}}N(r,\theta,\phi)\cos\theta\,d\Omega$$

$$H(r,-)=\int_{\text{outer hemisphere}}N(r,\theta,\phi)\cos\theta\,d\Omega.$$

Because the inward flow is only a percent or two of the outward flux,  $H(p,+)\gg H(p,-)$ .

For the 1-dimensional (radial) flow (Eq. 2-3) can be written

$$\frac{d}{-dr}[H(r,+)-H(r,-)]=a[h(r,+)-h(r,-)].$$

The excellent approximation of neglecting the return fluxes then yields the expression

$$\frac{dH(r,+)}{-dr}=a\,h(r,+). \tag{2-4}$$

*Precision.* It might seem that the precision with which the derivative  $dH(r+)/dr$  in Eq. 2-4 can be measured is low. This is, indeed, true if the lamp distance is small. On the other hand, Fig. 16 on p. 222 of Appendix A and Figs. 4-30, 4-36, and 5-10 in this report show that at large lamp distances the irradiance  $H(r,+)$  closely approximates a straight semilogarithmic line; that is to say, the long-range portion of the curve can be fitted by  $H(r_2+)/H(r_1+)=\exp[-K(r_2-r_1)]$  or  $dH(r+)/dr=-K\,H(r,+)$ , where  $K$  is an attenuation function for scattered light that is identified on p. 222 of Appendix A as being numerically similar to the attenuation function  $k$  for daylight scalar irradiance. Thus, Eq. 2-4 may be written

$$K\,H(r,+)=a\,h(r,+), \tag{2-5}$$

with the restriction that  $H(r,+)$  and  $h(r,+)$  must be measured at a sufficient lamp distance to make  $H(r,+)$  linear when plotted semilogarithmically, as in Fig. 16 on p. 222 of Appendix A. That restriction serves, however, to enable  $K$  to be measured to high precision by a convenient technique described in the following paragraph, thereby solving the precision problem that is seemingly inherent in Eq. 2-4.



## MEASUREMENT OF K

The spherical diffuse attenuation  $K$  for the light field far from a uniform spherical submerged light source was measured by mounting the 1000-watt inside frosted spherical diving lamp on the underwater cart, and measuring irradiance at a sufficiently long range to produce straight lines on a semilogarithmic plot of irradiance versus lamp distance, as in Fig. 16 on p. 222 of Appendix A. At Diamond Island it was standard procedure to measure irradiance  $H(r,+)$  at lamp distances of 90, 110, 130, and 150 feet and to plot these data as illustrated in Fig. 2-17. The nomographic scale in Fig. 2-17 enabled  $K$  to be directly with high precision.

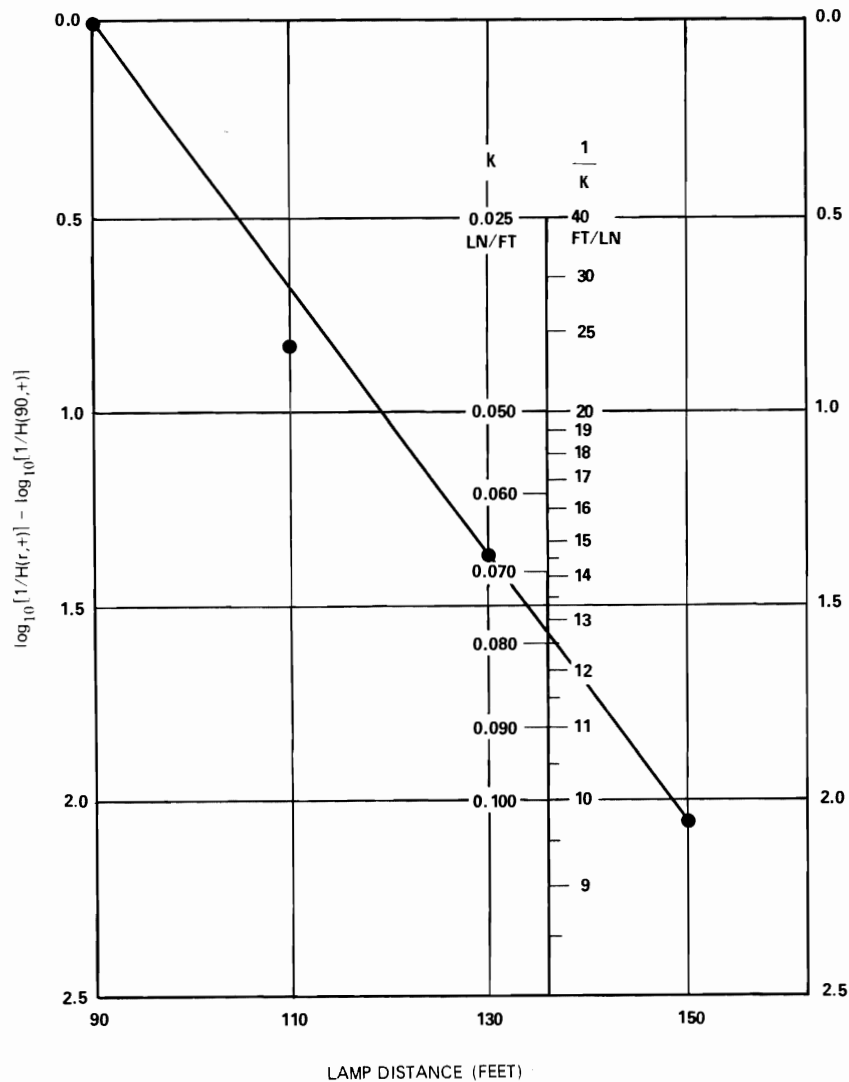


Fig. 2-17. Plot used in measurement of spherical diffuse attenuation coefficient  $K$ . The point below the line at lamp distance = 110 feet indicates that fish obscured part of the light being measured. Such errors were avoided by temporarily extinguishing the 1000-watt diving lamp and lighting another 50 feet away. When all fish had gone to the dummy lamp, it was turned off and the 1000-watt lamp was turned on. A valid irradiance measurement could then be made before the fish returned.

## MEASUREMENT OF THE RATIO $H(r,+)/h(r,+)$

Equation 2-5 may be written

$$a = K \frac{H(r,+)}{h(r,+)} \quad (2-6)$$

In the laboratory tank (see Section 7) two special irradiance collectors were used to measure  $H(r,+)$  and  $h(r,+)$ . These are shown in Fig. 2-18. They were mounted on a special cover for the measurement window. Figure 2-19 shows this cover and one of the collectors in place in the laboratory tank. An equivalent pair of collectors were used at Diamond Island. Each collector is irradiated, in turn, by a uniform spherical submerged lamp at a distance sufficient to fulfill the restriction on Eqs. 2-5 and 2-6 explained in the preceding section.

It will be noted in Fig. 2-18 that both collecting surfaces are supported by frustrums of cones which are painted glossy black. The primary intent of this design is to minimize irradiation of the rear side of the spherical collector by light reflected from the supporting structure. The shiny black conical surfaces also serve to direct unwanted flux away from the vicinity of the collector, thereby minimizing any local effects due to multiple scattering.

*Calibration.* A different degree of optical coupling exists between each collector and the multiplier phototube, which is located inside the measurement window. A calibration is, therefore, necessary. This is easily accomplished by means of the collimated underwater projector. It is brought close to the spherical collector; the projection lens nearly touches the ball. The uniform collimated beam of incandescent light or laser light produced by the projector, 50 mm in diameter, is more than large enough to cover either collector. If each element of collecting surface has cosine properties, both collectors will collect an equal amount of flux from the collimated beam, because their diameters are equal. The ratio of the photoelectric readings using the two collectors is the ratio of their respective optical couplings to the phototube.

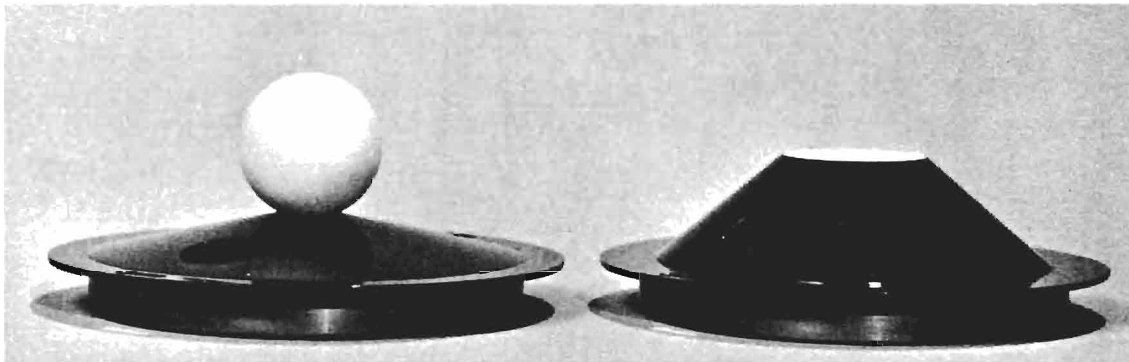


Fig. 2-18. Two special irradiance collectors used during measurement of the volume absorption coefficient (a).

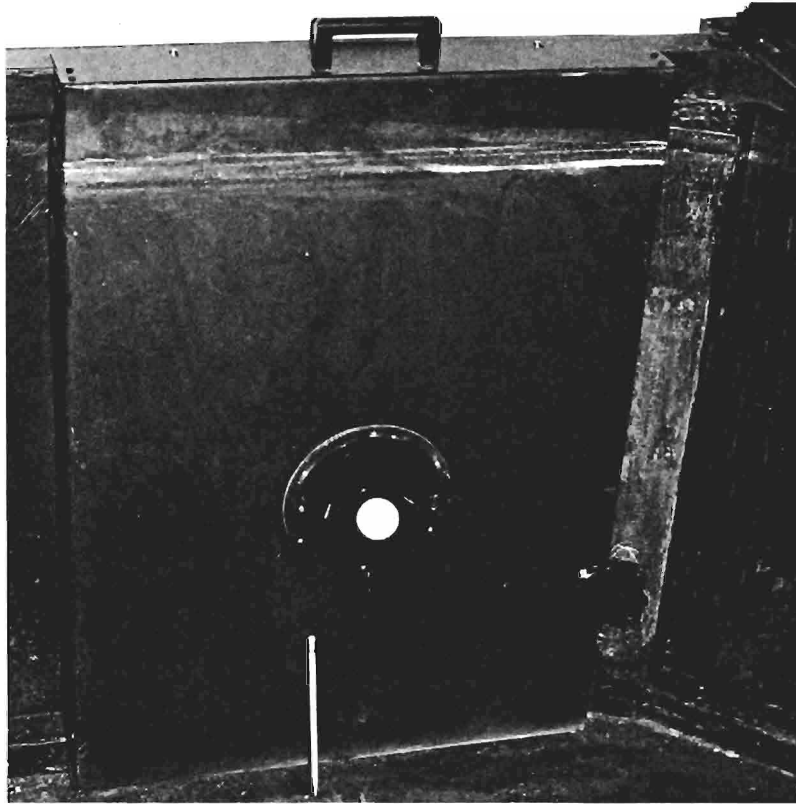


Fig. 2-19. Special irradiance collector mounted in a cover for the measurement window.

Let  $P'_H$  and  $P'_h$  be photoelectric readings (in the same relative unit) when the two collectors are irradiated by projector producing collimated irradiance  $H'$ . Then,

$$P'_H = C_H H' \quad \text{and} \quad P'_h = C_h H'$$

where  $C_H$  and  $C_h$  are coefficients of coupling for the plane and spherical collectors respectively. Hence,

$$\frac{C_H}{C_h} = \frac{P'_H}{P'_h} \tag{2-7}$$

Similarly, let  $P_H$  and  $P_h$  be the respective photoelectric readings when the two collectors are irradiated by the distant spherical lamp producing irradiances  $H(r,+)$  and  $h(r,+)$ . Then  $P_H = C_H H(r,+)$  and  $P_h = C_h h(r,+)$ , whence

$$\frac{H(r,+)}{h(r,+)} = \frac{P_H C_h}{P_h C_H} \quad (2-8)$$

Combining (2-7) and (2-8),

$$\frac{H(r,+)}{h(r,+)} = \frac{P_H P'_h}{P_h P'_H} \quad (2-9)$$

Combining Eqs. (2-6) and (2-9),

$$a = K \frac{P_H P'_h}{P_h P'_H} \quad (2-10)$$

Thus, the measurement of  $a$  is accomplished without measuring radiometric quantities in absolute units and without the loss of precision ordinarily associated with a derivative.

## COLLECTOR REQUIREMENTS

The method described above for *in situ* measurement of the volume absorption coefficient requires that *every element of area* on the surface of the spherical collector have cosine collection properties. This difficult requirement arises because each point on the spherical surface receives radiant flux from a unit solid angle centered on the direction  $(\theta, \phi)$  of an amount  $N(r, \theta, \phi) \int \cos i \, dA = \pi u^2 N(r, \theta, \phi)$ , where  $u$  is the radius of the sphere and  $i$  is the angle of incidence on the surface of the collector. The surface *must* respond properly to this flux in order to yield a valid answer. That is to say, each element of area must collect flux in a manner that is strictly proportional to  $\cos i$ . This is not easy to achieve, particularly at large angles of incidence, i.e., near grazing incidence.

The total flux received by the sphere from *all* directions is  $\pi u^2 \int_{4\pi} N(r, \theta, \phi) \, d\Omega \equiv \pi u^2 h(r, +)$ , and that intercepted by the plane irradiance collector is  $\pi u^2 H(r, +)^*$ . Since only the *ratio* of the outputs of the two collectors is used, and since both of the photoelectric readings represent flux collected by the *entire* collector, the finite size<sup>\*\*</sup> of the collectors does not affect the data.

---

\* The surface of the plane irradiance collector should also have cosine response, but the requirements are less severe because nearly all of the flux from the distant spherical lamp strikes the plane surface at small angles of incidence.

\*\* Spherical irradiance ( $h_{4\pi}$ ) is **not** involved here.

*Preparation of the Collector.* Great care was exercised in preparing and using the spherical collecting surface. Many kinds of table tennis balls were examined. None were found to be ideal for measuring absorption because of three major faults: (1) The surfaces showed residual gloss, particularly near grazing incidence. Many balls even exhibited a faint trace of an internal virtual image. Surface treatments, described below, improved the matteness of the best balls sufficiently to make them marginally useable. (2) Excess specular transmission rendered some balls unfit for use as spherical collectors. The ball must be cut in two in order to observe or measure the specular transmittance of its wall. (3) All balls have an overlapped, cemented, great circle seam. Seamless table tennis balls, formerly available, seem no longer to be on the market. The seam introduces a serious error in absorption measurements if the ball is mounted with the plane of the great circle seam perpendicular to the direction of the distant spherical lamp. This is intuitively obvious when it is recognized that the difference between the collection properties of the spherical and plane collectors stems from the way the field of scattered light "wraps around" the sphere.

Any table tennis ball selected for use in absorption measurements must be carefully cleaned with mild soap and water and/or detergents to remove finger grease. Various organic solvents may be used for the same purpose. Thereafter, the ball is handled only with gloves. The matte character of the surface can be improved by roughening it with pumice or some other mild abrasive.

Cement is used to attach the ball to its mount. Buoyancy force requires a strong bond. Difficulty with the strength of cement can, as a last resort, be solved by drilling tiny holes near the top and bottom of the ball, respectively, so that it floods. This expediency may produce cleaning problems and is suitable only when the absorption length of the water is very long compared with the diameter of the ball.

*Other Types of Collectors.* No known flat or spherical surface is perfectly matte. Departures from cosine collection properties at or near grazing incidence appear to be inevitable. The effect of such departures on the measurement of absorption coefficient are uncertain. Thus, the divergence relation method for measuring absorption coefficient, while potentially free from approximations, is affected by this experimental difficulty. The problem of cosine collection seems to have been well solved in the case of plane collectors by the exposed-edge design described by Smith.\* It may be that a sizeable, hollow, metal integrating sphere thickly and uniformly studded with many tiny exposed-edge plane collectors would represent a perfect spherical collector to within any necessary limits of radiometric precision and accuracy. The author has not yet had an opportunity to test this type of collector.

## **2.7 MEASUREMENT OF APPARENT RADIANCE DISTRIBUTION**

Power density (irradiance) on submerged surfaces is often insufficient information about their lighting. The direction from which the light arrives is important, particularly to the appearance of non-matte surfaces. The directional distribution of any given underwater lighting (see, for example, Fig. 2-1) was measured by producing that lighting on the measurement window of the laboratory tank (or the underwater tower) and measuring the resulting underwater radiance distribution with the Mark IV telephotometer (see Fig. 2-3) in the scanning mount shown in Fig. 2-20.

---

\* Smith, R. C. "An Underwater Spectral Irradiance Collector" *Journal of Marine Research* **27**, 3(1969).  
Also see: Austin, R. W. and Loudermilk, R. W. "An Oceanographic Illuminometer" SIO Ref. 68-11, July 1968.

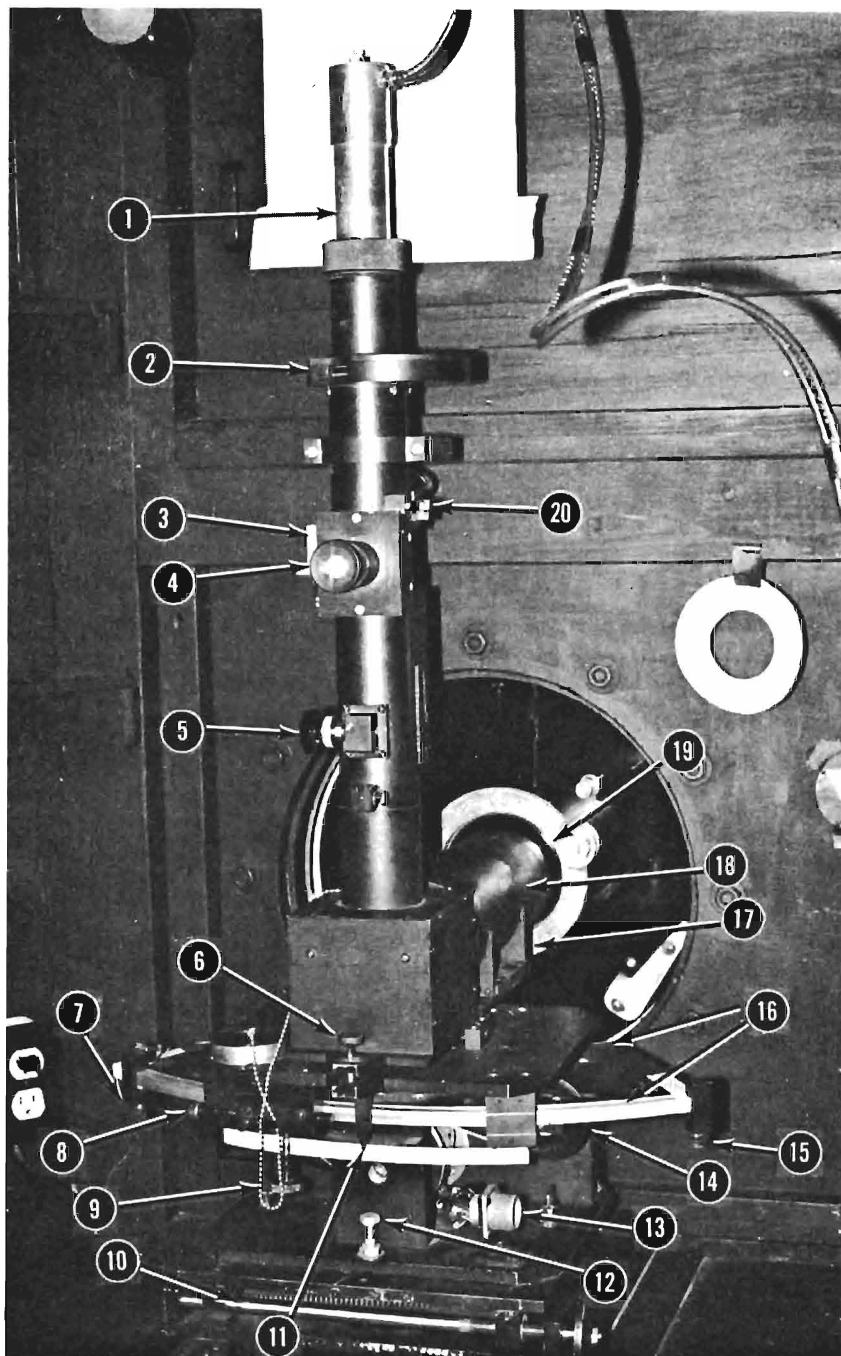


Fig. 2-20. Visibility Laboratory Mark IV Photoelectric Telephotometer in scanning mount at the measuring window of the laboratory tank. (1) One of several interchangeable multiplier phototubes, (2) Wheel containing glass neutral density filters (0.5 log steps), (3) Eyepiece mirror control lever, (4) Eyepiece with reticule for angular measurements, (5) Focus control with locking ring, (6) Vertical tilt adjustment, (6) Adjustable scan limit stop, (8) Fine horizontal adjustment, (9) Coarse horizontal adjustment, (10) Lead screw providing horizontal translation of optical axis, (11) Scale and pointer indicating horizontal angles, (12) Vertical adjustment of optical axis, (13) Electrical attachment for remote control of scan and synchronized recorder, (14) Synchronous scan motor with magnetic clutch, (15) Adjustable scan limit stop, (16) Arc of circular track centered on the optical window, (17) Mount for polarizer, (18) Stray light shield, (19) 4-inch diameter optical glass insert in plastic window of the tank, (20) Interchangeable field stops, 35 to 0.03 mr.

# 3. UNDERWATER LIGHTING FOR PHOTOGRAPHY

## 3.1 INTRODUCTION\*

The optical nature of ocean water imposes restrictions of two kinds on underwater photography. First, fine details tend to become progressively obliterated as the distance to the object is increased. Secondly, and usually of greater importance, the apparent contrast of underwater objects is severely attenuated by scattering processes within the water and often by absorption as well. The magnitudes of these effects will be discussed in this paper in terms of observable and measurable optical constants of water. Although a brief review of the optical nature of ocean water is included, considerable reliance has been placed on the reader to consult the referenced previous writings of the author and others. Interestingly, the principles which control underwater imagery are closely similar to those which govern imagery through the atmosphere with certain very important exceptions which arise either from the greatly enhanced role of absorption in water or from the unique optical properties of the scattering particles it contains. These differences between the atmospheric and the hydrologic media will be brought out in the course of the discussions which follow.

## 3.2 REFRACTIVE DETERIORATION OF IMAGERY

Natural waters contain refractive nonhomogeneities of two kinds: One, small-scale point-to-point variations in the refractive index due to temperature differences, and two, transparent biological organisms (plankton) which may range in size from microns to centimeters, from bacteria to jellyfish. The first of these nonhomogeneities are also found in the atmosphere where they are often referred to as atmospheric boil. Their effect in limiting the resolution of astronomical and terrestrial telescopes and long focal length cameras is well-known. Ordinarily, the thermal structures in water are of little consequence because their effect is ordinarily small compared with that of the transparent biological organisms. These have no true optical counterpart in the atmosphere because their refractive index matches that of water very closely, whereas water droplets in the atmosphere have a relative refractive index of 1.33 or more. The size of the organic particles in water is so large compared with the wavelength of light that scattering is produced chiefly by regular transmission through the large particle. The consequent deviations are very small. Even

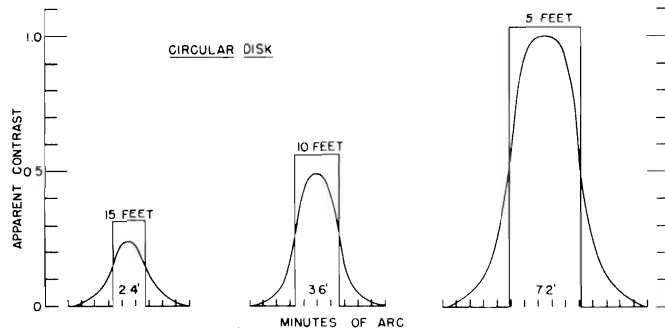
---

\* Sections 3.1, 3.2, 3.3, and 3.4 have been lifted almost verbatim from the author's paper entitled "Principles of Underwater Lighting" which appears on p. A-I-1 through A-I-7 in the Proceedings of the Seminar on Underwater Photo-Optics of the Society of Photographic Instrumentation Engineers held in Santa Barbara, California on 10 October 1966.

after passage through several such scatterers, imagery is not greatly disturbed except with respect to fine details. Nevertheless, these refractive effects cause the edges of objects to appear blurred and the apparent contrast of small objects to be reduced. Thus at the longer photographic ranges resolution is impaired and fine details are obliterated. An experimental study of this loss of resolution was performed several years ago at the author's Field Station at Diamond Island, Lake Winnepesaukee, New Hampshire, and a theoretical treatment was evolved, and is described in Appendix B of this report. It was found that the angular magnitude of the blur increases as the square root of the object-to-observer distance and that the apparent contrast of fine details is decreased inversely as the third power of the distance if the water is macroscopically uniform throughout the path of sight.

Figure 3-1 shows the result of one experiment performed at Diamond Island. A grey circular disk 1/8th-inch in diameter was photographed underwater along a horizontal path of sight in daylight. Under the prevailing lighting the apparent contrast of the grey material at a distance of five feet would have been unity with respect to the surrounding water if a somewhat larger piece of the material had been used. Due to the small size, however, refractive deterioration of the image caused contrast to be slightly reduced even at 5 feet and much more severely reduced as the object-to-camera distance was increased. In Fig. 3-1 rectangles have been drawn to illustrate the angular width and apparent contrast which would have been observed by a perfect camera in the absence of any refractive effects within the water. The curves represent experimental data obtained from the photographs after corrections had been applied for small losses in resolution attributable to the optical system and the photographic material. It will be noted that even in the center of the image contrast has been reduced. Outside the geometrical edge of the image, moreover, scattered light appears. Plainly, the edges of the object appear blurred and the apparent contrast has been reduced.

Fig. 3-1.  
Apparent contrast and angular size of a 1/8-inch diameter gray disk photographed through 5, 10, and 15 feet of lake water.



The three rectangles in Fig. 3-1 represent the angular size and apparent contrast which would have been available to the camera in the absence of refractive deterioration. The variation in angular size is, of course, a simple matter of object-to-camera distance. The reduction in contrast with distance is the result of scattering of daylight into the path of sight in accordance with principles described on pages 229 through 233 in Appendix A. Refractive deterioration has produced an additional contrast reduction factor which is displayed graphically by the difference in height between the rectangle and the curve. Obviously, this factor increases with object-to-camera distance. The three data in Fig. 3-1 are indicated by three points on Fig. 3-2, which is a plot of apparent contrast versus object distance. The resulting curve has been extrapolated to longer object distances by means of the principle that refractive deterioration of the image causes the apparent contrast of fine details to decrease inversely as the third power of the distance. Thus, in this log-log plot the extrapolation is based upon a straight line with a slope of  $-3$ .



It is evident from Fig. 3-1 that refractive deterioration produced no appreciable effect when the 1/8th-inch circular disk was closer than 5 feet from the camera. At this distance the object subtended 7.2 minutes of arc at the camera. The inverse cube nature of the phenomena is not displayed until the angular subtense is less than that associated with the third plotted point, i.e., beyond an object distance of 15 feet. There the object subtended 2.4 minutes. Obviously, curves for larger or smaller objects would form a regular family on Fig. 3-2, lying respectively right and left of the curve shown. Similarly, the position of the curve in Fig. 3-2 depends upon the concentration of scattering material in the water. Lesser or greater concentrations would produce a family of curves lying respectively right and left from the curve shown.

A means for assessing the practical consequences of refractive deterioration is illustrated by Fig. 3-3. This is identical with Fig. 3-2 except for an additional system of curves. The dashed line, marked  $e^{-\alpha r}$ , is a plot of the factor by which contrast is reduced with object distance due to the scattering of daylight along the horizontal path of sight. (See Appendix A, p. 231.) The lower solid line depicts the product of the two contrast reduction factors ascribable, respectively, to refractive deterioration and scattering of ambient light. If the grey disk were large, refractive deterioration would produce no contrast reduction near the center of the disk and, despite the slightly blurred edge, would have no effect on its visual detectability. In this case the large disk would be visually detectable at about 20 feet in the water to which Fig. 3-3 applies. In the case of the 1/8th-inch diameter circular disk, however, small angular size makes more apparent contrast necessary for visual detection. The short dotted line in Fig. 3-3 indicates the contrast required for the 1/8th-inch disk to be detected. In the absence of refractive deterioration the object is detectable at a distance of 14 feet as indicated by the intersection of the two dotted lines. Because of refractive deterioration, however, detection is possible at only 11 feet as indicated by the intersection of the dotted threshold curve and the lower solid line. Although this example refers to visual detection, it remains only to substitute the threshold curve for any photographic system in order to make a corresponding prediction of the range performance of that system.

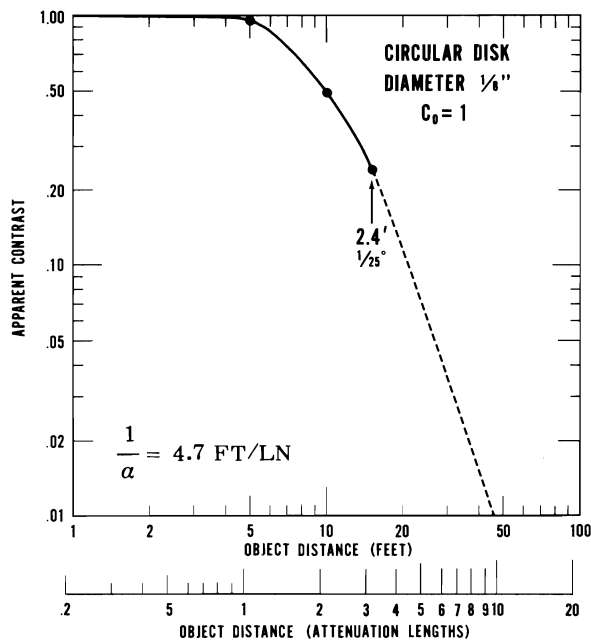


Fig. 3-2. Plot of data from Fig. 3-1.

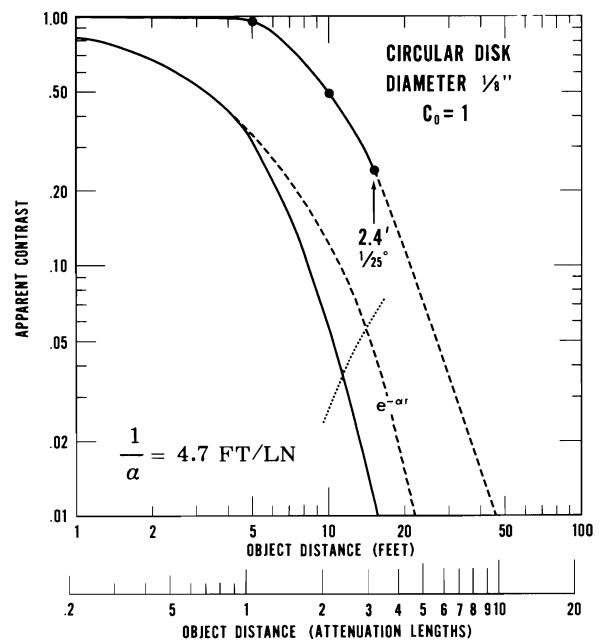


Fig. 3-3. Plot of data from Fig. 3-1.

Finally, it must be pointed out that the effect of refractive deterioration on underwater imagery does not depend upon the nature of the underwater lighting. That is to say, the curve in Fig. 3-2 will be the same whether the object is illuminated artificially or by daylight so long as its inherent contrast is the same.

### 3.3 THE OPTICAL NATURE OF NATURAL WATERS

At the bottom of Figs. 3-2 and 3-3 is an additional scale of object distance in units of attenuation length, a measurable index of water clarity. (See Appendix A, p. 216.) The inclusion of a scale of object distance in units of attenuation length implies that the data in Fig. 3-2 are applicable to other natural waters having greater attenuation lengths provided the diameter of the circular disk is increased proportionally.

Appendix A summarizes the optical nature of ocean water with the principles of underwater lighting specifically in mind. A discussion of the performance of collimated underwater light sources is given in Fig. 18 on page 224 of Appendix A for the case of irradiance on the axis of a uniform beam of green incandescent light having a divergence of approximately 3 milliradians (or 1/6th degree). This divergence was chosen in the belief that pulsed blue-green lasers for underwater use, when available, would produce beams having approximately this divergence. This has proved to be approximately true.

### 3.4 APPARENT CONTRAST OF ILLUMINATED UNDERWATER OBJECTS

The design of underwater illuminating systems can be studied on the basis of the concepts and data contained in this chapter and in Appendix A. No distinction need be made between light produced by the blue-green lasers used in the experiments described in this report and that produced by conventional sources, except due allowance for the very high peak power and short duration characteristics of the laser. No special effects due to coherence have been detected by extensive search. In fact, the radiation produced by the RCA underwater laser (see Sections 5 and 6) has not been found to exhibit appreciable coherent properties. It is best regarded as the equivalent of an incoherent or a thermal source producing light throughout a wavelength interval 25 angstroms wide centered at 0.53 microns. The light produced by the laser is linearly polarized with its E-vector perpendicular to the main axis of its beam cross-section. This state of polarization is preserved in transmission through natural waters to a truly amazing extent. For example, observations (See Section 5, Fig. 5-7) of the fractional polarization transmitted to various object distances from a linearly polarized, broad-beam incandescent source show that at four attenuation lengths, where 90% of the arriving light has experienced one or more scatterings, 90% of the light is still polarized. At an observation distance of 20 attenuation lengths, when less than one part in a million of the light arrives without having experienced a scattering, 82% of the light is still linearly polarized. Thus it is important to remember that the reflectance and scattering properties of objects associated with polarized irradiation must be used when the underwater blue-green laser is the irradiating source.

It is also important to note that the nature of the volume-scattering function depends upon the state of polarization of the light impinging on the elementary volume of water. It appears that the volume-scattering function for light from the underwater blue-green laser is identical with the volume-scattering function for blue-green light from an incandescent projector when equipped with a linear polarizer. (See Section 2.5)

Calculations of the apparent contrast of underwater objects irradiated by any kind of lighting are based upon the same set of equations for contrast reduction. That is to say, the basic triad of equations published by the author and his colleagues for use in problems relating to vision through the atmosphere\* apply equally well to the underwater case, and for every kind of lighting, natural or artificial, uniform or non-uniform, and in every kind of water, uniform or stratified, and along every path of sight. For example, consider the simple case depicted by Fig. 3-4. Here an underwater light source is located close beside a camera so that both may be regarded as being at the same distance  $R$  from an object near the axis of the irradiating beam. Some of the path of sight is within water lighted directly by the lamp, but a length  $A$  of path near the lens is outside the beam, as shown in Fig. 3-4. Each element of volume of length  $dr$  located at  $r$  along the path of sight is irradiated by the source. Its apparent radiance as seen from the camera is

$$dN = \sigma J e^{-\alpha r} \left[ r^{-2} e^{-\alpha r} + c_1 K r^{-1} e^{-K r} + c_2 K r^{-1} e^{-2K r} \right] dr,$$

according to Eq. (5) on page 222 of Appendix A. Here,  $\sigma$  is the volume-scattering function for the water in the direction specified by the geometry of Fig. 3-4.

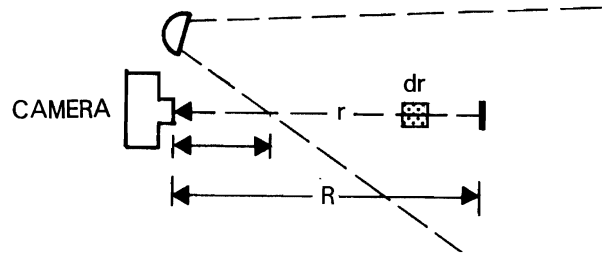


Fig. 3-4. Illustrating geometry of underwater lighting for photography.

The constants  $c_1 = 2.5/4\pi$  and  $c_2 = 17.5/4\pi$ . The apparent radiance of an entire illuminated path extending to infinity is:

$$N_{A,\infty}^* = \sigma J \left\{ \int_A^\infty r^{-2} e^{-2\alpha r} dr + c_1 K \int_A^\infty r^{-1} e^{-(\alpha+K)r} dr + c_2 K \int_A^\infty r^{-1} e^{-(\alpha+2K)r} dr \right\},$$

$$N_{A,\infty}^* \cong \sigma J A^{-1} \left\{ E_2[2\alpha A] + c_1 K E_1[(\alpha+K)A] + c_2 K E_1[(\alpha+2K)A] \right\} \equiv \sigma J A^{-1} E^*(A).$$

where  $E_2[2\alpha A]$ ,  $E_1[(\alpha+K)A]$ , and  $E_1[(\alpha+2K)A]$  are exponential integrals for which tables are available.\*\*

\*Seibert Q. Duntley, Jacqueline I. Gordon, John H. Taylor, Carroll T. White, Almerian R. Boileau, John E. Tyler, Roswell W. Austin, and James L. Harris, *Applied Optics* 3, Eqs. (6.3), (6.4), (6.5), 579 (1964).

\*\*Abramowitz, M. and Stegun, I. A. *Handbook of Mathematical Functions Nat. Bu. Stds. Appl. Math. Series 55* (1964) p. 238 ff.

Similarly,

$$N_{R,\infty}^* = \sigma_J R^{-1} E^*(R) .$$

$$\frac{C_R}{C_O} = 1 - \frac{N_{O,R}^*}{N_{O,\infty}^*} = \frac{N_{R,\infty}^*}{N_{A,\infty}^*}$$

By substitution:

$$\frac{C_R}{C_O} = \frac{A}{R} \frac{E^*(R)}{E^*(A)} .$$

Presumably similar, easy-to-use contrast reduction equations involving exponential integrals can be written for any geometry of underwater lighting and viewing. In some cases, inherent contrast is a simple function of the ratio of directional surface reflectances, but in the example chosen for illustrative purposes in this paper, the object appears against a water background. Thus,

$$C_O = \frac{\rho H_r}{\pi N_{R,\infty}^*} - 1 ,$$

where  $\rho$  is the directional reflectance of the object.

The foregoing concepts, data, and equations contained in or referenced by this section provide a means for optimizing underwater lighting and for predicting the performance of systems in terms of the observable optical properties of natural waters.

### 3.5 MEASUREMENTS OF APPARENT CONTRAST

The apparent contrast of a plane test surface lighted in a manner similar to that specified by Fig. 3-5 was measured at the Diamond Island field station in 1964; (see Table 3.1). The experiments employed the underwater steel tower and track shown in Fig. 4-15. The test surface was a square steel plate 1.5 feet

on each edge. It was coated with a matte gray paint having a submerged reflectance of 0.38 when measured in green light determined by a Wratten 61 filter. The plate was carried by the steel cart that traveled the underwater track, as shown in Fig. 4-10. The painted surface was vertical and faced the underwater tower; its center was at the same depth as the center of the measurement window in the underwater tower. Thus, the photoelectric telephotometer (see Fig. 2-3 and Fig. 2-20) within the tower looked out through the center of the measurement window along the axis of the underwater track to the center of the square test panel mounted on the moveable cart.

The test surface was irradiated by the same submerged light source that was used in the experiments upon which the first equation in the preceding section is based. That equation, given on page 223 of Appendix A, is based upon experiments described in detail by Appendix H. The light source is described on pages 3 and 4 of Appendix H; it is diagramed in Fig. 2 of that appendix.

The submerged lamp produced a circular cone of divergent incandescent white light with a nominal beam spread (see Fig. 2 in Appendix H) of 20-degrees. It was carried by a modified version of the cart shown in Fig. 4-6. All of the control mechanisms which protrude above the main frame of the cart in Fig. 4-6 were removed. A long ladder-like structure was attached to the top of the cart in a horizontal position and at right angles to the direction of the underwater track. The top of this "cross-track" was about 1 foot deeper than the center of the measurement window of the steel tower where the assembly was placed on the underwater track. The 20° light source was attached to the cross-track and could be placed at any "off-set" from the axis of the underwater track. Thus, the type of lighting geometry illustrated by Fig. 3-8 could be achieved. The mounting of the 20° underwater lamp included a large divided circle and the exit aperture of the lamp (a 6" diameter hole in the metal lamp box) was placed directly above the center of the divided circle. Thus, the axis of the 20° cone of light could be aimed in any horizontal direction. A setting of zero degrees on the divided circle made the axis of the cone of light parallel to the underwater track. Thus the value indicated on the divided circle was the angle  $\theta$  in Fig. 3-5.

The positions of the lamp and the test surface could be freely varied along the underwater track. As shown in Fig. 3-5, the lamp was offset a horizontal distance  $X$  from a point on the axis established by the telephotometer and the center of the test surface at distances  $Y$  from the test surface and  $Z$  from the window of the tower.

The field of view of the telephotometer was 0.25 degrees so that it was well within the boundaries of the test surface at all distances used in the course of the experiments.

When desired, the test surface could be removed from the experiment by rolling its cart to the remote end of the underwater track, 150 feet from the window of the underwater tower. Its presence was undetectable even very much closer. Telephotometer readings with the test surface removed to  $Y + Z = 150$  feet (36 attenuation lengths) were used as the apparent background radiance for computing the apparent contrast of the test surface; they are tabulated in Table 3.2.

Apparent contrast of the gray test surface (reflectance 0.38) for a variety of geometries ( $X, Y, Z$ ) were calculated from pairs of radiance measurements with the test surface in place and removed, respectively; these are tabulated in Table 3.1. The 20° cone of light was not always centered on the test surface, but in each case the position of the axis of the cone is specified by the angle  $\theta$ . Apparent contrast is affected by the aiming of the light beam. Generally, it is greatest when the beam is aimed to irradiate the test surface with its right edge, thereby minimizing the lighted water path through which the telephotometer must look, i.e., the "common volume" shared by the illuminating and viewing systems.

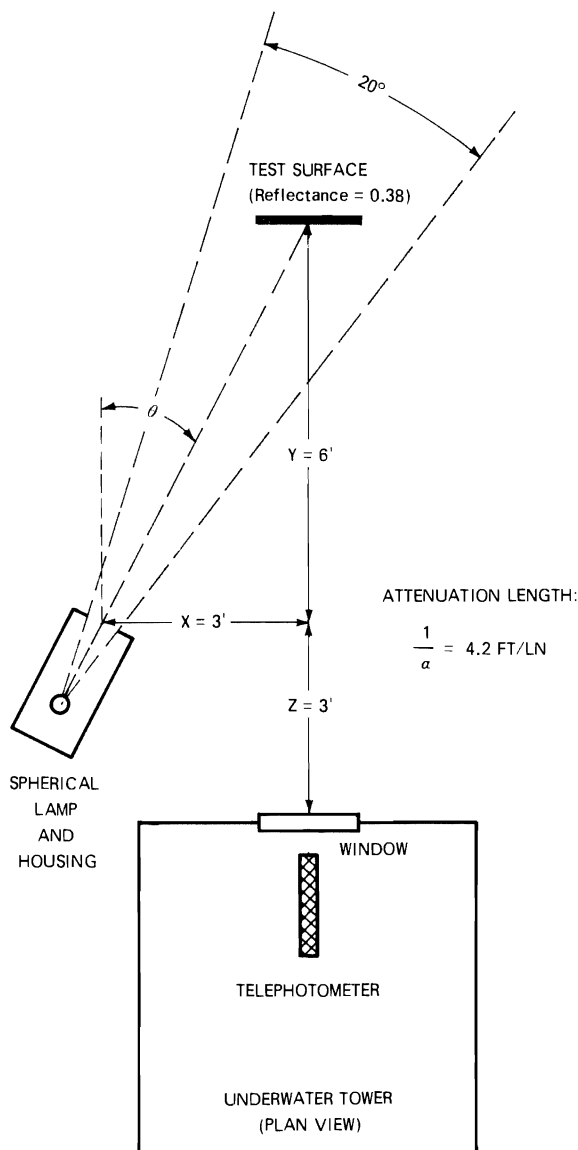


Fig. 3-5.

Plan view of an arrangement for measuring the apparent contrast of an illuminated submerged test surface.

### 3.6 POLARIZED UNDERWATER LIGHTING

Crossed polarizers profoundly increase the apparent contrast of the test surface, sometimes by an order of magnitude. This is accomplished, however, by a considerable reduction in light, because the effective transmittance of two polarizers in practical cases, is approximately 0.10 even if the test surface is a complete depolarizer. This is illustrated quantitatively in Table 3.1. For example, calculations based upon the first entries ( $X = 1'$ ,  $Y = 6'$ ,  $Z = 3'$ ) in Tables 3.1 and 3.2 show that insertion of the crossed polarizers lowered the radiance of the matte test surface by a factor of 11.5 (chiefly due to the transmittance of the two polarizers) whereas the apparent radiance of the background was reduced by a factor of 93. Thus, the ratio of the apparent radiance of the test surface to the apparent radiance of its background was increased by a factor of 8. It is important to note that the test surface *must* depolarize in order to produce a gain in apparent contrast when polarizers are used.

The use of single polarizers on either the light source or the telephotometer (camera) produced no significant gain in apparent contrast. Polarizers oriented to produce linear light with its E-vector vertical gave somewhat better results than with the E-vector horizontal in some geometries. No circumstance favoring a horizontal E-vector was found. Trials with circular polarizers failed to demonstrate any superiority from the standpoint of contrast enhancement over linear polarizers. It is a great practical advantage of circular polarizers that no "crossed" relation must be maintained.

**Table 3.1. Apparent Contrast of Gray Test Surface. (Submerged Reflectance = 0.38) (Green Light)**

		Z = 3'		Z = 6'		Z = 9'	
	$\theta$ Degrees	No Polarizers	Crossed Polarizers	No Polarizers	Crossed Polarizers	No Polarizers	Crossed Polarizers
Y = 6' X = 1'	4	21.9	185.	18.5	140.	11.0*	124.*
	9.5	2.99	22.4	2.99	30.0	2.23	24.2
	19.5	4.75	6.95	3.89	4.90	2.71	3.95
Y = 9' X = 1.5'	4	9.19*	(53)	8.15	49.0	5.32	32.0
	9.5	2.31	(11)	1.57	10.5	1.40	7.91
	19.5	2.08	3.36	2.55	3.36	1.63	2.72
Y = 12' X = 2'	4	3.90*	(22.)	3.46	20.8		
	9.5	0.82	( 4.8)	0.86	4.74		
	19.5	1.70	( 3.0)	1.40	2.80		
Y = 6' X = 2'	16.5					24.0	((170))
	26.5					5.87	(( 37))
	36.5					3.46	3.46
Y = 9' X = 4.5'	16.5	22.4	((150))				
	26.5	4.50	(( 38))				
	36.5	3.25	4.26				

- Note:**
1. Asterisk (\*) indicates that  $\theta = 0$  for this datum.
  2. Values in parentheses are extrapolations; values in double parentheses are less to be trusted.
  3. Green light selected by Wratten No. 61 filter.

**Table 3.2. Apparent Radiance of Background (Test Surface Removed; Relative Units; Green Light)**

		Z = 3'		Z = 6'		Z = 9'	
	$\theta$ Degrees	No Polarizers	Crossed Polarizers	No Polarizers	Crossed Polarizers	No Polarizers	Crossed Polarizers
Y = 6' X = 1'	4	$2.29 \times 10^{-3}$	$2.46 \times 10^{-5}$	$1.74 \times 10^{-3}$	$2.09 \times 10^{-5}$	$8.42 \times 10^{-4}$ *	$1.12 \times 10^{-5}$ *
	9.5	$3.31 \times 10^{-3}$	$3.31 \times 10^{-5}$	$2.63 \times 10^{-3}$	$2.63 \times 10^{-5}$	$2.09 \times 10^{-3}$	$1.51 \times 10^{-5}$
	19.5	$4.68 \times 10^{-3}$	$4.47 \times 10^{-5}$	$3.47 \times 10^{-3}$	$3.55 \times 10^{-5}$	$2.29 \times 10^{-3}$	$2.24 \times 10^{-5}$
Y = 9' X = 1.5'	4	$4.47 \times 10^{-5}$ *	$< 10^{-5}$ *	$9.55 \times 10^{-4}$	$1.23 \times 10^{-5}$	$1.66 \times 10^{-3}$	$9.77 \times 10^{-6}$
	9.5	$1.18 \times 10^{-4}$	$< 10^{-5}$	$1.41 \times 10^{-3}$	$1.79 \times 10^{-5}$	$8.71 \times 10^{-4}$	$1.29 \times 10^{-5}$
	19.5	$1.82 \times 10^{-4}$		$2.14 \times 10^{-3}$	$2.34 \times 10^{-5}$	$1.45 \times 10^{-3}$	$1.70 \times 10^{-5}$
Y = 12' X = 2'	4	$2.75 \times 10^{-5}$ *	$< 10^{-5}$ *		$< 10^{-5}$		
	9.5	$7.59 \times 10^{-5}$	$< 10^{-5}$		$1.10 \times 10^{-5}$		
	19.5	$1.35 \times 10^{-4}$	$< 10^{-5}$		$1.66 \times 10^{-5}$		
Y = 6' X = 2'	16.5					$2.88 \times 10^{-5}$	$< 10^{-5}$
	26.5					$4.77 \times 10^{-5}$	$< 10^{-5}$
	36.5					$5.01 \times 10^{-5}$	$< 10^{-5}$
Y = 9' X = 2'	16.5	$1.91 \times 10^{-5}$					
	26.5	$3.47 \times 10^{-5}$	$< 10^{-5}$				
	36.5	$4.90 \times 10^{-5}$					

- Note:**
1. Asterisk (\*) indicates that  $\theta = 0$  for this datum.
  2. Although radiance is tabulated to 3 places, the precision of the measuring system was not better than  $\pm 2$  percent. The data may also contain systematic non-linearities of this magnitude.
  3. Green light selected by Wratten No. 61 filter.

### 3.7 MAXIMUM RANGE OF UNDERWATER IMAGERY

One of the most surprising facts about underwater lighting is that at long range much more light reaches a distant object than is usually predicted. Consider an experiment diagramed in Fig. 3-6; a uniform spherical lamp is lowered at night directly beneath a downward-facing long-lens underwater camera in clear water having an attenuation length of 5 meters. The lamp is photographed at 3, 6, 9, and 12 at-



attenuation lengths below the camera. Each of the resulting pictures show an image of the bulb surrounded by a glow of forward-scattered light. Because of attenuation, the exposure required for the picture at the bottom is 1 000 000 times that for the picture at the top. The diameter of the scattered glow remains roughly independent of lamp distance, whereas the diameter of the image of the lamp decreases linearly with distance. It is not surprising, therefore, that as lamp distance is increased the irradiance received in the plane of the camera lens direct from the lamp diminishes more rapidly than does the component of irradiance due to the scattered glow. Figure 3-6 shows that both the image forming light and the scattered light pass through the lens but are separated in the film plane. Measurements in the film plane can, therefore, yield separate values of the two components of irradiance. If, however, the camera were to be replaced by a flat photocell facing the lamp, total irradiance would be measured. The solid curve in Fig. 3-7 is a plot of the total irradiance at the lens. The upper, dotted curve represents the image forming component alone. At long range the scattered component is greatly larger. For example, when the lamp is 40 meters below the camera, i.e., at a distance of 8 attenuation lengths, there is 170 times as much irradiance as would be expected on the basis of the simple  $\alpha$  calculation, but at this distance only one part of the light in 170 is capable of image formation. It is not surprising, therefore, that at some distance the image of the lamp falls below the contrast threshold of any viewing system. *The lamp will then be seen to disappear into its own glow.* In the case of direct underwater vision this occurs at about 15 attenuation lengths in *all* clear ocean waters. The use of much more powerful lamps produces only a slight increase

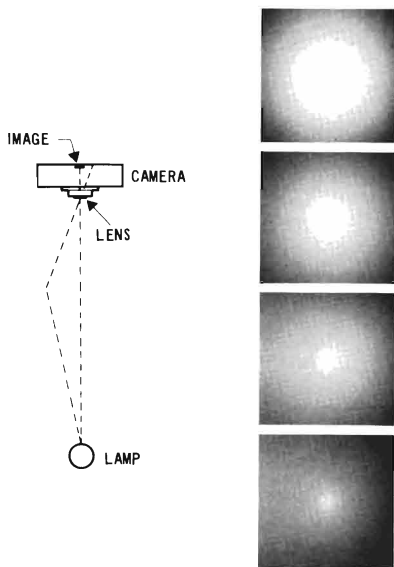


Fig. 3-6. Photographs of a uniform spherical lamp submerged vertically beneath an underwater camera.

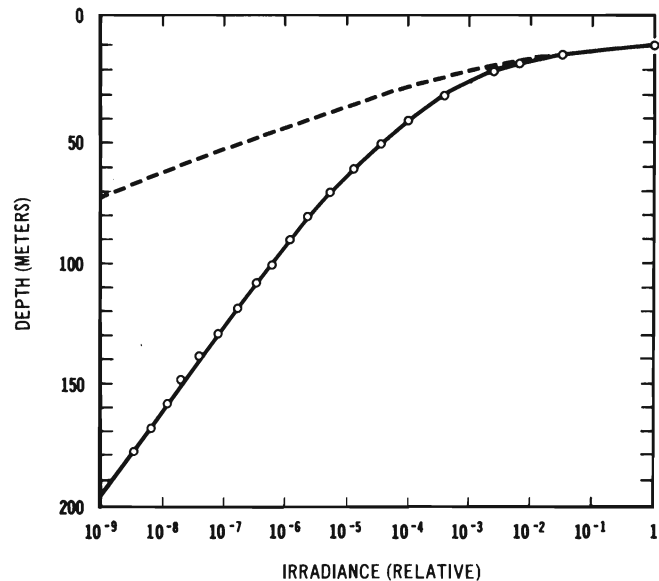


Fig. 3-7. Irradiance at the lens of the camera in Fig. 3-6. Dotted curve shows the image-forming component of the receiving light.

in visual range. Advanced electro-optical sensing systems having high quantum efficiency and ideally low internal noise can achieve only slightly more range. Since even a self-luminous object (like a lamp) becomes indistinguishable in its own glow of scattered light, there is a fundamental limiting range imposed by forward scattering properties of natural waters beyond which no object can be seen, even with virtually unlimited light power and the most advanced underwater viewing or photographic systems. Actually, the performance of existing systems fall well short of this limit. Thus, important improvements in existing techniques are possible.

### 3.8 LONG RANGE UNDERWATER PHOTOGRAPHY

It is interesting to explore various techniques of underwater lighting to see if the limiting range can be approached using ordinary photography. The pictures in the remainder of this section were taken in the laboratory tank described in Section 7. Figure 3-8 is intended to suggest an underwater camera and a nearby underwater lamp used to illuminate some object at a distance one attenuation length from the camera. It is easy to make good underwater photographs at this distance, as in Fig. 3-9, which serves to introduce the *cast of characters*. These are not swimmers but moored dummies. The upper swimmer is attired in trunks and flippers, whereas the lower swimmer is in a black wet-suit with a mask and light trunks. At a distance of one attenuation length this lighting technique produces acceptable photographic quality.

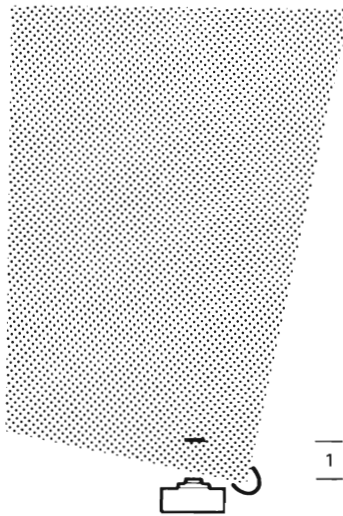


Fig. 3-8. Schematic plan view of underwater camera and nearby lamp irradiating a subject one attenuation length from the lens.

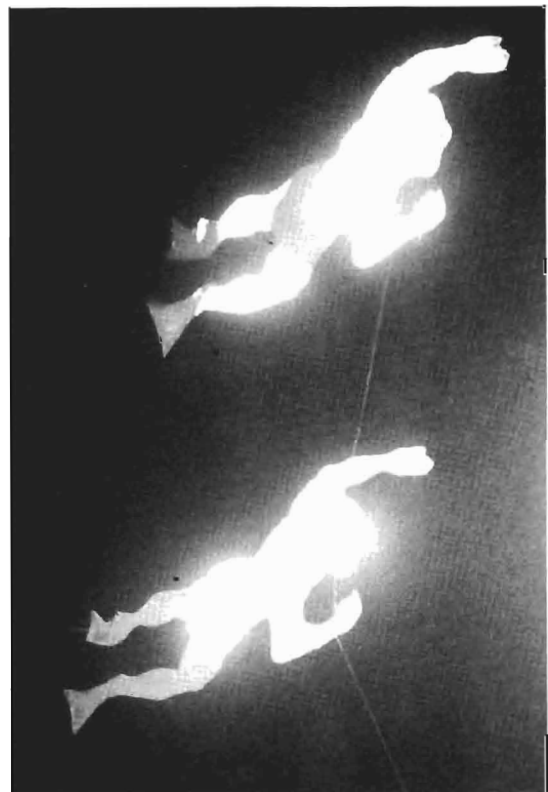


Fig. 3-9. Moored dummy swimmers photographed as shown in Fig. 3-8.

At longer underwater ranges the quality of underwater photographs made with cameras having attached lights are seriously degraded by scattered light within the volume of water which is common to both the illuminating and viewing systems; i.e., that part of the path of sight which is lighted by the lamp. Successful long range underwater photography requires elimination of scattering within the *common volume*. Three techniques are commonly used to suppress common volume scattering. Two of these aids are illustrated by Fig. 3-10, in which the diagram on the left represents the unaided condition with the object at 2 attenuation lengths from a camera having an attached or nearby light. In the center diagram, a light shield or *septum* has been added to shield most of the path of sight from direct light from the lamp. In the diagram on the right the lamp has been off-set to the side by a considerable distance. The entire path of

sight is still directly illuminated, but no part of the path is close to the lamp. Both inverse square law and attenuation by absorption and scattering operate to avoid the intense lighting of the water close to the camera lens; it is this brightly lighted water which contributes most to contrast loss in the unaided lighting arrangement shown in the left diagram. Offset of the lamp may be to the rear of the camera as well as to the side; this may have advantage when very large fields of view are to be photographed, but added lamp output is needed to compensate for the longer lamp to object distance.

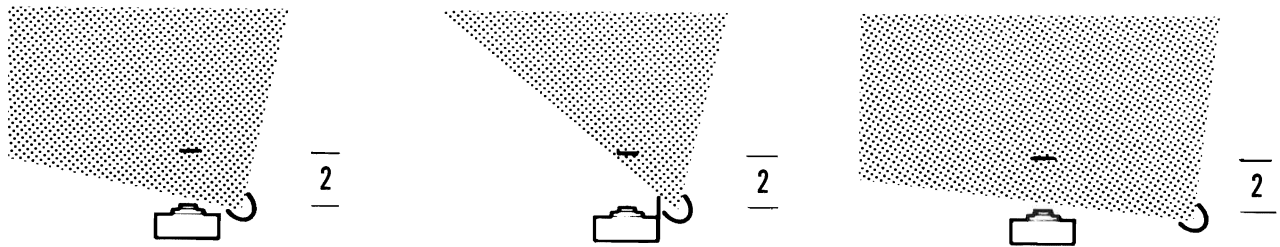


Fig. 3-10. Illustrating two methods for improving underwater photography by reducing the lighting on the water close to the lens.

A third aid in reducing common volume scattering is provided by crossed polarizers. Both the lamp and the camera must have polarizers and the object must depolarize in the process of reflection in order to be photographed. Absorption of light by the polarizers requires an increase in exposure time, lens speed, film speed, or lamp output by a factor of about ten.

The matrix of photographs in Figs. 3-11 and 3-12 illustrates the effects of the various modes of lighting discussed above on short, medium, and long range underwater photography. Photography at 2 attenuation lengths is shown by the three pictures on the top row. The figure on the left shows the lighting geometry for the first and second pictures; the geometry of the third picture is shown by the center diagram in Fig. 3-10. Consider first the unaided photograph on the left. It will be noted that the lamp irradiates the water path between the camera and the swimmer. Scattered light throughout this water path is added to the image forming light from the swimmer and serves to lower the available contrast. An obvious mechanism for suppressing the effect of scattering in the water is through the use of crossed polarizers. The second picture shows what can be achieved by means of placing a linear polarizer on the light source and a crossed linear polarizer on the camera. The background is darkened and the apparent contrast of the light portions of the swimmers is improved but it will be noted that the dark suit and dark trunks are barely discernible. Thus, actually more information concerning both swimmers but particularly the lower swimmer can be obtained from the lower contrast picture on the left. Another, perhaps better, way of improving the imagery is by means of an opaque partition or septum to darken the water between the camera and the swimmers. This is illustrated in the third picture. Here the images appear higher in contrast than in the unaided picture but the details of the dark suit are still visible.

Photography at 3 attenuation lengths is shown in the middle row of images of Fig. 3-11. The long path of lighted water between the camera and the swimmers has drastically reduced the contrast in the case of the unaided lighting depicted on the left. The second picture from the left illustrates the effect of polarizers. An opaque partition or septum was used in making the third photograph, and the final picture on the right represents the use of both the septum and the polarizers. At this range there is an obvious need for some aided photographic technique. The third picture, made with a septum is best at this range.

At 4 attenuation lengths the situation is as shown in the bottom row of pictures in Fig. 3-11. Combined use of both polarizer and septum produced an excellent picture of the top swimmer, but lack of depolarization by the dark suit of the lower swimmer seriously impaired this imagery compared with the photograph in the septum column.

At 5 attenuation lengths no image was recorded by conventional lighting, but something was achieved by a lateral separation of the lamp from the camera by several attenuation lengths. Such an off-set is not always practicable but if it can be done in the manner shown in the diagram in the top row in Fig.3-12, imagery sufficient to detect the presence of the swimmers can be achieved, as shown in the first (unaided) picture. The reason for this improvement is obvious: The lighting on the object is not much reduced by offsetting the position of the lamp relative to the camera, but the lighting on the water immediately in front of the lens is reduced greatly. This reduction in the veiling glare of lighted water enables the swimmers

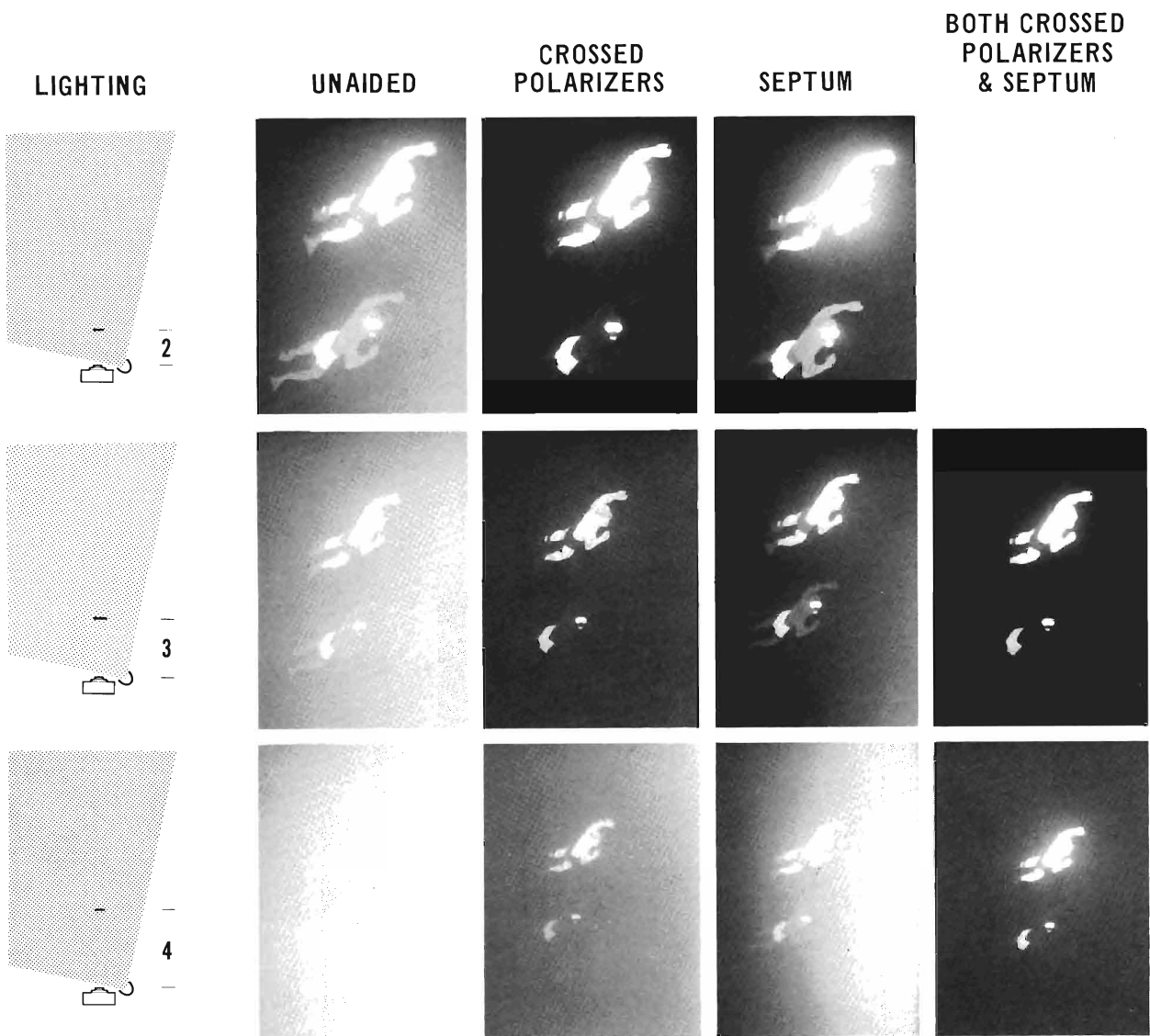


Fig. 3-11. Underwater photographs of moored dummies at 2, 3, and 4 attenuation lengths.

to be seen faintly. The aid given by crossed polarization or by the use of a septum was less dramatic with off-set lighting. Nevertheless, the pictures obtained with these techniques at 5 attenuation lengths are comparable in quality with those secured at 4 attenuation lengths without off-set.

At 6 attenuation lengths useable results were not obtained unless the lamp was moved out close to the swimmer and a septum was used to minimize the lighting of the common volume. In the picture on the right in the middle row polarizers have been added to further reduce the scattered light and to darken the background; the photographic quality is comparable with the best result obtained at 3 attenuation lengths.

The final picture in Fig. 3-12 was taken at a distance of 12 attenuation lengths. The lamp was near the moored dummy swimmers and a carefully adjusted septum darkened the common volume as much as possible. Crossed linear polarizers were used on both the lamp and the camera. Even so, there was a

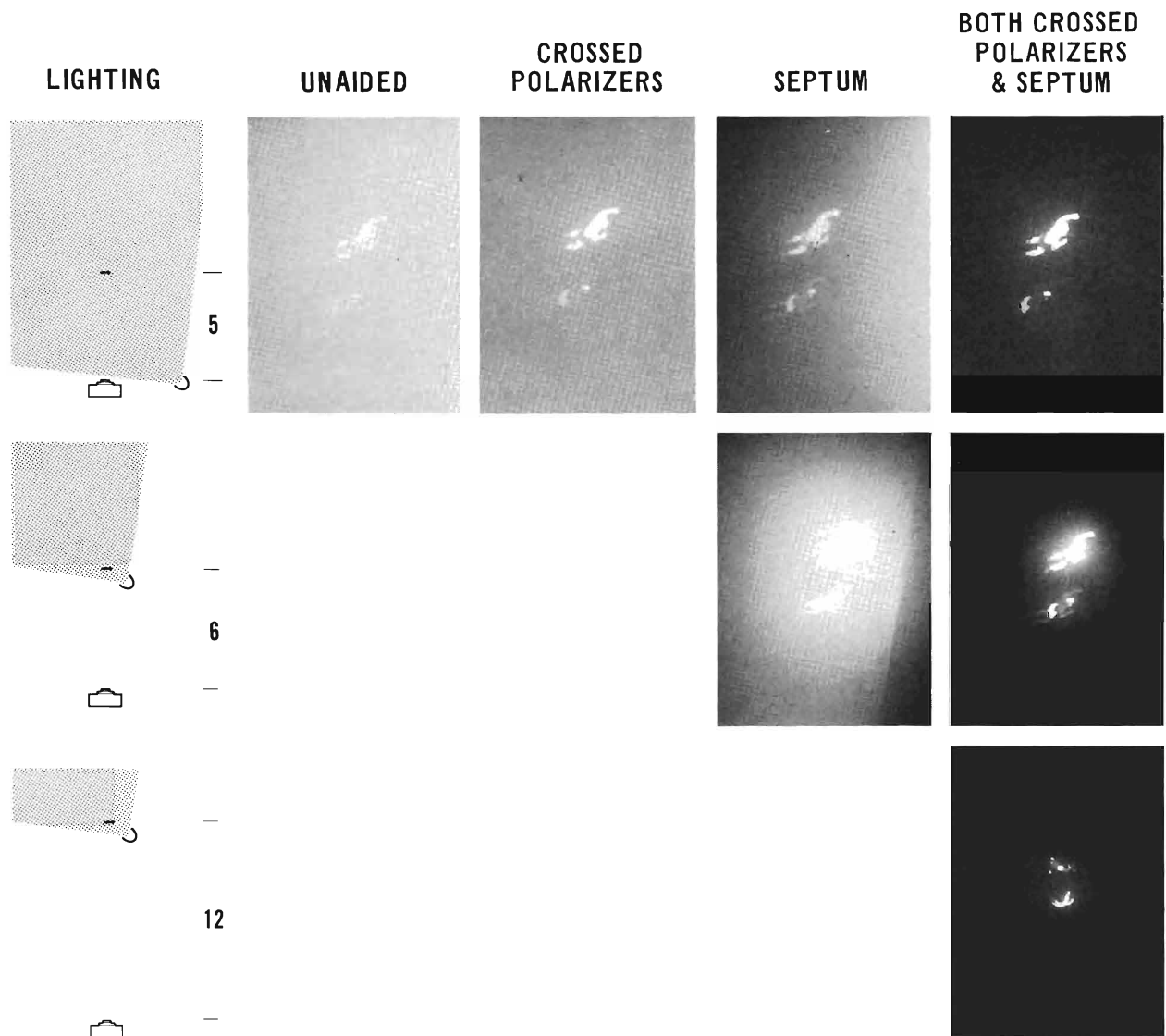


Fig. 3-12. Underwater photographs of moored dummies at 5, 6, and 12 attenuation lengths.

noticeable loss of contrast because the object is slightly veiled by the forward scattering of its *own* reflected light. Contrast enhancement in processing can overcome the minor loss of contrast, however, and good quality pictures can be obtained. An enlargement of the picture made at 12 attenuation lengths is shown in Fig. 3-13. It is to be remembered that this distance corresponds to 120 meters (394 feet) in average clear ocean water ( $1/\alpha = 10$  meters) or to 240 meters (787 feet) in exceptionally clear ocean water ( $1/\alpha = 20$  meters). The principal purpose of Fig. 3-12 is to illustrate that long range underwater photography is possible if the lights are close to the object and if adequate exposure can be provided.

There is, however, a limit to the photographic range which becomes apparent at slightly greater distances. Even with unlimited exposure, self-luminous objects in otherwise unlighted water disappear in their *own* forward scattered light beyond approximately 15 attenuation lengths. Contrast enhancement extends this limit only slightly.

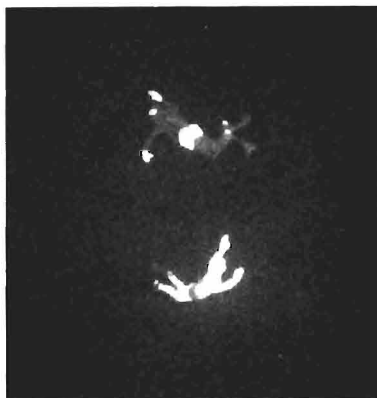


Fig. 3-13. Enlargement of the lower right photograph in Fig. 3-12, showing dummy swimmers moored 12 attenuation lengths from the camera.

### 3.9 EXPOSURE REQUIREMENTS

The range of underwater photography in terms of attenuation lengths is ordinarily limited by the available photographic exposure. One purpose of the equations given earlier in Section 3 is to enable exposure requirements to be calculated. The photographs in Figs. 3-11 and 3-12 were made at model scale in a laboratory tank with a Nikon camera containing Kodak Plus-X film and equipped with an F/2 lens. The lamp was a G.E. Type DVY. At distances of 1 or 2 attenuation lengths the exposure times were small fractions of a second, but at 5 or 6 attenuation lengths several minutes of exposure time was required. A time exposure for several hours was needed in order to obtain the picture at 12 attenuation lengths. Although long exposure times are feasible in the case of dummies moored in a tank, they are not available in the ocean with live objects and a mobile camera.

It must be remembered that very long range underwater photography requires not only large exposure but also that the object be self-luminous or lighted in an equivalent manner by having light only immediately adjacent to it. The latter option might seem to be impossible in most instances, yet this is exactly what is hoped for by those who are building systems using pulsed lasers for underwater imagery. Many of these lasers produce pulse durations of only a few nanoseconds. A laser pulse of 4 nanoseconds duration produces a train of light only about one meter long. When this light arrives at the object all of the water

closer to the camera is dark and the situation should be quite similar to having a lamp within a meter of the scene. Thus it would appear that the greatest hope, for truly long range underwater imagery is by means of pulsed lasers and gated electro-optical cameras.

### 3.10 SILHOUETTE PHOTOGRAPHY

Long range underwater imagery of silhouettes is easy if sufficient exposure is achievable. The maximum range at which opaque objects appearing as silhouettes against a distant extended source of light can be recorded in otherwise unlighted water is approximately 15 attenuation lengths. Beyond this distance the image becomes indistinguishable because of forward scattered light from outside the edges of the object. A silhouette photograph of a dummy moored at a distance of 12 attenuation lengths in the laboratory tank is shown in Fig. 3-14. The exposure time was several hours.

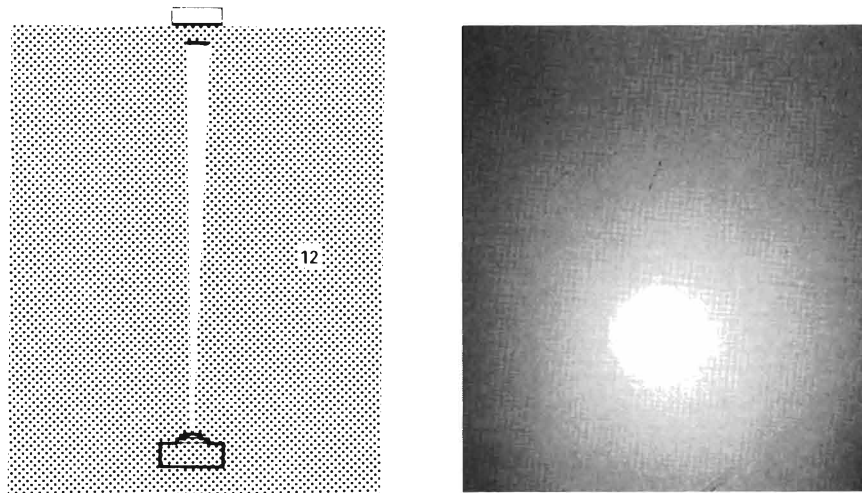


Fig. 3-14. Silhouette photograph of a dummy swimmer moored 12 attenuation lengths from the camera.

## 4. EXPERIMENTS WITH COLLIMATED LAMPS

### 4.1 SIMULATION OF UNDERWATER LASERS

Planning for experiments leading to an understanding of the properties of laser light in the oceans began early in 1961 when no blue-green laser suitable for submerged use existed or was expected to exist soon. Actually, the first such laser became available in 1964 but its eventual existence was only a matter of speculation in 1960. It was natural to ask: "Can an underwater laser be validly simulated by a projector producing a tiny, highly collimated beam from an ordinary source of light?" Answers to this question varied. No one was sure. Most were dubious.

The ruby lasers existing in 1960 produced millisecond pulses of coherent monochromatic red light in the form of well-collimated beams only a few millimeters in diameter. Already there was talk of Q-switching and other techniques that might enable pulse lengths to be shortened to microseconds or even nanoseconds with instantaneous power of a megawatt or greater.

There were perplexing doubts about possible nonlinear interactions between laser light and water. It was questioned whether the propagation of non-coherent light in water would be identical with that of coherent light. Some believed that studies of the behavior of steady light from a submerged incandescent projector would have no relevance to the behavior in water of light pulses as short as a few nanoseconds because such pulses would produce optical reverberations in the ocean. What if the optical relaxation time of water exceeds a few nanoseconds? It was suggested that the shape of the light pulse would be stretched or distorted in the process of transmission through the sea water, and that various forms of nonlinear absorption effects would take place. Energy might be lost, it was said, by the production of sound waves. There were reported observations of micro-bubble production when laser beams were focused in water: Would these destroy the beam by scattering? In short, there were in 1961 many unanswered scientific quandries which caused doubts to be expressed concerning whether any attempt should be made to experiment with steady burning conventional sources, even though optical systems could be constructed to produce beams of light similar in geometry to those expected from future lasers. It was said repeatedly that no incandescent projector should be called a "laser simulator" and, in fact, that term was dropped from usage by the Laboratory in deference to these objections. Experiments proceeded, however, with an incandescent projector used exactly as if a laser was being simulated.



In the clear light of hindsight, exploration of the properties of highly collimated small beams of incandescent light in water was most wise. It is now known that none of the effects enumerated in the preceding paragraph have any significant existence with respect to the performance of 1964-66 underwater lasers, whether steady burning or producing twenty-nanosecond, megawatt pulses. We have no evidence that the propagation of coherent light differs significantly from that of non-coherent light. No nonlinear effects, ringing, or pulse stretching due to propagation were observed.\* In fact, all irradiance and radiance data are identical from incandescent sources, doubled neodymium pulsed lasers, and continuous argon-ion lasers.

The fact that pulse stretching\* and nonlinear effects in water are not observed at the sub-megawatt power levels used in the work described by this report does not mean that these effects are not to be expected with much shorter pulses from high powered, mode-locked lasers. Clearly, there is a regime of such propagation phenomena that is associated with high powered pulses having durations comparable with the lifetimes of atomic or molecular states and transitions, but these complex phenomena do not, fortunately, seem to concern those using 20 nanosecond pulses.

The measured propagation characteristics of light from the steady incandescent projector were found to agree precisely with the propagation characteristics of light from a laser producing 20 nanosecond pulses provided that all geometrical properties of the respective light beams are identical; see Section 6.2. The same result was obtained with a steady burning argon-ion laser producing light having coherence length of several centimeters. The above statements are made on the basis of high quality experimental data and they support theoretical constructs that have evolved during the decade that has been occupied by the research, but in 1961 when the experiments were begun with the highly collimated incandescent projector there was no guarantee that the conclusions reached would have any relevance to the performance of lasers in the ocean. It is pleasing that the incandescent data given later in this section are applicable to performance of lasers, but even if this had not proved to be true the work in 1961 and 1962 would not have been wasted, because the experimental techniques and apparatus that were devised and built in those years made possible the laser experiments which came later. It is doubtful whether such successful techniques and equipment would have been developed using pulsed lasers alone, for laser observation is difficult and hazardous. The measurement techniques using cameras on fast oscilloscopes are vastly more cumbersome and somewhat less precise than those used to study light beams from incandescent lamps. Even the steady burning argon-ion laser is a difficult and dangerous light source compared with the incandescent projector.

#### THE COLLIMATED INCANDESCENT UNDERWATER PROJECTOR

In 1961 it was believed that submerged lasers might be expected to produce beams of light in water having a divergence of 1 to 3 milliradians and a diameter at the source of, typically, 1/2 inch (12.7 mm). Allowance should be made, it was said, for beam diameters as great as 50 mm. An incandescent projector was designed to meet these requirements. Fig. 4-1 is a photograph of it. A schematic diagram of the projector appears as Fig. 4 on p. 216 of Appendix A and the essential optical details are given in the caption of that figure. The diameter of the beam of light it produced could be reduced by an external stop to any desired value. The incandescent source was a zirconium concentrated-arc lamp manufactured by the Sylvania Company. The lamp housing was designed to accommodate four sizes of these lamps in prefocused

---

\* A form of pulse stretch due to path length differences was found in the scattered light far from the laser beam; see Section 6.6.

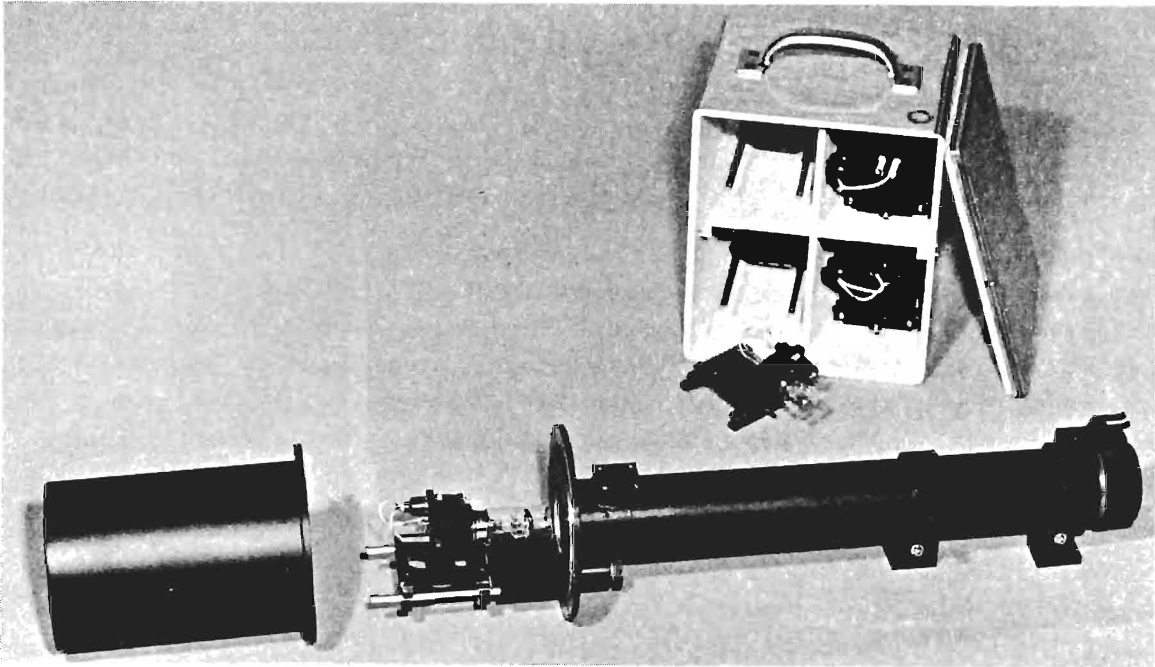


Fig. 4-1. Collimated incandescent underwater projector. See Fig. 4 on page 216 of Appendix A. Wooden case houses four sizes of concentrated-arc lamps in prefocused subassemblies.

subassemblies. Thus, the 2, 10, 25, and 100 watt models of the concentrated-arc could be used at will in order to vary the beam spread. The area of the arc crater in these lamps is roughly proportional to their power rating. The light beams they produced had divergences of 0.18, 0.80, 1.5, and 3.0 milliradians, respectively, at the full 50 mm beam diameter. These divergences were increased by diffraction when the beam diameter was reduced by the use of an external stop. For example, with a circular stop 1.27 mm (1/20 inch) in diameter the four beam divergences were 0.70, 1.3, 2.0, and 3.5 milliradians respectively.

*Collimation.* Adjustment of the collimation of the projector was accomplished by means of the device shown in Fig. 4-2. The small central tank was filled with water after the end of the underwater projector was pressed against an O-ring seal in the tank. The light emerging from the high quality plane window on the opposite side of the water tank was allowed to enter the telephotometer shown in Fig. 2-3. This instrument fitted the V-block supports which can be seen on the right in Fig. 4-2. The telephotometer served simply as a telescope. It was focused at infinity by sighting on some distant object, such as a

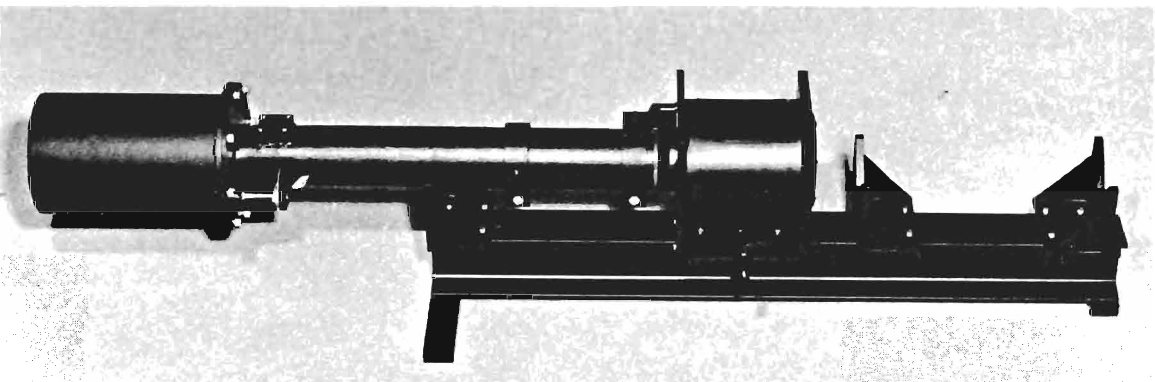


Fig. 4-2. Fixture for collimating the incandescent underwater projector. Telephotometer (See Fig. 2-3) fits in V-blocks on the right.

tree on some far-away hilltop, before being placed in the V-blocks. Both a neutral density filter and a Wratten No. 61 green filter were added to the eyepiece of the telephotometer so that the operator could look comfortably at the image of the arc crater formed by the system. He then adjusted the position of the zirconium arc to produce the sharpest image of the crater. This collimated the lamp. Once the adjustments on the subassembly were locked, the assembly could be removed and reinserted freely without requiring re-collimation. Thus, the four lamps in their respective subassemblies could be easily interchanged.

*Mounting Requirements.* Previous experience, gained at Diamond Island during the summer of 1960 with an underwater projector producing a beam having a spread of 43.5 milliradians (2.5 degrees), showed that the mounting for a highly collimated underwater lamp must be very stable and must have precise pointing controls. Attempts in 1960 to use the 43.5 mr lamp from a floating support demonstrated that such supports are useless. It was clear that both the projector and the measuring equipment must be supported rigidly from the bottom of the lake if successful measurements at high collimation were to be made.

## 4.2 THE FIRST UNDERWATER TOWER AND TRACK

A successful mounting system for experiments employing the highly collimated projector was constructed and used during the 1961 experimental season. It made use of a vertical cylinder of concrete 12 feet long with an inside diameter of 4.5 feet. It was placed on a rough platform of rocks arranged on the bottom of the lake. Portland cement concrete was poured into the cylinder from above until the lower 3.5 feet of the cylinder was filled. Since the cylinder was open at the bottom, the concrete also flowed down through the supporting rocks. Thus, the bottom of the cylinder was sealed by a massive concrete plug which anchored it to the rock foundation. Prior to putting the big cylinder in place, a window was cut in its side and fitted with a circular observation port 15 inches in diameter. The center of this port was 2.5 feet below the lowest level of water which occurred throughout the series of measurements.

The cylinder was tall enough to extend above the water surface. Its top was 2 or more feet above the level of the lake, depending upon seasonal differences in lake level. Pumps were used to remove the water from within the cylinder so that it could be occupied by the experimenter with his apparatus. A temporary wooden shelter was constructed on top of the concrete cylinder to provide laboratory space for recorders and electronic equipment. The installation was made in water about 12 feet deep at a location that was protected from the strong west and northwest storm winds and waves in the lake. It was near one corner of a large boathouse. A wooden footbridge was constructed between the boathouse and the top of the concrete cylinder to provide easy access. Figure 4-3 shows a photograph of the completed facility.

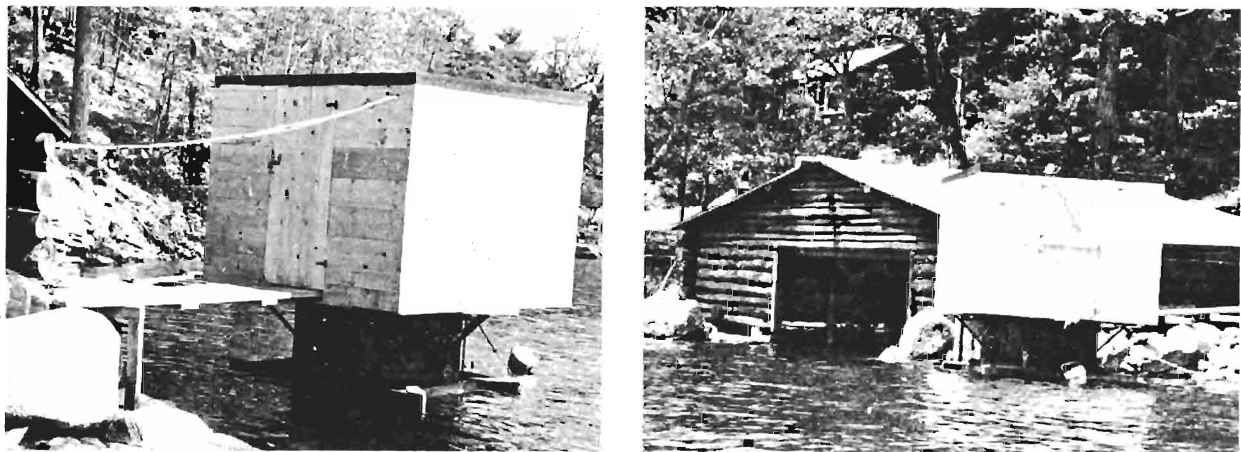


Fig. 4-3. First underwater tower at Diamond Island, 1961.

Access to the interior of the underwater tower was by means of a ladder, as shown in Fig. 4-4. A rigid table was provided to support the various photometers and cameras at the observation port. The circular underwater window, shown in Fig. 4-5, was made of Plexiglas 1-1/4 inches thick. Because this material showed birefringent patterns in polarized light (e.g., when used between crossed polarizers) a central insert of high quality, strain-free, optical glass 4 inches in diameter and 3/4 inches thick was provided. It is seen in Fig. 4-5, surrounded by a brass mounting ring. All telephotometry, photography, and measurements of radiance and irradiance were made through this glass insert. For irradiance measurements, a circular piece of translucent diffusing plastic was mounted on the brass ring in the water outside the window in such a way that it could be pivoted to positions either in front of the window or downward out of the way, as in Fig. 4-5. When the diffusing disk was in front of the window, the readings of the photoelectric telephotometer were proportional to the irradiance incident on the outer surface of the diffuser.\* A thin, blackened metal cover having a small central hole could be attached to the outer surface of the diffusing disk in order to limit and define the area of the disk used for the irradiance measurements.

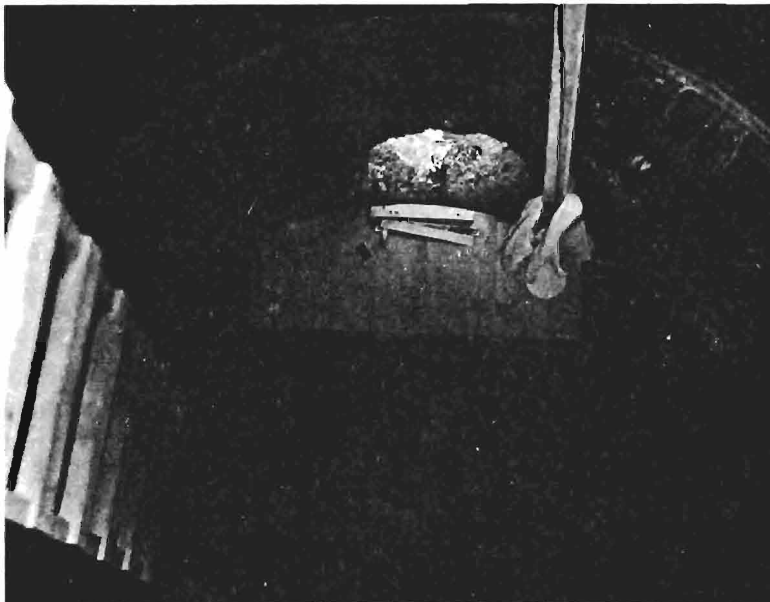


Fig. 4-4. Interior of the first underwater tower.

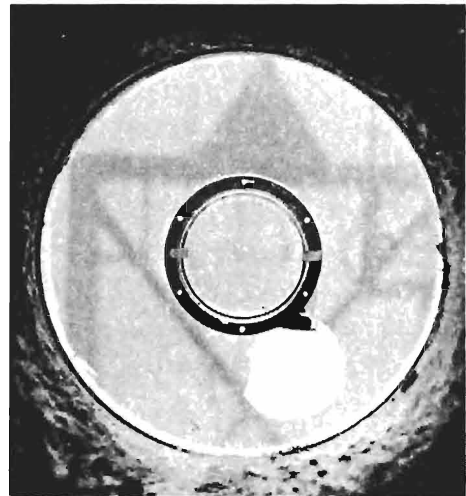


Fig. 4-5. Interior of the underwater window. Underwater cart is faintly visible beyond the window.

#### MOUNTING THE UNDERWATER PROJECTOR

It was essential that the underwater projector should be mounted in such a way that its distance from the measuring window could be varied. This was achieved by building a horizontal underwater trestle ("track") along the bottom of the lake. It was attached at one end to the outside of the concrete cylinder 2 feet below the center of the measuring port or 4.5 feet beneath the water surface and 7 or 8 feet above the lake bottom. It extended away from the underwater viewing port for a distance of 50 feet in a direction roughly parallel to the shoreline of the island which, at that place, ran in an approximately east-west direction. The cylindrical underwater observation "room", referred to as an underwater "tower", was situated at the west end of the track. The highly collimated underwater projector was carried along the track

\* See p. 4-15 and 4-18 for refinements of this technique, and discussion of the requirements to be met in order to obtain valid irradiance data.

by a four-wheeled cart fabricated of square-sectioned brass tubing, shown in Fig. 4-6. The cart could be pushed along the trestle and clamped in position at any distance from the tower.

Within the cart was a mounting for the "narrow beam lamp", as the projector came to be called. The projector could be rotated in a horizontal plane about a vertical axis passing through the second nodal point of its lens. The control for this rotation was brought to the water surface by means of the vertical column shown in Fig. 4-6. A sector plate at the surface enabled the lamp to be rotated through approximately 60° on either side of the axis of the track. Notches in the plate and a clamp mechanism, appearing to have somewhat the shape of a clothespin, Fig. 4-6, enabled the direction of the light beam to be set at known angles. A tangent-screw mechanism for fine horizontal adjustments was also provided in order that, at the center notch, the lamp could be adjusted until the light beam passed precisely through the center of the observation port; the tangent screw is obscured by the sector plate in Fig. 4-6.

The light beam also needed to be aimed precisely in a vertical plane. In order to accomplish this the lamp was pivoted about a horizontal axis located several inches from the lens (see Fig. 4-6). Small vertical displacements of the lens then provided vertical aiming of the light beam. The control was a knurled wheel which may be seen clearly in Fig. 4-6 at the top of the control column. This was attached to a threaded vertical shaft which extended downward through the center of the hollow control column to a tiny white ball which engaged a phosphor-bronze clip on the projector just above the lens. Rotation of the knurled control wheel thus moved the lens vertically through a sufficient range to enable the light beam to be positioned accurately in the center of the observing window.

At the extreme left of the sector plate (see Fig. 4-7) is a vertical rod which passed downward to the center of the front horizontal structural member of the cart. By pulling up on this rod the operator could release clamps just behind each of the two front rollers; the cart then rolled easily along the underwater track. Releasing the rod caused the clamps to lock the cart at any selected lamp distance. The distance of the lens of the underwater projector from the measuring aperture at the window of the underwater tower could be ascertained either by measuring with a steel tape above the water line from the tower to the top of the control column or by reading (underwater) the position of the cart by means of a steel tape fastened to the center of the track, as shown in the underwater photograph, Fig. 4-8.

*Spherical Lamp.* The cart also carried a 1000-watt spherical lamp for use in water clarity measurements by means of the techniques described in Sections 2.5 and 2.6. In Fig. 4-9 the spherical lamp is shown in position in front of the projector; Figs. 4-6 and 4-7 show it stowed in a protective housing at the right of the cart. The control handle was intended to protrude through the water surface.

## POSITIONING THE PROJECTOR

Unprotected swimmers had suffered greatly from cold during the night experiments in 1959 and 1960. It was desired, therefore, to minimize or eliminate the need to use a swimmer for moving the narrow beam projector along the track and to aim it.\*

The above-water system of controls for the narrow beam projector was devised to eliminate the need for anyone to enter the water. A pair of assistants in a rowboat could move the cart along the track, clamp it at any selected lamp distance, and adjust the light beam to the center of the measurement window by means of voice commands shouted by the experimenter inside the underwater tower or relayed for him by

---

\* Self contained underwater breathing apparatus (SCUBA) was unknown at Diamond Island in 1961 and wet suits for thermal protection were receiving their first trials.

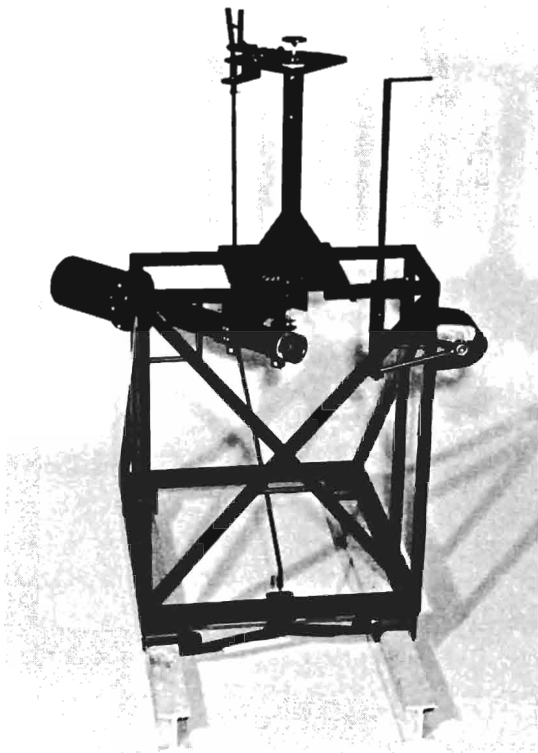


Fig. 4-6. Underwater cart and collimated projector in off-axis position.

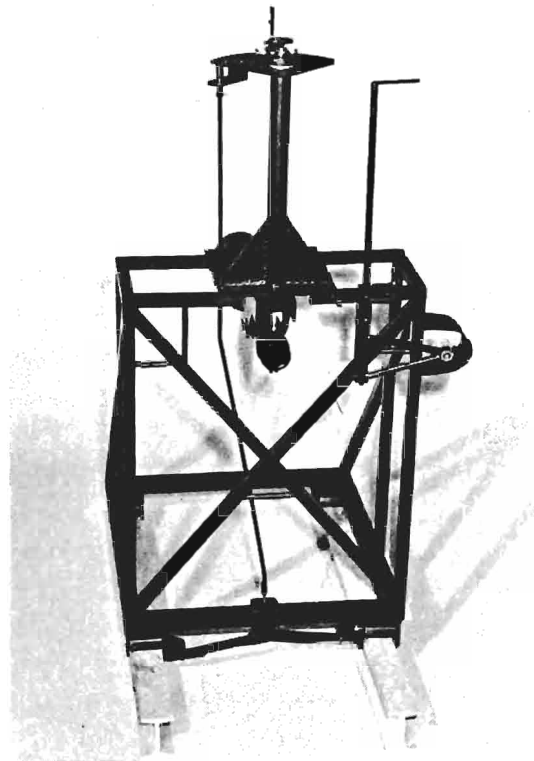


Fig. 4-7. Underwater cart and collimated projector in on-axis position.

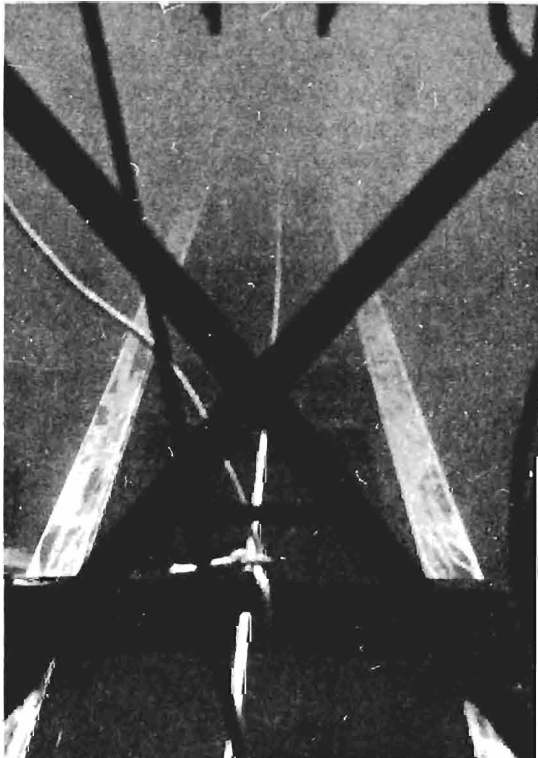


Fig. 4-8. Underwater track as seen through measurement window and underwater cart.

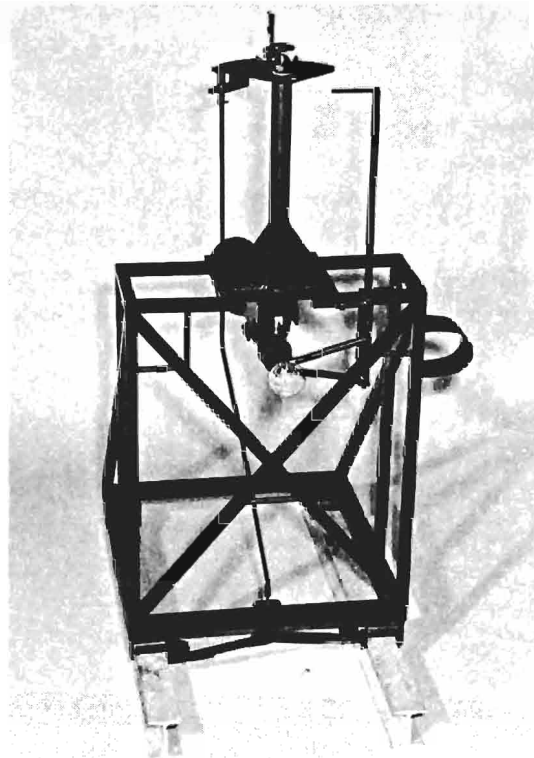


Fig. 4-9. Underwater cart with 1000-watt spherical lamp.

someone at the top of the tower. Thereafter, upon command, the assistants could rotate the light beam to any of the horizontal angles identified by the notches in the sector plate. On calm, quiet nights the rowboat technique worked fairly well. Unfortunately there were very few calm, quiet nights. Some good data were produced (with the help of swimmers), but the entire installation proved to have many shortcomings. These were corrected in 1962 when the second underwater tower and track were constructed.

#### THE 1961 DATA

The results of the experiments at Diamond Island in 1961 were published in the paper entitled "Light in the Sea," which is reproduced as Appendix A of this report. The 1961 results are on pages 218 to 225 and particularly in Figs. 9, 10, 12, 15, 17, 18, 20, 21, and 22.

### 4.3 THE SECOND UNDERWATER TOWER AND TRACK

The use of the first underwater tower, track, and cart during the summer of 1961 revealed many serious shortcomings. Drastic improvements were needed before the research potential of the highly collimated incandescent source could be realized or before meaningful explorations could be made of the properties of underwater lasers. The shortcomings of the 1961 equipment had a profound influence upon the design of the highly successful second generation installation that was made in the summer of 1962 and used subsequently for all of the underwater laser experiments at Diamond Island. The changes and the improved equipments are described in the following paragraphs.

#### DEPTH OF THE EXPERIMENT

The first underwater tower was designed to place the track and cart close enough to the water surface for the lamp controls to protrude into the air where they could be operated by an assistant in a small rowboat. The optical path for the light beam was chosen to be only two feet beneath the water surface and the controls were built accordingly. During the construction of the concrete tower, however, the measuring port was placed such that the depth of the light beam was about 2.5 feet. Thus, none of the control handles protruded above the water surface. This made the operation much more difficult than was planned. Finding the control handles in the dark without running into them with the rowboat was difficult at best and impossible in the presence of the small waves which were nearly always present. Use of the rowboat was soon abandoned; swimmers operated the lamp controls.

The existence of the control handles just below the water surface was detrimental because motion of the water due to waves produced forces on these parts that moved the projector and the light beam erratically. During a dishearteningly large part of the time the projector vibrated too much to enable data to be taken. Vibration became more serious, of course, when the collimated lamp was near the outer end of the 50-foot track. Even on nights when work could be done, there were often periods of an hour or more when a sudden breeze would force the work to stop. Such stoppages during the early morning hours were particularly discouraging and it was difficult to maintain the morale of tired men while waiting for the wind to die down. It became obvious that the shallow technique was impractical, especially for the future longer range underwater laser experiments. It was obvious that the facility must be reconstructed so that the experiment could be performed at a greater depth. The discussions were of an "all weather" capability.

Study of various interacting requirements resulted in a decision that the new installation would place the beam from the collimated lamp or the laser 6 feet beneath the surface and 3 feet above the underwater

track. This was a compromise between the desire to place the entire experiment so deep that it would never be affected by water waves and the need to restrict depth in the interest of swimmer performance. It was obvious that future experiments would require the continuous services of scuba divers, who would be required to make many ascents and descents between the surface, the underwater projector, the underwater track, and frequently, the lake bottom. Physiological difficulties due to frequent vertical transits would increase rapidly as depth was made greater.

The decision to place the optical axis of the experiment at a depth of only 6 feet was the result of considerable study. One of the factors considered was the optical effect of the water surface. Attenuation length in Lake Winnepesaukee in 1961 was about 5 ft/in. Although dark-painted rafts or floating curtains were to be used in order to eliminate the mirror-like air-water surface, it was nevertheless desired to have all solid reflecting objects located as far as possible from the light beam. The choice of 6 feet for the depth of the beam insured that the overhead rafts or curtains would be more than one attenuation length away from the beam. In 1966, when the most important laser data were taken, the water clarity was such that the curtains were about 1.5 attenuation lengths above the beam. The bottom of the lake was much farther from the light beam even at the shallowest point (near the tower). The lake bottom is covered by a thin layer of organic detritus which provides a diffuse reflectance of about 1.3 percent. This matches the reflection function of the water for diffused light almost perfectly. That fact is one of the major advantages of the Diamond Island location for the conduct of optical experiments underwater. Any light field is virtually unperturbed by bottom influence, a matter of the greatest importance in the studies of underwater daylight which were conducted during the first era at Diamond Island.

#### CONTROL OF BEAM ALIGNMENT

In 1961 the accurate pointing of the underwater light beam was extremely difficult and time consuming, particularly at the longer cart distances. Much of the difficulty resulted from the use of voice communication between the experimenter in the underwater room and the swimmer who attempted to follow his instructions. On most occasions the noise of wind and waves made it necessary for directions to move the beam up or down, toward the island or away from it, to be relayed by someone at the top of the tower. Every alignment of the light beam was a long, frustrating experience. Obviously, the experimenter, who could see the light beam entering his window, needed remote controls operated by his own hand. Such a system of lamp control was built in 1962.

*Remote Pointing Control.* The incandescent projector, and later the underwater laser, were mounted on top of a watertight steel box which contained the control mechanism. Wheels attached to this box made it a cart to travel along the underwater track, as shown in Fig. 4-10. Clamps located between the wheels on each side of the cart enabled it to be clamped rigidly to the flanges of the track. A heavy vertical steel column extending through the top plate of the box supported the narrow beam lamp. The vertical axis of the column passed through the lens of the projector. Thus, turning the column rotated the projector about its projection lens.

The projector was supported by a trunion mounting attached to a horizontal arm carried by the steel column. This provided a vertical adjustment for the light beam. Control was achieved by means of a small rod which occupied a vertical axial hole in the heavy steel column. This rod terminated in a small white ball which engaged a spring clip just beneath the projection lens. The control mechanism within the cart imparted a vertical motion to the rod, thus turning the projector about a horizontal axis through the trunion support and causing the light beam to be inclined slightly upward or downward.



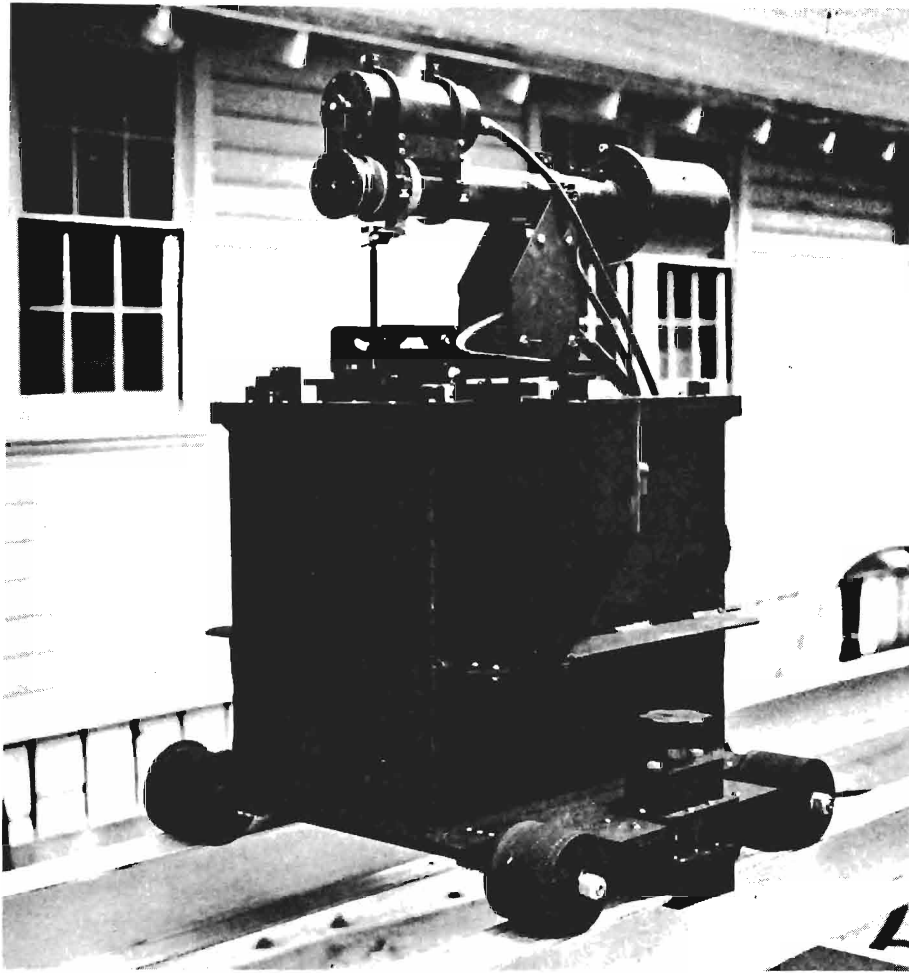


Fig. 4-10. Collimated underwater projector on second underwater cart.

Provision was made for the remote insertion and removal of an aperture stop for the projector. The mechanism can be seen in Fig. 4-10. It is a cylindrical case mounted on top of the projector above the projection lens. This case contains a rotary solenoid with its axle protruding forward toward the tower. This axle carries an arm, visible in the photograph, bearing an interchangeable aperture stop. A switch at the lower center of the control panel enabled the experimenter to insert or remove the stop at will. This was an important capability without which beam alignment at long lamp distances would have been impossible, for at long range the reduced beam passed by the stop is usually impossible to see until after it is precisely aligned with the eye of the observer.

The mechanism for accomplishing these motions was mounted to the top plate of the watertight compartment of the cart. It is shown in Fig. 4-11. The horizontal rotation enabled the beam to be swept from  $5^\circ$  on the island side of the axis of the underwater track to  $58^\circ$  on the opposite side of the axis, i.e., away from the island. A selsyn system sensed this rotation and indicated the direction of the light beam on a large dial on the experimenter's control panel, shown in Fig. 4-12.

Rate controls were provided on the control panel for both the vertical and horizontal drives. The upper switch, marked CW, OFF, CCW, controlled the azimuthal movement of the light beam and the lower

switch controlled the vertical motion. The middle switch controlled an auxiliary motor which operated the azimuth drive through a differential to provide a super-slow azimuth control for very fine pointing accuracy. This was essential at very large lamp distances. In the new configuration, 250 feet of track was available.

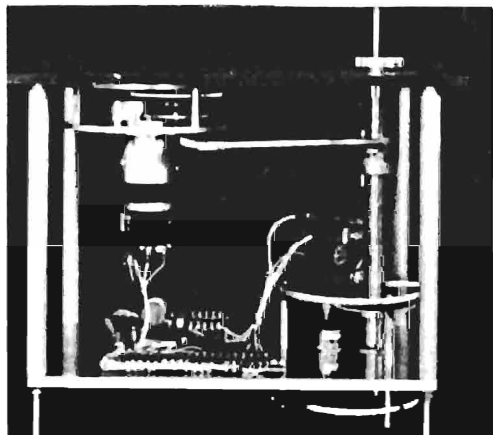


Fig. 4-11. Internal mechanism of second underwater cart.

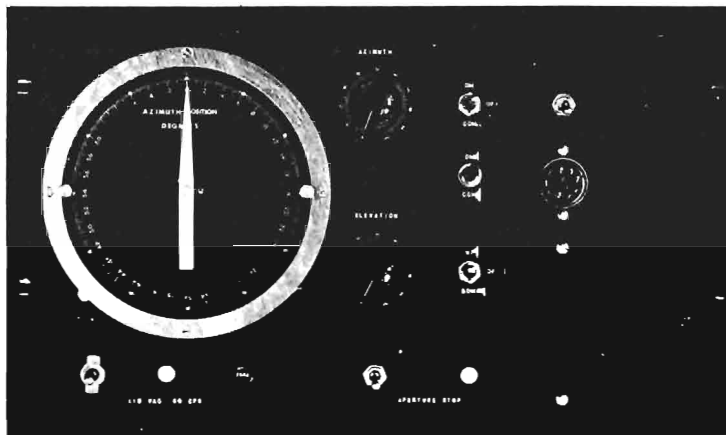


Fig. 4-12. Control panel for remote control mechanism in the underwater cart.

The wiring diagram of the cart control system is shown by Fig. 4-13 and the rear of the control panel is pictured in Fig. 4-14.

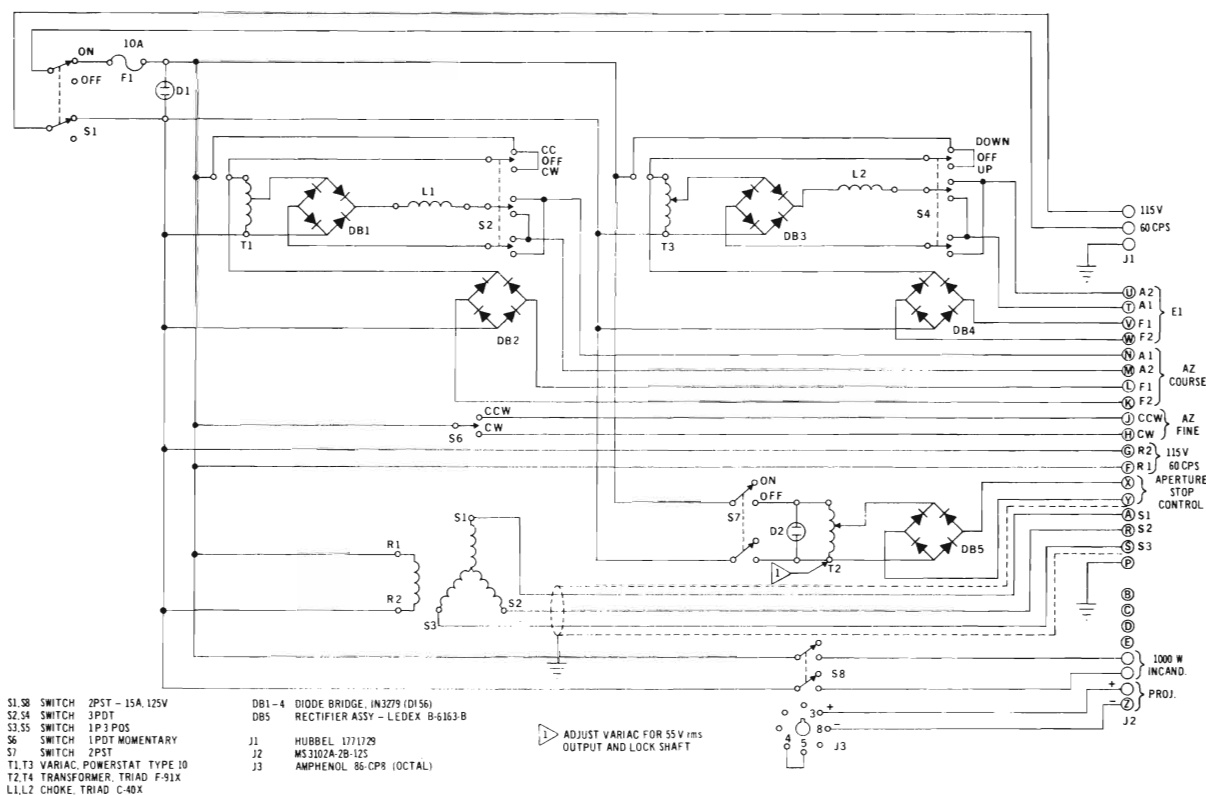


Fig. 4-13. Schematic wiring diagram of the control panel and pointing mechanism of the underwater cart.

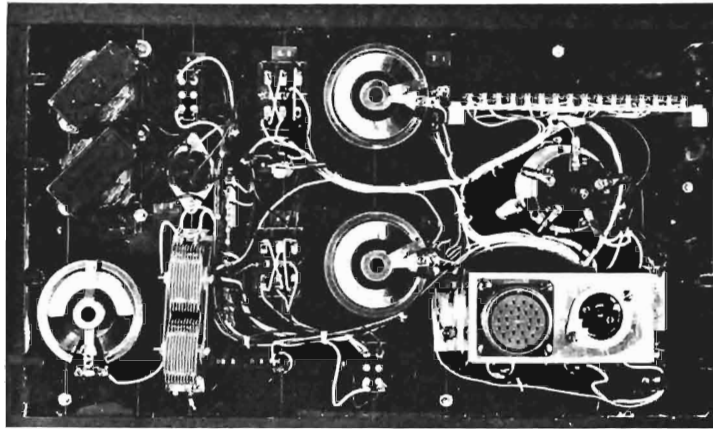


Fig. 4-14. Rear view of the control panel in Fig. 4-12.

#### MOVEMENT OF THE CART

It was the initial plan to provide the experimenter within the tower with means for moving the cart along the track by remote control. This was achieved. A long wire cable ran from an electrically driven drum at the top of the steel tower along the top of the "ties" of the track to the cart and thence to a pulley at the far end of the track. The cable returned to the tower along pulleys underneath the track and was attached to the drum. Thus, the cart could be pulled to or from the tower depending upon the direction of rotation of the electric motor which turned the drum. Spring operated clamps held the cart rigidly to the track unless they were released by activating electromagnets when the cart was to be moved. This system worked well so far as cart movement was concerned, but adequate provision had not been provided for the automatic handling of the many heavy electrical cables which were attached to the cart. Fouling of the cables and even damage to them occurred almost every time the cart was moved. Scuba divers were needed, therefore, to handle the electrical cables. Remote operation of the powerful cart drive created a hazard to the swimmers, whose hands could have been caught and crushed while endeavoring to manipulate the electrical cables. This risk was needless since the swimmers could move the cart and handle the cables simultaneously. They could also change stops, clean glass surfaces,\* and assist in beam alignment at long lamp distances.\*\* For all of these reasons the power drive for the cart was dismantled early in the 1962 series of experiments and was never used again. Scuba divers recruited locally were used throughout all of the remaining underwater experiments at Diamond Island.

#### APPLICABILITY OF DIAMOND ISLAND IRRADIANCE DATA TO OCEAN WATER

Although research at Diamond Island had, from the outset, been undertaken for the discovery of principles rather than for obtaining final data to be used in designing systems for use in oceans, it was natural

\* It was necessary to clean all glass surfaces in contact with lake water at three-hour intervals or oftener to insure that no errors in light measurement were caused by the accumulation of organic material on those surfaces.

\*\* At very long lamp distances (beyond 15 attenuation lengths) the light beam from the projector, even at full 50 mm aperture, was not visible unless it entered the eye of the experimenter. A swimmer at midrange could see the beam easily and position himself in it. A battery operated electric light bulb fastened to the back of the swimmer's head by attachment to the strap of his face mask could be seen by the experimenter, who operated the remote controls for pointing the projector until the swimmer was directly in front of the observation window. The swimmer next extinguished his lamp and moved aside. The beam from the projector was then visible to the experimenter, who could center it on the measuring aperture. Precise alignment of the projector at distances up to 25 attenuation lengths was achieved by this technique.

to speculate on the possibility that the lake data could be translated quantitatively to the ocean environment. The studies of forward scattering, including very small angle scattering, made with the first tower and track in 1961 (see pages 218, 219, and 220 of Appendix A) led to the belief that translation was possible with respect to irradiance on axis if certain geometrical scaling requirements were met. The requirements are described in the following section. This possibility was deemed to be so important that it had a major influence on the design of the second generation equipment and on the conduct of the experiments with the collimated incandescent projector in 1962 and with the submerged lasers in 1964 and 1965. Unfortunately, the first neodymium-doubled underwater green lasers produced beams that were so irregular in shape, in power distribution, and in reproducibility from pulse to pulse that little or no true significance attached to measurements of "irradiance-on-axis." Evolution of community interest, moreover, soon moved away from irradiance on-axis and toward total laser power delivered to surfaces larger than the geometrical size of the light beam. Thus, the spreading of laser beams by passage through water and the distribution of irradiance off-axis were the center of importance. The laser beam spread experiments in 1966 made clear the crucial role of absorption in determining the spreading of collimated beams of light in water. This discovery eliminated any hope of applying off-axis irradiance data from the lake to ocean water. (See Section 7.) Even on-axis irradiance by a circularly symmetric beam must be affected somewhat by beam spread, so that geometrical scaling is a necessary but not a fully sufficient requirement for translation between highly dissimilar types of water. Although section 7 of this report describes a much better approach to securing laser data applicable to the oceans, the principle of scaling is fully described in the following section of this report because of its influence on the design of the second generation equipment and the manner of its use.

#### THE PRINCIPLE OF SCALING

The conclusion (see Figs. 9, 10, 11, and 12 on pages 219 and 220 of Appendix A) that the volume scattering functions of Lake Winnepesaukee and of most ocean waters are remarkably similar at scattering angles less than 60 degrees led to the concept that measurements of irradiance on the axis of the collimated light beams in Lake Winnepesaukee could be applied to ocean water if all distances are expressed in attenuation lengths and if the light beams are *geometrically similar* in the lake and in the ocean; that is to say, if all of the scattering angles involved are the same in both cases. So far as the non-scattered photons which form the residue of the light beam at any distance are concerned this geometrical requirement is met if the ratio of the diameter of the collimated beam used in the lake to the diameter of the collimated beam used in the ocean is the same as the ratio of the attenuation length in the lake to the attenuation length in the ocean. The attenuation length of the lake in the green region of the spectrum centering at 530 nm, where all of the measurements were made, was about 5 feet in 1961. The attenuation length of the clearest ocean water at this wavelength is the order of 50 feet. The principle of scaling requires, therefore, that the light beam emitted by the underwater projector or the underwater laser at Diamond Island must have one-tenth of the diameter of the beam emitted by an underwater laser used in clearest ocean water.

In 1961 and 1962 there were no green lasers for underwater use although work to devise such equipment was in progress. The author was advised to assume that the beam of light produced by an underwater green laser for use in the oceans would be 1/2 inch in diameter. The requirement for scaling at Diamond Island meant that the collimated projector must emit a beam of light 1/20 of an inch in diameter in order to simulate the performance of the assumed laser in the clearest ocean water. If the oceanic average attenuation length at 530 nm is 25 feet, it follows that the diameter of the beam of light emitted by the

narrow beam source at Diamond Island should be 1/10 inch in order to simulate the performance of the assumed 1/2 inch diameter underwater laser in oceanic average water.

The above thought pattern dictated the design of the experiments in 1962 and the laser experiments which followed in 1964. In both instances the prime emphasis was in irradiance on-axis. A more general exploration of the light field produced by underwater lasers was, of course, also part of the program and, indeed, many off-axis measurements were made both in 1961, 1962, and throughout the underwater laser programs in 1964, 1965. They were the primary interest in 1966. Even in 1961, the mounting for the underwater narrow beam lamp was provided with a notched sector plate to allow the beam to be diverted through known angles from the axis of the underwater track. Nevertheless, the primary goal of the experiments for 1962 and 1964 were the measurements of irradiance on axis at all achievable ranges with light beams stopped down to diameters of 1/20 inch and 1/10 inch, respectively. This drastically reduced the power level of the experiment, particularly with the narrow beam incandescent projector. It meant also that the irradiance collector used must be smaller in diameter than 1/20 inch for the measurements to be made at small lamp distances where the beam diameter did not appreciably exceed 1/20 inch. At longer lamp distances spreading of the beam due to divergence and due to scattering processes in the water enabled larger irradiance collectors to be used but did not relax the requirement for extremely accurate pointing controls and highly stable mounting for both the underwater light source and the receiving aperture.

#### DESIGN OF THE SECOND UNDERWATER TOWER

The engineering design of the second generation tower, track, and pointing control equipment was set by the philosophy and requirements detailed in the preceding section. The severe loss of experimental time experienced in 1961 due to water waves and boat wakes dictated that the second generation installation should have "all-weather" capability. This was achieved (1) by conducting the experiment at greater depth, (2) by providing the experimenter with remote pointing controls for the light source, and (3) by providing underwater voice communication between the experimenter and the scuba divers who served as assistants in the experiment. The swimmers had air tanks and wet suits that enabled them to stay for hours if necessary at the depth of the experiment in order to move the cart along the track, change aperture stops on the light source and at the measuring window of the tower, clean all glass surfaces, and assist in beam alignment.

*Voice Communication.* Voice communication was provided by a row of underwater loudspeakers supported above the track just under the water surface by means of floats. The instructions of the experimenter could be heard from any working position. Reverse communication from the swimmer to the experimenter was needed only infrequently. Experience showed that the swimmer could tap on the rails of the underwater track with any metal object (such as a screwdriver or the handle of a diver's knife) and that these clicks were clearly audible to the experimenter inside the underwater tower. This was true because the second tower was made of steel rather than concrete.

*The Second Tower.* A model of the second underwater tower and track is shown in Fig. 4-15. It was square sectioned (rather than round as in the case of the concrete cylinder used previously) and about 5 feet square. Rings of I-beams inside the walls of the new tower stiffened the structure and provided convenient shelves for apparatus and convenient mountings for apparatus, flooring, ladders, etc. The same 18-inch diameter round underwater window was used in the new tower. The plastic window still contained the same 4-inch insert of strainfree high quality optical glass that had been used in the first tower.

*Modification of the Underwater Window.* Just outside the lower right edge of the circular glass insert, as viewed by the experimenter within the tower, the Plexiglas portion of the measuring window was pierced by an axle provided with O-ring seals. The experimenter could turn this axle from within the tower and thereby rotate any object attached to the shaft in the water. The outer end of the shaft bore a hub designed to receive a round plastic disk about 9.5 inches in diameter shown in Fig. 4-16. The disk contained a pattern of six holes 2.5 inches in diameter. The size and mounting of the disk was such that the center of each of these holes could coincide with the center of the optical glass insert in the measuring window and, thereby, with the optical axis of the experiment. Notches were milled in the outer edge of the plastic disk in positions such that a small roller attached to a spring-loaded arm mounted on the outer surface of the Plexiglas served as an accurate detent to center, successively, each of the six holes in the Plexiglas disk accurately in front of the glass window insert.

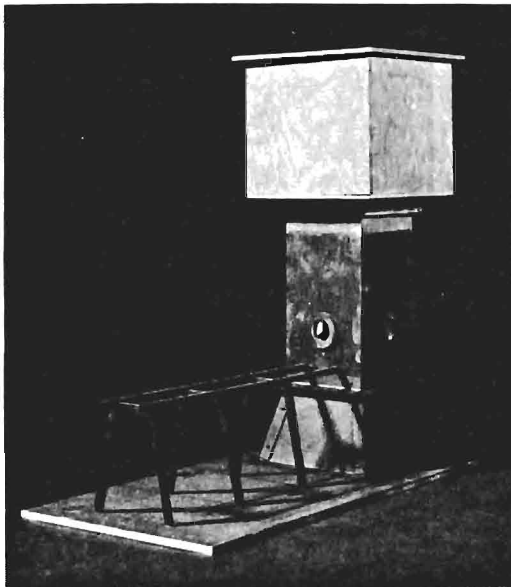


Fig. 4-15. Small wooden model of the second underwater tower and track.

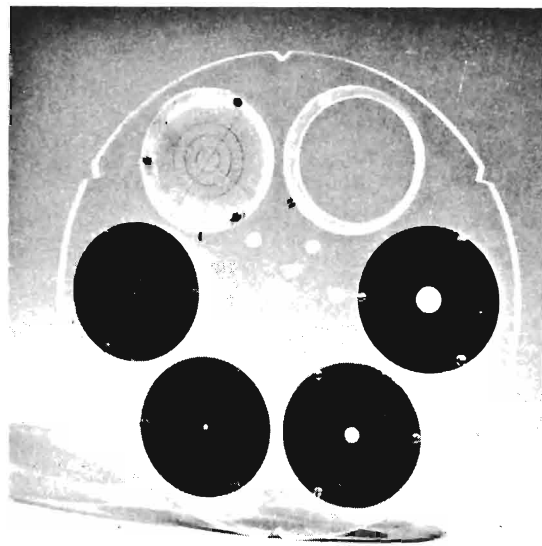


Fig. 4-16. The irradiance wheel.

*The Irradiance Wheel.* The Plexiglas disk or "wheel" as it was called (shown in Fig. 4-16) enabled irradiance on axis to be measured. Flat circular disks of any desired material could be inserted in the six 2-13/16 inch circular holes in the wheel. A considerable variety of different inserts were provided. Ordinarily, one insert consisted of a disk of diffusing plastic covered on the side away from the tower (i.e., toward the underwater lamp) by a thin blackened metal disk in which a sharp-edged circular hole 1/40 inch (0.635 mm) in diameter had been drilled. When a light beam 1/20 inch (1.27 mm) in diameter was centered on this insert, the light passing through it was considered to be proportional to the irradiance on axis of the light beam.

An exactly similar insert with a 1/20 inch diameter aperture was also in the wheel. This served an identical purpose when the light beam was 1/10 inch (2.54 mm) in diameter. It was also used when the lamp distance was such that the 1/20 inch (1.27 mm) light beam had spread to a (geometrical) diameter of 1/10 inch (2.54 mm). Changing the collector diameter from 1/40 inch to 1/20 inch increases the light available for measurement by a factor of four. Measurements recorded at both diameters enable the data to be reduced to a common basis; this procedure was called a "fold" in the data.

Two other positions in the irradiance wheel were occupied by similar irradiance collectors having larger diameters. Often 1/4 inch (6.35 mm) and 1/2 inch (12.7 mm) apertures were used so that "folds" could be made at greater lamp distances.

The remaining two positions in the irradiance wheel were nearly always reserved for aids in beam alignment. One of the positions was left open so that the experimenter had an unobstructed view of the light beam. The last position contained a transparent plastic disk lightly ground on the side toward the underwater lamp and provided with horizontal and vertical lines which crossed precisely on the axis of the experiment; i.e., at the center of the insert.

At very great lamp distances the light from the projector was difficult to see. The visual effect was that of a faint star seen against a black background. This star disappeared whenever the pupil of the experimenter's eye passed outside the light beam. Thus, he could trace the edge of the beam by systematic movements of his head. In such cases, the ground plastic reticle was replaced by an opaque stop having a round open hole slightly larger than the light beam. Head movements then enabled the experimenter to center the beam accurately in the open hole. This was a time-consuming adjustment.

*Limiting Range.* The greatest lamp distance at which data were obtained with the collimated projector or with the submerged laser was not set by sensitivity of the measuring sensor. In both cases longer ranges could have been used if more experimental time had been available! The time required for adjusting the light beam to the center of the measuring aperture increased with lamp distance so drastically that finally only one new lamp distance — one new point on a curve — could be added in an entire night by the alignment procedures described above. Instrumentation of several kinds could have been devised to make distant alignments much less time consuming, but project budgets were not sufficient. Neither were hours for experiments at the field station. Thus, data at sufficient range to establish whether the limiting slope is  $K$  or  $a$  in Fig. 4-31, although technically possible with the existing equipment, were not achieved.

All beam alignments were accomplished visually using light from the collimated projector, even in the case of experiments with the pulsed lasers that are described in section 7 of this report. Beyond 18 attenuation lengths, light from the projector could be seen only under conditions of full dark adaptation. Even on moonless nights the underwater background of scattered light was much too bright to see the lamp at such long distances. Attempts to do so had to be restricted to the night when the moon was new or to three or four nights before or after that event. Even then, truly long range alignments could not have been made without the "underwater tent" shown in Fig. 4-18. This aerial photograph of the field station at Diamond Island shows the "tent" attached to the second underwater tower. Buoyant rubberized fabric 12 feet wide and 90 feet long forms the dark section of the "roof" of the tent nearest the tower. The outer, lighter section is composed of strips of an older floating fabric laced into a 12 foot by 60 foot extension. The need for repairs to the lacing of this section is evident. At the end of the 150-foot "roof" is a wooden raft. This supported the chains to three heavy anchors which keep the free end of the tent in place. Floating 2 x 6 inch transverse wooden beams are visible at 12-foot intervals along the "roof"; anchors attached to the ends of these beams kept the floating structure straight.

The "tent" consisted of more than a fabric roof. Vertical side curtains of the same dark rubberized fabric hung from the "eaves" of the roof along the entire 150-foot length. These side curtains extended from the surface downward 12 feet. Their lower edge was anchored to the bottom of the lake by many lines. One end of the tent was closed by attachment to the tower, but the far end was open. The underwater tent was, of course, centered directly over the track on which was carried the collimated projector. With the



Fig. 4-18. Aerial view of the field of vision at Diamond Island showing the second underwater tower with its attached floating curtain. This is moored directly above the underwater track where all of the experiments described in Sections 5, 6, and 7 were conducted. Storm damage to the outer section of the curtain is evident. The boat landing, air track, and Laboratory building (top center) show clearly. The underwater tower is connected to the boathouse by a footbridge.

tent in place the background against which the projector appeared was, by measurement, 1000 times darker than without it. With this improvement in darkness, visual alignments were achieved at ranges beyond 19 attenuation lengths on a few very dark nights when the moon was new.

*Other Uses of the Underwater Tent.* The underwater tent served other important purposes besides enabling long range alignments to be made on very dark nights. It enabled shorter range measurements to be made under the lower levels of moonlight. It enabled measurements to be started earlier in the twilight and continued later into the dawn. It reduced ambient background in the case of K measurements (see Section 2.6), thereby increasing their precision. The tent also eliminated the mirror-like air-water surface which would have made K measurements invalid.



## TECHNIQUES OF IRRADIANCE MEASUREMENT

The use of the "wheel" for measurements of irradiance on-axis has already been described in the preceding section. Such measurements would be invalid, however, if steps were not taken to ensure that only light which passes through the small aperture in the center of the dark metal disk is measured. It is important therefore that an opaque metal cover be provided for both the wheel and the entire window. At Diamond Island, such a cover was put in place by divers after each alignment had been completed and the appropriate aperture of the wheel had been rotated into place. In the center of that cover was a shallow, concave, metal, conical depression, the center of which was precisely on axis. The apex of the conical depression was truncated to provide an opening about 30 mm in diameter. This was provided with a soft rubber ring that pressed gently against the metal insert in the wheel. With this cover in place no light could enter the tower except through the measuring aperture. The cover can be seen in Fig. 6-5.

In later experiments the same "wheels" were used for corresponding experiments performed in the laboratory tank. Fig. 4-19 shows a picture of the installation. The window and wheel were the same ones that were used at Diamond Island. The mounting ring that holds these parts is however smaller than the one used at the underwater tower because of mechanical constraints in the tank. The large, round Plexiglas window in this picture is 14 inches in diameter, whereas at Diamond Island it was 16 inches in diameter. The metal cover used in the laboratory tank is shown in Fig. 4-20. It hangs from the upper edge of the tank and covers the window completely. It is easily removable by the lifting handle at its top. The large, shallow cone at the center of the cover has a somewhat smaller hole than did the one used at the tower at Diamond Island, and the cone is mounted in a mechanism which enables it to be readily moved in and out until the opening is brought gently into contact with the metal surface of the insert in the "wheel".

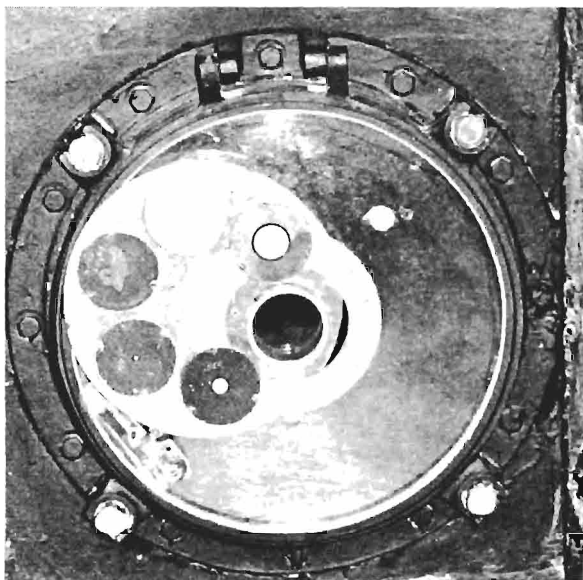


Fig. 4-19. Plexiglas disk ("irradiance wheel") containing four inserts for measuring irradiance, an alignment reticle, and a clear aperture is mounted on the measuring window inside the Laboratory tank described in Section 7.

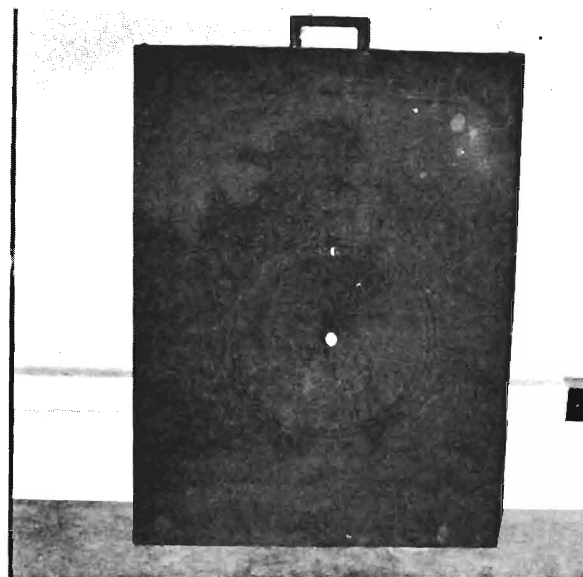


Fig. 4-20. Metal cover used in the Laboratory tank to prevent light from passing through the measurement window except through the irradiance collector. A shallow concave metal cone, having a small circular hole at its apex, made gentle contact with the irradiance wheel.

*Use of the EMI 9524-B Multiplier Phototube.* As mentioned previously, an EMI 9524-B end-on multiplier phototube was used at Diamond Island beginning in 1962. Its sensitivity is more than 1000 times greater than the selected RCA 931-A used in 1961. The EMI 9524-B has been used in nearly all experiments since that time. Other phototubes were used only for experiments with the pulsed laser or for incandescent irradiance measurements at very long ranges. The internal mounting for the EMI 9524-B multiplier phototube is shown in Fig. 4-21. That assembly is housed in an aluminum tubing that enabled the tube to be used either in the telephotometer mentioned previously or, in the case of irradiance measurements, in a fixture which attached it to the inner surface of the tower window. This mounting is shown in Fig. 4-22. The assembly was attached to the inner surface of the tower window by two mounting studs which were screwed into holes drilled part way through the Plexiglas window. This arrangement provided an extremely reproducible, yet easily removable, mounting for the multiplier phototube. Both ease of removal and reproducibility of replacement were essential, inasmuch as the unit had to be removed by the experimenter each time an alignment adjustment was made. This occurred, of course, each time the cart was moved to a new position on the underwater track.

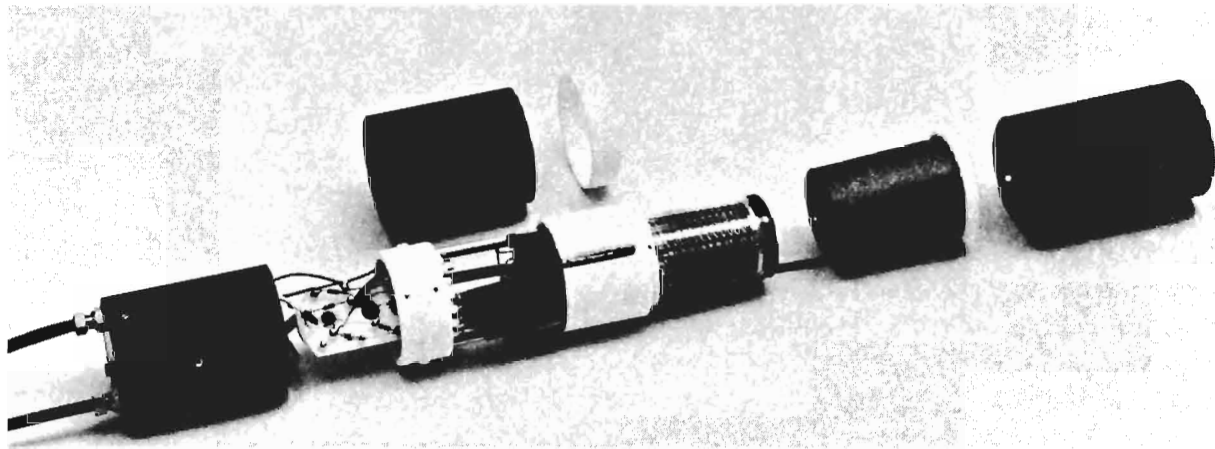


Fig. 4-21. Mounting for the EMI 9524-B Multiplier Phototube.



Fig. 4-22a



Fig. 4-22b

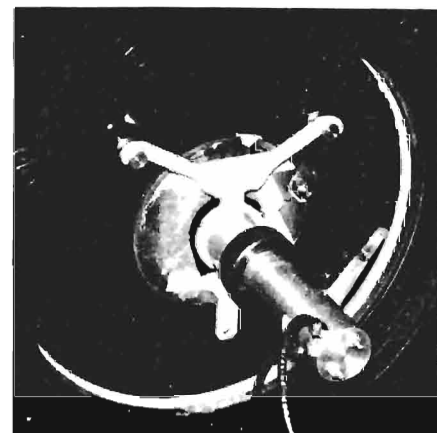


Fig. 4-22c

Fig. 4-22a. Inside (air) surface of the measurement window showing the 4-inch diameter optical glass insert in its brass mounting ring and two mounting studs for supporting the multiplier phototube, the integrating sphere, or the ultra-sensitive irradiator. Fig. 4-22b. Attachment fixture ("spider") for end-on multiplier phototube during irradiance measurements hangs from two mounting studs on the inner surface of the measurement window. Protective cover for optical glass insert is attached to the "spider" with tape. Fig. 4-22c. EMI 9524-B multiplier phototube in place at the measurement window.

*Irradiance Measurements at Long Range.* It was the intent of the 1962 program to measure the on-axis irradiance of the 1/10-inch diameter incandescent beams out to lamp distances sufficient to show the limiting slope of the irradiance-on-axis. Ranges well beyond 100 feet, i.e., beyond 20 attenuation lengths, were required. In fact, 150 feet of track was constructed and the remote pointing controls were designed to be adequate for the extremely delicate adjustments required to center the beam at even longer ranges.

*The Ultra-Sensitive Irradiometer.* Before a lamp distance of 100 feet was reached the EMI 9524-B multiplier phototube had insufficient sensitivity to measure the irradiance produced by the 1/10-inch diameter incandescent beam. In anticipation of the need for more sensitivity, an ultra-sensitive irradiometer based upon an EMI 9502-S multiplier phototube had been designed and constructed. That tube, in its black cylindrical housing, is shown on the left in Fig. 4-23. On the right is the mounting which attached it to the inner surface of the window with the same type of mounting hooks that were used with the EMI 9524-B multiplier phototube.

The assembled ultra-sensitive irradiometer is shown in Fig. 4-24. The black cylinder containing the EMI 9502-S multiplier phototube has been inserted in a thermostatically controlled, gas cooled refrigeration unit. Directly in front of the photocathode is a mechanical light chopper driven by an electric motor, located beneath the multiplier phototube. The light was chopped approximately 90 times per second. The electrical output was delivered to an amplifier-demodulator which drove a Brown strip chart recorder. The electronic assembly is shown in Fig. 4-25. The Brown recorder does not appear in this photograph but its place at the top of the rack is obvious.

A Smith-Florence regulated high voltage supply was used for the multiplier phototube. The voltage it supplied could be varied continuously by means of three thumbwheels, which can be seen at the top of the power supply panel in Fig. 4-25. In operation, the voltage on the multiplier phototube was adjusted manually to produce a fixed reading of the Brown recorder. The voltage indicated by the thumbwheel dials on the Smith-Florence power supply was then entered on a calibration curve to obtain a number proportional to irradiance. That curve was prepared at the Visibility Laboratory using incandescent standard lamps and inverse square law attenuation on a 3-meter photometric bench. A schematic diagram of the ultra-sensitive photometer is given in Fig. 4-26.

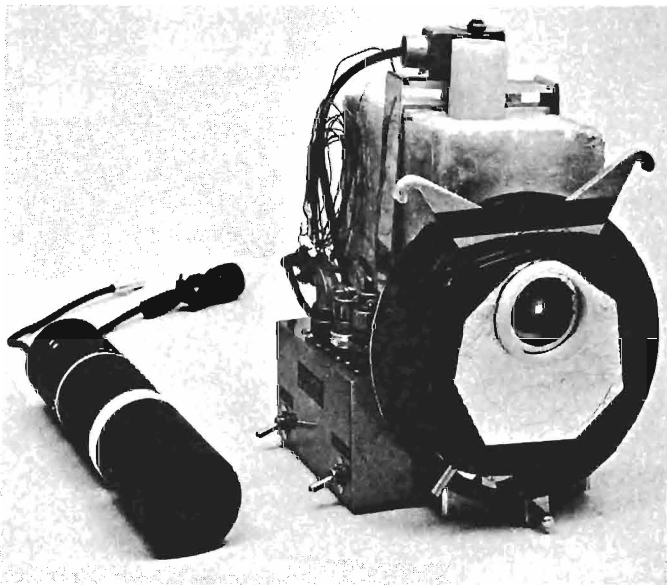
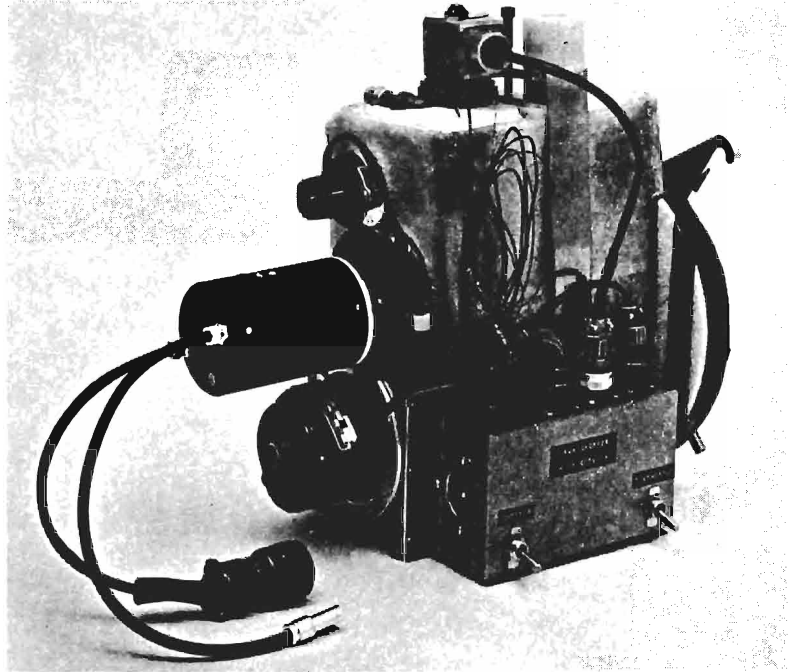


Fig. 4-23

Front view of ultra-sensitive irradiometer for attachment to the measurement window by means of the mounting studs shown in Fig. 4-22a. At the left is EMI 9502-S multiplier phototube in its black cylindrical housing.

**Fig. 4-24**

Rear view of ultra-sensitive irradiator. EMI 9502-S multiplier phototube in black cylindrical housing is inserted through the rear of the thermostated refrigeration jacket. Motor for driving the chopper disk is directly beneath the multiplier phototube.



**Fig. 4-25**

Amplifier-demodulator and variable voltage power supply for the ultra-sensitive irradiator. Strip chart recorder (Brown) has been removed from its position at the top of the mounting rack.



The temperature required to produce optimum signal to noise ratio with the EMI 9502-S multiplier phototube could be achieved simply and maintained conveniently with cooling provided by the expansion of compressed gas. An electronically controlled thermostatic chamber was provided, as shown in Figs. 4-23 and 4-24. A cylinder of compressed dry carbon dioxide gas was used at the Diamond Island field station for this purpose.

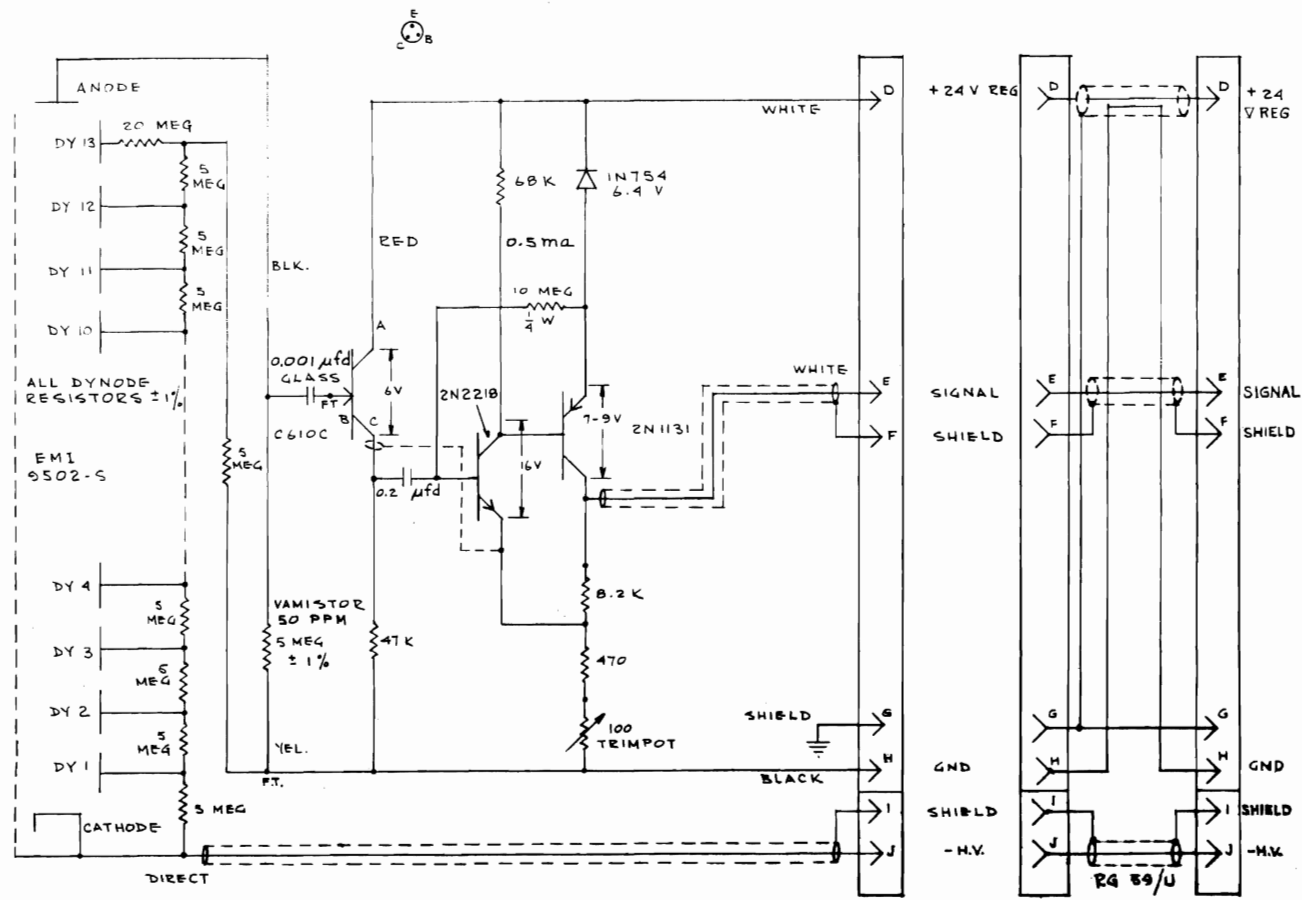
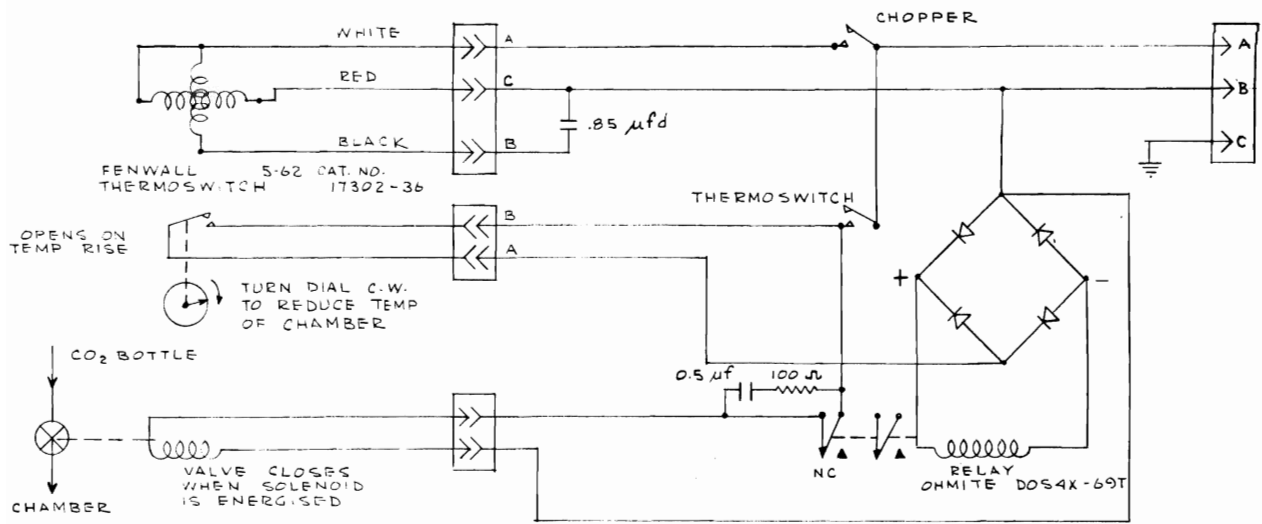
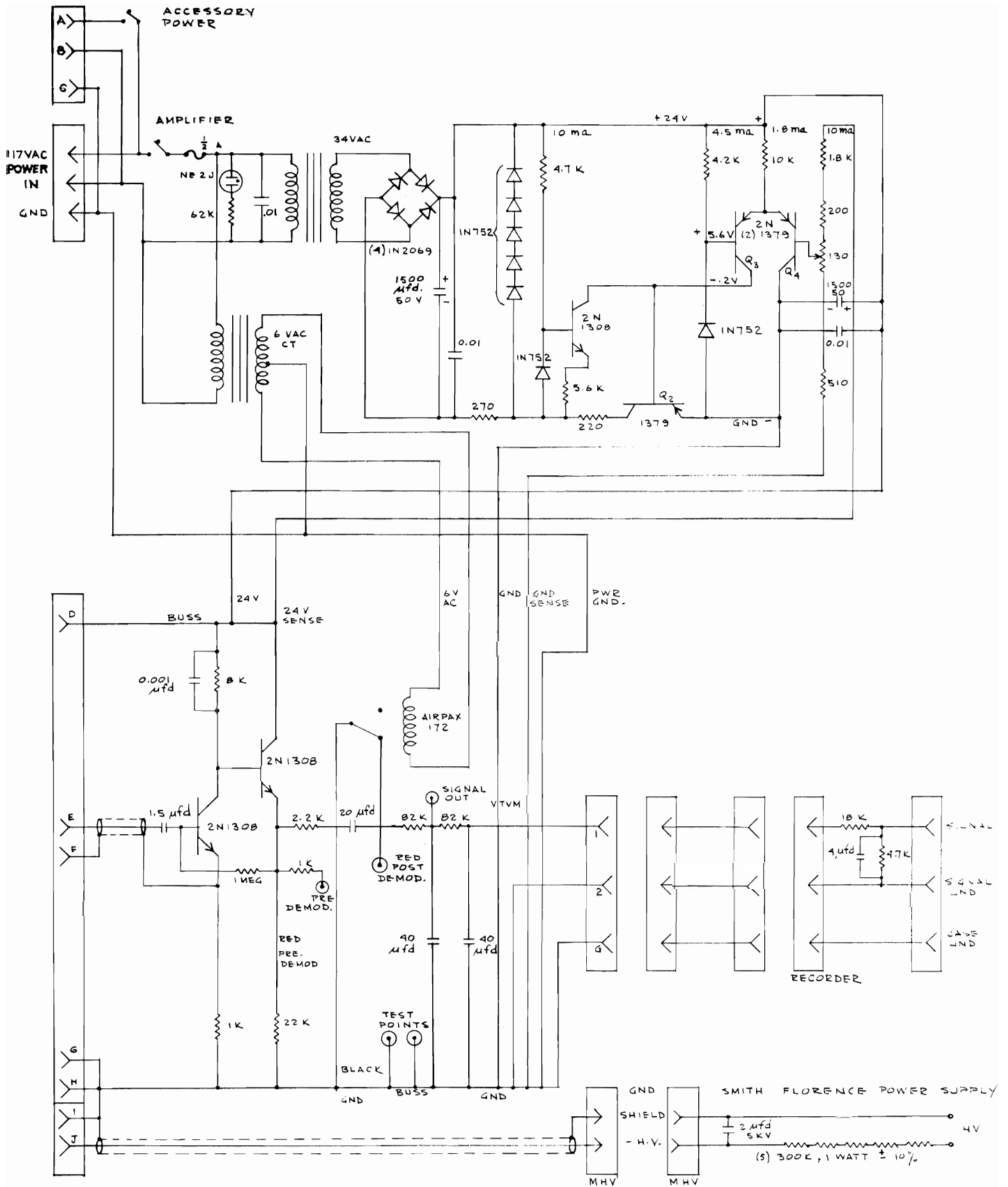


Fig. 4-26. Schematic wiring diagram of the ultra-sensitive irradiator.



Measurements on the photometric bench at the Visibility Laboratory showed that the ultra-sensitive photometer could measure irradiance levels 3000 times lower than could be measured with the EMI 9524-B multiplier phototube. This gain in sensitivity was, however, achieved only with a severe penalty in the length of time required to make a measurement. Whereas the indications of the EMI 9524-B system were nearly instantaneous, the ultra-sensitive system sometimes required as much as 20 minutes for a single reading. These readings were, however, remarkably repeatable.

The long range portion of the irradiance on-axis curves given in Section 4.4 were obtained with the ultra-sensitive photometer. They could not have been obtained with the EMI 9524-B system. As noted previously, a considerable time was required to make each visual alignment of the beam at the longest ranges. When this was added to the time required to take data with the ultra-sensitive irradiator, the experiments were forced to proceed so slowly that it was possible to add only one or two points to a curve by working from sunset to sunrise. Because of moonlight, only six or seven nights in any month were dark enough to permit the necessary visual alignments to be made, even beneath the underwater tent. Funds were not available to enable many long range data to be secured. Fiscal constraints alone prevented measurements from being made at still longer ranges than appear in the curves in Section 4.4. No sensitivity limit was approached. In fact, none of the data given in Section 4.4 required that the photocathode of the EMI 9502-S be cooled. Without cooling, its threshold was more than 200 times lower than that of the EMI 9524-B system; this was enough additional sensitivity to carry the curves as far as time permitted.

The level of darkness beneath the underwater tent was very low. Even after dark adaptation for nearly an hour, the experimenter could not detect the presence of the tower window after the protective outside cover had been removed. Neither could he see the small light beam from the distant incandescent projector. Yet, even without cooling, the ultra-sensitive photometer easily measured the irradiance it produced. When the projector was turned off, the readings of the ultra-sensitive photometer decreased, typically, by factors of 4 or even 10. Since the sensitivity of the ultra-sensitive photometer was more than sufficient, only working time limited the maximum range at which irradiance measurements were made. Instrumentation for rapid beam alignment would have extended the maximum range substantially, but such devices were not available.

#### **4.4 IRRADIANCE ON-AXIS**

The principal goal of the underwater experiments at Diamond Island in 1962 was the long range measurement of irradiance on-axis with the diameter of the light beam restricted in accordance with the principles of scaling described in Section 4.3. Thus, the diameter of the incandescent beam was reduced to a diameter of 1/20 inch as it emerged from the projector in order to simulate a 0.5 inch diameter beam used in clear ocean water having an attenuation length of 50 ft/in. Data were also collected with a beam diameter of 1/10 inch to simulate the performance of a 1/2 inch diameter laser used in "average" ocean water having an attenuation length of 25 ft/in. Except for the data reported in Figs. 4-35 and 4-36, which show a red-green comparison, all of the on-axis irradiance measurements were made in terms of green light as determined by a Wratten No. 61 filter that covered the cathode of the multiplier phototube.

A representative set of green light data is shown in Fig. 4-27. The underwater incandescent projector produced a beam 1/10 inch in diameter (2.54 mm or  $1.73 \times 10^{-3}$  attenuation lengths). The 25-watt Sylvania concentrated arc lamp was used in the projector so that the divergence of the light beam measured at 1/30 power points was 1.9 milliradians. This combination of beam diameter and beam divergence places the

transition between near-field and far-field conditions at a lamp distance of 0.91 attenuation lengths; that is to say,  $r' = 0.91$  attenuation lengths in equation 7 on page 223 of Appendix A. Figure 4-27 and all of the figures to follow in this section are semi-logarithmic plots of irradiance on-axis in relative units versus lamp distance in attenuation lengths. The expression  $e^{-\alpha r}$  is represented by a diagonal solid straight line having a position fixed by the choice of scales for the plot. Ten measurements of irradiance on-axis are shown by the plotted points. It will be noted that the measured irradiance follows the " $\alpha$ -line" throughout the first attenuation length and is only slightly beneath it when the lamp distance was two attenuation lengths. Thereafter, the measured irradiance falls below the  $\alpha$ -line, in a regular fashion.

The dotted line in Fig. 4-27 represents the function  $e^{-\alpha r}$  divided by the square of the ratio of the lamp distance  $r$  to the transition distance  $r'$ , as explained on page 223 of Appendix A in connection with the discussion of equation 7 and as illustrated by Fig. 18 and its caption on page 224. It will be clear from that discussion that if only monopath irradiance had been measured the data would have followed the dotted line. The measured irradiance, however, is the sum of the monopath irradiance and the multipath irradiance, as explained on page 223 of Appendix A. Thus, all of the long range data fall above the dotted

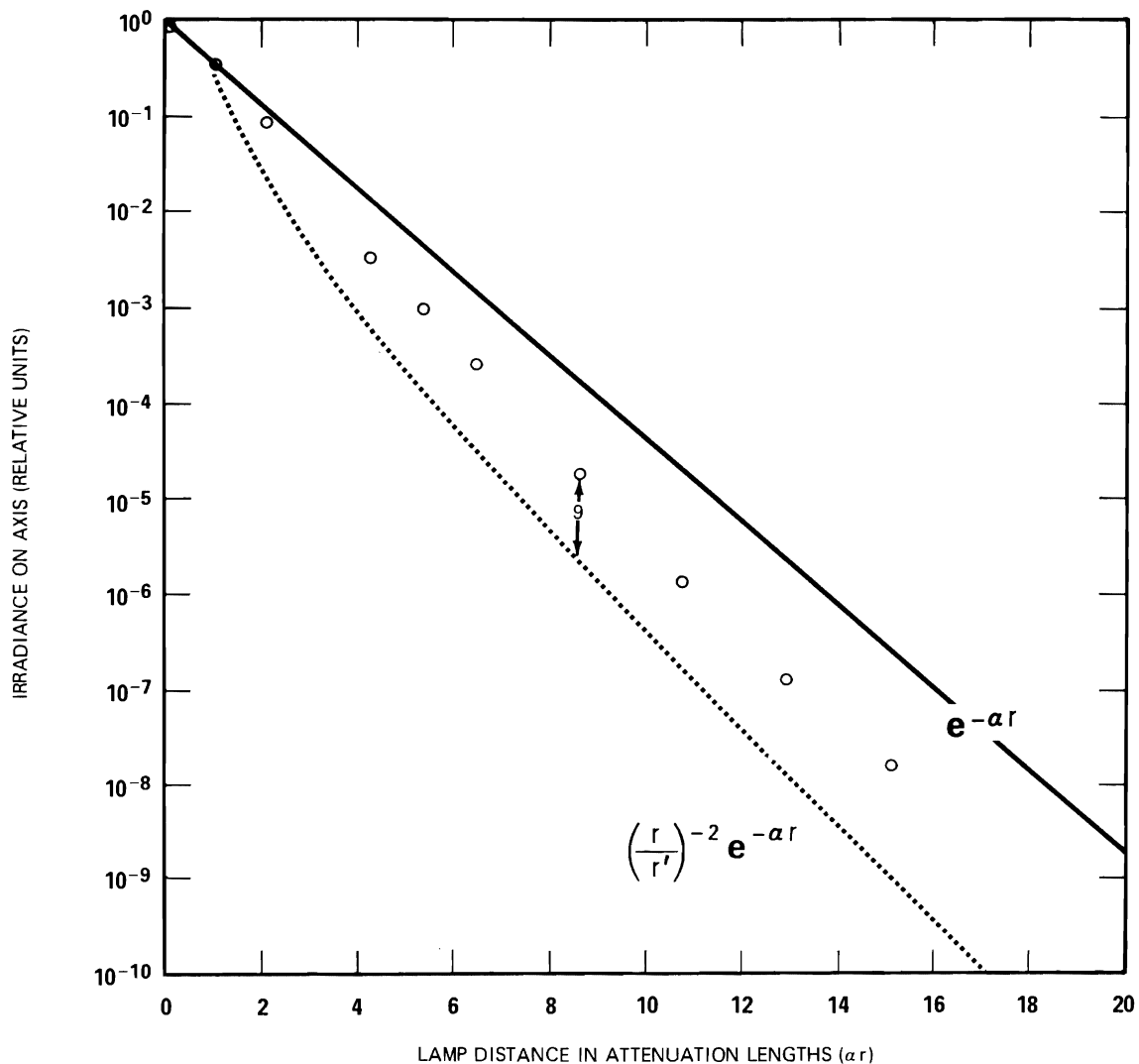


Fig. 4-27. Circles show irradiance on-axis. Green light. Beam diameter 1/10 inch. Beam divergence 1.9 milliradians. Monopath component of irradiance is shown by the dotted curve.



curve. Consider, for example, the point representing irradiance measured at a lamp distance of 8.6 attenuation lengths. This point lies vertically above the dotted line by a distance corresponding with a factor of 9 in irradiance. This means that 1/9 of the measured irradiance was monopath and 8/9 of it was multipath. No curve has been fitted to the experimental points plotted in Fig. 4-27, but it is obvious that such a curve would depart from the  $\alpha$ -line somewhere beyond one attenuation length, become parallel with it in the vicinity of 10 attenuation lengths, but show a converging tendency (a lessening of slope) at the longest ranges that were measured. This trend at long range can be observed even more prominently in Fig. 4-28 and subsequent plots of the on-axis irradiance data.

Figure 4-28 is similar in form to Fig. 4-27 and demonstrates that when irradiance on-axis is normalized at zero lamp distance, closely identical results are obtained by beams of light having the same beam diameter-to-beam-divergence ratio; that is to say, the same near-field to far field transition distance  $r'$ . Thus, in Fig. 4-28 the irradiance on-axis measurements denoted by the open circles relate to a beam diameter of 1/10 inch and a beam divergence of 3.2 milliradians ( $r' = 0.54$  attenuation lengths). The data repre-

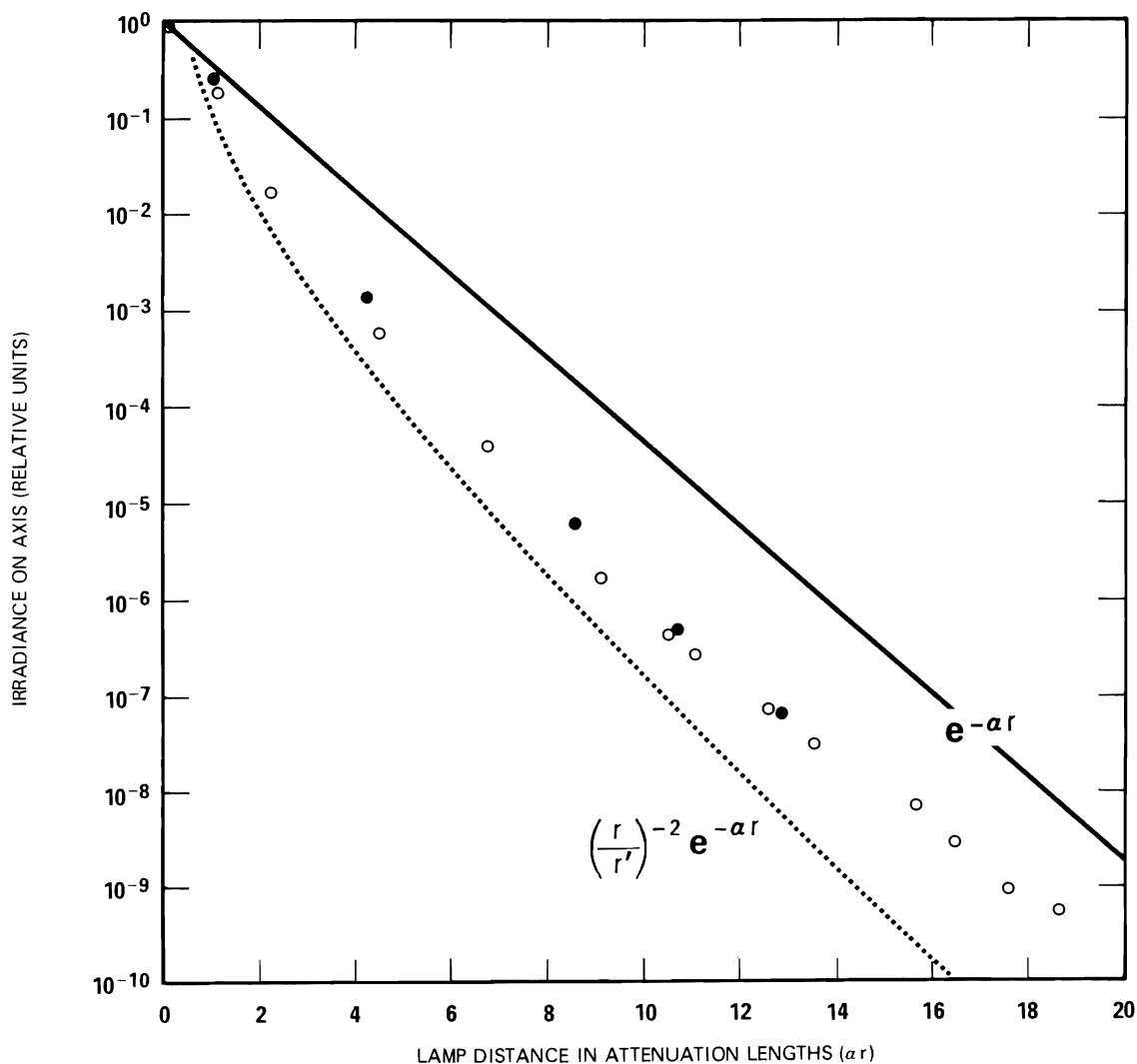


Fig. 4-28. Comparison of (nearly identical) normalized irradiance on-axis produced by geometrically different beams of green light having nearly identical near-field to far-field transition distance. Open circles: 1/10 inch beam diameter, 3.2 mr divergence. Solid circles: 1/20 inch beam diameter, 1.9 mr divergence.

represented by the solid points relates to a beam diameter of 1/20 inch and a beam divergence of 1.9 milliradians ( $r' = 0.46$  attenuation lengths). To the extent that these two values of  $r'$  are nearly equal, curves passed through the two sets of points would be nearly coincident. It must be noted that the two beams of light were substantially different in their total power. The power content of a light beam depends upon both the square of its diameter and the square of its divergence. The points represented by the open circles pertain to a beam whose power content is more than 11 times greater than that of the beam represented by the solid points. Irradiance-on-axis at any given distance is the same only after the data have been normalized at zero lamp distance.

The effect of beam divergence at small beam diameter is illustrated by Fig. 4-29. All four curves in this figure are for a beam diameter of 1/20 inch (1.27 mm or  $0.865 \times 10^{-3}$  attenuation lengths). The divergences of the beams represented by the four curves were respectively, 0.6, 1.2, 1.9, and 3.4 milliradians. These resulted from the use of the 2, 10, 25, and 100-watt Sylvania zirconium concentrated arc lamps in the collimated underwater projector. Solid black circles along the  $\alpha$ -line denote the  $r'$  points. The four curves display an inverse relation between on-axis irradiance and beam divergence, but it is important to note that all four of the curves have been normalized to unity at zero lamp distance. The gradual upturn

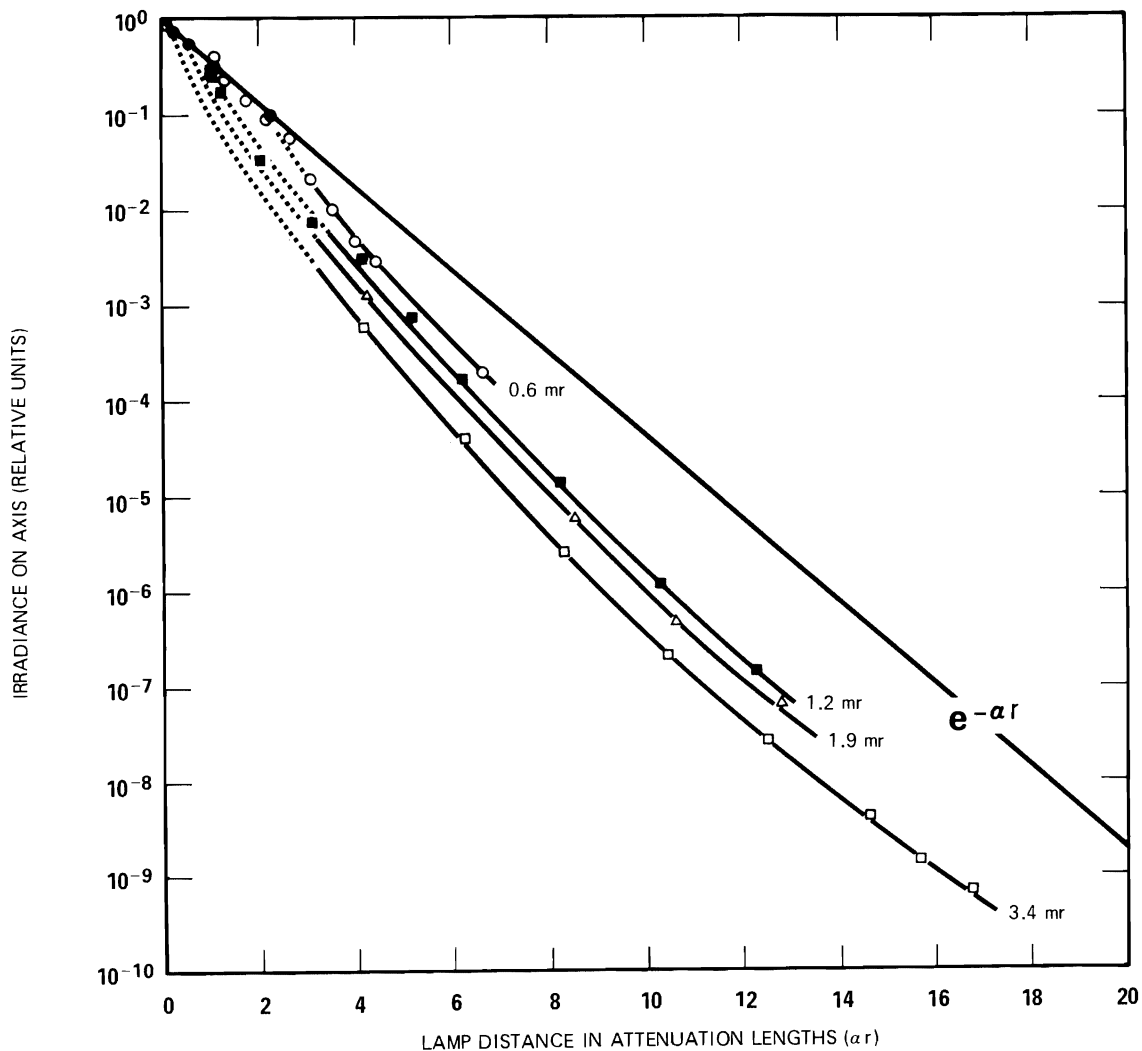


Fig. 4-29. Effect of beam divergence at small beam diameter.

of the curves beyond 10 attenuation lengths is clearly noticeable. Even at the longest distances measured, however the slope has not reduced to the value  $K$  displayed by the solid curve in Fig. 4-30 beyond 10 attenuation lengths. It is believed that the slope of all the curves diminishes the value  $K$  at sufficient range.

Measurements of the irradiance produced by a uniform spherical lamp are shown by the solid curve in Fig. 4-30. The lamp was a special version of the 1000-w incandescent "diving lamp" (No. MG-25/1) manufactured by the General Electric Company. It differed from the standard production item only in that the inside surface of the lamp had a white diffusing coating which prevented the filament structure from being seen and gave the underwater lamp a spherical distribution of intensity except in the direction of the lamp base, which was located in a direction opposite to that of the irradiator. This curve is closely analogous to the one in Fig. 16 on page 222 of Appendix A. The discussion given there applies in all respects to the curve in Fig. 4-30. It will be noted that the curve departs from zero lamp distance with a steep

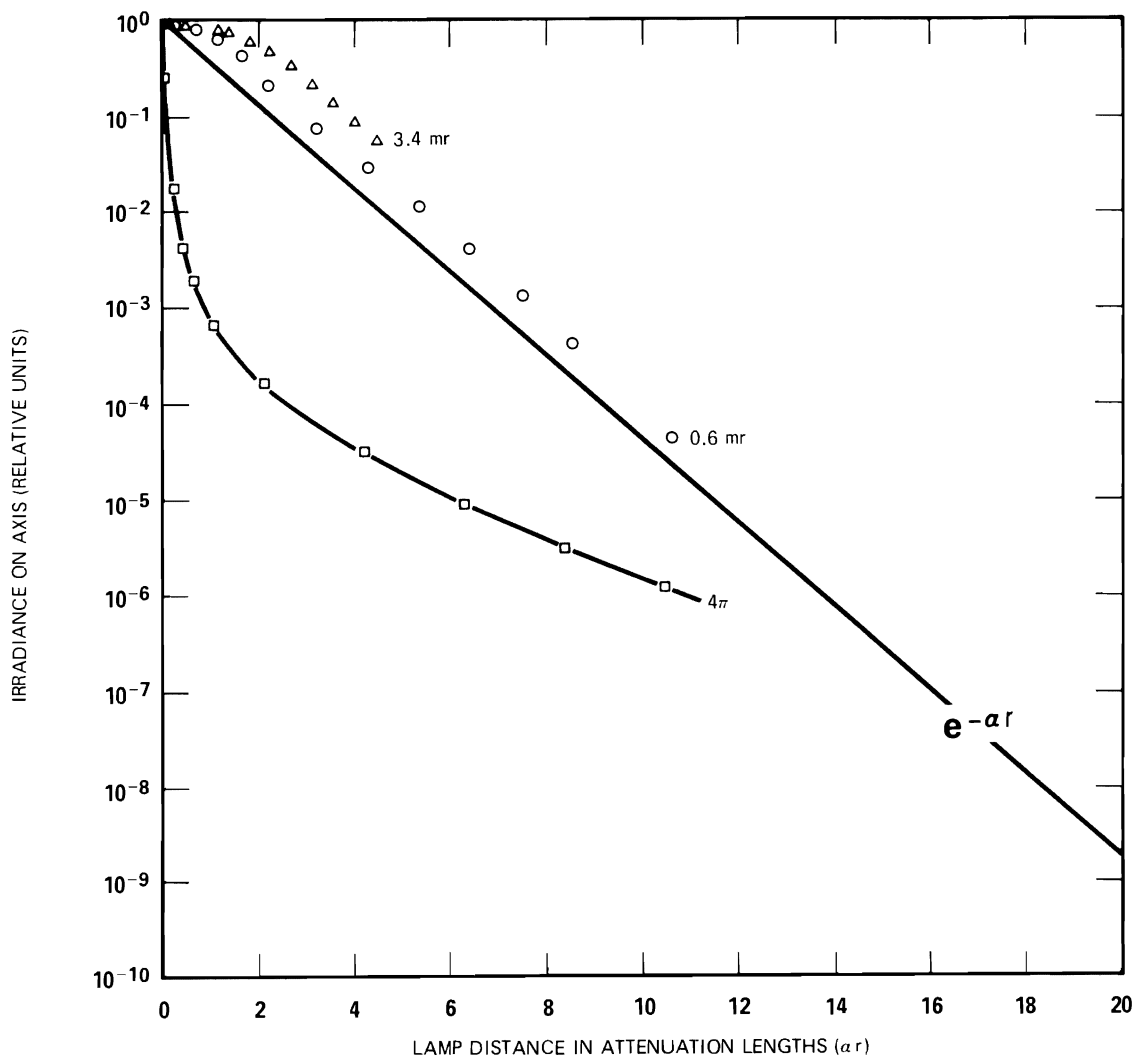


Fig. 4-30. Curve shows irradiance produced by a uniform spherical lamp. Circles and triangles show effect of beam divergence on irradiance on-axis produced by collimated beams 2 inches ( $1.73 \times 10^{-2}$  attenuation lengths) in diameter.

slope that is governed chiefly by the inverse square law in the manner shown by equation 3 on page 222 of Appendix A. At long range the curve becomes virtually a straight line with a slope of  $K$  in accordance with equations 4 and 5 of Appendix A. The notation " $4\pi$ " at the end of the curve denotes that it represents irradiance produced by a uniform, spherical, submerged source.

The circled points which lie above the  $\alpha$ -line in Fig. 4-30 are the result of measurements of irradiance on-axis produced by the underwater collimated projector used at its highest collimation (0.6 mr) and at 2-inch diameter (50 mm or  $17.3 \times 10^{-3}$  attenuation lengths). Because of the large beam diameter all of the measured points lie within the near-field of the projector. It will be noted that the row of circled points is approximately parallel to the  $\alpha$ -line. This suggests a possible technique for measuring the attenuation coefficient of water. It would be necessary only to measure irradiance along the axis of a large diameter highly collimated beam and determine the slope of a semilogarithmic plot of these data versus actual lamp distance. Such a measurement could not be regarded, however, as having fundamental significance inasmuch as the points lie above the  $\alpha$ -line in Fig. 4-30 by a factor of approximately 2.7. Thus, only one part in 2.7 of the measured irradiance results from monopath transmission and the remainder represents scattered light within the beam. The points denoted by triangles in Fig. 4-30 relate to measured values of irradiance on-axis of the same underwater projector when equipped with the 100-watt Sylvania zirconium concentrated-arc lamp so that it produced a divergence (at 1/30 power points) of 3.4 milliradians. The character of these data is closely similar to that of the circled points. The irradiance on-axis contains, however, a greater proportion of multipath light. Specifically, triangled points at long range lie above the  $\alpha$ -line in Fig. 4-30 by a factor of 5. Thus, 1/5 of the irradiance on-axis is monopath and 4/5 is multipath. It should be noted, however, that the data have been normalized to unity at zero lamp distance.

The triangle points in Fig. 4-30 appear again in Fig. 4-31, which also contains the lower curve from Fig. 4-29 (1/20 inch diameter, 3.4 mr) and two additional curves representing measurements of irradiance on-axis for the same lamp when the beam diameter is 1/10 inch (triangles) and 1/4 inch (solid squares). Thus, Fig. 4-31 displays the effect of beam diameter at a nominal divergence of 3.4 milliradians. Diffraction effects, of course, produce variations about the nominal value. For example, the measured divergence of the 2-inch beam at 1/30 power points was 3.04 milliradians but with the 1/20 inch stop it was 3.5 milliradians. It is the author's belief that at sufficient range all of these curves would achieve a  $K$  slope.

Figures 4-31 and 4-32 show irradiance on-axis data for 1/20 inch and 1/10 inch diameter beams at divergences of 1.9 and 1.2 milliradians. Comparison shows that the pair of curves approaches the  $\alpha$ -line as divergence decreases and that their separation diminishes. Figures 4-31, 4-32, and 4-33 show that the effect of beam divergence is rather minor for beams having diameters of 1/20 inch and 1/10 inch and divergences of 1.2 mr or greater. There is an abrupt change, however, when the collimation is reduced to a nominal value of 0.6 milliradians through the use of the 10-watt Sylvania zirconium concentrated-arc lamp. The data are given in Fig. 4-34. Not only is the irradiance on-axis much closer to the  $\alpha$ -line for the 1/20 inch diameter beam but the triangle points which represent data for the 1/10 inch diameter beam lie above the  $\alpha$ -line at short ranges! It must be remembered that all of the irradiance on-axis data have been normalized to unity at zero lamp distance. Nevertheless, at four attenuation lengths the on-axis irradiance produced by the 1/10 inch beam is more than 8 times greater than that produced by the 1/20 inch beam. It is interesting that, at short ranges, the highly collimated (0.6 milliradians) beam displays "large diameter" characteristics when the actual diameter is only 1/10 inches (2.54 mm or  $1.73 \times 10^{-3}$  attenuation lengths).

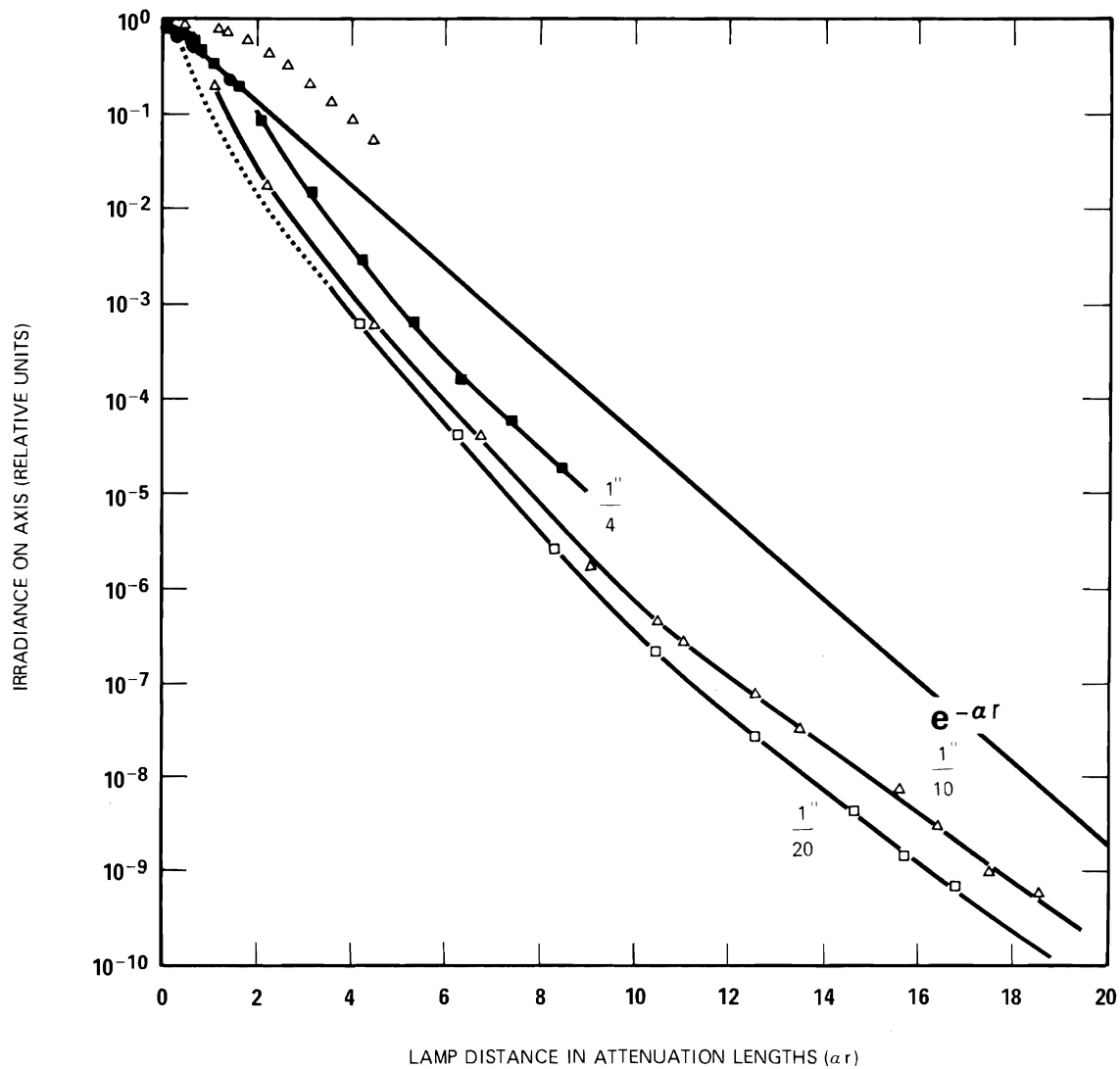


Fig. 4-31. Effect of beam diameter at 3.4 milliradians divergence.

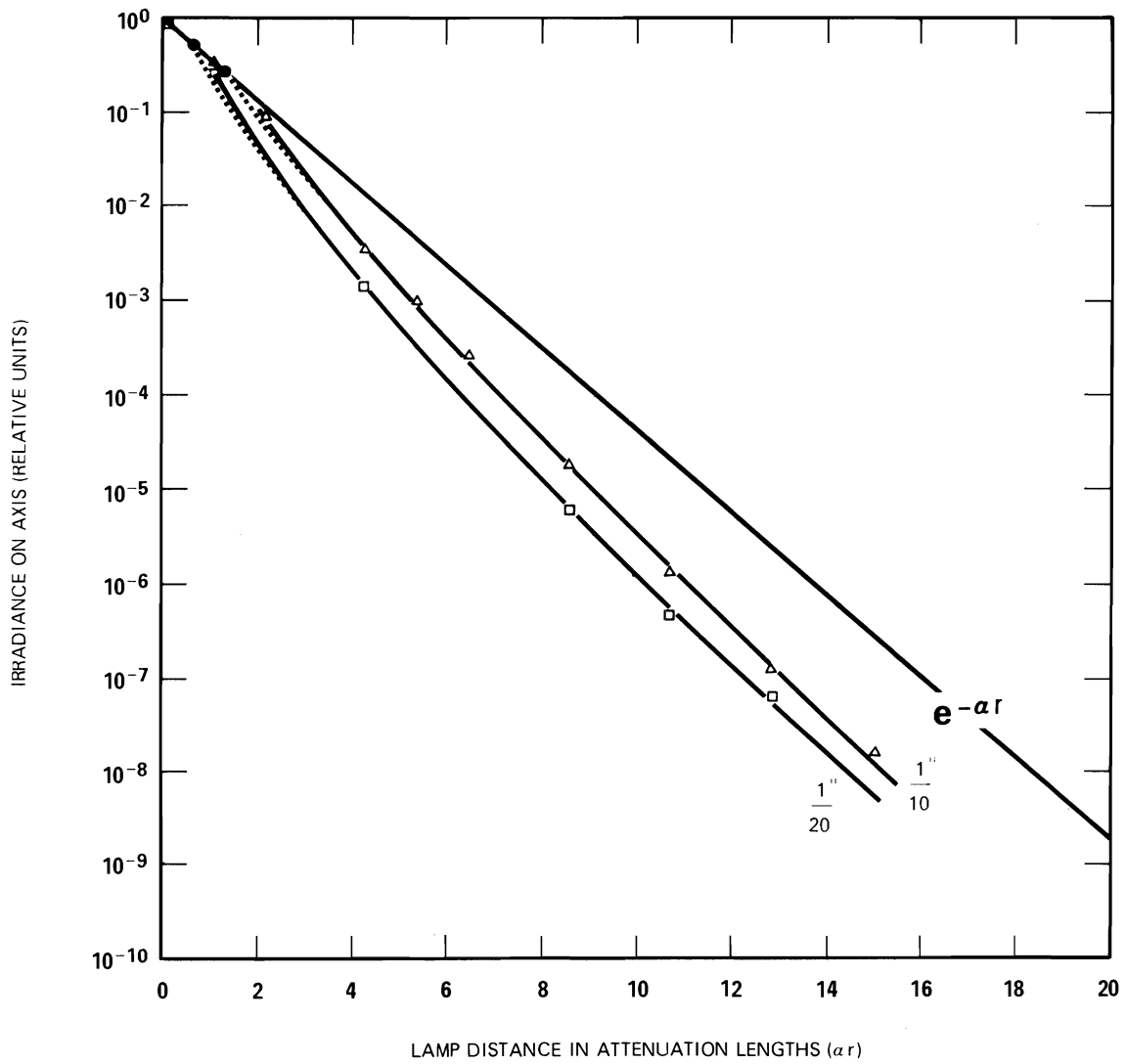


Fig. 4-32. Effect of beam diameter at 1.9 milliradians divergence.

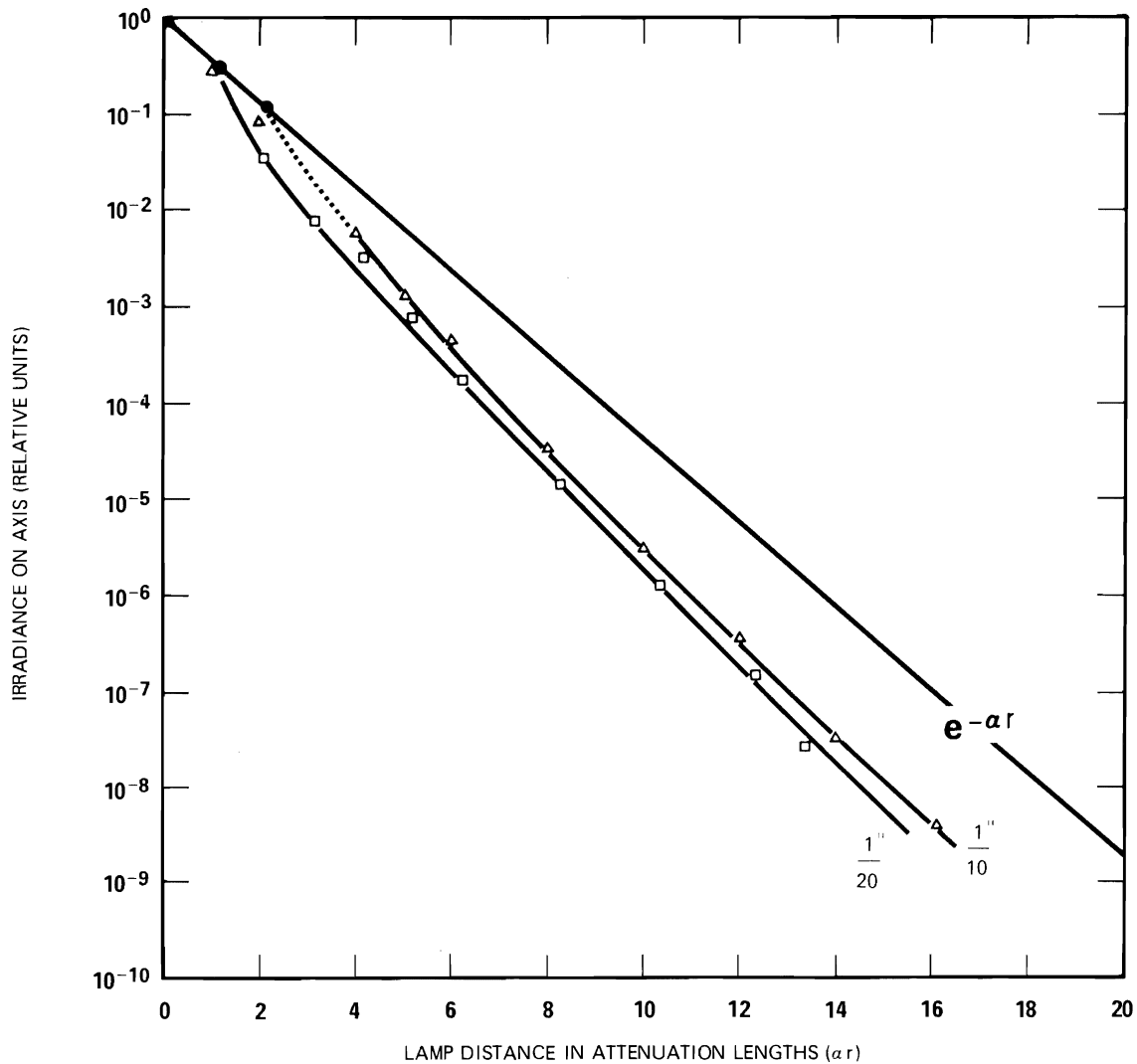


Fig. 4-33. Effect of beam diameter at 1.2 milliradians divergence.

#### IRRADIANCE BY RED LIGHT

All of the data presented in Figs. 4-27 through 4-34 were in terms of green light defined by means of a Wratten No. 61 filter attached to the EMI No. 9524-B multiplier phototube. Throughout these experiments there was often speculation on how the nature of the data would be affected by wavelength. In particular, would the irradiance on-axis produced by red light differ significantly from that produced by green light after allowing for diminished attenuation length at longer wavelength? Answers to this question were obtained by experiments made on 27 and 28 August 1962. The Wratten No. 61 green filter was removed from the phototube and replaced by a Wratten No. 25A red filter. The attenuation length for red light was then measured and found to be 1.87 feet (0.62 meters); the diffuse attenuation coefficient  $K$  was measured as 0.876 ln/m. Measurements of irradiance on-axis were then made with a beam diameter of 1/10 inch and a nominal beam divergence of 1.9 milliradians for comparison with the green light data depicted by Fig. 4-27. The comparison is shown by Fig. 4-35 in which the green light data, denoted by open circles, are the same data given in Fig. 4-27. Red light data are shown in Fig. 4-35 by solid circles. They agree quite closely with the green light measurements when all lamp distances are expressed in attenuation lengths for green

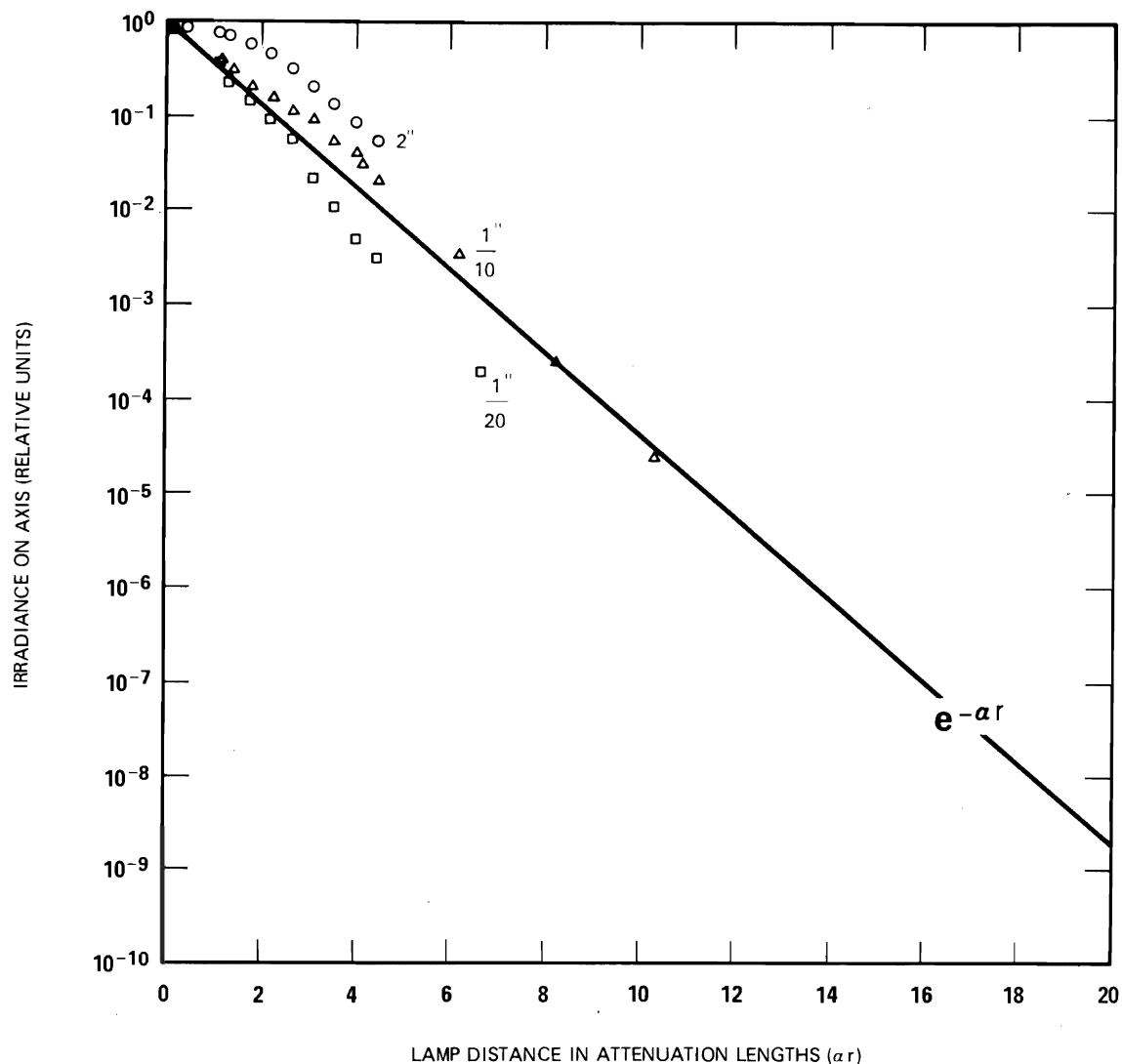


Fig. 4-34. Effect of beam diameter at 0.6 milliradians divergence.

light and red light, respectively. Thus, no significantly different new phenomena were observed by changing to red light.

Irradiance on-axis was also measured with red light after the 1/10 inch diameter stop had been removed from the projector so that the beam diameter for the second series of measurements was 2 inches (50 mm). These data are shown in Fig. 4-35 by solid triangles. They exhibit precisely the same type of behavior shown by 2-inch diameter beams of green light.

The experiments with red light were continued by reducing the beam diameter to 1/20 inch and measuring irradiance on-axis for comparison with corresponding green light data. This comparison is shown in Fig. 4-36 and illustrates again the lack of difference between red light and green light data when compared in terms of the respective red and green attenuation lengths.



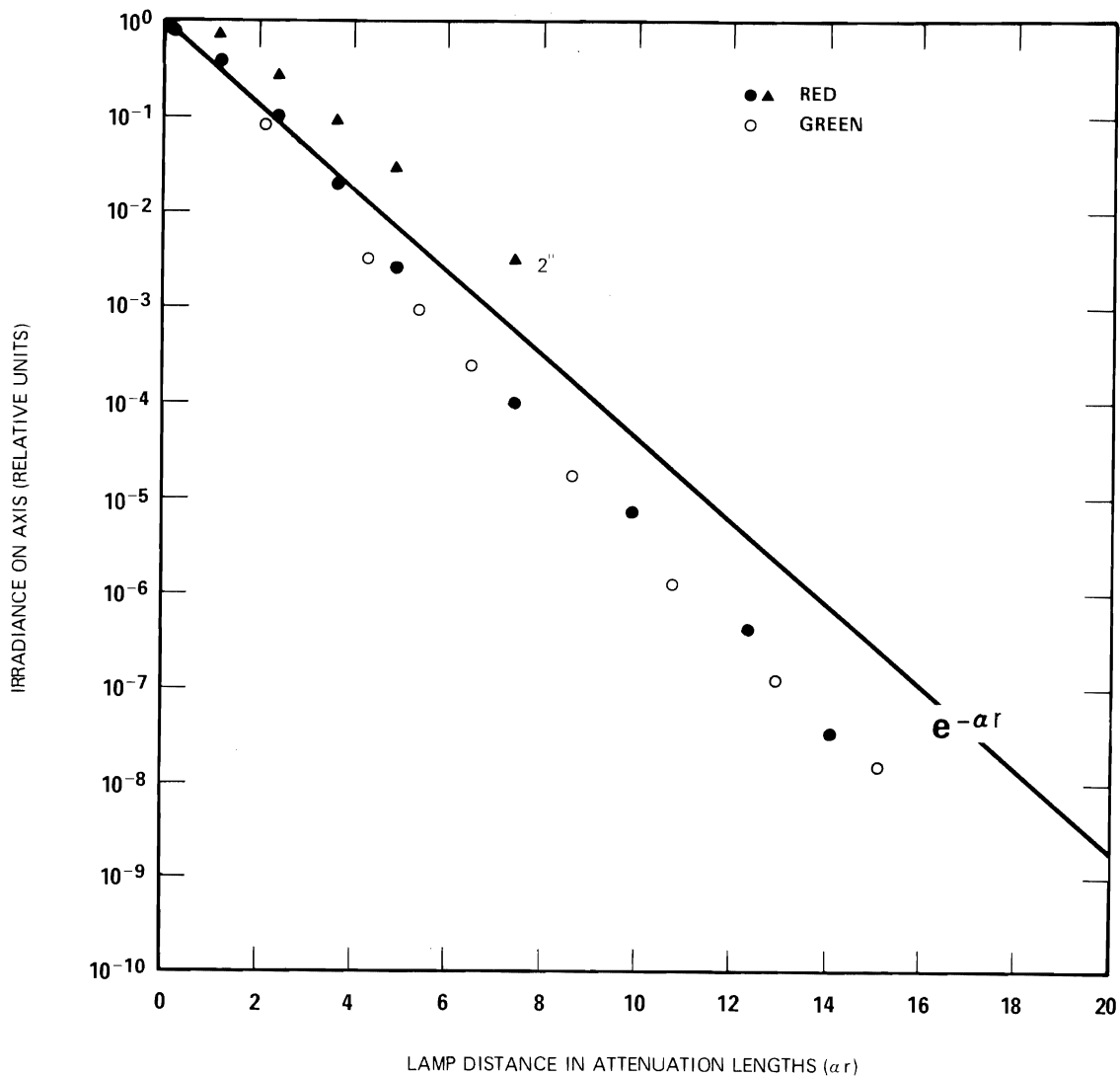


Fig. 4-35. Comparison of normalized irradiance on-axis produced by red light and green light. Beam diameter 1/10 inch. Beam divergence 1.9 milliradians.

A dramatic difference between the red and green data was found, however, when the irradiance produced by the uniform spherical source was measured. These data are also shown in Fig. 4-36. Although the character of these curves is similar, it is evident that they are approaching different asymptotes; thus, the diffuse attenuation coefficient  $K$  is substantially larger for red light than for green. This result follows directly from the fact that  $K$  is dominated by the absorption coefficient which, in turn, is controlled in the upper half of the visible spectrum by the absorption coefficient of pure water. This increases dramatically with wavelength. Thus the "4 $\pi$ " curve for green light intersects the  $\alpha$ -line at approximately 15.8 attenuation lengths whereas the corresponding intersection for red light is approximately 21 attenuation lengths. Except for this understandable difference, the nature of the irradiance function for a uniform point source is similar in terms of red light and green light.

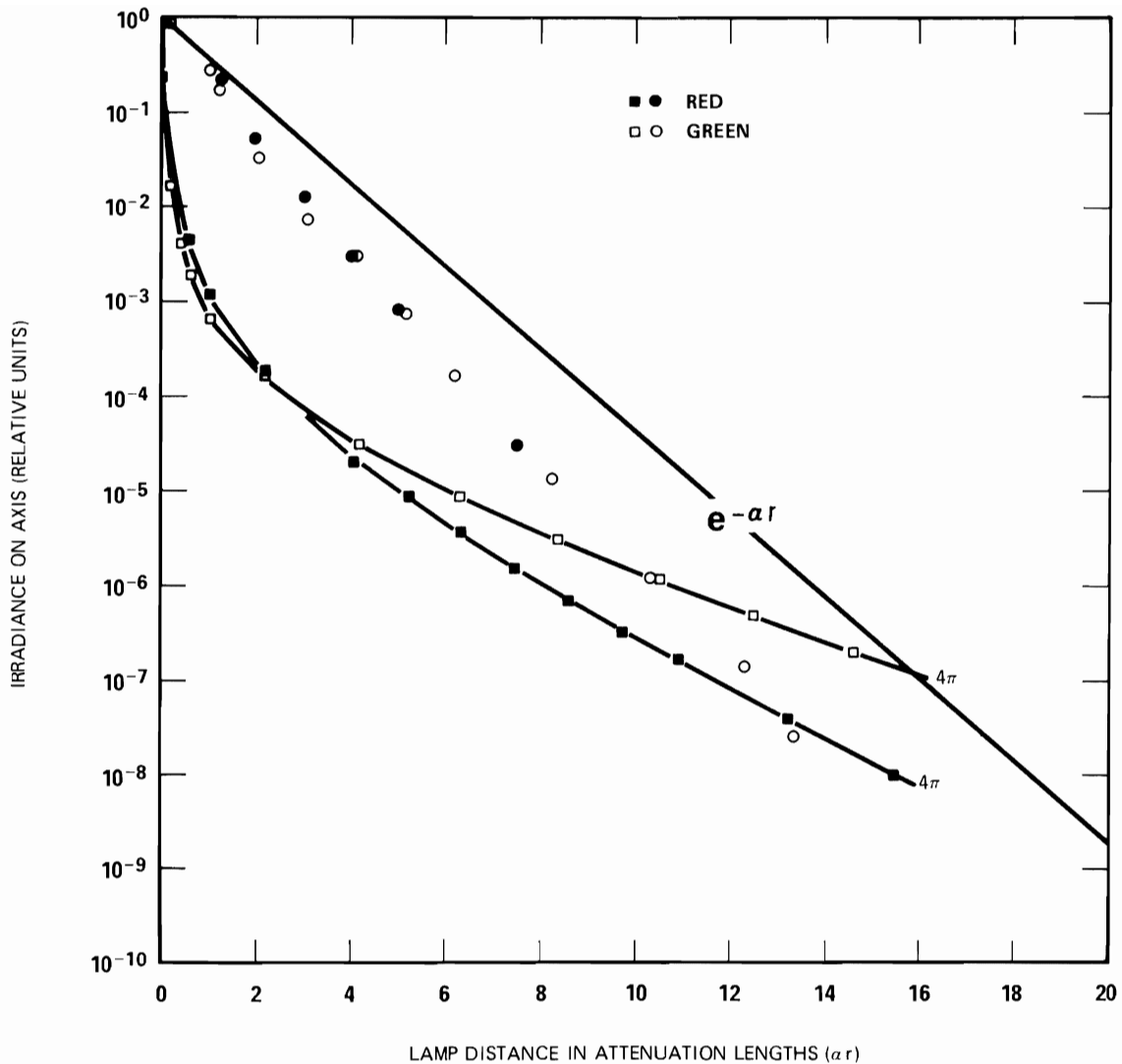


Fig. 4-36. Comparison of normalized irradiance on-axis produced by red light and green light. Beam diameter 1/20 inch. Beam divergence 1.9 milliradians. Solid curves compare irradiance produced by red light and green light from a uniform spherical source.

The author believes that if measurements of irradiance-on-axis had been extended to sufficient range the red and green curves would approach different asymptotes corresponding to red and green K values, respectively, just as did the irradiance functions for the red and green uniform spherical source.

#### COMPARISON WITH IRRADIANCE PRODUCED BY LASERS

Section 6 of this report describes experiments at Diamond Island in 1966 which showed that identical values of normalized irradiance-on-axis are produced, respectively, by a neodymium-doubled pulsed laser and by the incandescent collimated underwater projector *when the geometry of the beam of laser light and the geometry of the beam of incandescent light are made identical*. If this requirement is fulfilled the irradiance on-axis data presented in Figs. 4-27 through 4-34 are applicable to the 20 nanosecond pulses of light that were produced by the laser.

# 5. EXPERIMENTS WITH THE FIRST UNDERWATER LASER

## 5.1 INTRODUCTION

The U.S. Navy's first underwater green laser was made available to the Visibility Laboratory for experiments during the summer of 1964. It was developed by the Radio Corporation of America, Aerospace Systems Division, at Burlington, Massachusetts and has been described by Mr. Howard J. Okoomian in Applied Optics (Vol. 5, page 1441). It will not be necessary, therefore, to include a full description of the laser in this report. Certain details that were important determinants of the mountings for the laser and the manner of its use are presented in the following sections.

## 5.2 CHARACTERISTICS OF THE LASER

The first RCA laser for underwater use employed a neodymium glass rod to produce near infrared laser light at 1.06 micrometers. Frequency doubling was achieved by means of a small block of potassium dihydrogen phosphate (KDP) that was mounted within the laser cavity. It converted most of the 1.06 micrometer emission from the rod to 0.53 micrometer green light. A dichroic output mirror permitted almost no infrared to emerge from the laser.

The laser was Q-switched by means of a rotating glass prism. This caused the laser to produce pulses of green light approximately 20 nanoseconds in duration to half power points. The pulse had a steep rise to peak output which consumed approximately 7 nanoseconds and a more gradual nigrescence. During all of the experiments at Diamond Island the RCA lasers were used in the single pulse mode. This was effectively the only option in 1964 but later models of the RCA laser used at Diamond Island in 1965 and 1966 could have been used in a pulse repetition mode.

The RCA laser was self-contained. Its submersible case contained rechargeable batteries of sufficient capacity to charge the capacitor banks for about 100 flashes. Upon command, the energy stored in the capacitors was discharged through a mercury flash tube which pumped the neodymium rod. The only electrical connection from the submerged laser to the operator was a small cable which could be used either to trigger the flash or to charge the batteries. A small control box was available to the operator.

The performance of the first laser was disappointing from the standpoint of reliability. Had it not been for the fact that the Diamond Island field station was located within an easy drive of the RCA plant where the laser had been made, it is doubtful whether significant results would have been obtained. The unreliability of the laser was due at least in part to an explosion which had severely damaged it during use by the Navy which immediately preceded the experiments at Diamond Island. In fact, the beginning of these experiments was delayed while RCA replaced many damaged parts with pieces that had been used during the development of the laser but subsequently replaced with new construction before the laser was delivered to the Navy. Neither time nor funds existed to procure or construct new replacement parts for all of those that had been damaged. Some of the laser difficulties experienced at Diamond Island during 1964 were traced to damage of the solid state circuitry which controlled the pumping and Q-switching of the laser. No replacement for this electronic assembly was available after the explosion; its performance was erratic and unstable. Nevertheless, persistence enabled significant and usable data to be secured during the 1964 experiments. Later models of the RCA laser that were used at Diamond Island during 1965 and 1966 displayed none of the control circuit difficulties which plagued the 1964 operation. This is not to say that the 1965 and 1966 lasers were without service problems of various kinds, but the propinquity of the RCA laboratories and the willingness of their staff to assist in keeping the lasers running properly made successful field research possible.

### 5.3 MOUNTING THE UNDERWATER LASER

The RCA underwater laser is shown in Fig. 5-1 undergoing its first trials in air at Diamond Island. The entire mechanism, including the power supplies, were housed in a 2.5-foot length of 9-inch diameter steel pipe having heavy flanges at either end to which steel end plates were bolted. Large O-rings made the assembly watertight. The laser beam was emitted from a small window in one of the end plates, as shown in Fig. 5-1. Drawings of this case had been supplied to the Visibility Laboratory by RCA. A wooden mockup had been constructed in order to develop means for mounting the laser on the existing underwater cart, already described in Section 4 of this report and illustrated by Fig. 4-10.



Fig. 5-1. RCA underwater laser at Diamond Island. Left to right: Bailey, Pinkham, Duntley, Mather, and Kornstein.

The laser was very much larger and heavier than the collimated underwater projector for which the cart and its control mechanisms had been designed. This was not particularly serious because the laser was only slightly negatively buoyant when submerged. It was a comparatively simple matter to mount it on the arm of the underwater cart as shown in Fig. 5-2. A strap about the body of the laser about 9 inches from the forward end was used to secure it to a triangular box-shaped structure fastened to the horizontal arm of the underwater cart. The attachment between the triangular box and the strap surrounding the laser was a pivot, such that the laser could swing freely about a horizontal axis.

Vertical control of the light beam was accomplished by the same remote control mechanism described in Section 4. The front end of the laser rested on the same ball-tipped vertical control rod described there. This can be seen in Fig. 5-2 and in subsequent photographs directly beneath the laser window. The center of the small ball is directly beneath the glass-water surface of the window. Thus, just as in the case of the mounting for the narrow beam lamp, the laser was always rotated about a vertical axis which passed through the point at which the laser beam entered the water. A child's life belt was always strapped around the rear end of the laser case so that its upward thrust, acting through the central pivot, would cause the front end of the laser case to press solidly against the vertical control rod. Remote horizontal control of the laser beam was provided by the mechanism in the underwater cart in exactly the same way described in Section 4.

It was important to mount the laser at such a height above the underwater cart that the horizontal beam of light it produced would pass through the center of the observing window of the underwater tower. This made it necessary to orient the laser with its window at the bottom of the front end plate. Fortunately, it could be operated in any position. The triangular box mounting, shown in Fig. 5-2, was designed to place the laser beam at the proper elevation.

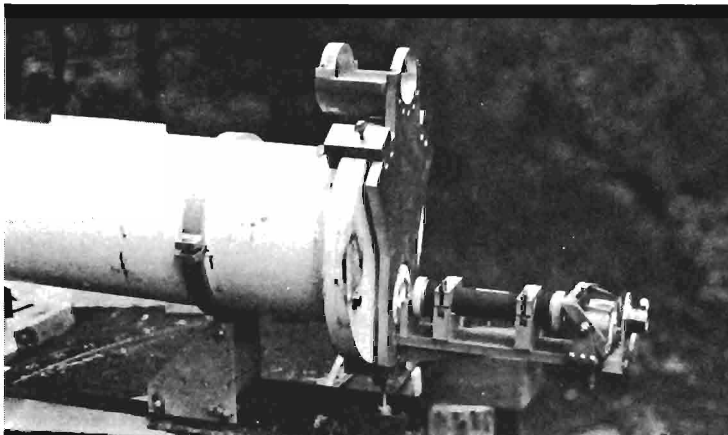


Fig. 5-2. RCA laser mounted on control arm of underwater cart. The clamp-on accessory support bracket is in place.

#### AIMING THE LASER

Throughout all of the experiments with the collimated underwater projector described in Section 4 it was possible to align the light beam visually. The experimenter was in virtually no danger of retinal damage, even if the direct beam from the incandescent projector inadvertently entered his eye. This was not true of the underwater laser. Direct alignment of the laser beam was out of the question, not only from the standpoint of eye hazard, but also because the single 20 nanosecond flashes produced by the laser could not be located accurately by direct observation. It should be explained that when an observer views a single flash on, say, a wall or screen, he finds it virtually impossible to identify the precise location of the bright spot because of involuntary eye movements. Persistence of vision causes the illusion that the spot

is present for a substantial fraction of a second during which the eye always changes its fixation. The actual position of the laser beam can be recorded by means of a sheet of photographic paper mounted on the wall. If an observer is asked to mark the position on this sheet of photographic paper where he believes the beam of light struck, it is nearly always found that (after development) the photographic record of the light beam is not at the point marked on the paper. Similarly, if two or more individuals observe a laser pulse they seldom agree about its location on the screen.

Photographic recording of the position of the laser beam is an impractically slow means to achieve precise aiming. It was essential to avoid the necessity of photographic beam alignment in the underwater laser experiments. Accordingly, the underwater collimated projector was used as an alignment device. The system is shown in Figs. 5-2, 5-3, and 5-4. A supporting metal plate was attached to the flanges of the laser by means of three clamps, two at the top and one at the bottom of the front face plate of the laser. A hole in this mounting plate was provided for the laser beam. The same collimated incandescent projector used throughout all of the experiments described in Section 4 was mounted at the top of this plate to provide a collimated beam of light for aiming purposes. In Figs. 5-3, 5-4, and 5-5 the collimated projector will be recognized because it is painted black. The 2-inch diameter beam of white light it produced entered a right-angle prism and was reflected directly downward to a second prism mounted at the end of a horizontal shelf attached to the bottom of the main mounting plate. This pair of prisms caused the 2-inch diameter beam of white light to leave the assembly horizontally along the optical axis of the optical bench. Obstruction of the laser beam by the lower prism was avoided by drilling a horizontal clearance hole through that prism. The laser beam passed freely through this hole, which shows clearly in Fig. 5-4. Vernier adjustments were provided in the mounting of the lower prism by means of which the large diameter white beam from the incandescent projector could be made coaxial with the laser beam.

The alignment procedure was simple. The laser was flashed upon a piece of photographic paper mounted on the back wall of the underwater tower. After development, the photographic paper was returned accurately to its position on the wall. Light from the incandescent projector was then allowed to shine on the wall and the vernier controls on the lower prism were adjusted by a swimmer until the 2-inch diameter white beam was centered on the recorded laser spot.

It will be noted in Figs. 5-2, 5-3, and 5-4 that the black cylinder containing a rotary solenoid is mounted above the projector, just as it was in Fig. 4-10. In this case, however, the arm attached to the solenoid carried an opaque metal disk so that the white light beam could be remotely interrupted by the experimenter without extinguishing the concentrated arc lamp. Thus, the white light beam was available to the experimenter in making his alignment but could be extinguished before the laser was flashed for measurement purposes.

The use of the collimated incandescent projector enabled all of the alignment techniques described in Section 4 to be employed in the experiments with the underwater laser. This capability was of utmost importance in accomplishing the goals of the research within the available hours of experimental time. If it had been necessary to make all alignments of the laser by photographic procedures, no night would have been long enough to obtain significant data and nights dark enough to enable visual alignment at long range would have been too few to obtain the desired results. The importance of this technique of laser alignment to the success of the research cannot be overemphasized.

*Appearance of the Aiming Pattern.* It is interesting to note that the visual appearance of the lens of incandescent projector when used with the prism system attached to the laser was not a uniform circular

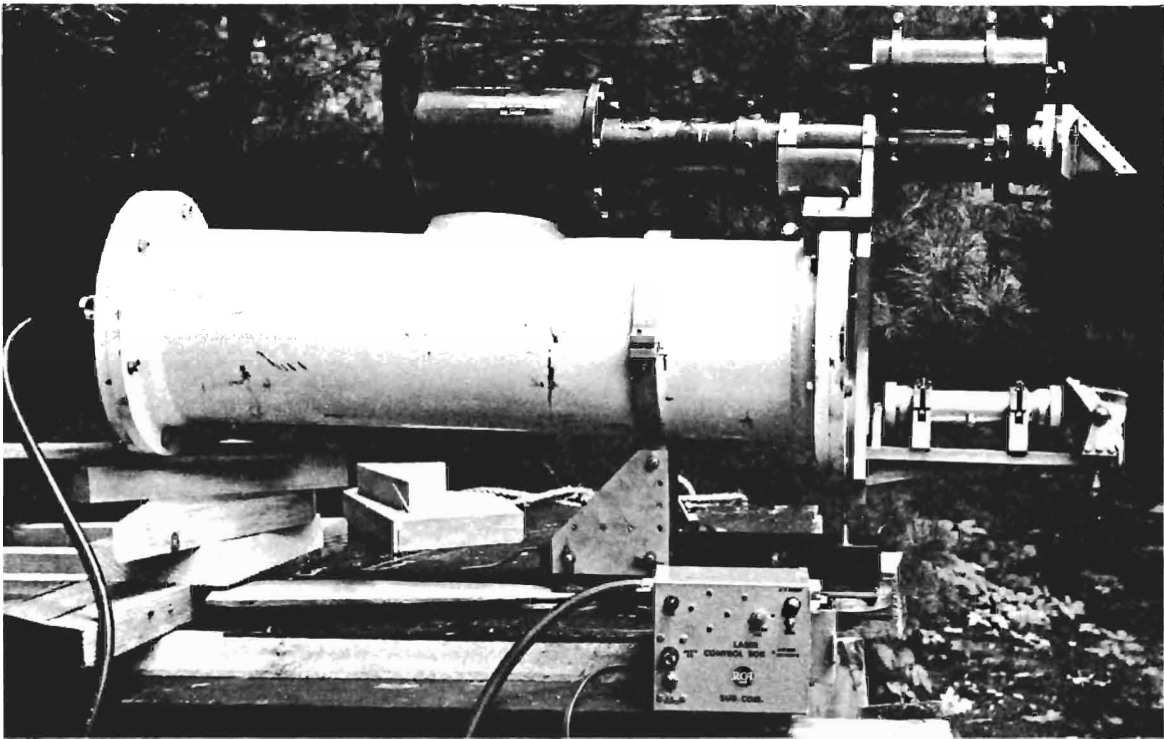


Fig. 5-3. Underwater laser with collimated projector used as an alignment device.

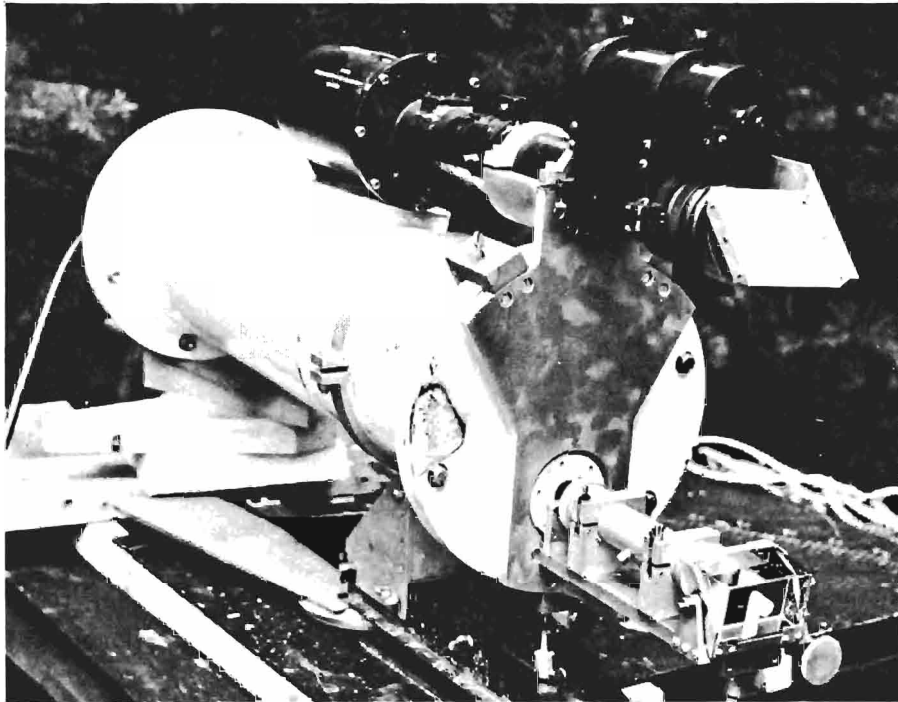


Fig. 5-4. Front view of underwater laser.

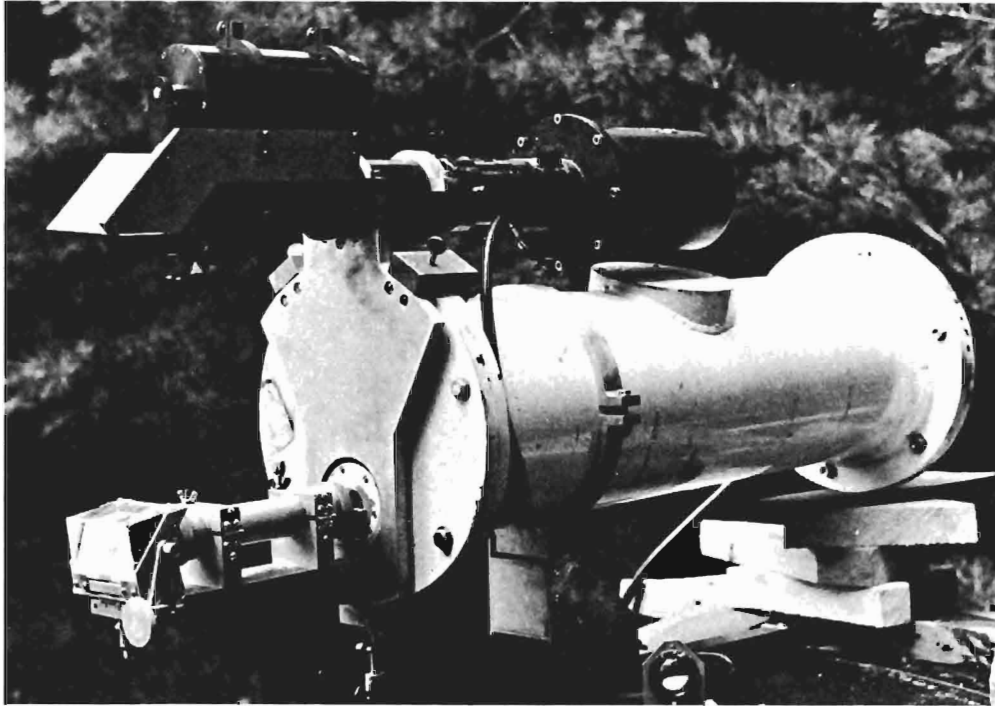


Fig. 5-5. Underwater laser with alignment accessories.

white disk of light. It contained a dark central spot because of the horizontal clearance hole for the laser beam and, in addition, a dark vertical shadow directly beneath that hole, because the "tunnel" through the prism prevented light from the lamp from reaching the reflecting hypotenuse of the lower prism. Thus, a vertical black column extended from the bottom of the white circular disk of light up to its center. The upper termination of this vertical column was, of course, rounded. The fact that the lower prism was separated by approximately 12 inches from the lens of the projector served to introduce parallax between the black column and the circular aperture. Thus, operation of the remote azimuth control by the experimenter produced the effect of moving the vertical black column horizontally across the face of the projector aperture. This formed an excellent optical sight. Its precision was nearly independent of the range at which the projector was viewed. The remote azimuth control was operated by the experimenter until the black column appeared to be centered on the face of the projector aperture. The remote vertical controls were then operated to place rounded upper part of the shadow column precisely in the center of the circular disk of light from the projector. The effect was strikingly like that of certain forms of rifle sights; the precision of pointing by this means was excellent, even at extreme range.

#### ATTACHMENTS TO THE LASER

The horizontal shelf which supported the lower prism also provided mounts for several attachments to the laser. The first of these was simply a mounting for the insertion of an exterior aperture stop. For example, measurements of irradiance on-axis were made during 1964 and 1965 using the underwater laser so that the laser results could be compared with those obtained with the incandescent projector. Since most of the data given in Section 4.4 made use of beam diameters as small as 1/10 inch or 1/20 inch, the laser beam was reduced to these diameters by means of an external stop. This was a disk of metal containing a small central hole. It was supported in a holder immediately in front of the laser window (see Fig. 5-3).



Between the aperture stop and the lower prism at the outer end of the shelf were two mounting brackets which could be used to support various attachments. In Fig. 5-3 these brackets hold an air-filled, white, horizontal tube closed at either end by means of high-quality glass windows. Another (black) tube contained a Dove (see Fig. 6-7) prism, by means of which the laser beam could be rotated about its axis. Unlike the incandescent projector, the divergence of the laser beam was roughly elliptical. Photographs of the beam from the laser are shown in Fig. 5-8. The major axis of the ellipse is inclined, approximately at 23 degrees from the vertical. The laser light is linearly polarized with its E-vector in the direction of the minor axis of the ellipse. For most experiments it was desired to have control over the orientation of the E-vector. This capability was provided by the Dove prism.

#### THE LASER IN WATER

The mountings and alignment devices shown in Figs. 5-3, 5-4, and 5-5 proved to be very satisfactory when the laser was put into the water on its underwater cart. All of the remote controls worked as well as they had with the incandescent underwater collimated projector used alone.

A night (flash) photograph (Fig. 5-6) taken downward through the water surface shows the laser mounted on the underwater cart and track. The depth of the laser is six feet. The track is 9 feet deep. Figure 5-7, taken through the measurement window of the underwater tower, shows the experimenter's view of the laser in action. The green beam of the laser is diverted toward the right of the observing window. The original color photographs of Figs. 5-6 and 5-7 were by Charles Haney of the US Naval Air Development Center.

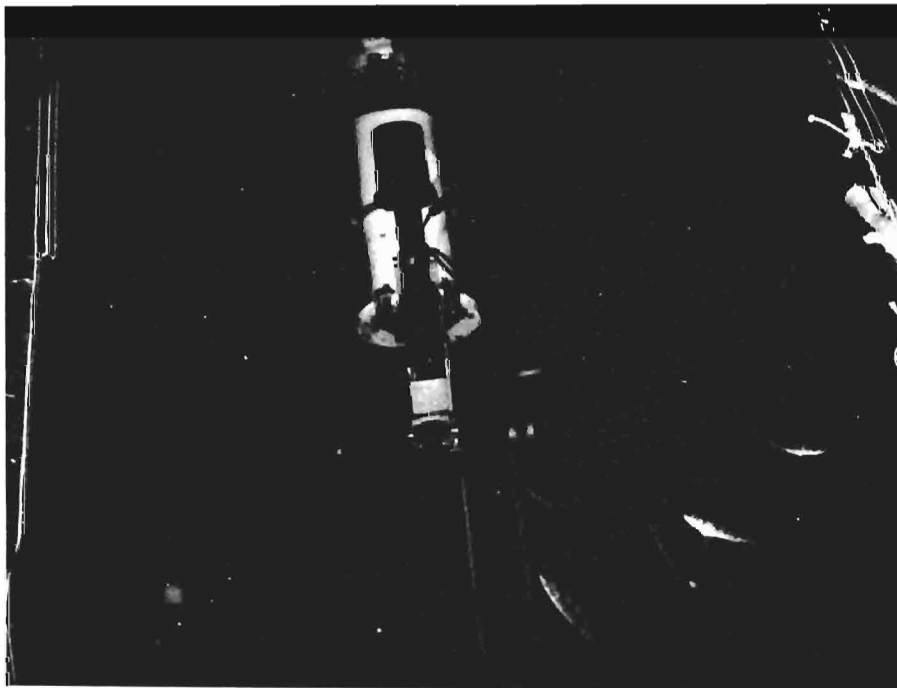


Fig. 5-6. Underwater laser in place on the underwater cart and track. Interested fish were frequent observers.

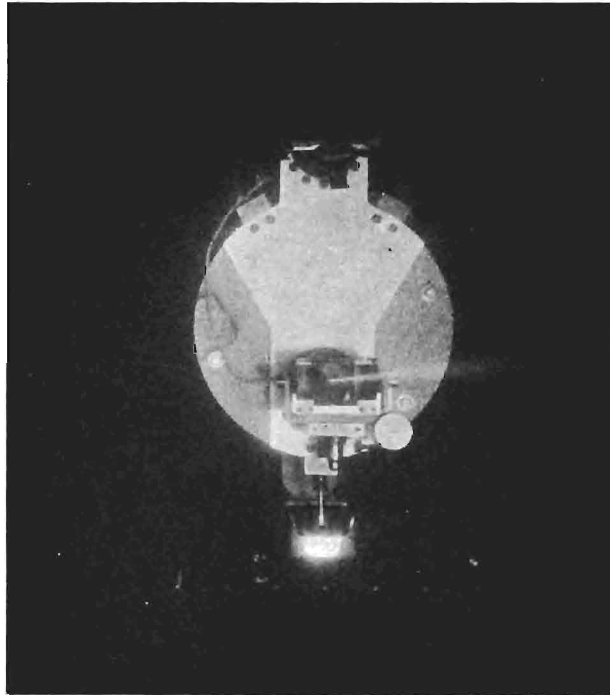


Fig. 5-7. Experimenter's view of the laser from the underwater tower. The laser beam is diverted to the right.

#### 5.4 DIVERGENCE OF THE UNDERWATER LASER

Photographic studies were made to ascertain the divergence and the diameter of the beam from the first RCA underwater laser. These studies are described in a letter dated 17 August 1964 from the author to ONR. The following paragraphs relate to Fig. 5-8 and are quoted almost verbatim.

“The side view of the apparatus shows a small vertical metal plate between the laser and the laser polarizer. This metal plate was a mounting into which a thin circular disk of metal could be inserted in order to stop down the laser beam. In order to get a valid comparison between the laser and the incandescent sources, and in order to obtain data that can be scaled to clearer water, it was necessary to introduce such a stop. The data shown by the triangle points in figure I am sending you with this letter were obtained with the laser beam stopped down to a diameter of 0.050" by means of a stop introduced in the manner just described. It was necessary, of course, to ascertain the effect of this stop on the divergence of the beam, and consequently I made a series of photographic determinations of beam spread with and without the stop in place. One of the photographic figures I am sending you with this letter is a composite plate which is a photographic representation of an assemblage of 17 polaroid prints which I made for the purpose of

ascertaining the beam spread of the laser. Please refer to pictures 1 through 5 at the top of [ Fig. 5-6 ]. These were made with the polaroid back from the oscilloscope camera by mounting it flat against the inside surface of the window of the tower. The unobstructed beam from the laser fell directly upon the polaroid material. The Wratten neutral density gelatin filter was fastened across the aperture of the polaroid film back to limit the exposure. The photographic reproduction has been carefully made at unit magnification with respect to the original polaroid pictures so that the spots on the plate are exactly the same size as those on the original polaroid prints. Prints 1 through 5 were made without stopping down the laser. The distance from the window in the laser case to the window of the tower was 13.5 ft when these pictures were made; that is to say, 13.5 ft of lake water separated the window of the laser from the window of the tower. By trial and error a Wratten neutral density filter was found which provided a minimum exposure on the photographic film. This is shown in picture No. 1. This Wratten filter was then changed for one having 0.5 less density. Three exposures were then made of three successive laser flashes. The laser was cooled for 1 minute between these flashes. These three pictures are Nos. 2, 3, and 4 on the plate. It is obvious that the power output of the laser was not identical in these three pictures, but this is typical of the way the laser was operating. The water contained a large amount of biological life, including an occasional large "bug" which shows as a dark shadow in the picture. The "granular" appearance of the edges of the beam in the pictures is the result of the transparent organisms in the 13.5 ft of water between the laser and the film. The contrast of the photographic material was high. We were using the same 10000-speed Polaroid oscilloscope film with which we were making the oscilloscope pictures. There is a comparatively sharp edge to the spot of light in the picture, an effect which I desired in order to get a measure of the beam spread. Under these circumstances, of course, the size of the spot depends upon the exposure. The beam spreads measured from photographs 2, 3, and 4 represent a cross-section through the beam at something like the  $1/3$  power point. This corresponds approximately with the criterion I used for determining (by photoelectric techniques) the beam spread of the incandescent light beam, and this was my reason for selecting this particular photographic exposure level. In order to ascertain something of the shape of the flux distribution of the laser beam, I took photograph No. 5, using a neutral filter which transmitted 1.0 log units more light than did the filter used in taking photograph No. 1. Thus the beam portrayed in photograph 5 is representative of the  $1/10$ th power contour.

RCA has estimated the diameter of the beam as it emerges from the laser to be  $3/16$ " in diameter. The prism assembly prevented me from bringing the laser close to the window of the tower but I was able to get it into a position such that approximately 1 foot separated the window of the laser case from the Polaroid material. In this position I took pictures 6, 7, and 8 which correspond in exposure to pictures 1, 2, and 5 above. Thus picture 7 is intended to represent the diameter of the laser beam at the  $1/3$  power contour and picture 8 represents the  $1/10$  power contour at this distance. Measurements of picture 7 and comparison with measurements of pictures 2, 3, and 4 enable the maximum and minimum beam spreads to be calculated. Similarly, measurements of pictures 5 and 8 enable the beam spread to the  $1/10$  power point to be measured. Another pair of photographs not shown in this plate were intended to provide similar measurements at the  $1/30$ th power point. The data are tabulated below.

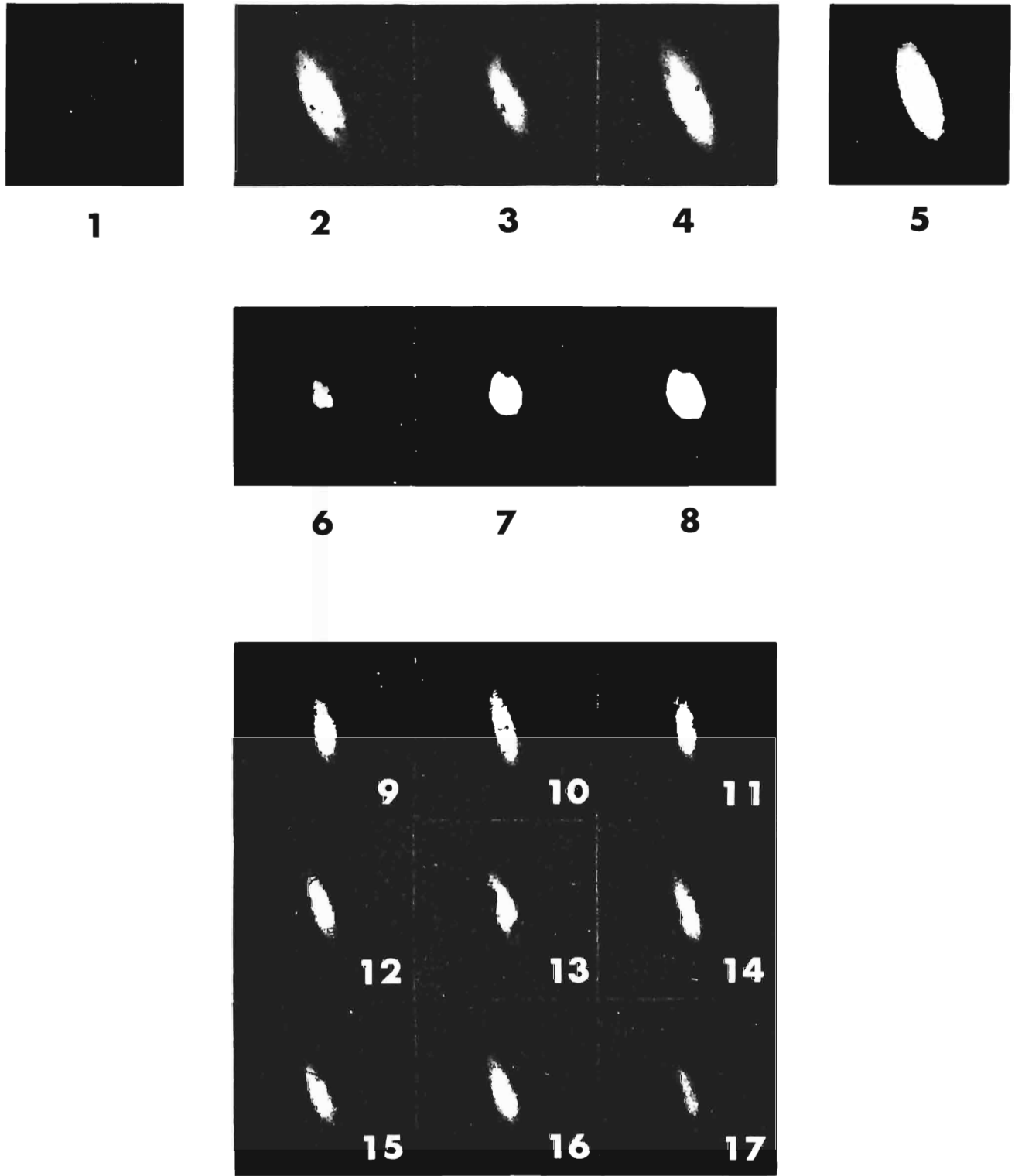


Fig. 5-8. Photographic recordings of the laser beam after passing through lake water. (Full scale)

## LASER BEAM SPREAD

(milliradians)

Fraction of Peak Power	Maximum	Minimum
1/3	1.67	0.37
1/10	2.38	0.64
1/30	5.00	2.33

It is interesting to note that RCA gives a nominal beam spread for the laser of 3 milliradians by 1 milliradian. This rating is based upon visual estimates of the size of the laser beam on the wall of the Laboratory. In view of the characteristics of human vision under such circumstances and the fact that the RCA measurements were made in air rather than in water, it would appear that there is no disagreement between their rating and the values I obtained.

Pictures 1 through 8 [in Fig. 5-8] refer to the unobstructed laser beam. I repeated the beam spread measurements with the 0.050" circular stop in place as previously described. Pictures 9 through 17 show successive firings of the laser with this stop in place and 12.0 ft of water separating the window and the laser case from the window of the tower. Nine pictures were made in order to illustrate the variability of the successive flashes. The photographic exposure in the case of all of these 9 pictures was adjusted to correspond with the 1/3 power point; that is to say, these pictures are comparable with pictures 2, 3, and 4. Using measurements from these pictures and an initial beam diameter of 0.050", I have calculated the average beam spread with the 0.050" stop in place to be 1.73 by 0.38 milliradians. By comparison with the values for the unobstructed beam given in the table above for the 1/3 power point, it is evident that the insertion of the stop has made no important difference to the divergence of the laser beam.

All of the pictures of the laser beam show the oval spot to be inclined to the vertical by an average value of 24°. It will be noted from the photographs of the laser mounting that the laser window was located directly beneath the cylinder axis. Thus the major axis of the elliptical beam is neither radial with respect to the axis of the case nor tangential but inclined 24° to the radial (vertical direction.)"

### 5.5 POLARIZATION OF LIGHT FROM THE UNDERWATER LASER

The first studies of the state of polarization of the light from the first underwater laser were described in the letter of 19 August 1964 from the author to ONR, as follows:

"I was interested to ascertain whether the light emerging from the laser was polarized. I investigated this by bringing the laser as close to the tower window as possible and placing Polaroid sheeting in the circular filter wheel which can be mounted on the outside of the tower window. Thus the laser beam traversed an unobstructed path consisting of about 1 foot of water, a sheet of Polaroid

linearly polarizing material, a plastic diffusing disk, the glass window of the tower, about 1" of air before arriving at the cathode of the multiplier phototube. Time did not permit me to do a full study of the state of polarization of the light being emitted from the laser. There is no question that the light is polarized. The only measurements I secured were with the analyzer oriented to transmit the component of light having its E-vector vertical and, a second measurement, with its E-vector horizontal. Thus I was able to determine from the oscilloscope pictures that the ratio of irradiance at the photocathode produced by light having its E-vector horizontal to light having its E-vector vertical was 13.7. These measurements do not indicate whether the emitted light is linearly polarized or elliptically polarized. If it is linearly polarized and if the axis of the axis of polarization is associated with the axes of the ellipse, then it would appear that the E-vector of the emitted light is associated with the minimum diameter of the ellipse.

Measurements of polarization transmittance by natural water were made at Diamond Island in 1962 and are shown in [Fig. 5-9]. The data in that figure were obtained as follows: The same incandescent light source shown in Fig. 3-5, producing a 20° divergent beam, was equipped with a linear sheet polarizer such that the light entering the water at the lamp was linearly polarized. A photoelectric irradiance meter was equipped with a rotatable linear sheet polarizer mounted in the water just in front of the collecting surface of the irradiance meter. This instrument was used to measure the irradiance at the center of the beam produced by the underwater lamp at distances out to 29 attenuation lengths [ $1/a = 4.2 \text{ ft/ln}$ ]. Each point in [Fig. 5-9] represents the fraction of the measured irradiance which is linearly polarized at the receiver. At each lamp distance one measurement of irradiance was made with the axis of the analyzer parallel with that of the polarizer and another with the analyzer in the crossed position. The ratio of the difference to the sum of these two readings is the fraction of irradiance which is polarized, i.e., the percentage polarization at the irradiance meter.

[Figure 5-9] shows that more than 75 percent of the light received at 28 attenuation lengths has the same state of polarization as that with which it left the lamp.

The dashed portion of the curve beyond 30 attenuation lengths in [Fig. 5-9] is an arbitrary extrapolation of the data. If it is correct, nearly half of the light has its original state of polarization at a distance of 50 attenuation lengths from the lamp.

A similar measurement of polarization transmittance was made at Diamond Island in 1964 using the underwater laser. The lamp distance was 22.7 attenuation lengths [ $1/a = 4.4 \text{ ft/ln}$ ]. The laser polarizer was used for the first time. It was mounted in such a fashion that the laser light it transmitted had its E-vector horizontal. The average of several oscilloscope pictures showed that the irradiance at the tower was 83 percent polarized."

This datum is plotted at the point marked L in Fig. 5-9. It indicates that the retention of polarization by light from the RCA laser is only slightly better than in the case of the 20 degree divergent incandescent beam. A measurement of polarization transmittance using a small beam of light from the collimated incandescent projector would have provided a better comparison, but this was not accomplished. Later studies confirmed that the light emitted by the underwater laser was nearly linearly polarized with its E-vector parallel to the minor axis of the elliptical cross-section of the light beam.

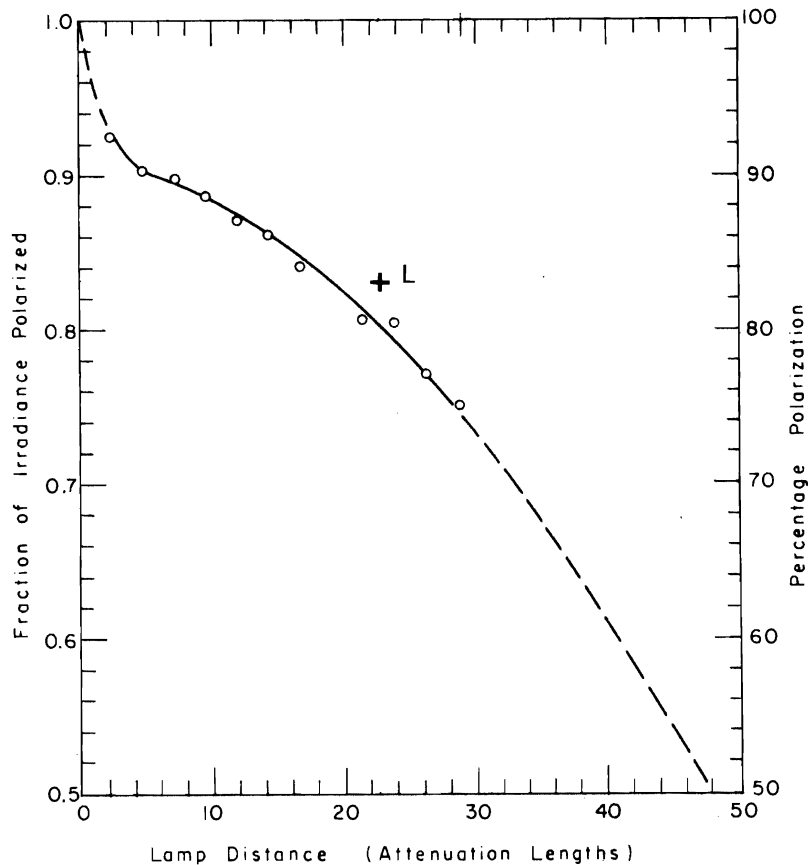


Fig. 5-9. Polarization transmittance of lake water.

## 5.6 MEASUREMENTS OF IRRADIANCE ON-AXIS

The primary thrust of the 1964 experiments with the first RCA underwater laser was the measurement of irradiance on the axis of the laser beam. These data were regarded as being the information of greatest interest to those concerned with small, distant receivers. It was presumed that irradiance off-axis would be less than on-axis, so that the latter could be regarded as setting an upper limit to reception range. This presumption was, of course, to be explored.

The techniques employed were exactly like those already described in Section 4 in connection with measurements of irradiance on the axis of the collimated incandescent projector. Although translation of the data to clear ocean water was a secondary goal, nearly all of the laser data was taken with the beam stopped down to diameters of 1/10 inch and 1/20 inch to facilitate scaling the results to clear ocean conditions, just as was done in the case of the 1962 incandescent beam data given in Section 4.

Troubles with the partially damaged laser, previously mentioned, prevented the 1964 series of experiments from covering all of planned conditions. They also reduced the precision of the data. Nevertheless, laser irradiance on axis was measured to approximately 17 attenuation lengths with a 1/10 inch diameter beam and to 12 attenuation lengths with a 1/20 inch beam. Ironically, the 1964 irradiance on-axis data raised more questions than it answered. A careful repeat of the work, performed in 1965, only served to confirm the reality of the quandaries. Finally, in 1966 the earlier findings were explained and experimen-

tal proof obtained that incandescent light and light from the RCA laser have identical beam propagation characteristics when compared under identical beam geometries. Specifically, this laser light is *not* converted to multipath irradiance at a different space rate than is incandescent light. The series of experiments which led finally to this conclusion despite intervening periods of doubt are described by Sections 5 and 6 in the order in which they were performed. Interest in other more important and scientifically significant propagation characteristics of laser light in natural water dominated the research from 1965 to 1970, as described in Sections 6 and 7.

## ELECTRONIC TECHNIQUE

The irradiance-on-axis measurements which dominated the 1964 series at Diamond Island differed from those done with the collimated underwater projector only in the electronic system used to measure the irradiance. The 20-nanosecond laser pulses could not be measured with the DC photometric system that was used in obtaining the data described in Section 3. The multiplier phototube was replaced by an RCA-7767 and its output was displayed on a Techtronic 585 oscilloscope and recorded with a Polaroid oscilloscope camera. The pulse was used to trigger the sweep of the oscilloscope and the delay line enabled the shape of the entire pulse to be recorded. Wratten neutral filters were inserted in front of the photocathode to avoid saturation of the phototube. The small usable dynamic range of the phototube-oscilloscope system made it necessary to change these filters for virtually every change in laser position on the track. Calibration of the neutral filters was of utmost importance. Their transmittance was measured in place using the DC electronic photometer system described in Section 2; the linearity of this system was calibrated at frequent intervals on an inverse-square-law photometric bench employing incandescent standard lamps and narrow-band green filters centered on the laser wavelength, 530 nanometers.

The 1965 and 1966 RCA lasers contained a beam splitter which placed a sample of the outgoing pulse on a vacuum diode phototube in order to monitor the power of each pulse. The output of this monitor was displayed on a Techtronic 545 oscilloscope and recorded by a Polaroid oscilloscope camera. Pulse-to-pulse variability under good operating conditions is illustrated by pictures 9 through 17 in Fig. 5-8. The linearity of the monitor photometric system was calibrated at frequent intervals by means of Wratten neutral filters having transmittances measured as described in the preceding paragraph.

## THE 1964 LASER DATA

Success in obtaining valid irradiance data had not been achieved when ONR representatives visited the experimental site at Diamond Island during July, 1964. This was due chiefly to erratic performance of the damaged laser. Continuing repairs soon produced usable laser pulses and irradiance data were secured. A laser beam diameter of 1/20 inch was used and the irradiator had a diameter of 1/40 inch. The prevailing attenuation length was 4.74 ft/ln. Following an abridged reduction of some of the oscillograms a letter report was sent to ONR on 19 August 1964. Exerpts from that letter, after some minor editing, is as follows:

“During the nights immediately following your visit to our laser experiment at the Diamond Island field station last month, we had the good fortune of securing usable performance from the laser part of the time and I was able to secure enough data to define the character of the propagation of the laser beam out to



approximately 19 attenuation lengths. I was disappointed in not being able to carry the curve further because I was successful in aligning the beam on the detector out to more than 30 attenuation lengths and I had sufficient sensitivity to perform these measurements, but by the time I had reached these lamp distances the laser had become unusably erratic in its power output, and I was unable to obtain any usable data beyond 19 attenuation lengths.

The laser data are represented by the triangles in (Fig. 5-10). They do not represent all of the data I took at these lamp distances. At nearly every lamp distance I made several oscilloscope pictures in order to minimize the variability in power output of the laser and also to minimize the probability that one of the many fish in the vicinity partially obscured the laser beam. There has been time to measure only one oscilloscope picture at each distance. The oscilloscope

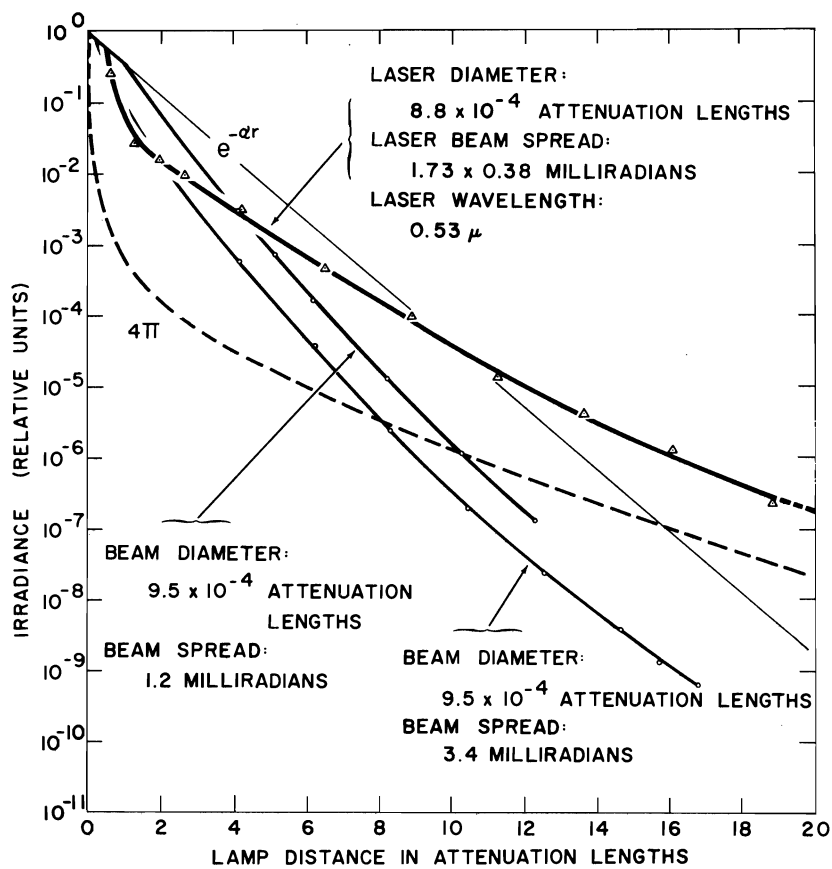


Fig. 5-10. 1964 measurements of irradiance on-axis using the underwater laser and the underwater collimated incandescent projector. Dashed curve is irradiance from a uniform spherical lamp.

traces are not identical but I have attempted to select ones which appeared to me "typical." Not until I have been able to measure all of the oscilloscope traces and study their effect upon the curve can I speak with any real confidence about the detailed shape of the function.

The oscilloscope technique for measuring these short pulses afforded a dynamic range not greater than about two-thirds of a log-cycle. It was necessary, therefore, to make a photometric "fold" in connection with virtually every point. The curve was generated step-wise beginning at zero lamp distance so that an error in any point affects the position of all of the succeeding points on the curve. Thus, errors are cumulative from left to right. The final curve which I will evolve on the basis of all the oscilloscope pictures may intersect the alpha-line at quite a different point than the preliminary curve. Nevertheless, preliminary inspection of all the oscilloscope pictures gives no reason to expect any change in the fundamental character of the curve. It seems safe to conclude already that the laser beam behaves in much the same fashion as does the beam from an incandescent lamp having similar beam diameter and beam spread. As illustrated by the curve passed near the triangle points, the laser beam follows the alpha-line until the near field-far field transition is reached after which the irradiance on axis shows an inverse square dependence and, therefore, a rapid attenuation until multipath effects take over. At long range the irradiance on axis seems clearly to approach the K-slope which characterizes the spherical ( $4\pi$ ) source at long range. Thus the light which was received at long range has experienced small-angle forward scattering and exhibits multipath propagation. The dotted section to the right of the last triangle point is parallel to the dashed line which represents data on the ( $4\pi$ ) spherical lamp in order to emphasize that, even in the range between 16 and 19 attenuation lengths, the curve laser has nearly reached parallelism with the curve for the spherical lamp, i.e., the K slope.

The dotted curve in Fig. 5-10 represents the performance of the spherical lamp. The two lower curves represent the performance of the collimated incandescent projector with a 1/20 inch diameter stop at Diamond Island during 1962. It is too soon to conclude that the laser beam is converted to multipath radiation more quickly than is the incandescent beam. The laser curve [in Fig. 5-10] represents only a small sample of the new data; its reduction has been hasty. Careful study of all of the oscillograms may yield a different curve."

All of the 1964 oscilloscope pictures were later restudied and re-measured. No way had been available to monitor the highly variable pulse-to-pulse variations in the power output of the damaged laser. All measurements had, however, been repeated several times to make statistical treatment of the data possible. The statistical restudy of all 1964 oscillograms did not change the curve in Fig. 5-9 sufficiently to bring it into agreement with the incandescent data. The final points are represented by triangles in Fig. 6-1, where they are compared with corresponding data that were secured with RCA's much improved 1965 underwater laser.

# 6. LASER LIGHT IN LAKE WATER

## 6.1 INTRODUCTION AND SUMMARY

Preliminary use of the first RCA underwater laser at the Diamond Island field station during the summer of 1964 had developed successful techniques for experiments with submerged pulsed lasers, had explored some polarization effects and certain beam characteristics of the laser, and had seemed to show that on-axis irradiance produced by the laser differed basically from that produced by the collimated underwater incandescent projector. (See Section 5.6). Further exploration of that difference was one mission of the 1965-66 program; it was found that identical normalized irradiance is produced if (and only if) the geometry of the beam of laser light is made the same as the geometry of the beam incandescent light. (See p. 6-9 end of section "Measurements in Water")

Extensive measurements were made of off-axis irradiance by scattered light from laser beams. It was found that big objects may receive very large amounts of scattered radiant power far outside the geometrical limits of the beam, often with considerable pulse stretch. On the other hand, measurements of the distribution of received radiance showed that small receivers on or near the axis need a field of view only 5 or 6 degrees in angular diameter in order to receive virtually all the light available to them.

## 6.2 STUDIES OF IRRADIANCE ON-AXIS

The first experiment conducted in 1965 was a repetition of the earlier measurements of irradiance on axis which led to the data shown in Fig. 5-7. The irradiance was measured for light produced by an improved RCA green laser and by the collimated incandescent projector equipped with a 100-watt zirconium arc lamp which caused the unit to produce a uniform beam spread of 3.4 milliradians. Just as in the 1964 experiments, both the laser and the incandescent source were equipped with circular stops 0.050 inches in diameter. The RCA green laser used in the 1965 experiments was the second such laser produced by that company and was physically identical with the first such laser, used at Diamond Island in 1964. Laser

No. 2 performed very well throughout all of the 1965 experiments. Initially the power output had considerable pulse-to-pulse variability but an effective system for monitoring the power output of the laser was available so that the data points could be corrected effectively. Adjustments gradually improved the stability of the laser output. The effective help of RCA in maintaining the fine performance of the laser is very gratefully acknowledged.

Irradiance on the axis of the beam was measured as a function of lamp distance and the results are shown by the solid curve in Fig. 6-1. This curve has been fitted to round points representing each individual measurement; these points are shown in the figure. For purposes of comparison, points from the 1964 measurements of the same function are shown by squares. These data differ slightly from those plotted in Fig. 5-7 because they represent the result of averaging all of the oscilloscope pictures taken in 1964 whereas the points in Fig. 5-7 were derived from single oscilloscope pictures at each distance. The 1964 and 1965 laser data are in excellent agreement.

The lower (dashed) curve in Fig. 6-1 represents irradiance on-axis produced by the narrow beam incandescent projector. This curve has been fitted to the ensemble of points collected in 1965 and also in 1962 using the same lamp and the same photoelectric receiving system. The 1962 points are denoted by triangles; the 1965 points by circles. It is obvious that very close agreement was obtained between the measurements made in 1962 and 1965.

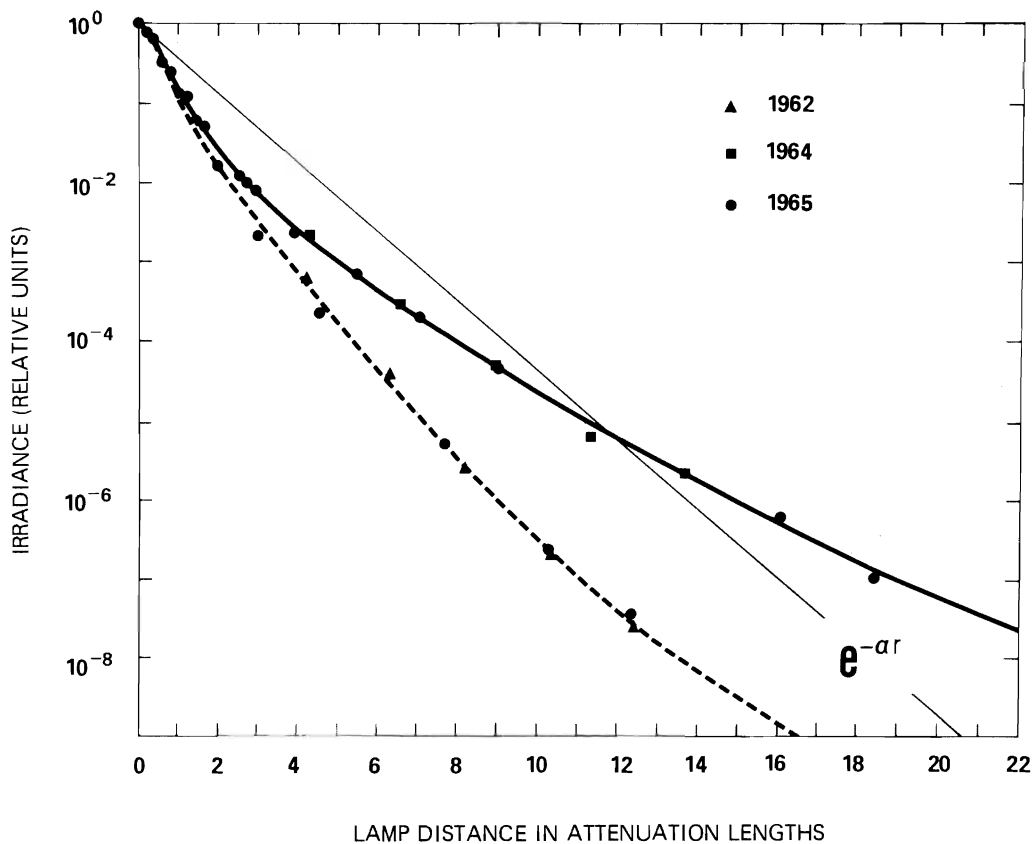


Fig. 6-1. Irradiance On-Axis produced by the RCA underwater laser (solid line) and by the underwater collimated incandescent projector (dashed line). When the geometry of the beam of laser light was made identical with the geometry of the beam of incandescent light, the solid curve became identical with the dashed curve.

It is clear that the on-axis irradiance produced by the narrow beam incandescent projector differed from the irradiance on-axis produced by the underwater green laser in a reproducible fashion and by amounts that are far beyond experimental error. Speculations concerning the causes and meaning of these differences were, of course, made. Since the difference in curve shape is not attributable to spectral band pass effects (See Sec. 2.4), it was natural to inquire whether coherence is responsible for the observed differences, but tests failed to discover any measurable coherence in the laser light. RCA states that the output of their laser is not monochromatic but consists of a pattern of many spectrum lines spread over a spectral range of approximately  $40^{\circ}\text{A}$ . The complex asymmetrical beam spread and the nonuniform distribution of flux within the beam suggest that this laser light source is essentially non-coherent. Measurements of the coherence of the green laser were attempted by a visiting team of investigators from the U. S. Naval Ordnance Test Station, China Lake, California, who came to Diamond Island during 1965 experimental sessions for the purpose of making this and other measurements. They did not detect coherence in the laser output. The author made photographic studies using a double slit technique, but no fringes were observed under circumstances such that they would have been produced by light having a coherence length of 1 millimeter.

#### COMPARISON OF BEAM STRUCTURES

It was obvious that the light produced by the RCA underwater laser had a much different beam structure than did the collimated underwater incandescent projector. It was suspected from the outset that this might be the cause of the difference in shape between the two curves in Fig. 6-1. Eventually, in 1966, it was demonstrated that this was, in fact, true. The experiments leading to that conclusion are described in the paragraphs which follow.

The incandescent projector produced a uniform circular cone of light having a well-defined, symmetrical distribution. The laser, on the other hand, produced a highly irregular beam pattern which cannot be adequately described by the word elliptical. Further insight into the nature of the beam from second harmonic green lasers can be obtained from the photograph which constitutes Fig. 6-2. This is the beam produced by a second harmonic green laser built by the Lear-Siegler Corporation. This laser is similar in many respects to that made by RCA except that the KDP crystal is outside the resonant cavity.\* The beam produced by the Lear-Siegler laser was less confined by stops than the RCA laser and therefore the pattern produced by the optical processes within the KDP crystal are more obvious. It is evident from this picture that the peak emission is actually part of a circular fringe produced by the crystal. The "ellipse" is therefore not elliptical but curved, not uniform but with a peculiar gradient which causes the distribution of flux within the beam to be nonsymmetrical with respect to the short axis of the "ellipse," and surrounded by side lobes and what appears to be a pattern of scattered light. It must be remembered that the data plotted in Fig. 6-1 represent irradiance on the axis of the beam; that is to say, the flux collected by a tiny receiver much smaller in diameter than the beam and located precisely at its center. It is not surprising, therefore, that the irradiance at the center of the beam changes with distance in a different way in the case of the uniform, symmetrical, circular beam produced by the projector than in the highly asymmetrical, nonuniform beam produced by the laser.

\*The RCA laser used at Diamond Island in 1966 (the fifth RCA underwater laser), unlike the first two lasers, had the KDP crystal outside the laser cavity. This change was made only because no KDP crystal having sufficiently good optical quality for use inside the cavity could be found in 1966. Several desirable advantages were lost by the change. For example, less of the 1.06 micrometer infrared was converted to 530 nanometer green light. The final output of the 1966 laser was chiefly infrared with a small component of green. This made the beam more dangerous to human eyes when the laser was adjusted in air and it opened the possibility of spectral errors in measurements.

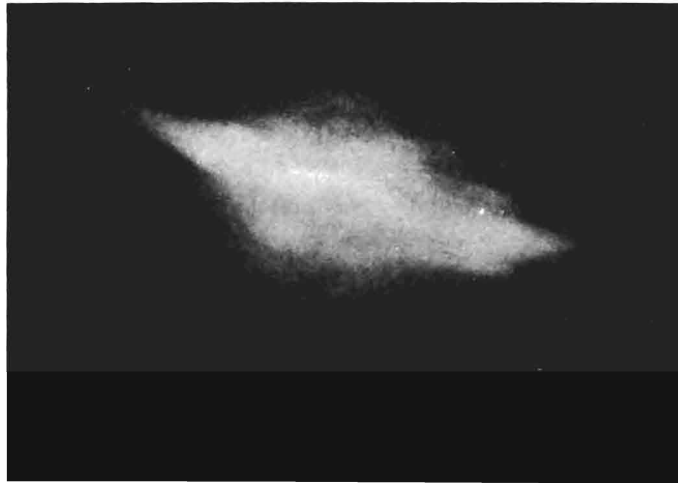


Fig. 6-2. Photograph of the beam pattern produced by a second harmonic green laser built by the Lear-Siegler Corporation. The KDP crystal was outside the resonant cavity, just as in the case of the 1966 RCA underwater laser.

#### EFFECT OF BEAM STRUCTURE

An important although minor part of the program of experiments at Diamond Island in 1966 was a further exploration of the effect of beam structure on axial irradiance. Clearly, as shown in Fig. 6-1, the normalized irradiance on-axis produced by the RCA laser differed from that generated by the collimated underwater incandescent projector. It was asked: Would the two curves in Fig. 6-1 come together if both the laser and the incandescent projector produced geometrically identical beams? That question was answered affirmatively in 1966 by the experiments next to be described.

There seemed little hope of building an incandescent projector that would match the complex beam pattern produced by the RCA laser shown in Fig. 6-2. On the other hand, it appeared possible to use the laser as the source of light for the collimated underwater projector. This was accomplished as shown in Fig. 6-3. The lamp housing of the underwater projector (see Fig. 4-1) was removed, as in Fig. 6-3a. The 100-watt zirconium concentrated-arc lamp was replaced (see Fig. 6-3b) by a metal plate and tube containing an opaque diaphragm with an on-axis circular hole having the same size and location that had previously been occupied by the luminous crater of the concentrated-arc lamp; it was, therefore, at the focal point of the collimator lens and determined the beam-spread of the projector. When this aperture was illuminated uniformly the underwater projector produced a beam of light geometrically identical with that which it emitted when the 100-watt concentrated-arc lamp was in place. A new watertight lamp housing was added, as shown in Fig. 6-3c; laser light was admitted through a window in the end plate of this housing, see Fig. 6-3d. The assembly was mounted in front of the RCA laser, as shown in Figs. 6-3e and 6-3f.

The new lamp housing shown in Fig. 6-3c contained a mechanism illustrated by Fig. 6-4. The position of this mechanism was controlled by an external knob (see Fig. 6-3c). The knob had 3 positions, established by detents. In the central position the internal arrangement was as shown in Fig. 6-4b; laser light entering through the window in the end plate of the housing then fell upon the hole in the diaphragm (see Fig. 6-3b). With the control knob in the position shown in Fig. 6-4c a metal cell containing two separated diffusing disks were brought into place close to the hole in the diaphragm; the laser beam then

passed through this diffusing system before reaching the diaphragm. Since the diffusers were stationary they did not alter the coherence length of the laser beam.\*

In order to measure irradiance on-axis the laser-projector system had to be pointed precisely on the tiny irradiance-measuring aperture at the window of the underwater tower. Incandescent light for beam alignment was provided by an automobile lamp, which could be swung into position behind the diaphragm, as shown in Fig. 6-4a. The irradiance produced with this lamp was not measured because the filament structure of the lamp did not result in a simple, smooth beam pattern. All incandescent irradiance data were secured with the concentrated-arc lamp in the projector.

*The Air Track.* The first step in exploring the effect of beam structure was to ascertain whether the beam of light produced by the new laser-projector system was geometrically identical with that generated by the projector when used with the 100-watt concentrated-arc lamp. This test was performed in air in order that no transmission property of water would be involved. The essential features of the underwater tower and track were duplicated on land. A small shed similar to and slightly larger than the lower part of the underwater tower was constructed and equipped with experimental facilities which duplicated the tower as closely as possible. One hundred feet of track was provided. The facility is shown in Fig. 6-5 and in an aerial view, Fig. 6-6.

The underwater cart is in place on the track in Fig. 6-5, as is the collimated underwater incandescent projector. A plastic window with an optical glass insert exactly like the one in the underwater tower was installed in the "air tower." The experiment employed the same plastic irradiance wheel, diffusers, and stops used underwater. The same cover used for the window of the underwater tower is in place in Fig. 6-5. The same multiplier phototube, electronics, and recorders were used. The projector was modified only by providing forced ventilation in the lamp housing and attaching a thin water cell having a plane window to the outer surface of the projection lens. That attachment was necessary because the lens was designed for use with water in contact with its external surface.

*Measurements on the Air Track.* The azimuth drive of the underwater cart was used to make sweeps of the light beam across the tiny irradiance collector, thereby producing curves of the light distribution in the beam from the projector. Beam diameters of 1/10 and 1/20 inches were used in order to duplicate experimental conditions of Figs. 5-8 and 6-1. These measurements were repeated at several lamp distances out to 100 feet. Exactly similar procedures were used to explore the distribution of light from the projector-laser system.† This work was made much slower and less accurate by the necessity, imposed by the pulsed laser, to make oscilloscope pictures flash-by-flash, point-by-point. As expected, a residue of the laser beam structure was found when the direct laser beam was focused on the hole in the diaphragm of the projector, as in Fig. 6-4b. When the diffusing system was used before the diaphragm, as in Fig. 6-4c, the beam pattern formed by the projector using laser light was found to be identical with the beam it produced with the concentrated-arc lamp.

---

\*No appreciable coherence was evidenced by the light from the RCA laser. One of several tests for coherence was made with a double slit assembly. This was an attachment to the projector, such that the slits were irradiated by the collimated beam. No fringes were observed or detected by photography. In these tests no diffuser was used; i.e., the mechanism inside the lamp housing was in the configuration pictured in Fig. 6-4b.

† In order to guard against the possibility of error in photoelectric measurement due to the copious 1.06 micrometer infrared light emitted by the 1966 RCA laser, copper sulfate was added to the water cell outside the projection lens; it was also used throughout the measurements of the incandescent beams.

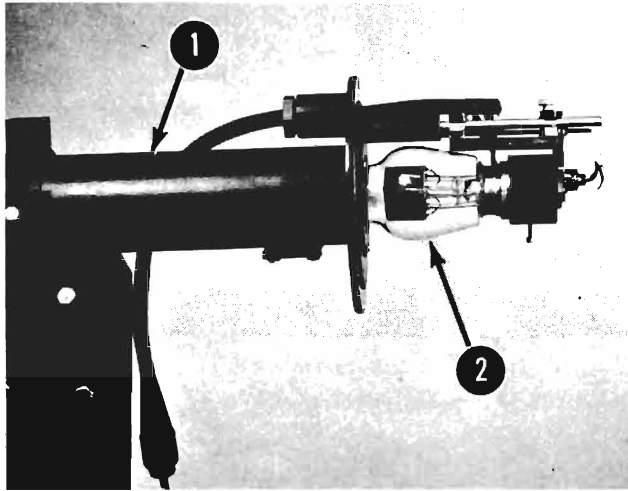


Fig. 6-3a.

Underwater collimated incandescent projector (See Fig. 4-1) with lamp housing removed. (1) Main tube of the collimated underwater incandescent projector, (2) 100-watt zirconium concentrated-arc lamp.

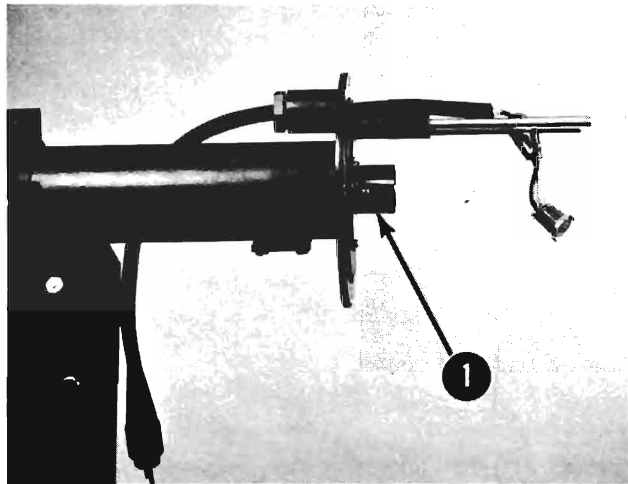


Fig. 6-3b.

Lamp has been removed. A metal diaphragm with an on-axis circular hole having the same size and position previously occupied by the crater of the concentrated-arc lamp has been added. (1) Tube containing a metal diaphragm with an on-axis circular hole having the same size and the same position previously occupied by the crater of the concentrated-arc lamp.

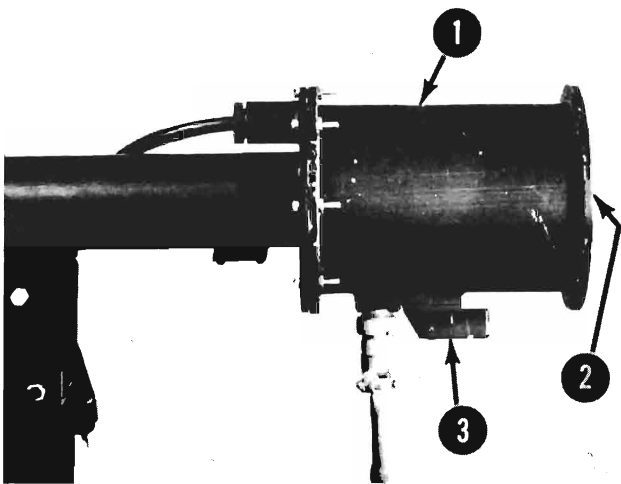


Fig. 6-3c.

New lamp housing having a rear window through which laser light enters. Control knob operates internal mechanism shown in Fig. 6-4. (1) Watertight lamp housing. (2) Laser light enters through a window in this end plate, (3) Control knob for mechanism shown in Fig. 6-4.



Fig. 6-3d.

Rear view of lamp housing showing window to admit the laser beam. (1) Window for laser beam to enter the projector.

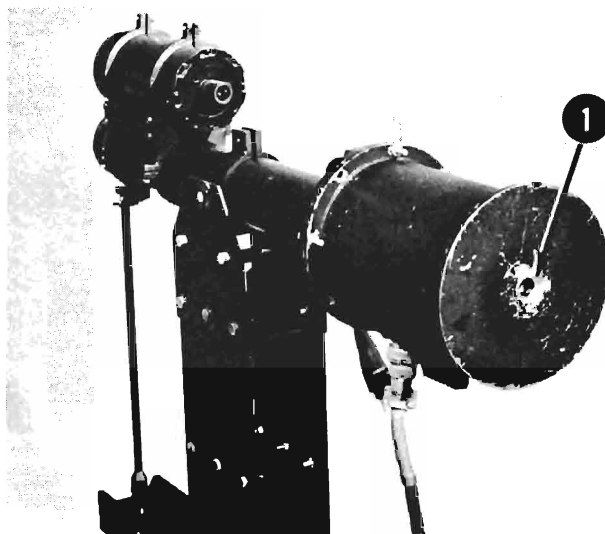


Fig. 6-3e.

RCA underwater laser mounted in position to inject its beam into the projector.

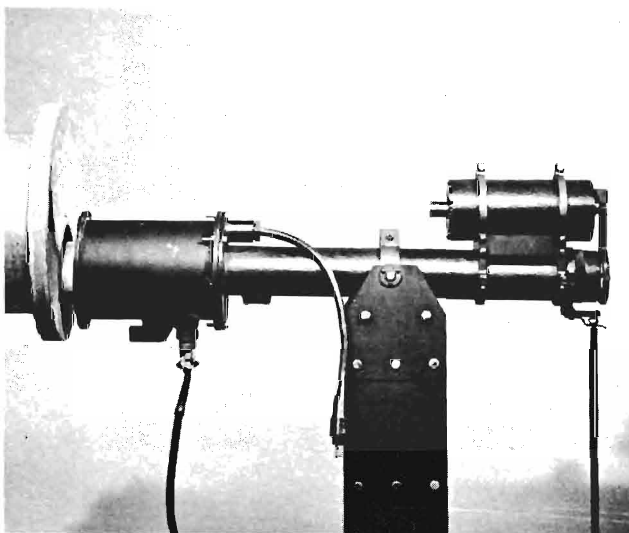
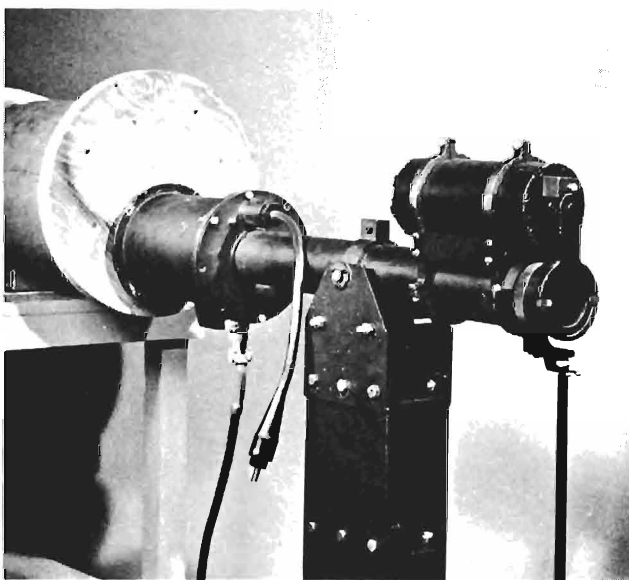
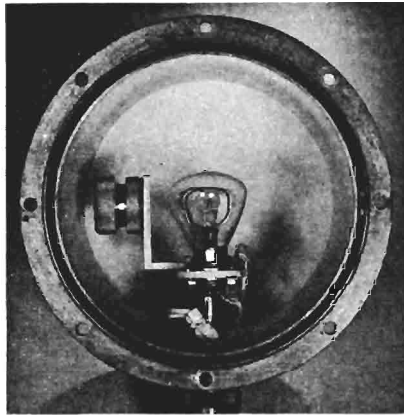


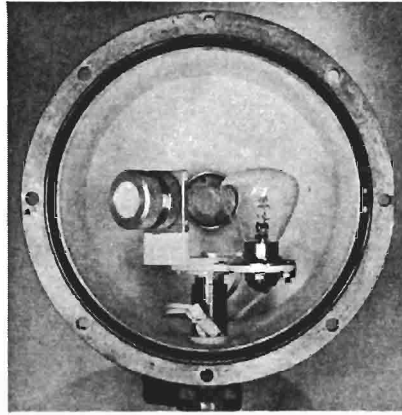
Fig. 6-3f.

Front view of RCA underwater laser attached to the modified underwater collimated projector.

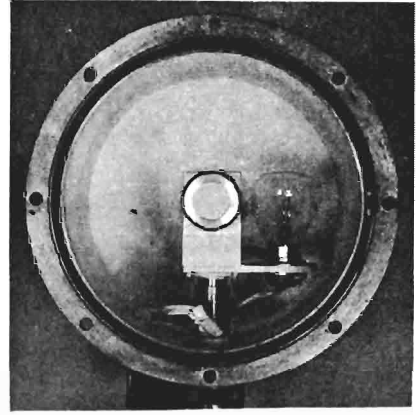




6-4(a)



6-4(b)



6-4(c)

Fig. 6-4. Interior of new lamp housing for the underwater collimated projector, showing 3-position internal mechanism. (a) Automobile lamp on-axis to provide light for visual alignment of the underwater projector. (b) Open pathway for laser beam to irradiate the on-axis beam-forming aperture (see Fig. 6-3b). (c) Diffuser inserted in the path of the laser beam.

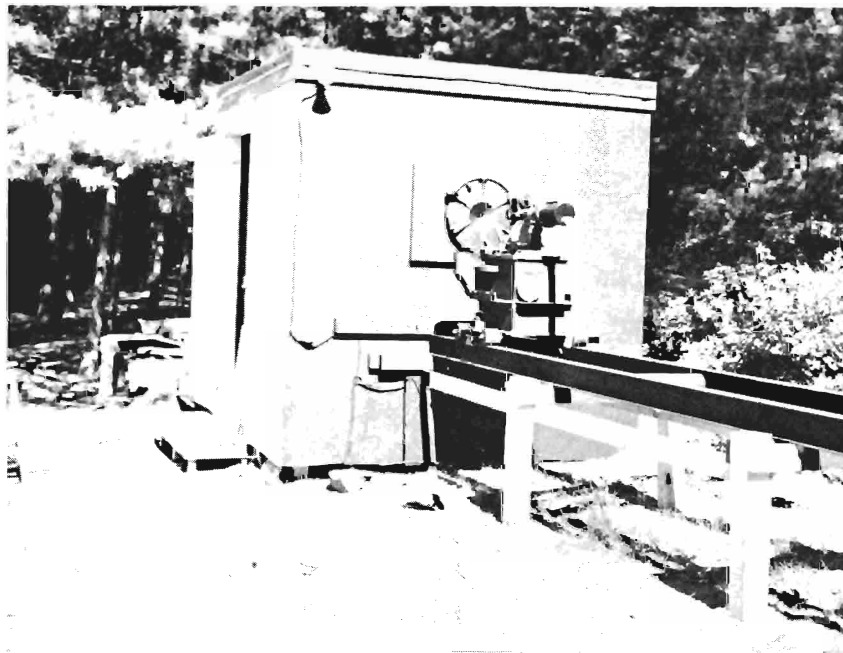


Fig. 6-5. "Air tower" and air track with underwater cart and collimated underwater incandescent projector. The laser-projector system (See Fig. 6-3f) was also used on the same mounting.



Fig. 6-6. Aerial view showing air tower and air track situated between the boat landing and the Laboratory building. Boat house and underwater tower, with curtain floating over the underwater track, is at lower right.

*Measurements in Water.* The experiment was transferred from the air track and "air tower" to the underwater track and underwater tower. No difference was found in the normalized irradiance on-axis produced by the collimated underwater projector using laser light or incandescent light from the concentrated-arc lamp. Both the laser and the incandescent arc produced values of irradiance-on-axis that matched the lower (dotted) curve in Fig. 6-1. Thus, it was demonstrated that identical values of normalized irradiance on-axis are produced, respectively, by a neodymium-doubled pulsed laser and by the collimated underwater incandescent projector when the geometry of the beam of laser light and the geometry of the beam of incandescent light are made identical.

#### MEASUREMENTS OF INTEGRATED IRRADIANCE

Experience with the RCA laser in 1964 served as a warning that a follow-on program based upon detailed mapping of the distribution of irradiance within the beam at each lamp distance was impracticable. It was decided, therefore, to integrate optically over the geometrical pattern of the beam and part of its surroundings by means of a flux-collecting aperture large compared with beam dimensions. This was achieved by fitting the window of the underwater tower with an integrating sphere having an entrance aperture as large as permitted by the optical glass insert in the 16-inch diameter Plexiglas window of the tower. Thus, the integrating sphere had an entrance aperture 4 inches in diameter. Only at extreme ranges did the major diagonal of the elliptical beam produced by the RCA laser become as large as 4 inches. The integrating sphere which was mounted inside the tower and in contact with the optical glass window integrated all of the flux which entered the 4-inch entrance port and delivered a proportional sample of this flux to the cathode of the multiplier phototube which was attached to a small side port on the sphere. In this way the half-inch photocathode of the end-on multiplier phototube was able to respond to the integrated flux entering the 4-inch diameter entrance port of the integrating sphere. Normal experimental precautions were

taken by means of interior baffles within the integrating sphere to make sure that no flux from the bright spot on the back of the sphere could reach the photocathode without multiple reflections on the sphere walls. Figure 6-7 shows the integrating sphere mounted on the measuring window inside the tower.

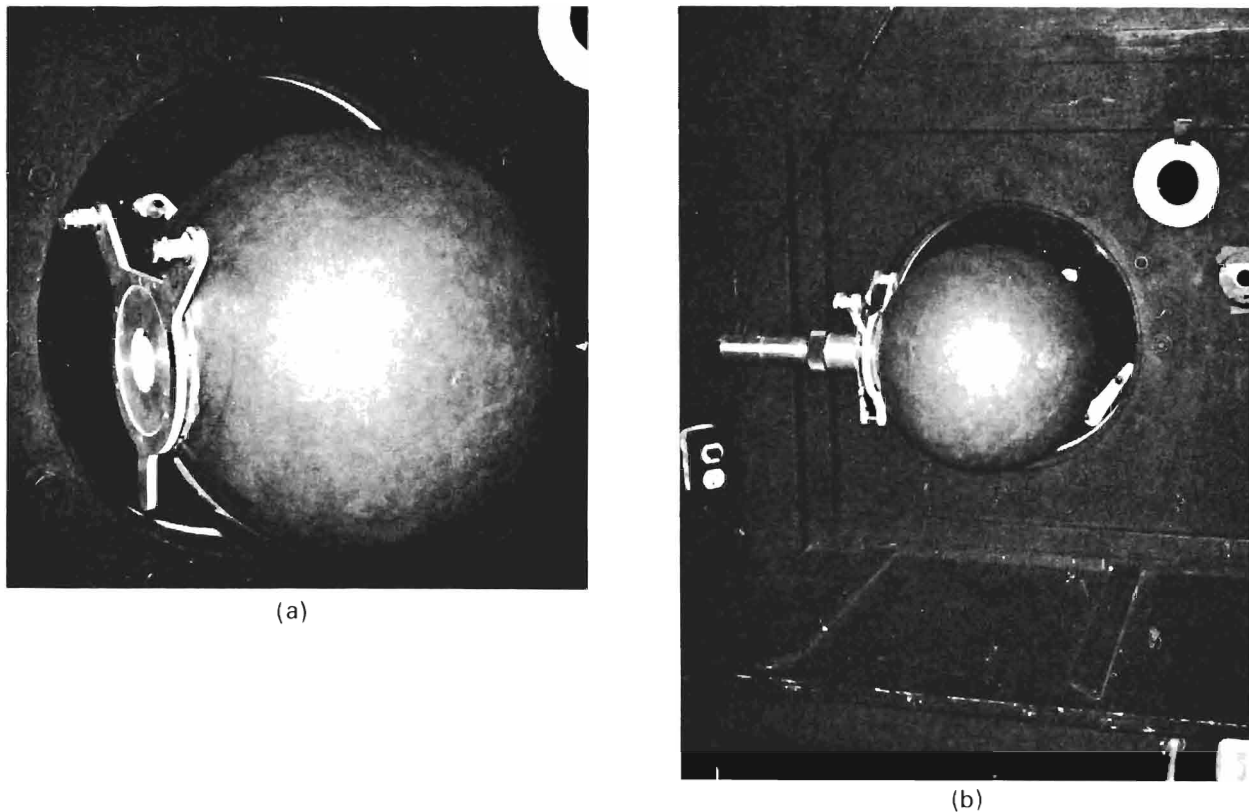


Fig. 6-7. Rear view of integrating sphere attached to inner (air) surface of the measurement window. (a) Without multiplier phototube. (b) With multiplier phototube in place.

Figure 6-8 is a plot of the integrated radiant flux collected by the 4-inch aperture at various lamp distances. For this experiment the full beam of the laser was used. A dramatic change in the shape of the curve is apparent when Fig. 6-8 is compared with Fig. 6-1. There is no evidence of the transition between near-field and far-field. Under all circumstances the curve is above the "alpha-line." Throughout the range of lamp distances from 1 to nearly 5 attenuation lengths, the curve is nearly parallel to the alpha line and approximately a factor of 2 above it. Beyond 5 attenuation lengths the curve begins to rise, its slope diminishes until, beyond 20 attenuation lengths, its slope agrees with the diffuse attenuation coefficient  $K$ , as indicated by the broken line which is used to extrapolate the last experimental point. Thus, just as in the case of irradiance measured at very long distances from lamps of any kind, the radiant flux collected by the 4-inch aperture is attenuated with distance at the  $K$ -rate.

A similar experiment was made using the narrow beam incandescent source. The resulting curve of integrated irradiance vs. lamp distance duplicated Fig. 6-8 exactly. Thus, the act of integrating the flux distribution over a diameter comparable to that ascribable to the total beam pattern causes the differences between the laser beam and the incandescent beam, which show so prominently on the axis, to disappear.

All evidence of the inverse square nature of the on-axis irradiance in the far-field portion of the curve has also disappeared. Thus integration over the beam and its immediate surroundings has caused the geometrical differences between the two beam geometries to cancel out, and the differences between near-field and far-field beam structures to no longer be noticeable. Obviously in applications in which the collection aperture or the reflector of the beam equals or slightly exceeds the cross-sectional dimensions normally ascribed to the "beam," the applicable propagation characteristics of the light field are as displayed by Fig. 6-8. Only when the receiver aperture is small compared with beam dimensions do the kind of effects shown by Fig. 6-1 appear. It is significant, however, that at long range the propagation is governed by the K-rate of attenuation. Since this is true both on the axis of the beam and for the integrated irradiance produced by the whole beam, it follows that all portions of the beam will be attenuated at the K-rate at long lamp distances, although the onset of this favorable rate of attenuation may be different throughout the beam pattern.

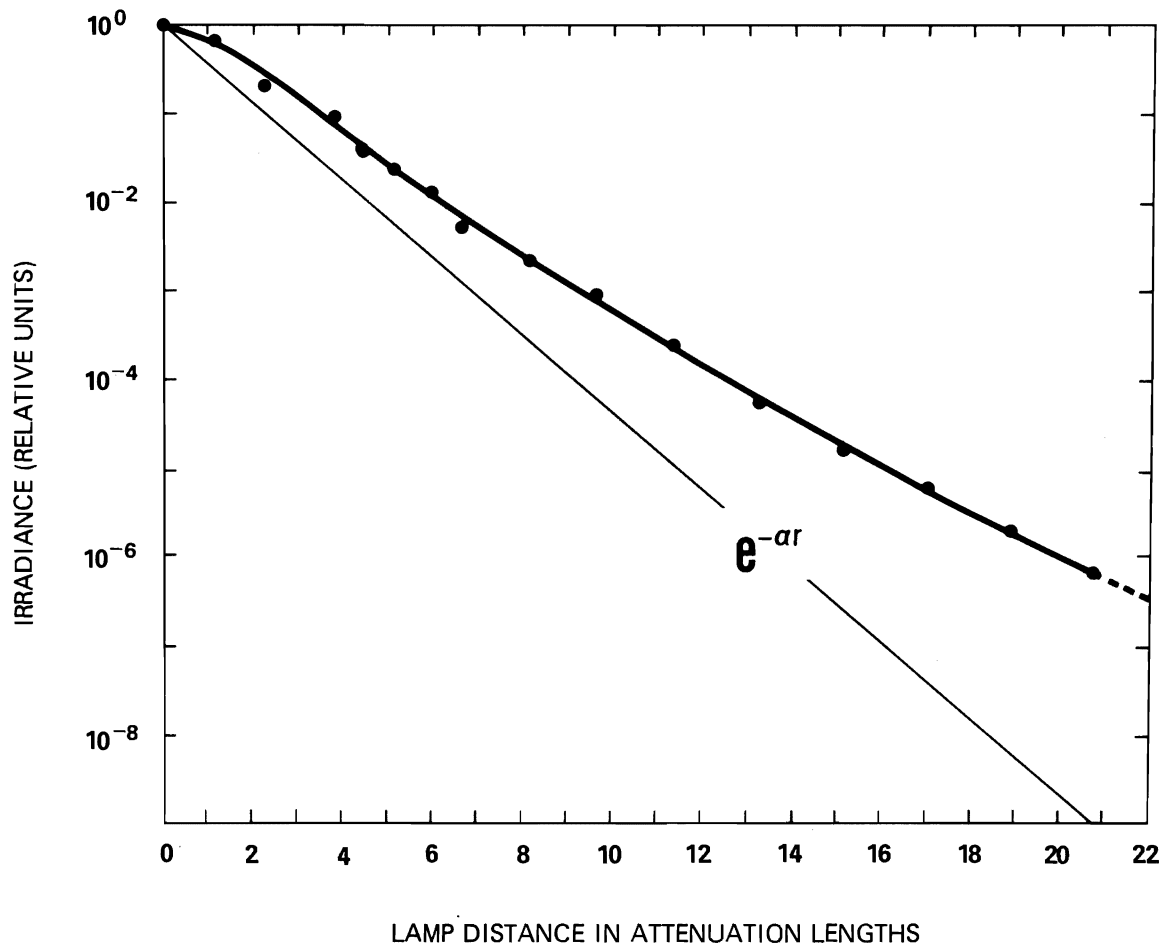


Fig. 6-8. Integrated irradiance collected by the integrating sphere at various laser distances.

## EFFECT OF COMPRESSED DIVERGENCE

There has been an intuitive feeling on the part of some of those concerned with underwater lasers that more favorable transmission characteristics can be obtained by using an optical system to compress the beam. Several laboratories have conducted experiments with beam-compression optics added to the laser. In order to make a test of this hypothesis, an optical system capable of compressing the divergence of the laser beam by a factor of 10 was constructed. This is simply a 10-power telescope focused on infinity. The scope was constructed of available high quality lenses and provided with a watertight enclosure having plane windows.

A fixture was built such that the telescope could be easily added (or removed) from the path of the light from the underwater laser; it is shown in Figs. 6-9 and 6-10. The fixture was an attachment to the existing shelf, shown in Figs. 5-3, 5-4, and 5-5. The upper assembly involving the collimated underwater incandescent projector (see Fig. 5-3) was not used because it was optically incompatible with the telescope. The lower prism was not removed from the shelf (see Figs. 6-9 and 6-10) but it played no part in the experiment because the laser beam passed through the clearance hole in the prism. The fixture was provided with adjustments for aligning and centering the axis of the telescope with the laser beam. In order to insure adequate clearance of all of the stops within the telescope, the diameter of the laser beam was reduced to 0.050 inches by means of a stop in the water close to the laser output aperture.

It was necessary to devise a new system for aiming the laser, since the system described in Section 5 and illustrated in Fig. 5-1 could not be used. A small collimated underwater incandescent projector, shown in Fig. 6-11 was designed to fit in the brackets of the shelf attached to the laser. Figure 6-12 shows the small projector in place. This alignment lamp used a 10-watt zirconium concentrated-arc lamp to produce a collimated beam of white light having approximately the same diameter and divergence as did the laser through the 0.050" diameter beam stop (see Fig. 6-10). This beam was visible from the underwater tower and could be used to center the laser beam on the measuring aperture. It was much more difficult to use than the aiming system shown in Fig. 5-3; the time required for alignment was substantially increased. Swimmers had to remove the alignment lamp after each alignment and replace it after the laser flashes had been recorded by the oscilloscope cameras. Only if the alignment beam returned to its original position in the entrance aperture of the integrating sphere were the data accepted. Many sets of data had to be discarded, particularly at large lamp distances, because the alignment was found to be disturbed in the process of removing the alignment lamp and replacing it again. Nevertheless, integrated irradiance data were secured with and without the beam compressing telescope to a lamp distance of more than 17 attenuation lengths. No improvement in integrated irradiance at any distance resulted from the ten-fold reduction in beam divergence.

Figure 6-13 shows the result of measuring the flux collected by the integrating sphere at various lamp distances. The solid curve has been passed near the points representing the performance of the laser without the telescopic attachment. The shape of this curve is quite similar to that shown by Fig. 6-8, the only difference being the effect of reducing the diameter of the beam at the source. The measurements were repeated after the divergence compressing optics had been added and the results are shown by stars. Obviously no appreciable effect was produced. The stars lie slightly below the solid line, presumably because of loss of light within the telescope. It may be noted that a 10-fold compression of divergence is necessarily accompanied by a 10-fold increase in beam diameter at the exit pupil of the telescope and by a 100-fold increase in the distance at which the near-field-far-field transition takes place within the beam

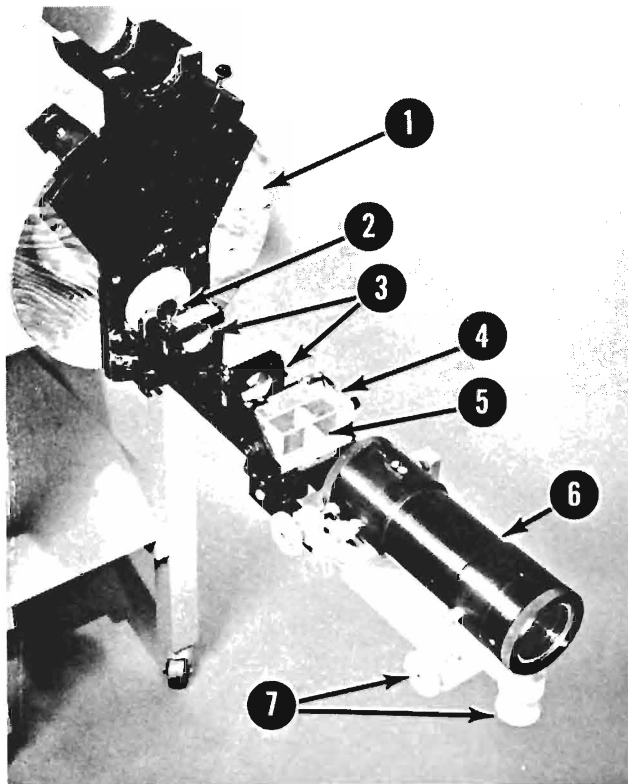


Fig. 6-9.

Beam-compressing telescope attachment for RCA underwater laser. (1) Mock-up of RCA laser, (2) 0.050 in. diameter beam stop, (3) Mountings for alignment lamp, (4) Prism, (5) Clearance hole for laser beam, (6) 10X telescope, (7) Alignment adjustments for telescope.

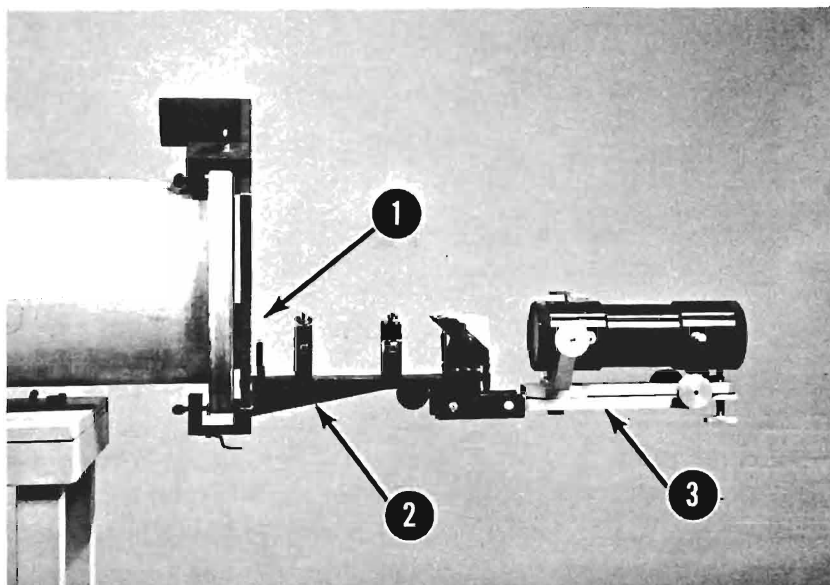


Fig. 6-10. Side view of beam-compressing telescope. (1) 0.050 in. diameter beam stop, (2) Shelf attached to laser, (3) Mount for telescope.

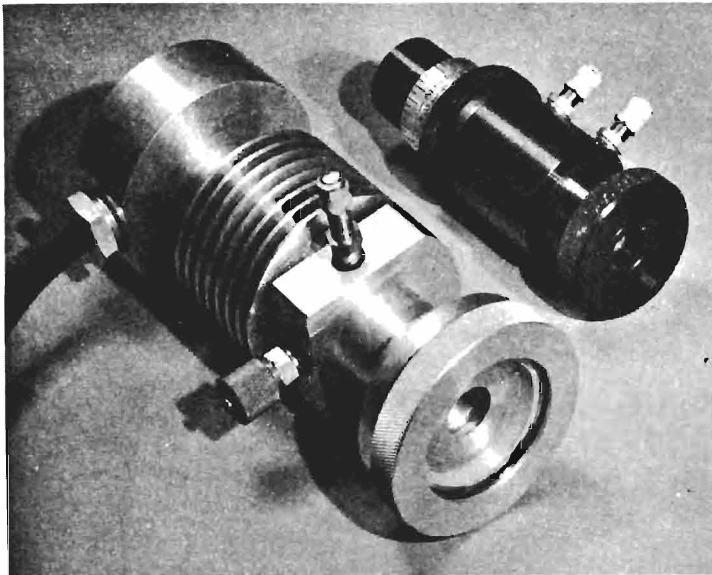


Fig. 6-11.

Small collimated underwater incandescent projector used for beam alignment with the beam-compressing telescope. Black cylindrical device (upper right) contains a dove prism, sometimes used to rotate the laser beam about its axis.

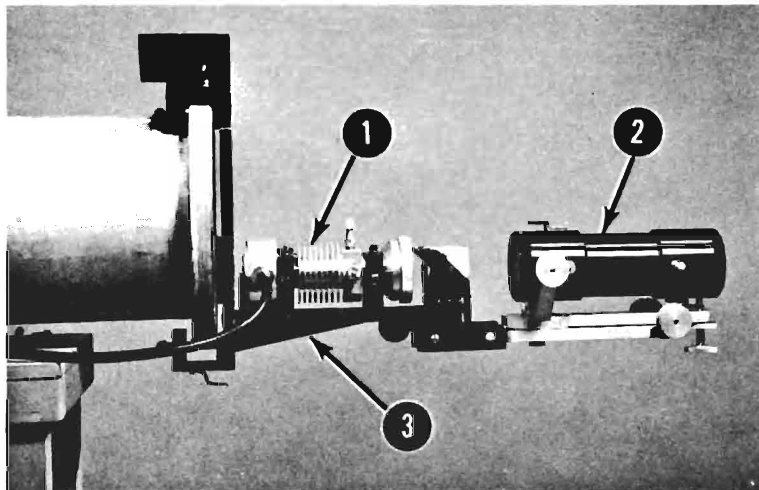


Fig. 6-12.

Small collimated underwater incandescent projector in position for use in beam alignment. (1) Alignment lamp, (2) 10X telescope, (3) Shelf attached to laser.

pattern. The transition point for the normal beam, which occurs (see Fig. 6-1) at a lamp distance of 0.4 attenuation lengths, is extended to 40 attenuation lengths by the use of the beam-compressing optics. Thus, in Fig. 6-13 virtually all of the data represented by the solid line are in the far-field portion of the beam whereas all of the data represented by the stars are for conditions within the near-field portion of the beam having compressed divergence. This is further evidence that no measurable difference is found between the near-field and far-field conditions with respect to the integrated radiant flux in and near the beam.

#### TWO-WAY SYSTEMS

It is interesting to consider the sort of propagation characteristics that should be found with a two-way underwater system in which a narrow beam source (laser or conventional), is used to irradiate a dif-



fuse perfectly reflecting object comparable in size to the 4-inch aperture of the integrating sphere used in obtaining data for Figs. 6-8 or 6-13. After reflection by such an object the flux will spread just as it does from a divergent source. The two-way power characteristic can then be inferred simply by combining the experimentally determined curve for a divergent source, such as that shown by the dashed line in Fig. 5-7, with the data on the flux content of the outgoing beam, illustrated by Fig. 6-8. A simple means for making this combination is as follows. At each lamp distance measure downward from the upper boundary of the figure to the curve in Fig. 6-8 and, at the same lamp distance, measure downward to the dashed curve in Fig. 5-7. Since the scale of irradiance is logarithmic, these two values should be added together in order to provide a point on the two-way transmission characteristic. The result of performing this construction at each lamp distance is illustrated in Fig. 6-10. It will be noted that for very small lamp-to-object distances the inverse square characteristic of the return path after diffuse reflection is dominant. In the portion of the curve between 1 and 2 attenuation lengths, the characteristic is parallel to the "2 alpha line" which is shown on the figure. At long lamp-to-object distances, beyond 9 attenuation lengths, the line is virtually straight and at the 2K-slope.

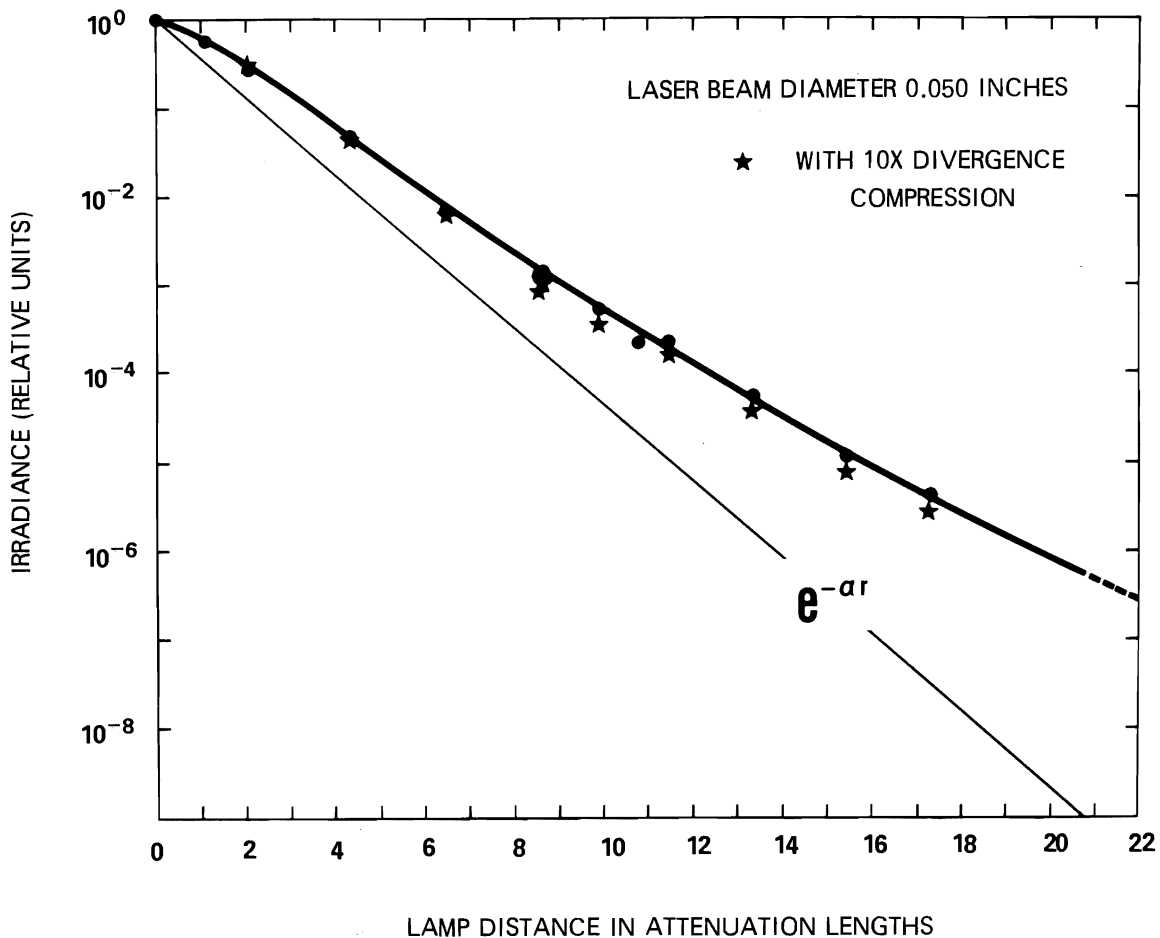


Fig. 6-13. Integrated irradiance collected by the integrating sphere at various laser distances, with (stars) and without (solid circles) the divergence compressing telescope shown in Fig. 6-9.

## THE POWER BARRIER

It is an interesting consequence of Fig. 6-14 that the first 7 or 8 attenuation lengths of lamp distance can be regarded as a *power barrier*, in the sense that beyond that distance increased range is obtained with increased power in accordance with the 2K-slope rather than (say) the 2-alpha slope. The ratio  $\alpha/K$  is, typically, 2.7 in clear ocean water. In Fig. 6-14 irradiance at the receiver aperture is reduced by a factor of approximately  $10^8$  in the first 8 attenuation lengths of 2-way path and by a factor of roughly  $10^4$  in the second 8 attenuation lengths.

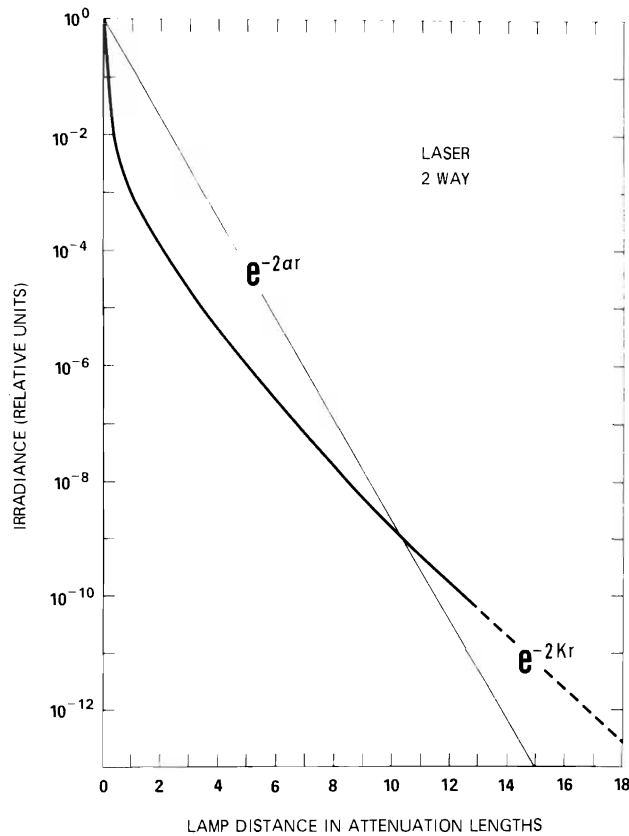


Fig. 6-14. Received irradiance from a 4-inch diameter perfectly reflecting diffuse object at various distances in a 2-way laser system.

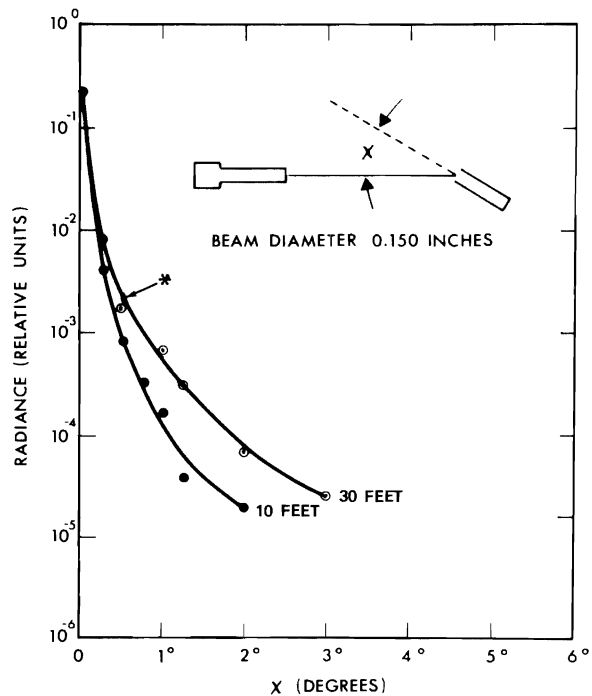
## 6.3 RADIANCE DISTRIBUTIONS

When a photograph is made of an on-coming laser beam, the impression is obtained that the radiance distribution drops dramatically at the edge of the beam and that very little radiance is derived from portions of the field of view which make appreciable angles with the axis of the beam. This concept is supported quantitatively in Fig. 6-15 which depicts the result of radiance distribution measurements made by means of a photoelectric telephotometer having a field of view one-fourth degree in angular diameter. This telephotometer was placed with the center of its entrance pupil on the axis of the narrow beam incandescent source and the unit was then rotated about the center of the measurement window as shown at the top

of Fig. 6-15. The diameter and divergence of the beam from the incandescent narrow beam projector were arranged to simulate that produced by the RCA underwater laser. Measurements were made at lamp distances of 10 feet and 30 feet and the results are shown by the two curves in Fig. 6-15. These curves illustrate the dramatic decrease in apparent radiance of the light field and show that the apparent radiance has dropped by four orders of magnitude only 2 or 3 degrees from the axis of the beam. The angular coverage of the radiance distribution is seen to be slightly greater when measurement is made at the lamp distance of 30 feet than when a 10-foot lamp distance is used. An attempt was made to measure the radiance distribution at a lamp distance of 50 feet but the sensitivity of the photoelectric photometer was insufficient to perform this measurement beyond approximately two-thirds of a degree. Up to that point, however, the curve was identical in shape with that obtained at 30 feet. The most distant 50-foot point is indicated in Fig. 6-15 by an arrow terminating in an asterisk.

Fig. 6-15.

Angular distribution of received radiance from the underwater laser at ten feet and thirty feet.



#### 6.4 RECEIVER FIELD OF VIEW

Many investigators have been concerned over the proper field of view to incorporate in receivers for laser beams, i.e., in 1-way systems. Throughout the Diamond Island experiments it has been normal policy to use receivers with complete hemispherical collection capability as typified, for example, by the aperture of an integrating sphere. Figure 6-15 indicates that no such wide-field collection aperture is necessary and suggests that an angular radius of the field of view as small as 2 or 3 degrees should suffice to collect most of the available flux. As a test of this belief, the telephotometer was aimed directly at the narrow beam source and its field of view was increased by means of changing field stops so that its field of view was increased successively to from 1/4 degree to 1/2, 1, 1-1/2, and 2 degrees. The result of this

procedure is given in Fig. 6-16. It should be noted that this figure plots the angular diameter of the receiver field of view whereas the data in Fig. 6-15 relate to the angular radius of the field of view. The curves in Fig. 6-16 would indicate that receivers having fields of view 5 or 6 degrees in angular diameter should be adequate.

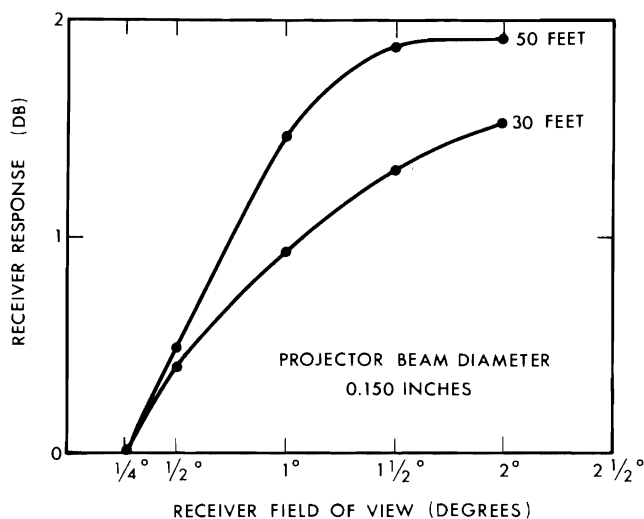


Fig. 6-16. Receiver response for various receiver fields of view at projector distances of 30 and 50 feet. Projector and receiver are coaxial.

## 6.5 DIAMETER OF THE RECEIVER APERTURE

Questions concerning receiver field of view discussed in the preceding paragraph should be distinguished carefully from effects having to do with the diameter of the receiver aperture or the diameter of the object used to reflect the light from an underwater laser. In order to gain information concerning the distribution of irradiance on the surface of a sphere centered on the source of the light beam, a limited series of experiments were made during the 1965 series in which the collimated underwater incandescent projector was rotated about its exit pupil in the manner depicted by the small sketch in Fig. 6-17. In this case the photoelectric telephotometer was replaced by a photoelectric irradiance meter having a small collection aperture (0.010 inches diameter). Data were obtained at a lamp distance of 30 feet as shown by the round points through which a curve has been passed. Data could not be secured between approximately 1/10th degree and 3 degrees because of the interference of mechanical structures (window edges, reinforcing rings, and instrument mountings) at the window of the underwater tower. Nevertheless the shape of the function seems quite well defined. Photoelectric sensitivity was sufficient to measure the irradiance curve only to 10 degrees. The purpose of taking these data with the incandescent narrow beam lamp was conceived as establishing a guide line for a similar curve to be done with the laser. This experiment was conducted on the last scheduled night of operations during 1965 and on that occasion the laser developed a malfunction before any data were obtained. The laser was returned to the RCA laboratories for repairs but no further data could be taken because both time and funds were exhausted. Thus, laser data corresponding with Fig. 6-17 were not secured in 1965.\*

\* Measurements of off-axis irradiance dominated the experimental program in 1966 and thereafter. Lasers were used almost exclusively.

The curve in Fig. 6-17 clearly indicates that the 4-inch diameter aperture in the integrating sphere was by no means large enough to include all of the flux or even a large fraction thereof. For example, at 30 feet the last point (at approximately 10 degrees) corresponded with a linear offset on the irradiated plane of about 5.3 feet. Obviously, an integrating sphere with an aperture 5.3 feet in radius would have been necessary to have collected all of the flux in the irradiation pattern out to the last point plotted on the figure. How much of the total flux this represented cannot be ascertained from these data. Since the area of a circular zone on the irradiated plane and centered about the axis of the beam is linearly related to the radius of the zone, an integration is necessary in order to interpret the data shown in Fig. 6-17 in terms of the fraction of the total flux which is incident on the portion of the irradiated spherical surface contained within a circle of any given radius. An arbitrary log-linear extrapolation was made of the irradiance data beyond 10 degrees in Fig. 6-17 so that a cumulative integral curve could be generated. This calculated result is shown in Fig. 6-18. It predicts that half of the total flux on the irradiated surface falls outside a circle more than 5 feet in diameter or at an angle  $\phi = 9.5^\circ$  in terms of the geometry depicted at the top of Fig. 6-17. This illustrates that the cloud of scattered light accompanying the beam, dim though its irradiance may be, contributes importantly to the total flux reflected by a large object when irradiated by a small beam of light and that the shape of curves like Fig. 6-8 must be profoundly influenced by the diameter of the collecting surface. These deductions were explored much more fully during the series of experiments at Diamond Island during 1966. The shape of the curve in Fig. 6-8, for example, is explained in terms of the 1966 data by Fig. 8 of the letter quoted in Section 6.6.

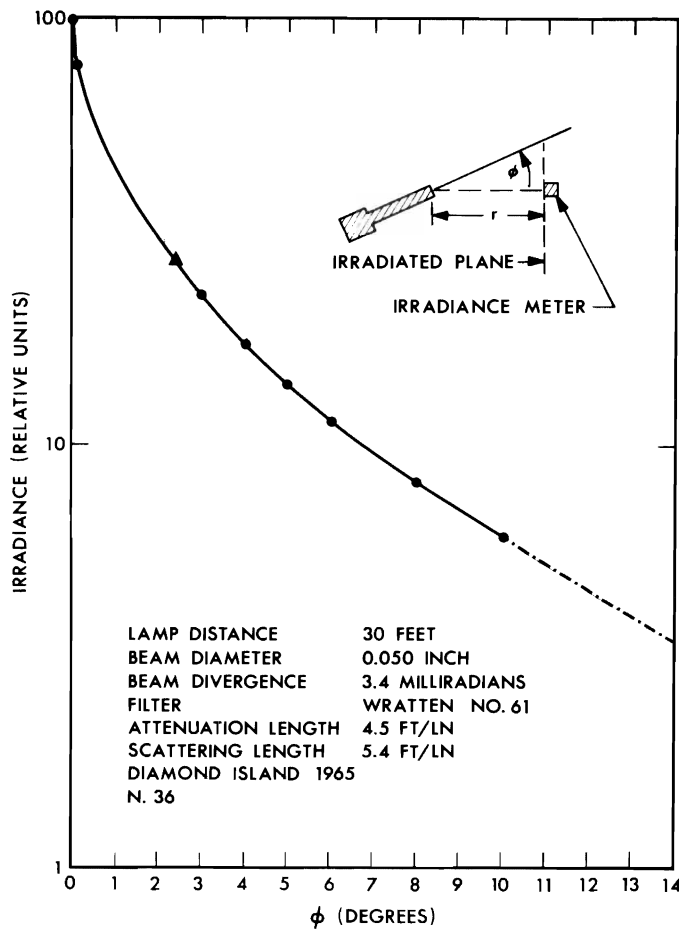


Fig. 6-17

Off-axis irradiance at a lamp distance of 6.7 attenuation lengths.

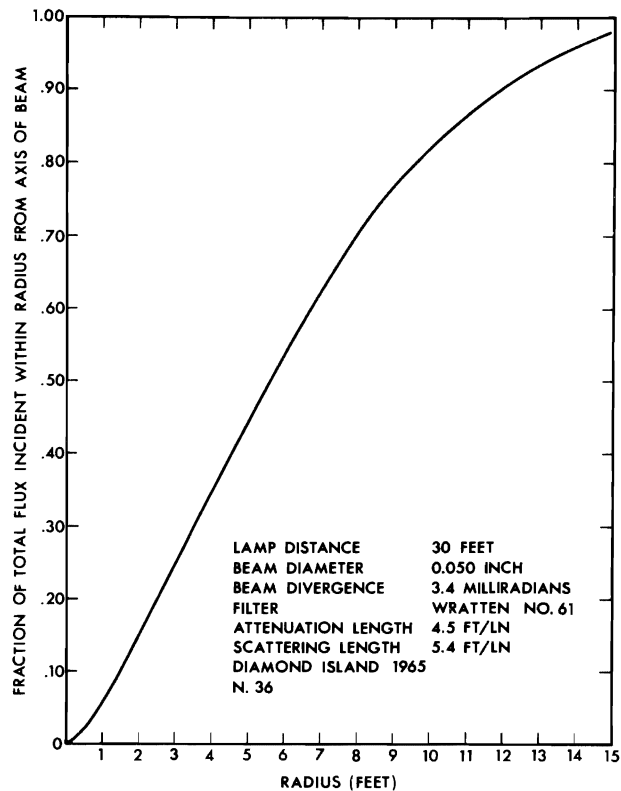


Fig. 6-18. Integral of Fig. 6-17.

## 6.6 STUDIES OF IRRADIANCE OFF-AXIS

The principal experiments at the Diamond Island field station during July and August 1966 concerned the distribution of off-axis irradiance produced by the underwater green laser. Measurements were made at angles up to 58 degrees from the beam and at lamp distances out to more than 19 attenuation lengths. These data were obtained by mounting the underwater laser on the remote-control cart which ran along the track outside the measurement window of the underwater experimental tower at Diamond Island and rotating the laser in a horizontal plane about the point at which the laser beam left the laser case and entered the water. The mechanical drives for this cart, constructed in 1962, limited the horizontal angular rotation to 58 degrees. As will be seen from the data which follow, this was a sufficient angle for the purposes of the research. Angular scans were made at lamp distances of 0, 5, 15, 30, 45, 60, 75, and 90 feet. Preliminary reduction of the off-axis irradiance laser data revealed many basic principles. It also explained the causes of certain important effects that had been observed earlier.\* A letter report dated 10 December 1966 presented the preliminary data and interpreted it. That letter was made available by ONR through the Defense Documentation Center as No. AD 647791 and has been widely quoted throughout the report literature. It is reproduced here from the original typed pages:

\* For example, the shape of the curve in Fig. 6-8 is explained by the curve marked "integrating sphere data" in Fig. 7 in the letter-report of 10 December 1966.

It is the purpose of this letter to make a preliminary report of the principal results I obtained at the Diamond Island Field Station last summer with the RCA underwater green laser which was loaned to us by the U.S. Naval Air Development Center. The research was supported jointly by ONR under contract Nonr-2216(14) and by NADC under contract N 62269-3097. The results are summarized by the figures attached to this letter. This letter and its figures continue and extend my letter of 12 March 1966 to Mr. Isakson and my previous letters, all of which concern the studies I have made in previous years with the underwater green laser under contract Nonr-2216(14). All of this material will be included in a summary report which is now in preparation.

The experiments at the Diamond Island Field Station during July and August 1966 followed the plan discussed on pages 9, 10, and 11 of my letter to Mr. Isakson of 12 March 1966. The principal topic of the present letter concerns the distribution of flux on an irradiated surface perpendicular to the axis of the beam produced by the underwater green laser at angles up to  $58^\circ$  and at lamp distances out to more than 19 attenuation lengths. Various other ancillary investigations arising from the discussions contained in my letter to Mr. Isakson of 12 March 1966 were made and will be reported in detail later. For the sake of completeness, however, a summary statement of the findings on some of these topics can be given as follows:

1. The differences between the on-axis irradiance produced by the narrow beam incandescent projector and the irradiance on axis produced by the underwater green laser illustrated by the curves in Fig. 3 attached to my letter of 12 March 1966 to Mr. Isakson and discussed on page 3 of that letter were found to be attributable to the differences in beam geometry between the light produced by the two sources, as suggested on page 4 of my letter of 12 March 1966. When the radiation produced by both lamps was compared under conditions of identical beam geometry, the on-axis irradiance curves, like those in Fig. 3, were found to agree.

2. Further studies of narrow angle forward scattering were made with the newly completed coaxial scattering meter constructed by the Visibility Laboratory for NADC and operated at Diamond Island by NADC personnel. Concurrent independent measurements of the attenuation coefficient and the absorption coefficient of the water enabled former results concerning the magnitude and importance of narrow angle forward scattering to be verified and inferences drawn concerning the nature of the scattering at even smaller forward angles than have yet been measured.

3. The measurements depicted by Fig. 10 attached to my letter to Mr. Isakson of 12 March 1966 concerning the distribution of light on a surface at right angles to the beam produced by the narrow beam projector at a lamp distance of 30 feet were repeated and extended somewhat in angle from the axis. Good agreement with the curve in Fig. 10 was found and the calculations and conclusions drawn from these data and illustrated by Figs. 11 and 12 of my letter of 12 March 1966 were thereby supported. Similar data were obtained using the narrow beam incandescent projector at other lamp distances. These will be reported in detail later but it may be said in summary that they are in agreement with corresponding data obtained with the underwater green laser,

which will be reported in detail later in this letter. Thus, all of the underwater lighting distributions thus far measured are identical for the light from the narrow beam incandescent projector and the RCA underwater green laser when both have similar beam geometry.

#### Power Distributions Produced by the Laser

The principal goal of the experiments performed at the Diamond Island Field Station during 1966 was a study of the distribution of radiant power produced underwater by the RCA green laser over a wide range of angles from the beam and as a function of lamp distance. These data were obtained by mounting the underwater laser on the remote-control cart which runs along the track which extends horizontally from the sensor port of the underwater experimental tower at Diamond Island and rotating the laser in a horizontal plane about the point at which the laser beam left the laser case and entered the water. The mechanical drives for this cart, constructed in 1962, limited the horizontal angular rotation to  $58^\circ$ . As will be seen from the data which follow, this was a sufficient angle for the purposes of the research. Angular scans were made at lamp distances of 0, 5, 15, 30, 45, 60, 75 and 90 feet. The beam pattern of a typical second harmonic neodymium green laser is shown in Fig. 4 of my letter of 12 March 1966. Although this was the beam produced by such a laser built by the Lear-Siegler Corporation, it represents rather well the beam pattern made by the 1966 model RCA green laser because the KDP crystal is outside the resonant cavity in both lasers. Detailed beam pattern studies were made and will be reported later. Also, detailed irradiance distributions within the geometrical confines of the laser beam were measured at some distances and these will also be reported later. Inasmuch as this level of angular detail is not necessary for the principal investigation reported herein, experimental time was saved by using an integrating sphere having an opening 4 inches in diameter to measure the average irradiance near the center of the pattern where the extreme asymmetries are encountered. After the beam had been rotated sufficiently from the optical axis above the cart track, the angular dependence on beam geometry had smoothed out sufficiently so that only two directions of measurement were necessary in order to get a sufficiently complete specification of the power distribution. Because the angular rotation mechanism within the cart allowed for only horizontal motions of the laser beam, an attachment containing a dove prism was built for the laser so that the direction of the major axis of the "ellipse" could be controlled at will. Irradiance distributions as a function of beam rotation angle were made with the major axis of the "ellipse" horizontal and vertical, respectively. At angles beyond  $7^\circ$  rotation of the dove prism produced no measurable effect. That is to say, at off-axis angles in excess of  $7^\circ$  the light produced by the laser had circular symmetry with respect to the axis of the beam.

Figure 1 depicts the measured value of irradiance out to off-axis angles of  $58^\circ$  at the various lamp distances listed in the preceding paragraph. During most of these measurements the water was characterized by an attenuation length of 4.54 ft/ln, an absorption coefficient of 0.0446 ln/ft, a diffuse attenuation coefficient K of 0.0523 ln/ft, and an attenuation coefficient to absorption coefficient ratio of 4.94. It was, of course, impossible to obtain the many hundreds of oscilloscope pictures required for this study in a single night. The optical constants of the water varied slightly from night to night so that data obtained on occasions when the water had slightly different properties have been adjusted in proportion to attenuation lengths so that they conform as closely as possible to the values given above. In all such cases the water had a greater attenuation length than 4.54 ft/ln; the greatest value which occurred during the taking of the irradiance data shown in Fig. 1 was 4.94 ft/ln. The irradiance data shown by Fig. 1 represents the peak value



of the oscilloscope traces. The measurements were made with an RCA No. 7767 multiplier phototube and a Tektronix Model 585 oscilloscope. This equipment has sufficient temporal resolution to exhibit the pulse shape of the light arriving at the irradiance collector. Examination of the oscilloscope traces makes it clear that there is a considerable pulse spread when the measurements are made at long distance and at large angles from the axis of the laser beam. Figure 2 shows typical waveforms selected because the peak amplitudes chanced to be the same. The dashed curve shows the waveform as received by the irradiance collector at 90 feet from the laser and only  $0.1^\circ$  off the axis of the beam. The solid curve shows the waveform received at the same lamp distance but with the laser rotated to place the measuring irradiance meter  $58^\circ$  off the axis of the beam. Integration of the area under these curves shows that 2.1 times as much power is included in the oscillogram depicting conditions at  $58^\circ$  than is included in the curve measured at  $0.1^\circ$  from the laser beam axis. Corresponding measurements of what I have called the "pulse stretch factor" have been made from a few other oscilloscope pictures at other lamp distances and other angles from the beam. This work is by no means complete since there are literally thousands of oscilloscope pictures which can be studied in this way. The results thus far have been summarized by some straight-line models depicted by Figs. 3 and 4. This model of the pulse stretch factor has been used for preliminary correction of the irradiance data in Fig. 1. Since the effect is not large, particularly at the smaller angles where the principal contributions to the total power are found, it is probable that no more elaborate and detailed study of the pulse stretch factor will change the conclusions of this study. Nevertheless, it is expected to look at this matter in greater detail when time permits.

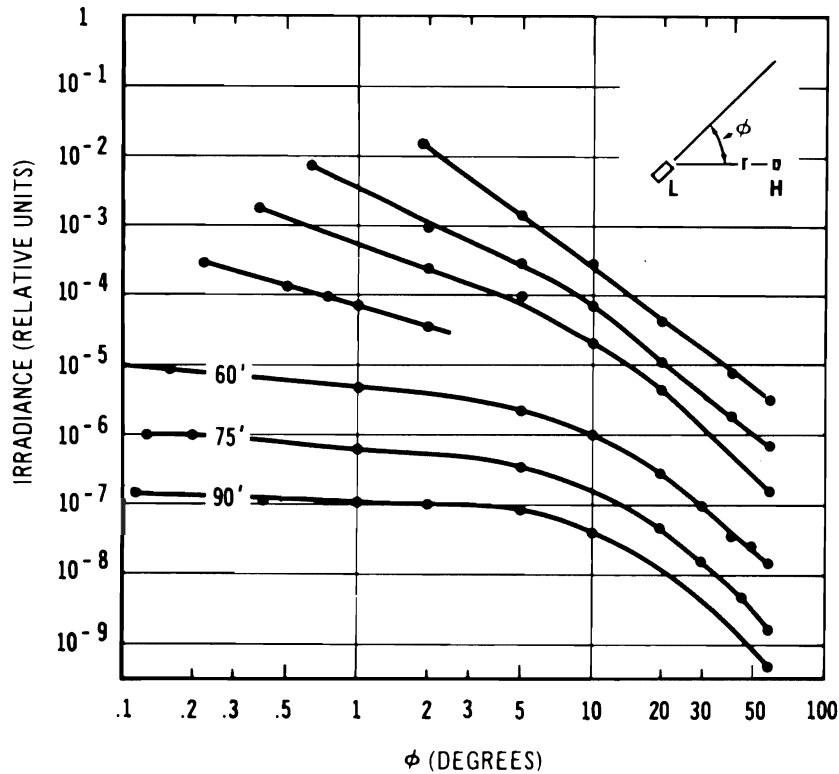


Figure 1

Figure 2

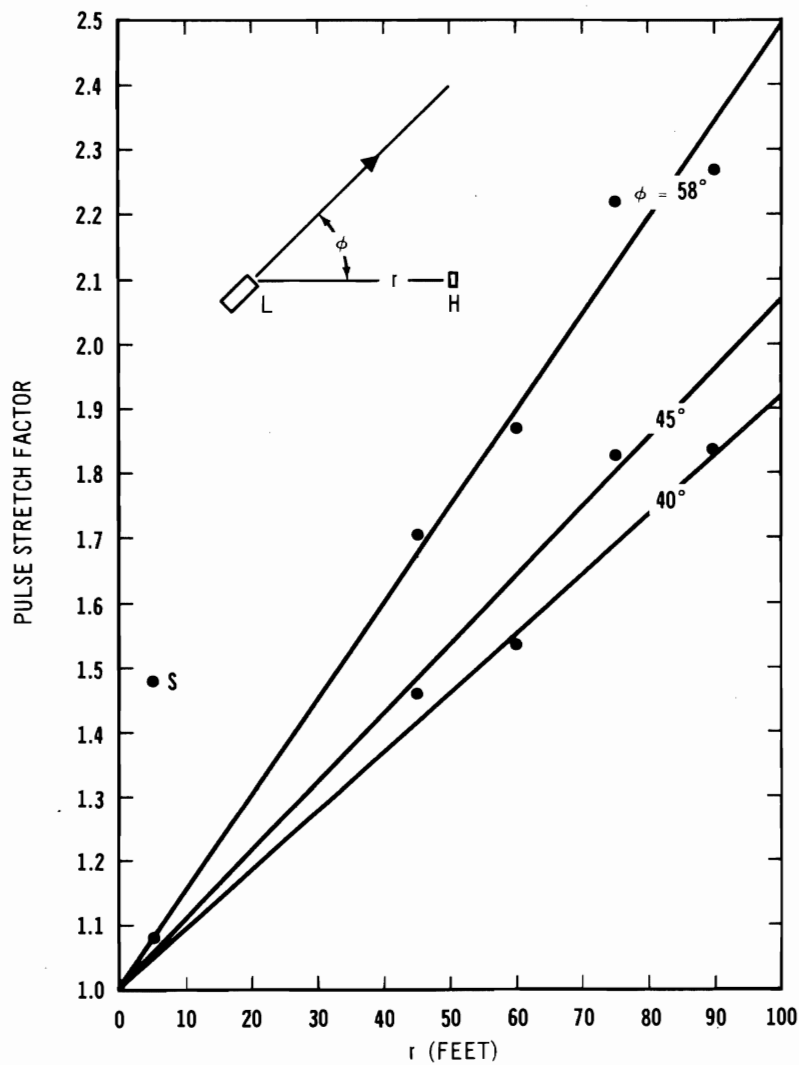
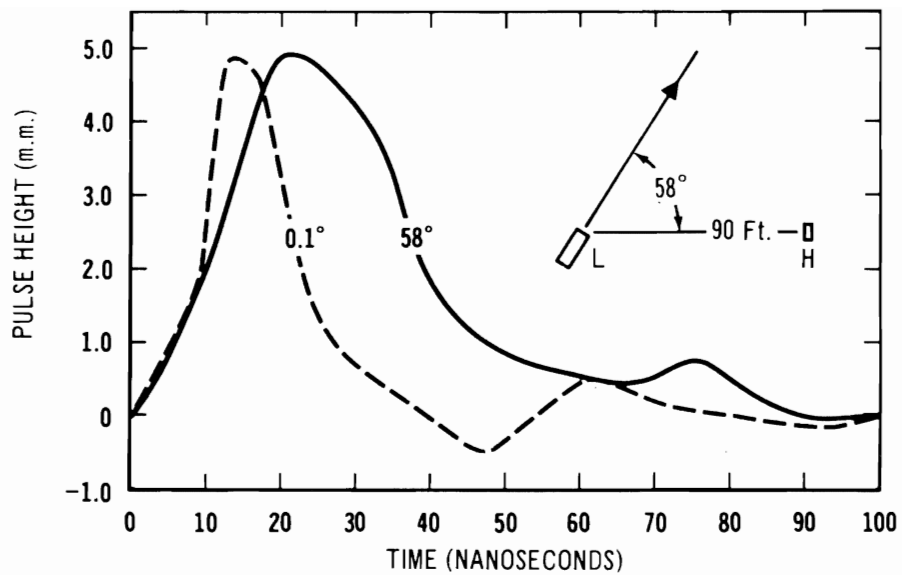


Figure 3

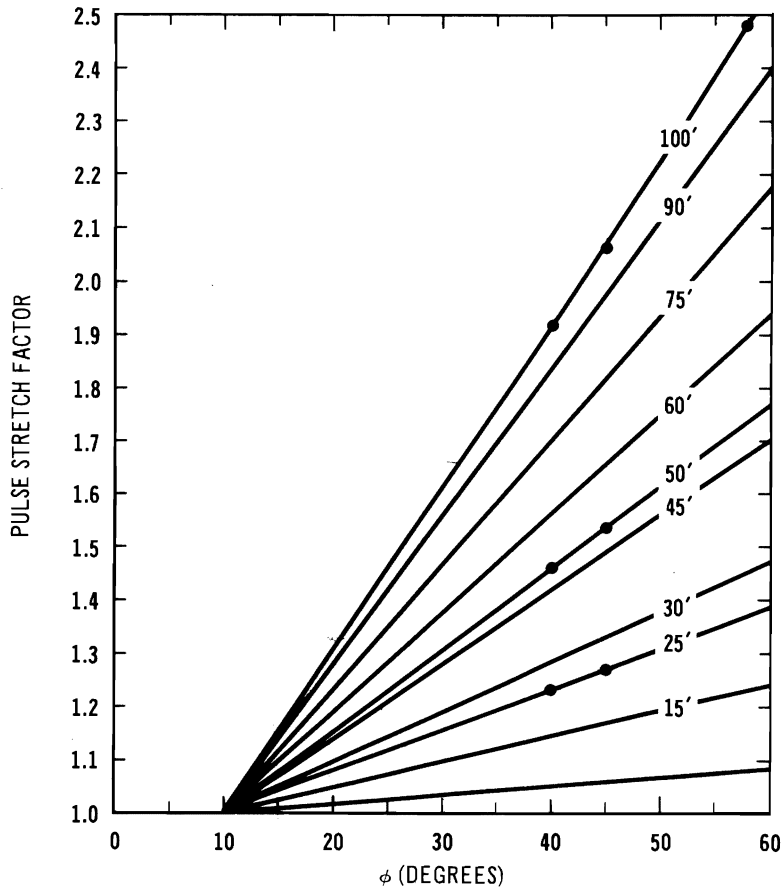


Figure 4

A computer program was prepared so that the irradiance data in Fig. 1 could be converted readily into information concerning the total radiant power received by a surface at right angles to the laser beam within a circle bounded by any selected angular radius from the beam. The result of such computer integration, corrected for pulse stretch factor on the basis of Figs. 3 and 4, is shown in Fig. 5.

The small diagrams appearing in the upper right hand corners of both Figs. 1 and 2 are plan views which illustrate how the laser beam was rotated in a horizontal plane with respect to the fixed irradiance meter in order to study the distribution of radiant power at off-axis angles. The small diagram in the lower left hand corner of Fig. 5 illustrates that this procedure is equivalent to leaving the laser beam fixed in space and moving the irradiance collector along the arc of a circle of radius  $r$  through off-axis angles as depicted by the dashed circular arc. The computer program referred to in the preceding paragraph produces values, in relative units, of the total power received by an imaginary concave, spherical surface centered on the point at which the laser beam enters the water and bounded by the angular radius  $\gamma$ . Figure 5 has a logarithmic scale of total power within the angular radius  $\gamma$  and a linear scale of attenuation lengths. The lower dashed straight-line in this figure depicts the function  $e^{-ar}$ . This line is an invariant of the coordinates because lamp distance is plotted in attenuation lengths ( $ar$ ). The upper dashed line in Fig. 5 represents the function  $e^{-ar}$ , where the

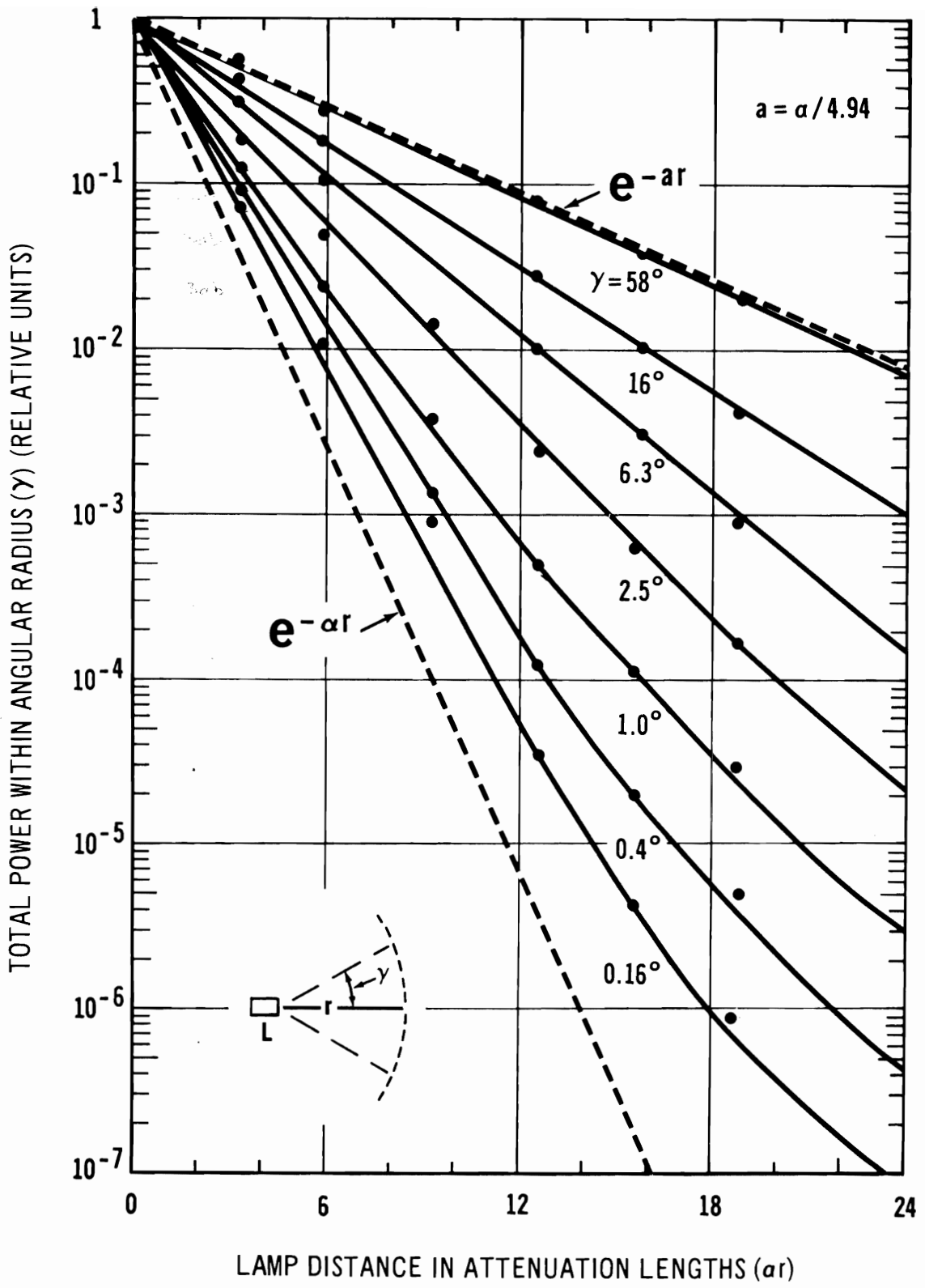


Figure 5

absorption coefficient  $a$  has the magnitude  $a/4.94$  in accordance with the measured optical properties of the water given earlier in this letter.

It will be noted that the observed total power within the maximum angular radius for which data were obtained ( $\mathcal{N} = 58^\circ$ ) is represented by a straight line which lies just beneath the dashed line representing the function  $e^{-ar}$ . Figure 5 also contains curves for integrations at various lamp distances for values of angular radius ( $\mathcal{N}$ ) of 16, 6.3, 2.5, 1.0, 0.4, and 0.16 degrees respectively. Throughout the first twelve attenuation lengths, these data can be represented by straight lines but small amounts of upward curvature are shown by the data, particularly for small values of angular radius ( $\mathcal{N}$ ). It is evident from Fig. 5 that rotation of the laser through  $58^\circ$  was sufficient for the purposes of this investigation inasmuch as integration over a complete sphere surrounding the laser ( $\mathcal{N} = 180^\circ$ ) could not exceed the total power represented by the function  $e^{-ar}$ , that is to say, the upper dashed straight-line boundary in Fig. 5. This statement is necessarily true of any light source, narrow beam, broad beam or spherical, in a steady state condition. The question of whether the short duration pulse produced by the underwater green laser as depicted by the dashed curve in Fig. 1 can be regarded as a quasi-steady state distribution of radiant power is answered experimentally by the manner in which the total power integral approaches an asymptote as  $\mathcal{N}$  approaches  $58^\circ$ , and theoretically by an independent study of the  $\Delta$  function response of natural waters which has been made and will be reported in detail later. The upper dashed straight line representing the function  $e^{-ar}$  in Fig. 5 is therefore regarded as an absolute upper bound for the total power in the space surrounding the beam produced by an underwater laser.

The existence of the function  $e^{-ar}$  as an upper bound to the power produced by the underwater laser leads to an interesting speculation concerning the nature of the curves in Fig. 5 if extended to very long ranges. Clearly, the irradiance distribution produced by the laser becomes progressively less sharply peaked as lamp distance increases. At very long ranges it must approach a nearly uniform distribution. Nevertheless, any residual non-uniformity must be in the nature of an increased irradiance at and near the axis of the beam. Thus it can be confidently stated that the total power within a  $16^\circ$  cone can never be less than the power within the  $58^\circ$  cone reduced in proportion to the ratio of the solid angle of the  $16^\circ$  cone to the solid angle represented by the  $58^\circ$  cone. Thus at very long ranges, an upper bound to the power within the  $16^\circ$  cone can be constructed as a straight line parallel to the boundary represented by the function  $e^{-ar}$ , i.e., parallel to the upper dashed line in Fig. 5, and positioned beneath the curve for  $\mathcal{N} = 58^\circ$  by a factor which is the ratio of the respective solid angles subtended by  $58^\circ$  cone and  $16^\circ$  cone, respectively. Let it be assumed that, at long range, the curve for  $\mathcal{N} = 58^\circ$  is a straight line parallel to the upper dashed boundary and separated from it by no more than the separation of the  $\mathcal{N} = 58^\circ$  line in Fig. 5. Upper boundaries at long range can then be plotted for each of the successively smaller values of  $\mathcal{N}$  in Fig. 5. This has been done in Fig. 6 at an arbitrarily selected lamp distance to 44 attenuation lengths, as shown by the points plotted in that figure. Straight lines having the same slope as the function  $e^{-ar}$  were then passed through these plotted points and joined arbitrarily to the curves in Fig. 5, producing thereby an upper bound model for the distribution of power produced by an underwater laser at the very long range. It must be understood that these extrapolations are not founded upon any data since no experimental measurements were made at ranges beyond those indicated by the points near 19 attenuation lengths in Fig. 5. The range limitation on the 1966 laser data was not set by sensitivity or by laser power. The limitation was imposed chiefly by the non-availability of time and funds to continue the experiment at longer range. Calculations indicate that laser power was available to perform the experiment at Diamond Island out to at least 40 attenuation lengths. No practical barrier to obtaining such long-range data is known.

Figures 5 and 6 can be used to ascertain the power received by an object of fixed size at any range. When the object is very close to the laser it obviously subtends a very large solid angle so that the power it receives is indicated by the upper dashed boundary on Fig. 5. As distance increases the angular subtense of the object diminishes so that at appropriate ranges a circular object, for example, will subtend the various values of  $\gamma$  depicted by Figs. 5 and 6. Appropriate points can be plotted on each of the curves and the plotted points connected to produce a plot of the total power received by a circular object as a function of lamp distance. The result of such a use for Figs. 5 and 6 is illustrated by Fig. 7 wherein this has been done for 5 different circular objects having angular radii of 30 feet, 10 feet, 3 feet, 1 foot, and 1/6th foot, respectively. Experimental data for an object 1/6th foot in angular radius is available because the integrating sphere used to obtain the integrated value at the center of the laser beam has an opening 1/6th foot in radius (diameter = 4 inches). The experimental points obtained with the integrating sphere are plotted in Fig. 7.

Figures 5 and 6 can also be used to ascertain the angular radius within which any arbitrary amount of power is contained at any given lamp distance. These are simply a family of straight lines parallel to the dashed upper boundary,  $e^{-ar}$ , as illustrated by Fig. 8. Values read from that figure are plotted in Figs. 9 and 10.

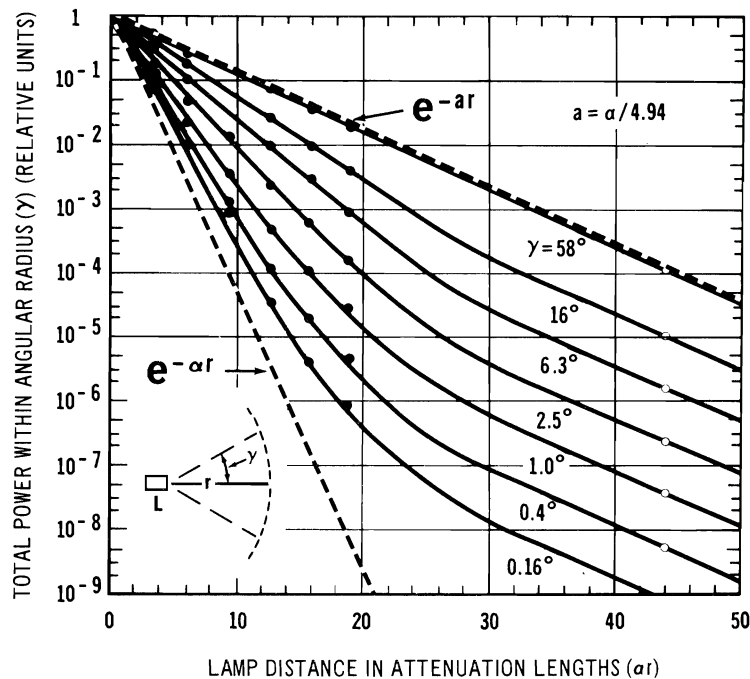


Figure 6

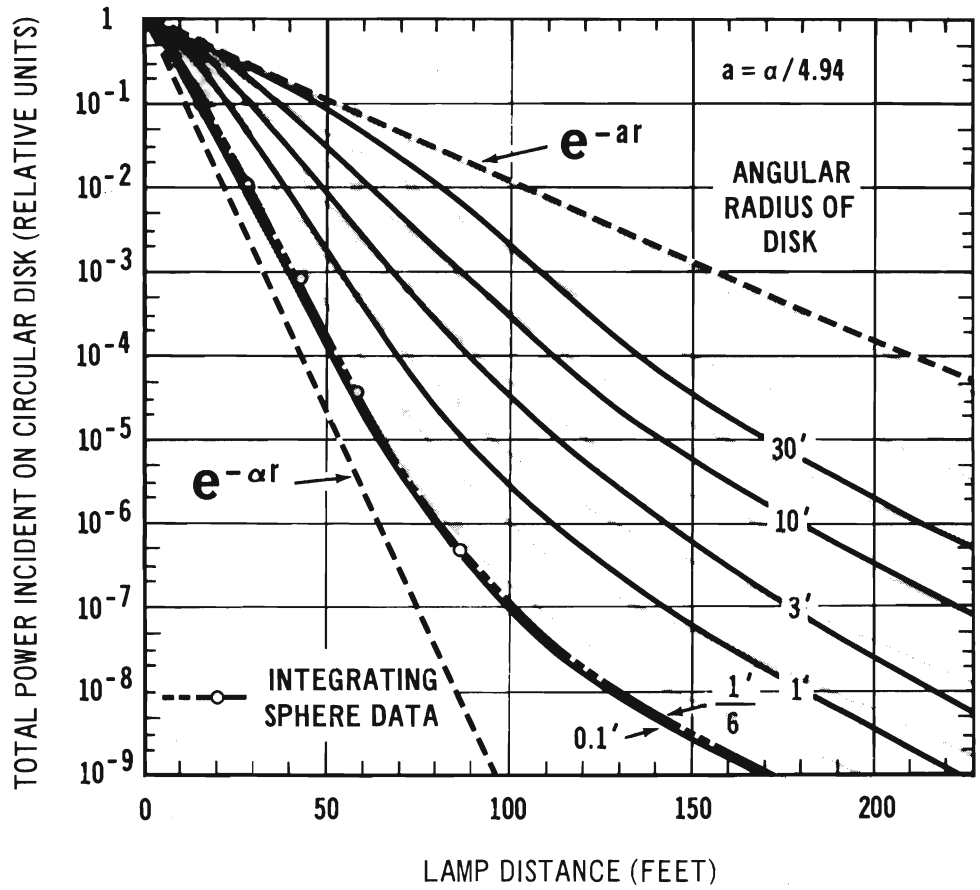


Figure 7

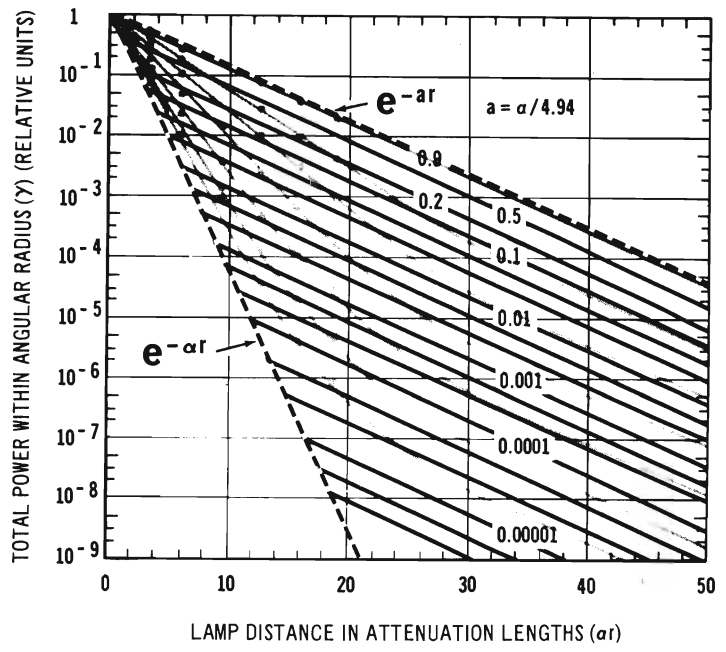


Figure 8

Figure 9

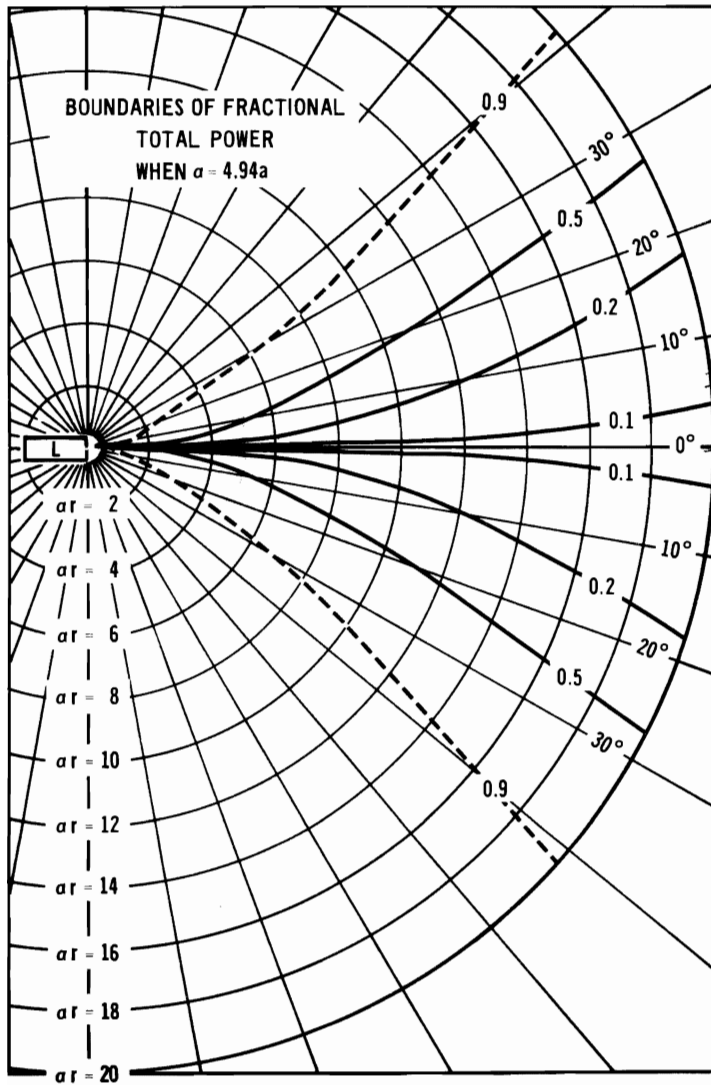
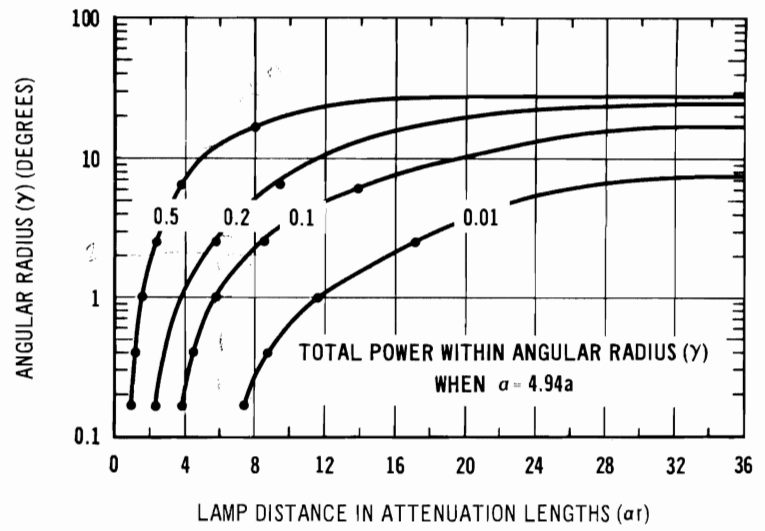


Figure 10



It must be remembered that all of the figures attached to this letter are drawn for the specific case of natural water in which the attenuation coefficient is 4.94 times as great as the absorption coefficient. This is reflected in the position of the upper dashed boundary line in Figs. 5, 6, 7, and 8. The position of this line depends upon the  $\alpha/a$  ratio. The lower boundary, representing the function  $e^{-\alpha r}$ , is an invariant of the coordinates and does not depend upon the value of  $\alpha$ . Thus, the angular opening between the upper and lower boundary lines in these figures will be different for various natural waters and will also depend upon wavelength, inasmuch as the absorption coefficient of the water molecule is a steep function of wavelength. There is good reason to believe that the principles and general form of functions like those depicted by the figures attached to this letter will typify any natural water but it must be remembered that the figures attached to this letter apply quantitatively only when  $\alpha = 4.94a$ .

#### FURTHER STUDY OF THE PRELIMINARY RESULTS

The Diamond Island off-axis irradiance data have, of course, received considerable study since December 1966. Slowly accumulating additional facts from experiments the author has made in a laboratory tank, or from certain experiments by others, and indications drawn from model studies performed on computers have aided in improving the original interpretations. Surprisingly, very few conclusions have been altered. The most significant alteration in Figs. 5 and 6 of the letter report concerns the nature of the curves beyond 10 attenuation lengths. It is clear that the curve for  $\gamma = 58^\circ$  does not parallel the upper dashed curve (the "a-line"). This is shown by a restudy of the hundreds of oscillograms made at Diamond Island and by all subsequent experiments. Better corrections for pulse stretch lower the curves in Fig. 5 significantly at large  $\gamma$  and large  $\alpha r$ . The same trend appears in all of the new data given in Section 7. Thus, extrapolation of the power curves at the a-slope to longer ranges, as is done in Figs. 6, 7, and 8 of the preliminary report, is wrong.

#### QUALITY OF THE 1966 OFF-AXIS DATA

The quality of the off-axis irradiance data taken at Diamond Island is not high, for at least three reasons:

(1) Measurements were rarely repeated on subsequent nights because the total time for the program was fund limited. Manpower available for data reduction was insufficient to keep pace with the experiments. Thus, questions did not arise in time to enable specific measurements to be checked. Cumulative fatigue made procedural errors on the part of divers and scientists inevitable as the 20-night sequences progressed.

(2) Although the 1966 laser was vastly improved over earlier models, it had service problems that would have been insurmountable without the expert and dedicated assistance of the nearby RCA laboratory. Residual output variations, even after monitor corrections, were damaging to the irradiance data because of the very large number of sequential "folds" required; the usable open range of the light measuring system covered less than a factor of five.

(3) Successive plankton blooms and water temperature changes resulting from storms produced minor variations in the optical properties of the water throughout the six-week data acquisition period that were significant in terms of the off-axis laser experiments. Attempts were made to correct the irradiance data to some common set of water conditions, but residual uncertainties remained that would have been eliminated if all of the data could have been taken on a single night.

#### DATA WITH HIGHER FIDELITY

The preliminary reduction of the 1966 off-axis laser irradiance data, presented in the letter report of 10 December 1966, disclosed most of the governing optical principles. Thus, the primary goal of the off-axis program at Diamond Island was achieved. The quantitative reliability of the preliminary results is, however, less satisfactory. Extensive careful reviews of all of the basic irradiance and water property data were subsequently made with the goal of achieving power curves having higher fidelity.

Small night-to-night changes in the optical properties of the water was deemed to be the source of greatest uncertainty in the basic data. A review of these changes and of the operating performance of all apparatus, including the laser, showed that the most consistent and reliable set of experimental conditions occurred on the nights of 15, 16, 17, and 22 August 1966. Enough data were obtained on those four nights to determine the desired set of total power curves. It was decided, therefore, to treat these data alone as an independent set, having higher reliability than does the preliminary composite study of data from all occasions.

Improved pulse-stretch corrections were made to each irradiance datum. The measurements of all optical constants of the water were reviewed and linear averages of  $\alpha$  and  $a$  were adopted as nominal values representative of the set. Table 6.1 gives these values for the four nights and their linear averages.

**Table 6.1. Attenuation Coefficient Absorption Coefficient**

Date	$\alpha$ (ln/meter)	$a$ (ln/meter)	$\frac{\alpha}{a}$
15 August 1966	0.671	0.186	3.61
16 August 1966	0.682	0.168	4.06
17 August 1966	0.722	0.158	4.57
22 August 1966	0.644	0.163	3.95
Average	0.680	0.169	4.03

The resulting revised laser power data are plotted in Fig. 7-1 of the next section, where they are compared with corresponding laser power measurements made in the ocean-simulation laboratory tank.

# 7. LASER LIGHT IN SIMULATED OCEAN WATER

## 7.1 INTRODUCTION AND SUMMARY

Underwater laser experiments during 1964, 1965, and 1966 at the Visibility Laboratory's field station on Diamond Island in Lake Winnepesaukee, New Hampshire showed that the spreading of scattered radiant power of collimated beams depends upon the ratio ( $a/a$ ) of the volume attenuation coefficient to the volume absorption coefficient.\* At Diamond Island this ratio was significantly larger than in typical ocean water. It was clear that laser beams would spread less in the ocean and, therefore, that data from Diamond Island could not be used for the engineering design of laser systems to be used at sea. It was also obvious that the needed engineering data could not be obtained by further experiments at Diamond Island.

At the request of ONR in 1967, the Visibility Laboratory made a survey of potential sites where a "Diamond Island Experiment" could be conducted in clear ocean water. That survey, described in Section 7.2, was discouraging. No ideal site (or facility afloat) was found in United States waters, Atlantic or Pacific. Only one available site was judged to be worth further study. This was at Mala on the southwest coast of Maui, Hawaii. Even there conditions were marginal and the cost of the experiment would have been substantial. By late 1967 the Office of Naval Research found it impossible to secure the funds needed for the desired experiment in ocean water. It then approved a Visibility Laboratory proposal to perform laser beam spread experiments at model scale in a laboratory tank using simulated ocean water. This was distilled water (or its equivalent) to which dyes and scattering agents were added until, at the laser wavelength, the resulting fluid had optical properties identical with ocean water except that the attenuation length (reciprocal attenuation coefficient) for a beam of laser light was the order of a tenth that of clear ocean water. Thus, 5 meters of path in the tank could produce the same optical effects as a 50-meter path in the ocean.

---

\*Since attenuation, absorption, and total scattering are connected by the relation  $a = a + s$ , it is obvious that beam spread in water can be characterized equally well by the ratios  $s/a$  or  $s/a$ . These ratios appear in various other connections throughout the literature of radiative transfer and hydrologic optics; they sometimes are given names like "the albedo for single scattering" or "the probability of photon survival." Obviously,  $s/a = 1 - (a/a)$  and  $s/a = (a/a) - 1$ . The ratio  $a/a$  is used throughout this report because its role in controlling beam spread is so clear when Figs. 7-20, 7-23, 7-24, 7-25, and 7-40 are compared.

More than a year was lost by administrative delays of several kinds that were beyond the power of the Visibility Laboratory to avoid. The simulation studies finally began under circumstances of extreme austerity. Success in carrying them through was possible only because of financial assistance from the Naval Air Development Center, the Naval Ordnance Laboratory, the Sea Grant College Office of the National Science Foundation, and the University of California.

By the end of 1970 high quality laser underwater propagation data suitable for engineering use existed for typical clear ocean water ( $\alpha/a = 2.5$ ) and also for a wide range of other  $\alpha/a$  ratios. Thus, design data exist which are applicable to laser wavelengths other than 530 nanometers and to many kinds of ocean water. These data were fitted by an empirical equation suitable to be used with a computer for engineering purposes, including design optimization by parametric studies. The equation is intended to be applicable to any kind of natural water, any wavelength, and a wide range of underwater distances and off-axis angles. A computer program for this equation has been programmed and given extensive trials. It has been used to predict the laser propagation characteristics of waters (or wavelengths) having more extreme  $\alpha/a$  ratios than any yet modeled in the laboratory.

Validity of the model scale technique was tested by simulating Lake Winnepesaukee water in the laboratory tank. Figure 7-17 compares data from the tank (curves) with data from the lake (points). The agreement is excellent.

The remainder of this report is devoted to an account of the 1967 ocean site survey and the subsequent laboratory studies of the propagation of laser light through model scale simulations of ocean waters.

## **7.2 SURVEY OF SITES FOR A LASER EXPERIMENT IN THE OCEAN**

During 1967 the Visibility Laboratory searched for an ocean site at which laser irradiance off-axis could be measured in clear ocean water by the same techniques used at Diamond Island.

### **USE OF DRY DOCKS**

An early suggestion was the use of a dry dock. The Navy made a test filling of the large dock at Roosevelt Roads, Puerto Rico with this use in mind. Excessively rapid biological growth and the unavailability of sufficiently clear water made this site unsuitable. All other large dry docks, such as those near the entrance to Pearl Harbor, Honolulu were unavailable. The only floating dry docks large enough for the experiment if conducted in clear ocean water were in Apra Harbor, Guam. Both were permanently anchored in water too turbid to be of use for the experiment. Considerable attention was given to the possibility of conducting a short range experiment in a small World War II concrete floating dry dock that was available in San Diego. The cost of refurbishing, towing, and operating this unit proved to be out of the question, and its small size (about 300 feet) made its suitability marginal at best.

### **LOCAL SITES**

No suitable local sites on California shores or islands were found where favorable water clarity, depth, shelter and other requirements were met sufficiently to enable a Diamond Island type underwater tower and track to be built and used successfully.

## SITES NEAR NAVAL BASES

Outstanding cooperation and interest on the part of Navy personnel at Guam, Hawaii, and Antigua caused special attention to be given to the possibilities in these areas, but without success. Anecdotal accounts of idyllic, land locked shallow lagoons (crocodile free) with water "clear as air" on various Pacific islands appear to be inaccurate. Such lagoons are usually associated with land structures from which there is sufficient silted run-off to make the water (when measured) disappointingly unclear in comparison with normal off-shore clear ocean water. One location on an underwater shelf near the harbor entrance on the inner side of the Glass Breakwater in Apra Harbor, Guam seemed interesting until the Navy began construction of a docking facility on that site.

## OTHER SITES

The search included detailed inspection by land, sea, and air of all possibilities on Guam, Midway, the Hawaiian Islands, Florida, the Keys, the Bahamas (including the AUTEK facility), Bermuda, Puerto Rico, the Virgin Islands, and other Caribbean locations including Antigua. Navy personnel supplemented this search by independent inspection of various suggested sites. Many experienced Navy divers were interviewed for suggestions. Off-shore tropical reefs were often mentioned as having clear water. The cost of establishing, maintaining, powering, and staffing a Diamond Island-type operation on an unprotected off-shore reef appears to be large. Neither is it clear that these locations are safe for scuba divers to be in the water at night illuminated frequently by underwater working lights.

## THE MOST LIKELY SITE

A large abandoned commercial pier at Mala near Lahina on the southwest coast of Maui, Hawaii seemed to be the only available, practical, and suitable site discovered by the survey. Here the water clarity appeared to be marginal, just as did the best of all coastal locations. More extended measurements of water properties at Mala are needed before the site should be selected.

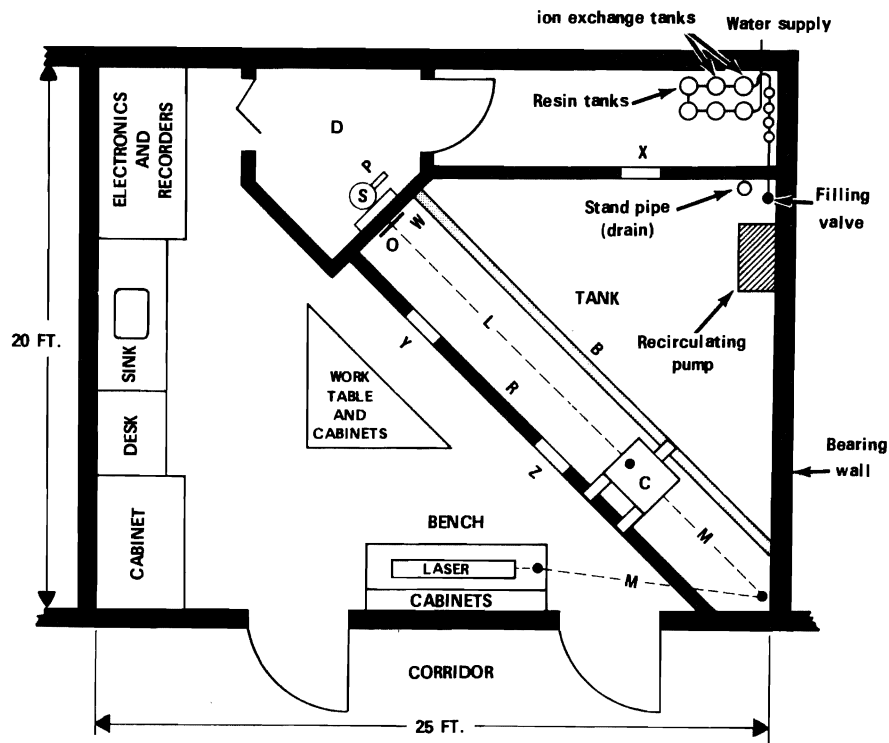
## REPORT OF THE SITE SURVEY

The Visibility Laboratory engineer who visited the sites submitted a detailed report to ONR. Excerpts from that report are given in Appendix E. The lack of a truly ideal ocean site or facility afloat together with the impact of restrictions in funding precluded laser studies at sea. In their stead, preparations began for laser experiments at model scale in simulated ocean water.

## 7.3 THE LABORATORY TANK

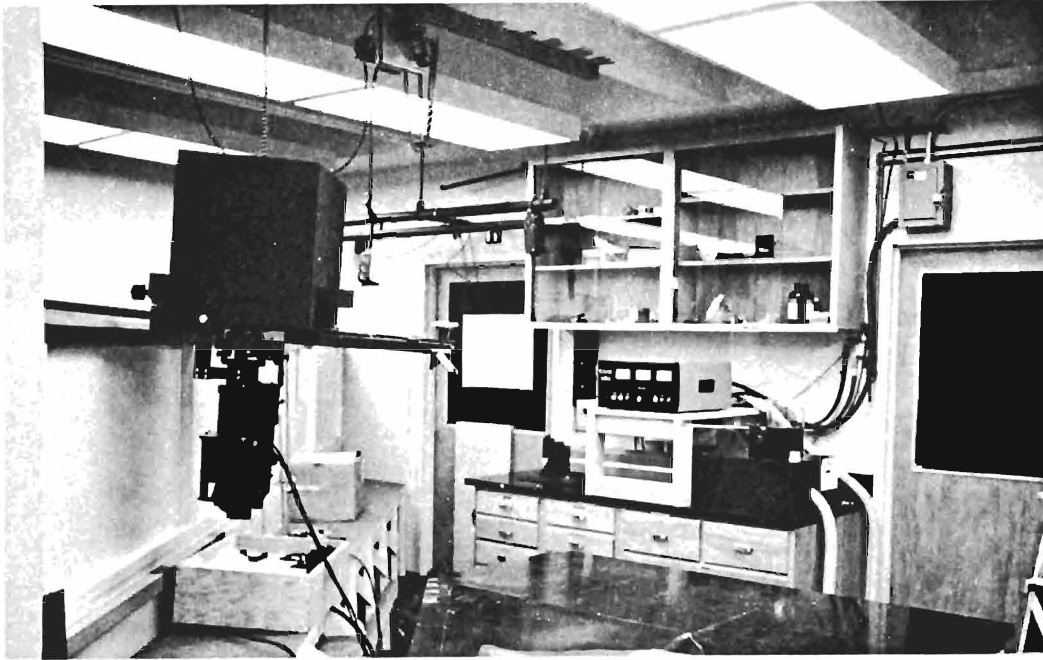
A unique laboratory tank was constructed to enable underwater laser experiments to be made at model scale in simulated ocean water. The essential features of the underwater tower and track at Diamond Island were duplicated in a 20 x 25 foot room of Sverdrup Hall at the Scripps Institution of Oceanography. The tank, roughly triangular and two feet deep, holds about 2000 gallons of water. An approximate replica of the lower part of the underwater tower of Diamond Island is at one corner of the tank. A schematic plan

of the installation is shown in Fig. 7-1 and photographs of it are in Fig. 7-2. The longest laser beam path through water in this tank is 5.5 meters. The axis of the underwater beam is 1 foot below the water surface and 1 foot above the bottom of the tank. It is also 1 foot from that wall of the tank which parallels the track. These 1 foot spacings between the laser beam and 3 boundaries of the tank were chosen to correspond in terms of attenuation lengths with the 6 foot depth of the laser beam at Diamond Island and, consequently, its 6 foot separation from the 3 surfaces of the underwater tent. At Diamond Island  $\alpha = 0.75 \text{ ln/m}$ ; in the tank dyes and scattering particles were added until  $\alpha = 0.75 \times 6 = 4.5 \text{ ln/m}$ . Thus, in both cases the laser beam was 1.37 attenuation lengths from the nearest boundary. In tank water the attenuation length is 0.222 m/ln, and the 5.50 meter maximum lamp distance represents 24.8 attenuation lengths.

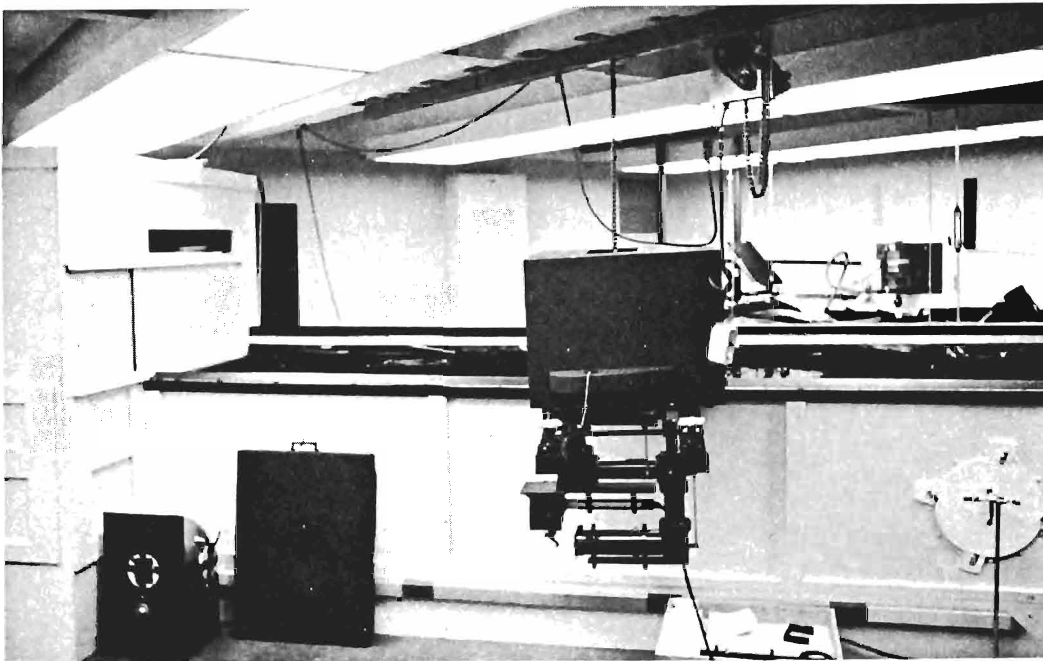


- X, Y, and Z - Observing ports with external covers.
- L - Dashed line is the underwater portion of the laser beam path.
- M - Dashed lines are the above-water portions of the laser beam path
- C - Above-water cart which runs on V-rail and flat top (above-water) I-beam B. The cart C contains the same pointing control mechanism used at Diamond Island.
- R - V-rail
- B - I-beam
- W - Same measurement window used at Diamond Island.
- O - Same irradiance wheel used at Diamond Island.
- S - Same integrating sphere used at Diamond Island.
- P - Same multiplier phototube used at Diamond Island.
- D - Black-painted, darkened measurement room corresponding to the lower part of the underwater tower at Diamond Island.

Fig. 7-1. Laboratory tank for optical simulation of ocean waters at model scale, located in Room 2215 of Sverdrup Hall, Scripps Institution of Oceanography, University of California, San Diego.



(a)



(b)

Fig. 7-2

- (a) Laboratory room (see Fig. 7-1) showing argon-ion laser (center), diagonal wall of laboratory tank (left), and cart hanging from a chain hoist on a ceiling track. Black upper box contains control mechanism; lower mechanism is submersible prism system; see Fig. 7-3b.
- (b) Laboratory room showing diagonal wall of tank (center) and measurement room (left).

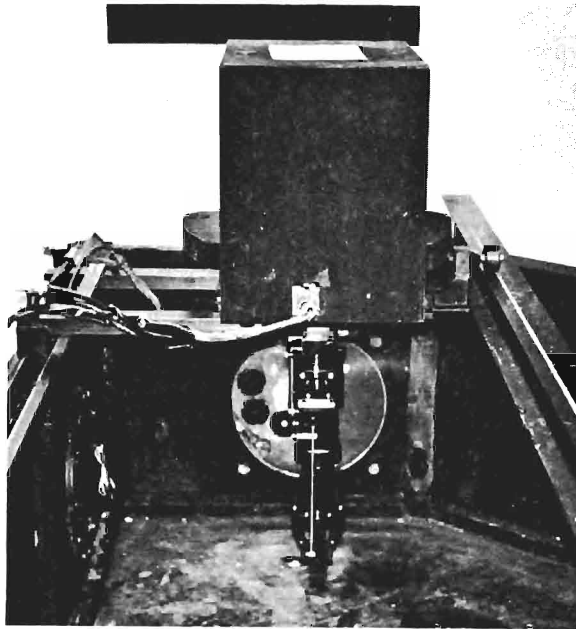


Fig. 7-3a

Interior of empty laboratory tank, facing measurement room. Cart spans between V-rail (left) and I-Beam (right) and carries control mechanism (upper box) and submersible prism system. Measurement window with irradiance wheel is visible behind submersible assembly. Interior surfaces of tank are black fiber glass with additional paint.

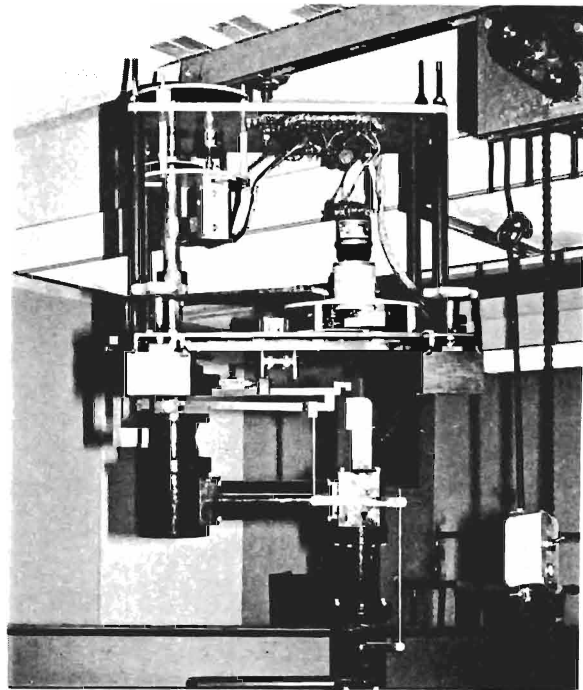


Fig. 7-3b

Cart hanging from ceiling track and chain hoist. Upper control mechanism (cover removed) points underneath laser beam by rotating submerged assembly about a vertical axis and by tilting a prism (lower right).

The same techniques and devices used at Diamond Island were employed in the laboratory experiments. For example, the laser pointing control mechanism from the underwater cart was refitted for use at the tank. In this case the track was built in air above the water surface, and the new cart containing the original control mechanism is in air above the new track, as shown in Fig. 7-3. Whereas the laser and the incandescent projector were supported above the control mechanism at Diamond Island, the corresponding items hang below it in the new tank. This was accomplished by inverting the entire control mechanism assembly when mounting it on the new cart.

A triangular rail is mounted on top of the hypotenuse edge of the triangular tank. This serves to support and guide the cart by means of V-blocks, visible at the left in Fig. 7-3a. The other side of the cart is supported by a single roller which runs on an I-beam spanning the tank, as diagramed in Fig. 7-1. The heavy underwater cart used at Diamond Island is still there. In its place a light wooden box serves as a dust cover for the control mechanism; see Fig. 7-3a.

Figure 7-4 shows that the same type of measurement window used in the underwater tower at Diamond Island was installed in the tank. The same 4-inch diameter optical glass insert in the 1.25-inch thick main Plexiglas window is used. The same irradiance wheel used at Diamond Island is in place. A large metal cover is placed over the entire window whenever an irradiance measurement is made. The cover is shown in place in Fig. 7-5a. The cover contains a large, shallow metal cone with a small hole at its apex. The only light that can enter the measurement room behind the window must pass through this hole in the cover;



directly behind it is the irradiance wheel, so that the size of the irradiance measuring surface is determined by the selected stop in the irradiance wheel. The window cover in Fig. 7-5 plays exactly the same role as the port cover used at Diamond Island and shown in place at the window of the air tower in Fig. 6-6.

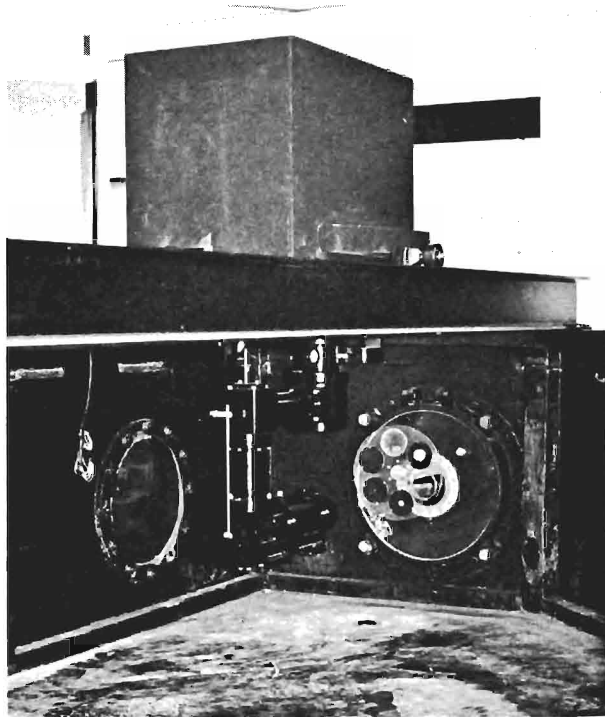


Fig. 7-4

Interior of empty laboratory tank showing measurement window with irradiance wheel (right), control cart with submersible prism assembly (center), and observation port (left). Laser beam (above water surface) enters fixed white circular window at top of prism system and is injected into water toward measurement window at bottom of prism assembly.

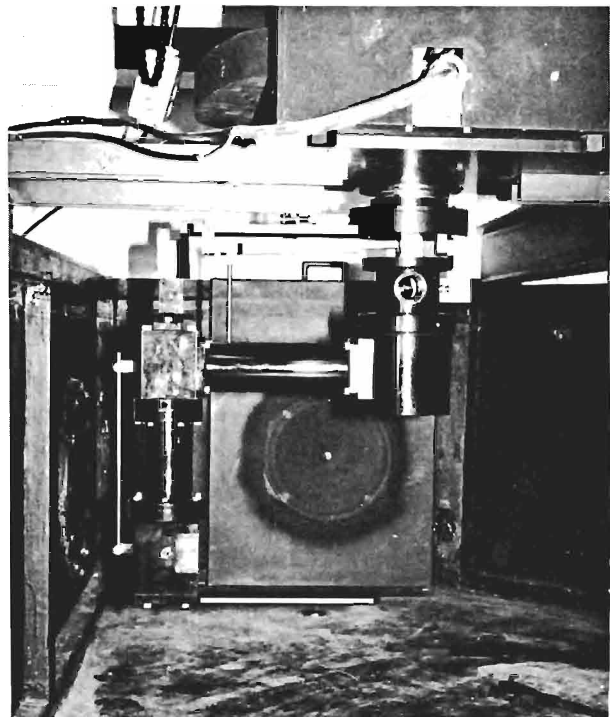


Fig. 7-5a

Interior of empty laboratory tank showing metal cover in place over measurement window. Large shallow metal concave cone has a hole at its apex to admit light to the irradiance wheel. All irradiance data at Diamond Island were taken with this light-collecting system, but the off-axis irradiance measurements in the laboratory tank made use of the collector shown in Fig. 7-5b. When the submerged prism system is used without an air-tube (like the ones shown in Figs. 7-13 and 7-14) the volume scattering function can be measured. The irradiance collector is then replaced by a telephotometer located behind the center of the measurement window. All optical properties of the water used in the experimental tank can be measured with laser light by means of the submerged prism system.

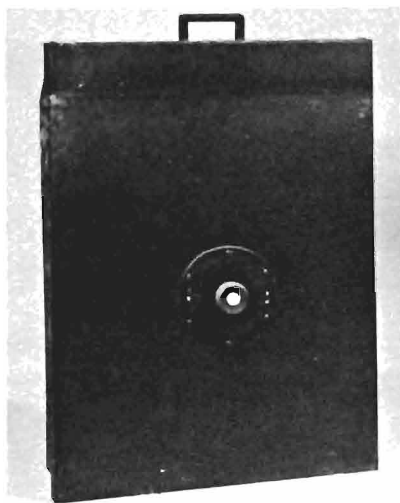


Fig. 7-5b

Alternate window cover equipped with improved irradiance collector [see R. C. Smith, *Jour. of Marine Research* 27, 341, (1969)]. All off-axis irradiance measurements in the laboratory tank were made with this type of collector.

The room which houses the tank has a white ceiling. Any light emerging from the water surface is reflected from the ceiling back into the tank and causes serious errors in the data, because water having  $\alpha = 4.5 \text{ ln/m}$  attenuates much more strongly than air. Therefore, a light-tight, opaque, black plastic cover supported by a light framework of aluminum rods is used to cover the triangular corner of the tank beyond the I-beam (see Fig. 7-1). Cover for the rectangular area of water surface between the I-beam and the V-rail is provided by a segmented floating black rubber curtain, much as was done at Diamond Island. The rubber material is the same used to make wet-suits for divers and is reinforced on one side with a black nylon fabric backing. The rubber sheeting was floated with the fabric side down because, when submerged, it is extremely matte and eliminates completely the mirror-like air-water surface.

The tank is made of wood but lined on the inside with black fiber glass. Paint is added to modify the submerged reflectance of the tank walls and bottom according to the needs of the experiment, the shade of gray being chosen to match the reflectance of the particular water used. Thus, the boundaries of the tank are "camouflaged" to represent the optical equivalent of a limitless volume of water. Considerable effort is always expended in cleaning and preparing the tank prior to each filling.

## 7.4 SIMULATION OF NATURAL WATERS

In all natural water the collimated light produced by a laser experiences sequential scattering, chiefly at very small forward angles, such that the beam is gradually transformed from its original highly collimated state to a cloud of forward moving diffused light that spreads far beyond the confines of the beam geometry. All aspects of this phenomenon except those which involve the velocity of light can be accurately observed at model scale in laboratory simulations of natural waters. Since the solutes in ocean water have no detectable effect on the scattering or absorption<sup>†</sup> of visible light, the simulation can advantageously be based upon pure water. To this may be added dyes in true solution (i.e., molecular dispersion) to increase the absorption coefficient of the fluid in inverse proportion to the reduced spatial dimensions of the experiment. Similarly, scattering particles having low relative refractive indices and a proper distribution of sizes can be added to bring the volume scattering coefficient to the required level. This procedure has the very important advantage that exact values of both the volume absorption coefficient and the volume scattering coefficient become known from simple, accurate, *in situ* measurements of the volume attenuation coefficient during the synthesis of fluid. Any value of attenuation coefficient can be reached. Any ratio of scattering to absorption coefficients can be achieved. Thus, any natural water (and any laser wavelength) can be simulated at the desired model scale.

### PREPARATION OF HIGH-PURITY WATER

The experimental tank constructed for the model scale experiments holds about 2000 gallons. This quantity of pure water can be expensive. Distilled water delivered by tank truck and pumped through a hose contained too much particulate matter. Bottled distilled water is costly and impractical. Tap water cleared by a recirculating filter nearly always contains too much chlorine to enable stable dye concentrations to be maintained. A satisfactory source of water was achieved with the system of filters shown in Fig. 7-6.

---

<sup>†</sup>Organic decomposition products ("yellow stuff") excepted.

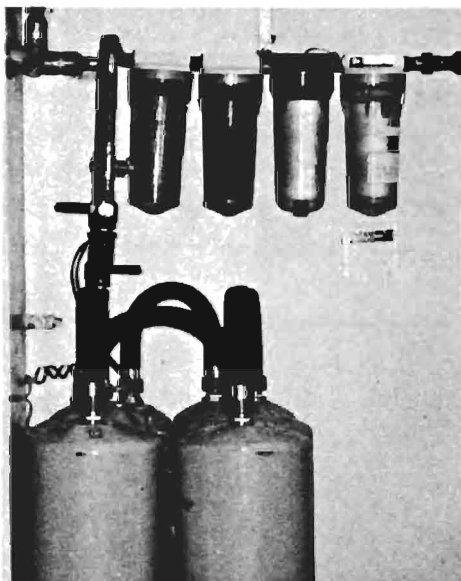


Fig. 7-6

Filter system used to prepare tap water for use in the ocean simulation tank. For description, see text.

The incoming tap water passes first through six large vertical gray tanks which stand on the floor and then through four cartridge-type filters mounted on the wall. Two of the gray tanks are for anion exchange, two are for cation exchange, and the remaining two contain a microreticular resin which removes iron salts, chlorine, and most of the organic material in the water, particularly bacteria. The first cartridge filter contains cotton string, the second activated charcoal, and the third is a plastic millipore-type filter which takes out particles down to 5 micrometers in diameter. The final cartridge contains a pleated membrane (Gelman) filter which removes particles down to 0.45 micrometers in diameter. The resulting water is low conductivity, chlorine free, and bacteria free. If the experimental tank is cleaned carefully and rinsed thoroughly with this water before filling is begun, an attenuation length of 12 to 14 meters/ln is usually achieved. A trace of formalin is added immediately to insure that no form of bacterial or other organic growth will occur.

All of the data were obtained with the green line of the argon-ion laser at 514.5 nanometers. At this wavelength it is believed that the volume absorption and volume scattering coefficients of the high purity water are approximately equal. Thus, it has been our practice to assume that if  $\alpha = 0.072 \ln/m$ ,  $a = s = 0.036 \ln/m$  in the high purity water.

The time required to fill the 2000 gallon tank through the filter system is about 9 hours. The six large filter tanks must be replaced after each fill. The cartridge filters serve for many fillings.

#### PREPARATION OF SIMULATED OCEAN WATER

Let it be assumed, for the purpose of an example, that clear ocean water having  $\alpha/a = 2.50$  is to be simulated in the tank by a fluid having an attenuation length  $1/\alpha = 0.222 \text{ m/ln}$ ; i.e.,  $\alpha = 4.50 \ln/m$ . Then the fluid must have an absorption coefficient  $a = 1.80 \ln/m$  and a volume scattering coefficient  $s = 2.70 \ln/m$ . Either the absorbing dye (Nigrosin, Central Scientific Co. No. 39680)\* or the scattering agent may be added first. For purposes of the example, let it be assumed that the black dye is added first to the water

---

\* Nigrosin (Cenco No. 39680) was selected after testing many dyes in the 514 nm laser beam because it showed less fluorescence than any other suitable dye tested. A Wratten No. 64 green filter was mounted over the photocathode of the multiplier phototube in order to suppress the (probably negligible) residual red fluorescence of Nigrosin.

in the tank until the measured volume attenuation coefficient  $\alpha = a + s = 1.80 + 0.036 = 1.836 \text{ ln/m}$ . Thereafter the scattering agent is added until  $\alpha = a + s = 1.80 + 2.70 = 4.50 \text{ ln/m}$ .

The tank is provided with a circulating system consisting of an electric pump which collects water near the surface near the corner of the tank furthest from the laser track and distributes it through a network of plastic pipes that cover the entire bottom of the tank. These pipes stand on plastic legs about 3 inches above the bottom of the tank and contain many tiny holes on their under surfaces. Thus, many tiny jets of water continuously scrub the bottom of the tank to insure that no settled scattering particles remain there. Thus, the tank has a continuous forced vertical circulation that overturns the entire water volume hourly. After each addition of dye there must be a sufficient time to insure complete mixing. Ordinarily, the addition of dyes or scatterers is made through the pump. About 30 minutes seems to be an adequate waiting time to insure complete mixing before meaningful  $\alpha$  measurements are made.

## SELECTION OF A SCATTERING AGENT

All natural waters appear to be characterized by intense forward scattering, particularly at very small angles. In fact, as shown on page 220 of Appendix A, the forward portion of the volume scattering function is remarkably similar in all natural waters. This observation opens the way for a laboratory simulation of natural waters. Discovery of a scattering agent that, when added to pure water, produces the same shape of volume scattering function in forward directions as do all natural waters is the principal requirement for valid simulations. So far as the forward propagation of laser light is concerned, the shape of the volume scattering function to the side and rear is of no consequence because such scattering contributes only an undetectable fraction of the total forward scattered power.

Measurements of the volume scattering function at Diamond Island and in ocean waters are discussed in Section 2 and illustrated by Fig. 2-15. The search for a scattering agent that produces a curve of this shape has been a long one. Trials of newly suggested materials may be continued indefinitely. The earliest material used for simulation work was silica gel. This comes in many grades and one was found that seemed marginally satisfactory if vigorously stirred to prevent the settling of the largest particles. These are, of course, the scattering elements of greatest importance in determining forward scattering characteristics.

*Biological Scatterers.* Because the forward scattering properties of natural waters has been chiefly attributed to transparent biological microscopic organisms large compared with the wavelength of light, it would seem that laboratory simulation could be achieved most accurately by growing a culture of such organisms in the tank. This approach has been tried by the author and his colleagues on several occasions and abandoned for many practical reasons. The cultures are difficult to maintain precisely constant for days or even hours. A delicate balance must be maintained involving nutrients, waste products, acidity, temperature, oxygen, and other factors. Biological contaminants, including massive blooms of bacteria, produce unwanted optical effects. Adjustment of the concentration of scatterers tends to be slow and uncertain. To summarize, biological scattering systems in an optical tank are insufficiently stable and controllable for quantitative radiometric studies.

*Inorganic Scatterers.* The best scattering materials found thus far for simulating natural waters are pharmaceutical mixtures of aluminum hydroxide and magnesium hydroxide that are sold for the relief of stomach distress. There are many brands of these "stomach gels," and all are significantly different when used as scattering agents. The one employed in obtaining all of the data given in this report was Rexall Aluminox. Not only did this product give the best match to the volume scattering function of natural waters in forward directions (see Fig. 7-7) but it had much less tendency to settle out than the other pharmaceutical preparations tested. The only serious difficulty encountered with Aluminox occurred during summer months when the water temperature was above 75 degrees Fahrenheit; flocculation then occurred. It has not been verified that all manufacturer's lots of Aluminox have the same desirable scattering properties that are exhibited by the particular bottles we purchased.

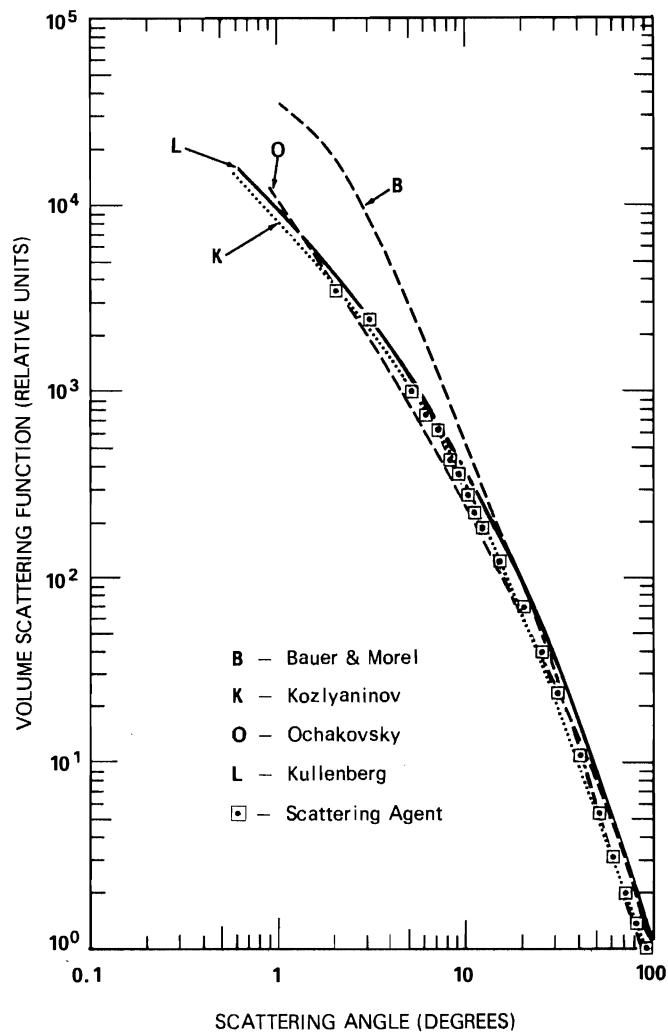


Fig. 7-7. Normalized volume scattering functions for ocean waters reported by four investigators using dissimilar instruments, different spectral regions, and different ocean locations illustrate first order similarity between 10 and 100 degrees. Departures between 1 and 10 degrees may be due to different size distributions of large particles.

Points within squares represent simulated ocean water used in the laboratory tank. The scattering agent was Rexall Aluminox, a preparation of aluminum and magnesium hydroxides.

## 7.5 INSTALLATION AND USE OF THE LASER

The laser used to secure all of the data given in this section was a Coherent Radiation Laboratory Model 52 Argon-ion Laser. It was installed, as shown in Fig. 7-1, on a bench separated from the experimental tank. The installation is shown in Fig. 7-8. The laser is mounted to a steel plate fixed to the top of the laboratory bench. The power supply and control panel were supported above the laser by a small wooden table. The light emerged the left end of the laser as seen in Fig. 7-8 and was deviated upward by means of a prism system. The prism assembly is shown in Fig. 7-9. The two dispersing prisms operated near the Brewster angle serve to disperse the laser spectrum so that a circular stop further along in the system could accept only a single laser line. Also shown in Fig. 7-9 is a rotary solenoid which is a part of the safety system for the laser. An arm attached to the solenoid carried a small black cup that intercepted the laser beam close to the laser unless the arm was raised by activation of the solenoid. This safety cup was tied into various forms of interlocks in the interest of eye safety.

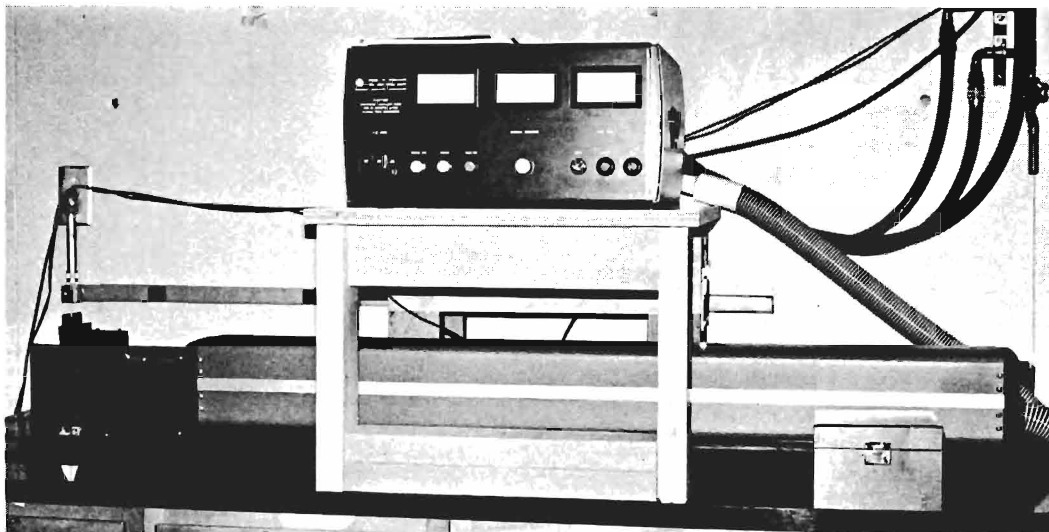


Fig. 7-8. Coherent Radiation Laboratory Model 52 argon-ion laser and power supply.

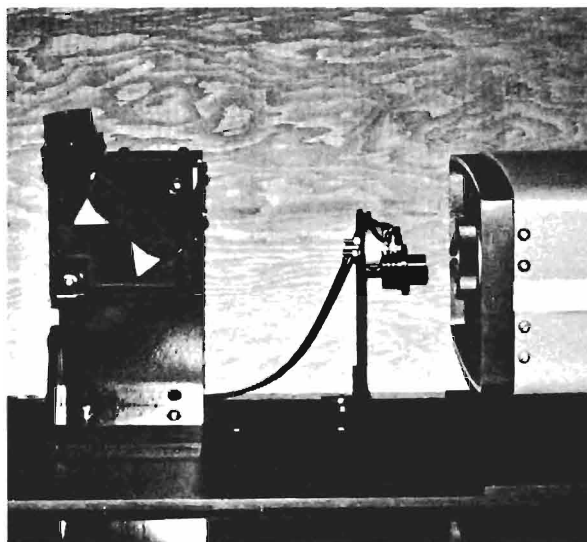


Fig. 7-9.

Prism assembly used to isolate 514.5 Å green line used for all data collection.

The laser installation with light covers in place is shown in Fig. 7-10. The laser beam was taken horizontally above the laboratory door to a prism located directly above the point at which the light beam was to enter the experimental tank. The beam was contained within tubing throughout its path. A relay lens imaged the exit aperture of the laser with unit magnification approximately at the point where the light beam emerged from the last prism, just above the water surface. The assembly was supported by a tubular I-beam hung from the ceiling and from the adjacent wall. The descending member of the system is shown in greater detail in Fig. 7-11. The laser beam emerged horizontally from the window at the lower end of this vertical section. When the tank was filled to its normal water line, faintly visible along the walls of the tank, the light beam was approximately 3 cm above the water surface. If unobstructed, the laser beam traversed the length of the tank to a point directly above the measurement window and 3 cm above the water line. Ordinarily it was intercepted somewhere along the track by a mechanism supported by the cart which contained the laser beam pointing control mechanism. The ascending member of the system is shown in Fig. 7-12. The adjustable stop which isolated the argon green line at 514.5 nm was located at the top of the vertical pipe on the right.

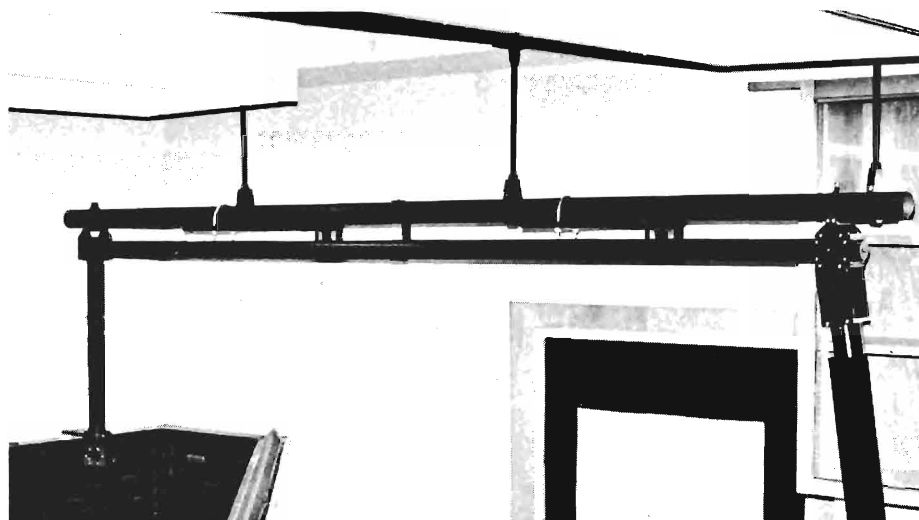


Fig. 7-10. Enclosed path for laser beam (lower tube) supported by tubular "I-beam" attached to ceiling and wall.

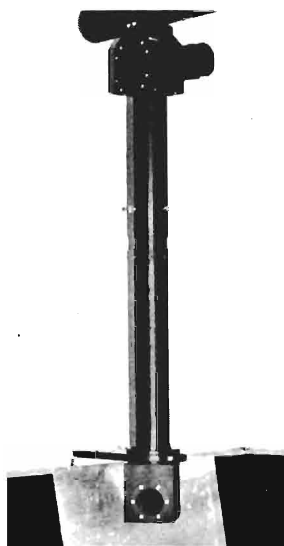


Fig. 7-11. Tubing for descending laser beam has prism boxes at top and bottom. Beam emerges horizontally from circular window facing camera; it is 3 cm above the water surface when the tank is filled to its normal level.

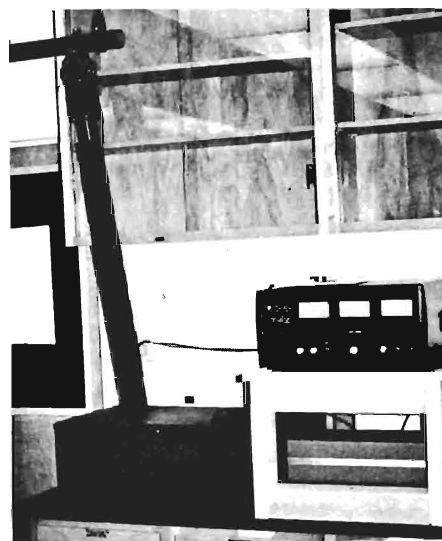


Fig. 7-12. Laser and power supply with covers in place.

Figure 7-13 shows the mechanism attached to the underside of the cart. During use much of this mechanism is in water. The normal water line is indicated in this figure by an arrow. Three centimeters above the tip of the arrow is the window which intercepts the horizontal beam. A prism system within the lower part of the mechanism directs the laser beam downward, thence horizontally to the left (in Fig. 7-13) to a prism which directs it vertically downward to final prism which sends the beam horizontally to the right through an empty tubing that terminates in a plain glass window directly beneath the axis of rotation provided by the pointing control mechanism. In the position shown, the laser beam emerges horizontally into water exactly at the axis of rotation. It then proceeds to the right (in Fig. 7-13), at right angles to the axis of the track. The beam entered the water one foot beneath the surface, one foot above the bottom of the tank, and slightly more than one foot from the nearest side wall. All of this structure turned about the vertical axis except the piece containing the upper window, which intercepts the laser beam in air. Thus, operation of the pointing control drives in the cart causes the beam to perform a horizontal sweep which, if desired, makes a complete 360 degree rotation.

Ordinarily, the laser beam is sent directly toward the measuring window. Vertical adjustment of the beam is accomplished remotely by means of a control mechanism in the cart. The adjustment is accomplished through a system of levers which can be seen in Fig. 7-13. These turn the lower prism in the underwater assembly.

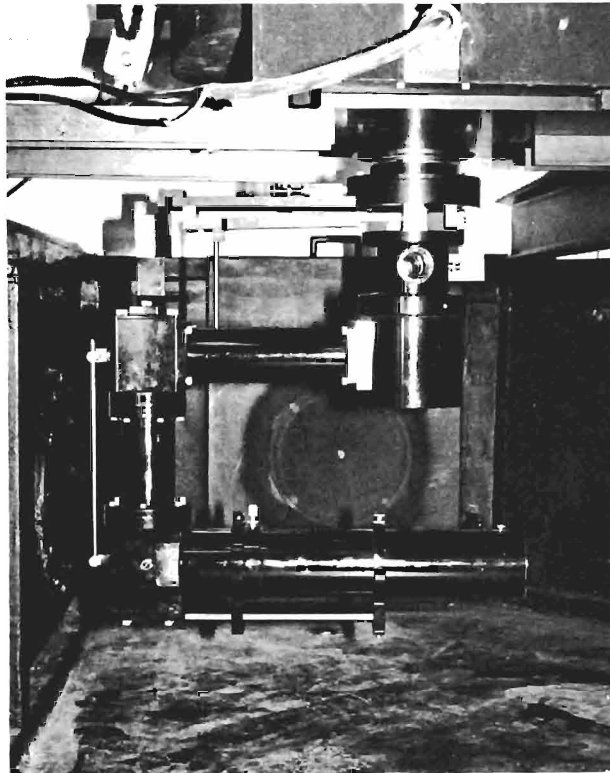


Fig. 7-13

Prism assembly of the beam pointing control system beneath its supporting cart in the (empty) laboratory tank. With removable air-tube in place, the laser beam enters the water directly beneath the vertical axis of the rotation. Compare with Fig. 7-5a.

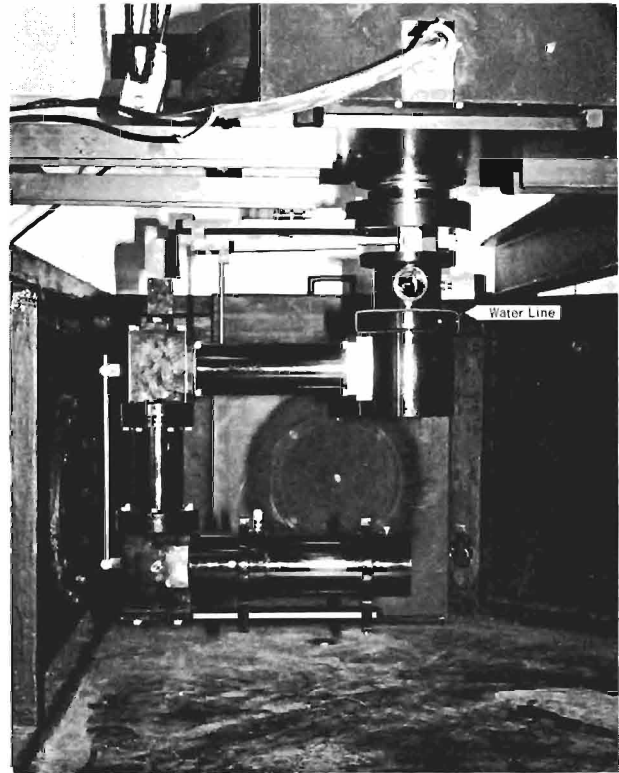


Fig. 7-14

Removable horizontal air-tube shown in Fig. 7-13 has been replaced by a longer one to enable total beam power entering the water to be measured; see text.



The principal interest in these experiments concerns off-axis irradiance. It suffices, therefore, to take an average value of the irradiance close to the axis of the track. This is accomplished by removing the window cover and mounting the integrating sphere on the inside of the measurement window. The laser beam enters the center of 4-inch diameter circular window of the integrating sphere. With it goes some forward scattered light. After the photoelectric reading has been recorded the beam is rotated horizontally to the right enough to make it miss the opening of the integrating sphere. A second reading is made. The integrating sphere is then removed and an irradiance collector and window cover is put in place. Another reading is made to establish a photometric fold in the data. Thereafter, all irradiance measurements are made by means of the special irradiance collector shown in Fig. 7-5b.

Comparison of Fig. 7-5a with Fig. 7-13 shows that the lower horizontal tubing can be removed so that the light beam enters the water not at the vertical axis of rotation of the system but at a considerable distance away. This configuration enables the volume scattering function to be measured with laser light. For this measurement the telephotometer looks out through the measurement window along the axis of the track.

If Fig. 7-13 is compared with Fig. 7-14 it will be observed that the removable horizontal tube in the former has been replaced with a longer horizontal tube in Fig. 7-14. This longer tube is provided in order to permit measurement of the total power in the laser beam where it enters the water. The empty tube in Fig. 7-14 is long enough so that with the assembly in the position shown in Fig. 7-4 the cart can approach the measurement window close enough that end of the long horizontal tube can be brought within a millimeter or two of the surface of the optical glass insert in the measurement window. Thus the laser beam traverses a negligible amount of water before entering the glass window and the integrating sphere. In this way the total beam power can be measured without attenuation by water.

#### CONSTANCY OF POWER IN THE LASER BEAM

The submerged prism assembly of the beam pointing control system enabled the laser beam to be centered on the measuring window and then swept horizontally to any angle, so that off-axis irradiance could be measured. Such a rotation of the prism system would, however, have caused the state of polarization of the light injected into the water to vary had it not been for the incorporation of a set of wave plates and linear polarizers within the prism train. Even so, rotation was accompanied by a significant change in the power of the laser beam as it entered the water. This change was eliminated by mounting a thin glass beam splitter to receive the laser beam just after it entered the water, as shown in Fig. 7-15. A small fraction of the beam was reflected vertically into a small integrating sphere. A proportional sample of the flux in that cavity was fed to a submerged multiplier phototube that controlled the power input to the laser. This feedback system eliminated all detectable variations in the power of the light beam as it entered the water whether caused by prism rotation, mechanical vibrations of the optical system, line voltage changes, or fluctuations within the laser. The output of the submerged monitor multiplier phototube was displayed continuously on a recording potentiometer-type strip chart recorder (Brown) so that the experimenter could verify that no detectable variations in laser beam power had occurred throughout the measurements.

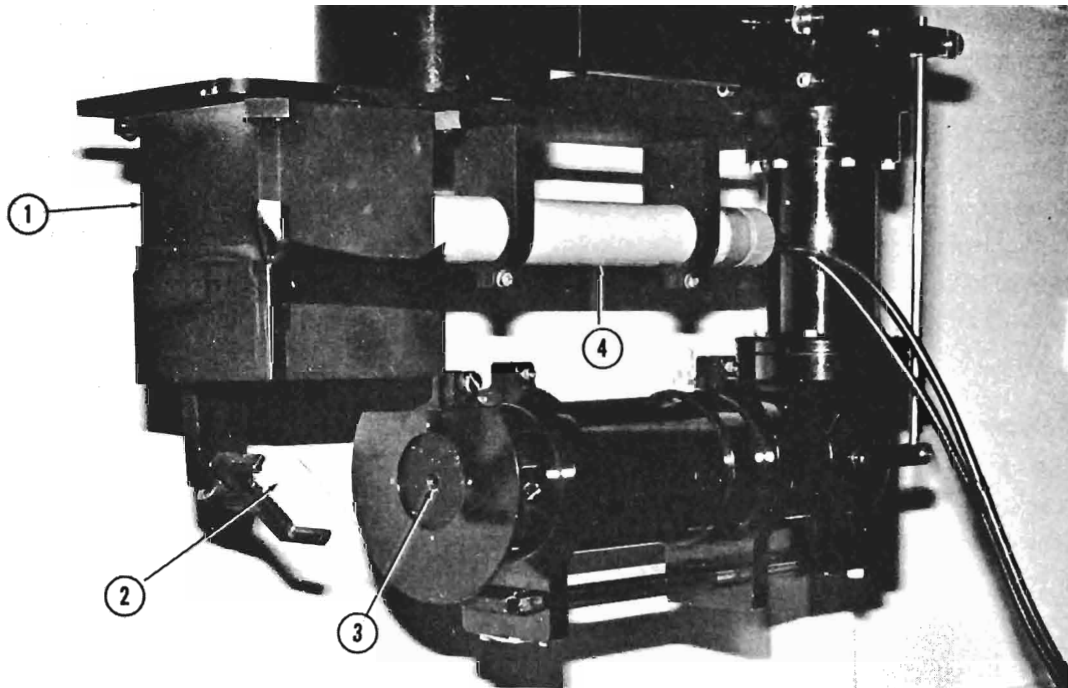


Fig. 7-15. Submergible light-beam pointing control system with beam splitter, and multiplier phototube for maintaining total beam power constant.

(1) integrating cavity; (2) beam splitter; (3) stop to eliminate weak satellite laser beams caused by inter-reflections between prism and window surfaces; (4) multiplier phototube in submergible housing.

## 7.6 STUDIES OF IRRADIANCE OFF-AXIS

It was the principal object of the laboratory tank to produce a family of curves like those generated at Diamond Island, but applicable to clear ocean water. This objective was achieved. The results are recorded in figures which follow. Actually, much more than this was achieved. Laser propagation has been measured in waters having a wide range of  $a/a$  ratios. Before explorations of ocean conditions could proceed, however, it was essential to simulate the  $a/a$  ratio of the water at Diamond Island and measure this in the tank for comparison with the measurements made previously at Diamond Island.

### COMPARISON WITH FIELD DATA

The total power received by a spherical cap centered on a laser beam at various distances was measured at the Visibility Laboratory's field station at Diamond Island, New Hampshire in 1966. Both the distance of the cap and its angular radius were varied. In all cases the center of the spherical surface was at the point where the laser beam entered the water; see diagram on page 7-32.

The light source used was a submergible RCA frequency-doubled neodymium-ion glass laser producing 20 nanosecond pulses of low-coherence light having a nominal wavelength of 530 nanometers. The water was characterized by an attenuation length of 1.4 m/ln and a beam spread parameter  $a/a = 4.04$  at the laser wavelength. The quality of the best of these field data was only moderate by laboratory standards.

Corresponding measurements were made in the laboratory tank using 514.5 nanometer light from a steady burning argon-ion laser configured to produce high coherence. The water had an attenuation length of 0.225 m/ln and a beam spread parameter  $\alpha/a = 4.00$  at the laser wavelength. Figure 7-17 shows computer plotted curves of these data. They are plotted in terms of the dimensionless source distance  $\alpha r$  from 0 to 23 attenuation lengths. The angular radius of the spherical cap ( $\gamma$ ) is from 0.1 to 100 degrees, as indicated by a vertical column of numbers at the right of the diagram.

Four columns of black dots in Fig. 7-17 represent comparison data obtained at Diamond Island. The satisfactory agreement between the two bodies of data strongly supports the validity of off-axis irradiance measurements at model scale in simulated natural waters.

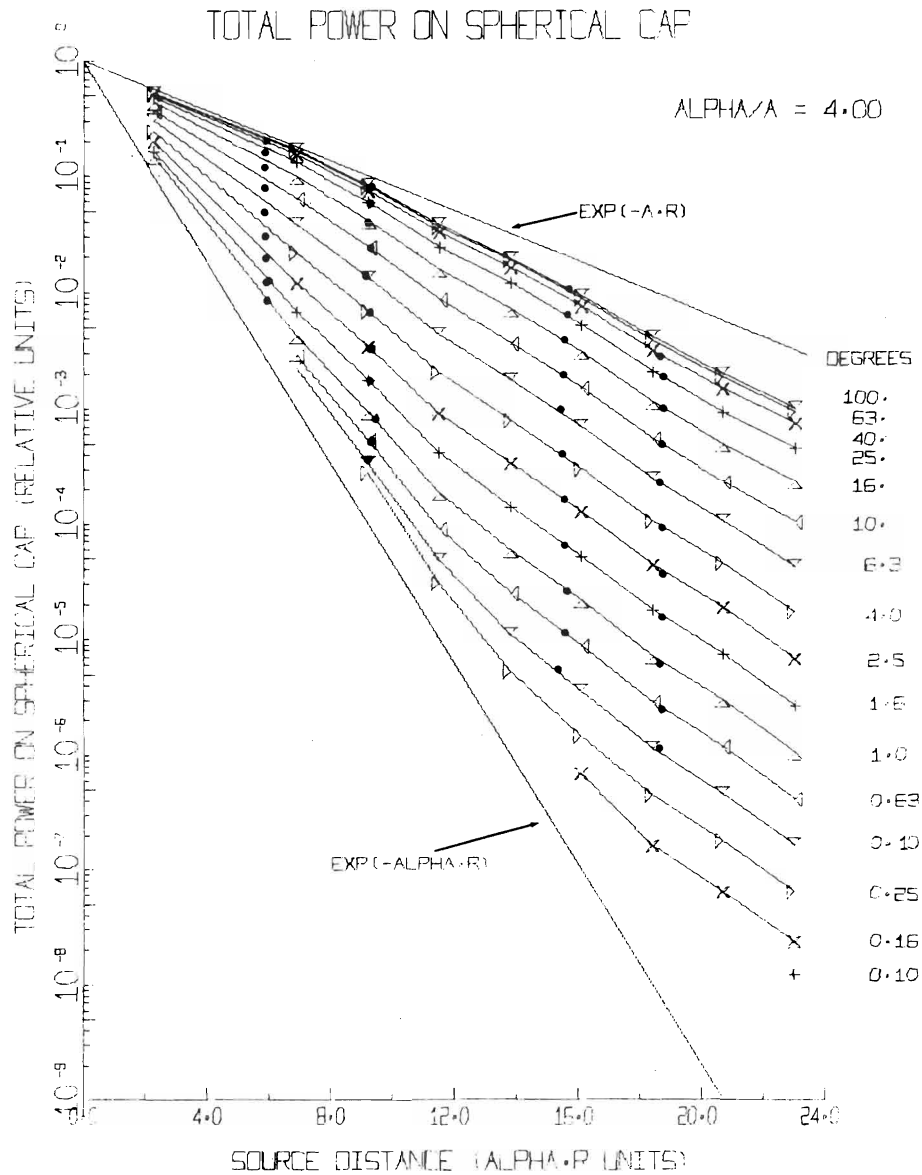


Fig. 7-17

## EFFECT OF POLARIZATION

The laser light was inherently polarized. The final element of the prism train was a linear polarizer which insured that the output beam would have a fixed state of polarization. Tests disclosed that off-axis irradiance is remarkably unaffected by the state of polarization of the laser beam.† A minor effect (a few percent) on measured irradiance can be detected at small off-axis angles below 3 or 4 degrees. At greater angles the effect of polarization quickly vanishes. The greatest off-axis angle at which the difference in irradiance between vertical and horizontal E-vector positions exceeded the threshold of photoelectric detection (about 0.1 percent) at any range in any water was 7 degrees. The irradiance collector was not polarization sensitive. All irradiance data in this report were taken with the E-vector vertical.

## EFFECT OF BEAM SHAPE

The laser beam has circular cross-sectional symmetry, but cylindrical lenses (up to 16 diopters) were sometimes put in the water outside the air tube to produce assymetry. The major axis of the resulting fan-shaped beam could be rotated by turning the cylindrical lens in its own plane. Much as in the case of polarization, beam shape and orientation had no detectable effect on measured irradiance beyond off-axis angles of 3 degrees or less.

## 7.7 IRRADIANCE OFF-AXIS IN CLEAR OCEAN WATER

Clear ocean water was simulated in the laboratory tank by making the beam spread parameter  $\alpha/a = 2.5$ . (Actually,  $\alpha/a = 2.49$ .) Figure 7-18 shows the measured off-axis irradiance (points) and curves drawn through these points by the computer.

The rising trend of these data at off-axis angles ( $\gamma$ ) greater than  $80^\circ$  was observed consistently but has not yet been fully explored. It may be attributable to the rapidly increasing volume of lighted water which contributes effectively to the received irradiance.

---

† The volume scattering function (a single-scatter, highly directional quantity) **does** depend on the state of polarization, particularly with polarization-sensitive detectors.

# IRRADIANCE

$\text{ALPHA}/\lambda = 2.49$

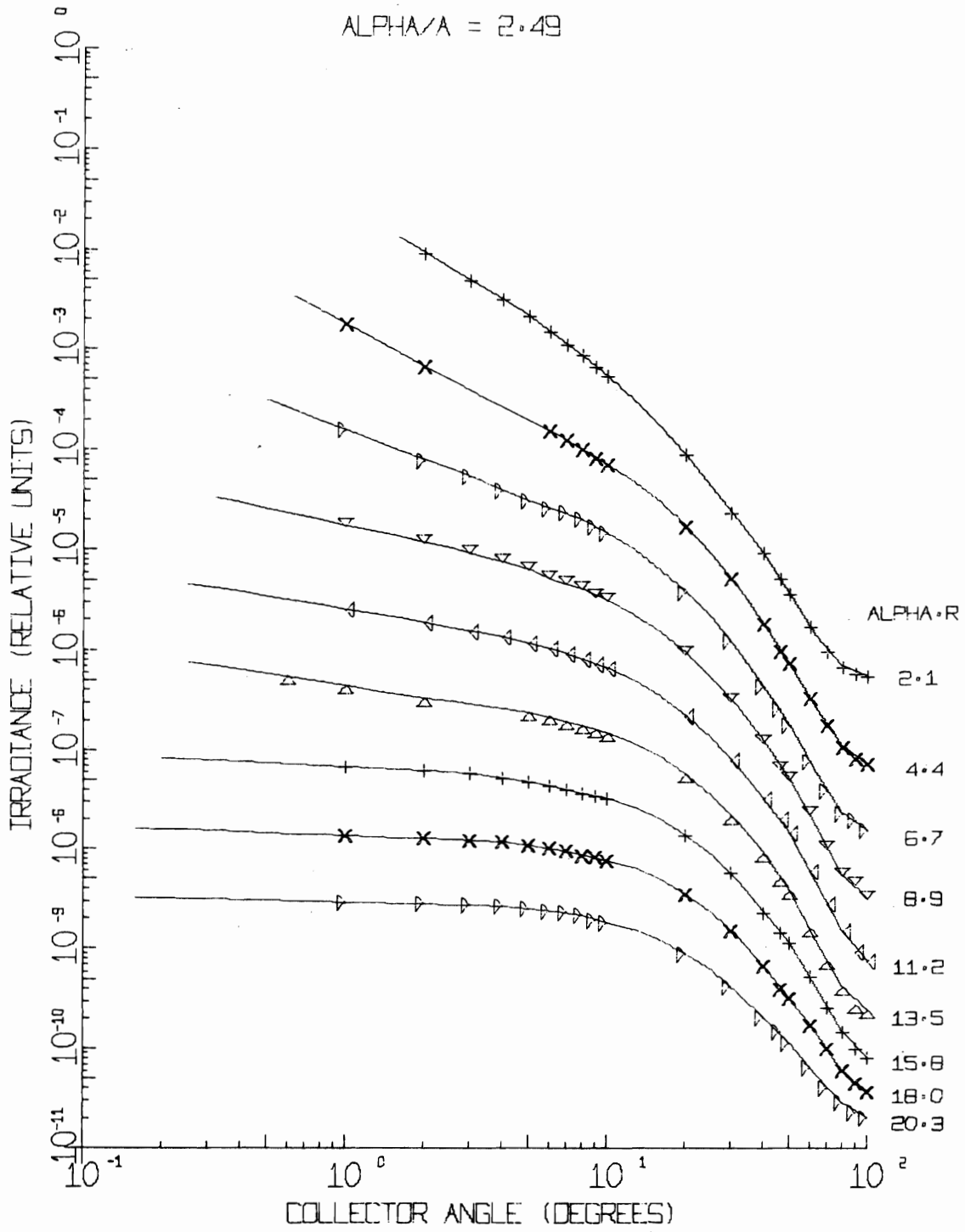


Fig. 7-18

The irradiance data in Fig. 7-18 have been integrated to produce a family of curves in Fig. 7-19. These show the total power on spherical caps having angular radius  $\gamma$ .

The nearly spherical nature of the irradiance functions below  $\gamma = 10^\circ$  are responsible for the long, nearly straight, inclined portions of the power curves at long dimensionless distances ( $\alpha r$ ). The same information is displayed in another, more familiar form, by Fig. 7-20. It will be noted that the spread of the curves in Fig. 7-20 is less than those in Fig. 7-17, which represents water for which  $\alpha/a = 4.0$ .

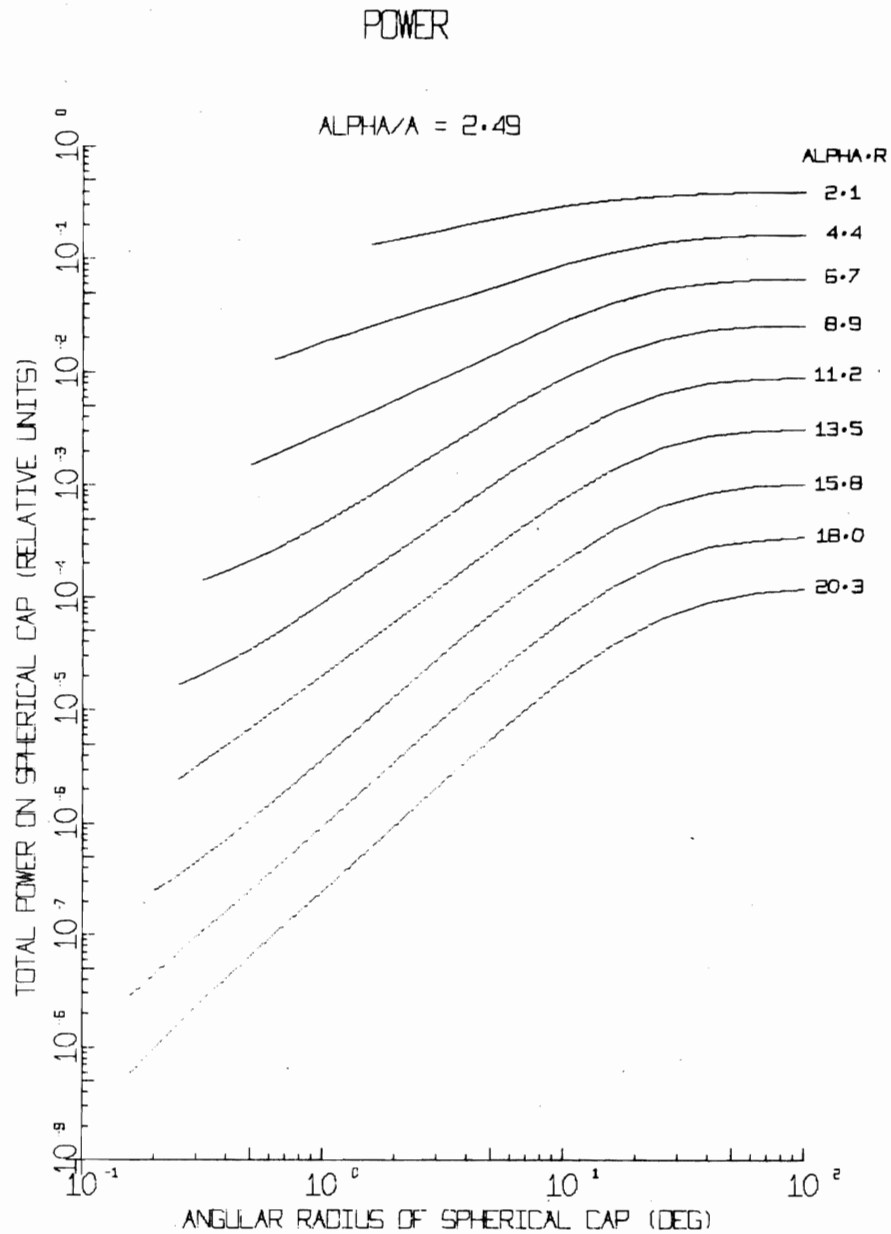


Fig. 7-19

The equation for spectral irradiance  $H(\gamma)$  produced at any off-axis angle  $\gamma$  by a laser having monochromatic power output  $P$  is

$$\frac{H(\gamma)}{P} = \frac{10^{A-C} \gamma^B}{2\pi r^2 \sin \gamma} \quad (7-1)$$

where:

$$A = 1.260 - 0.375 (\alpha r) [0.710 + 0.489 (\alpha/a)^{-1}] - [1.378 + 0.053 (\alpha/a)] 10^{-(\alpha r)} [0.268 + 0.083 (\alpha/a)],$$

$$B = 1 - 2(10^{-D}),$$

$$C = \frac{1}{3} \left[ \left( \frac{\gamma^{3/2} + E^{3/2}}{E^{3/2}} \right)^{2/3} - 1 \right]$$

$$D = (\alpha r) [0.018 + 0.011 (\alpha/a) + 0.001725 (\alpha r)], \text{ and}$$

$$E = [13.75 - 0.501 (\alpha/a)] - [0.626 - 0.0357 (\alpha/a)] (\alpha r) + [0.01258 + 0.00354 (\alpha/a)] (\alpha r)^2.$$

Inspection of the equation shows that the computed numerical answer is in terms of irradiance per unit of laser power. That is to say, if the equation predicts an irradiance  $H$  at some off-axis angle and at an actual distance of, say, 100 feet, this means that the irradiance at that point in the light field is  $H$  watts per square foot for each watt of total beam power produced by the laser.

Inspection of the right hand member of Eq. (7-1) shows that the denominator has a form which arises from the differential solid angle and a numerator which is governed by three exponents,  $A$ ,  $B$ , and  $C$ , identified below. The functions  $A$  and  $B$  control the magnitude and slope, respectively, of the irradiance curves at an off-axis angle of about  $1^\circ$ . The function  $C$  controls the shape of the irradiance curves at large off-axis angles. It will be noted that  $A$ ,  $B$ , and  $C$  are functions of the dimensionless distance  $\alpha r$ , the beam spread parameter  $\alpha/a$ , and, in the case of  $C$ , also the off-axis angle  $\gamma$ .

#### FIDELITY OF THE IRRADIANCE EQUATION

Equation (7-1) was developed from the laboratory data listed in Table 7-2. The fidelity with which it represents the experimental results can be judged from Figs. 7-38 through 7-41. In these figures the data are represented by points and the curves were plotted from Eq. (7-1). It is believed that the data for  $\alpha/a = 2.49$  and  $\alpha/a = 5.88$  are of slightly higher quality than those for  $\alpha/a = 3.29$  and  $4.86$ . Accordingly, somewhat more weight was given to them in fitting the constants in Eq. (7-1).

The comparisons between the data and the computer generated curves based upon Eq. (7-1) seem clearly to demonstrate that the equation is adequate for use in the engineering design of laser systems for use in water. Parametric studies for optimization of such designs should be straightforward and as reliable as the input data  $\alpha$  and  $a$ .

# TOTAL POWER ON SPHERICAL CAP

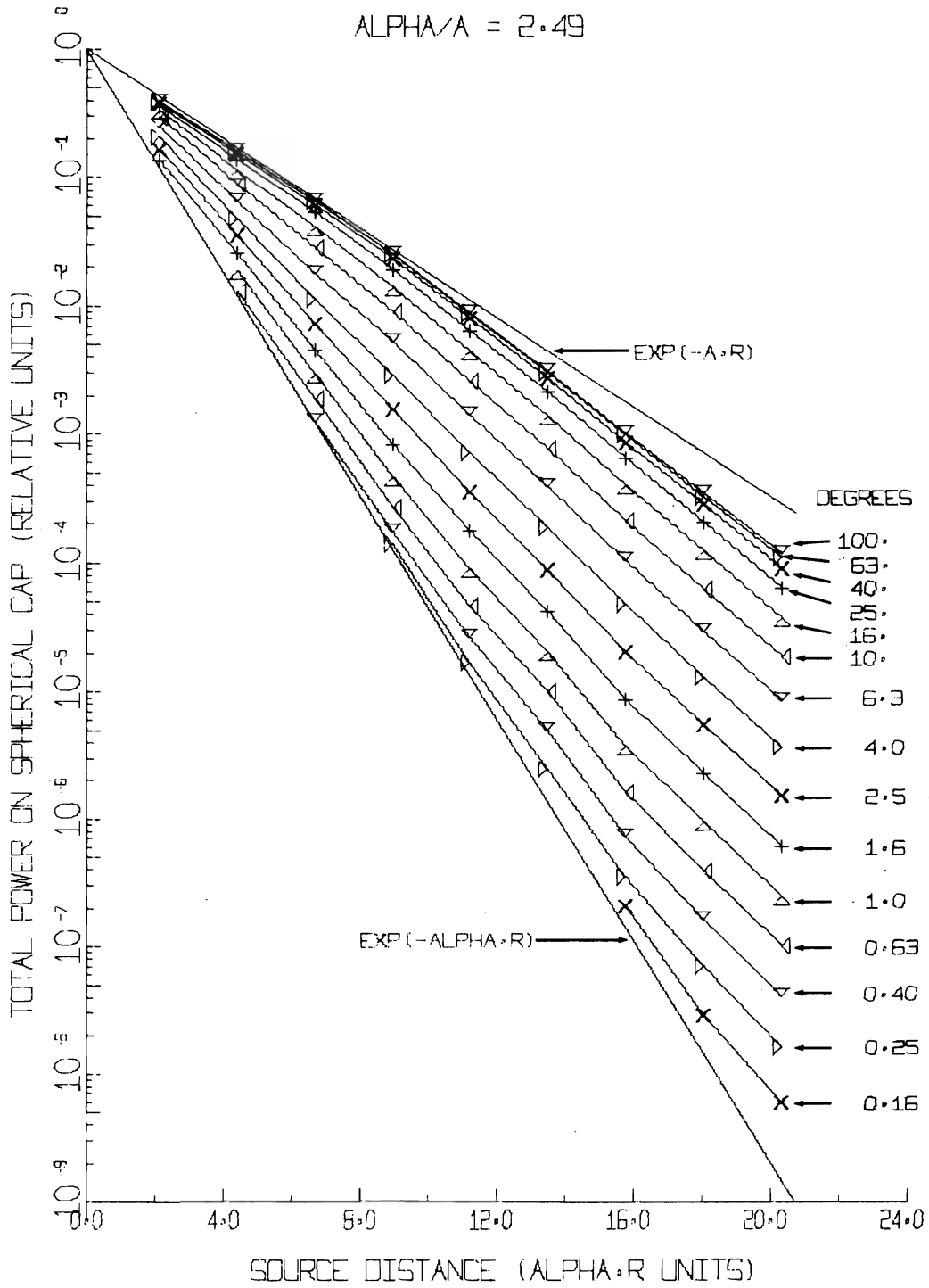


Fig. 7-20



The spreading of laser beams in water is illustrated in polar coordinate form by Fig. 7-21. The figure is drawn as if a laser submerged in uniform water at the origin of the plot is injecting a beam of light upward along the  $0^\circ$  radial. The first curve is the boundary within which 10 percent of the total power reaching the distance  $\alpha r$  is contained; it should be thought of as generating a surface of revolution about the  $0^\circ$  radial; i.e., about the laser beam. The raggedness of the 0.9 fractional power boundary is caused by the necessity for taking small differences between large numbers during the computation.

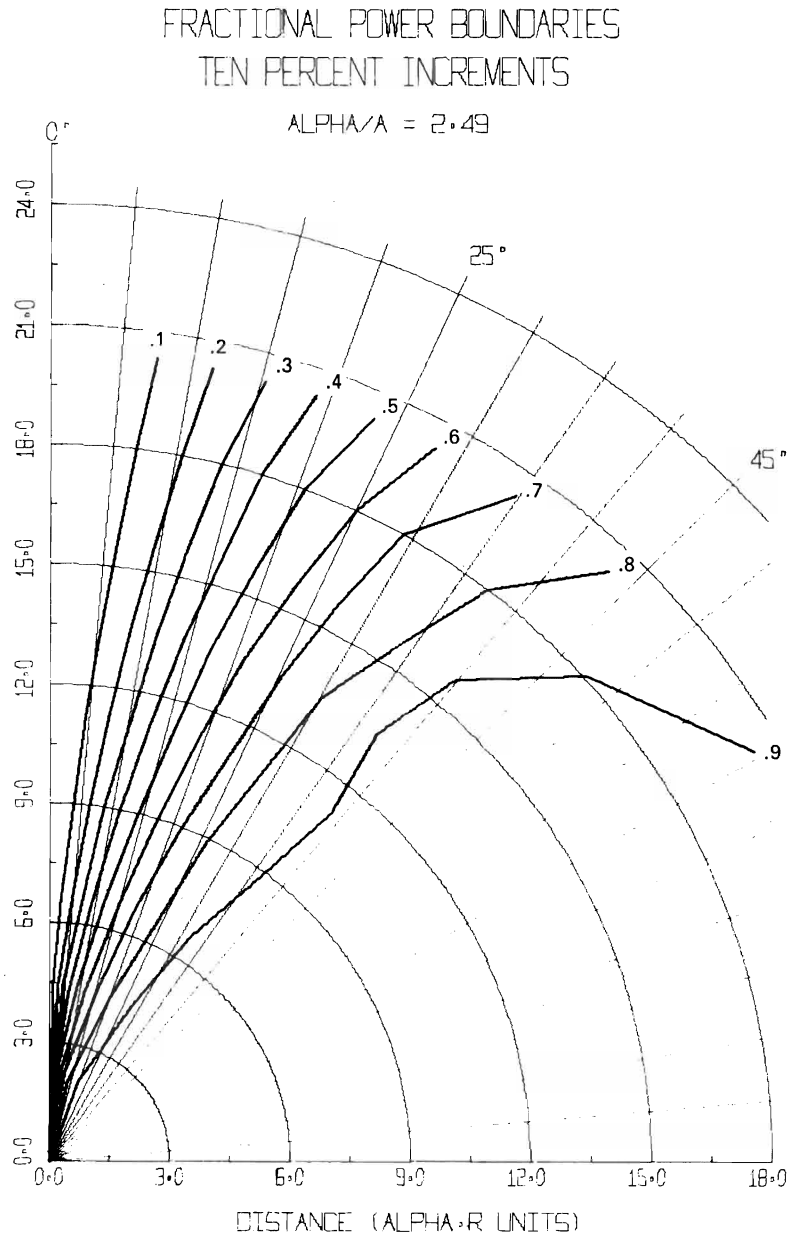


Fig. 7-21

## 7.8 OFF-AXIS IRRADIANCE IN OTHER WATERS

Very clear ocean water occurs in vast central ocean areas, but waters having higher ratios of  $a/a$  are prevalent on continental shelves and elsewhere. Beam spread ( $a/a$ ) and water clarity ( $1/a$ ) do not vary together in any simple way throughout the oceans. This complexity is illustrated by Table 7-1, in which locations are arranged in descending order of water clarity (first column) and beam spread (second column), respectively. The numerical values were generated chiefly from data published by Jerlov. They pertain to blue light rather than green.

**Table 7-1. Comparison of Ocean Waters**

Water Clarity (Attenuation Length) (465 nm)		Beam Spread ( $a/a$ ) (465 nm)	
Eastern Mediterranean	15.4 m/ln	Western Pacific	3.6
Sargasso Sea	14.1	Sargasso Sea	3.5
Western Pacific	11.8	Caribbean	3.5
Red Sea	9.8	Northeastern Atlantic	3.1
Caribbean	8.7	Eastern Mediterranean	3.1
Northeastern Atlantic	6.3	Red Sea	2.2
Galapagos Islands	5.2	Galapagos Islands	2.1
Diamond Island (530 nm)	1.4	Diamond Island (530 nm)	4.0

Six waters ranging from  $a/a = 2.49$  to  $a/a = 5.88$  were measured in the laboratory tank. Data for each water (except  $a/a = 4.00$ ) are given by a set of four plots like Figs. 7-18 through 7-21 in section 7.7. These plots show off-axis irradiance, total power on spherical caps, and fractional power boundaries throughout the space surrounding the laser beam. The 6 sets of figures are listed in Table 7-2.

**Table 7-2. Data for Simulated Ocean Waters**

$a/a$	Figure Numbers
2.49	7-18 through 7-21
3.29	7-22 through 7-25
4.00	7-17
4.57	7-26 through 7-29
4.86	7-30 through 7-33
5.88	7-34 through 7-37

IRRADIANCE

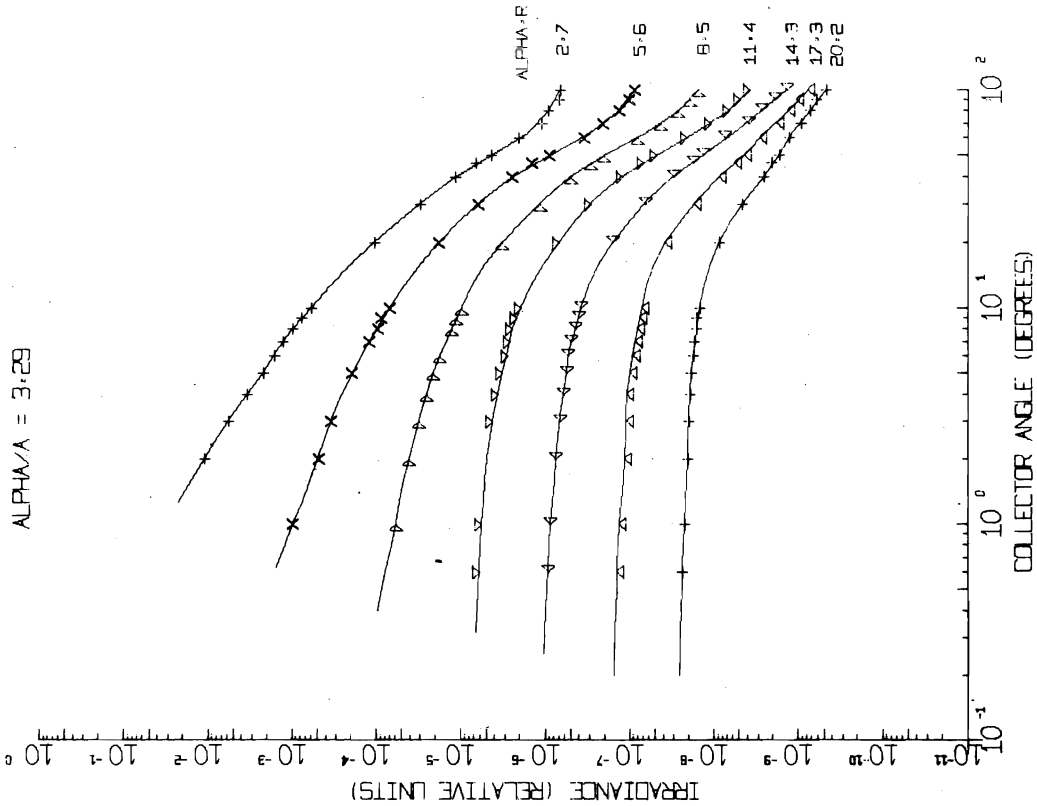


Fig. 7-22

POWER

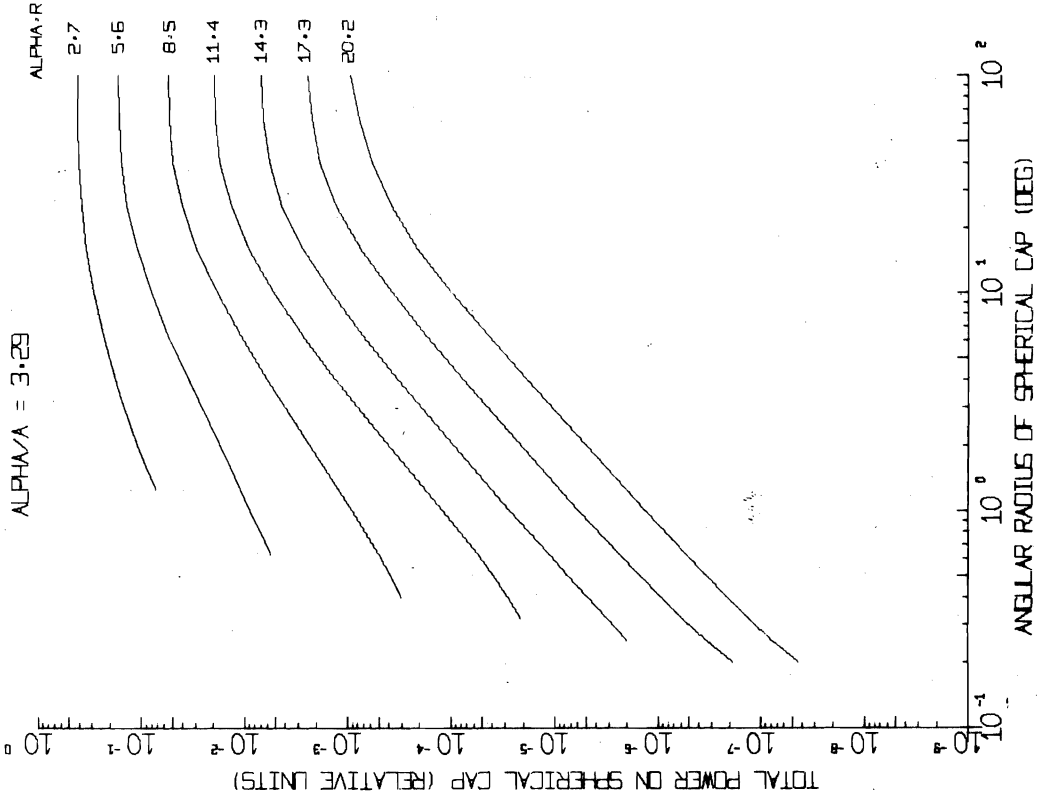


Fig. 7-23

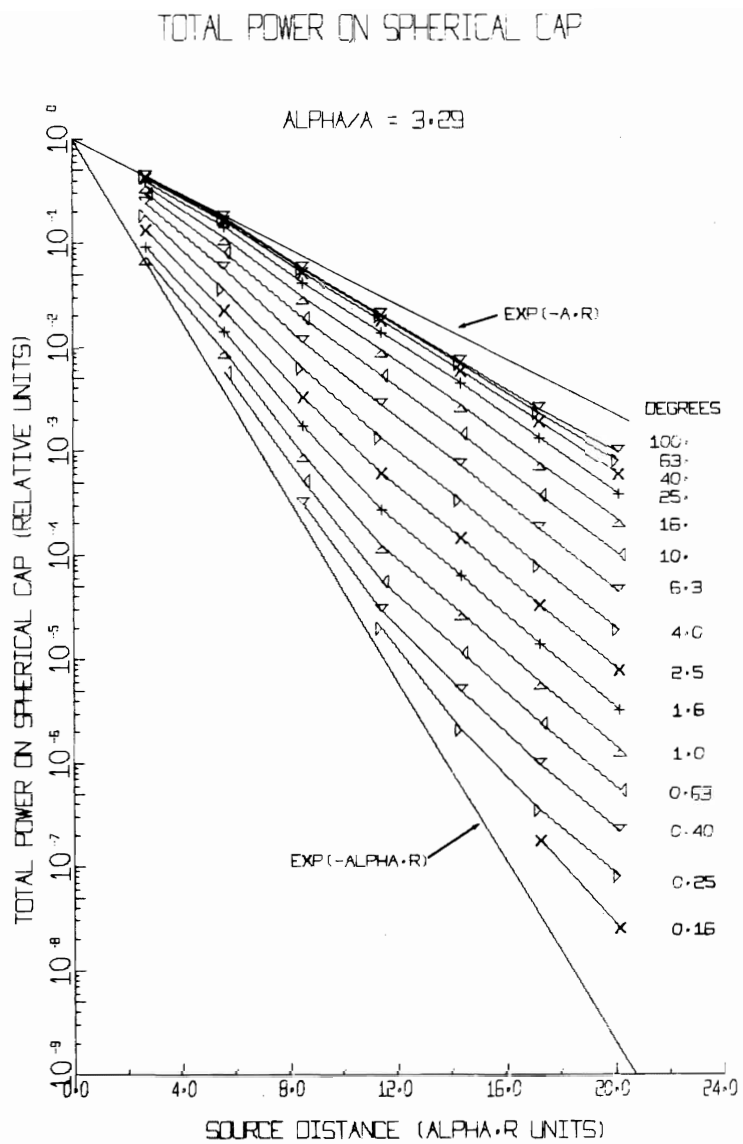


Fig. 7-24

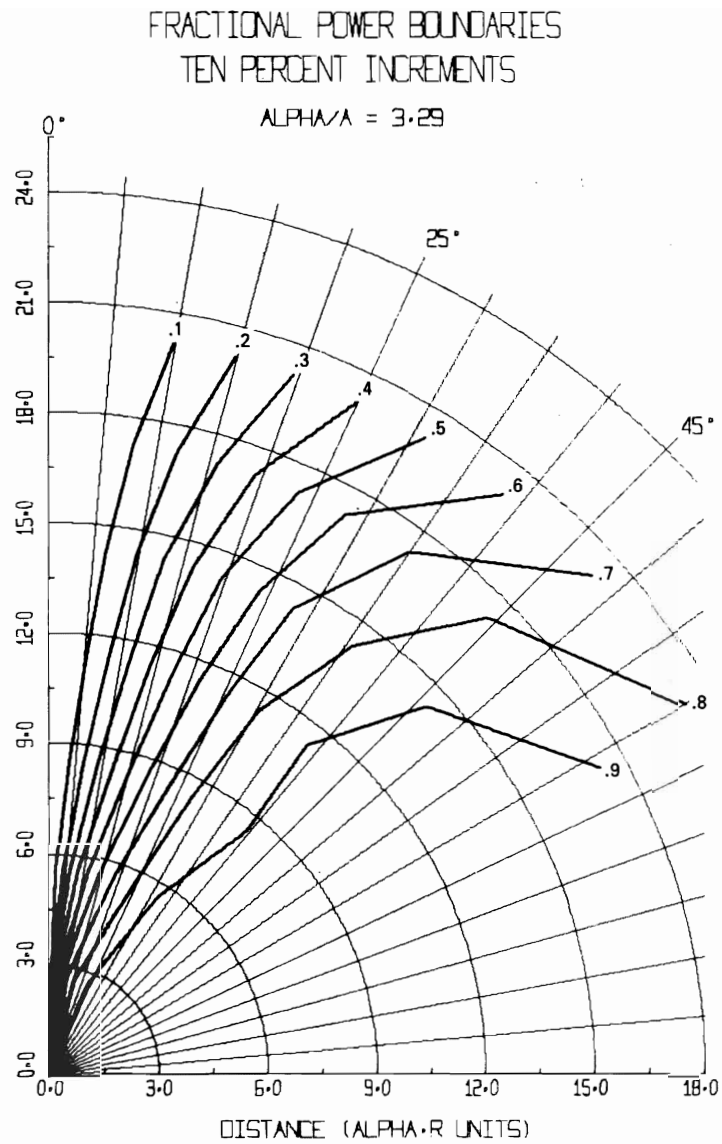


Fig. 7-25

IRRADIANCE

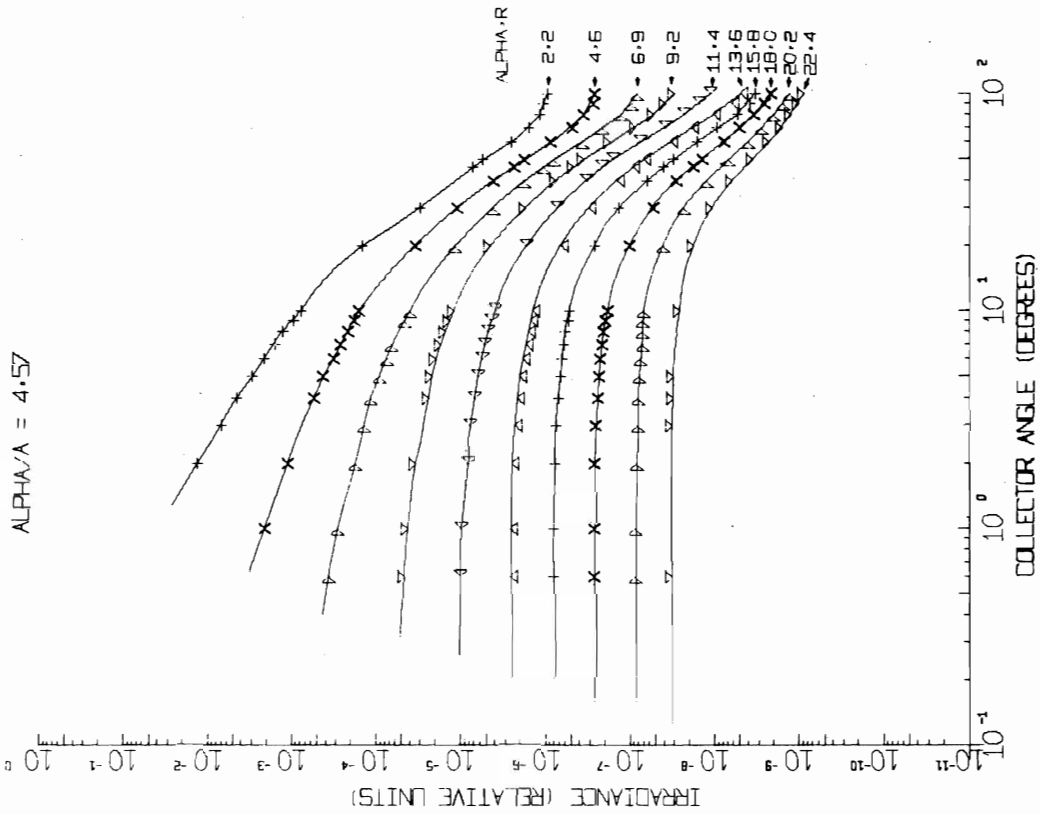


Fig. 7-26

POWER

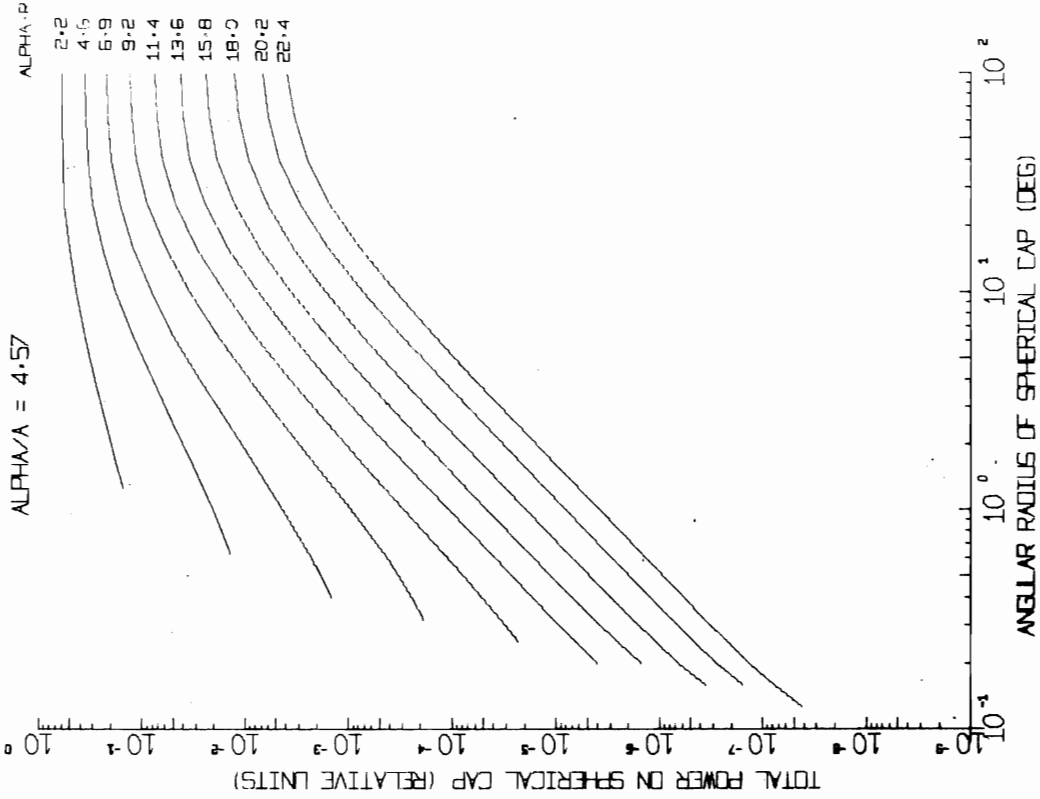


Fig. 7-27

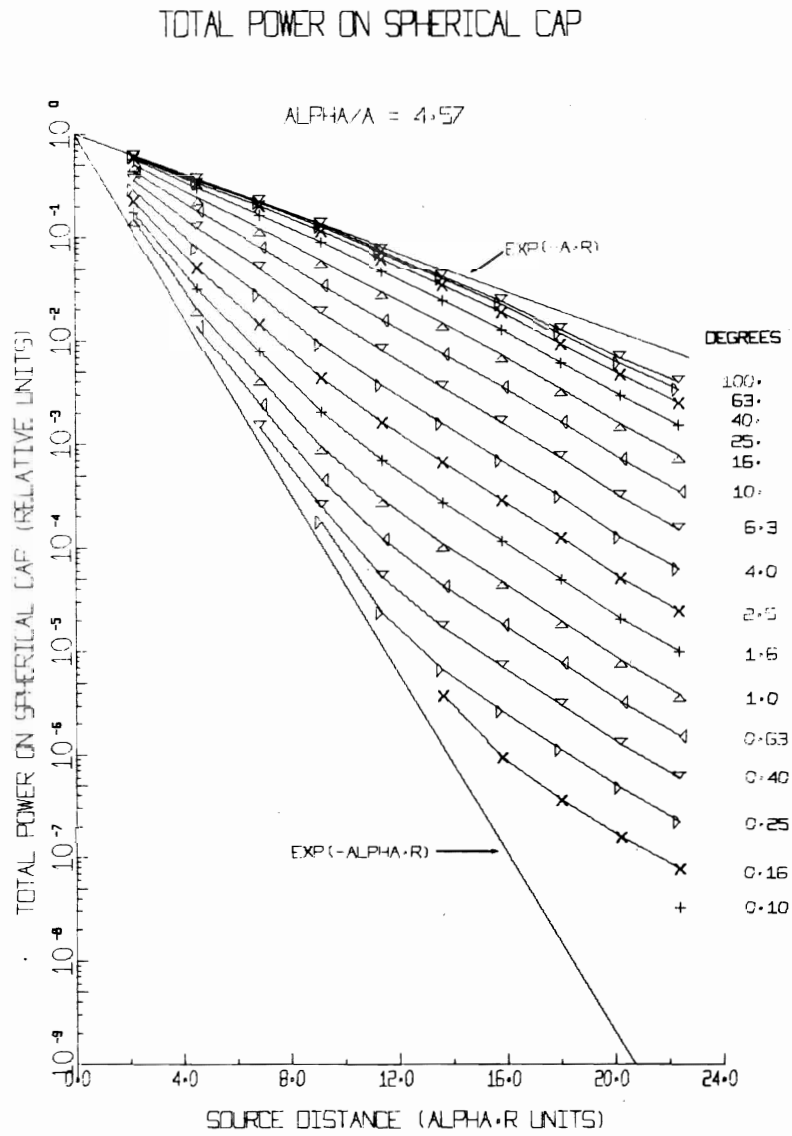


Fig. 7-28

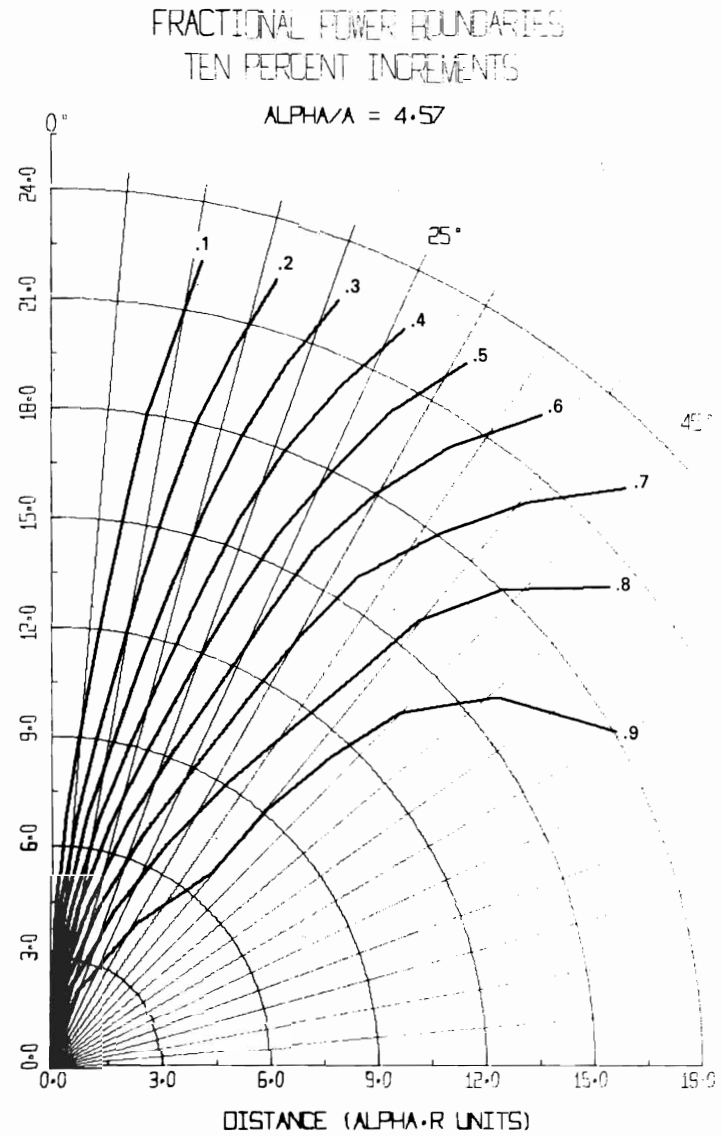


Fig. 7-29

IRRADIANCE

ALPHA/A = 4.86

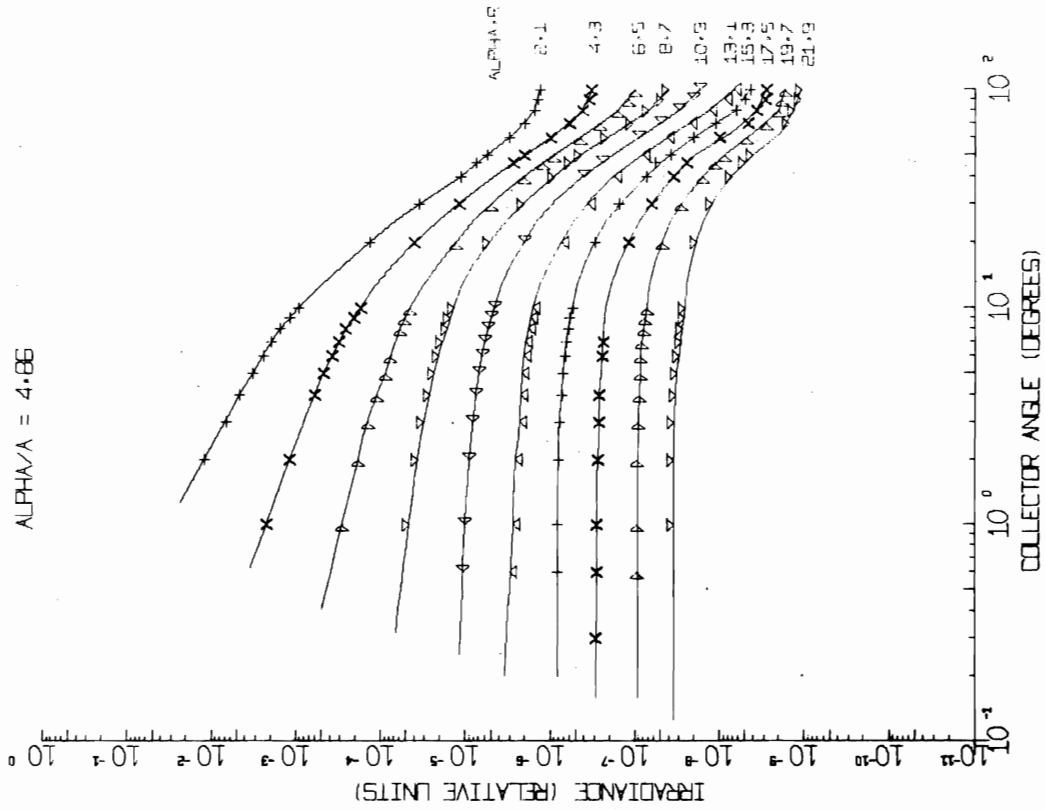


Fig. 7-30

POWER

ALPHA/A = 4.86

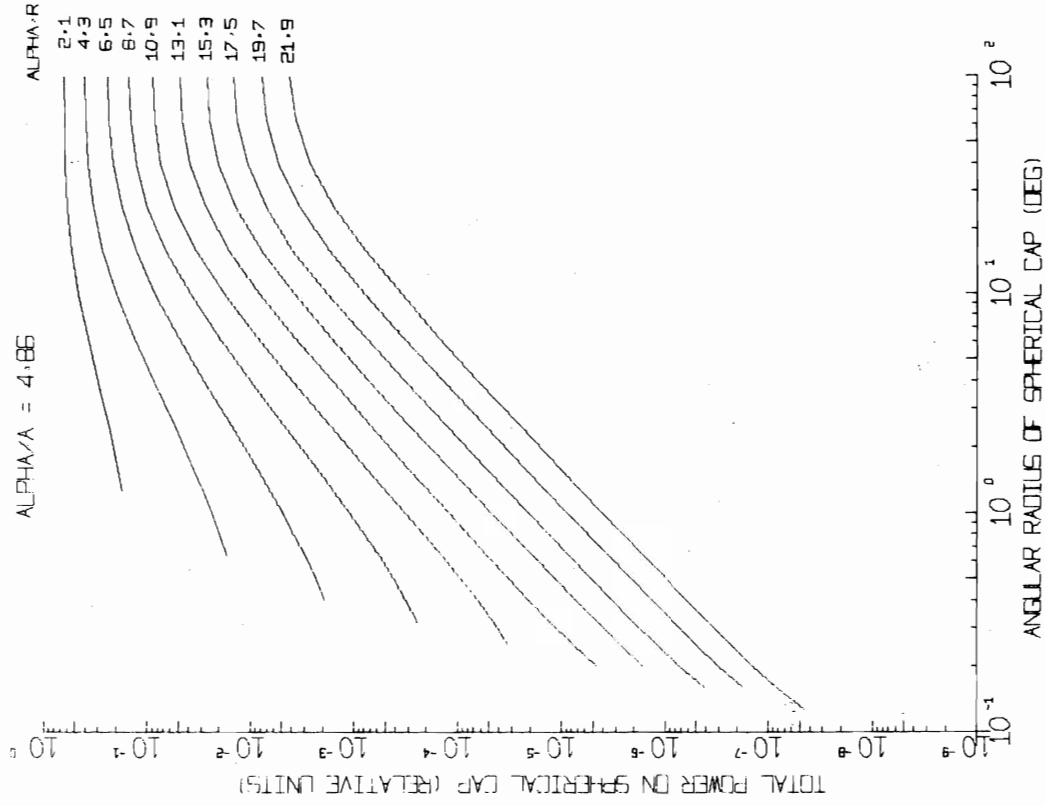


Fig. 7-31

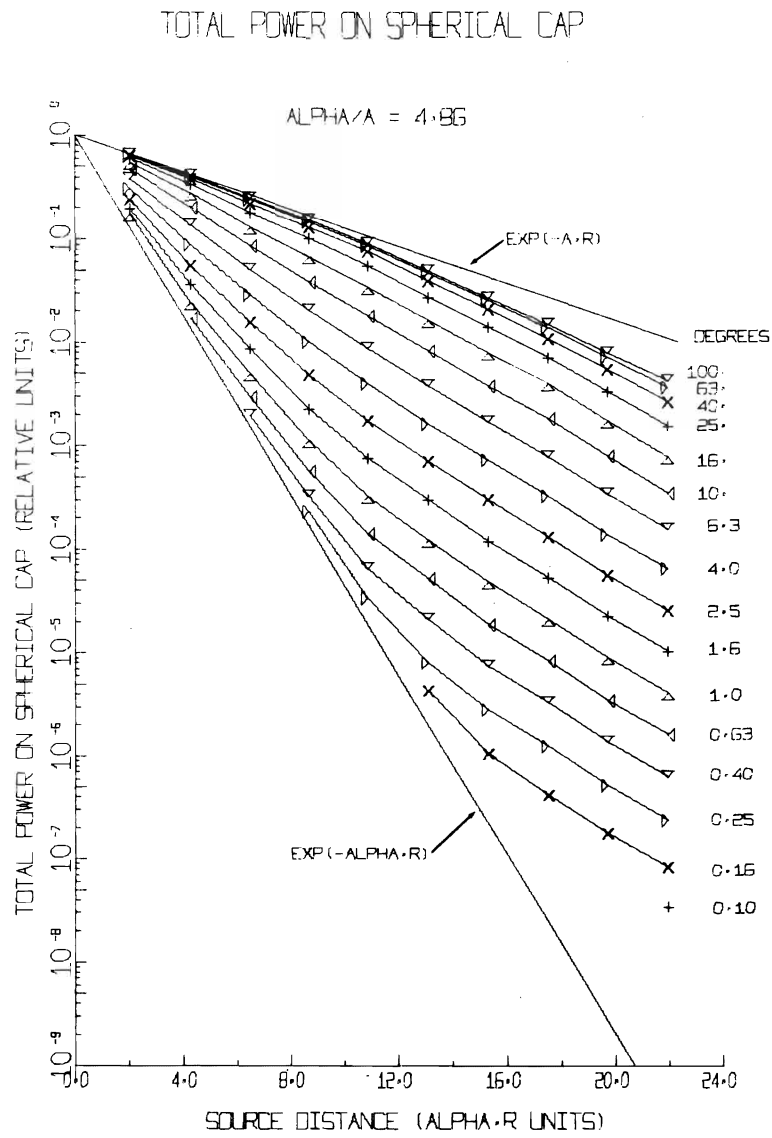


Fig. 7-32

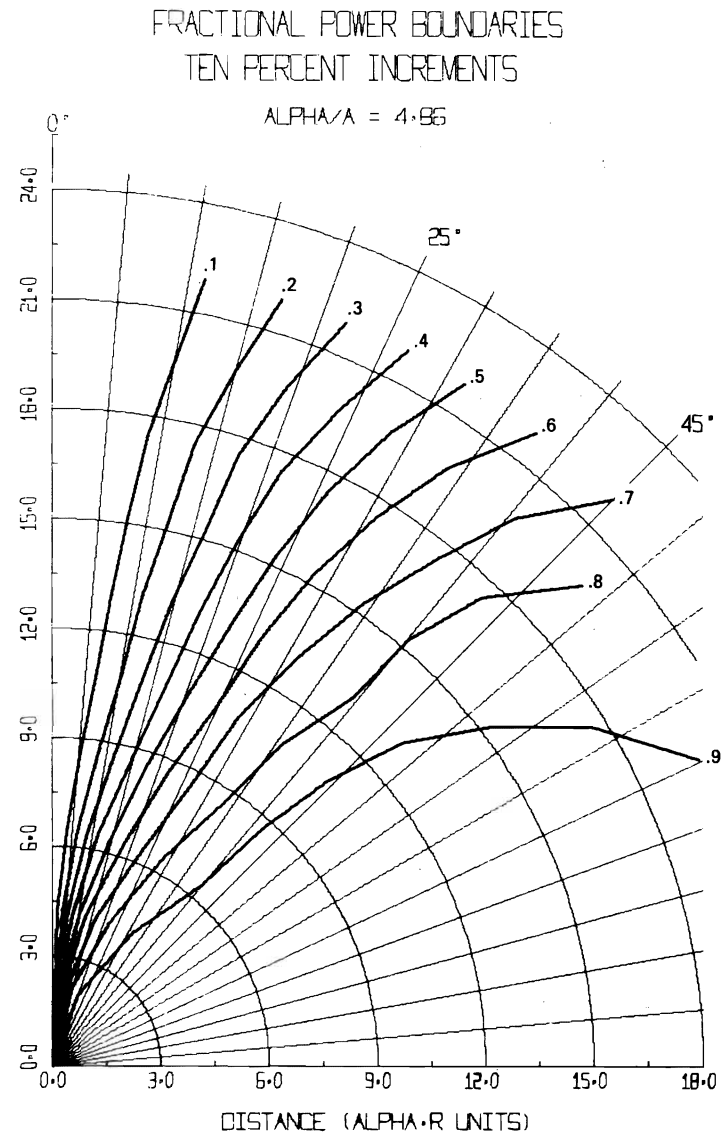


Fig. 7-33



IRRADIANCE

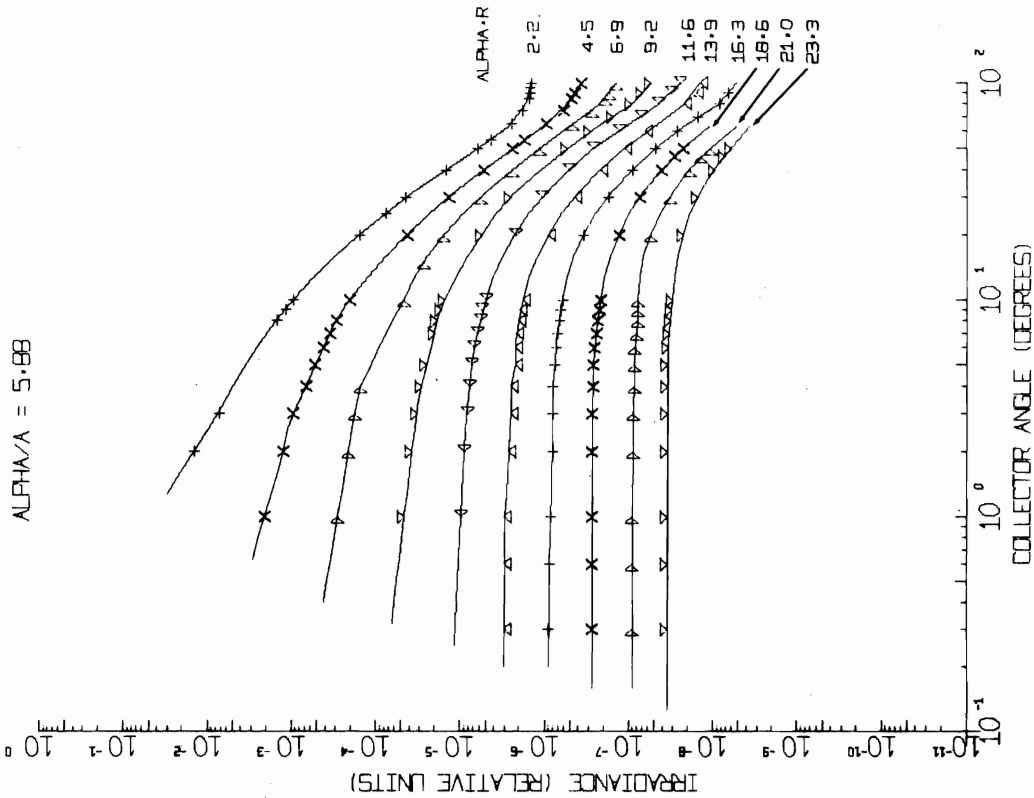


Fig. 7-34

POWER

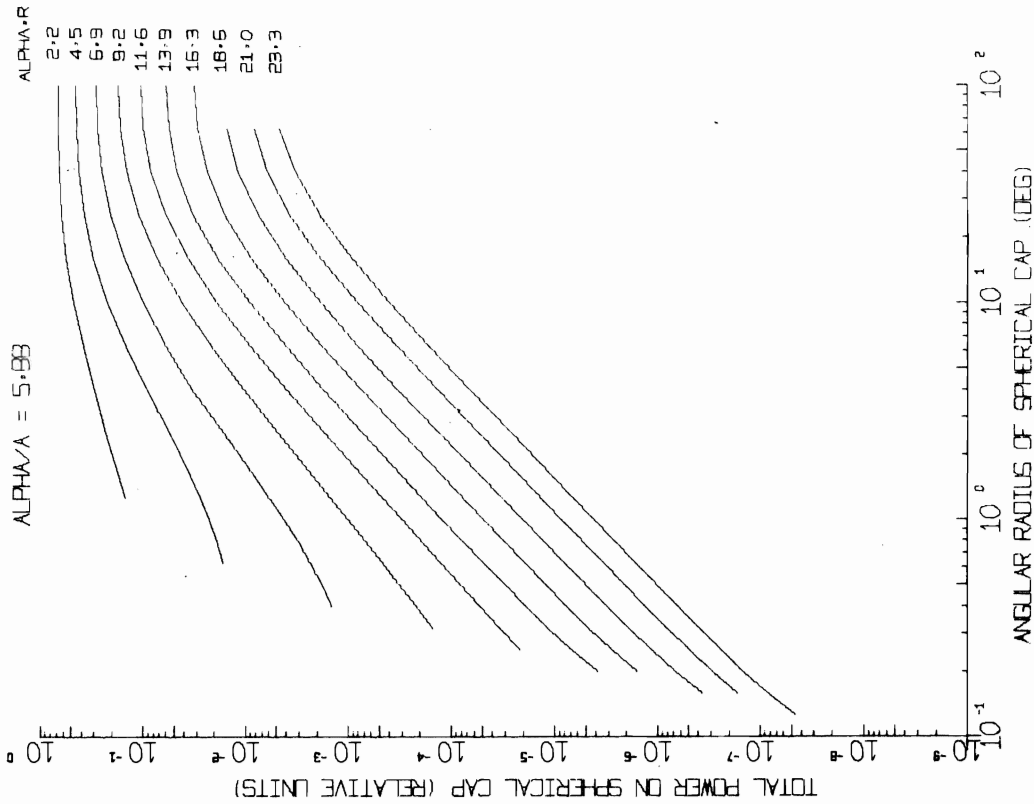


Fig. 7-35

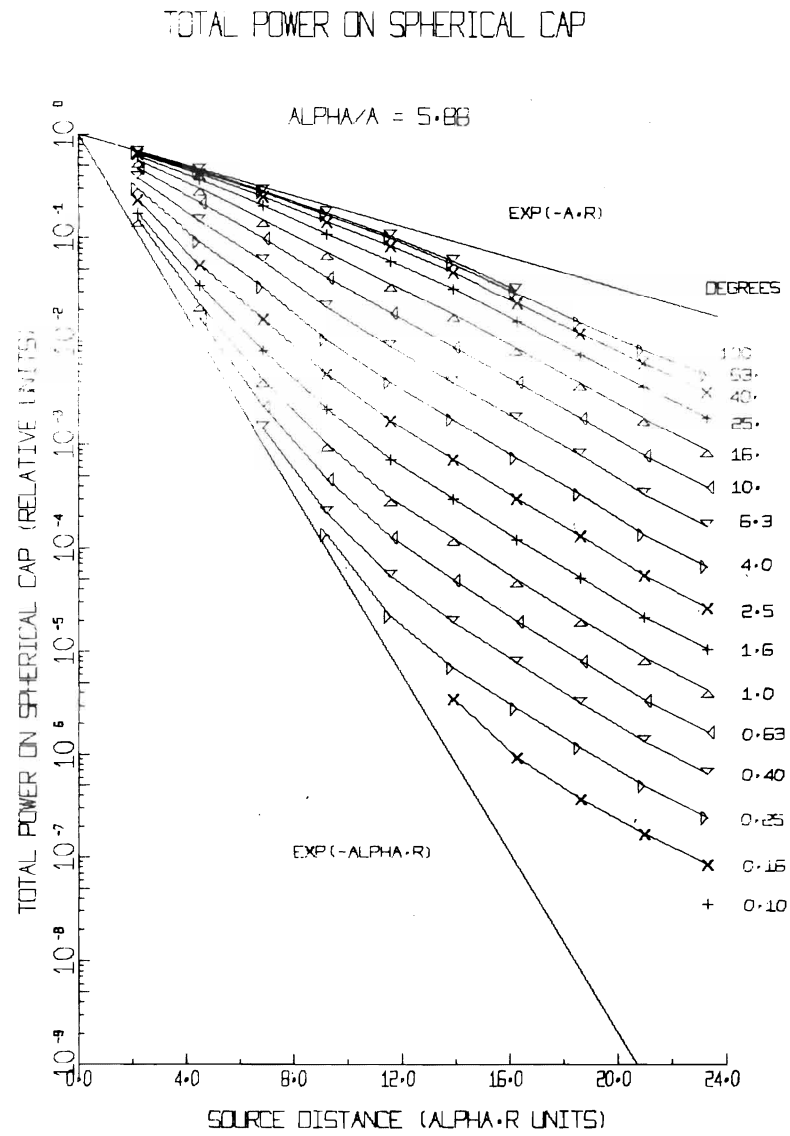


Fig. 7-36

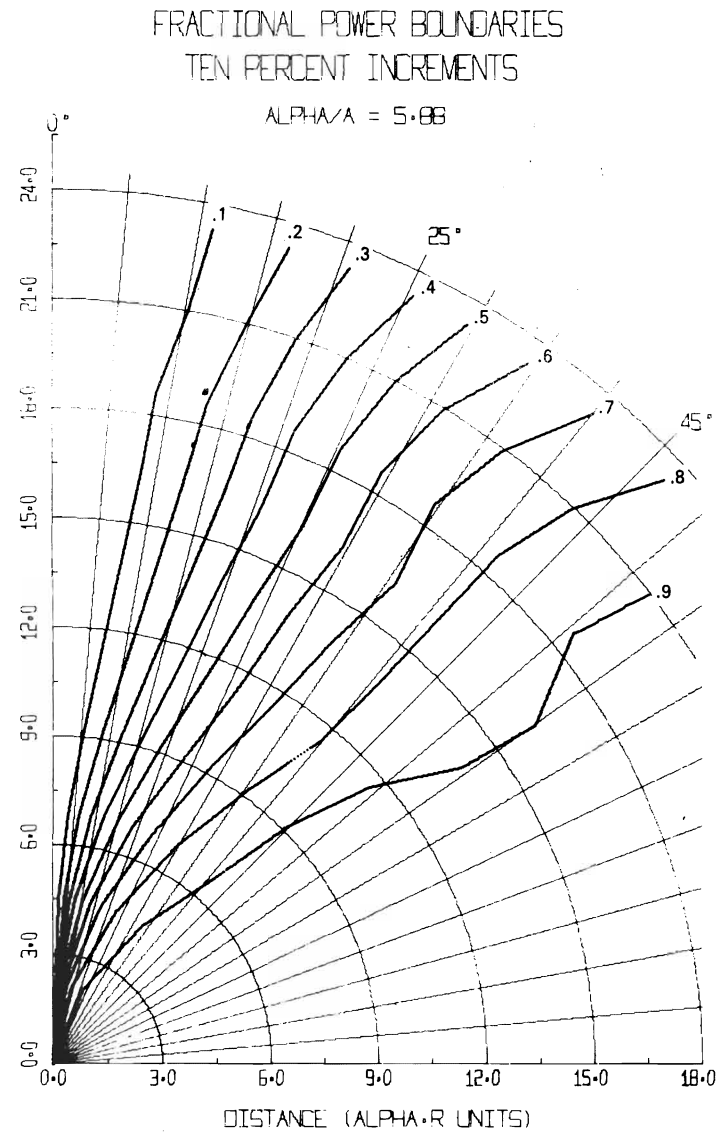


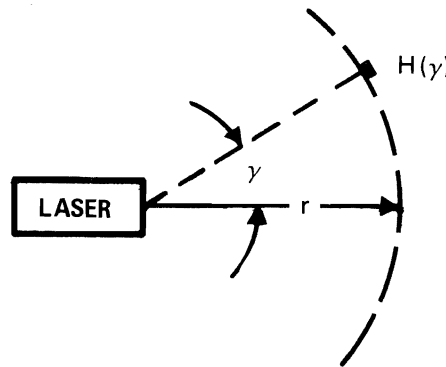
Fig. 7-37

## 7.9 AN EQUATION FOR ENGINEERING USE

It is obvious that engineers will need data on the performance of underwater laser systems in other types of water and at other wavelengths than those that have been measured in this study. They will also need data at intermediate distances. There is a need, therefore, for tractable closed-form equations that summarize all of the findings and data that are displayed by the preceding plots and serve automatically to interpolate these results for other waters, other wavelengths, and other distances. Computer programs based on such equations will enable design compromises to be explored by means of parametric calculations.

An empirical equation for off-axis irradiance was produced and computer tested at ranges from 0.5 to 21 attenuation lengths.\* It has been compared against data from the tank having  $a/a$  ratios ranging from 2.5 to 5.88. It has been used to predict irradiance functions and power functions from  $a/a = 2.0$  to 10. In these extrapolations beyond our present experimental data, the predicted irradiance curves and power curves look very reasonable. We believe that the equation is an engineering tool for parametric studies that can be used to predict the irradiance produced by underwater lasers in virtually any kind of natural water, at any wavelength, at any off-axis angle up to  $90^\circ$ , and at any range from 0.5 to, at least, 20 attenuation lengths.

The diagram below illustrates the geometry to which the equation applies. It represents a submerged laser sending a beam horizontally to the right. Irradiance is measured at a constant radius  $r$  from the point at which the light beam enters the water. The off-axis angle is measured by  $\gamma$ . When the irradiance data are integrated to obtain the total power on a spherical cap,  $\gamma$  is the angular radius of the cap.



\*An early, apparent success in formulating an empirical equation for engineering use had the form  $P(\gamma) = P e^{-(ar)} (a/a)^\rho$ , where  $P(\gamma)$  is the total power received by a centered, spherical cap of angular radius  $\gamma$ ,  $P$  is the total beam power produced by the laser, and  $\rho$  denotes a function of  $a/a$ ,  $ar$ , and  $\gamma$  in a structure of incomplete gamma-functions. Although this equation fitted the power curves well, it was soon discovered that the partial derivative of  $P(\gamma)$  with respect to  $\gamma$  did not represent the irradiance data. Inasmuch as these data are the ones of primary importance from an engineering standpoint the early equation was abandoned. Subsequent effort was devoted entirely to obtaining an empirical equation for off-axis irradiance. The ultimate result was equation 7-1 as given in this section.

The equation for spectral irradiance  $H(\gamma)$  produced at any off-axis angle  $\gamma$  by a laser having monochromatic power output  $P$  is

$$\frac{H(\gamma)}{P} = \frac{10^{A-C} \gamma^B}{2\pi r^2 \sin \gamma} \quad (7-1)$$

where:

$$A = 1.260 - 0.375 (\alpha r) [0.710 + 0.489 (\alpha/a)^{-1}] - [1.378 + 0.053 (\alpha/a)] 10^{-(\alpha r)} [0.268 + 0.083 (\alpha/a)],$$

$$B = 1 - 2(10^{-D}),$$

$$C = \frac{1}{3} \left[ \left( \frac{\gamma^{3/2} + E^{3/2}}{E^{3/2}} \right)^{2/3} - 1 \right]$$

$$D = (\alpha r) [0.018 + 0.011 (\alpha/a) + 0.001725 (\alpha r)], \text{ and}$$

$$E = [13.75 - 0.501 (\alpha/a)] - [0.626 - 0.0357 (\alpha/a)] (\alpha r) + [0.01258 + 0.00354 (\alpha/a)] (\alpha r)^2.$$

Inspection of the equation shows that the computed numerical answer is in terms of irradiance per unit of laser power. That is to say, if the equation predicts an irradiance  $H$  at some off-axis angle and at an actual distance of, say, 100 feet, this means that the irradiance at that point in the light field is  $H$  watts per square foot for each watt of total beam power produced by the laser.

Inspection of the right hand member of Eq. (7-1) shows that the denominator has a form which arises from the differential solid angle and a numerator which is governed by three exponents,  $A$ ,  $B$ , and  $C$ , identified below. The functions  $A$  and  $B$  control the magnitude and slope, respectively, of the irradiance curves at an off-axis angle of about  $1^\circ$ . The function  $C$  controls the shape of the irradiance curves at large off-axis angles. It will be noted that  $A$ ,  $B$ , and  $C$  are functions of the dimensionless distance  $\alpha r$ , the beam spread parameter  $\alpha/a$ , and, in the case of  $C$ , also the off-axis angle  $\gamma$ .

#### FIDELITY OF THE IRRADIANCE EQUATION

Equation (7-1) was developed from the laboratory data listed in Table 7-2. The fidelity with which it represents the experimental results can be judged from Figs. 7-38 through 7-41. In these figures the data are represented by points and the curves were plotted from Eq. (7-1). It is believed that the data for  $\alpha/a = 2.49$  and  $\alpha/a = 5.88$  are of slightly higher quality than those for  $\alpha/a = 3.29$  and  $4.86$ . Accordingly, somewhat more weight was given to them in fitting the constants in Eq. (7-1).

The comparisons between the data and the computer generated curves based upon Eq. (7-1) seem clearly to demonstrate that the equation is adequate for use in the engineering design of laser systems for use in water. Parametric studies for optimization of such designs should be straightforward and as reliable as the input data  $\alpha$  and  $a$ .

IRRADIANCE

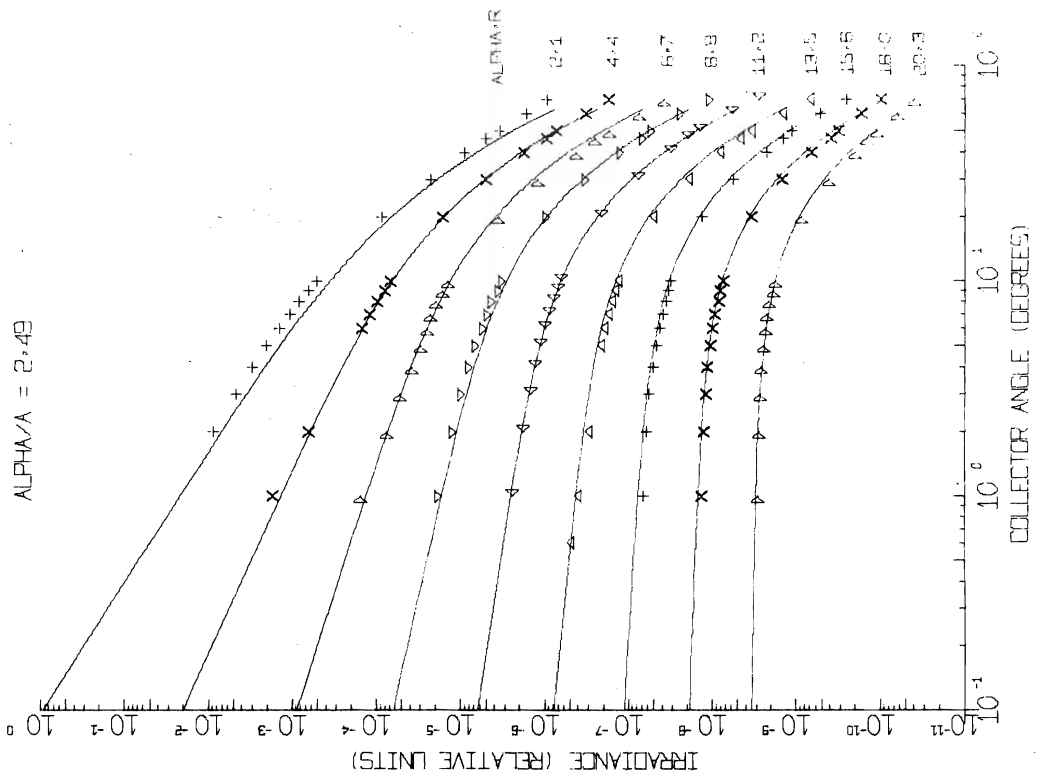


Fig. 7-38

IRRADIANCE

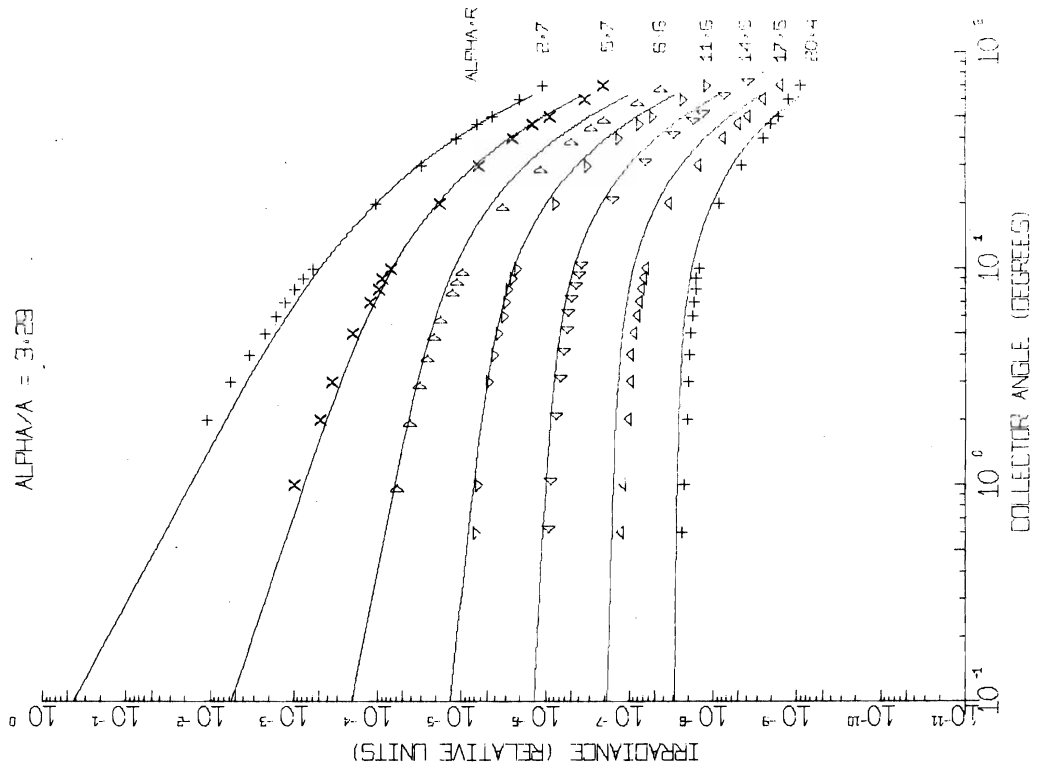
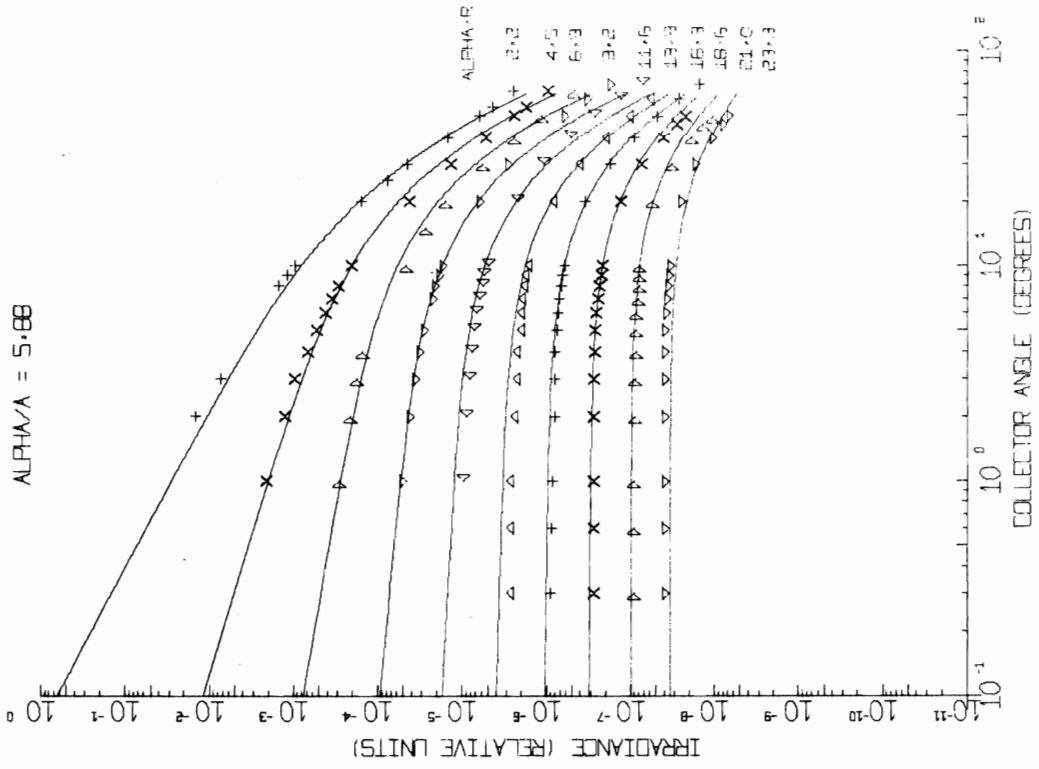


Fig. 7-39

IRRADIANCE



IRRADIANCE

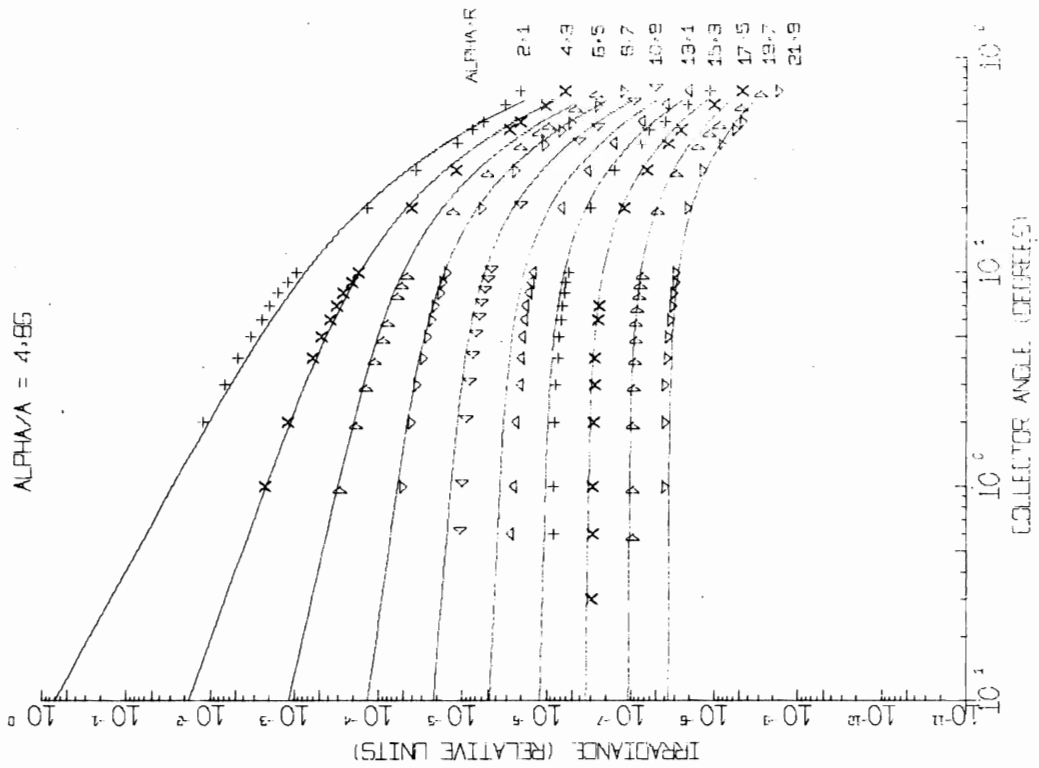


Fig. 7-41

Fig. 7-40

Off-axis irradiance displayed in Figs. 7-18, 7-38, and similar plots is given in relative units. Users wishing numerical values like those produced by Eq. (7-1) should multiply relative irradiance read from these figures by  $4.98 \times 10^3$ . This factor allows for the finite size of the irradiance collector shown in Fig. 7-5b.

### 7.10 SPECIAL USES OF THE EQUATION

It is interesting to use Eq. (7-1) to explore the effect of even smaller values of the beam spread parameter  $\alpha/a$ . Predicted irradiance distributions for  $\alpha/a = 2.00$  are given in Fig. 7-42; corresponding curves for total power on spherical caps are in Fig. 7-43. Sets of predicted power curves for  $\alpha/a = 1.50$ , and 1.25 are in Figs. 7-44 and 7-45, respectively. The dramatic "closing of the fan" is obvious. This result predicts improved resolution in underwater imagery whenever  $\alpha/a$  is small, subject however to certain restrictions set forth in the following paragraph.

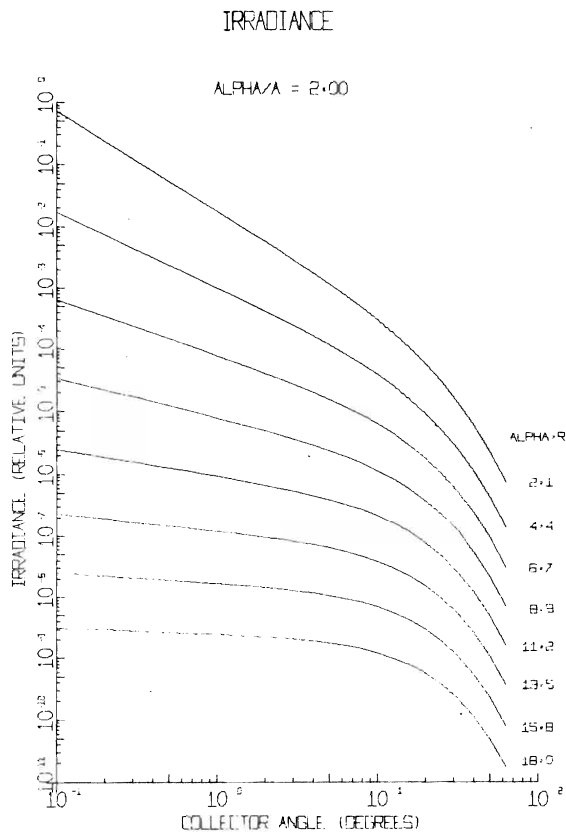


Fig. 7-42

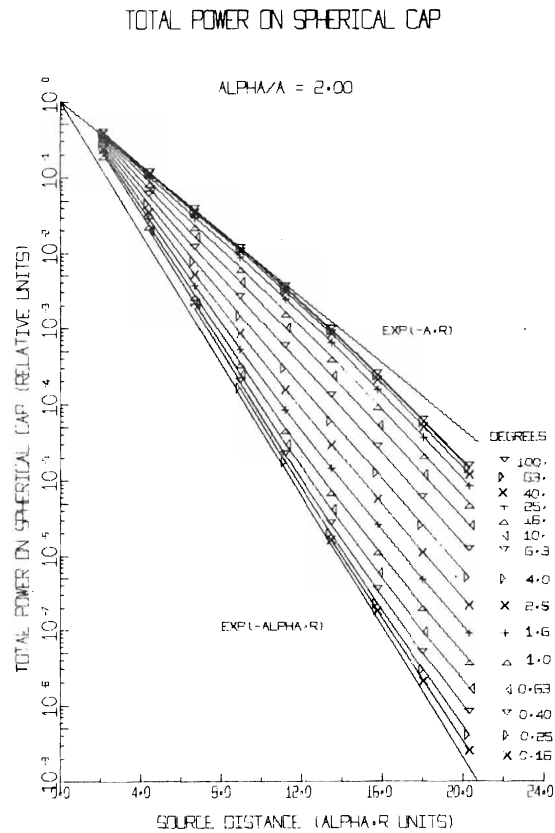


Fig. 7-43

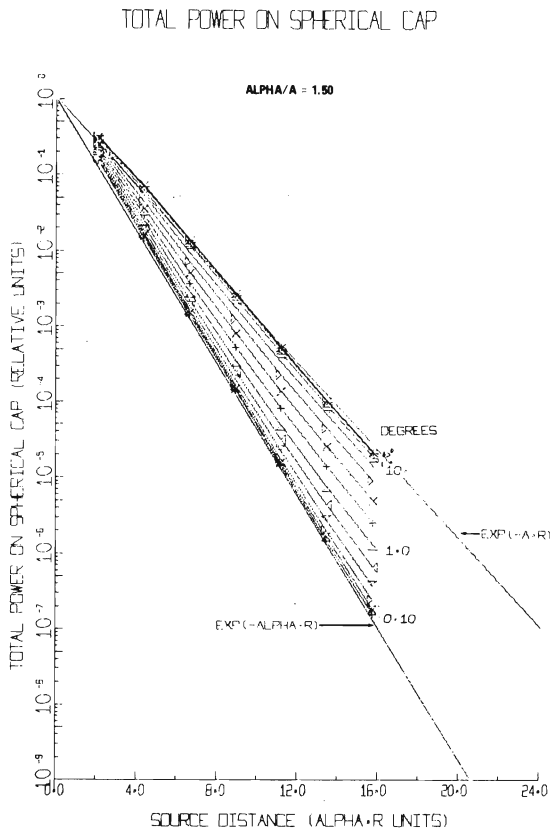


Fig. 7-44

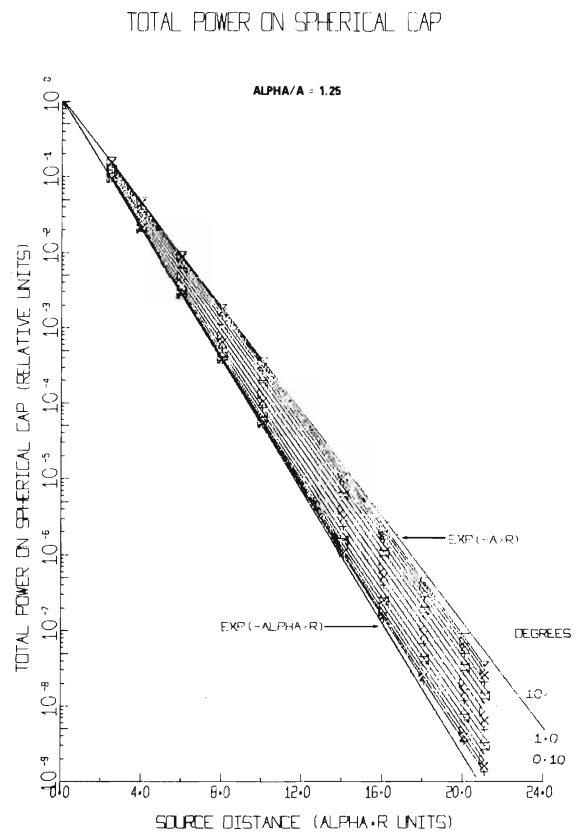


Fig. 7-45

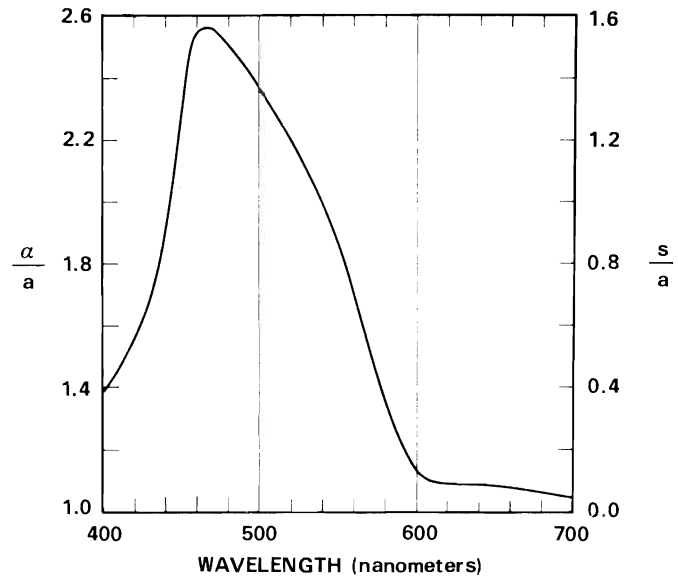
#### OFF-AXIS IRRADIANCE AT OTHER WAVELENGTHS.

Distributions of off-axis irradiance can be calculated by means of Eq. (7-1) for light beams of any wavelength for which the constants  $\alpha$  and  $a$  are known. Optical oceanographic data, while presently not extensive, are becoming increasingly available. Instrumentation for their measurement at sea is improving and becoming more common. Monochromatic data on  $\alpha$  and  $a$  throughout the usable spectrum are rare and sorely needed. Fig. 7-46 is an attempt to infer the spectral shape of the beam spread parameter  $a/a$  from classical published measurements by E. O. Hulburt (J. Opt. Soc. Am. **35**, 698(1945)) on distilled water and the assumption that the total volume scattering coefficient is, to a first approximation, independent of wavelength; it illustrates that beam spread diminishes significantly as wavelength is increased from the green region of the spectrum through the yellow to the orange. This implies improved resolution and image quality, as suggested by Figs. 7-20 through 7-45. It should be noted, however, that the attenuation length ( $1/\alpha$ ) decreases as wavelength increases (see Fig. 2-8). At any fixed actual distance ( $r$ ), therefore, an increase in wavelength requires that the power curves be read at successively larger values of the dimensionless distance ( $\alpha r$ ) in progressing from Fig. 7-20 through Figs. 7-43, 7-44, and 7-45. Thus, there is an inherent compensation which makes any increase in resolution gained by using successively longer wavelengths be a much smaller, less dramatic effect than might be inferred from a casual inspection of the above sequence of figures. Additionally, it is important to recall that greater  $\alpha r$  requires increased power or longer integration time.



Fig. 7-46

Hypothetical variation of beam spread parameter  $a/a$  with wavelength in clearest ocean water, illustrating that the spectral region having greatest transparency (minimum attenuation coefficient  $\alpha$ ) produces the greatest beam spread. This curve is based on the attenuation coefficient data of Hulbert (J. Opt. Soc. Am. **35**, 698 (1945) for distilled water and the assumptions (1) that these apply to clearest ocean water, (2) that the total spectral volume scattering coefficient  $s$  of clearest ocean water is the same at all wavelengths, and (3) that  $s = 0.6 \alpha$  at 480 nanometers.



## 8. DESIRABLE FURTHER WORK

The body of data and the engineering equations presented in the foregoing sections, as well as numerous other findings and conclusions throughout the report, have achieved the goals for which the program was undertaken. Engineers involved in the design of underwater lighting for imagery and underwater communication now have information needed for optimizing the design of equipment. Nevertheless, some valuable continuing research, identified below, can and should be done.

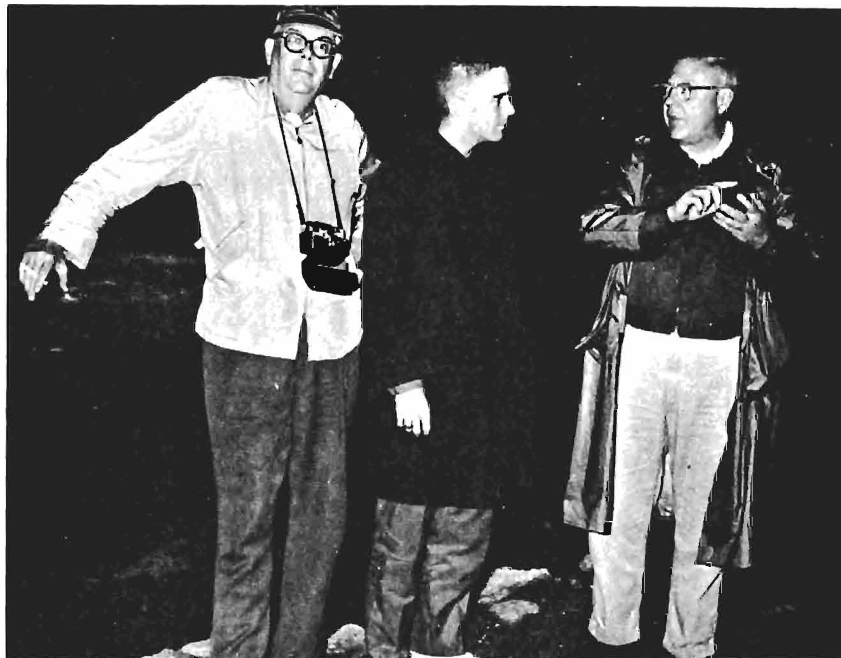
Light from lasers producing trains of sub-nanosecond pulses, perhaps in the regime of 10's of picoseconds may be affected by Type 2 pulse stretch and possibly by nonlinear effects of several kinds. A fruitful path for future research lies in continued experiments using the short pulses generated by mode locked lasers, but these cannot be performed meaningfully at model scale since the velocity of light in water is fixed. Full scale experiments in the ocean are needed, not only in connection with sub-nanosecond systems, but also to verify the results described in this report of the laboratory model scale studies of quasi-steady laser light propagation.

Application of Eq. 7-1 to the prediction of the underwater lighting produced by submerged luminaires is now feasible with computers, since the output of any luminaire may be regarded as a properly weighted ensemble of small beams of light. The contribution due to each such beam throughout the lighted field can be found by means of Eq. 7-1 and these contributions can be summed. Submarine irradiance by daylight and skylight can be calculated in an analogous way. Thus, a basis has been provided for development of procedures for many forms of illuminating engineering in water.

Optical oceanographic data, particularly monochromatic optical constants of ocean waters as functions of depth, are insufficiently available and are sorely needed.

## 9. ACKNOWLEDGEMENTS

The Physics Branch of the U. S. Office of Naval Research did much more than support the research described by this report. It provided continuing high level technical participation from the outset. Regular visits to the field station at Diamond Island by Frank B. Isaacson, Head of the Physics Branch, and by other ONR physicists including Francis T. Byrne, Thomas B. Dowd, Charles E. Steerman, and Bruce A. Finlaysen were working sessions that made penetrating studies of the data being obtained and formulated research plans. Additional ONR visits to the Visibility Laboratory in San Diego produced invaluable in-depth scientific discussions. The long program could not have been carried through without the continuing, dedicated participation of the ONR scientists.



Frank B. Isaacson and Bruce A. Finlaysen from the Physics Branch of the U. S. Office of Naval Research at Diamond Island with S. Q. Duntley on the rainy night of 23 August 1966.

The three RCA underwater lasers used in successive years at Diamond Island were loaned by the U. S. Navy Bureau of Ships (1964), the U. S. Naval Ordnance Test Station (1965), and the U. S. Naval Air Development Center (1966). In 1965 Floyd Kinder, Gerry Gilbert, James Jurnigan, and others represented NOTS at Diamond Island, where they used the underwater tower, track, and facilities with equipment of their own for independent experiments. In 1965 and 1966 NADC representatives Lawrence Ott, Charles Haney, Robert E. Morrison and others were at Diamond Island for extended periods to participate in the experiments. At NADC, Cyrus Beck and George Eck joined in many technical discussions. NADC contracts with the Visibility Laboratory provided for the development of some of the instruments used at Diamond Island; they also shared in paying certain costs of these field experiments. Later, an NADC contract paid for constructing the laboratory tank described in Section 7 of this report. The argon-ion laser used with that tank was bought with funds from the U. S. Naval Ordnance Laboratory Center. The basic instrumentation of the laboratory tank and most of the research funds were from ONR.

Research in lighting for underwater photography was funded via ONR by the U. S. Geological Survey of the Department of Interior. The USGS was represented at Diamond Island by Raymond Nelson during the 1965 experiments.

The underwater laser experiments at Diamond Island were made possible by the outstanding support of the Radio Corporation of America, who made the three underwater lasers that were used in successive years. The RCA laboratories, located in nearby Burlington, Massachusetts, gave immediate service on the submergible lasers. Without their splendid cooperation the nearly continuous experimental schedules could not have been maintained and the program would not have achieved its goals. RCA engineers Edward Kornstein, Howard Okoomian, Tom Knowland, Anthony Luce, and Bertram Clay serviced the lasers both in their laboratory and at Diamond Island.

The research on underwater lighting at Diamond Island could not have been performed without the facilities established there by the U. S. Navy during the 1948-1959 era of research on submarine daylight. Captain Dayton R. E. Brown, USNR, of the U. S. Navy Bureau of Ships was responsible in large measure for enabling the field station to be developed and equipped. For a considerable period during the 1950's the field station at Diamond Island was operated by the Bureau of Ships, through Captain Louis B. Melson, Capt. D. R. E. Brown, and many other officers. Capt. Brown's personal participation in the research at Diamond Island during the 1950's was an important contribution to that work; the subsequent underwater laser program used all of the field station facilities which he had been instrumental in establishing.

The owner of Diamond Island, engineer Fredrick C. Spooner, hosted the research during its initial years and participated in the construction of some of the field station facilities. His continuing cordial interest throughout the subsequent underwater laser program contributed importantly to its success. The cooperation and assistance of David Spooner is also gratefully acknowledged.

A major fraction of all employees of the Visibility Laboratory, past and present, have participated in the research at Diamond Island. Only a few whose specific contributions to the research on underwater lighting was major will be mentioned. First among these is Clarence Fred Pinkham, who superintended the field station from 1949 to 1966 and participated in its every technical activity. No experiment mentioned in this report can be accurately recounted without describing Fred Pinkham's important role. Even the work in the laboratory tank was conducted with facilities which he constructed.

All of the Diamond Island non-laser data in this report were recorded by engineer Charles W. Saunders. The corresponding technical role for the experiments with submerged lasers was by engineer Floyd D. Miller. On-the-spot reduction of the non-laser data was by Roger A. Howerton. Physics graduate student John C. Mather reduced all laser data at Diamond Island. The laser data taken in the laboratory tank were recorded and reduced by graduate student Wayne H. Wilson. Graduate students Gilbert Van Dyke and Morgan Morley assisted. Operation of the underwater laser and other submerged devices was by a team of scuba divers supervised by graduate student Don Clewell.

The engineering design of the special optical, mechanical, and electronic equipment used at Diamond Island and in the laboratory tank is the work of a talented team of engineers, designers, and technicians under the guidance of Research Engineer Roswell W. Austin and Senior Development Engineer Theodore J. Petzold. Principal Photographer John C. Brown made important contributions to Section 3 and to many other portions of this report.

Special mention must be made of the versatile contributions of engineer James Cameron Bailey to every aspect of the experiments at Diamond Island in 1965 and 1966, and to the construction of the laboratory tank facility. He also made the survey of ocean sites described in Section 7.2.

The equation for engineering use given in Section 7 is the work of graduate student Wayne H. Wilson. His extensive computer studies of all laser data, including both those from Diamond Island as well as from the laboratory tank, are responsible for all of the computer-drawn figures in Section 7. Wilson's role in all of the latter stages of the work described by this report cannot be overemphasized.

Special mention must be made of the important salary support to this program provided by the University of California and the Sea Grant College Program.

## Light in the Sea\*

SEIBERT Q. DUNTLEY

*Visibility Laboratory, Scripps Institution of Oceanography, La Jolla, California*

(Received 27 August 1962)

Light in the sea may be produced by the sun or stars, by chemical or biological processes, or by man-made sources. Serving as the primary source of energy for the oceans and supporting their ecology, light also enables the native inhabitants of the water world, as well as humans and their devices, to see. In this paper, new data drawn from investigations spanning nearly two decades are used to illustrate an integrated account of the optical nature of ocean water, the distribution of flux diverging from localized underwater light sources, the propagation of highly collimated beams of light, the penetration of daylight into the sea, and the utilization of solar energy for many purposes including heating, photosynthesis, vision, and photography.

### INTRODUCTION

AN interest in the aerial photography of shallow ocean bottoms prompted the author to begin, nearly 20 years ago, a continuing experimental and theoretical study of light in the sea. Some of the principles discovered or extended and generalized by the author and his colleagues are summarized in this paper. Early discussions with E. O. Hulburt and D. B. Judd as well as publications by many investigators<sup>1</sup> provided a valuable starting point. By 1944 the author was using a grating spectrograph, specially designed by David L.

\* Most of the investigations described in this paper were supported by the Office of Naval Research and the Bureau of Ships of the U. S. Navy. Grants from the National Science Foundation have also aided the work. At certain times in the past the research was supported by the National Defense Research Committee and by the U. S. Navy's Bureau of Aeronautics.

<sup>1</sup> See E. F. DuPré and L. H. Dawson, "Transmission of Light in Water: An Annotated Bibliography," U. S. Naval Research Laboratory Bibliography No. 20, April, 1961 for abstracts of 650 publications by over 400 authors in more than 150 Swiss, German, French, Italian, English, and U. S. journals and other sources from 1818 to 1959.

MacAdam, in a glass-bottomed boat off the east coast of Florida to obtain the spectroradiometric data shown in Fig. 1; the presence of reefs and sandy shoals show clearly in the green region of the spectrum.<sup>2</sup> When the spectrograph was flown in an airplane 4300 ft above the same ocean locations, the radiance spectra shown in Fig. 2 were obtained.<sup>3,4</sup> The data in Figs. 1 and 2, displayed in colorimetric form by Fig. 3, exhibit many intricate and beautiful phenomena which are manifestations of some of the physical principles discussed in this paper.

The importance of light in the sea is apparent when it is recalled that solar radiation supplies most of the energy input to the ocean and supports its ecology

<sup>2</sup> S. Q. Duntley, *Visibility Studies and Some Applications in the Field of Camouflage*, Summary Tech. Rept. of Division 16, NDRC (Columbia University Press, 1946), Vol. II, Chap. 5, p. 212.

<sup>3</sup> See J. G. Moore, *Phil. Trans. Roy. Soc. (London)* **A240**, 163 (1946-48) for a method of using such data to determine depth and attenuation coefficients of shallow water.

<sup>4</sup> See G. A. Stamm and R. A. Hengel, *J. Opt. Soc. Am.* **51**, 1090 (1961) for data on the spectral irradiance incident on the underside of an aircraft flying above the ocean.

through photosynthesis. The biological productivity of an acre of ocean has been estimated to be, on a world-wide average, comparable to that of an acre of land. Most of the surface of our "water planet" is covered by seas and its atmosphere contains great quantities of water in the form of vapor and clouds. Light in the sea enables the native inhabitants of the water world to find their food and to evade attack. Nowhere in nature is protective coloration more perfectly or dramatically displayed than in the feeding grounds of the sea. Man and his cameras may view underwater scenes by means of daylight or with the aid of artificial lighting devices. Many biological organisms, including some living at very great depth, produce their own light at or near the wavelength for which water is most transparent, presumably both for vision and for signaling. All of these

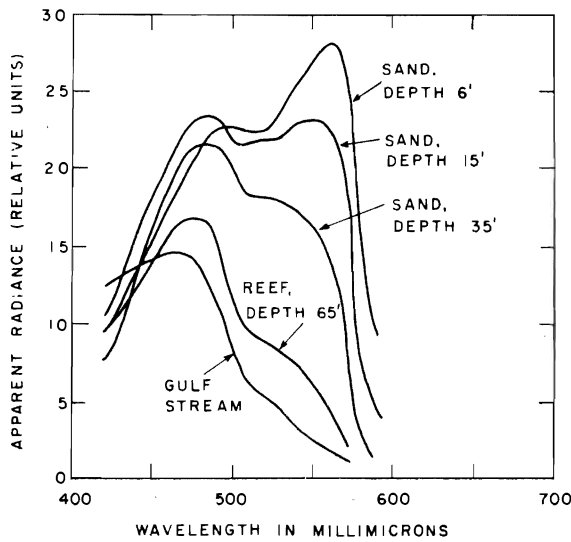


FIG. 1. Spectroradiometric curves of light from the nadir reaching a spectrograph mounted in a glass-bottomed boat over shoals off Dania, Florida (March 1944). Spectral resolution: 7.7 mμ; spatial resolution:  $2.0 \times 10^{-6}$  sr.

aspects of light in the sea can be treated by describing the optical nature of ocean water, the distribution of flux diverging from localized underwater light sources, the propagation of highly collimated beams of light, and the penetration of daylight into the sea. An integrated account of these topics is the subject of this paper.

OPTICAL NATURE OF OCEAN WATER

Most of the optical properties of ocean water as well as many of the principles which govern the propagation of light in the sea can be studied by injecting a highly collimated beam of monochromatic light into otherwise unlighted water and measuring all aspects of the resulting distribution of flux. This investigative approach even provides a basis for understanding the distribution of daylight in the sea and the submarine lighting pro-

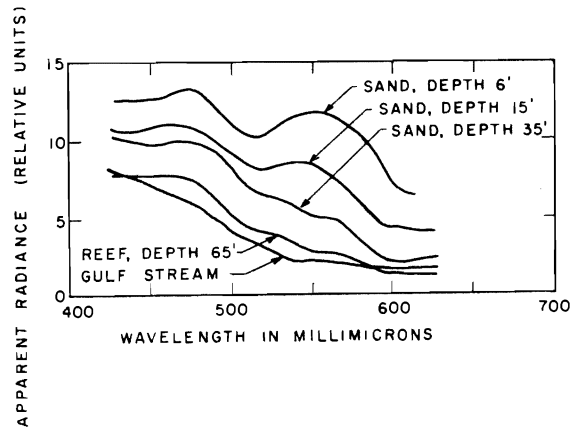


FIG. 2. Spectroradiometric curves of light from the nadir reaching a spectrograph in an airplane 4300 ft above the same ocean locations as in Fig. 1. Spectral resolution: 7.0 mμ; spatial resolution:  $3.2 \times 10^{-6}$  sr.

duced by artificial underwater light sources, for any optical input to the water may be represented by an appropriate superposition of highly collimated, monochromatic beams. The following paragraphs describe a variety of experiments which have been made by using a collimated, underwater light source, shown schematically in Fig. 4, at the Visibility Laboratory's Field Station at Diamond Island, Lake Winnepesaukee, New Hampshire.

Attenuation of a Collimated Beam

If a collimated beam of monochromatic light is injected into macroscopically homogeneous water by

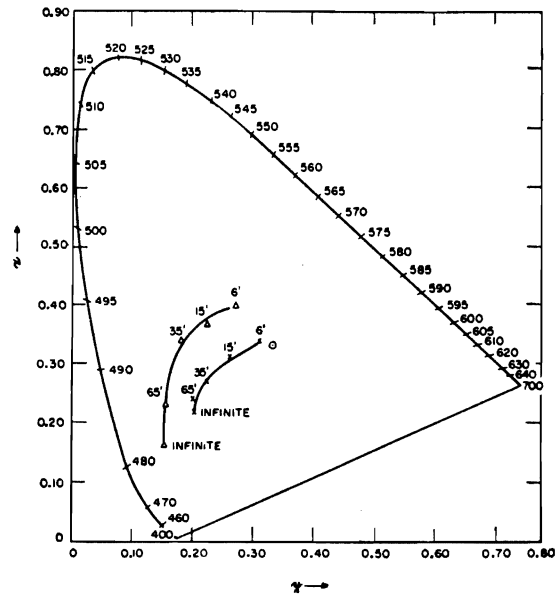


FIG. 3. CIE chromaticity diagram showing loci of the colors of ocean shoals as seen from an altitude of 4300 ft (shorter curve) and from a glass-bottomed boat (longer, upper curve). The points were calculated from the spectral radiance data in Figs. 1 and 2. The circled point represents CIE source C.

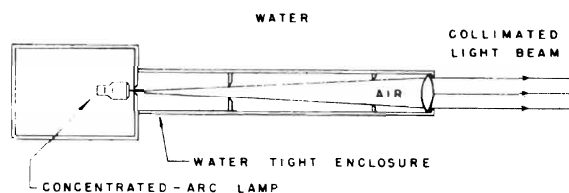


FIG. 4. Schematic diagram of the highly collimated underwater light source represented by a cross-hatched block in Figs. 5, 6, 7, 13, 20, and 21. This source was used in obtaining part or all of the data presented in Figs. 9, 10, 12, 17, 18, 20, and 22. Interchangeable 2, 10, 25, and 100 w zirconium concentrated-arc lamps in a water-tight air-filled enclosure produce nominal total beam spreads of 0.010°, 0.046°, 0.085°, and 0.174°, respectively, when used with a Wratten No. 61 green filter and a specially constructed air-to-water collimator lens having an effective first focal length of 495 mm. This lens, designed for the author by Justin J. Rennilson, is a cemented doublet 55 mm in diameter having radii  $r_1 = 269.75$  mm,  $r_2 = r_3 = 102.60$  mm,  $r_4 = -325.0$  mm and axial thicknesses  $t_1 = 3.0 \pm 0.2$  mm,  $t_2 = 6.5 \pm 0.2$  mm. The first element is of Hayward LF-2 glass ( $N_D = 1.5800 \pm 0.0010$ ;  $\nu = 41.0$ ) and the second is of Hayward BSC-1 ( $N_D = 1.5110 \pm 0.0010$ ;  $\nu = 63.5$ ). The free aperture is 50.0 mm. The first back focal length of the doublet with its last surface in water is 493.88 mm. The air-glass surface was treated for increased light transmission. The achromatization is such that with the 2-W concentrated-arc lamp the extreme ray divergence is 0.0031°, 0.0039°, and 0.0109° at 480, 520, and 589 m $\mu$ , respectively, when the lamp is used in fresh water having a temperature of 20°C. A Wratten No. 61 green filter was used during all of the experiments with this lamp, but it does not appear in Fig. 4 because it was always incorporated in the photometer or the camera. An external circular stop (not shown) can be mounted in the water close to the lens whenever a smaller beam diameter is desired.

means of an underwater projector, as suggested by Fig. 5, it is found that the residual radiant power  $P_r^0$  reaching a distance  $r$  without having been deviated by any type of scattering process is

$$P_r^0 = P_0 e^{-\alpha r}, \quad (1)$$

where  $P_0$  represents the total flux content of the beam as it leaves the projector. The zero superscript on  $P_r^0$  denotes the zero scattering order, i.e., nonscattered radiant power. The spectral volume attenuation coefficient  $\alpha$ , defined by Eq. (1), has the dimension of reciprocal length and can be expressed in natural log units per meter (ln/m), natural log units per foot (ln/ft), etc; it is a scalar point function of position which may vary along any underwater path of sight if the water is macroscopically nonhomogeneous.

The attenuation of a beam of light by water results from two independent mechanisms: scattering and absorption. Scattering refers to any random process by which the direction of individual photons is changed without any other alteration. Absorption includes all of the many thermodynamically irreversible processes by which photons are changed in their nature or by which the energy they represent is transformed into thermal kinetic energy, chemical potential energy, and so on. Transformation of photon energy into thermal kinetic

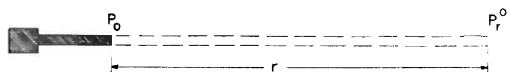


FIG. 5. Illustrating the geometry of Eq. (1). The cross-hatched block represents the collimated underwater light source (projector) shown schematically in Fig. 4.

energy of the water is the major absorption mechanism in the ocean. Photosynthetic conversion of light into chemical potential energy is, of course, measurable and vital to the existence of life in the sea. Visible light fluorescence and transpectral effects are ordinarily too minute to be detected in ocean water. The volume attenuation coefficient  $\alpha$  is the sum of the volume absorption coefficient  $a$  and the total volume scattering coefficient  $s$ : thus  $\alpha = a + s$ .

**Wavelength dependence.** The attenuation coefficient of all water (pure, distilled, or natural) varies markedly with wavelength. Typical data are summarized in Table I, wherein the reciprocal of the volume attenuation coefficient, called attenuation length, has been tabulated rather than attenuation coefficient for three reasons: (1) a distance is easier to visualize and to remember than a reciprocal distance; (2) visibility calculations and many experiments by swimmers show that any large

TABLE I. Attenuation length of distilled water at various wavelengths.<sup>a-c</sup>

Wavelength m $\mu$	Attenuation length (1/ $\alpha$ ) meters/ln
400	13.
440	22.
480	28.
520	25.
560	19.
600	5.1
650	3.3
700	1.7

<sup>a</sup> E. O. Hulburt, J. Opt. Soc. Am. 35, 698 (1945).

<sup>b</sup> For ultraviolet attenuation data see L. H. Dawson and E. O. Hulburt, J. Opt. Soc. Am. 24, 175 (1934).

<sup>c</sup> For near infrared attenuation data see J. A. Curcio and C. C. Petty, J. Opt. Soc. Am. 41, 302 (1951).

dark object (such as a dark-suited swimming companion) is just visible at a horizontal distance of about 4 attenuation lengths when there is sufficient underwater daylight; (3) many physicists like to characterize any absorbing-scattering medium (such as water) by the mean free path for a photon in the ordinary kinetic theory sense; this is the attenuation length 1/ $\alpha$ . The term, "20-meter water," signifying water having an attenuation length of 20 m/ln, facilitates verbal discussions.

Water possesses only a single important window, the peak of which lies near 480 m $\mu$  unless it is shifted toward the green by dissolved yellow substances. Such yellow solutes, usually prominent in coastal waters, consist of humic acids, melanoidins, and other compounds which result from the decomposition of plant and animal materials. Clear ocean water is so selective in its absorption that only a comparatively narrow band of blue-green light penetrates deeply into the sea<sup>5</sup> (see Fig. 1) but this radiation has been detected at depths greater than 600 m with a multiplier phototube photometer.<sup>6</sup>

<sup>5</sup> J. E. Tyler, Limnology and Oceanography 4, 102 (1959).

<sup>6</sup> S. Q. Duntley, Natl. Acad. Sci.—Natl. Research Council Publ. 473, 79 (1956).

Many have wondered whether there exists any fine structure in the volume attenuation function which was beyond the spectral resolution available to the investigators whose results are summarized by Table I. Is there, for example, a narrow-band window of high transmission? It is the consensus of most physicists that the atomic and molecular structures involved in water provide no reason to expect any significant fine structure in the spectral attenuation function. A careful spectroscopic examination of the region from 3750 to 6850 Å with a resolution of 0.2 Å and sensitivity sufficient to detect a variation of 0.02 ln/m in the attenuation coefficient has been reported by Drummeter and Knestrick.<sup>7</sup> They detected no fine structure, i.e., no narrow-band window.

### Water Clarity

The clearest body of ocean water of large extent is reputed to be in the Sargasso Sea, a vast region of the Atlantic Ocean east of Bermuda. Jerlov has reported very clear water between Madeira and Gibraltar,<sup>8</sup> as

TABLE II. Attenuation length of the Atlantic Ocean for wavelength 465 m $\mu$  at various depths in the vicinity of Madeira and Gibraltar.<sup>a</sup>

Depth meters	Attenuation length (1/ $\alpha$ ) meters/ln
0-10	19
10-25	20
25-50	18
50-75	15
75-90	16

<sup>a</sup> N. G. Jerlov, Kgl. Vetenskap. Vitterh. Handl. F.6, Ser. B, BD8.N:01 (1961).

summarized by Table II. Although clearer water was found at 10 m depth than at 90 m at this location, the reverse is often true elsewhere. Optical oceanographic data are not numerous. Jerlov's measurements during the Swedish Deep Sea Expedition of 1947-48 are classical examples. Table III shows some of these data selected to typify certain indicated locations.<sup>9</sup>

DuPré and Dawson<sup>1</sup> give many references to water-clarity data; users of published data should note carefully whether the attenuation coefficients reported are expressed in ln/m or in log/m and whether the values refer to the attenuation coefficient  $\alpha$  for nonscattered light, as in a collimated beam, or to some form of *diffuse attenuation coefficient*  $K$ , discussed later in this paper. No single number can adequately specify the clarity of any natural water because two independent mechanisms, absorption and scattering, govern water

<sup>7</sup> L. F. Drummeter and G. L. Knestrick, U. S. Naval Research Laboratory Rept. No. 5642 (1961).

<sup>8</sup> N. G. Jerlov, Kgl. Vetenskap. Vitterh. Handl. F.6, Ser. B, BD8. N:0 11 (1961).

<sup>9</sup> N. G. Jerlov, Reports of the Swedish Deep Sea Expedition of 1947-48 (1951), Vol. III, p. 49, Table 27.

TABLE III. Attenuation length of ocean water for wavelength 440 m $\mu$  at various locations.<sup>a</sup>

Location	Attenuation length (1/ $\alpha$ ) meters/ln
Caribbean	8
Pacific N. Equatorial Current	12
Pacific Countercurrent	12
Pacific Equatorial Divergence	10
Pacific S. Equatorial Current	9
Gulf of Panama	6
Galapagos Islands	4

<sup>a</sup> N. G. Jerlov, Reports of the Swedish Deep Sea Expedition of 1947-48 (1951), Vol. 3, p. 49, Table 27.

clarity. Even for monochromatic light, at least two coefficients, such as  $\alpha$  and  $K$ , are required, and a more complete specification requires data on the volume scattering function  $\sigma(\vartheta)$ , defined in the paragraphs which follow.

Daylight, abundant in the mixed layer near the surface, supports the growth of phytoplankton in the biologically productive regions of the oceans. These, in turn, feed a zooplankton population. The transparent planktonic organisms, ranging in size from microns to centimeters, scatter light and thereby produce optical attenuation. Settling of the plankton, particularly after death, tends to produce a high concentration of these scatters just above the thermocline which ordinarily exists at the lower boundary of the mixed layer in the sea.<sup>10</sup> Below the thermocline lies clearer water which may be optically uniform for tens or hundreds of meters before some different water mass is encountered. Interestingly, the optical structure of the ocean resembles, in a sense, that of the atmosphere if depth is considered as analogous to altitude and a proper allowance is made for the decrease of atmospheric density with height.

### Scattering

Scattering of light in the sea is predominantly due to transparent biological organisms and particles large compared with the wavelength of light. The magnitude of the scattering is, therefore, virtually independent of wavelength.<sup>11</sup> The variation of attenuation length with

<sup>10</sup> Multiple thermoclines often form in the upper portion of the sea; the maximum optical attenuation is associated with the maximum vertical temperature gradient and frequently falls on a secondary thermocline. Internal waves shift the scattering layer vertically. See E. C. La Fond, E. G. Barnham, and W. H. Armstrong, U. S. Navy Electronics Laboratory Rept. 1052 (July 1961), p. 15. Also see J. Joseph, Deut. Hydrograph. Z., Nr. 5 (1961).

<sup>11</sup> Scattering is also contributed by fine particles, by molecules of water, and by various solutes, but these contributions are usually quite minor and often difficult to detect. Even in very clear, blue ocean water scattering by water molecules produces only 7% of the total scattering coefficient and is dominant only at scattering angles near 90°, where it provides more than 2/3 of the scattered intensity (see reference 8); although the magnitude of this small component of scattering varies inversely as the fourth power of wavelength ( $\lambda^{-4}$ ), it is so heavily masked by nonselective scattering due to large particles that total scattering in the sea is virtually independent of wavelength. The prominent blue color of clear ocean water, apart from sky reflection, is due almost entirely to selective absorption by water molecules.



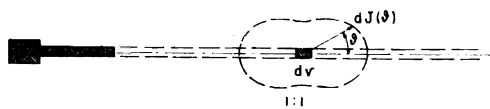


FIG. 6. Polar diagram illustrating Rayleigh scattering by pure water. The ratio of the light scattered into the rear hemisphere to that scattered into the forward hemisphere is 1 to 1. The cross-hatched block represents the collimated underwater light source shown schematically in Fig. 4.

wavelength (see Table I) is due almost wholly to selective absorption.

In the blue region of the spectrum, centering at 480  $m\mu$ , approximately 60% of the attenuation coefficient of clear, blue ocean water is due to scattering and 40% is due to absorption; e.g.,  $s=0.030 \ln/m$  and  $a=0.020 \ln/m$ .<sup>8</sup> In all other spectral regions absorption is overwhelmingly predominant in very clear water.

Since scattering is virtually independent of wavelength its detailed nature is best revealed by means of experiments conducted at or near the wavelength of minimum absorption. This means experiments with blue light in clear, blue ocean water and experiments with green light in greenish coastal and lake waters.

**Scattering by pure water.** Consider a scattering experiment performed in pure water, that is, in water molecules containing no dissolved or particulate matter whatsoever. As in Fig. 6, consider an element of volume  $dv$  receiving collimated, nonpolarized, monochromatic irradiance  $H$  to act as source of scattered light, producing radiant intensity  $dJ(\vartheta)$  at scattering angle  $\vartheta$ . Scattering by the water molecules will be Rayleighian, with  $dJ(\vartheta) \sim \lambda^{-4}$  and with the shape of the intensity function  $dJ(\vartheta)$  characterized by  $(1+0.835 \cos^2\vartheta)$  (see reference 12). Since even the most elaborately prepared distilled water samples show particulate matter when examined in a light beam, scattering by truly pure water has probably never been measured.

**Scattering by distilled water.** A colleague, John E. Tyler, has performed scattering experiments in many samples of commercial distilled water<sup>13</sup>; Fig. 7 shows a typical result. Obviously, the scattering produced by this sample of distilled water is very different from that

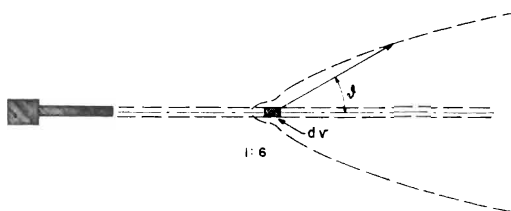


FIG. 7. Polar diagram illustrating measured scattering by a typical sample of commercial distilled water. The ratio of the light scattered into the rear hemisphere to that scattered into the forward hemisphere is 1 to 6 for this water sample. Data are by Tyler (see reference 13). The scale of this polar plot is smaller than that used in Fig. 6.

<sup>12</sup> L. H. Dawson and E. O. Hulburt, *J. Opt. Soc. Am.* 31, 554 (1941).

<sup>13</sup> J. E. Tyler, *Limnology and Oceanography* 6, 451 (1961).

predicted for pure water. The predominant forward scattering is caused by a comparatively few large particles. The dotted curve may be regarded either as a polar plot of the radiant intensity  $dJ(\vartheta)$  or of the volume scattering function  $\sigma(\vartheta)$ , defined by the equation  $dJ(\vartheta) = \sigma(\vartheta) H dv$ , where  $H$  is the irradiance produced by the collimated lamp on the volume  $dv$ . The dimension of  $\sigma(\vartheta)$  is reciprocal length; typical units are reciprocal steradian-meters or reciprocal steradian-feet. The polar curve in Fig. 7 is not complete; it begins at  $\vartheta = 22 \frac{1}{2}^\circ$  and stops at  $\vartheta = 165^\circ$ . All conventional scattering meters designed to be used *in situ* possess the limitation that they cannot measure scattering at small angles. Fortunately, the total scattering coefficient  $s$ , defined by the relation

$$s = 2\pi \int_0^\pi \sigma(\vartheta) \sin\vartheta d\vartheta,$$

is insensitive to the magnitude of small-angle forward scattering. Unfortunately, however, the propagation of highly collimated light does depend importantly on small-angle scattering.

**Small-angle scattering.** The author has devised a special (coaxial) *in situ* scattering meter to supply the missing forward part of the curve. Figure 8 is a schematic diagram of the instrument. It shows the optical system adjusted to measure the volume scattering function at a scattering angle of  $1/2^\circ$ . Such a datum was obtained with the coaxial scattering meter at the Diamond Island Field Station and determines the upper end of the upper curve in Fig. 9. This may be the first *in situ* measurement of small-angle scattering by natural water. The very large scattering found at small scattering angles is believed to have been caused primarily by re-

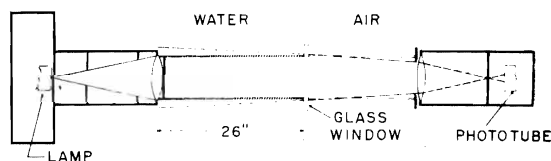


FIG. 8. Coaxial scattering meter for *in situ* measurement of the volume scattering function at small scattering angles. In this schematic drawing the vertical scale has been exaggerated five times over the horizontal scale in order to illustrate the principle of the device more clearly. The collimated underwater light source shown in Fig. 4 is used with the addition of an external opaque central stop which results in the formation of a thin-walled hollow cylinder of light. This traverses 26 in. of water to a high-quality glass window behind which, in air, is a photoelectric telephotometer with a  $2^\circ$  total field of view. The light source and the telephotometer are coaxial, but the latter is equipped with an external stop small enough to exclude the hollow cylinder of light so that only light scattered by the water is collected. The cylindrical scattering volume is indicated by cross-hatching. The upper limit of the scattering angle is determined by the field of the telephotometer and the lower limit is set by the size of its external stop, i.e., by the entrance pupil. A detailed geometrical analysis of the configuration depicted above shows that the scattering is measured at  $0.47 \text{ deg} \pm 0.15^\circ$ ; this datum is used as the volume scattering function for  $1/2^\circ$  scattering angle in Figs. 9 and 10. Photometric calibration of the scattering meter is achieved by removing the external stop on the telephotometer.

fractive deviations produced by the passage of the collimated light beam through transparent plankton having an index of refraction close to that of water. The curve shape at small scattering angles is chosen to suggest that the magnitude of the volume scattering function may merge tangentially with that of the irradiating beam at vanishingly small angles.

Chemists have, for many years, made laboratory measurements of very small-angle scattering from tiny volumes of scattering materials.<sup>14</sup> Koslyaninov<sup>15</sup> has reported volume scattering measurements at angles down to 1 deg by means of a shipboard laboratory apparatus using water samples brought on board for measurement. Figure 10 shows the data of Koslyaninov for the East China Sea superimposed upon the lake data from Fig. 9 after normalization at a scattering angle of 90°, as denoted by the small circle in the figure. The forward-scattering portions of the curves are similar in shape.

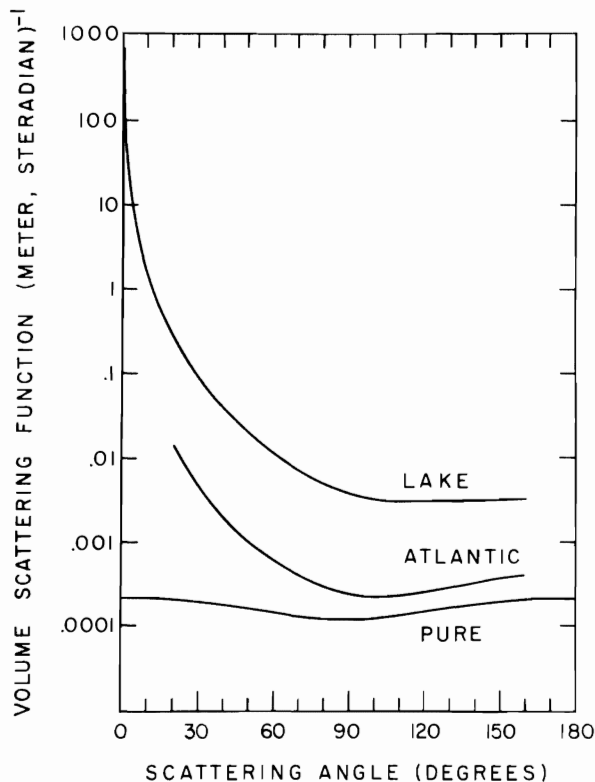


FIG. 9. Volume scattering function curves for pure water (Dewson and Hulburt, see reference 12), the Atlantic between Madeira and Gibraltar (Jerlov, see reference 8), and the Diamond Island Field Station, Lake Winnepesaukee, New Hampshire. The upper curve (lake) represents *in situ* measurements at 5° intervals between scattering angles 20° >  $\theta$  > 160° by means of a conventional type, pivoted-arm scattering meter and a single datum at  $\theta = 0.5^\circ$  obtained *in situ* with the coaxial scattering meter shown schematically in Fig. 8; the data are of 20 August 1961; and are for green light isolated by means of a Wratten No. 61 filter.

<sup>14</sup> H. F. Aughey and F. J. Baum, *J. Opt. Soc. Am.* **44**, 833 (1954).

<sup>15</sup> M. V. Koslyaninov, *Trudy Inst. Okeanol. Acad. Nauk S.S.S.R.* **25**, 134 (1957).

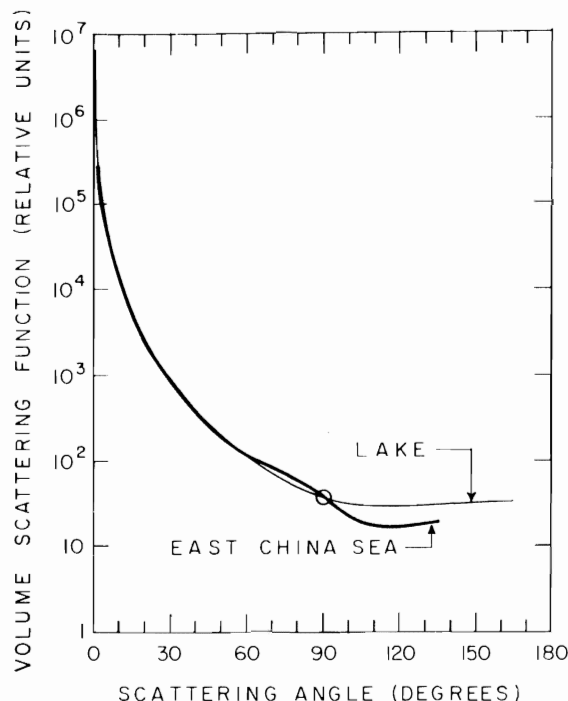


FIG. 10. Comparison of the shape of the *in situ* volume scattering function data for Lake Winnepesaukee, New Hampshire, from Fig. 9 with the shape of a curve representing the *in vivo* scattering data obtained by Koslyaninov (see reference 15) using a shipboard laboratory apparatus and a sample of water taken from the East China Sea. The curves have been normalized at a scattering angle of 90° (circled point) for purposes of shape comparison. Koslyaninov used blue light isolated by means of an absorption filter having an effective wavelength of 494 m $\mu$ ; he reported data at scattering angles of 1, 2.5, 4, 6, 10, 15, 30, 50, 70, 110, and 144 deg. The curves are similar in shape for scattering angles less than 60°.

*Comparison with distilled water.* Figure 11 shows a comparison of *in situ* scattering measurements by Tyler<sup>13</sup> of commercial distilled water and clear Pacific water. Ocean water scatters more light than does distilled water but the similarity of the shape of the curves is striking and interesting in its implication of the predominant role of large particle scattering.

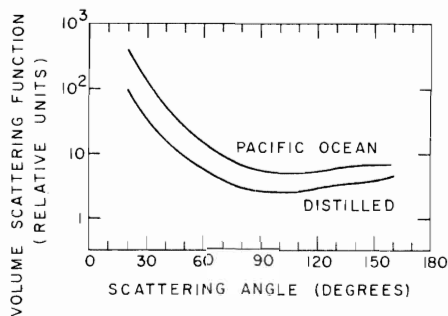


FIG. 11. Comparison of *in situ* scattering data by Tyler (see reference 13) in clear Pacific ocean water near Catalina with comparable data for a typical sample of commercial distilled water. Both curves were obtained with the same pivoted-arm scattering meter and are in the same relative units. The data are for green light isolated by means of a Wratten No. 61 filter.

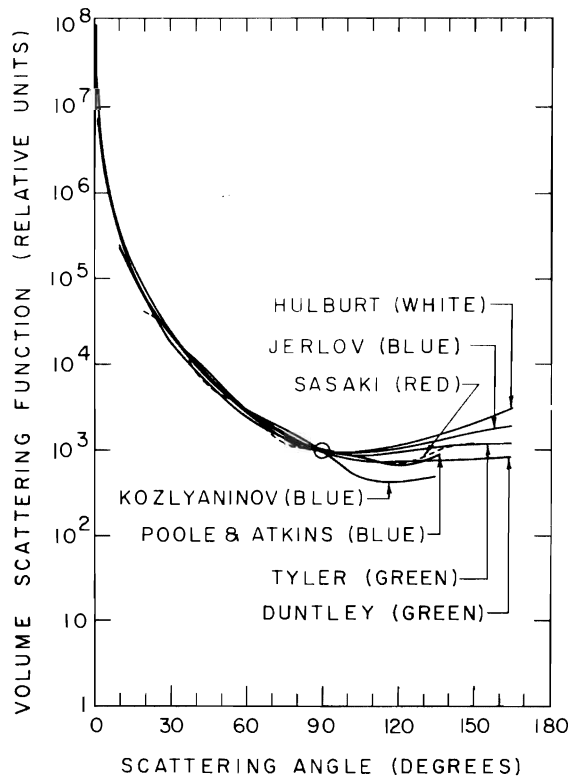


Fig. 12. Comparison of scattering data by seven investigators using dissimilar instruments in seven different parts of the world. All curves are superimposed at a scattering angle of  $90^\circ$ , as indicated by the circled point. Gross similarity in curve shape is apparent in the forward ( $0 < \theta < 90^\circ$ ) scattering directions despite major differences in water clarity ( $2 \text{ m}/\ln < 1/\alpha < 20 \text{ m}/\ln$ ), spectral region, geographical location, instrumental design, and experimental technique. Most of the scattering in natural waters is caused by transparent organisms and particles large compared with the wavelength of light. The scattering is believed to result chiefly from refraction and reflection at the surfaces of these scatterers. As a consequence, scattering at small forward angles predominates and polarized light tends to preserve its polarization. To the extent that all scattering curves have identical shapes the scattering by natural waters can be specified in terms of some single number, such as the total volume scattering coefficient  $s$  or the volume scattering function at some selected angle.

*Comparison between natural waters.* A comparison of the scattering properties of natural waters is afforded by Fig. 12, which shows a superposition of measurements by seven different investigators using seven dissimilar instruments in seven different parts of the world. Three of the measurements were made with blue light, two were made with green light, the dashed curve was obtained with red light, and one investigator employed white light. The attenuation lengths of the waters ranged  $2 \text{ m}/\ln$  for the author's lake data to  $20 \text{ m}/\ln$  in the case of Jerlov's data for the Atlantic. It appears that the shape of the forward portion of the volume scattering function is remarkably similar in all of these natural waters, but that significant differences occur in the character of the backscattering they produce.

Although it is a useful first-order concept that natural waters are somewhat similar in the shape of their

volume scattering functions, it is important to note therefore that measurable differences apparently exist and that ocean water masses might therefore be identified by their scattering function curves.

*Multiple scattering.* The propagation of light in the sea is complicated by multiple scattering. Consider, as in Fig. 13, a plane surface irradiated at normal incidence by the collimated lamp shown in Fig. 4. Every point on the plane receives scattered light from every volume element within the light beam. It receives, moreover, multiply scattered light from every elementary volume of water near the beam. In fact, every volume element within the sea is irradiated by every other volume element both inside and outside the beam. The figure illustrates how irradiation is produced throughout the plane by second-, third-, and fourth-order scattering.

Although theoretical treatments of the effects of multiple scattering on the distribution of light in the sea both from underwater sources and from daylight have been undertaken with partial success by several workers, no fully practical solution has yet been evolved. Some derivations include only secondary scattering and neglect higher-order effects. Others, following the practice of neutron physics, assume the scattering to be virtually isotropic, that is to say, the shape of the volume scattering function is assumed to be spherical or nearly so; this is, of course, highly unrealistic. Four patterns of approach characterize the theories: (1) *Multiple integration* using the volume scattering function, the attenuation coefficient  $\alpha$ , and the inverse square law; these treatments suffer from complexity, are never complete, and may neglect sizeable components of flux but some useful approximate solutions have been achieved in special cases. (2) *Diffusion theory.* This applies rigorously only to isotropic or very mildly non-isotropic scattering systems which are not found in the sea; nevertheless, considerable success has been achieved in the prediction of *irradiance* at long ranges; diffusion theory is, however, unable to yield much information concerning the directional characteristics of the underwater light field. (3) *Radiative transfer.* This method is based upon equations of transfer, sometimes in vector form; these integro-differential equations are solved in practice by iterative procedures on the largest electronic computers. (4) *Monte Carlo procedures.* These also require the use of large electronic computers. Al-

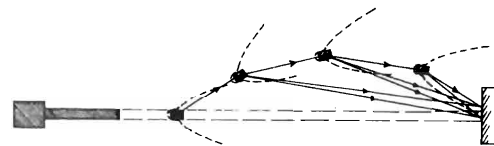


Fig. 13. Illustrating the irradiation of an object by multiply scattered light at arbitrary points inside and outside the light beam. The dotted curve associated with each cross-hatched volume element has the shape shown in Fig. 7 and represents a polar plot of the volume scattering function. The need for additional scattering data at small forward angles is obvious.

though, *in principle*, either of the two latter approaches appears to be capable of handling all underwater light propagation problems, neither has thus far achieved appreciable practical success in the treatment of point source or collimated beam geometrics, for the calculations are too massive for even the largest of electronic computers. Success has, however, been achieved for the case of daylight in the sea,<sup>16</sup> wherein the development of theory and the evolution of practical computation procedures followed quickly after experimental explorations of underwater daylight radiance distributions had produced a body of data, described later in this paper, from which valid assumptions could be made and against which predictions could be checked. This experience prompted the author to begin a program of experimental explorations of the distribution of light produced by submerged divergent light sources and by collimated lamps underwater. These explorations are still in progress, but some of the conclusions reached thus far are summarized in the following section.

#### DIVERGENT LIGHT IN THE SEA

Marine organisms which emit nearly hemispherical flashes of light are found at virtually all depths in the sea. Underwater lighting for vision, television, or photography is often accomplished by means of incandescent lamps or flash tubes which approximate point sources and emit divergent flux. Quantitative prediction of the irradiation produced by such lamps at the object, on its background, and throughout the observer's path of sight can enable optimum lighting arrangements and camera positions to be planned in advance and exposure to be predicted with sufficient accuracy to permit high-contrast photographic techniques to be employed effectively.

#### Apparent Radiance at the Object

Every underwater object and every elementary volume of water irradiated by a submerged divergent light source is lighted by an apparent radiance distribution which depends upon the radiant intensity distribution of the lamp, the optical properties of the water, and the lamp distance. This radiance distribution can be seen, photographed, and measured by an observer stationed at the position of the object. To such an observer a receding, uniform, spherical lamp appears to be surrounded by a glow of scattered light which becomes proportionately more prominent as lamp distance is increased, until at some range, often 18 to 20 attenuation lengths, the lamp image can no longer be discerned and only the glow is visible. The glow, however, may be seen for a considerably greater distance, depending upon the radiant intensity of the source and the ambient level of light in the sea.

*Apparent radiance of the lamp.* Densitometric meas-

<sup>16</sup> W. H. Richardson and R. W. Preisendorfer, Scripps Inst. Oceanog., Ref. 60-43 (1960).

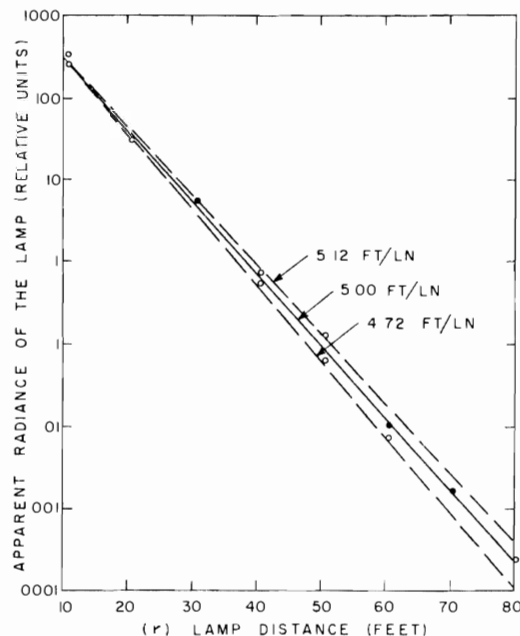


FIG. 14. Apparent radiance of a uniform, spherical underwater lamp at various distances, illustrating the exponential nature of the attenuation of apparent lamp radiance with distance. Photographic photometry was employed using a Wratten No. 61 filter and Eastman Plus X 35-mm film (Emulsion No. 5061-64-16A) developed to unity gamma in D-76. Exposure time at  $f/1.5$  varied from 1.75 msec at a lamp distance of 10.5 ft to 180 000 msec when the lamp was 80 ft from the camera. The source of light was a 1000-W incandescent "diving lamp" (No. MG25/1) manufactured by the General Electric Company. The 3-in. spherical lamp envelope was sprayed with a white gloss lacquer in order to produce a uniform translucent white covering which gave the lamp the same radiant intensity in all directions (to within  $\pm 7\%$ ) except toward the base, which was turned away from the camera. Two or more exposure times differing by 5- or 10-fold were used at each lamp distance. Open circles represent data from a single time of exposure; solid points indicate that identical values of apparent radiance were obtained from negatives made with two different exposure times. A solid straight line, representing an attenuation length  $1/\alpha = 5.00$  ft/ln, has been drawn near the points. Dashed lines corresponding to attenuation lengths of 4.72 ft/ln and 5.12 ft/ln, respectively, represent values measured by means of a light-beam transmissometer before and after the all-night experimental session. Cooling of the water during the night correlated with the observed increase of attenuation length, presumably due to plankton shrinkage. Data are of 26 August 1959 at Diamond Island Field Station.

urements of the lamp images in a series of photographs of a receding spherical underwater light source produced the results shown in Fig. 14, wherein the close fit of the data to the solid straight line shows that the apparent radiance of the lamp is attenuated exponentially, as the equation

$$N_r = N_0 e^{-\alpha r}, \quad (2)$$

where  $N_r$  is the apparent radiance at distance  $r$ ,  $N_0$  is the inherent radiance of the lamp surface, and  $\alpha$  is the attenuation coefficient for apparent radiance. The dashed lines, constructed from data secured with a light-beam transmissometer designed to conform with the requirements of Eq. (1), provide evidence that numerically identical attenuation coefficients  $\alpha$  apply in

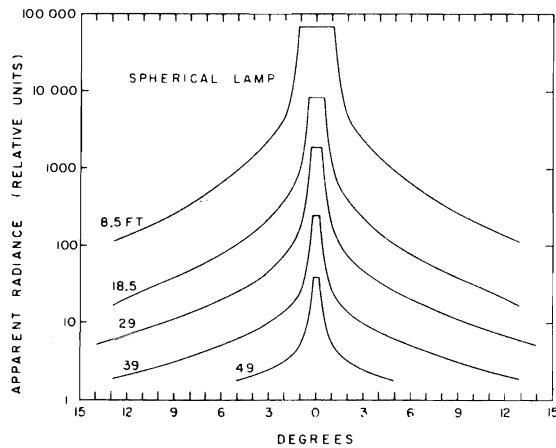


FIG. 15. Angular distribution of apparent radiance produced by a uniform, spherical, underwater lamp at distances of 8.5, 18.5, 29, and 39 feet. The lamp was identical to the one described in connection with Fig. 14. The photometry was by means of an automatic scanning, photoelectric, telephotometer having a circular acceptance cone  $0.25^\circ$  in diameter and with its spectral response limited by a Wratten No. 61 filter. Attenuation length was 5.1 ft/ln. Data are of 3 August 1961 at the Diamond Island Field Station.

Eqs. (1) and (2), indicating thereby that images are formed by photons transmitted without being scattered and that the contribution of scattered light to the exposure of the image portion of the negative was negligible.

*Apparent radiance of the glow.* Distributions of the apparent radiance of the glow surrounding the distant lamp were obtained by densitometry of the same series of photographs, but more accurate results have been achieved by means of an automatic scanning photoelectric telephotometer which was more free from stray light than was the camera. Distributions of apparent radiance as measured photoelectrically from the target position are shown in Fig. 15. The irradiance on any surface of the target facing the lamp can be computed from these curves and, if the reflectance and gloss characteristics of the target surfaces are known, the inherent radiance of the target in any specified direction can be calculated. If, moreover, the volume scattering function of the water and its attenuation length are known, calculations of inherent background radiance, path radiance, and apparent target contrast can be made from Fig. 15.

### Irradiance at the Object

The surface of any underwater object is irradiated by (1) direct (nonscattered) light from the lamp and (2) scattered light. The *nonscattered* or *monopath irradiance*  $H_r^0$  produced at normal incidence by a lamp radiant intensity  $J$  at distance  $r$  is given by the relation

$$H_r^0 = J e^{-\alpha r} / r^2. \quad (3)$$

In addition to  $H_r^0$ , the object is irradiated by the scattered or *multipath irradiance*  $H_r^*$ . Thus the *total*

*irradiance*  $H_r = H_r^0 + H_r^*$ . Since  $H_r$  can be measured (see Fig. 16) and  $H_r^0$  can be calculated by means of Eq. (3),  $H_r^*$  can be found by subtraction; thus,  $H_r^* = H_r - H_r^0$ .

Diffusion theory<sup>17,18</sup> based upon the assumption of isotropic scattering suggests that

$$H_r^* = JK e^{-Kr} / 4\pi r, \quad (4)$$

where  $K$  is an attenuation coefficient for scattered light. If this  $K$  is given a value numerically equal to the attenuation function for daylight scalar irradiance  $k$ , as discussed later in the portion of this paper devoted to daylight in the sea, Eqs. (3) and (4), when summed, fit the data of Fig. 16 within experimental uncertainty both at short and at long lamp distances; between 10 ft (2 attenuation lengths) and 70 feet (14 attenuation lengths), however, the measured total irradiance is as much as twice the predicted values. A semiempirical modification of Eq. (4) which, added to Eq. (3), fits the data of Fig. 16 within experimental error is

$$H_r^* = 2.5(1 + 7e^{-Kr})JK e^{-Kr} / 4\pi r. \quad (5)$$

*Effect of beam spread.* Underwater sources of divergent light are seldom completely spherical in their radiant intensity distribution. Many underwater lamps

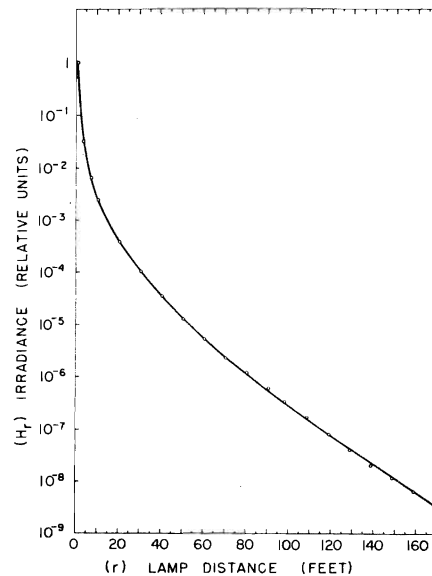


FIG. 16. Total irradiance produced at various distances by a uniform, spherical underwater lamp at the Diamond Island Field Station. The solid curve was passed through the data points by means of a least-squares procedure. The lamp was identical with the one described in connection with Fig. 14. The photometry was by means of an underwater photoelectric irradiance meter facing directly toward the lamp. The spectral response of the irradiator was limited by means of a Wratten No. 61 green filter. The attenuation length of the water was 5.0 ft/ln. Data are of 26 August 1959.

<sup>17</sup> S. Glasstone and M. C. Edlund, *Elements of Nuclear Reactor Theory* (D. Van Nostrand and Company, Inc., Princeton, New Jersey, 1952), p. 107.

<sup>18</sup> R. W. Preisendorfer (private communication).

emit roughly conical patterns of flux 20° or more in total angular extent. Monopath irradiance is, of course, unaffected by the beam spread, and the effect on multipath irradiance is not large unless the lamp produces a highly collimated beam. Experiments with an underwater light source having a continuously variable beam spread down to 20° resulted in an empirical modification of Eq. (5) to the form

$$H_r^* = (2.5 - 1.5 \log_{10} 2\pi/\beta) \times [1 + 7(2\pi/\beta)^{1/2} e^{-Kr}] JK e^{-Kr} / 4\pi r, \quad (6)$$

where  $\beta$  is the total beam spread. Equation (6) should not be used for beam spreads less than 20°.

Equations (4), (5), and (6) have been tested by the author only at the Diamond Island Field Station, but because of the similarity in the shape of the volume scattering functions of natural waters, as illustrated by Fig. 12, they may have nearly universal applicability as approximations for engineering purposes.

COLLIMATED LIGHT IN THE SEA

Underwater projectors producing beam spreads small compared with 1° exhibit distinctive properties. When seen from the position of the irradiated target, the head-on appearance of a distant, highly collimated lamp is remarkably similar to that of a broad-beam lamp at some lesser range. Thus, the bright disk-shaped image of the lamp is surrounded by a glow of scattered light, having an apparent radiance distribution like that shown in Fig. 17. Although it is difficult to distinguish a distant collimated lamp from a distant divergent source when each is observed from within its beam, radiance distribution measurements reveal subtle differences, the nature of which can be seen by comparing Figs. 15 and 17.

The appearance presented by a moderately distant, slightly averted collimated lamp is, however, very different from that of its divergent counterpart because the intense small-angle scattering, common to all natural waters, produces a readily visible, sharply defined, nearly cylindrical luminous column extending toward the observer from the collimated lamp. Near the lamp and on the axis of this column the monochromatic monopath irradiance normal to the beam at distance  $r$  is  $H_r^0 = H_0 e^{-\alpha r}$ , where the irradiance  $H_0$  in the water at the lens of the projector is given by  $H_0 = J\psi^2 D^{-2}$  in terms of radiant intensity  $J$ , total beam spread  $\psi$ , and diameter  $D$  of the light beam. Beyond the distance  $r' = D/\psi$ , at which the lens replaces the source as the aperture stop of the irradiating system,  $H_r^0$  is given by

$$H_r^0 = J e^{-\alpha r} / r^2 = H_0 e^{-\alpha r} (D/\psi r)^2 = H_0 e^{-\alpha r} / (r/r')^2 \quad (7)$$

if diffraction is negligible.

The dashed lines in Fig. 18 illustrate the foregoing relations applied to the case of three collimated lamps having a divergence of 1/6° and exit pupil diameters of 1/300, 2/300, and 8/300 of an attenuation length,

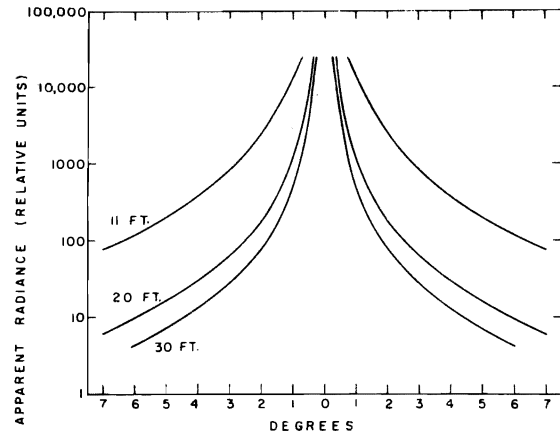


FIG. 17. Apparent radiance produced by scattering from the beam of the highly collimated underwater lamp shown in Fig. 4. The photometry was by means of an automatic scanning, photoelectric telephotometer having a circular acceptance cone 0.25° in diameter and with its spectral response limited by a Wratten No. 61 filter. The beam from the lamp had a divergence of 0.01°; it was directed toward the telephotometer and filled the entrance pupil of that instrument at all times. Lamp distances of 11, 20, and 30 ft were used. Tests of the telephotometer showed that the data in Fig. 17 are free from stray-light effects. Attenuation length of the water was 6.7 ft./in. The data are of 11 August 1961 at the Diamond Island Field Station.

respectively. For these three lamps the distances  $r'$  are 1.15, 2.30, and 9.20 attenuation lengths. The points at  $r=r'$ , beyond which Eq. (7) applies, lie within the diagram for both of the two smaller lamps and are indicated by triangles. In all cases, diffraction will lower the curves.

The total irradiance  $H_r$  on the axis of a collimated beam exceeds the monopath irradiance  $H_r^0$  by the multipath contribution  $H_r^*$ ; i.e.,  $H_r = H_r^0 + H_r^*$ . This is illustrated by the experimental data points shown in Fig. 18 and the solid curves which have been fitted to them. In the case of the two smaller lamps the multipath contribution was not detected at ranges shorter than  $r'$ , indicated by the triangle points, but this is not true in the beam from the large-diameter lamp where  $H_r^*$  and  $H_r^0$  are approximately equal throughout much of the range of distances covered by the data. The steadily increasing separation of the solid and dashed curves in each of the lower pairs implies that multipath irradiance becomes dominant at large lamp distances.

Data such as those in Fig. 18 can be used to calculate the ratio of monopath to multipath irradiance; i.e.,  $H_r^0/H_r^*$ . This ratio, independent of the intensity of the lamp or its radiant power output, is a measure of the beam content of the light; it is the ratio of image-forming light transmitted by the water path to the non-image-forming (scattered) light arriving at the irradiated object. Applications dependent on the retention of narrow-beam geometrical characteristics, of coherence, or of single-valued transmission time may require that some usable fraction of the irradiance consist of nonscattered (monopath) light. Figure 19 is a

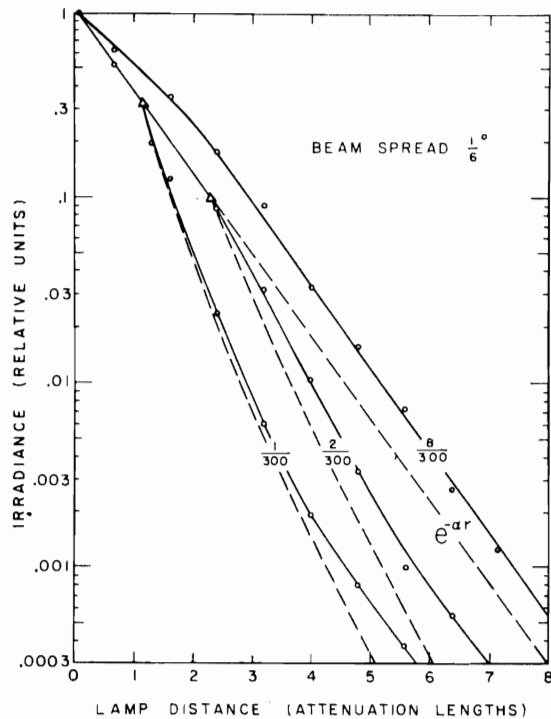


FIG. 18. Irradiance normal to the axis of the beam of light having a divergence of  $1/6^\circ$  produced by a collimated underwater lamp (Fig. 4) at distances up to 8 attenuation lengths is shown by the data points and the solid lines for beam diameters of  $1/300$ ,  $2/300$ , and  $8/300$  of an attenuation length. The data are of 14 August 1961 at the Diamond Island Field Station; attenuation length  $1/\alpha = 6.3$  ft./ln. Dashed lines represent the monopath irradiance in each case computed from Eq. (7). Geometrical divergence reduces the axial monopath irradiance at all lamp distances beyond the points marked by triangles, which occur at 1.15 and 2.30 attenuation lengths for the two smaller lamps and at 9.20 attenuation lengths (not shown) for the largest lamp. Spreading of the beam by diffraction also reduces the monopath irradiance at all lamp distances, often dramatically. In a plot involving dimensionless lamp distance (such as Fig. 18), the dashed lines cannot be drawn to include the potentially major effect of diffraction because the wavelength of light is independent of the attenuation length, but they should be appropriately lowered when the figure is interpreted in terms of actual dimensions. The vertical separation between the dashed and the solid curves in each pair is a measure of the multipath irradiance. *Caution:* The data in this figure relate only to the axis of an aplanatic underwater projection system having a beam spread  $\psi = 1/6^\circ$ ; they should *not* be scaled by the ratio  $D/\psi$ ; they do *not*, for example, apply to the case of  $\psi = 1/60^\circ$  and lamp diameters  $D = 1/3000$ ,  $2/3000$ , or  $8/3000$  attenuation length.

plot of  $H_r^0/H_r^*$  for divergent sources. It shows that for a beam spread of  $20^\circ$ ,  $H_r^* = H_r^0$  at 1.4 attenuation lengths and that multipath irradiance predominates at large lamp distances. Experiments now in progress with light beams of small diameter and high collimation may produce corresponding curves for collimated lamps.

*Irradiance near a highly collimated beam.* All of the foregoing discussion has concerned irradiance produced on the axis of a collimated beam. Measurements of irradiance outside the light beam at various distances from the collimated lamp are shown in Fig. 20.

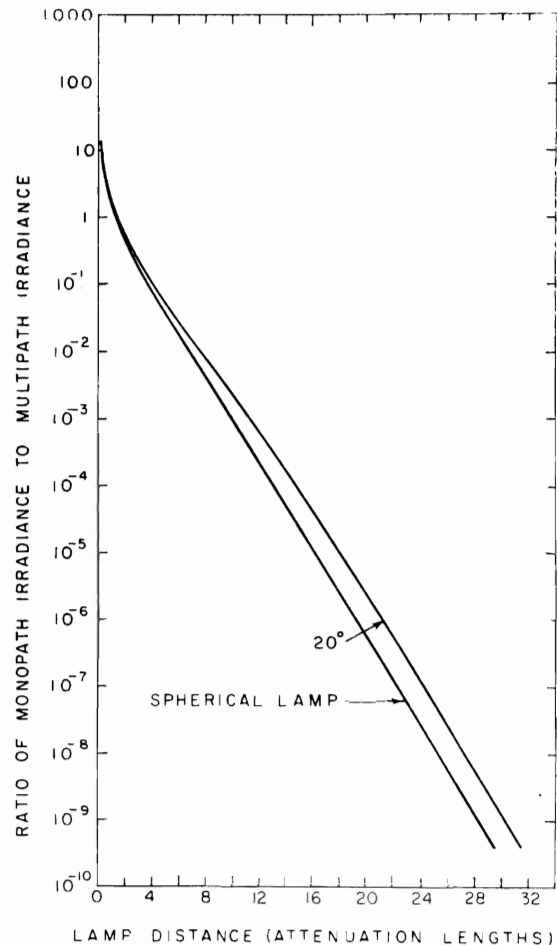


FIG. 19. Ratio of monopath irradiance to multipath irradiance produced by a uniform spherical lamp (lower curve) and by the same source mounted within a blackened enclosure (box) which limited its emittance to a circular cone  $20^\circ$  in total angular diameter (upper curve). In producing these curves, monopath irradiance  $H_r^0$  was calculated by means of Eq. (3) and multipath irradiance  $H_r^*$  was obtained by subtracting  $H_r^0$  from the total irradiance data given by Fig. 16 for the unrestricted spherical lamp and from corresponding data for the  $20^\circ$  case.

### Refractive Deterioration of High Collimation

No discussion of the properties of highly collimated underwater light or image-forming rays would be complete without mention of certain commonly encountered refractive effects which limit the resolution of fine detail and tend to destroy high collimation. Natural waters often contain refractive nonhomogeneities of two kinds: (1) small scale point-to-point variations in refractive index due, for example, to temperature differences; and (2) transparent biological organisms (plankton) which may range in size from microns to centimeters. The effects of these optical nonhomogeneities has been observed by allowing the beam from the 2-in.-diameter  $0.01^\circ$  divergent lamp shown in Fig. 4 to fall on an underwater viewing screen after traversing any convenient water path or by photographing the effect with an underwater camera having no lens, in the manner

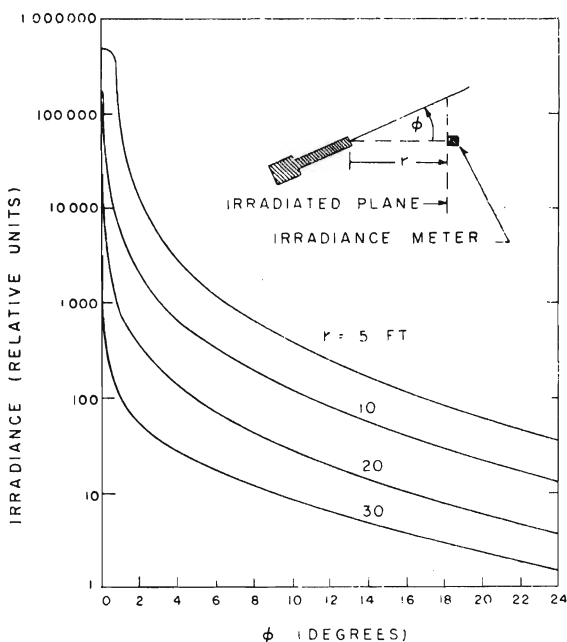


FIG. 20. Irradiance outside a collimated beam of light. Beam divergence: 0.046°; beam diameter: 2-in. Filter: Wratten No. 61. Attenuation length 4.8 ft/lm; Diamond Island.

suggested by Fig. 21. If such a photograph is made in well-mixed distilled water, only a uniform white field is recorded, but if the distilled water is allowed to stand, a pattern of shadows appears as thermal structures develop. If transparent plankton are added, their refractive shadows are superimposed.

Figure 22 is a photograph of the pattern obtained when such a picture was taken in the clear, natural water at the Diamond Island Field Station in Lake Winnepesaukee, New Hampshire. In this case the light beam passed through 10 ft of lake water. The circular shadows were caused by transparent plankton somewhat less than 1 mm in size whose refractive index differed only slightly from that of water. No effects due to thermal tubulons have been identified in this picture. The light beam was horizontal and 30 in. beneath the surface of the water. A shutter speed of 1/50 second was used because the pattern was in constant restless motion, primarily due to slight wave action, but also due to plankton movements and possibly to thermal drifts.

*Loss of resolution.* Wavefronts passing through natural waters are distorted by these refractive effects. The edges of objects appear blurred and the apparent contrast of small objects is reduced. Thus, resolving power is impaired and fine details are obliterated. It is said that in some clear, south-sea waters the concentration of transparent plankton is so great that a swimmer cannot distinguish his toes even though his foot is clearly visible at high contrast. Conditions are much less severe at the Diamond Island Field Station, where

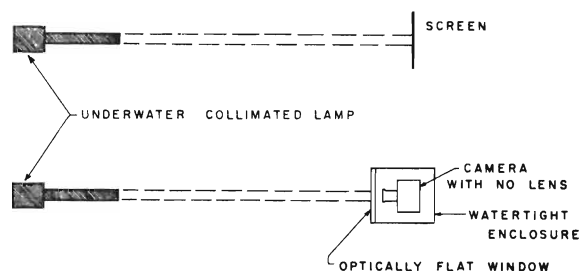


FIG. 21. Techniques for observing (upper figure) and recording (lower figure) the effects of refractive inhomogeneities on the transmission of a highly collimated beam of light through natural water.

magnification is necessary to make the loss of resolution obvious.

An experimental study of this loss of resolution was performed several years ago at the Diamond Island Field Station and a theoretical treatment of the effect was evolved.<sup>19,20</sup> At Diamond Island the loss of resolution was comparable to that caused by the on-axis aberrations of a flat water-to-air window of 1/4-in.-thick commercial plate glass when 10 ft of water separated the object from the camera. The angular magnitude of the blur increases as the square root of the object-to-camera distance, and the apparent contrast of fine details is decreased inversely as the third power of the distance in macroscopically uniform water.<sup>20</sup>

DAYLIGHT IN THE SEA

Most of the light in the sea is from the sun and the sky. In sunny weather each square meter of the water surface may be irradiated by as much as one kilowatt of solar power. Approximately 95% of this power en-

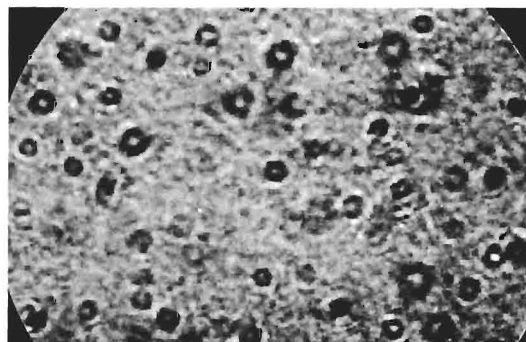


FIG. 22. Photograph of the light distribution from the collimated underwater lamp (Fig. 4) after traversing 10 ft of water in the manner shown schematically in Fig. 21. Camera: Contax without lens. Exposure time: 1/50 sec. Film: Eastman Plus-X. Development: normal, D-76. Beam spread: 0.01°. Beam diameter: 2 in. Attenuation length: 5.6 ft/lm; Diamond Island; 22 August 1961. The diameter of the outer black circular border (caused by the opening in the camera body) measured 1.3 in. on the negative.

<sup>19</sup> S. Q. Duntley, W. H. Culver, F. Richey, and R. W. Preisendorfer, *J. Opt. Soc. Am.* 42, 877(A) (1952).

<sup>20</sup> S. Q. Duntley, W. H. Culver, F. Richey, and R. W. Preisendorfer, *J. Opt. Soc. Am.* (to be published).



ters the water and is absorbed somewhere beneath the surface. Daylight is the principal source of energy for the sea, supplying it with heat and supporting its ecology through photosynthesis. Nearly half of the irradiation is infrared, most of which is absorbed within a meter of the surface. As much as one-fifth of the daylight may be ultraviolet and this can penetrate somewhat more deeply if the concentration of dissolved organic decomposition products ("yellow substance") is low. Fortunately, the peak of the solar spectrum is not far from the wavelength (480 m $\mu$ ) of greatest transparency in clear ocean water. Blue-green light, representing less than one-tenth of the total incident solar power, penetrates so deeply into the sea that it has been detected photoelectrically below 600 m. Visibility, important to inhabitants of the underwater world, is possible chiefly because of this blue-green light.

### Directional Distribution of Daylight Underwater

Sunlight entering at the surface becomes progressively more diffuse with depth until a state of diffusion is reached which (1) is characteristic of the water mass, (2) is independent of the solar altitude and the prevailing sky condition, and (3) is invariant with further increases in depth unless optically different water is encountered. This behavior of daylight in water, a subject of conjecture for more than 30 years, was probably first definitively postulated by Whitney<sup>21,22</sup> in brilliant speculations based neither upon adequate radiance distribution data nor upon a valid theoretical analysis but chiefly upon insightful interpretations of irradiance measurements. Whitney's hypothesis could not be confirmed until 1957, when an eight-year experimental program, initiated by the author and conducted in its later stages chiefly by several of his colleagues, culminated in the definitive radiance distribution data of Tyler.<sup>23</sup> These data were obtained with superlative equipment representing nearly a decade of apparatus development. The experiments were conducted in a mountain lake containing optically uniform water of very great depth. This lake (Pend Oreille, Idaho) was used only after many futile attempts had been made to find sufficiently uniform, deep water at sea and in other lakes. Even at Pend Oreille optical uniformity occurs only for a few days during the spring of each year. The Pend Oreille data show an unmistakable, systematic trend toward the formation of a characteristic (or *asymptotic*) distribution of underwater daylight radiance. A series of figures developed from Tyler's tabulated Pend Oreille data<sup>23</sup> and described in the section which follows summarize this experimental evidence for the *asymptotic radiance distribution* hypothesis and illustrate the progressive transformation of the light field from the sunny condition near the surface to the characteristic diffuse distribution which prevails at great

depth. A theoretical proof of the existence of characteristic diffuse light (asymptotic radiance distribution) in natural waters has been given by Preisendorfer<sup>24</sup> and confirmatory experimental data in other natural waters have been obtained by Jerlov and Fukuda<sup>25</sup> and Sasaki.<sup>26</sup>

### Depth Profiles of Underwater Radiance

The most usable graphical representation of the distribution of daylight radiance in the sea is a family of radiance distribution profiles like those in Fig. 23. Con-

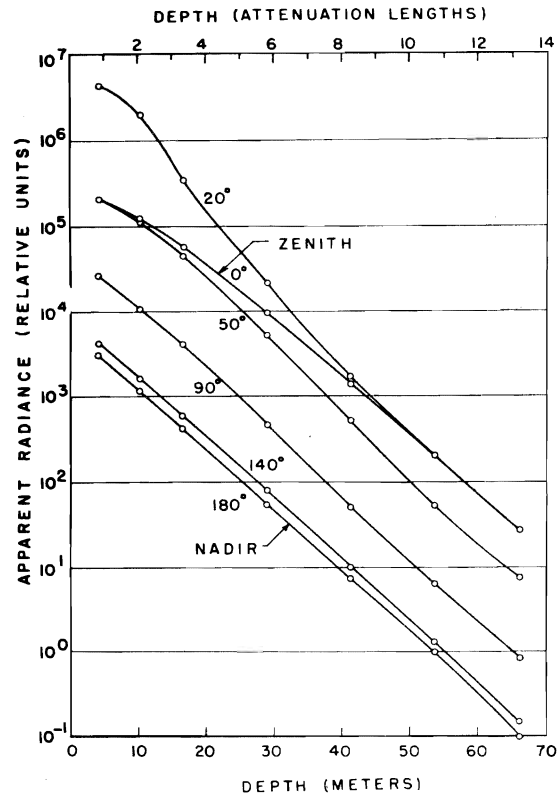


FIG. 23. Depth profiles of underwater apparent radiance for several paths of sight (i.e., zenith angles) in the plane of the sun on a clear, calm, cloudless, sunny day (28 April 1957) at Pend Oreille, Idaho. The circles denote data by Tyler (see reference 23). The solar zenith angle was 33.4°. The submerged photoelectric radiance photometer measured blue light by means of an RCA 931A multiplier phototube equipped with a Wratten No. 45 filter; its field of view was circular and 6.6° in angular diameter. The water was nearly uniform in its optical properties; i.e., the attenuation length (as measured by means of a light beam transmissometer having a tungsten source, an RCA 931A phototube, and a Wratten No. 45 filter) was 2.52 m/ln just beneath the surface and increased very slightly at a steady rate to 2.62 m/ln at a depth of 61 m; that is to say, the change in attenuation length with depth was barely detectable. Additional families of radiance profiles in vertical planes at other azimuths can be constructed from Tyler's tables, which also provide corresponding data for overcast conditions. All such sets of profiles are remarkably similar at great depth. Parallel profiles signify that the radiance distribution has its asymptotic form.

<sup>21</sup> L. V. Whitney, *J. Marine Research* 4, 122 (1941).

<sup>22</sup> L. V. Whitney, *J. Opt. Soc. Am.* 31, 714 (1941).

<sup>23</sup> J. E. Tyler, *Bull. Scripps Inst. Oceanog.* 7, 363 (1960).

<sup>24</sup> R. W. Preisendorfer, *J. Marine Research* 18, 1 (1959).

<sup>25</sup> N. G. Jerlov and M. Fukuda, *Tellus* 12, 348 (1960).

<sup>26</sup> T. Sasaki, *Bull. Japan. Soc. Sci. Fisheries* 28, 489 (1962).

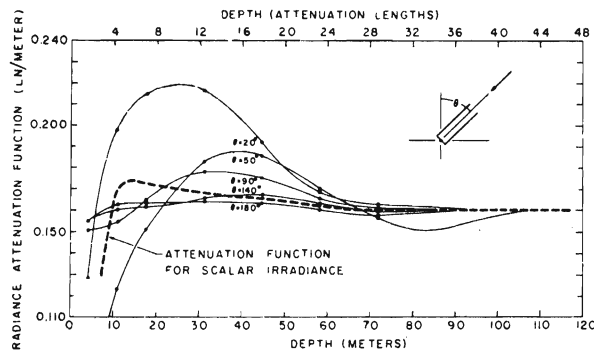


FIG. 24. The solid curves are radiance attenuation functions (i.e., slopes) of the depth profiles of apparent radiance in Fig. 23. The circled points are from Tyler's attenuation function tables (see reference 23). The dashed curve is the attenuation function for scalar irradiance; i.e., the slope of the depth profile of scalar irradiance, a radiometric quantity proportional to the response of a spherical diffuse collector such as that at the top of the instrument pictured in Fig. 25. The transformation of the light field to its asymptotic form is illustrated by the convergence of the radiance attenuation functions to a common, steady value at sufficient depth.

ceptually, each curve represents the results of lowering vertically into the sea a radiance photometer having a fixed zenith angle and azimuth. The unique utility of such profiles arises from the fact that the contrast transmittance of any path of sight in the day-lighted sea is given by the ratio of the apparent background radiances at the *terminals of the path* multiplied by the beam transmittance of the path [see Eq. (8)]. This important general theorem is rigorously true despite any degree of stratification or nonhomogeneity possessed by the water and despite any amount of nonuniformity in the lighting throughout the path of sight. Radiance distribution profiles like those in Fig. 23 enable the apparent background-radiance ratio to be read for any pair of terminal points regardless of the shape of the profile.

In Fig. 23 each curve is nearly, but not quite, straight and nearly, but not quite, parallel with its fellows. When, at sufficient depth, all of the profiles are parallel, the asymptotic radiance distribution prevails.

### Radiance Attenuation Functions

The inverse slope of the semilogarithmic underwater radiance distribution profiles in Fig. 23 is called the *radiance attenuation function*. It is symbolized by  $K(z, \theta, \phi)$ , where  $z$  refers to depth,  $\theta$  specifies the zenith angle of the radiance photometer, and  $\phi$  denotes its azimuth. Figure 24, developed from similar ones by Preisendorfer,<sup>27,28</sup> is a plot of the radiance attenuation functions (slopes) of the radiance profiles shown in Fig. 23. The curves in Fig. 24 have been extrapolated beyond the greatest depth explored by Tyler's measurements in order to illustrate the asymptotic radiance distribution

<sup>27</sup> R. W. Preisendorfer, Scripps Inst. Oceanog. Ref. 58-59, (1958).

<sup>28</sup> R. W. Preisendorfer, Scripps Inst. Oceanog. Ref. 58-60, (1958).

concept more completely. Differential equations for the radiance attenuation functions have been evolved by Preisendorfer.<sup>27</sup>

### Attenuation Function for Scalar Irradiance

The slope of a vertical profile of scalar irradiance  $h(z)$ , a radiometric quantity measurable by means of a spherical diffuse collector, is called the *attenuation function for scalar irradiance* at depth  $z$  and is denoted by  $k(z)$ . This function is shown by the dashed curve in Fig. 24. The limiting value  $k(\infty)$  of  $k(z)$  is a convenient experimental parameter for describing the optical properties of the sea because (1)  $k(z)$  approaches its asymptotic value at less depth than do the radiance attenuation functions, and (2) it is easier to measure. Figure 25 shows a water-clarity meter proposed by the author and constructed

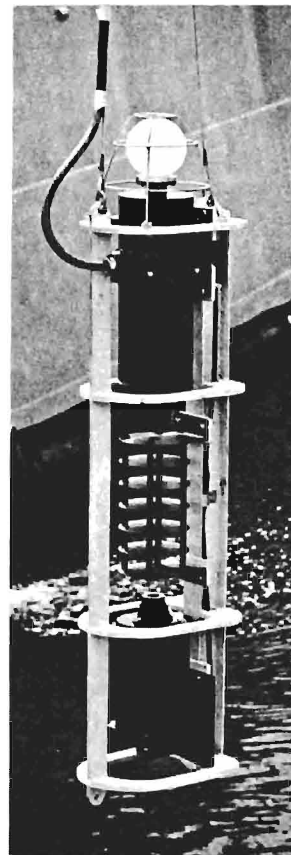


FIG. 25. Water-clarity meter for measuring depth profiles of scalar irradiance  $h(z)$  and attenuation coefficient  $\alpha(z)$  at sea. The hollow, translucent, white sphere at the top of the instrument is the collector for the measurement of scalar irradiance. Attenuation is measured by means of a highly collimated beam of light, produced by a projector in the lower compartment, which travels upward to a photoelectric telephotometer in the upper chamber. Baffles are used to minimize the effect of daylight in near surface measurements. The use of multiplier phototubes enables this equipment to produce profiles of scalar irradiance at depths greater than 10 attenuation lengths. A pressure transducer is incorporated in the instrument to indicate its depth. Due to the spherical nature of the irradiance sensor, the orientation of the instrument is not important; it can, if desired, be oriented horizontally (see reference 29).

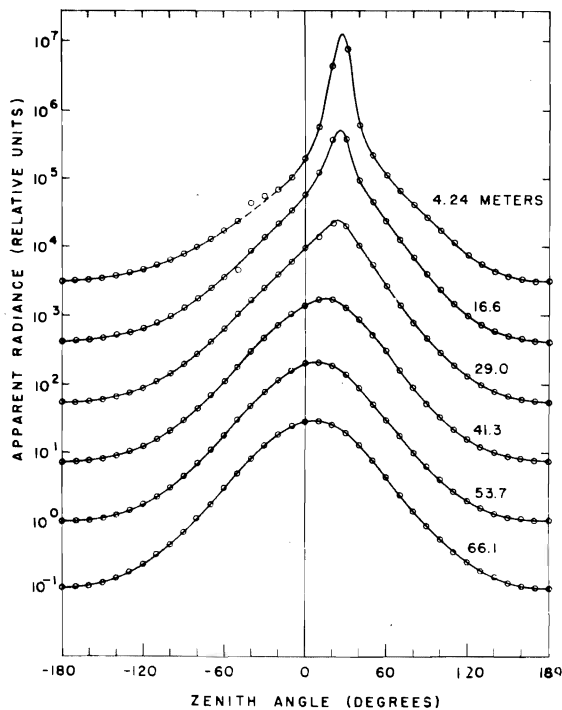


FIG. 26. Underwater radiance distributions in the plane of the sun on a clear, sunny day at depths of 4.24, 16.6, 29.0, 41.3, 53.7, and 66.1 m, respectively. The circles denote data by Tyler (see reference 23) at Pend Oreille, Idaho, 28 April 1957. The solar zenith angle was  $33.4^\circ$ . For additional experimental details see Fig. 23. At the shallowest depth measured (4.24 m), the peak of the radiance distribution is at a slightly greater zenith angle than refracted rays from the sun ( $24.4^\circ$ ); see Fig. 29. At progressively greater depths the distribution becomes less sharply peaked and the maximum moves toward zero zenith angle. The radiance distribution is nearly in its asymptotic form at 66.1 m, the greatest depth at which data were taken. Corresponding trends appear in similar plots of data obtained by Sasaki in ocean water near Japan (see reference 26) and in Gullmar fjord by Jerlov and Fukuda (see reference 25).

by his colleagues,<sup>29</sup> which measures simultaneous vertical profiles of scalar irradiance  $h(z)$  and attenuation coefficient  $\alpha(z)$  in routine oceanographic surveys.

### Shapes of the Underwater Radiance Distribution

The shapes of a typical family of underwater radiance distributions in the plane of the sun at progressively greater depths are shown by Fig. 26, which includes the same data plotted in Fig. 23. At shallow depths the distribution is sharply peaked, approximately in the direction of the refracted rays from the sun. At increasingly greater depths the distribution becomes less sharply peaked and the maximum moves progressively toward the zenith. The change in curve shape is better illustrated by Fig. 27, wherein the upper four curves of Fig. 26 have been superimposed at their respective maxima.

The lower two curves in Fig. 26 do not appear in Fig. 27 because their shape does not differ from that of the 41.3-m curve within the precision of the data. It may be noted, therefore, that the form of the radiance dis-

tribution changes throughout only the first 41 m of depth (about 16 attenuation lengths or *optical depths*). At that depth, however, the shift of the maximum toward the zenith is incomplete and continues to change rapidly as depth is progressively increased. Figure 28 shows how the maximum of the underwater daylight distribution shifts toward the zenith with increasing depth; it suggests, by extrapolation, that a depth of 20 attenuation lengths (100 m) or more is required in order for the true asymptotic radiance distribution to be reached.

### Irradiance Profiles

When the underwater radiance distribution has its asymptotic form, the irradiance incident on a plane oriented in any direction will decrease exponentially with depth at the same rate as will the irradiance on planes oriented in any other directions. A family of semilogarithmic profiles of the irradiance on planes oriented in various directions is merely a group of parallel straight lines having a slope corresponding to  $k(\infty)$ , the limiting value of the attenuation function for scalar irradiance. In most ocean water the irradiance  $H(z, -)$  on the upper surface of a horizontal plane at any depth  $z$  is approximately 50 times as great as the irradiance  $H(z, +)$  on the lower surface of the same plane; the irradiance on planes oriented in all other directions at this depth lies between  $H(z, -)$  and  $H(z, +)$ .

At lesser depths, where the underwater radiance distribution departs from its asymptotic form, the semilogarithmic irradiance profiles differ somewhat from parallelism and straightness. Such perturbations are, however, comparatively minor and for many purposes they are negligible. For example, some of the attenuation functions at a depth of 2.5 ft on an overcast day

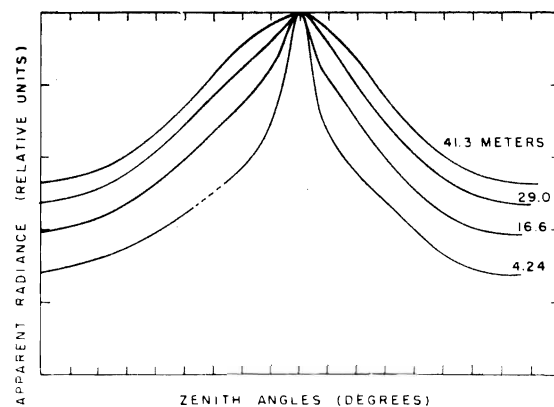


FIG. 27. In this figure the underwater radiance distribution curves for depths 4.24, 16.6, 29.0, and 41.3 m from Fig. 26 have been superimposed at their respective maxima in order to compare their shapes. The radiance curves for depths 53.7 and 66.1 m are not shown since, within the limits of experimental error, their shapes are identical with the curve for 41.3 m depth. Thus, the *shape* of the underwater radiance distribution has nearly completed its transformation to the asymptotic form at 41.3 m depth. The maximum of the curve has not, however, reached zero zenith angle at this depth and is, in fact, changing at maximum rate; see Fig. 28.

<sup>29</sup> R. W. Austin, Scripps Inst. Oceanog. Ref. 59-9, (1959).

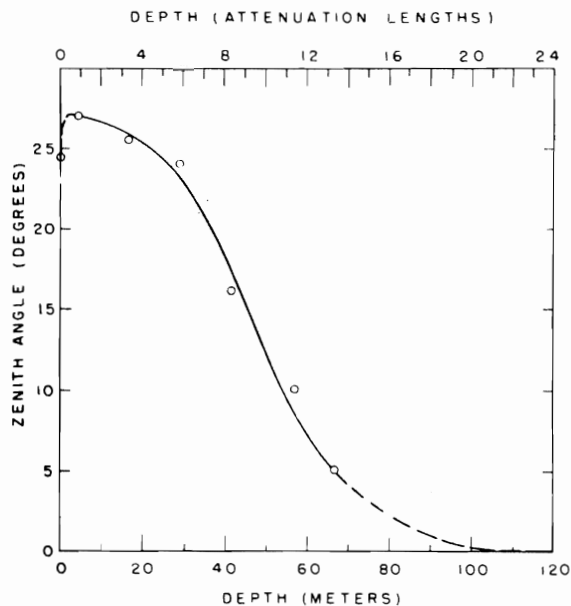


FIG. 28. Illustrating how the peaks of the underwater daylight radiance distributions shown in Fig. 26 shift toward zero zenith angle with increasing depth. At shallow depths in these data the peak occurs at a greater zenith angle than the direction (underwater) of rays from the sun. The extrapolated (dashed) portion of the curve suggests that a depth of more than 100 m is required to bring the peak to zero zenith angle; i.e., to complete the transformation of the light field to its asymptotic form.

(28 August 1959) at Diamond Island were  $K(2.5, -) = 0.067 \text{ ln/ft}$ ,  $k(2.5) = 0.063 \text{ ln/ft}$ ,  $K(2.5, +) = 0.051 \text{ ln/ft}$ , and  $\alpha(2.5) = 0.18 \text{ ln/ft}$ .

### Contrast Transmittance

*Introduction.* Underwater sighting ranges are always short compared with sighting ranges in clear air. Nearly all objects, therefore, subtend so large a visual angle when seen underwater that the exact size of the object is of almost no consequence. Except for very tiny objects or the fine details of larger ones, underwater sighting ranges depend almost entirely upon the contrast transmittance of the path of sight when ample daylight prevails. Along horizontal paths of sight dark objects (such as black-suited swimmers) approach detection threshold near the distance  $4/\alpha(z)$  when viewed against a water background, although bright objects (including light sources) can be seen further.<sup>30</sup> For objects of sufficient angular size, horizontal daylight sighting ranges underwater are remarkably similar to horizontal daylight sighting ranges in the atmosphere if both are expressed in attenuation lengths. This quantitative similarity does not hold, however, when the path of sight is inclined either upward or downward because water, unlike air, absorbs light so strongly that all aspects of

<sup>30</sup> Along any underwater path of sight a remarkable proportion of the objects ordinarily encountered can be seen at limiting ranges between 4 and 5 times the distance  $1/[\alpha(z) - K(z, \theta, \phi) \cos \theta]$ , regardless of their size or the background against which they appear, provided ample daylight prevails [see Eqs. (14) and (15)].

daylight in the sea diminish rapidly with depth. Contrast reduction along inclined paths of sight through optically uniform water are treated after certain general principles have been discussed.

*General case.* A completely general phenomenological treatment of the reduction of apparent contrast by any scattering and absorbing medium has been given by the author and two of his colleagues in an earlier paper<sup>31</sup> concerned with the atmosphere; Eq. (1) through (10) of that paper and the discussions which accompany them apply also to the reduction of contrast along all underwater paths of sight, and the notation employed in reference 31 has been used throughout the present paper, except that  $z$  is used to denote depth (rather than altitude) and is positive from the sea surface downward. Although, in the interest of brevity, only one [Eq. (7)] of those equations is discussed here, they constitute the foundation for all of the relations which follow in this paper.

Equation (7) in reference 31 states that the ratio of the apparent contrast  $C_r(z, \theta, \phi)$  of an object at distance  $r$  from an observer at depth  $z$  along a path of sight having zenith angle  $\theta$  and azimuth  $\phi$  to the inherent contrast  $C_0(z_t, \theta, \phi)$  of a target at depth  $z_t$  is

$$C_r(z, \theta, \phi) / C_0(z_t, \theta, \phi) = \frac{T_r(z, \theta, \phi) {}_b N_0(z_t, \theta, \phi)}{{}_b N_r(z, \theta, \phi)}, \quad (8)$$

where  $T_r(z, \theta, \phi)$  is the beam transmittance of the path of sight for image-forming light and  ${}_b N_0(z_t, \theta, \phi) / {}_b N_r(z, \theta, \phi)$  is the ratio of the apparent radiances of the background at the *terminals* of the path of sight. This equation is rigorously true despite any amount of non-uniformity in the water or in its lighting. Profiles of underwater radiance, such as those in Fig. 23, provide the two background radiance values required by Eq. (8) and the beam transmittance can be found from a profile of attenuation length by means of Eq. (16) in reference 31. It should be noted that the beam transmittance  $T_r(z, \theta, \phi)$  must include the factor  $[n(z)/n(z_t)]^2$  required by geometrical optics when the refractive index  $n(z)$  of the medium at the observer differs from that at the target  $n(z_t)$ , as in the case of underwater observation through a flat face plate or a plane window.

*Uniform water.* If the underwater path of sight lies entirely within a single optically uniform stratum and if the profile of monochromatic apparent radiance (see Fig. 23) can be approximated by a straight line and represented by the differential equation

$$dN(z, \theta, \phi) / dr = -K(z, \theta, \phi) \cos \theta N(z, \theta, \phi), \quad (9)$$

where  $r \cos \theta = z_t - z$ , Eq. (10) of reference 31 can be replaced by differential equations of transfer for spectral field radiance

$$dN(z, \theta, \phi) / dr = N_*(z, \theta, \phi) - \alpha(z) N(z, \theta, \phi), \quad (10)$$

<sup>31</sup> S. Q. Duntley, A. R. Boileau, and R. W. Preisendorfer, *J. Opt. Soc. Am.* **47**, 499 (1957).

and for apparent spectral target radiance

$$d {}_t N(z, \theta, \phi) / dr = N_*(z, \theta, \phi) - \alpha(z) {}_t N(z, \theta, \phi). \quad (11)$$

Equations (9), (10), and (11) can be combined and integrated throughout the path of sight to produce the important relation

$$\begin{aligned} {}_t N_r(z, \theta, \phi) = & {}_t N_0(z, \theta, \phi) \exp[-\alpha(z)r] \\ & + N(z, \theta, \phi) \exp[+K(z, \theta, \phi)r \cos \theta] \\ & \times \{1 - \exp[-\alpha(z)r + K(z, \theta, \phi)r \cos \theta]\}, \quad (12) \end{aligned}$$

where  ${}_t N_r(z, \theta, \phi)$  is the apparent spectral radiance of the target and  ${}_t N_0(z, \theta, \phi)$  is its inherent spectral radiance. In Eq. (12) the first term on the right represents

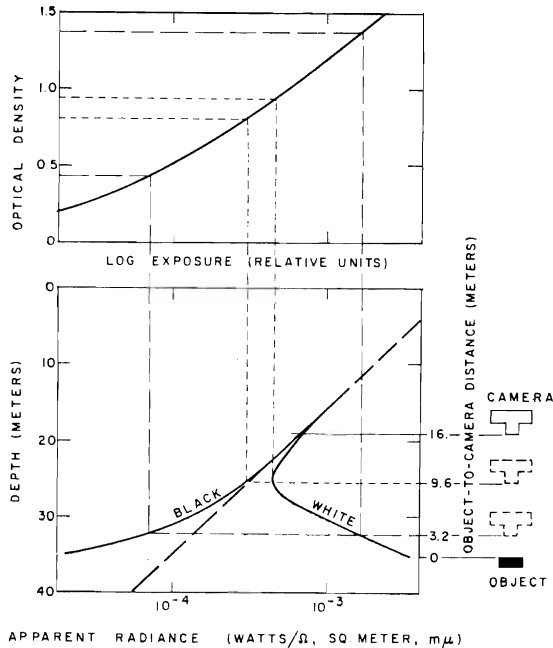


Fig. 29. Illustrating the effect of (vertical) object-to-camera distance on the apparent radiance (lower figure) and the photographic contrast (upper figure) of an object having both white and black areas submerged 35 m beneath the surface of deep, optically uniform water characterized by an attenuation length  $(1/\alpha)$  of 3.2 m/ln,  $(\alpha/K)=2.7$ ,  $H(z,+)/H(z,-)=0.02$ , and asymptotic radiance distribution. The prevailing spectral irradiance on the surface of the water is assumed to be  $1 \text{ W/m}^2, \text{ m}\mu$ .

As a downward-looking camera is lowered from the sea surface, the apparent radiance presented by the water decreases at the rate of  $K=0.116 \text{ ln/m}$ , as shown by the diagonal dashed line in the lower figure. At 19 m depth (i.e., an object-to-camera distance of 16 m or 5 attenuation lengths) the apparent radiances of the object differ but little from that of the surround. When the camera is 9.6 m (i.e., 3 attenuation lengths) above the target, the white area presents an apparent radiance significantly greater than the surround (diagonal dashed line) but the black area appears only slightly darker than the water background. Near this camera position the two terms in the right-hand member of Eq. (12) are equal, so that  $dN(z, \pi, 0)/dr=0$ ; at greater camera depths the second term predominates. When the camera is 3.2 m or 1 attenuation length above the object, both the black and the white areas of the target differ markedly in apparent radiance from the surround (diagonal dashed line). The upper figure illustrates, by means of the characteristic curve of a negative material, the range of photographic densities corresponding with object-to-camera distances of 3.2 m (dashed lines) and 9.6 m (dotted lines).

residual image-forming light from the target and the second term represents radiance due to scattering of light in the sea throughout the path of sight, i.e., the path radiance  $N_r^*(z, \theta, \phi)$ . A graphical illustration of Eq. (12) is provided by Fig. 29, which shows how black objects and white objects submerged in deep water appear to emerge gradually from the background as they are approached from above by a descending, downward-looking underwater observer or camera.

In Eq. (12),  $\alpha(z)$  and  $K(z, \theta, \phi)$  are considered to be constants throughout the path of sight. In uniform water this is true of  $\alpha(z)$  but not of  $K(z, \theta, \phi)$  unless the radiance distribution is asymptotic. Figure 24 illustrates how  $K(z, \theta, \phi)$  changes with  $z$  and  $\theta$  in the plane of the sun; corresponding figures can be constructed from Tyler's tables<sup>23</sup> to illustrate changes with  $\phi$ . Such data should be used to ascertain the variation of  $K(z, \theta, \phi)$  on the particular segment of the path of sight to be used; the degree of approximation represented by Eq. (12) [and by Eqs. (14), (15), and (16)] can then be estimated. Because underwater sighting ranges rarely exceed  $2/K$ , the effect of  $K$  variation is seldom appreciable, except near the surface of the sea. General equations, remarkably similar in form to Eqs. (12), (14), (15), and (16), have been written by Preisendorfer (private communication); these involve, for example,

$$\exp \left\{ - \int_0^r [\alpha(z) - \cos \theta K(z, \theta, \phi)] dr' \right\}$$

instead of

$$\exp[-\alpha(z)r + \cos \theta K(z, \theta, \phi)r];$$

they are also applicable to nonuniform water and even to multi-media paths of sight.

Equation (12) also specifies the apparent radiance of any background against which a target may be seen; when used for this purpose the presubscript  $t$  (for target) should be changed to  $b$  (for background). Subtraction of the background form of Eq. (12) from Eq. (12) itself yields the relation

$$\begin{aligned} {}_t N_r(z, \theta, \phi) - {}_b N_r(z, \theta, \phi) \\ = [{}_t N_0(z, \theta, \phi) - {}_b N_0(z, \theta, \phi)] \exp[-\alpha(z)r]. \quad (13) \end{aligned}$$

Equation (13) implies that along any underwater path of sight, radiance differences are transmitted with exponential attenuation at the same space rate as image-forming rays.

The two forms of Eq. (12) can be combined with the defining relations for inherent spectral contrast,  $C_0(z, \theta, \phi)$ , and apparent spectral contrast  $C_r(z, \theta, \phi)$ , which are, respectively,

$$C_0(z, \theta, \phi) = [{}_t N_0(z, \theta, \phi) - {}_b N_0(z, \theta, \phi)] / {}_b N_0(z, \theta, \phi),$$

and

$$C_r(z, \theta, \phi) = [{}_t N_r(z, \theta, \phi) - {}_b N_r(z, \theta, \phi)] / {}_b N_r(z, \theta, \phi).$$

When this is done, the ratio of inherent spectral con-

trast to the apparent spectral contrast is found to be

$$\begin{aligned} C_0(z, \theta, \phi) / C_r(z, \theta, \phi) &= 1 - [N(z, \theta, \phi) / {}_b N_0(z, \theta, \phi)] \\ &\times \{1 - \exp[\alpha(z)r - K(z, \theta, \phi)r \cos \theta]\}. \end{aligned} \quad (14)$$

If  ${}_b N_0(z, \theta, \phi) = N(z, \theta, \phi)$ , as in the special case of an object suspended in deep water, Eq. (14) reduces to

$$C_r(z, \theta, \phi) = C_0(z, \theta, \phi) \times \exp[-\alpha(z)r + K(z, \theta, \phi)r \cos \theta]. \quad (15)$$

Whenever the underwater daylight radiance distribution has, effectively, its asymptotic form, the radiance attenuation function  $K(z, \theta, \phi)$  is a constant, independent of  $z$ ,  $\theta$ , and  $\phi$ . Equation (15) may then be written

$$C_r(z, \theta, \phi) / C_0(z, \theta, \phi) = \exp[-\alpha + K \cos \theta] r. \quad (16)$$

The right-hand member of Eq. (16), sometimes called the *contrast reduction factor*, is independent of  $\phi$ , the azimuth of the path of sight. This and other implications of Eq. (16) were discovered by the author in the

course of early experiments as illustrated, in part, by Figs. 30 and 31.

*Horizontal paths of sight.* Along horizontal paths of sight  $\cos \theta = 0$  in Eqs. (9), (12), (14), (15), and (16), which show that both the apparent radiance and the apparent contrast of objects seen horizontally underwater change with distance in a manner dependent on  $\alpha$  but not on  $K$ . When  $\cos \theta = 0$ , Eq. (10) indicates that some unique *equilibrium radiance*  $N_q(z, \pi/2, \phi)$  must exist at each point such that the loss of radiance within the horizontal path segment is balanced by the gain, i.e.,

$$dN_q(z, \frac{1}{2}\pi, \phi) / dr = 0 = N_*(z, \frac{1}{2}\pi, \phi) - \alpha(z)N_q(z, \frac{1}{2}\pi, \phi). \quad (17)$$

Even in nonuniform water there is an equilibrium radiance for each element of horizontal path although this may differ from point to point. Inclined paths of sight do not have a true equilibrium radiance, as will be clear from Eq. (9), but they possess an exponential counterpart which is illustrated by the diagonal dashed line in Fig. 29.

A method<sup>32</sup> for measuring the attenuation coefficient

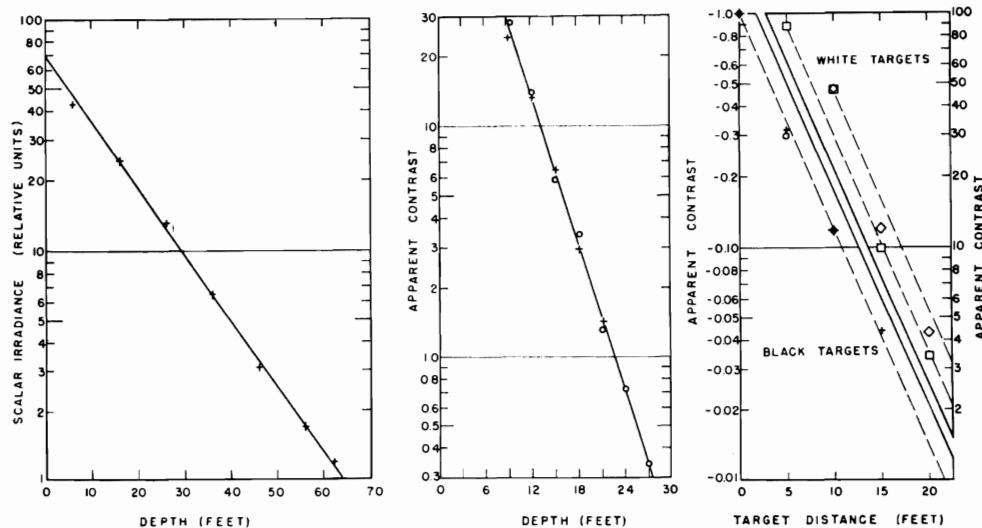


FIG. 30. Interrelated experiments from the September 1948 series at the Diamond Island Field Station: (Left) Semilogarithmic depth profile of scalar irradiance obtained by lowering a 6-in.-diameter, air-filled, hollow, translucent, opal glass sphere having a photovoltaic cell sealed in an opening at its bottom. The straightness of the curve indicates optical homogeneity of the water and a depth invariant attenuation coefficient  $k(z) = 0.066$  ln/ft. (Center) Semilogarithmic plot of the absolute apparent contrast of a horizontal, flat, white target lowered vertically beneath a telephotometer mounted in a small, hooded, glass-bottomed boat; calm water, clear sky, low sun. The long, straight portion of the curve illustrates Eq. (15) and its slope indicates that  $\alpha(z) + K(z, \pi, 0) = 0.247$  ln/ft. Because the sun was low the radiance distribution was approximately asymptotic, so that  $K(z, \pi, 0) \approx k(z) = 0.066$  ln/ft and, by subtraction  $\alpha(z) = 0.181$  ln/ft or the attenuation length  $1/\alpha = 5.5$  ft/ln. (Right) Two semilogarithmic plots of apparent contrast vs target distance along 60°-downward-sloping paths of sight for black targets (lower portion) and white targets (upper portion) have been combined to demonstrate (1) that the apparent contrast is exponentially attenuated with target distance at the same space rate for both light targets and dark targets, (2) that this space rate is independent of azimuth, and (3) that Eq. (16) is valid. All four paths of sight have the same zenith angle,  $\theta = 150^\circ$ , but the azimuth angles relative to the plane of the sun are  $\phi = 0$  (circled points) and  $\phi = 45^\circ$  (crosses),  $\phi = 95^\circ$  (diamonds) and  $\phi = 135^\circ$  (squares). The dashed straight lines are constructed parallel and, in accordance with Eq. (16), they have a slope  $0.181 - 0.066 \cos 150^\circ = 0.214$  ln/ft. These lines were passed through the uppermost datum point of each series without regard to the lower points; the lines are provided solely to facilitate judgment of the slope and linearity of the data. Photographic underwater telephotometry; green light, calm water, clear sky, low sun.

<sup>32</sup> S. Q. Duntley, J. Opt. Soc. Am. 37, 994(A) (1947) and U. S. Patent No. 2,661,650.

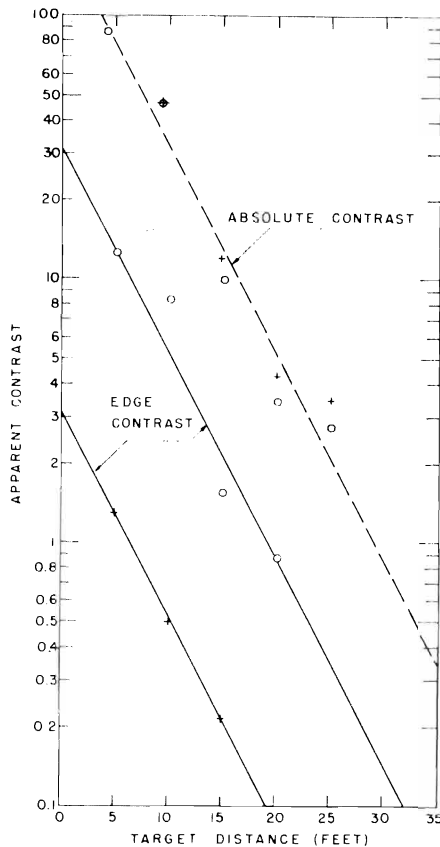


FIG. 31. Comparison of apparent absolute contrast with apparent edge contrast of white targets for two horizontal underwater paths of sight having azimuths relative to the direction of the sun of  $95^\circ$  (crosses) and  $135^\circ$  (circles), respectively. The three lines are parallel and correspond to an attenuation length  $1/\alpha = 5.65$  ft/ln. The data are of 24 September 1948 at Diamond Island. Photographic telephotometry; green filter.

$\alpha(z)$  is suggested by Eq. (17) and the fact that in optically uniform water  $qN(z, \frac{1}{2}\pi, \phi) = N(z, \frac{1}{2}\pi, \phi)$ ; thus

$$\alpha(z) = N_*(z, \frac{1}{2}\pi, \phi) / N(z, \frac{1}{2}\pi, \phi). \quad (18)$$

In Eq. (18),  $N_*(z, \frac{1}{2}\pi, \phi)$  can be approximated by the apparent radiance of a very black object, such as an opening in a small black box, located at a unit distance which is small compared with the attenuation length, and  $N(z, \frac{1}{2}\pi, \phi)$  is the apparent radiance of the unrestricted water background. This technique is especially convenient for documenting conditions in underwater photography by daylight. The value of  $\alpha(z)$  so obtained agrees precisely with data obtained by (1) properly designed light beam transmissometers, (2) measurements of the apparent contrast of underwater objects observed along horizontal paths of sight, and (3) underwater telephotometry of the apparent radiance of the surface of a distant submerged frosted incandescent lamp or other diffusely emitting source.

*Field experiments.* Experimental explorations of the distribution of daylight in the sea and underwater image transmission phenomena were begun by the author in 1948 and are still in progress. Most of the physical prin-

ciples discussed in this paper were discovered or generalized early in the course of these experiments. The data guided a collaborative development of the foregoing equations by Dr. Rudolph W. Preisendorfer and the author.<sup>33-35</sup>

Experiments were conducted concurrently in lakes and at sea almost from the beginning because optical principles can be explored better and more inexpensively in lakes whereas the magnitude of the optical constants of ocean waters can be measured only at sea. Most of the data used in this paper to illustrate principles were obtained at a field station established by the author in 1948 at Diamond Island in Lake Winnepesaukee, New Hampshire. Examples of data from the field station are provided in Fig. 30. These data, taken from the 1948 series, illustrate several important principles which are implied and summarized by Eq. (16). Figure 30 shows that the attenuation coefficients  $k(z)$  and  $\alpha(z)$  obtained by means of a depth profile of scalar irradiance and measurements of the apparent radiance of a white object lowered vertically (in the manner of a Secchi disk) can be used with Eq. (16) to predict the apparent contrast of any object, black or white, along various underwater paths of sight. Measurements of apparent contrast with highly refined photoelectric equipment have been made along many paths of sight and under many kinds of lighting conditions in the course of the field station experiments; all of these experiments support the validity of Eqs. (15) and (16).

The water-clarity meter pictured in Fig. 25 produces a profile of scalar irradiance similar to that shown in Fig. 30 and, therefore, a measure of  $k(z)$ ; it also measures the attenuation coefficient  $\alpha(z)$ , providing, thereby, the necessary input information for using Eq. (16) to calculate contrast reduction, since  $K = k(z)$ .

Telephotometry of either black or white targets along any two paths of sight having different inclinations (i.e., zenith angle  $\theta$ ) yields two values of the contrast attenuation coefficient ( $\alpha - K \cos\theta$ ) from which  $\alpha$  and  $K$  can be found. The use of a horizontal path for determining  $\alpha$ , and a downward vertical path for determining  $\alpha + K$ , is often a convenient choice.

*Absolute contrast.* The water immediately surrounding a submerged white object sometimes appears to glow. This effect is caused by the intense small-angle forward scattering of light which is reflected by the target in directions adjacent to that of the observer. The effect is most noticeable when a strongly lighted white object is observed against a dark background. The apparent radiance of the scattered glow has been found to be attenuated at the same space rate as the target itself; this is shown by Fig. 31 wherein the semi-logarithmic attenuation curves for apparent *absolute contrast* and apparent *edge contrast* are parallel. Apparent absolute contrast is relative to the apparent background

<sup>33</sup> S. Q. Duntley, Proc. Armed Forces-Natl. Research Council Vision Committee 23, 123 (1949); 27, 57 (1950); 28, 60 (1951).

<sup>34</sup> S. Q. Duntley and R. W. Preisendorfer, MIT Rept. N5ori 07864 (1952).

<sup>35</sup> R. W. Preisendorfer, Scripps Inst. Oceanog. Ref. 58-42 (1957).

radiance that would be observed if the target were absent; apparent edge contrast is relative to the apparent background radiance which appears immediately adjacent to the target. Ordinarily, few underwater objects are white enough to cause the two types of contrast to differ significantly. When the glow is prominent, absolute contrast is usually the more meaningful measure of object detectability, but a full treatment of this topic can be made only in context with details concerning the characteristics of the detector (eye, camera, etc.), a matter beyond the scope of this paper.

**Absorption**

If radiant power in the sea is to be useful for heating or for photosynthesis it must be absorbed. The monochromatic radiant power absorbed per unit of volume at any depth depends upon the amount of power received by the volume element and the magnitude of the absorption coefficient; i.e., upon the product of the scalar irradiance and the volume absorption coefficient.<sup>36</sup> A more frequently useful relation<sup>37</sup> has been evolved as follows: The net inward flow of radiant power to any element of volume  $dv$  in any horizontal lamina of thickness  $dz$  at depth  $z$  in the sea is

$$\frac{dP(z)}{dv} = -\frac{d}{dz} \{H(z, -) - H(z, +)\} = -\frac{d}{dz} \left\{ H(z, -) \left[ 1 - \frac{H(z, +)}{H(z, -)} \right] \right\}. \quad (19)$$

The ratio  $H(z,+)/H(z,-)$ , sometimes called the *reflection function* of water, has been found by experiment to be virtually independent of depth and to have a value of  $0.02 \pm 0.01$  for most natural waters unless large quantities of suspended matter are present; the reflection function is rigorously independent of depth when the underwater daylight radiance distribution has its asymptotic form in optically uniform water. To the extent to which 2% effects are negligible, Eq. (19) becomes

$$dP(z)/dv \approx H(z,-)K(z,-), \quad (20)$$

since, by definition,  $K(z,-) = -[dH(z,-)/dz]/H(z,-)$ . Thus, the radiant power absorbed per unit of volume at any depth in the sea can be measured simply by lowering an upward-facing, diffusely collecting, flat photocell and determining the product of the magnitude and slope of the resulting profile of downwelling irradiance, as illustrated by Fig. 32.

Alternatively, the quantity  $\{H(z,-) - H(z,+)\}$  can be measured directly by lowering an assembly of two diffusely collecting, flat photocells mounted back to back so that one faces upward and the other downward. Such an assembly, sometimes called a *janus cell*, can

<sup>36</sup> R. W. Preisendorfer, Scripps Inst. Oceanog. Ref. 58-41, (1957).

<sup>37</sup> S. Q. Duntley, Natl. Acad. Sci./Natl. Research Council Publ. 473, 85 (1956).

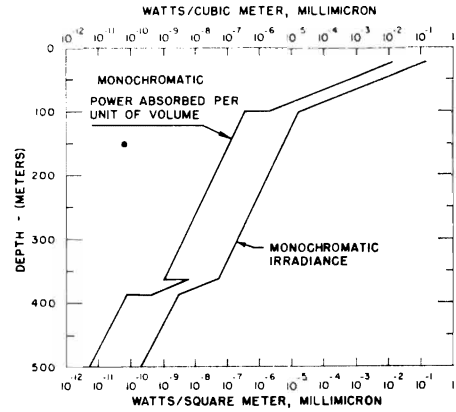


FIG. 32. Superimposed semilogarithmic plots of monochromatic downwelling irradiance vs depth and monochromatic radiant power absorbed per unit of volume vs depth illustrate the (approximate) relation between these quantities expressed by Eq. (20). Monochromatic downwelling irradiance is the total monochromatic radiant power per unit of area received by the upper surface of a horizontal plane at arbitrary depth  $z$ . The product of this irradiance and its depth attenuation function (slope of its depth profile) is, within about 2%, equal to the monochromatic power absorbed per unit of volume. Thus, at a depth of 50 m in Fig. 32,  $H(50, -) = 6.3 \times 10^{-3} \text{ W}/(\text{m}^2, \text{m}\mu)$ ,  $K(50, -) = 0.114 \text{ ln}/\text{m}$ , and  $dP(50)/dv \approx (6.3 \times 10^{-3})(0.114) = 7.2 \times 10^{-4} \text{ W}/(\text{m}^3, \text{m}\mu)$ . Neither of the curves in this figure represent specific experimental data, but the irradiance profile is typical of the Pacific Ocean off California. The presence of a deep scattering layer is shown below 350 m.

be used to measure  $dP(z)/dv$  by means of Eq. (19) in turbid waters for which  $\{1 - [H(z,+)/H(z,-)]\}$  is not negligible.

**CONCLUSION**

Although no research program is ever fully completed and the author hopes to participate in studies of light in the sea for many years to come, the investigations which, with many colleagues, have been made thus far, coupled with the findings of other workers all over the world, have produced a sufficient quantitative understanding of the optical properties of ocean water and the behavior of underwater light to provide scientific guidance and optical engineering methods for those persons whose interests or occupations involve light in the sea.

**ACKNOWLEDGMENTS**

The long research program, spanning two decades, from which this paper is drawn has involved too many persons to permit complete acknowledgment here. Special mention should be made, however, of the important technical contributions of Dr. David L. MacAdam, Willard P. Greenwood, Capt. Dayton R. E. Brown, Professor George E. Russell, John Frankovitch, Frederick C. Spooner, Robert W. Sandberg, Walter Rutkowski, Robert J. Uhl, Frances Richey, Dr. Rudolph W. Preisendorfer, Roswell W. Austin, Almerian R. Boileau, John E. Tyler, Justin J. Rennilson, William Hadley Richardson, Dr. William H. Culver, Theodore J. Petzold, Charles W. Saunders, Jr., Sidney Lindroth, Alden D. J. Hooton, Roger A. Howerton, and Clarence Fred Pinkham who, since 1949, has superintended nearly all of the field operations.



## BIBLIOGRAPHY OF REPORTS DESCRIBING RELATED EXPERIMENTS 1948 – 1958

- Duntley, S. Q., "Interim Report on Exploratory Studies of the Physical Factors which Influence the Visibility of Submerged Objects," Proceedings of the AF/NRC Vision Committee, 23rd Meeting (1949), p. 123.
- Duntley, S. Q., "Temporal Factors which Influence the Visibility of Submerged Objects." Proceedings of the AF/NRC Vision Committee, 26th Meeting (1950), p. 98
- Duntley, S. Q., "The Reflectance of Submerged Objects," J. Opt. Soc. Am. **40**, 795, (A) (1950).
- Duntley, S. Q., "The Visibility of Submerged Objects. I" Proceedings of the AF/NRC Vision Committee, 27th Meeting (1950), p. 57.
- Duntley, S. Q., "The Visibility of Submerged Objects. II" Proceedings of the AF/NRC Vision Committee, 28th Meeting (1951), p. 60.
- Duntley, S. Q., "The Reflection of Light by Water Waves," J. Opt. Soc. Am. **41**, 287 (A) (1951).
- Duntley, S. Q., "The Visibility of Submerged Objects," Visibility Laboratory, (Contract N5ori 07864, MIT 1952).
- Duntley, S. Q., "The Inherent Contrast of Submerged Objects," Proceedings of the AF/NRC Vision Committee, 30th Meeting (1952), p. 100.
- Duntley, S. Q., "Refractive Limitations on Resolving Power in Underwater Photography," J. Opt. Soc. Am. **43**, 821 (A) (1953).
- Duntley, S. Q., "Measurements of the Distribution of Water Wave Slopes," J. Opt. Soc. Am. **44**, 574 (1954).
- Duntley, S. Q., Uhl, S. J., Austin, R. W., Boileau, A. R., Tyler, J. E., "Underwater Photometer," J. Opt. Soc. Am. **45**, 904 (A) (1955).
- Duntley, S. Q. and Tyler, J. E. "Apparent Color of Underwater Objects," J. Opt. Soc. Am. **45**, 405 (A) (1955).
- Duntley, S. Q., "The Penetration of Light into the Sea," Proceedings of the Symposium on Aspects of Deep-Sea Research, Committee on Undersea Warfare, National Academy of Sciences, National Research Council Publ. 473 (1957), p. 79.
- Tyler, J. E., "Measurement of Light in the Sea," J. Opt. Soc. Am. **45**, 904 (A) (1955).
- Tyler, J. E., "Monochromatic Measurement of the Volume Scattering of Natural Waters," J. Opt. Soc. Am. **47**, 745 (1957).
- Tyler, J. E. and Richardson, W. H., "Nephelometer for the Measurement of Volume Scattering Function in Situ," J. Opt. Soc. Am. **48**, 354 (1958).
- Tyler, J.E., "Measurement of Light in the Sea," Proceedings of the Ninth Pacific Science Congress – 1957, **16**, 237 (1958).
- Tyler, J. E., "Comparison of Light Distribution Above and Below Water," J. Mar. Res. **16**, 96 (1958).

SIO REFERENCE 59-39  
Bureau of Ships  
Contract NObs-72092  
Index Number NS 714-100  
June 1959

FIELD TEST OF A SYSTEM FOR  
PREDICTING VISIBILITY BY SWIMMERS  
FROM MEASUREMENTS OF THE CLARITY OF NATURAL WATERS

S. Q. Duntley, J. E. Tyler, and J. H. Taylor

I. INTRODUCTION AND SUMMARY

1. Introduction

A continuing program concerned with the visibility of submerged objects has been in progress within the Visibility Laboratory for more than a decade. Early experimental and theoretical work<sup>1,2</sup> provided a basis for predicting visibility by swimmers from instrumental measurements of water clarity. Further investigations, theoretical and experimental, and instrumental developments of many kinds verified and extended the original work and enabled this Laboratory to provide the U. S. Navy Hydrographic Office with an accurate water clarity meter<sup>3</sup> and nomographic charts<sup>4</sup> for the interpretation of its readings in terms of the limiting range at which swimmers can sight any flat, horizontal object lying on the bottom of the sea.

---

<sup>1</sup> Duntley, S. Q., "Interim Report on Exploratory Studies of the Physical Factors which Influence the Visibility of Submerged Objects," Minutes and Proceedings Armed Forces-NRC Vision Committee, 23d meeting, March 1949 (p. 123).

<sup>2</sup> Duntley, S. Q., "The Visibility of Submerged Objects;" Final Report under Contract NSori-07831, NSori-07864, and NObs-50378; August 1952.

<sup>3</sup> Austin, R. W., "Water Clarity Meter Operating and Maintenance Instructions," SIO Ref. No. 59-9, Visibility Laboratory, Univ. of Calif., La Jolla, Contract NObs-72092, February 1959.

<sup>4</sup> Duntley, S. Q., "Nomographs for Calculating Visibility by Swimmers," Report No. 3-1, May 1958, Contract NObs-72039.

In providing the Navy with water clarity measuring equipment and the associated nomographic charts, the Laboratory has a responsibility for providing evidence of the over-all validity of the system. A careful review of all experimental evidence relative to the components of the system disclosed that (1) no sufficiently critical test of an underwater sighting range prediction had ever been made and (2) that experiments with earlier instruments showed a disturbing lack of close agreement between the apparent contrast of underwater objects calculated by means of the contrast reduction equation and corresponding values of apparent contrast measured directly with photographic or photoelectric telephotometers. There is, however, considerable evidence that the equation is valid when supplied with water clarity constants derived from direct contrast reduction measurements.

### 1.2 The New Water Clarity Meter

The lack of close agreement between the two methods for obtaining the water clarity constants was believed to be attributable to perturbations of the underwater light-field due to the presence of the target, if large, and to the presence of the measuring apparatus. Both water clarity meter readings and telephotometer observations are affected, but ordinarily to different extents. There is, moreover, a perturbation of the underwater light-field by the presence of the swimmer in the case of visual target sightings. Agreement between the different methods for measuring water clarity constants and their applicability to sighting range predictions requires that the effective perturbation of the light-field match in all three instances.

During the design of the new water clarity meter for the Navy, Dr. R. W. Preisendorfer of the Visibility Laboratory was asked to make a theoretical exploration of underwater light-field perturbations. His results,<sup>5</sup> which relate to effects due to the presence of the target only, were used to establish design criteria for the new instrument. Great care was exercised to reduce the perturbations far below those of any previous hydrophotometer and to endeavor to match the residual effects with those which are always produced by the presence of a human observer.

### 1.3 The Field Test

It was necessary, obviously, to conduct a field test to ascertain whether the intent of the instrumental design had been successfully realized, i.e., to see if the water clarity constants obtained by means of the instrument provide a valid measure of contrast reduction as seen by swimmers or as observed with a telephotometer. A field test for this purpose was conducted at the Diamond Island Field Station of the Visibility Laboratory during the summer of 1958 and is described in this report. The successful result constitutes evidence that the clarity meter and nomograph method for predicting underwater sighting range works as a system.

The  $\alpha$ -measuring equipment used for the field test embodied the same basic optical design as the water clarity meter constructed for the Navy. In the field test the K-measuring portion of the water clarity

---

<sup>5</sup> Preisendorfer, R. W., "A General Theory of Perturbed Light Fields with Application to Forward Scattering Effects in Beam Transmittance Measurements," SIO Ref. 58-37, Visibility Laboratory, Univ. of Calif., La Jolla, Contract NObs-72092, 1 May 1958.

meter was a physically separate unit. The coefficient  $K$  was determined by measuring the vertical gradient of downwelling irradiance; this was accomplished by means of an upward facing photovoltaic cell covered by a matte-surfaced diffusing plate which, by test, evaluated flux in proportion to the cosine of the angle of incidence, thus measuring the irradiance on the surface of the plate. Absorption filters were used to correct the photocells to photopic response.

#### 1.4 Experimental Procedure

Contrast reduction was measured by means of an underwater photoelectric telephotometer in a carefully prepared perturbation-minimized mounting and compared with values predicted by theory on the basis of data from the water clarity meter. Concurrently, underwater sighting ranges were determined under identical viewing conditions by an experienced observer and compared with ranges predicted from the water clarity meter readings.

#### 1.5 Conclusions

All of the data are in excellent agreement; they constitute experimental evidence that:

- (1) the new water clarity meter provides values of the water clarity constants,  $\alpha$  and  $K$ , which are valid for predicting the apparent contrast of underwater subjects by means of equation (1), and
- (2) the sighting ranges predicted by the nomographic charts are valid when based upon values of  $\alpha$  and  $K$  from the new water clarity meter.

2. MEASUREMENTS OF APPARENT CONTRAST2.1 Introduction

It was discovered experimentally during Visibility Laboratory underwater experiments in 1948<sup>1</sup> and subsequently derived analytically<sup>2,6</sup> that the apparent contrast of any submerged object observed against a deep-water background is reduced exponentially as the object-to-observer distance ( $r$ ) is increased along any path of sight having uniform (homogeneous and isotropic) optical properties, as follows:

$$C_r = C_o e^{-(\mathcal{X} - K \cos \theta)r} \quad (1)$$

Here  $C_r$  and  $C_o$  are apparent contrast and inherent contrast respectively. The contrast attenuation coefficient is  $(\mathcal{X} - K \cos \theta)$ , where  $\theta$  is the zenith angle of the path of sight and the water clarity constants  $\mathcal{X}$  and  $K$  are, respectively, the volume attenuation coefficient<sup>\*</sup> and the diffuse attenuation coefficient.

The water clarity meter is designed to measure  $\mathcal{X}$  and  $K$ , and these coefficients can also be obtained by measuring the contrast attenuation coefficient  $(\mathcal{X} - K \cos \theta)$  for two or more paths of sight having different zenith angles  $\theta$ . Conversely, the apparent contrast of any object seen against a deep-water background can be measured

---

\* The constant  $\mathcal{X}$  is also sometimes referred to as the beam attenuation coefficient, since it specifies the attenuation of a beam of photons.

<sup>6</sup> Preisendorfer, R. W., "Model for Radiance Distribution in Natural Hydrosols," SIO Ref. 58-42, Visibility Laboratory, Univ. of Calif., La Jolla, Contract NObs-72092, 1 August 1959.

at any given object-to-observer distance or it can be calculated from values of  $\alpha$  and K from the water clarity meter. The field test data will be presented in the latter form in this report since apparent contrast (or, alternatively, the contrast reduction factor) is regarded as the datum of primary significance.

The measurements of apparent contrast, as well as the visual sighting-range measurements described in section 3 of this report, were made from a specially constructed barge having an underwater room with windows 30 inches below the surface of the water. This research barge, constructed in 1948 and depicted in references (1) and (2), was equipped in 1949 with an underwater track extending 28 feet in front of the window and supported at its outer end by a float. The track carries a small car on which targets of any kind can be mounted. This unique research facility has been used throughout the years for many contrast reduction studies and other researches in hydrologic optics.

The Diamond Island Field Station is a uniquely favorable site for experiments of this type owing to the optical uniformity of the water (i.e., the lack of vertical stratification), to the constancy of K and  $\alpha$ , to the convenient degree of water clarity, the lack of bottom influence on the light-field, and to several other favorable factors. The tests described in this report were performed at this location for a small fraction of the cost of carrying out the same work at sea.

Theory<sup>6,7</sup> and experiment<sup>9</sup> have demonstrated that the magnitude of the diffuse attenuation coefficient  $K$  depends upon the distribution of light within the water. During sunny weather the variation of  $K$  with depth near the surface may not be negligible. In order to minimize any variation of  $K$  with depth and to enable more perfect minimization of the effect of the presence of the barge on the underwater light field, all of the 1958 field tests were conducted under overcast skies or prior to sunrise. This choice of lighting condition was realistic inasmuch as the nomographic charts are for objects lying on the bottom where the lighting distribution often differs but little between sunny and cloudy conditions.

## 2.2 Experimental Details

The experimental equipment shown in Figure 1, consisted of an underwater room with windows 30 inches below the water surface. An optical bench track 28 feet long was mounted outside one of the windows.

- 
- <sup>6</sup> Preisendorfer, R. W., "Directly Observable Quantities for Light Fields in Natural Hydrosols," SIO Ref. 58-46, Visibility Laboratory, Univ. of Calif., La Jolla, Contract NObs-72092, July, 1958.
- <sup>7</sup> Preisendorfer, R. W., "Some Practical Consequences of the Asymptotic Radiance Hypothesis," SIO Ref. 58-60, Visibility Laboratory, Univ. of Calif., La Jolla, Contract NObs-72092, September, 1958.
- <sup>8</sup> Tyler, J. E., Richardson, W. H., and Holmes, R. W., "The Optical Properties of Lake Pend Oreille," SIO Ref. 58-80, Visibility Laboratory, Univ. of Calif., La Jolla, 3 December 1958, Contract NObs-72092.



The outboard end of the track could be adjusted in depth to obtain angles up to  $45^\circ$  from the horizontal. A small cart on the track carried the target and could be manually adjusted to any desired path length by means of rope A and the counterweight. The target itself was over-weighted on the outboard side of its hinge pin and could be raised by rope B or allowed to fall back in a matter of seconds. In order to reduce the perturbation of the light field, created by the presence of the underwater room and floats, the side C of the room facing the optical bench was camouflaged with canvas painted to reflect a luminance equal to equilibrium luminance in the horizontal direction. In addition to this, a six-foot air path was provided by the air tube to insure that the target-to-barge distance would be large for small path lengths  $r$ . The water between the air tube and the window was shielded from light by means of a black cloth. The target was a metal disc covered with black Norzon cloth which had previously been soaked to remove any excess water-soluble dye. When this target was in contact with the air tube window, the telephotometer reading was less than  $10^{-4}$  of the maximum reading of background luminance.

For inclined paths of sight an auxiliary window was mounted inside the room. Its angle corresponded to the angle of observation. This auxiliary window provided an air-glass-water interface that was perpendicular to the line of sight.

Measurements of apparent target luminance  $B_r$  and background luminance  $B$  were made with a reflex telephotometer employing a 931A multiplier phototube corrected for photopic response, a log-chassis

## APPENDIX C

and a Brown recording potentiometer. Calibration of the telephotometer system was done on a special photometer bench using the inverse square law to achieve a  $10^5$  range in light level. Three complete calibrations were run for the measurements reported here, one just before the telephotometer measurements began, one on completion of the horizontal path data and one on completion of the inclined path data. The known instrument error revealed by these calibrations has been converted to variability in  $1 - B_r/B$  and is shown graphically in Figures 2 and 3 (dotted lines). As  $B_r/B$  approaches 1 the precision of the "black-target" experiment becomes increasingly poor.

The angular field of view of the telephotometer was  $1.05^\circ$  (full cone angle). The target slightly more than filled this field at the maximum path lengths.

A flat-plate irradiance collector (shown in Figure 1) was used to obtain experimental values of the diffuse absorption coefficient  $K$  and an hydrophotometer (not shown) was used to measure the volume attenuation coefficient  $\kappa$  in the vicinity of the target. All the measurements were made using a bandwidth corresponding to that of the C.I.E. luminosity curve.

Data were taken during periods of relative calm and also when the sun was obscured by clouds or horizon. Since the ratio of apparent luminance to background luminance is independent of the level of illumination, data could be taken under variable lighting conditions by operating the target rapidly.

### 2.3 Horizontal Paths of Sight.

For horizontal paths of sight, ( $A = 90^\circ$ ) and black targets ( $B_0 = 0$ ) Equation 1 predicts that the apparent contrast  $C_r$ , will be exponentially attenuated at a rate determined by  $\alpha$  alone, see Equation 2 :

$$1 - \frac{B_r}{B} = e^{-\alpha r} = -C_r \quad (2)$$

It can be seen from Equation 2 that when  $r = 0$ ,  $(1 - B_r/B)$  must equal 1 and that the slope of the plot of  $(1 - B_r/B)$  vs  $r$  on semi-log paper (Figure 2) should be  $-\alpha$ , the volume attenuation coefficient.

The points in the semi-log graph of Figure 2 are values of  $(1 - B_r/B)$  computed from telephotometer data. The slight but systematic departure of the points from linearity is introduced by perturbation of the light field, that is, shadowing of the path near the air tube which results in values of  $B_r$  that are disproportionately low compared with  $B$ . The straight line of Figure 2 is not drawn through the points but has a slope equal to the numerical value of  $\alpha = .490/\text{meter}$  as measured with the hydrophotometer.

It can be seen from Figure 2 that except for residual perturbation, the contrast reduction is valid for submerged

horizontal paths and the value of  $\alpha$  obtained with our hydro-photometer can be used to predict apparent contrast along such paths.

#### 2.4 Inclined Paths of Sight.

For inclined paths of sight Equation 1 may be written

$$1 - \frac{B_r}{B} = e^{-(\alpha - K \cos \theta) r} \quad (3)$$

Equation 3 predicts that for black targets seen along inclined paths of sight the apparent contrast will be exponentially attenuated at a rate determined by the expression  $(\alpha - K \cos \theta)$ . As before, when  $r = 0$ ,  $(1 - B_r/B)$  must be 1.

The points of Figure 3 are computed from telephotometer data taken before sunrise and during a day of sometimes broken overcast, with the track angle  $\theta$  set at  $121.2^\circ$ . Evidence of perturbation of the light field is now missing owing partly to deeper operation and partly to the angle of the track. As before, the straight line is not drawn through the points but has the numerical value of  $(\alpha - K \cos \theta)$  computed from hydrophotometer determinations of  $\alpha$  and flat-plate determinations of  $K$ . In this case the average value of  $\alpha$  from 14 determinations was .585/m, the average value of  $K$  from 14 determinations was .350/m.

It can be seen from Figure 3 that the apparent contrast of the target was predicted correctly by means of the contrast reduction equation (1) and values of the water clarity constants and  $K$  obtained from independent instrumental measurements.

### 3. MEASUREMENTS OF SIGHTING RANGE

#### 3.1 Introduction

Sighting ranges for a small black target were determined by a young, well-trained observer concurrently with the measurements of apparent contrast and the water clarity constants. The observer removed the telephotometer at the underwater window of the research barge (see Figure 1) and viewed the target through the air-tube. In this way the perturbation of the light-field was precisely the same low value attained in the case of the apparent contrast measurements. The target was a small, black, conical cavity 0.311 inches in diameter at the open end, facing the observer; it was mounted to the movable cart by means of a transparent Lucite bracket. The observer was unable to see the cart at any time because of the limited field of view afforded by the air-tube so that, near threshold, the target appeared as a small black disc in an otherwise unstructured field.

#### 3.2 Experimental Procedure

The luminance of the underwater light field was measured at frequent intervals throughout the experiment by means of a carefully calibrated Macbeth illuminometer equipped with a telescopic attachment

which limited its field of view to a small portion of the air-tube window. A Wratten No. 40 filter was found to provide an excellent color match of the 2360° K Macbeth comparison field with the greenish light coming from the water; the transmission of this filter for light of 2360° K color temperature was calculated from spectrophotometric data in the usual manner. Additional monitoring of the luminance level was provided by placing the photoelectric telephotometer at another underwater window in order to produce a strip-chart record of the underwater luminance it observed throughout the period of observations. Analysis of these records showed that the coefficient of variance (s/m) of the underwater luminance did not exceed 0.17 during either of the series of observations reported. This was, of course, a measure of the stability of the overcast under which the experiments were performed.

The observer (male, age 21) had more than a year of experience in laboratory visual threshold measurements. His thresholds were well stabilized and closely duplicated those of the Tiffany data within the range of adaptation levels and angular target subtenses involved in the field test. Before departing for the field station the observer underwent extensive practice on a simulation of the planned experiment, and at the field station he practiced freely with the actual underwater viewing task until it was familiar to him. Because of this practice there is reason to believe that learning effects had vanished before the sighting range data were taken, and that the observer's responses were stable in the field environment.

The observations were made by the method of adjustment, the observer moving the target along the track by means of a pull cord. At the outset of the experiment the car was at the outer end of the track, far beyond the point at which the target disappeared. The observer was careful to use no fixed over-run, so that he had no mechanical or kinesthetic position cues. He then moved the target toward himself until he detected its presence and an assistant recorded the target position as indicated by a steel tape attached to the car.

The observer then moved the target close to the air-tube window and permitted it to recede slowly by allowing the pull cord to slip through his fingers. When the target disappeared he stopped the cart and an "out" distance was measured. This process was repeated ten or more times, depending upon the stability of the overcast. Great care was taken to accept data only when the water was so completely calm that there was no relative motion of the target with respect to the barge. This additional stringent requirement reduced the number of occasions when data could be taken to two. In both cases the path of sight was  $30.8^\circ$  downward from horizontal, i.e., zenith angle  $\theta = 120.8^\circ$ .

### 3.3 Sighting Range Data

Sighting range data were obtained on 13 August and 17 August; these were the only two occasions during the expedition when observing conditions fulfilled all requirements and contrast reduction data were available.

Figures 4 and 5 display these data graphically in combination with apparent contrast values calculated from water clarity constants measured by means of the water clarity meter. In each figure the plotted points show the average "out" distance, the average "in" distance, and the mean of both "out" and "in" distances. The curve connecting these points shows apparent contrast as a function of target distance expressed in terms of visual angle.

### 3.4 Calibration of the Observer

After the observer had returned to the laboratory his contrast thresholds were measured for the same type of visual task which he had encountered in the field. An accurate simulator was constructed in which a circular target was presented by projection on an unstructured, uniformly bright screen which could be moved throughout the same range of distances encountered in the field experiment, due allowance having been made for refractive effects at the underwater windows. The field-of-view restriction imposed by the six-foot air-tube was duplicated. The luminance levels in the simulator duplicated those which prevailed during the field experiment, and thresholds were measured by varying the target distance in a realistic manner. The method of adjustment was used, as in the field experiment, and the means of "in" and "out" distances are given in Table 1. These data differ from classical (e.g., Tiffany) thresholds primarily because of adaptive and accommodative effects due to the presence of the air-tube. These visual effects and their implications are to be discussed in more detail in a separate report.



Table I  
Laboratory Visual Thresholds

Adaptation Luminance (ft-L)	Target Contrast	Threshold Target Size (min)
4.09	.0206	6.22
4.09	.0295	4.99
8.05	.0198	5.60
8.05	.0291	4.85
8.05	.0360	4.53

### 3.5 Comparison of Observed and Predicted Sighting Ranges

The dotted curves on Figures 4 and 5 have been drawn through the threshold points listed in Table 1 and indicated by crosses.

At the intersection of the solid and dotted curves the apparent contrast of the target equals the contrast threshold for the observer, and the target would, therefore, be predicted to be just visible at this visual angle (target distance.) It will be noted from Figure 4 that the predicted sighting range is 15.2 feet whereas the mean of the observed sighting ranges was 15.6 feet. In Figure 5 the predicted and observed sighting ranges are in precise agreement.

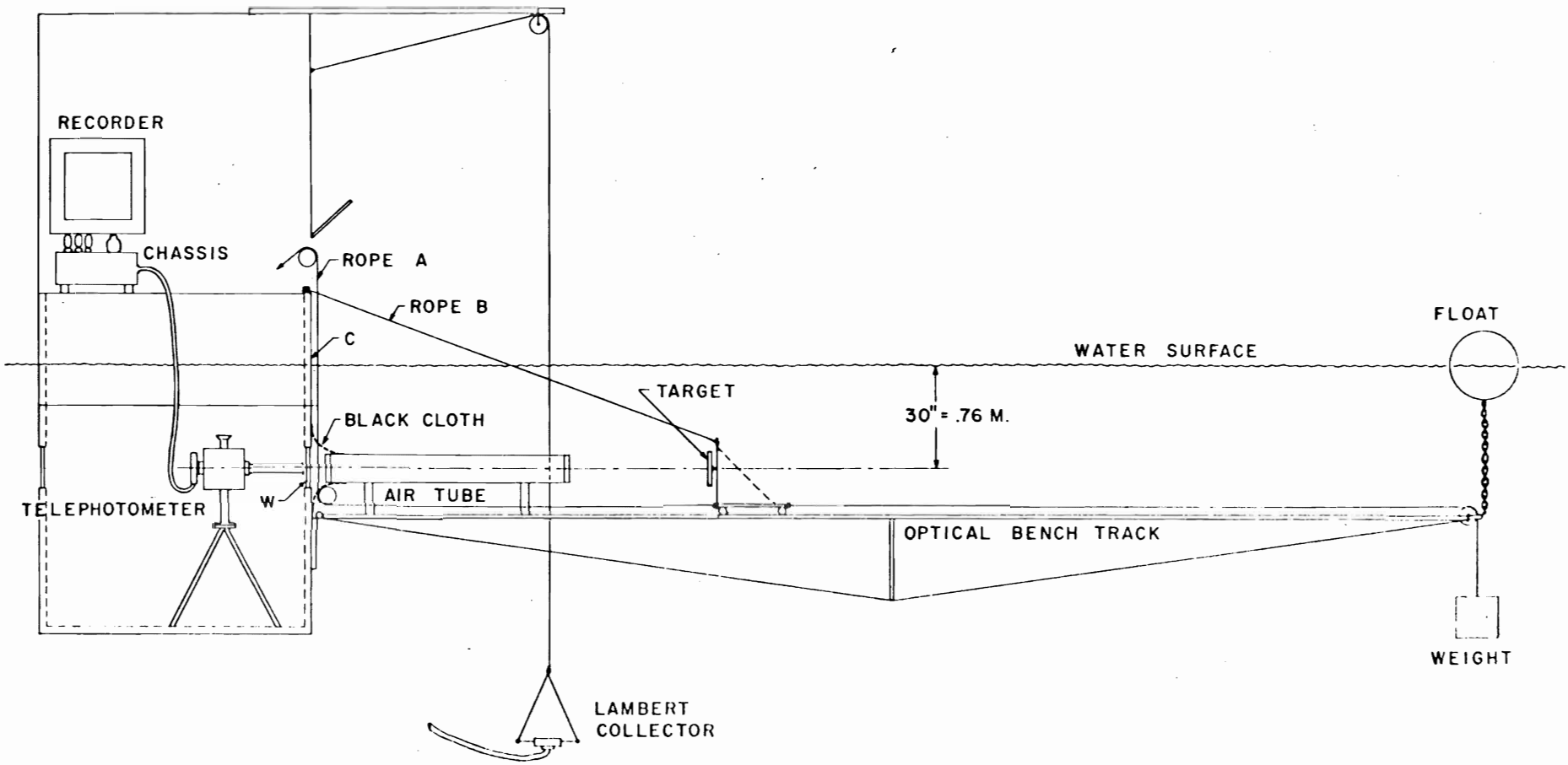
### 3.6 Conclusions

The agreement between the predicted and observed sighting ranges exhibited by the data in figures 4 and 5 constitutes evidence of the validity of the basic method for predicting underwater sighting

ranges from water clarity meter data, the contrast reduction equation, and visual contrast thresholds. Since the nomographic charts for predicting visibility by swimmers are an embodiment of this method, the results of the field test provide a careful spot-check of the validity of the clarity meter-and-nomograph system.

The field test provides experimental evidence that:

- (1) the new water clarity meter provides values of the water clarity constants,  $\alpha$  and  $K$ , which are valid for predicting the apparent contrast of underwater objects by means of equation (1), and
- (2) the sighting ranges predicted by the nomographic charts are valid when based upon values of  $\alpha$  and  $K$  from the new water clarity meter.



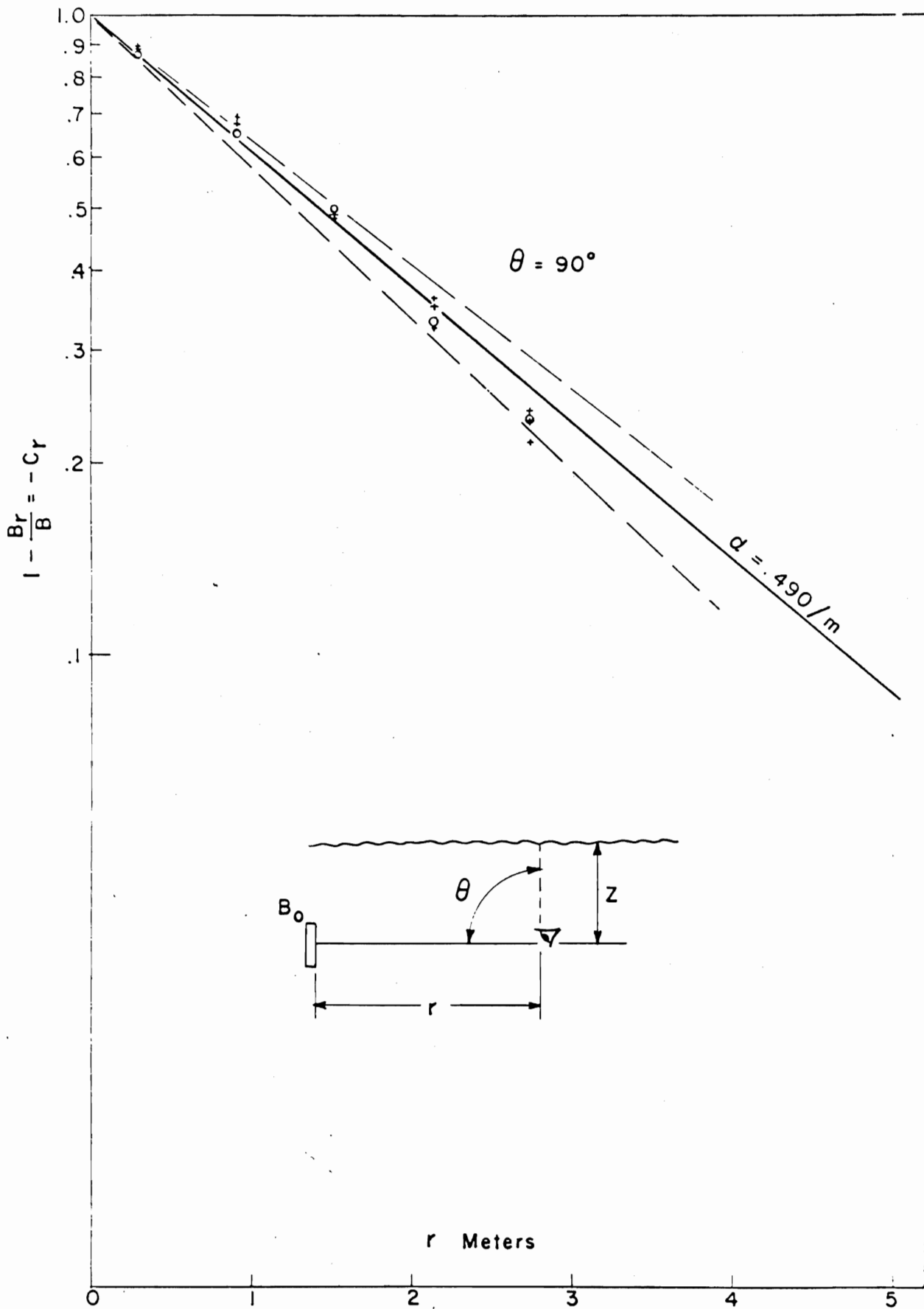


FIG 2

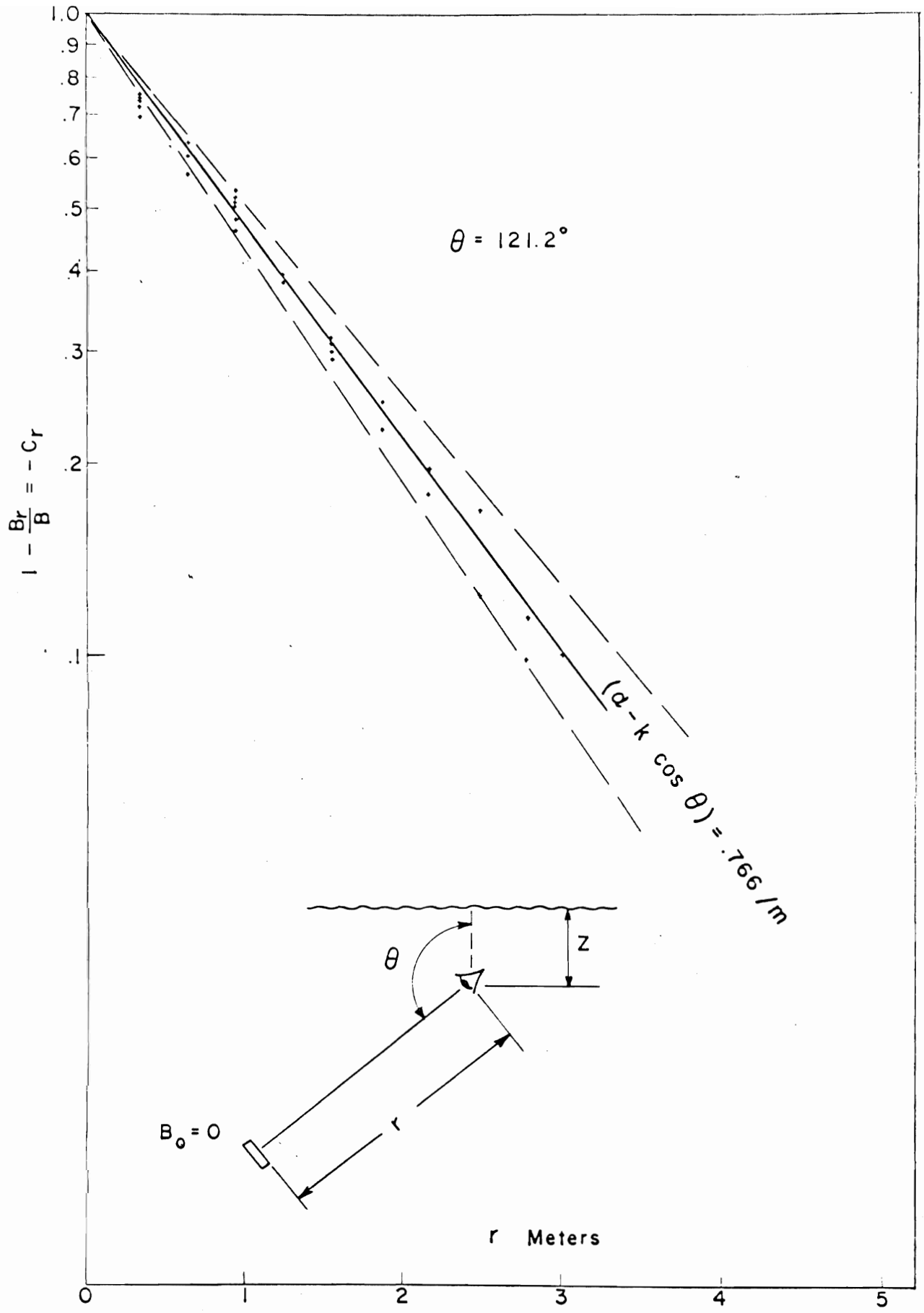
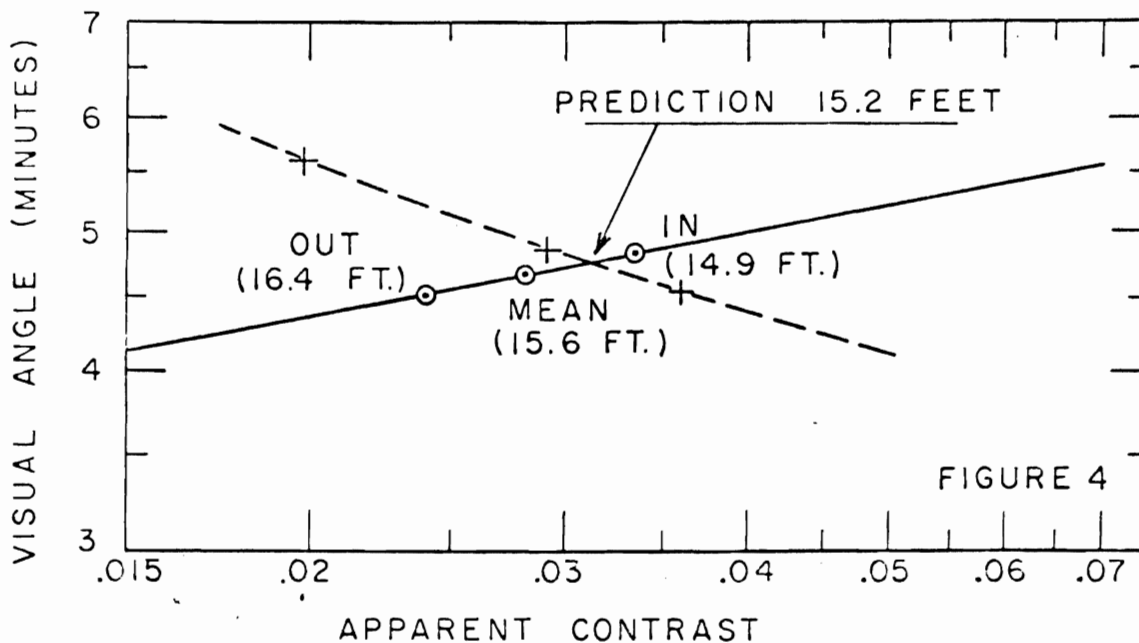


FIG. 3

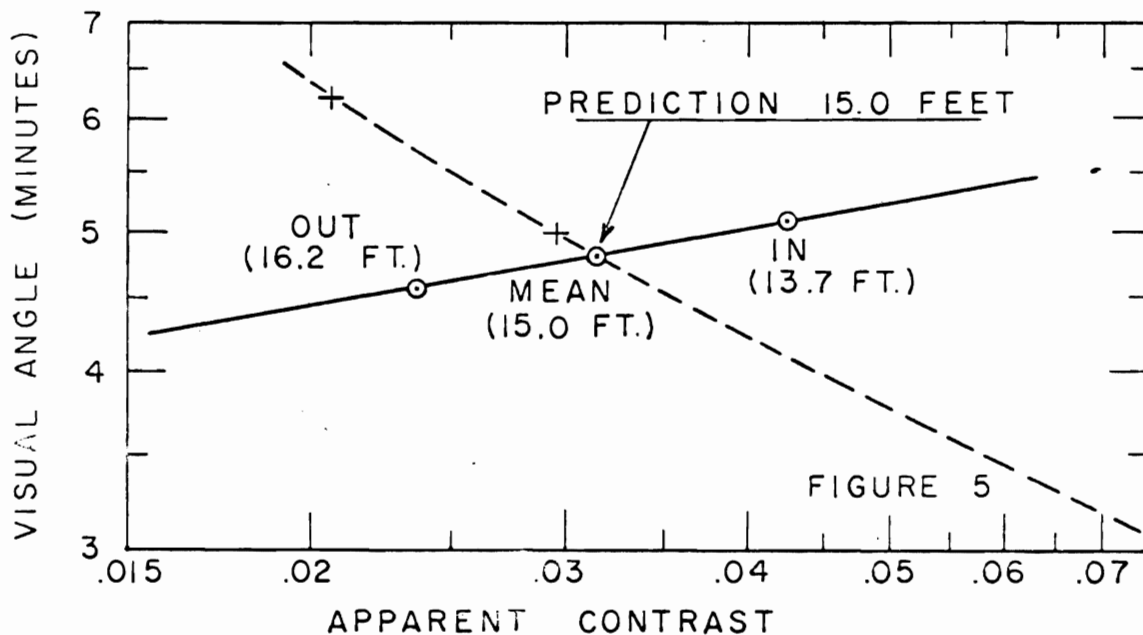
13 AUGUST 1958  
BACKGROUND LUMINANCE  
8 FOOT LAMBERTS

TARGET DIAMETER 0.311 IN.  
PATH DEPRESSION 30.8°



17 AUGUST 1958  
BACKGROUND LUMINANCE  
4 FOOT LAMBERTS

TARGET DIAMETER 0.311 IN.  
PATH DEPRESSION 30.8°



## Reduction of Contrast by Atmospheric Boil\*†

SEIBERT Q. DUNTLEY, WILLIAM H. CULVER,‡ FRANCES RICHEY,§ AND  
RUDOLPH W. PREISENDORFER

*Scripps Institution of Oceanography, University of California, La Jolla, California*

(Received 26 May 1958)

It is shown that the probability of receiving light from an object viewed through a turbulent atmosphere follows a normal Gaussian distribution. Furthermore the root-mean-square angular deflection of the points of any object will be proportional to the square root of the object-to-observer distance. From relations of the type described in the examples it is possible to predict the apparent contrast throughout a given scene, provided the inherent contrast distribution, the optical air state, and the range of the target are known. The optical air state for a given condition of atmosphere can be measured by using a telephotometer and a series of long thin black bars of varying widths.

### INTRODUCTION

ONE of several factors determining the form of the image of a distant object is the time-varying distortion caused by inhomogeneities in the refractive index of the atmosphere. As is well known, the shimmer of distant objects is caused by spatial and temporal variations in the index of refraction of rising columns of hot air, with the resulting disturbance of the propagated electromagnetic radiation. This disturbance causes time-varying distortion of the image and loss of fine detail.

This phenomenon is of particular interest to the geodesist, because it limits the precision with which a telescope can be pointed at a distant object,<sup>1</sup> and to the astronomer, because it blurs the images of the stars and limits his resolving power.

Experiments on time-varying characteristics of optical transmission through an inhomogeneous atmosphere have been made by Riggs, Mueller, Graham, and Mote,<sup>2</sup> who found that for a horizontal path length of several hundred meters the average apparent instantaneous displacement of a point on a target was greater than 3 sec of arc with a maximum displacement of 9 sec. The instantaneous displacements of points separated by more than 5 min of arc were uncorrelated.

Some of the time-varying characteristics of the shimmer effect are slow enough to be discernable to the eye, but much of the effect is so rapid that only time-averaged values of the radiance of the image are important for visual observation.

The analytic treatment of the propagation of electromagnetic waves through inhomogeneous media has been

considered by a large number of investigators. The rigorous solution of the problem by perturbation methods in terms of the statistical parameters of the inhomogeneities yields results in very untractable forms, especially for one interested in the transmission of optical images. Results derived from approximate models have been useful for specific problems. The use of the approximation of geometric optics yields results in a form that is most easily used in problems of optical-image transmission, particularly for the consideration of the time-averaged image.

The validity of the geometrical optics approximation of a particular case can be ascertained by the value of the quantity  $a^2/\lambda r$ , where  $a$  is a representative size of a turbulent element,  $\lambda$  is the wavelength of light, and  $r$  is the distance from the turbulence to the observer. If  $a^2/\lambda r \gg 1$  the geometrical optics approximation is valid.<sup>3</sup>

For a slit of width  $a$  the size of the diffraction pattern is equal to the geometric image of the slit when  $a^2/\lambda r = 1$ . Thus the criterion above is seen to be plausible.

The problem of transmission through an inhomogeneous medium has been treated by (using the geometrical optics approximation) Bergmann<sup>4</sup> and Chandrasekhar.<sup>5</sup> The results of this paper are consistent with some of those of Chandrasekhar but are derived from less restrictive assumptions.<sup>6</sup>

For an investigator interested in image transmission

\* This paper was prepared under a contract between the University of California and the Bureau of Ships, U. S. Navy. Contribution from The Scripps Institution of Oceanography, University of California, New Series.

† Presented in part before the Thirty-Seventh Annual Meeting of the Optical Society of America, October 1952, and abstracted in *J. Opt. Soc. Am.* **42**, 877A (1952).

‡ Present address: Institute for Defense Analysis, Washington, D.C.

§ Present address: E. H. Plesset Associates, Inc., Los Angeles, California.

<sup>1</sup> F. E. Washer, and H. B. Williams, *J. Opt. Soc. Am.* **36**, 400 (1946).

<sup>2</sup> L. A. Riggs, C. G. Mueller, C. H. Graham, and F. Mote, *J. Opt. Soc. Am.* **37**, 415 (1947).

<sup>3</sup> H. G. Booker, and W. E. Gordon, *J. Geophys. Res.* **55**, 241 (1950).

<sup>4</sup> P. G. Bergmann, *Phys. Rev.* **70**, 486 (1946).

<sup>5</sup> S. Chandrasekhar, *Monthly Notices Roy. Astron. Soc.* **112**, 475 (1952).

<sup>6</sup> The literature of astronomical and terrestrial seeing has virtually ignored the contrast-reducing effects of atmospheric boil. [See Coleman and Rosenberg, *J. Opt. Soc. Am.* **40**, 507 (1950).] Studies relating atmospheric stratification and transient physical phenomena (e.g., shadow bands) to transient image phenomena (e.g., scintillation) [see G. Keller, *Astron. J.* **58**, 113 (1953), and *J. Opt. Soc. Am.* **45**, 845 (1955), and *Astron. Nachr.* **283**, 85 (1956)] as well as the many experimental and theoretical investigations of the dancing, pulsation, and tremor disk of images do not pertain directly to the *time-averaged*, extended-medium case discussed in this paper. Slightly more related are the atmospheric transfer functions of Ramsay [J. V. Ramsay, *Optica Acta (Paris)* **6**, 344 (1959)] and Scott [R. M. Scott, *Phot. Soc. Eng.* **3**, 201 (1959)] or image measurements like those of Djurle and Bäck [E. Djurle and A. Bäck, *J. Opt. Soc. Am.* **51**, 1029 (1961)].

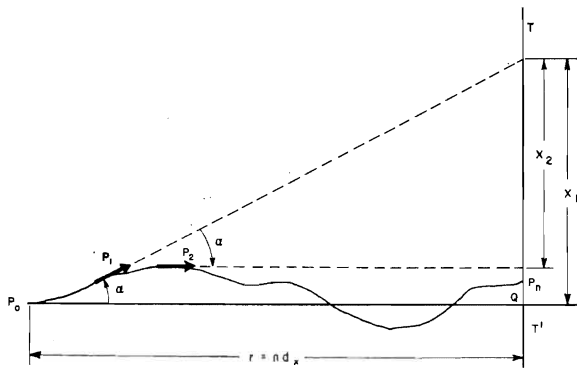


FIG. 1. Illustrating the geometry of the derivation of  $\Phi$ .

the distortion property of an inhomogeneous medium is usefully described in terms of the distortion of a point source. More precisely, let a given point in the object space be designated by the pair of direction components  $(\psi'_x, \psi'_y)$ , and let the point be assigned a unit isotropic radiance. The exact form of  $(\psi'_x, \psi'_y)$  will be given later. If the distortion action of the medium changes sufficiently rapidly over an interval of time, the successive images  $(\psi_x, \psi_y)$  of  $(\psi'_x, \psi'_y)$  appear essentially as a continuum of points (a blur) in the image space. For the purposes of this discussion, a function  $\Phi$  is defined which assigns to each object point  $(\psi'_x, \psi'_y)$  the time-averaged radiance  $\Phi(\psi_x - \psi'_x, \psi_y - \psi'_y)$  of the image point  $(\psi_x, \psi_y)$ . The time-averaged radiance distribution  $\bar{N}$  on the image space is then representable as a convolution of the function  $\Phi$  with the radiance distribution  $N$  on the object space

$$\bar{N}(\psi_x, \psi_y) = \int_{\Psi} N(\psi'_x, \psi'_y) \Phi(\psi_x - \psi'_x, \psi_y - \psi'_y) d\psi'_x d\psi'_y, \quad (1)$$

where  $\Psi$  is the object space, namely, the collection of all directions  $(\psi'_x, \psi'_y)$ . Since the location of the observer is held fixed throughout the entire discussion, the location symbol  $\mathbf{x}$  has been suppressed in the radiance function notation [ordinarily written  $N(\mathbf{x}, \psi_x, \psi_y)$ ].

In the following discussion attention is given to the statistics of the deviations undergone by a ray traversing a path between a point source and a screen some distance away. Because of an optical reciprocity law this derivation applies equally well to an extended field of view, from which light is received by a "point" receiver such as an eye or a lens.

#### METHOD OF APPROACH

A theoretical treatment for transmission through any inhomogeneous medium<sup>7</sup> has been evolved which is based on the following considerations: The path of sight is assumed to lie within a (spatially and tem-

<sup>7</sup> Including the oceans and other bodies of water, wherein refractive inhomogeneities may result from suspensoids, including transparent planktonic organisms in addition to any inhomogeneities of the water itself.

porally) uniformly turbulent medium made up of uncorrelated optically inhomogeneous regions with dimensions small compared to the distance through which the ray travels. Each light ray undergoes a large number of deflections. Only small-angle deflections need be considered. Using only these assumptions we may consider the following.

Figure 1 shows the path of a light ray emitted at  $P_0$  traversing a turbulent medium toward an arbitrarily oriented screen  $TT'$  a distance  $r$  from the source. The plane of the figure is perpendicular to  $TT'$  and passes through the path  $P_0Q$  of the undeviated ray. Two perpendicular axes—the  $x$  and  $y$  axes—lie in  $TT'$ . A segment  $TQT'$  of the  $x$  axis is shown. The  $y$  axis is normal to the plane of the figure and goes through  $Q$ . The ray now travels from  $P_0$  to a point  $P_1$  determined by the condition that the ray will have turned through an angle whose projection on the plane of the figure is of a small fixed magnitude  $\alpha$  (in radians). In accordance with our assumptions, the distance along the segment  $P_0P_1$  is large compared to the dimensions of the centers of turbulence. The projection (in the manner shown in the figure) of  $P_1$  falls on  $TT'$  a distance  $x_1$  away from  $Q$ . As the ray continues along its path from  $P_1$  it will undergo further deflections. When its direction has been changed through another angle whose projection in the plane of the figure is of the same magnitude  $\alpha$ ,  $P_2$  is projected on the screen, where it falls a distance  $x_2$  away from the projection of  $P_1$ .

In the same way the remainder of the path of the ray is divided up into segments representing equal angles of deviation  $\alpha$ , and the projection of each endpoint  $P_i$  is mapped onto the screen  $TT'$ . Finally  $x_n$  will be the  $x$  distance on  $TT'$  of the projection of  $P_n$  from the projection of  $P_{n-1}$  where  $P_{n-1}P_n$  is the last such path segment traversed by the ray before it strikes the screen. No generality is lost if  $P_n$  is taken to lie on  $TT'$ . Since the distance over  $P_iP_{i+1}$  is large compared to the dimensions of the centers of turbulence, it follows that the curvature of the ray between  $P_i$  and  $P_{i+1}$  is uncorrelated with its curvature during its past or future history so that the directions of projected path segments are uncorrelated.

The magnitude of  $x_i$  can be found in the following way from the small angle assumption. If  $D_i$  is the distance from  $P_i$  to  $TT'$ , then  $x_i = D_i \alpha$ . For a large number  $n$  of deflections, the value of  $D_i$  will approach an average value given by  $(n-i) d_x$ , where  $d_x$  is the average distance between  $P_i$  and  $P_{i+1}$ . Then  $x_i = (n-i) \alpha d_x$ . The algebraic sign associated with any particular  $x_i$  has equal probability of being  $+$  or  $-$ . It can then be seen that the distance from the point  $Q$  to the point  $P_n$  can be found by summation over all the  $x_i$ 's with the appropriate signs.

Because the  $x_i$ 's are uncorrelated, they can be considered to be the steps in a one-dimensional *random walk*: Let  $x_n$ , the last of the  $x_i$ 's, be the (signed) length



of the first step in the random walk,  $x_{n-1}$  the length of the second and so on. Therefore the absolute magnitude of the  $j$ th step will be  $j\alpha d_x, j=1, \dots, n$ . The size of the steps in this one-dimensional random walk thus increase linearly with each step.

DETAILS OF THE DERIVATION

The probability distribution for a one-dimensional random walk can be calculated in the following way. The mean-square deviation  $\sigma^2(n)$  of the distribution for a walk of  $n$  steps is equal to the sum of the mean-square deviations for each step

$$\sigma^2(n) = \sum_{j=1}^n \sigma_j^2,$$

where

$$\sigma_j = j\alpha d_x$$

is the (signed) length of the  $j$ th step. Therefore,

$$\sigma^2(n) = \sum_{j=1}^n j^2 \alpha^2 d_x^2 = \alpha^2 d_x^2 \left[ \frac{n(n+1)(2n+1)}{6} \right].$$

For large  $n$  the expression in brackets approaches  $\frac{1}{3}n^3$ . Therefore,

$$\sigma^2(n) = \frac{1}{3} \alpha^2 d_x^2 n^3.$$

From a special central-limit theorem due to Liapounoff,<sup>8</sup> it can be shown that the angular probability distribution approaches a normal distribution whose mean is the position on the screen reached by the undeviated ray. Liapounoff's theorem states the following: let  $x_1, x_2, x_3, \dots$ , be independent random variables, and denote  $n_j$  and  $\sigma_j$  as the mean and standard deviation of  $x_j$ . Suppose that the third absolute moment of  $x_j$  about its mean

$$\rho_j^3 = \text{Expectation} (|x_j - m_j|^3)$$

is finite for every  $j$  and define  $\rho^3$  as

$$\rho^3 = \sum_{j=1}^n \rho_j^3.$$

Then if the condition  $\lim_{n \rightarrow \infty} [\rho(n)/\sigma(n)] = 0$  is satisfied, the result is that the sum

$$x = \sum_{j=1}^n x_j$$

is asymptotically normal.

This can be applied to the case of the above random walk in the following way:

$$\rho^3(n) = \alpha^3 d_x^3 \sum_{j=1}^n j^3 = \alpha^3 d_x^3 \left[ \frac{1}{4} n^2 (n+1)^2 \right].$$

<sup>8</sup>H. Cramer, *Mathematical Methods of Statistics* (Princeton University Press, Princeton, New Jersey, 1946), pp. 215-216.

For large  $n$

$$\rho^3(n) = \frac{1}{4} \alpha^3 d_x^3 n^4,$$

and

$$\lim_{n \rightarrow \infty} \left[ \frac{\rho(n)}{\sigma(n)} \right] = \lim_{n \rightarrow \infty} \frac{n^{4/3}}{n^{3/2}} = \lim_{n \rightarrow \infty} n^{-1/6} = 0,$$

and thus the hypothesis of Liapounoff's theorem is satisfied.

Hence it is shown that a continuum of rays starting with a given initial direction and which traverse a medium whose optical properties are uniformly turbulent will give rise to a continuum of terminal points on the target plane such that the density of the points projected onto the  $x$  axis follows a normal distribution.

Since

$$r = n d_x,$$

we may write, alternatively,

$$\sigma_x^2(r) = \alpha^2 r^3 / 3 d_x, \text{ for fixed } \alpha.$$

Thus the spread of the Gaussian probability distribution increases as the 3/2 power of  $r$ . We now introduce the angular variable  $\psi_x \equiv x/r$ . In terms of  $\psi_x$ , the spread of the probability distribution  $P_r(\psi_x)$  is proportional to  $r^{1/2}$ . The normalized Gaussian probability distribution with root-mean-square deviation given by

$$\sigma_x(r) = +(\alpha^2 r / 3 d_x)^{1/2}$$

is

$$P_r(\psi_x) = \frac{1}{(2\pi)^{1/2} \sigma_x(r)} \exp \left\{ -\frac{1}{2} \left[ \frac{\psi_x}{\sigma_x(r)} \right]^2 \right\}.$$

The above derivation may be extended to the two-dimensional case. The new derivation is similar in all details to the former. In particular the same angle  $\alpha$  is used. However, the projections of all ray segments are now onto the  $y$  axis in the plane  $TT'$ , and in general a new average distance  $d_y$  must be introduced. The result is

$$P_r(\psi_y) = \frac{1}{(2\pi)^{1/2} \sigma_y(r)} \exp \left\{ -\frac{1}{2} \left[ \frac{\psi_y}{\sigma_y(r)} \right]^2 \right\},$$

$$\psi_y \equiv \frac{y}{r}, \quad \sigma_y(r) = \left( \frac{\alpha^2 r}{3 d_y} \right)^{1/2}.$$

In general the two-dimensional probability distribution is of the form

$$\begin{aligned} \mathcal{P}_r(\psi_x, \psi_y) &= \\ &= \frac{1}{2\pi \sigma_x(r) \sigma_y(r) (1 - \rho^2)} \\ &\times \exp \left( \frac{-1}{2(1 - \rho^2)} \left\{ \left[ \frac{\psi_x}{\sigma_x(r)} \right]^2 - \frac{2\rho \psi_x \psi_y}{\sigma_x(r) \sigma_y(r)} + \left[ \frac{\psi_y}{\sigma_y(r)} \right]^2 \right\} \right), \end{aligned}$$

where  $\rho$  is the correlation coefficient between  $P_r(\psi_x)$  and  $P_r(\psi_y)$ . Along a horizontal path of sight the vertical displacement of a point would be expected to be uncorrelated with the horizontal displacement. In this case

$$\mathcal{P}_r(\psi_x, \psi_y) = \frac{1}{2\pi\sigma_x(r)\sigma_y(r)} \times \exp\left(-\frac{1}{2}\left[\left(\frac{\psi_x}{\sigma_x(r)}\right)^2 + \left(\frac{\psi_y}{\sigma_y(r)}\right)^2\right]\right).$$

If the turbulence is isotropic, i.e., if  $d_x = d_y = d$ , then

$$\sigma_x(r) = \sigma_y(r) = (\alpha^2 r / 3d)^{1/2} = \sigma(r).$$

If we set  $\psi^2 = \psi_x^2 + \psi_y^2$ , then under these assumptions ( $\rho = 0$ ,  $d_x = d_y$ ) we have

$$\mathcal{P}_r(\psi_x, \psi_y) = [1/2\pi\sigma^2(r)] \exp\{-\frac{1}{2}[\psi/\sigma(r)]^2\}.$$

The foregoing formulas give the probability that the terminal point  $P_n$  on  $TT'$  of a light ray aimed along  $P_0Q$  lies in the direction  $(\psi_x, \psi_y)$  as seen from  $P_0$ . By tracing the light ray in the opposite direction, these formulas admit the following interpretation: they give the probability that the image of the point  $(\psi_x, \psi_y)$  on  $TT'$  is at the origin  $(0,0)$  of  $TT'$ . For fixed  $r, \mathcal{P}_r$  is thus the required function defined in (1).

#### OPTICAL AIR STATE

The lower limit on the size of  $\alpha$  is determined by the condition that the direction of successive steps be uncorrelated. This condition will be fulfilled if (as assumed above) the average distances  $d_x$  and  $d_y$  between successive  $P_i$ 's is large compared to the dimensions of the inhomogeneities of the medium. It follows that the quantities  $A_x = (\alpha^2/3d_x)$  and  $A_y = (\alpha^2/3d_y)$  are properties only of the medium and not of the target. The pair of numbers  $(A_x, A_y)$  is called the *optical air state* of the medium and gives a useful measure of the optical turbulence of the atmosphere. If the turbulence is isotropic, the *optical air state* is a single number  $A = A_x = A_y$ . In most applications the turbulence is essentially isotropic. The assumptions  $\rho = 0$ ,  $A_x = A_y$  will be in force for the remainder of the paper. As a consequence we may write

$$P_r(\psi_x) = [1/(2\pi Ar)^{1/2}] \exp[-(\psi_x^2/2Ar)],$$

$$P_r(\psi_y) = [1/(2\pi Ar)^{1/2}] \exp[-(\psi_y^2/2Ar)],$$

and

$$\mathcal{P}_r(\psi_x, \psi_y) = P_r(\psi_x)P_r(\psi_y) = \frac{1}{2\pi Ar} \exp\left(-\frac{\psi^2}{2Ar}\right), \quad (2)$$

where

$$-\infty < \psi_x < +\infty, \quad -\infty < \psi_y < +\infty, \quad \psi^2 = \psi_x^2 + \psi_y^2.$$

#### TIME-AVERAGED APPARENT RADIANCE

Actual computations of the time-averaged apparent radiance distribution  $\bar{N}_r$  can now be carried out by means of formula (1) in which the explicit expression (2) for the function  $\mathcal{P}$  is used. A particularly useful formula for  $\bar{N}_r$  arises in the following special but important context: let a target occupy a subregion  $\Psi_t$  of object space  $\Psi = \{(\psi_x', \psi_y') : -\infty < \psi_x' < \infty, -\infty < \psi_y' < \infty\}$ ; let the apparent radiance distribution  $N_r$  over  $\Psi_t$  be uniform and of magnitude  ${}_tN_r$ . Let the remaining portion  $\Psi_b$  of the object space (the background of the target) have uniform apparent radiance of magnitude  ${}_bN_r > 0$ . Then, from (1)

$$\begin{aligned} \bar{N}_r &= \int_{\Psi} N_r \mathcal{P}_r \\ &= \int_{\Psi_t} N_r \mathcal{P}_r + \int_{\Psi_b} N_r \mathcal{P}_r + \int_{\Psi_t} {}_bN_r \mathcal{P}_r - \int_{\Psi_t} {}_bN_r \mathcal{P}_r \\ &= ({}_tN_r - {}_bN_r) \int_{\Psi_t} \mathcal{P}_r + {}_bN_r. \end{aligned}$$

This result, in more detail, states that

$$\begin{aligned} \bar{N}_r(\psi_x, \psi_y) \\ &= ({}_tN_r - {}_bN_r) \int_{\Psi_t} \mathcal{P}_r(\psi_x - \psi_x', \psi_y - \psi_y') d\psi_x' d\psi_y' + {}_bN_r \end{aligned} \quad (3)$$

for all  $(\psi_x, \psi_y)$  in  $\Psi$ .

A perusal of the derivation of  $\mathcal{P}_r$  would show that (3) (and in fact any formula making use of the derived  $\mathcal{P}_r$ ) is strictly applicable only to those regions  $\Psi_t$  of  $\Psi$  which are angularly small. It is precisely this kind of target, however, which is of primary concern in contrast-reduction problems involving atmospheric boil. These targets have their time-averaged radiance greatly influenced by their background radiance. On the other hand, the time-averaged background radiance of such targets is virtually unaffected by the target's radiance.

#### TIME-AVERAGED APPARENT CONTRAST

The introduction of the notion of contrast greatly facilitates the solution of visibility problems. Let  $(\psi_x, \psi_y)$  and  $(\psi_x', \psi_y')$  be any two points in either image or object space. The *contrast*  $C(\psi_x, \psi_y)$  of  $(\psi_x, \psi_y)$  with respect to  $(\psi_x', \psi_y')$  is defined as

$$C(\psi_x, \psi_y) = [N(\psi_x, \psi_y) - N(\psi_x', \psi_y')]/N(\psi_x', \psi_y'),$$

where  $N$  is a given radiance distribution,  $N(\psi_x', \psi_y') > 0$ . As an example consider the apparent radiance distribution  $N_r$  defined in the preceding section. Let  $(\psi_x', \psi_y')$  be an arbitrary fixed point in  $\Psi_b$ . Then the apparent con-

trast function  $C_r$  on  $\Psi$  has the following form:

$$C_r(\psi_x, \psi_y) = \begin{cases} C_r & \text{for } (\psi_x, \psi_y) \text{ in } \Psi_t, \\ 0 & \text{for } (\psi_x, \psi_y) \text{ in } \Psi_b. \end{cases} \quad C_r \equiv (iN_r - bN_r) / bN_r,$$

In this context we can say that the target  $\Psi_t$  has a contrast  $C_r$  with respect to its background  $\Psi_b$ . In accordance with the general definition of contrast, the time-averaged apparent contrast function  $\bar{C}_r$  necessarily has the form

$$\bar{C}_r(\psi_x, \psi_y) = [\bar{N}_r(\psi_x, \psi_y) - \bar{N}_r(\psi_x', \psi_y')] / \bar{N}_r(\psi_x', \psi_y').$$

Now let  $(\psi_x', \psi_y')$  be an arbitrary fixed point in  $\Psi_b$ . In view of the comments of the preceding section, we may for all important cases write  $\bar{C}_r(\psi_x, \psi_y)$  as

$$\bar{C}_r(\psi_x, \psi_y) = [\bar{N}_r(\psi_x, \psi_y) - bN_r] / bN_r, \quad (4)$$

where  $(\psi_x, \psi_y)$  is any point in  $\Psi$ . By adopting this convention, (3) yields the following approximate but highly useful contrast formula

$$\bar{C}_r(\psi_x, \psi_y) = C_r \int_{\Psi_t} \mathcal{P}_r(\psi_x - \psi_x', \psi_y - \psi_y') d\psi_x' d\psi_y'. \quad (5)$$

From this we immediately deduce the general facts that

$$|\bar{C}_r(\psi_x, \psi_y)| \leq |C_r| \quad \text{for all } (\psi_x, \psi_y) \text{ in } \Psi,$$

and the handy rule of thumb for very small targets of area  $\mathcal{A}$  and arbitrary shape

$$\bar{C}_r = C_r (\mathcal{A} / 2\pi Ar^3). \quad (6)$$

This points up among other things an inverse-cube decay of  $\bar{C}_r$  with range  $r$ . This relation may be used to explain in simple terms the loss of fine detail on targets as the observer-target distance is increased. For by subdividing the given target into sufficiently small elements each of area  $\mathcal{A}$ , (6) will describe the time-averaged contrast of the element against its background consisting of the remainder of the target area. Now while the flux from the element falls off at a rate proportional to  $r^{-2}$ , the contrast (and hence the detectability) of the element falls off at a rate proportional to  $r^{-3}$ . In short, fine detail on a receding target is lost at a greater rate than the flux from the entire target. As a consequence, the detail on a target is lost from view sooner than the target itself. Despite the concession to complexity made in (4), the resulting formula (5) faithfully reproduces the main features of the time-averaging affect of atmospheric boil phenomena, as the following examples illustrate.

**EXAMPLES**

**A. Long Straight Edge**

Consider an infinitely long straight boundary between two regions of object space each with a distinct uniform apparent radiance (Fig. 2). For this example, the

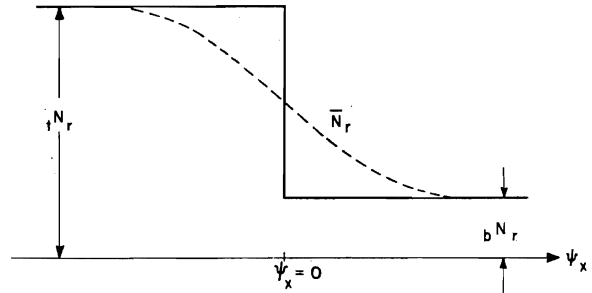


FIG. 2. Illustrating the time-averaged radiance profile of a shimmered edge (example A).

target  $\Psi_t$  consists of all points  $(\psi_x, \psi_y)$  such that  $\psi_x \leq 0$ . The background  $\Psi_b$  is the complementary region of all points  $(\psi_x, \psi_y)$  such that  $\psi_x > 0$ .  $\Psi_t$  is assigned the uniform apparent radiance  $iN_r$ . From (3) with (2)

$$\begin{aligned} \bar{N}_r(\psi_x, \psi_y) &= (iN_r - bN_r) \left\{ \frac{1}{2\pi Ar} \int_{-\infty}^0 \int_{-\infty}^{\infty} \right. \\ &\quad \times \exp \left[ -\frac{1}{2} \frac{(\psi_x - \psi_x')^2 + (\psi_y - \psi_y')^2}{Ar} \right] d\psi_x' d\psi_y' \left. \right\} + bN_r \\ &= (iN_r - bN_r) \left[ \frac{1}{(2\pi Ar)^{1/2}} \int_{\psi_x}^{\infty} \exp \left( -\frac{\psi_x'^2}{2Ar} \right) d\psi_x' \right] + bN_r. \end{aligned}$$

$\bar{N}_r$  is plotted in Fig. 2.

The time-averaged apparent contrast is, by (5):

$$\bar{C}_r(\psi_x, \psi_y) = \frac{C_r}{(2\pi Ar)^{1/2}} \int_{\psi_x}^{\infty} \exp \left( -\frac{\psi_x'^2}{2Ar} \right) d\psi_x'.$$

The limits

$$\begin{aligned} \lim_{\psi_x \rightarrow \infty} \bar{C}_r(\psi_x, \psi_y) &= 0, \\ \lim_{\psi_x \rightarrow -\infty} \bar{C}_r(\psi_x, \psi_y) &= C_r, \end{aligned}$$

which hold for all  $\psi_y$ , agree with the values one would

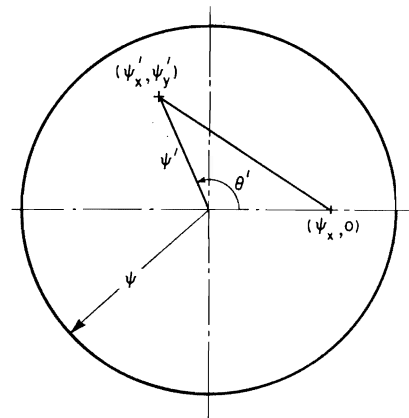


FIG. 3. Diagram for the derivation in example D.

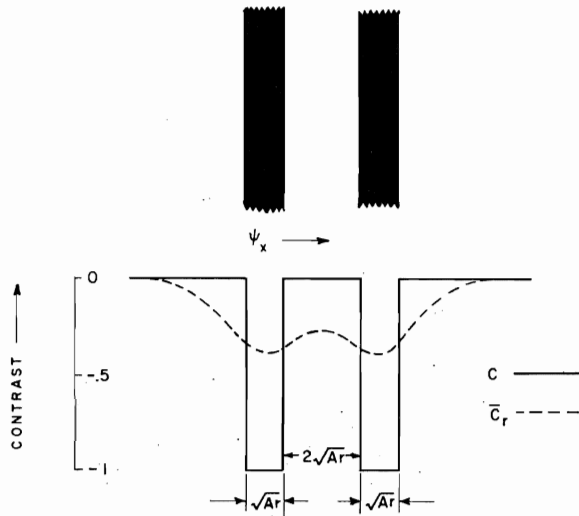


FIG. 4. The characteristic shape of the time-averaged contrast profile of two long black bars of the dimensions shown.

expect on the basis of the values of the unshimmered contrast  $C_r$  discussed in the preceding section.

**B. Long Thin Bar**

A long thin bar may be represented by the subregion  $\Psi_t$  of  $\Psi$  consisting of all points  $(\psi_x, \psi_y)$  such that  $-a \leq \psi_x \leq a$ . All other points of  $\Psi$  form the background  $\Psi_b$ .  $\Psi_t$  is assigned the uniform radiance  $tN_r$ ,  $\Psi_b$  the radiance  $bN_r$ . Then from (5) with (2)

$$\begin{aligned} \bar{C}_r(\psi_x, \psi_y) &= \frac{C_r}{2\pi Ar} \int_{-a}^a \int_{-\infty}^{\infty} \exp\left[-\frac{1}{2} \frac{(\psi_x - \psi_x')^2 + (\psi_y - \psi_y')^2}{Ar}\right] \times d\psi_x' d\psi_y' \\ &= \frac{C_r}{(2\pi Ar)^{\frac{1}{2}}} \int_{\psi_x - a}^{\psi_x + a} \exp\left(-\frac{\psi_x'^2}{2Ar}\right) d\psi_x'. \end{aligned}$$

It is easy to verify that  $|\bar{C}_r|$  attains a maximum at the point  $(0,0)$ .  $\bar{C}_r(0,0)$  is the extreme contrast attained by  $\bar{C}_r$  over  $\Psi$ , i.e.  $\bar{C}_r(0,0)$  is either a maximum [if  $\bar{C}_r(0,0)$  is positive] or a minimum [if  $\bar{C}_r(0,0)$  is negative]. It is clear from the geometry in this and the preceding example that  $\bar{C}_r$  is independent of  $\psi_y$ . Some contrast profiles of shimmered bars are shown in Fig. 5. Observe that the widths of the bars are given in terms of the dimensionless parameter  $(Ar)^{\frac{1}{2}}$ . These facts will be of some use in the discussion of the measurement of  $A$ .

**C. Rectangle**

A rectangle in  $\Psi$  centered on the origin is defined as the subregion  $\Psi_t$  consisting of all points  $(\psi_x, \psi_y)$  such that  $-a \leq \psi_x \leq a$ ,  $-b \leq \psi_y \leq b$ . From (5) with (2), after

some reductions,

$$\begin{aligned} \bar{C}_r(\psi_x, \psi_y) &= \frac{C_r}{2\pi Ar} \left[ \int_{\psi_x - a}^{\psi_x + a} \exp\left(-\frac{\psi_x'^2}{2Ar}\right) d\psi_x' \right] \\ &\quad \times \left[ \int_{\psi_y - b}^{\psi_y + b} \exp\left(-\frac{\psi_y'^2}{2Ar}\right) d\psi_y' \right]. \end{aligned}$$

The computations of  $\bar{C}_r$  for a rectangle can therefore be carried out by using the results of example B.

**D. Circular Disk**

A circular disk  $\Psi_t$  in  $\Psi$  centered on the origin and of angular radius  $\psi$  is the set of all points  $(\psi_x, \psi_y)$  such that  $\psi_x^2 + \psi_y^2 \leq \psi^2$  (Fig. 3). From (5) with (2) the associated contrast expression is:

$$\begin{aligned} \bar{C}_r(\psi_x, \psi_y) &= \frac{C_r}{2\pi Ar} \iint_{\psi_x'^2 + \psi_y'^2 \leq \psi^2} \exp\left[-\frac{1}{2} \frac{(\psi_x - \psi_x')^2 + (\psi_y - \psi_y')^2}{Ar}\right] \times d\psi_x' d\psi_y'. \end{aligned}$$

An examination of the function  $\bar{C}_r$  would show that in this case  $\bar{C}_r([\psi_x^2 + \psi_y^2]^{\frac{1}{2}}, 0) = \bar{C}_r(\psi_x, \psi_y)$  (circular symmetry). It is therefore sufficient to consider the evaluation of

$$\begin{aligned} \bar{C}_r(\psi_x, 0) &= \frac{C_r}{2\pi Ar} \iint_{\psi_x'^2 + \psi_y'^2 \leq \psi^2} \exp\left[-\frac{1}{2} \frac{(\psi_x - \psi_x')^2 + \psi_y'^2}{Ar}\right] \times d\psi_x' d\psi_y'. \end{aligned}$$

Adopting the following transformation of coordinates:  $\psi_x' = \psi' \cos\theta'$ ,  $\psi_y' = \psi' \sin\theta'$ , we have

$$\begin{aligned} \bar{C}_r(\psi_x, 0) &= \frac{C_r}{2\pi Ar} \int_0^\psi \exp\left[-\frac{(\psi'^2 + \psi_x^2)}{2Ar}\right] \left[ \int_0^{2\pi} \exp\left(\frac{\psi' \psi_x \cos\theta'}{Ar}\right) d\theta' \right] \psi' d\psi'. \end{aligned}$$

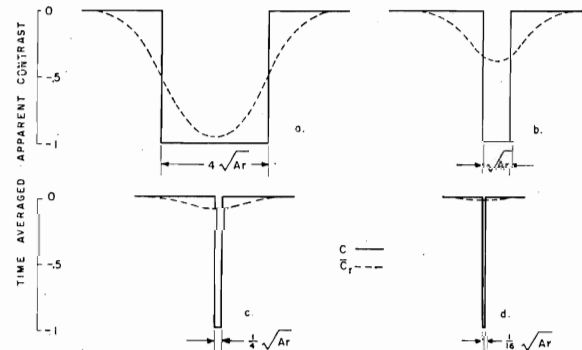


FIG. 5. Illustrating the characteristic time-averaged contrast profiles of long black bars as a function of bar width.

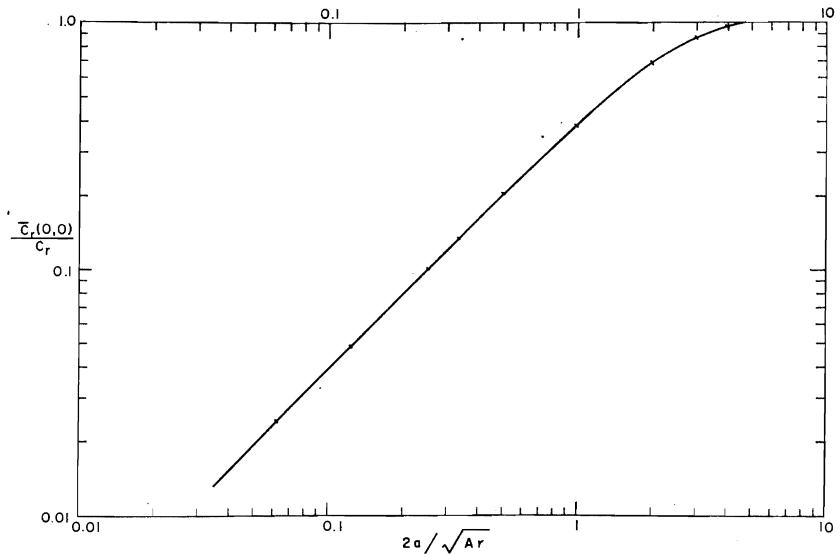


FIG. 6. Graph used in the experimental determination of A.

The inner integral is readily evaluated:

$$\int_0^{2\pi} \exp(z \cos\theta') d\theta' = 2 \int_0^\pi \cos(iz \sin\theta') d\theta' = 2\pi I_0(z),$$

$$z = \frac{\psi' \psi_x}{Ar},$$

where  $I_0$  is a modified Bessel function of the first kind, of zero order, which has the series representation

$$I_0(z) = \sum_{k=0}^{\infty} \frac{(z/2)^{2k}}{(k!)^2}.$$

Hence

$$\bar{C}_r(\psi_x, 0) = \frac{C_r}{Ar} \int_0^\psi \left[ \sum_{k=0}^{\infty} \frac{(\psi' \psi_x / 2Ar)^{2k}}{(k!)^2} \right] \exp\left[-\frac{(\psi'^2 + \psi_x^2)}{2Ar}\right] \psi' d\psi',$$

which may be rewritten as

$$\bar{C}_r(\psi_x, 0) = C_r e^{-\phi_x} \sum_{k=0}^{\infty} \frac{\phi_x^k}{(k!)^2} \Gamma(\phi; k+1),$$

where

$$\Gamma(a; k+1) = \int_0^a y^k e^{-y} dy$$

defines the incomplete gamma function, for which tabulations exist,<sup>9</sup> and  $\phi_x = \psi_x^2 / 2Ar$ ,  $\phi = \psi^2 / 2Ar$ . It is easy to check that  $|\bar{C}_r|$  is a decreasing function for increasing  $\psi_x$ , so that  $|\bar{C}_r|$  attains a maximum at (0,0). Thus if  $|\bar{C}_r(0,0)|$  is below a threshold contrast, the entire disk is undetectable. The formula for  $\bar{C}_r(0,0)$  is

<sup>9</sup> K. Pearson, *Tables of the Incomplete Gamma Function* (Cambridge University Press, Cambridge, England, 1946).

readily obtained:

$$\bar{C}_r(0,0) = C_r \Gamma(\psi^2 / 2Ar; 1) = C_r [1 - \exp(-\psi^2 / 2Ar)].$$

For angularly small disks

$$\bar{C}_r(0,0) = C_r (\alpha / 2\pi Ar^3),$$

where  $\alpha = \pi(\psi r)^2$  and which agrees with (6). If  $\psi = \infty$ , i.e., if the disk is infinitely large, then since  $\Gamma(\infty; k+1) = k!$ , the general expression yields

$$\bar{C}_r(\psi_x, \psi_y) = C_r e^{-\phi_x} \sum_{k=0}^{\infty} \frac{\phi_x^k}{(k!)} = C_r,$$

as expected.

### E. Two Long Thin Bars

One example of the effect of atmospheric boil on the ability to resolve two objects which are close together is illustrated in Fig. 4. Two identical black bars of angular width  $(Ar)^{1/2}$ , separated an angular distance  $2(Ar)^{1/2}$ , have their contrast profiles smeared into a characteristic shape shown by the dashed curve. The object space contrast of  $-1$  at the center of each bar is invariably raised to  $-0.6$  in the image space, and the zero contrast at the center of the gap between the bars is invariably pulled down to  $-0.74$ . Such predictable features of shimmered contrast profiles can be used to generate an experimental procedure for determining A, one of which is appended below.

### MEASUREMENT OF OPTICAL AIR STATE

For a bar whose width  $2a$  is less than  $5(Ar)^{1/2}$ , the values  $|\bar{C}_r(\psi_x, \psi_y)|$  are measurably less than  $|C_r|$ . Figure 5 depicts the contrast profiles of four long black bars (hence  $C_r = -1$ ). The width of each differs by a

factor of four from its predecessor. From example B,

$$\bar{C}_r(0,0) = \frac{-1}{(2\pi)^{\frac{1}{2}}} \int_{-a/(Ar)^{\frac{1}{2}}}^{a/(Ar)^{\frac{1}{2}}} \exp(-\frac{1}{2}t^2) dt.$$

By means of this integral, each choice of the ratio  $2a/(Ar)^{\frac{1}{2}}$  leads to a corresponding value  $\bar{C}_r(0,0)$ . These correspondences are graphed in Fig. 6. The experimental procedure consists in measuring  $\bar{C}_r(0,0)$  for each bar by scanning the bar with a telephotometer at a given range  $r$ . The four corresponding values of  $2a/(Ar)^{\frac{1}{2}}$  are then picked from the graph. Since  $r$  is fixed, and  $2a$  is known for each bar,  $A$  can then be determined.

We observe finally that before using the graph in

Fig. 6 the measured values  $\bar{C}_r(0,0)$  must be corrected to remove the reduction effect on the contrast induced by the scattering and absorption mechanisms of the atmosphere. For horizontal paths of sight, with the usual uniformity properties, the corrected values are given by  $\bar{C}_r(0,0) \exp(+r/L)(bN_r/bN_0)$ , where  $L$  is the attenuation length of the atmosphere.<sup>10</sup>

#### ACKNOWLEDGMENT

The authors wish to acknowledge the contributions made by T. A. Magness of the Marine Physical Laboratory of the Scripps Institution of Oceanography.

<sup>10</sup> S. Q. Duntley, A. R. Boileau, and R. W. Preisendorfer, *J. Opt. Soc. Am.* **47**, 499 (1957).

## MALA WHARF

(An excerpt from the log of the search for an ocean site for an underwater laser experiment.)

One day was spent flying around all of the islands, except Kauai, in a Marine C-47. A number of color photographs were taken to show bays and shorelines. A general consensus led to one spot on the west (lee) shore of Maui at Lahaina. A 1000-ft long condemned, concrete wharf there could provide a platform for the caisson and some laser locations. The wharf was built many years ago but was little used by cargo ships because of danger from Kona (SW) winds. During the daylight hours current averages 1 to 2 knots. This presents a problem. At night when winds are down, the current should not be too great, but this is only a speculation because there was no way to measure it. The sketch depicts, roughly, the Mala Wharf.

Horizontal visibility just off the end of the wharf was 83 feet, measured by horizontal sightings of a red bottomed boat from six feet under the surface. This observation was done in full 11:00 AM sunlight. The shadow of the boat undoubtedly enhanced perception.

Measured from the shore, the first 400 feet of wharf was considered unusable because the water is too shallow. The usable 600 feet of wharf could be extended out to the required 1000 feet by building under-surface pilings (with buoy markers) for laser mountings. The north side of the wharf would be the better location for the caisson. Heavy timbers should be lashed to the opposite side of the concrete pilings to afford protection from possible southwest (Kona) winds. The best weather is from March to November. Normal waves in the area are about 1 foot high with occasional swells to just over 2 foot.

Permission for the use of the wharf could be secured from Mr. Fujio Matsuda, Director, Department of Transportation, Division of Harbors, State of Hawaii, Honolulu.

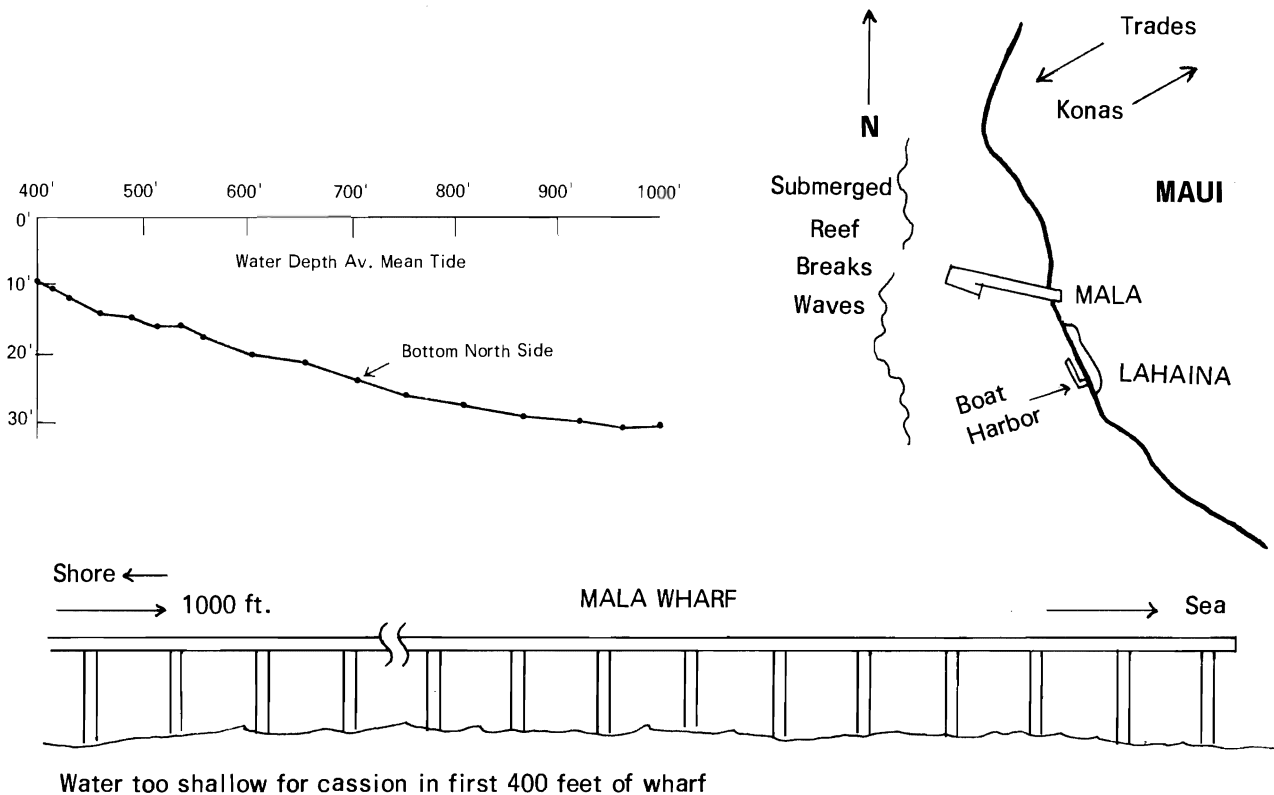


## Image Transmission by the Troposphere I\*

SEIBERT Q. DUNTLEY, ALMERIAN R. BOILEAU, AND RUDOLPH W. PREISENDORFER  
*Scripps Institution of Oceanography,† University of California, La Jolla, California*

(Received November 15, 1956)

Quantitative treatment of the apparent luminance of distant objects and the reduction of apparent contrast along inclined paths of sight through real atmospheres has been accomplished by means of optical data taken from an aircraft in flight. Sample data from a single flight are used to illustrate some of the principles involved. Correlation has been found between the humidity profile of the atmosphere and its optical properties.

### INTRODUCTION

DISTANT objects are usually viewed, photographed, or televised by means of some path of sight through the atmosphere. Conventional principles of geometrical and physical optics suffice to describe the nature of the final image except for effects due to the atmosphere. In most circumstances, however, the configuration of the image and its information content is affected, often seriously, by its transmission from the object to the receiver. The atmosphere can be regarded as a transmission link in the object-to-image chain and the concomitant effect of the pertinent optical atmospheric properties can be regarded as governing its *image transmission*.

This paper is intended as the first of a series describing the results of an extensive on-going research program which has already been in progress for several years. Results from numerous theoretical and experimental investigations of image transmission phenomena are ready to be reported and further research of many kinds is in progress. Experimental results from a single flight comprise the factual content of this first paper and the equations are limited to certain general relations needed for the practical utilization of the data; this is in keeping with the scope of the oral version of the paper as presented at the Cambridge meeting of the International Commission on Optics.

The specially instrumented B-29 aircraft used to collect the data reported in this paper has, on other flights, secured data up to 30 000 ft under several different atmospheric and lighting conditions; and subsequent papers in the series will present data from these and other flights. The optical properties of the troposphere are of special interest because most viewing takes place through it. Roughly three-fourths of the atmosphere lies within the troposphere and because this lower

air often contains haze, clouds, dust, and rain it seriously affects image transmission more frequently than do the higher strata. Exploration of image transmission phenomena in the stratosphere must await an opportunity to instrument a vehicle having greater altitude capability.

### SOME GENERAL PRINCIPLES‡

#### Introduction

In the absence of appreciable atmospheric boil<sup>1</sup> the apparent radiance of any distant object is the sum of two independent components: (1) residual image-forming light from the object that has traversed the atmospheric path without having been scattered or absorbed; (2) radiance created by the scattering of ambient light throughout the path of sight, including sunlight, skylight, earth-shine, etc. Only the first component contains information about the object, for the second is the result of scattering processes throughout the path of sight and is, therefore, independent of the nature of the object. In this paper the image transmission of any path of sight will be specified in terms of the transmittance of the entire path and the path radiance. No theoretical model for the atmosphere is needed; consequently, nearly all restrictive assumptions are avoided and the equations can be used to describe any path of sight through all real isotropic atmospheres with any lighting condition. To be useful in practice, these equations must be supplied with data and these are becoming available as a result of the flight research program now in progress.

#### Notation

The notation used in this paper has been adopted with great care and on the basis of experience accumulated over many years. It is designed to fulfill many

\* Presented at the Fourth Congress of the International Commission of Optics, held in Cambridge-Boston, Massachusetts, March 28-April 3, 1956. Published with financial assistance from UNESCO and the International Union of Pure and Applied Physics.

† Contribution from the Scripps Institution of Oceanography, University of California, New Series No. 921. This work has been supported by the Geophysical Research Directorate of the Air Force Cambridge Research Center and the Bureau of Ships of the U. S. Navy under contracts NObs-43356, NObs-50274, NObs-72039, and NObs-72092.

‡ The principles presented in this paper and in subsequent papers of this series were formulated in unpublished lecture notes used within the Visibility Laboratory of the Scripps Institution of Oceanography which include, generalize, and extend earlier work by the authors and others (R. W. Preisendorfer, "Lectures on photometry, hydrological optics, atmospheric optics," Fall, 1953, Vol. I).

<sup>1</sup> Duntley, Culver, Culver, and Preisendorfer, *J. Opt. Soc. Am.* 42, 877A (1952); publication of this paper is planned.



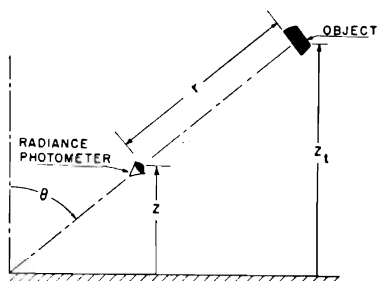


FIG. 1. Illustrating the geometry of the path of sight.

requirements: It is suited to the terrestrially-based system of altitudes and directions in which flight data must be taken and it is fully compatible with the more powerful vector notation required for the generalized theoretical treatments of image transmission and radiative transfer phenomena to follow. It is compatible also with the notation commonly used in several mathematically allied fields of physics, as for example, neutron diffusion theory. It is extendable to hydrological optics, a natural counterpart of meteorological optics, in which the authors of this paper are deeply interested.

The basic symbol employed for the spectral radiance is  $N$ , and the symbol for luminance is  $B$ . The altitude of the photometer is denoted by  $z$ , the height above mean sea level. The direction of any path of sight is specified by a zenith-angle  $\theta$  and an azimuth angle  $\phi$ , the photometer being directed upward when  $0 \leq \theta < \pi/2$ , as in Fig. 1;  $z$ ,  $\theta$ , and  $\phi$  are always written as parenthetical attachments to the parent symbol. When the post subscript  $r$  is appended to any symbol, it denotes that the quantity pertains to a path of length  $r$ . The subscript 0 always refers to the hypothetical concept of a photometer located at zero distance from the object, as, for example, in denoting the *inherent* radiance of a surface. Pre-subscripts identify the object, thus the pre-subscript  $b$  refers to background, and  $t$  to object or visual target. Thus, the (monochromatic) *inherent spectral radiance* of an object  $t$  at altitude  $z_t$  as viewed in the direction  $(\theta, \phi)$  is  ${}_t N_0(z_t, \theta, \phi)$  and the corresponding apparent radiance observed in the direction  $(\theta, \phi)$  at any other altitude  $z$  is  ${}_t N_r(z, \theta, \phi)$  where  $z_t = z + r \cos \theta$ . A post-superscript \*, or post-subscript \* is employed as a mnemonic symbol signifying that the radiometric quantity has been generated by the scattering of ambient light reaching the path from *all directions*. Thus  $N_r^*(z, \theta, \phi)$  is the spectral path radiance observed at altitude  $z$  in the indicated direction, and  $(N_{*z}, \theta, \phi)$  is used to denote *path function*, a quantity defined later in this paper.

The (monochromatic) *apparent spectral radiance* of any distant object  $t$  is

$${}_t N_r(z, \theta, \phi) = T_r(z, \theta, \phi) [{}_t N_0(z_t, \theta, \phi) + N_r^*(z, \theta, \phi)], \quad (1)$$

where the first term on the right is the residual image-forming light from the object and the second term is the path radiance due to scattering processes throughout

the path.  $T_r(z, \theta, \phi)$  is the spectral transmittance of the path for image-forming rays; it includes the factor  $[n(z)/n(z_t)]^2$  required by geometrical optics whenever the index of refraction of the medium at the observer  $[n(z)]$  differs from the index of refraction of the medium at the target  $[n(z_t)]$ . In the case of paths of sight through the troposphere the departure of  $[n(z)/n(z_t)]^2$  from unity is negligible. The transmittance of the path is a property of the atmosphere throughout the path and is independent of the distribution of the ambient lighting; in the case of any path of sight through the troposphere it is the same for upward or downward transmissions, thus  $T_r(z, \theta, \phi) = T_r(z_t, \pi - \theta, \pi + \phi)$  where  $z_t = z + r \cos \theta$ . Because forward scattering generally exceeds backward scattering, reversibility is not true of the path radiance  $N_r^*(z, \theta, \phi)$  except for a few symmetrical lighting conditions, such as (1) horizontal paths of sight under a uniform overcast, and (2) a horizontal path at right angles to the plane of the sun provided both the radiance distributions of the sky above and the earth below the path are symmetrical with respect to the plane.

The image transmitting properties of the atmosphere can be separated from the optical properties of the object by the introduction of the *contrast* concept:

The *inherent spectral contrast*  $C_0(z_t, \theta, \phi)$  of an object is, by definition,

$$C_0(z_t, \theta, \phi) = [{}_t N_0(z_t, \theta, \phi) - {}_b N_0(z_t, \theta, \phi)] / {}_b N_0(z_t, \theta, \phi). \quad (2)$$

The corresponding definition for *apparent spectral contrast* is

$$C_r(z, \theta, \phi) = [{}_t N_r(z, \theta, \phi) - {}_b N_r(z, \theta, \phi)] / {}_b N_r(z, \theta, \phi). \quad (3)$$

The apparent and inherent background radiances are related by the expression

$${}_b N_r(z, \theta, \phi) = T_r(z, \theta, \phi) [{}_b N_0(z_t, \theta, \phi) + N_r^*(z, \theta, \phi)]. \quad (4)$$

### Theorems

Subtracting Eq. (4) from Eq. (1) yields the relation

$$[{}_t N_r(z, \theta, \phi) - {}_b N_r(z, \theta, \phi)] = T_r(z, \theta, \phi) [{}_t N_0(z_t, \theta, \phi) - {}_b N_0(z_t, \theta, \phi)]. \quad (5)$$

Thus, radiance differences are transmitted along inclined paths with the same attenuation as that experienced by each image-forming ray.

If Eq. (5) is divided by the apparent radiance of the background  ${}_b N_r(z, \theta, \phi)$  and combined with Eq. (3), the result can be written:

$$C_r(z, \theta, \phi) = T_r(z, \theta, \phi) \times [{}_t N_0(z_t, \theta, \phi) / {}_b N_r(z, \theta, \phi) - {}_b N_0(z_t, \theta, \phi) / {}_b N_r(z, \theta, \phi)]. \quad (6)$$

When the inherent radiance of the background is very dark, as in the case of an object at high altitude, the second term in the brackets on the right side of Eq. (6) may be negligible.

Combining Eqs. (2) and (6) yields the expression

$$C_r(z, \theta, \phi) / C_0(z, \theta, \phi) = T_r(z, \theta, \phi) \cdot N_0(z, \theta, \phi) / N_r(z, \theta, \phi). \quad (7)$$

The right-hand member of Eq. (7) is an expression for the *contrast transmittance* of the path of sight; it is independent of the optical properties of the object. Equation (7) is the law of contrast reduction by the atmosphere expressed in its most general form.<sup>2</sup>

An interesting variant of Eq. (7) formed by combination with Eq. (4) is the following expression in which *contrast transmittance* is characterized in terms of path radiance and inherent background radiance:

$$C_r(z, \theta, \phi) / C_0(z, \theta, \phi) = 1 - [N_r^*(z, \theta, \phi) / N_r(z, \theta, \phi)]. \quad (8)$$

The apparent indeterminateness of Eqs. (7) and (8) when applied to the case of objects outside the atmosphere can be avoided by the use of the limiting form of Eq. (6), as follows:

$$C_r(z, \theta, \phi) = T_r(z, \theta, \phi) \cdot N_0(z, \theta, \phi) / N_r(z, \theta, \phi). \quad (9)$$

It should be emphasized that Eqs. (1) through (9) are completely general; they apply rigorously to any path of sight regardless of the extent to which the scattering and absorbing properties of the atmosphere or the distributions of lighting exhibit nonuniformities from point to point. No theoretical model of the atmosphere is involved and no restrictive assumptions have been made. The equations can be used in treating all real atmospheres and all real lighting conditions. This is in sharp distinction to treatments of the subject which are based upon theoretical models of the atmosphere which invariably involve major assumptions such as horizontal uniformity, exponential lapse rate of air density, vertical uniformity of particle size distribution, negligible earth curvature, etc.

### Equation of Transfer

Image-forming light is lost by scattering and absorption in each elementary segment of the path of sight and contrast-reducing path radiance is generated by the scattering of the ambient light which reaches the segment from all directions. The quantitative description of this scattered component of path-segment radiance involves a quantity called the *path function* and denoted by the symbol  $N_*(z, \theta, \phi)$ , where the mnemonic subscript symbol  $*$  is used both to suggest light reaching the path segment from all directions and to denote that the quantity is a point function. The parenthetical symbols  $(z, \theta, \phi)$  indicate that the path function depends upon the direction of image transmission and upon the location of the segment in the path of sight. The path function depends upon the directional distribution of

<sup>2</sup> Equation (7) is a generalization of Eq. (15) on p. 183 of S. Q. Duntley, *J. Opt. Soc. Am.* **38**, 179 (1948).

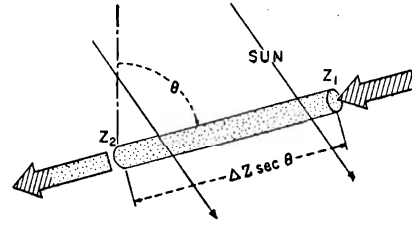


FIG. 2. Illustrating the derivation of the equation of transfer. Δz is defined as z1 - z2, so that Δr = Δz sec θ is always non-negative. The difference ΔN(z, θ, φ) between output and input is N(z2, θ, φ) - N(z1, θ, φ).

the lighting on the segment due to its surroundings; it can be operationally defined in terms of the (limiting) ratio of the path radiance associated with a short path to the path length by the relation  $N_*(z, \theta, \phi) = \lim(\Delta r \rightarrow 0) \times N_{\Delta r}(z, \theta, \phi) / \Delta r$ . In experimental practice, the path length Δr should be sufficiently short that no change in the ratio can be detected if Δr is made shorter. Apparatus for path function measurement has been built and will be described elsewhere.

The loss in image-forming light due to attenuation by scattering and absorption within any path segment is proportional to the amount of image-forming light present; the coefficient of proportionality will be written in the reciprocal form 1/L(z), and L(z) will be referred to as the *attenuation length*. L(z) is a function of position within the path of sight; it does not depend upon the image transmission direction unless the aerosol is anisotropic, as sometimes occurs in the case of falling snow; it is independent of the manner in which the path segment is lighted by the sun or sky; it is a physical property of the atmosphere alone. Attenuation includes loss of image-forming radiance by absorption and by scattering. Absorption refers to any thermodynamically irreversible transformation of monochromatic radiant energy including, primarily, conversion of light into heat but also fluorescence phenomena, photochemical processes, etc. Attenuation by scattering results from any change of direction sufficient to cause the radiation to fall outside the summative radius of the detector mosaic.

In any path segment of length Δr = Δz sec θ, as illustrated by Fig. 2, the difference ΔN(z, θ, φ) between output and input radiance is attributable to a gain term  $N_*(z, \theta, \phi) \Delta r$  and a loss term  $N(z, \theta, \phi) \Delta r / L(z)$ , so that  $\Delta N(z, \theta, \phi) = N_*(z, \theta, \phi) \Delta r - N(z, \theta, \phi) \Delta r / L(z)$ . This relation may be rewritten

$$\Delta N(z, \theta, \phi) / \Delta z \sec \theta = N_*(z, \theta, \phi) - N(z, \theta, \phi) / L(z). \quad (10)$$

In conformity with usage in other fields of physics Eq. (10) will be referred to as the *incremental form of the equation of transfer*. It is implicit in this equation that Δz must be taken sufficiently small so that over this interval L(z) and  $N_*(z, \theta, \phi)$  may be regarded as constants within the precision of experimental data.

Equation (10) is a steady-state equation of continuity,<sup>3</sup> based upon the conservation of energy principle; it refers only to nonemitting atmospheres, since an additional term would be needed to represent emission of radiation in the path, as by fluorescence, recombination phenomena, particle excitation, etc. Self-radiosity within the visible spectrum appears to be of negligible importance in the troposphere. Equations (1) and (4) may be regarded as integral forms of the equation of transfer.

The equation of transfer and the concepts of attenuation length and path function share the same generality as the concepts associated with Eqs. (1) through (9): No theoretical model atmosphere has been employed; each of the equations in this paper is applicable to all real isotropic atmospheres, all lighting conditions, and all paths of sight. The use of the equation of transfer in numerical summation procedures involving experimental data will be illustrated in a later section of this paper. Only when Eq. (10) is simulated by a differential equation and an analytic integration performed does the introduction of a theoretical model for the atmosphere become necessary; this will not be done in the present paper.

### Equilibrium Radiance

Many image transmission phenomena are most clearly understandable in terms of the concept of *equilibrium radiance*. This concept is a natural consequence of the equation of transfer, which indicates that some unique *equilibrium radiance*  $N_q(z, \theta, \phi)$  must exist at each point such that the loss of radiance within the path segment is balanced by the gain, i.e.,  $\Delta N_q(z, \theta, \phi) = 0$ . Thus

$$0 = N_*(z, \theta, \phi) - N_q(z, \theta, \phi)/L(z), \quad \text{so that} \\ N_q(z, \theta, \phi) = N_*(z, \theta, \phi)L(z) \quad (11)$$

and the equation of transfer (10) may be rewritten as follows:

$$\Delta N(z, \theta, \phi)/\Delta z \sec\theta = [N_q(z, \theta, \phi) - N(z, \theta, \phi)]/L(z). \quad (12)$$

Equation (11) shows that each segment of every path of sight has associated with it an equilibrium radiance, and Eq. (12) states that the average space rate of change in image-forming radiance caused by the path segment is in such a direction as to cause the output radiance to be closer to the equilibrium radiance than is the input radiance. This segment-by-segment convergence of the apparent radiance of the object to the dynamic equilibrium radiance is illustrated by the data in Fig. 6 of this paper.

<sup>3</sup> The equation of transfer has been generalized to the transient case, and rigorously derived for an arbitrary optical medium, using the concepts of measure theory. R. W. Preisendorfer, "A mathematical foundation for radiative transfer theory," Doctoral dissertation, U.C.L.A., May 1956. An exposition of this theory has been submitted for publication in the Journal of the Optical Society of America.

When the path of sight is horizontal and optically uniform both in terms of the composition of the aerosol and its lighting, the equilibrium radiance is identical with the apparent radiance of the horizon. The apparent radiance of distant objects inherently more radiant than the equilibrium value decreases toward the equilibrium radiance as an asymptote; conversely the apparent radiance of any dark distant object approaches the same asymptote.

### Equilibrium Contrast

Many of the foregoing equations can be rewritten in terms of *equilibrium contrast*,  $C_q(z, \theta, \phi)$ , which is defined by the relation

$$C_q(z, \theta, \phi) = [N_r(z, \theta, \phi) - N_q(z, \theta, \phi)]/N_q(z, \theta, \phi). \quad (13)$$

Notation of the type defined by Eq. (13) enables the equation of transfer (10) to be written

$$\Delta C_q(z, \theta, \phi)/\Delta z \sec\theta = -C_q(z, \theta, \phi)/L(z) \quad (14)$$

or

$$\Delta C_q(z, \theta, \phi)/C_q(z, \theta, \phi) = -\Delta z \sec\theta/L(z), \quad (15)$$

provided that the equilibrium radiance  $N_q(z, \theta, \phi)$  is constant on the segment of path under discussion. In this case the fractional change in equilibrium contrast depends only upon the ratio of the length of the path segment to the attenuation length. The negative signs throughout Eqs. (14) and (15) signify that equilibrium contrast decreases in absolute magnitude in the segment.

## EXPERIMENTAL METHODS

### Introduction

The apparent radiance of any distant object can be computed by means of Eq. (1) if the transmittance of the path of sight and the path radiance are calculated from experimental data. This can be done from profiles of attenuation length and path function for the path of sight by means of the relations

$$T_r(z, \theta, \phi) = [n(z)/n(z_i)]^2 \prod_{i=1}^m \exp\{-\Delta r/L(z_i)\} \\ = [n(z)/n(z_i)]^2 \exp\{-\Delta r \sum_{i=1}^m 1/L(z_i)\} \quad (16)$$

and

$$N_r^*(z, \theta, \phi) = \Delta r \sum_{i=1}^m T_{r_i}(z, \theta, \phi) N_*(z_i, \theta, \phi), \quad (17)$$

where the vertical height  $|z_i - z|$  of the path is divided into  $m$  equal segments of length  $\Delta z$ , and  $\Delta r = \Delta z \sec\theta$ .  $L(z_i)$  and  $N_*(z_i, \theta, \phi)$  are the mean values of  $L$  and  $N_*$  in the  $i$ th segment.  $r_i = (i-1)\Delta r$ ,  $i = 1, \dots, m$ .

Attenuation Profile

An experimental technique for measuring the vertical profile of attenuation length in horizontally uniform atmospheres has been devised around an air-borne version of an instrument based upon principles described earlier.<sup>4,5</sup> Figure 3 shows this attenuation meter mounted on the B-29 aircraft used by the Visibility Laboratory in its flight research program. The optical system is shown diagrammatically in Fig. 4. The for-



FIG. 3. Specially instrumented B-29 aircraft used to collect the data presented in this paper. The long cylindrical apparatus on top of the fuselage is the *attenuation meter*, shown schematically in Fig. 4. The smaller cylindrical device which appears slightly forward of the attenuation meter is the sky-scanning telephotometer. It consists of an end-on type multiplier phototube mounted at the focal point of a parabolic front-surfaced mirror 12 in. diam. Scanning is accomplished automatically by means of a turret and trunion mounting; scanning time for the entire hemisphere is 90 sec. Field of view, adjustable by means of interchangeable field stops, was circular, 5° in angular diameter in the case of the data shown in Fig. 6. Sensitivity is sufficient to map even the darkest high-altitude night skies. Spectral response is controlled by absorption filters. A similar (downward-viewing) telephotometer is mounted beneath the aircraft but is not shown by this photograph.

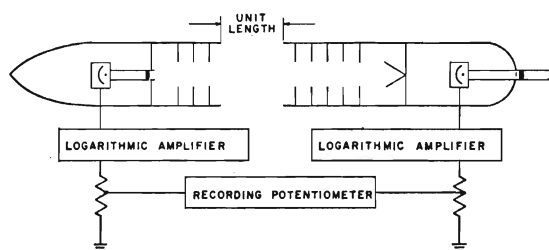


FIG. 4. Schematic diagram of the air-borne attenuation meter. The forward photoelectric telephotometer measures the equilibrium radiance; the rear telephotometer measures the radiance of a path of unit length. The latter radiance is numerically equal to the horizontal path function in the direction of flight. Multiplier phototubes and Sweet-type logarithmic circuits enable direct recording of the ratio of these radiances, i.e., of the attenuation length [see Eq. (11)]. Wind-tunnel tests of the aerodynamic design showed ambient pressure throughout the unit path. Light trap design, stray-light treatment, and photoelectric sensitivity are sufficient to enable measurement of attenuation lengths up to 200 nautical miles when the phototube spectral sensitivity is rendered photopic by means of absorption filters.

<sup>4</sup> S. Q. Duntley, U. S. Patent No. 2,661,650.

<sup>5</sup> S. Q. Duntley, J. Opt. Soc. Am. 39, 630A (1949).

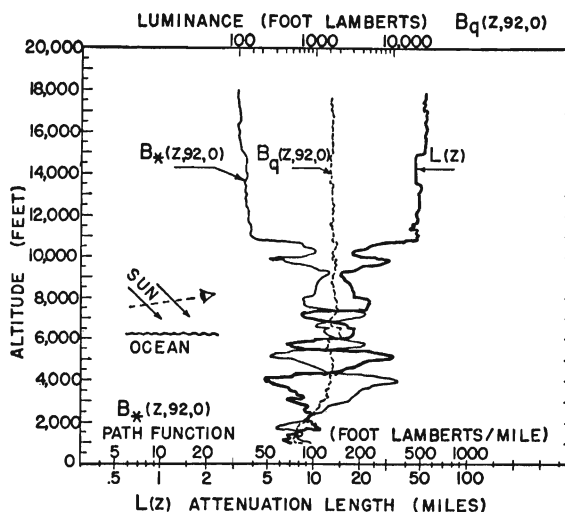


FIG. 5. Measured profiles of path function and attenuation length over the Atlantic Ocean off the coast of Florida, March 10, 1956. Flight 77. Sun position: zenith angle = 48°, azimuth = 140° clockwise from true north. Path function: zenith angle  $\phi = 92^\circ$ ; azimuth  $\theta = 0^\circ$  from the plane of the sun. Sky condition: cloudless, blue. Approximately 36 hr after the passage of a major front. Very light ground haze with top at 4000 ft. The profile of equilibrium luminance was computed by means of Eq. (11).

ward telephotometer is directed toward the horizon and measures the equilibrium radiance of the horizontal path of sight in the direction of flight of the aircraft. The rear telephotometer measures the radiance of a path of unit length; this is numerically equal to the path function. The attenuation length is the ratio of the equilibrium radiance to the path function, as shown by Eq. (11). Recording potentiometers within the aircraft record the outputs of both telephotometers as well as their ratio.

Despite the use of multiplier phototubes, the low level of radiance produced by scattering processes in clear high altitude air precluded the use of narrow-band interference or absorption filters in the airborne attenuation meter. Because it was not possible to measure the spectral radiances called for by the equations given in this paper, each phototube was carefully corrected by means of specially constructed absorption filters to measure luminous quantities. For reasons of rigor the equations in this paper are written with the symbol  $N$ , denoting spectral radiance, but it will be understood that these same equations have been used with  $N$  replaced by  $B$ , denoting luminance, in the treatment of the illustrative data shown in Figs. 5 through 8.

During the flight for which data is given in this paper, the aircraft maintained a constant (southerly) heading and a fixed attitude which held the attenuation meter pointed at the desired portion of the horizon sky while making a controlled, rapid descent from 18 000 ft to 1000 ft at a rate of approximately 1500 ft per min. The resulting profiles of path function, equilibrium luminance, and attenuation length are shown in Fig. 5.

It will be noted that the equilibrium luminance (horizon luminance) was nearly independent of altitude. Repeated descents have demonstrated that the major details of these curves are repeatable.

The transmittance of any inclined path of sight having terminal altitudes between 1000 and 18 000 ft can be calculated from the attenuation profile in Fig. 5 by means of equations corresponding to Eq. (16).

### Path Function Profiles

The aircraft is not equipped for the direct measurement of path functions for vertical and inclined paths of sight. It is capable, however, of measuring the radiance of the sky in any direction, above or below, during flight. A photoelectric telephotometer is located in a trunion mounting on top of the fuselage near the forward end of the attenuation meter, as shown in Fig. 3. This instrument performs an automatic scan of the entire sky above the aircraft in approximately 90 sec. Another telephotometer in a fixed vertical mount provides a continuous record of the radiance of the zenith during the controlled rapid descent described in the preceding section. A corresponding pair of telephotometers is mounted on the bottom of the fuselage. Figure 6 shows zenith luminance data secured by the fixed telephotometer during the same descent to which Fig. 5 applies. Similar profiles of sky luminance for any upward path of sight inclined at angles  $\theta$ ,  $\phi$  can be constructed from the record of the sky-scanning telephotometer, which is designed to be operated continuously during the descent.

The profile of the path function for any path of sight can be calculated from the sky radiance profile and the attenuation profile by means of Eq. (10) after rearrangement as follows:

$$N_*(z, \theta, \phi) = \Delta N(z, \theta, \phi) / \Delta z \sec \theta + N(z, \theta, \phi) / L(z). \quad (18)$$

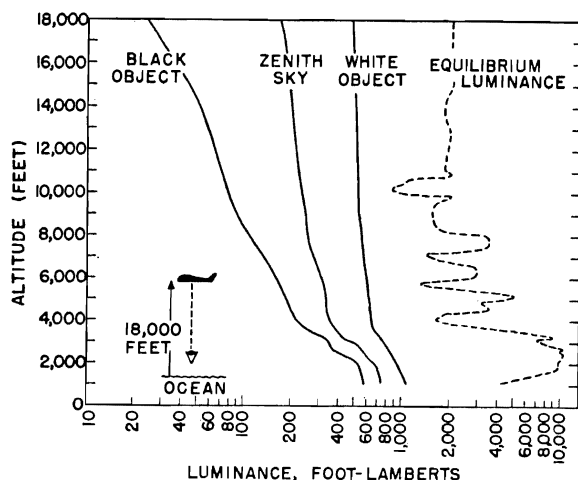


FIG. 6. Measured profile of the luminance of the zenith sky. Flight 77. Calculated profiles of the apparent luminance of black and white objects at 18 000 ft. Calculated profile of vertical equilibrium luminance.

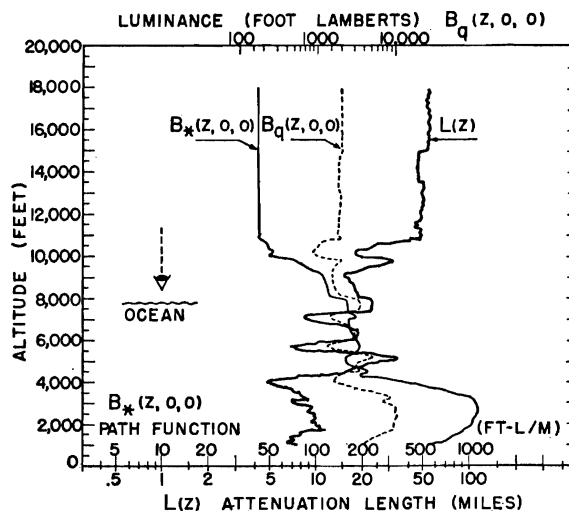


FIG. 7. Calculated profiles of vertical path function and vertical equilibrium luminance. Flight 77. The profile of attenuation length is identical with that in Fig. 5.

Figure 7 shows the result of such a calculation for the vertical path of sight which corresponds with the zenith luminance profile given in Fig. 6.

### Equilibrium Radiance Profiles

An expression for the equilibrium radiance for each element of any path of sight can be found by combining Eqs. (11) and (18) as follows:

$$N_q(z, \theta, \phi) = L(z) (\Delta N(z, \theta, \phi) / \Delta z \sec \theta) + N(z, \theta, \phi). \quad (19)$$

Figure 6 shows the result of the use of Eq. (19) for a calculation of the equilibrium luminance profile for the upward vertical path of sight; the same profile appears in Fig. 7.

In every case the radiance of the sky  $N(z, \theta, \phi)$  as observed from any altitude  $z$  is the path radiance generated by the portion of the path above the observer. That is,  $N(z, \theta, \phi) = N_{\infty}^*(z, \theta, \phi)$ , where  $0 \leq \theta < \pi/2$ . Because  $N(z, \theta, \phi) = 0$  outside the atmosphere (except for light from the stars) and  $N(z, \theta, \phi) > 0$  within, it follows from Eq. (19) that the equilibrium radiance exceeds the apparent radiance of the clear sky and, therefore, the measured radiance of a clear sky increases as the photometer descends.

When clouds are present or when the image transmission direction is upward, the apparent radiance reaching any particular path segment may exceed the equilibrium radiance for that segment, so that a decrease of apparent radiance is possible. In such cases it often happens that the apparent radiance of highly radiant objects decreases while that of objects of small inherent radiance increases. Illustrative data for upward-transmitting paths of sight are planned for presentation in a subsequent paper.

**Profiles of Apparent Object Luminance**

Profiles of the apparent luminance of any specific object can be calculated for any path of sight provided that the inherent luminance of the object in the direction of interest is known. Two such profiles appear in Fig. 6; they refer to hypothetical "black" and "white" objects, respectively, located at a fixed altitude of 18 000 ft and viewed from directly below on the occasion to which the data in this paper applies. The profiles were calculated by means of Eq. (1). Alternatively, they could have been generated step-wise by successive applications of either Eq. (10) or Eq. (12). The complexity which characterizes the attenuation, path function, and equilibrium luminance profiles is scarcely noticeable in these vertical profiles of apparent object luminance. In the case of paths of sight inclined at large zenith angles, however, the object luminance profiles exhibit the complexities due to atmospheric structure much more prominently.

**Profiles of Apparent Contrast**

Figure 8 shows profiles of apparent object contrast generated by means of Eq. (3) from the apparent luminance profiles in Fig. 5. The same profiles could have been generated by use of the Eq. (7).

**METEOROLOGICAL CORRELATIONS**

The complex profiles of attenuation length and path function can only be the result of sharply defined layers of scattering particles. Repeated descents have demonstrated that the major features of the profiles are reproducible in space and time; the layers must, therefore,

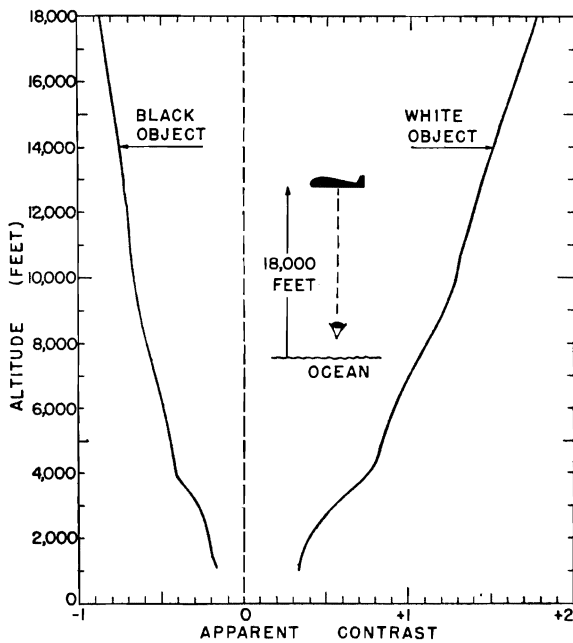


FIG. 8. Calculated profiles of the apparent contrast of black and white objects at 18 000 ft. Flight 77.

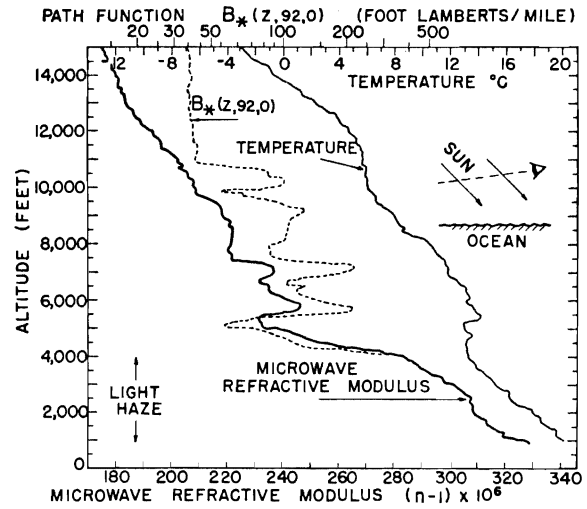


FIG. 9. Profiles of microwave refractive modulus, path function, and free air temperature. Flight 77. Correlations between the profiles of microwave refractive modulus and path function can be noted.

be horizontal strata of great extent which characterize the air mass. Such strata must also be observable in terms of nonoptical meteorological phenomena. Initial attempts to discover correlations with the temperature and humidity profiles produced routinely by the meteorological services from radiosonde observations met with failure. This was attributed to the long time constant associated with the humidity sensing elements carried by the balloons. It was believed necessary to measure the humidity profile during the controlled rapid descent of the B-29 with equipment having a fractional second time constant in order to record faithfully the presence of strata only a few feet in thickness. This was accomplished by means of an airborne microwave refractometer<sup>6</sup> of the type described by Crain and Deam.<sup>7</sup> The microwave refractive index recorded by this instrument is governed primarily by the water vapor concentration in the atmosphere; it is related to pressure, temperature, and the partial pressure of water vapor by an equation derived by Debye and discussed by numerous authors in connection with microwave propagation.<sup>8</sup> An expression for the partial pressure of water vapor obtained from the usual microwave approximation of Debye's equation is:

$$\epsilon = \frac{(\text{microwave refractive modulus})(\text{Kelvin temp.})^2}{(77.6)(4810)} - \frac{(\text{total pressure})(\text{Kelvin temp.})}{4810}$$

<sup>6</sup> The authors are indebted to Mr. Thomas J. Obst, Director of Range Development, Patrick Air Force Base, for suggesting the use of the microwave refractometer, and for arranging for the availability of this equipment for the flight experiment described in this paper.

<sup>7</sup> C. M. Crain and A. P. Deam, *Rev. Sci. Instr.* **23**, 149 (1953).

<sup>8</sup> E. K. Smith, Jr., and S. Weintraub, *J. Research Natl. Bur. Standards* **50**, 39 (1953).

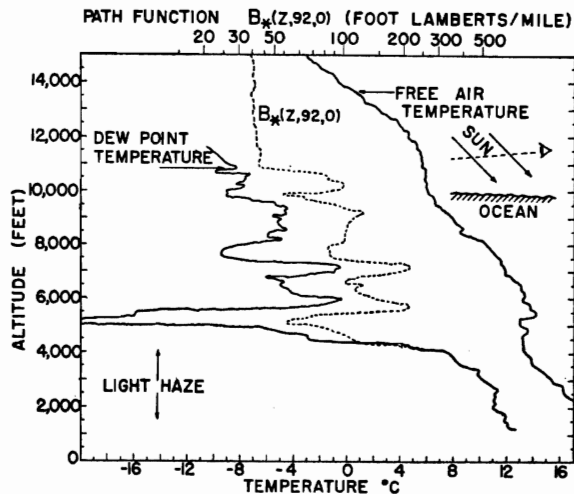


FIG. 10. Profile of dew point temperature calculated by means of Debye's equation from the profile of microwave refractive modulus in Fig. 9. Profiles of path function and free air temperature are identical with those in Fig. 9. Correlations between profiles of dew point temperature and path function are obvious.

In this equation  $\epsilon$  is in millibars, the Kelvin temperature is of the stratum, the total pressure is in millibars, and the *microwave refractive modulus* of the stratum for microwaves is defined by the expression  $(n-1) 10^6$ , where  $n$  is the refractive index of the stratum.

An Air Force C-131 equipped with a microwave refractometer flew in formation with the B-29 throughout the descent during which the optical data reported in this paper was secured. The resulting profile of microwave refractive modulus is shown in Fig. 9. The profile of horizontal path function from Fig. 5 also appears in Fig. 9 for purposes of comparison.

Debye's equation was used to calculate a humidity profile from the microwave data. This profile, expressed in terms of dew-point temperature, is given in Fig. 10. The close correlation between humidity and path function is obvious.

The following speculations on the reasons for the observed correlation are offered: In terms of visible

light water vapor exhibits virtually no absorption and it contributed only molecular scattering, the magnitude of which is too small to be responsible for the observed effects. The atmosphere invariably contains, however, suspended material such as sea-salt ions, silica, ammonia, or oxides of nitrogen and sulfur which can form condensation nuclei for water droplets. A tenuous haze of these tiny droplets will form in any stratum having a water vapor content above some critical minimum. These droplets will grow until the vapor pressure just outside the curved surface of the drop equals the partial pressure of water vapor in the surrounding air.<sup>9</sup> Liquid droplets ranging from  $4 \times 10^{-7}$  to more than  $10^{-4}$  cm are known to be present in the atmosphere.<sup>10</sup> In the case of spherical water droplets small in diameter compared with a wavelength of light that component of the scattering coefficient which is due to droplets increases as the sixth power of their diameter,<sup>11</sup> assuming the number of droplets per unit of volume to remain fixed. In view of this, the observed correlation between the path function and the humidity within tenuous haze layers appears to be understandable.

#### ACKNOWLEDGMENTS

The number of individuals involved in an experimental program of the complexity, scope, and duration of the flight research partially described by this paper is too great to be listed properly here. Special mention should be made, however, of the technical contributions of Brig. Gen. Victor A. Byrnes, USAF, through whose efforts the program was initiated; Lt. Col. George E. Long, USAF; Major Joseph X. Brennan, USAF; and research pilot Capt. Robert L. Baron, USAF. Important contributions to the detailed design of the apparatus were made by John M. Hood, Roswell W. Austin, W. Joseph Woodside, Thomas H. Glenn, Romuald Anthony, Merrill D. Hobt, and David J. A. Hooton.

<sup>9</sup> W. E. K. Middleton, *Vision through the Atmosphere* (Toronto Press, Toronto, 1952), Chap. 3.

<sup>10</sup> C. Junge, *Nuclei of Atmospheric Condensation*, Compendium of Meteorology (American Society for Metals, Cleveland, 1951).

<sup>11</sup> Lord Rayleigh, Proc. Roy. Soc. (London) A90, 219 (1914).

October 1960  
Contract NObs-72039  
Task 5  
Report No. 5-11

MEASUREMENTS OF THE TRANSMISSION OF LIGHT  
FROM AN UNDERWATER POINT SOURCE

By

S. Q. Duntley

1. INTRODUCTION AND SUMMARY

This report describes underwater measurements of the transmission of light from a submerged uniform point source and compares these data with the predictions of certain simple equations. Although the data relate only to a single example of natural water they conform with certain general principles, so that applicability of the results to most natural waters is probable.



## 2. THE EXPERIMENT

The experiment was conducted in Lake Winnepesaukee, New Hampshire during August 1959. A photoelectric irradiance photometer was mounted at an underwater window of an anchored, floating barge. A train of black-painted rafts, each ten feet long, was attached to the barge in front of the photometer window, as shown in Figure 1. These rafts served to support the light source at selected distances from the photometer and to also eliminate specular reflection at the water surface. The measurements were made on a moonless night when no ambient light was detectable by the photometer. Photometric photographs were also made from the underwater window in order to measure the apparent radiance of the source.

### 2.1 The Light Source

The source of light was a 1000 watt incandescent "diving lamp" manufactured by the General Electric Company. It was operated at rated current and voltage through a Sorenson model 3000 S regulator. The lamp, designed for underwater burning, had a spherical envelope 3 inches in diameter. It was spray-painted with W. P. Fuller No. 7786 gloss white lacquer in order to produce a uniform translucent white covering. After being painted, the lamp was found to produce the same radiant intensity in all directions to within  $\pm 7$  percent except toward the base, which was always turned away from the photometer. Provision was made for mounting the lamp beneath any selected raft

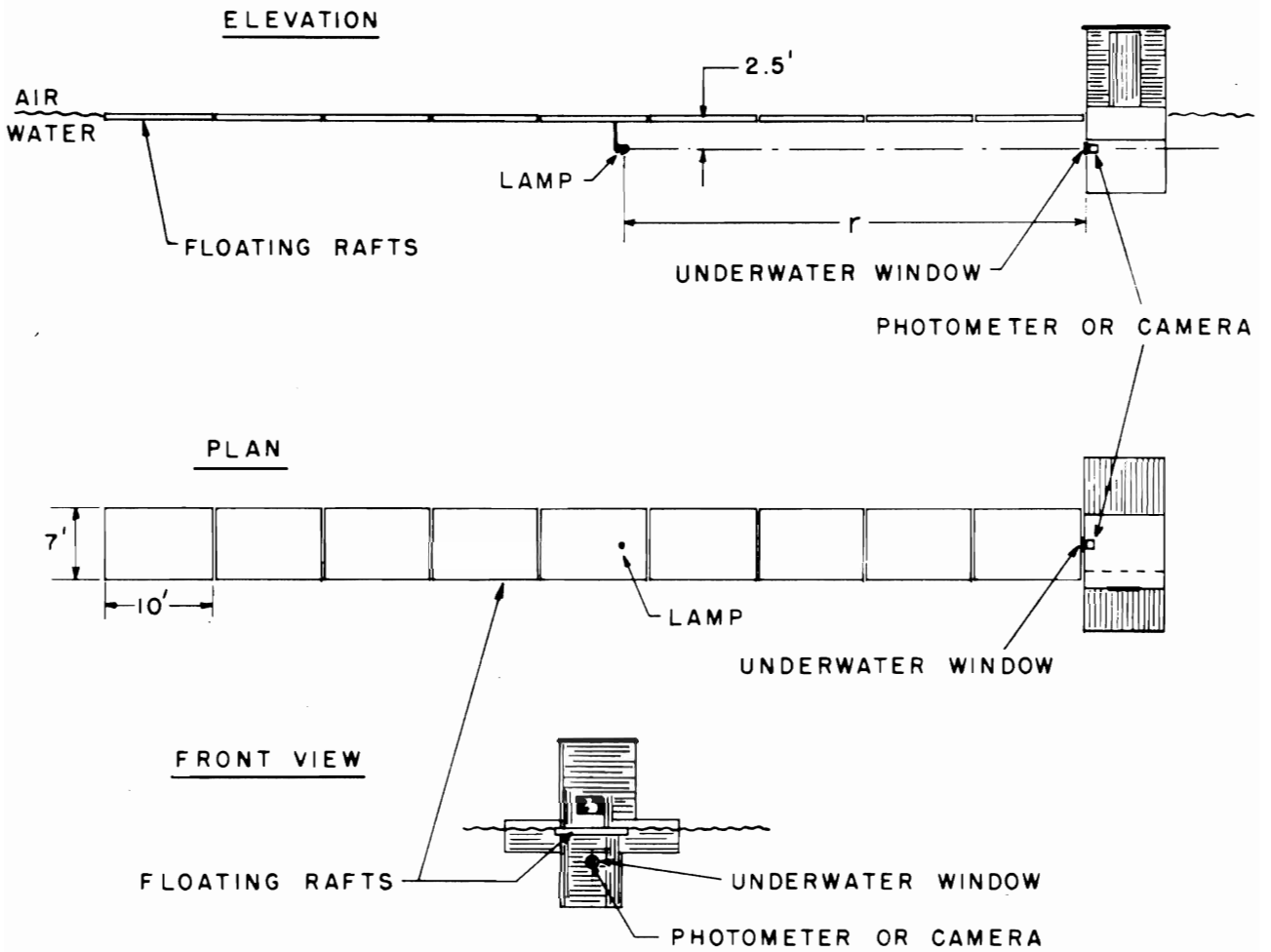


FIGURE 1

by means of a vertical pipe fitted at its lower end with a right-angle elbow to hold the lamp with its base horizontal. The depth of the lamp was always 30 inches. This depth corresponded with the center of the observation window in the barge.

## 2.2 The Irradiance Photometer

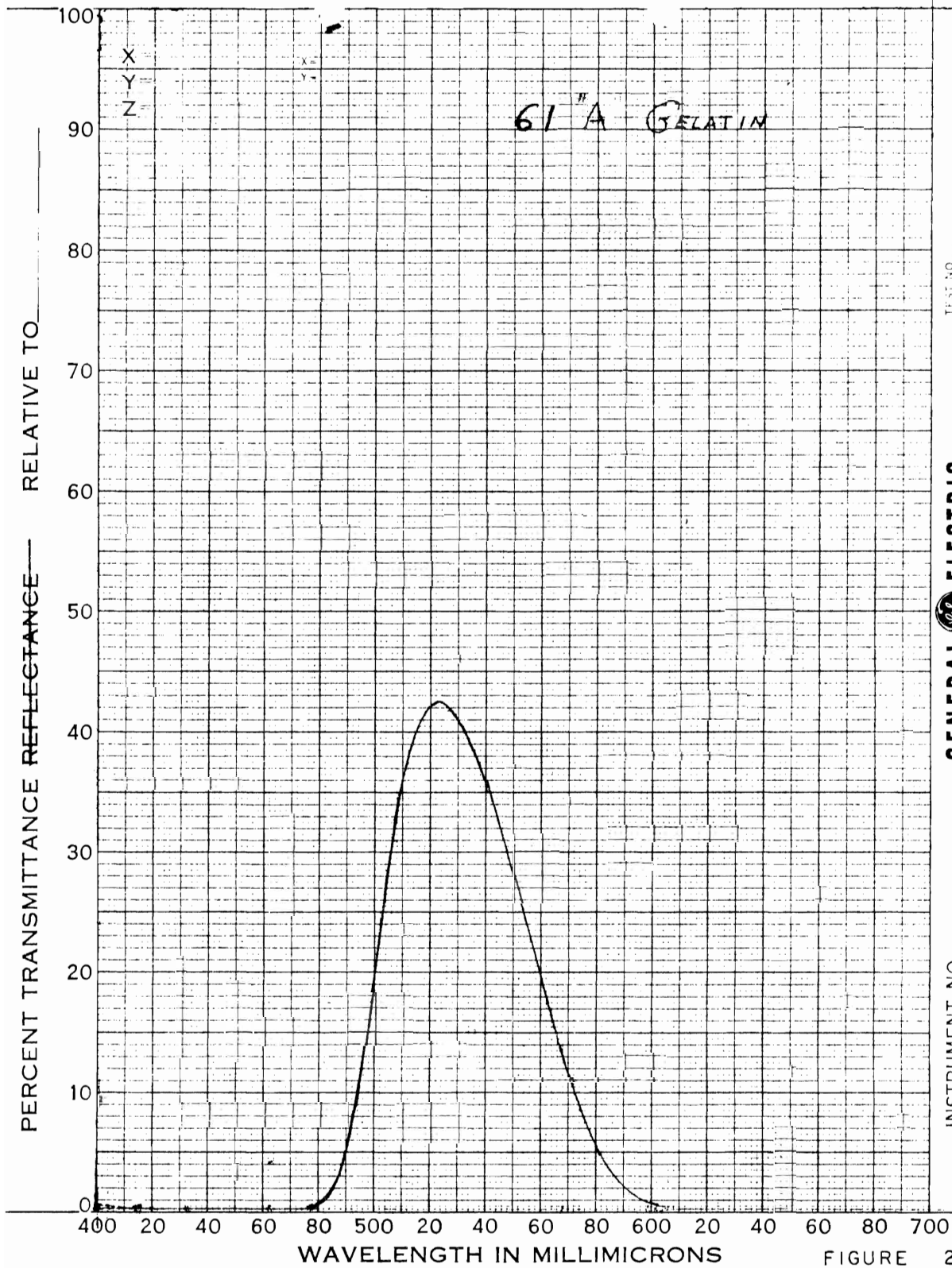
The irradiance photometer consisted (1) of a sheet of translucent white plastic mounted in the water just outside the barge window and (2) a selected 931-A multiplier phototube in a light-tight metal housing placed just inside the barge window. An aperture in the housing admitted light from the rear surface of the white plastic sheet to the phototube. Neutral filters, made from pieces of uniformly fogged photographic film, were inserted as necessary between the photocell housing and the window in order to keep the photoelectric readings on scale. The multiplier phototube was connected to a Sweet-type 4-cycle logarithmic photometer circuit which had been linearized to within  $\pm 0.02$  logarithmic units by means of a standard lamp and an inverse-square-law attenuator. A Brown strip-chart recording potentiometer was used to record the data. The strip-charts were read with a specially constructed rule embodying the detailed calibration data for the photometer. The reproducibility of the photometer and the stability of its calibration was such that the over-all photometric precision is believed to have been approximately  $\pm 1$  percent except at the lowest light levels where noise was appreciable.

### 2.3 The Color Filter

A Wratten No. 61 gelatin filter was fastened to the surface of the 931-A multiplier phototube in order to limit the spectral response of the photometer to a narrow band in the green portion of the spectrum, as shown by Figure 2. This filter was chosen in the belief that the water exhibited minimum absorption at the wavelength interval it transmits. A duplicate filter, mounted in B glass, was used with the camera described in the following section.

### 2.4 The Camera

A Zeiss Contax III camera fitted with an F/1.5 Zeiss Summar lens of 5.0 centimeters focal length was used as a radiance photometer to measure the apparent radiance of the submerged spherical lamp. Eastman Plus X 35 millimeter film having Emulsion No. 5061-64-16A was used. It was developed for 10.5 minutes in D-76 at  $68^{\circ} \pm 0.5^{\circ}\text{F}$  in a Nikor tank with minor agitation and jar at 30 second intervals in order to produce unity gamma as read on the high-resolution projection densitometer which was used to evaluate the negatives. A Wratten No. 61 filter was used on the camera at all times. Sensitometric calibration was by means of photography in air of a 24-step gray scale prepared from specially formulated, spectrophotometrically neutral gray paints. The gray scale steps, each 2" x 3", were separated by 0.06 reflection density units as measured by a photoelectric telephotometer located



TEST NO. \_\_\_\_\_  
 BY \_\_\_\_\_  
 DATE \_\_\_\_\_

INSTRUMENT NO. \_\_\_\_\_  
**GENERAL ELECTRIC**  
**RECORDING SPECTROPHOTOMETER**

N. P. 62581

FIGURE 2

at the camera position, approximately 20 feet from the gray scale. The sensitometric calibration exposures were made before and after the experiment; all of the photographic data given in this report were from a single roll of film. The effect of shutter speed on the shape of the characteristic curve of the film was investigated independently and found to be negligible.

#### 2.41 Shutter Calibration

The exposure times in the experiment described in this report varied from 1.75 milliseconds to 180,000 milliseconds. The longer intervals were timed with a stop watch but the shorter were produced by the camera shutter mechanism. In preparation for the experiment, the camera was sent to the Zeiss service station in New York for shutter lubrication and overhaul. The performance of the shutter was then studied by means of a high precision oscillographic technique. It was found to be reproducible to within  $\pm$  2 percent at the center of the field with mean values of 1.75, 3.0, 6.0, 10.0, 30, 52, 112, 175, 420, and 4000 milliseconds respectively at the 10 different shutter speed settings.

## 2.5 Minimization of Reflection Effects

An optically boundless, homogeneous body of water with no reflecting surfaces to affect the light-field produced by the submerged lamp is required for the experiment described by this report. This condition was approximated as closely as practical limitation permitted. The available barge had its observation window 2.5 feet beneath the water surface and only horizontal or near-horizontal viewing was possible. The lamp, therefore, was held at a depth of 2.5 feet. Reflection effects were minimized and, it is believed, adequately eliminated (1) by providing a "roof" of floating rafts to eliminate the air-water boundary and (2) by painting the under surfaces of these rafts and the side of the barge with matte black paint having a submerged reflectance of approximately 1.5 percent, a value chosen to match the measured reflectance function of the water. The visual impression gained by looking out through the barge window was of a highly uniform and symmetric light field with no evidence of specular glints or other unwanted reflected light.

## 2.6 Experimental Procedure

Photoelectric irradiance data were obtained with the lamp at 10", 4', 7'4", 10'6", and at (approximately) 10 foot intervals out to 168'. Photographs of the lamp were made at a distance of 10.5 feet and at ten foot intervals out to 80.5 feet, beyond which photography was not practicable.

### 2.7 Apparent Radiance of the Lamp

Data on the apparent radiance of the lamp at various distances are shown in Figure 3. These data were obtained by photographic photometry. In most cases two or three exposure times differing by 5 or 10 fold were used at each lamp distance and the resulting points are plotted in the figure. A small numeral 2 beside a point indicates that identical values of apparent radiance were obtained from negatives made with two different exposure times. It is interesting to note that exposure time ranged from 1.75 milliseconds at 10.5 feet to 180,000 milliseconds at 80.5 feet. Extremely calm water conditions were required in order to obtain meaningful photographs at the longer exposures.

Figure 3 is semi-logarithmic. The close fit of the data to a straight line on this plot supports the hypothesis that the apparent radiance of the lamp is attenuated exponentially, as in the equation

$$N_r = N_o e^{-\alpha r} \quad (1)$$

where  $N_r$  is the apparent radiance at distance  $r$ ,  $N_o$  is the inherent radiance of the lamp surface, and  $\alpha$  is the attenuation coefficient for apparent radiance. In Figure 3 a straight line representing  $\alpha = 0.200$  natural log-units per foot is drawn near the data points.



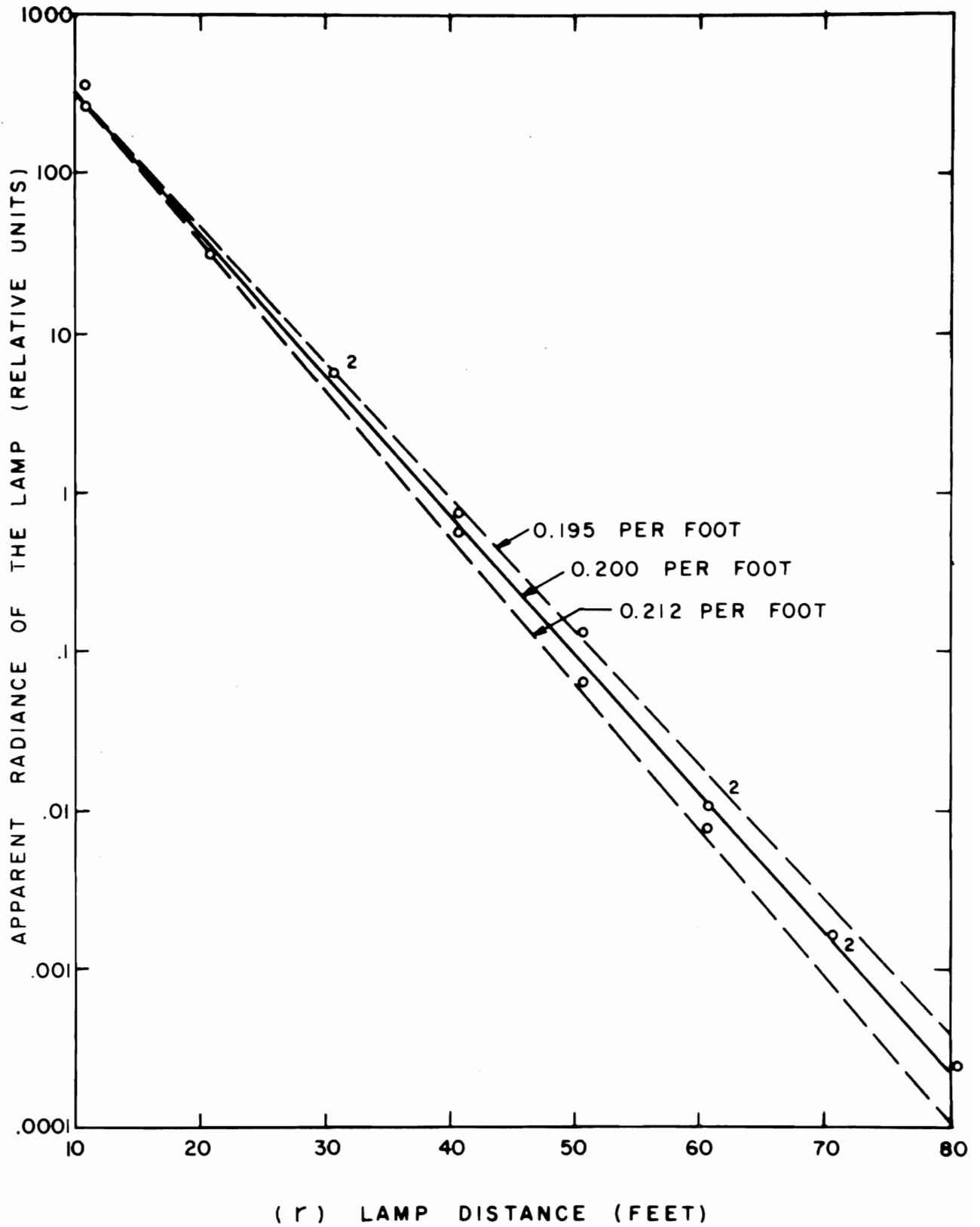


FIGURE 3

## 2.71 Comparison with Hydrophotometer Data

Just prior to the photometric experiments, which lasted throughout the night, a hydrophotometer was used to measure the attenuation coefficient for a highly collimated beam of light. The measured value of this attenuation coefficient was 0.212 natural log-units per foot. The lower dashed line in Figure 3 depicts this rate of attenuation.

The hydrophotometer was used again after the photometric experiments had been completed and an attenuation coefficient of 0.195 natural log-units per foot was measured. This value is represented by the upper dashed line in Figure 3. The small decrease in attenuation coefficient may represent an instrumental variability or it may signify that the standing crop of marine organisms diminished slightly as the water temperature fell during the night.

It is interesting to note that virtually all of the apparent radiance values fall between the dashed lines. This strongly supports the hypotheses that the contribution of multiply scattered light to the apparent radiance of the lamp is negligible and that the mono-path (i.e., non-scattered) component  $H_r^0$  of irradiance produced by the submerged lamp is given by the relation

$$H_r^0 = \frac{J}{r^2} e^{-ar}, \quad (2)$$

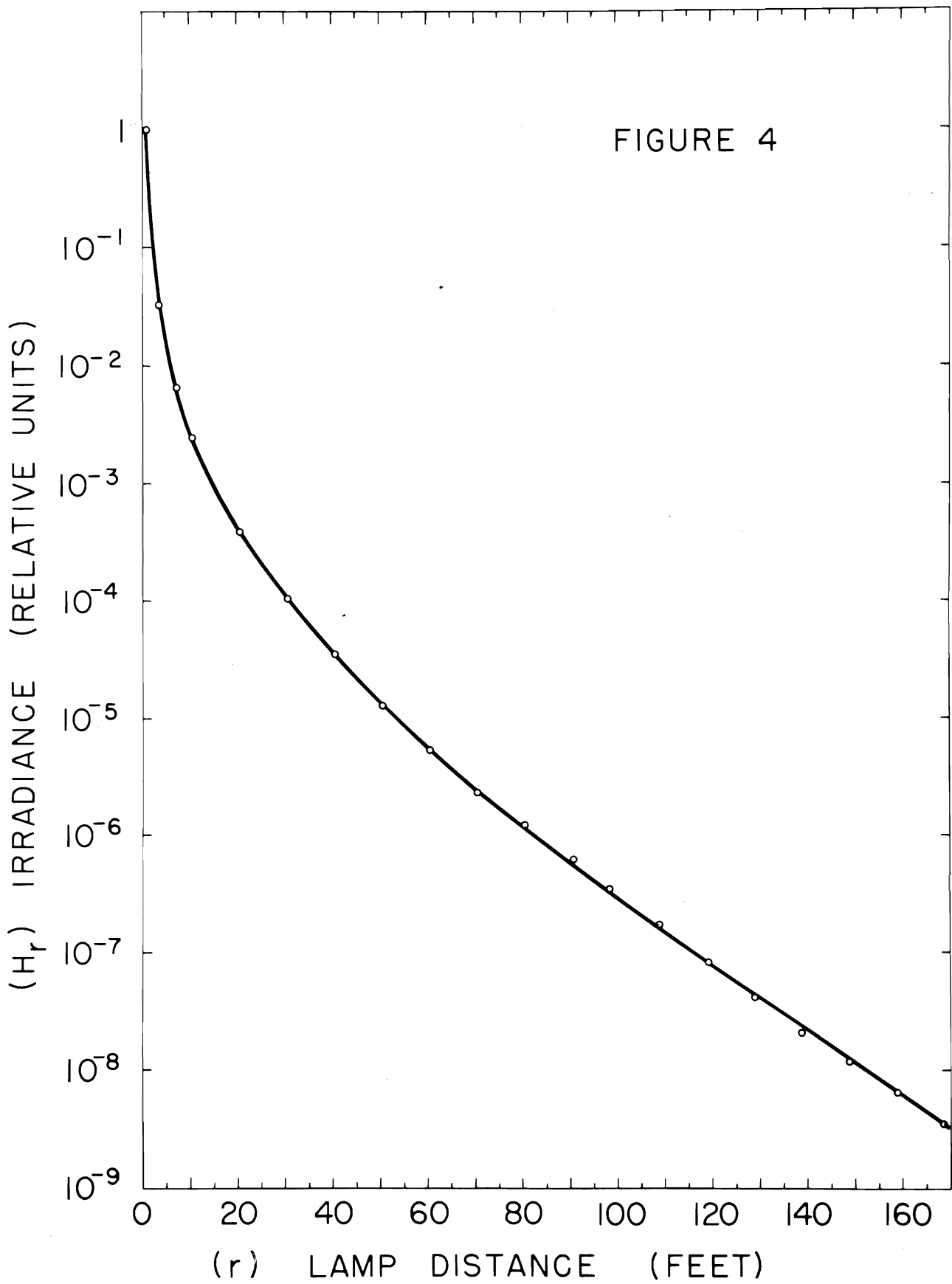
where the irradiance  $H_r^O$  is on a plane perpendicular to direction of the flux at distance  $r$  from the lamp,  $J$  is the radiant intensity of the lamp in the direction of the observation, and  $\alpha$  is the attenuation coefficient for collimated light as measured by a hydro-photometer.

The component  $H_r^*$  of irradiance due to multi-path transmission (i.e., multiply scattered light) can readily be deduced from the irradiance measurements described in the following section since the total irradiance  $H_r$  must be the sum of the mono-path and multi-path components; that is,

$$H_r = H_r^O + H_r^* . \quad (3)$$

## 2.8 Irradiance Produced by the Lamp

The irradiance produced by the underwater lamp at various distances was measured by means of the photoelectric irradiance photometer described in section 2.2 of this report. The data are plotted as crosses (+) in Figure 4. A smooth curve was fitted to these points by a least-squares procedure and appears as the solid line in Figures 4 and 5. The primary goal of the research described by this report was to evolve a simple equation capable of describing this curve in terms of measurable inherent or apparent optical properties of the water. Progress toward that goal is described in the following section.



### 3. THEORY

#### 3.1 Rigorous Methods

A rigorous treatment of the submerged point source is an imposing theoretical problem in the domain of radiative transfer. Such a treatment has been set forth by Preisendorfer using his discrete-space method.<sup>1</sup> The resulting solution is iterative in character and application of it to practical problems requires the use of a large electronic computer. A program for the IBM 7090 at Wright-Patterson Air Force Base is soon to be prepared by the Air Force on the basis of Preisendorfer's theory, but even after this advanced technique is available, a simple, approximate, theoretical or empirical equation in closed form will be of use.

#### 3.2 The Diffusion Theory Approximation

Theoreticians concerned with neutron transport and related phenomena have used diffusion theory to derive relations which are adaptable to multipath (i.e., multiply scattered) transmission by water. Most of these derivations assume isotropic scattering, a very improper assumption with respect to most natural waters, wherein the volume scattering function may range over more than 1000 to 1. The diffusion theory relation for irradiance has been found, however, to fit the measured data closely at large distances from the source and,

---

<sup>1</sup> Preisendorfer, R. W., "Two Fundamental Methods of Solving Point-Source Problems in Discrete-Space Radiative Transfer Theory," SIO Ref. No. 59-71, December 1959.

as will be shown later in this section, empirical modifications can be devised which extend the usefulness of this mathematical model to all source distances.

### 3.2.1 Derivation

The diffusion theory derivation for the flux produced by multiple isotropic scattering from a distant uniform point source appears in various books. For example, equation (5.49.1) on page 107 of Glastone and Edlund's, "Elements of Nuclear Reactor Theory," (New York, von Nostrand's Press, 1952) is  $\phi = e^{-Kr}/4\pi D r$ . Following suggestions by Preisendorfer, this relation can be expressed in the notation of hydrologic optics<sup>2</sup> as follows:

$$h(r,+) + h(r,-) = D(r,+)H(r,+) + D(r,-)H(r,-) = \frac{J_0 e^{-K(r,+)r}}{4\pi a/K^2(r,+)}$$

where  $K^2(r,+) = D(r,+)a[\bar{D}(r,+)a + 2b]$

but  $H(r,-)$  and  $b$  can be neglected since in most natural waters

$H(r,-) \cong 0.02 H(r,+)$  and  $b \cong 0.02 a$ . Thus,

$$H(r,+) = \frac{J_0 e^{-K(r,+)r}}{4\pi a} K(r,+) \quad (4)$$

If, at large  $r$ ,  $K(r,+)$  is approximately independent of  $r$ ,

---

<sup>2</sup> Preisendorfer, R. W. and Tyler, J. E., "The Measurement of Light in Natural Waters, Radiometric Concepts and Optical Properties," SIO Ref. No. 58-69, 17 November 1958.

then the diffusion theory approximation for the irradiance produced by a distant uniform point may be written

$$H_r^* = JK (4\pi r)^{-1} e^{-Kr}, \quad (5)$$

where the attenuation coefficient  $K$  is for some configuration of diffused light.

### 3.2.2 Comparison with Experiment

In view of the algebraic form of equation (5), the smoothed irradiance data which form the basis of the curve in Figure 4 were multiplied by  $r$  and replotted. At the longer distances this semi-logarithmic plot was an excellent straight line with a slope of 0.0570 natural log-units per foot. This value of  $K$  was also calculated algebraically from the relation:

$$\frac{H_1^*}{H_2^*} = \frac{r_2}{r_1} e^{-K(r_1 - r_2)} \quad (6)$$

which results from writing equation (5) successively for two distances, 1 and 2, dividing one of these equations by the other.

Equations (2) and (5) were combined with equation (3) as follows:

$$H_r = J \frac{e^{-ar}}{r^2} + J \frac{Ke^{-Kr}}{4\pi r} \quad (7)$$

The constants  $\alpha = 0.20$  per foot and  $K = 0.057$  per foot were inserted and  $J$  was arbitrarily assigned to make the calculated value of  $H_r$  agree with the photoelectric data at long range. Values of  $H_r$  at various distances were then computed and are plotted as solid dots in Figure 5. The solid curve in Figure 5 is identical with that in Figure 4 and represents the smoothed irradiance data.

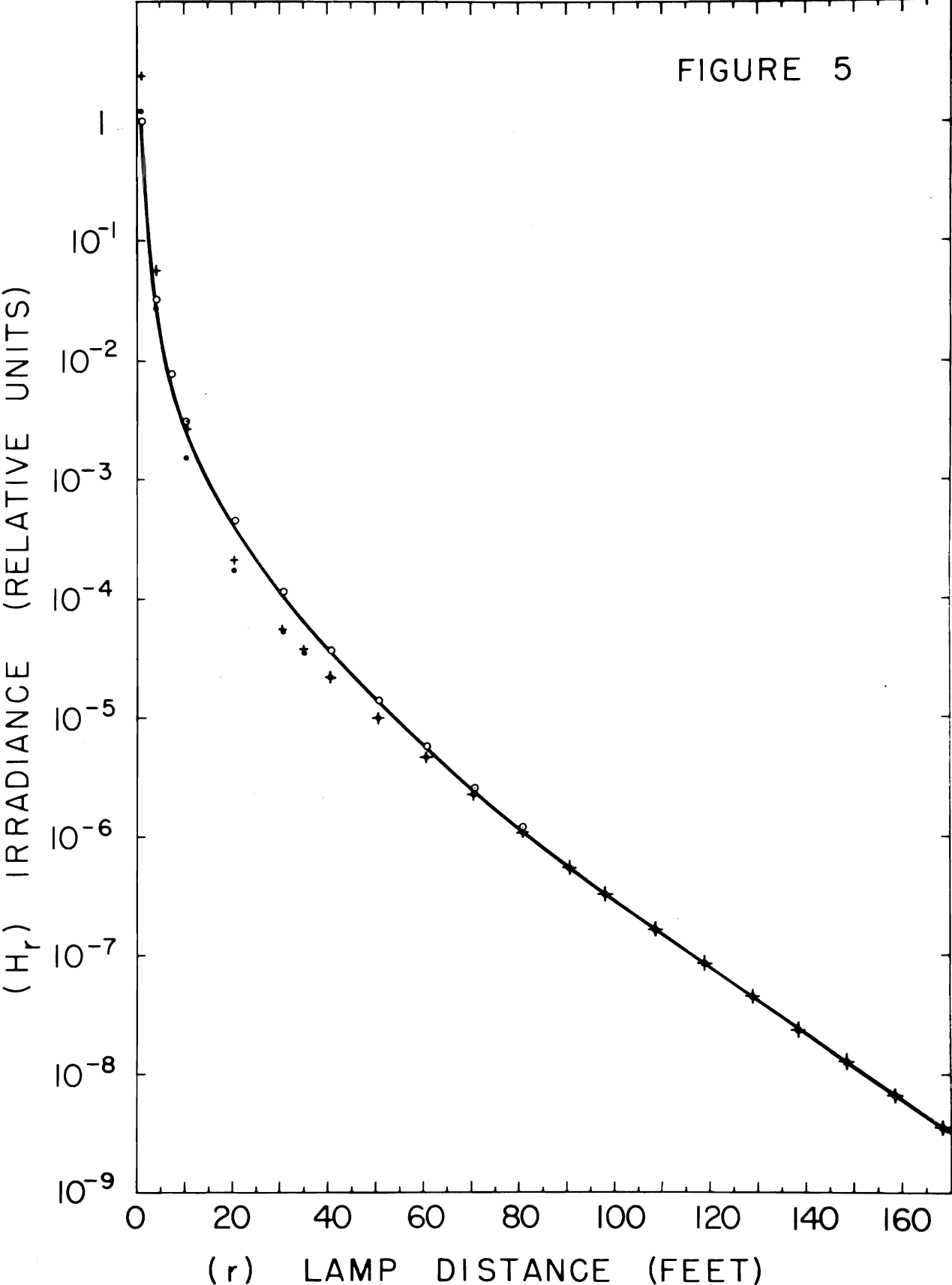
The agreement of the solid dots with the data curve in Figure 5 is most encouraging, although they predict less irradiance than was measured at intermediate distances.

### 3.2.3 Comparison of $K$ with other Attenuation Coefficients

Thirty-six hours after the irradiance and apparent source radiance data were obtained calm, overcast, daylight conditions permitted three apparent optical properties of the water  $k$ ,  $K(+)$ , and  $K(-)$  to be measured by means of appropriate submersible photoelectric irradiance photometers equipped with Wratten No. 61 gelatin filters. At that time the hydrophotometer indicated an attenuation coefficient  $\alpha = 0.179$  natural log-units per foot. The measured values of the three diffuse attenuation coefficients for overcast daylight at a depth of 2.5 feet were  $k = 0.0633$  natural log-units per foot,  $K(+)$  = 0.0512 natural log-units per foot, and  $K(-)$  = 0.0698 natural log-units per foot, respectively.



FIGURE 5



The measured attenuation coefficient for multipath transmission from the submerged point source was reported in the preceding section as  $K = 0.0570$  natural log-units per foot. This value appears to lie between  $k$  and  $K(+)$ , probably somewhat closer to  $k$ . Later experiments in other natural waters should explore this observation carefully. The finding that  $K$  and  $k$  are probably interchangeable for practical purposes is an important result of the experimental study described in this report.

### 3.3 Empirical Corrections

#### 3.3.1 Constant Factors

Trials quickly demonstrated that no constant factor applied to the second term of equation (7) will cause it to fit the data. For example, the crosses (+) in Figure 5 show how the fit is affected by changing the factor 4 to 2 in the denominator of the second term of equation (7).

#### 3.3.2 Range Dependent Corrections

A more fruitful approach was suggested by equation (4), wherein  $K(r,+)$  is dependent upon the lamp distance  $r$ . Inasmuch as  $K(r,+) = a D(r,+)$  if  $b$  is negligible, a change of  $K(r,+)$  with  $r$  should result from the gradual alteration of the directional distribution of radiance in the water as the source is approached.

In the absence of a theoretical model for the range-dependance of the distribution function  $D(r,+)$ , several empirical algebraic forms were tried. The most promising of these is represented by the equation

$$H_r = J \frac{e^{-ar}}{r^2} + J \frac{u(1+ve^{-Kr})}{4\pi r} \frac{Ke^{-w(1+ze^{-Kr})Kr}}{4\pi r} \quad (8)$$

where  $u$ ,  $v$ ,  $w$ , and  $z$  are arbitrary constants.

Numerical trials soon showed that the data could not be fitted if  $u = w$  and  $v = z$ , i.e., the attenuation factor within the exponent must differ from that without. This observation indicates that the simple concept of a single-valued, range-dependent attenuation function or distribution function is an over-simplification of the physical situation. This is not surprising in view of the complexity of Preisendorfer's rigorous theory.

Since different forms of attenuation function must be used within and without the exponential, it is believed that convenience will be served by reducing the exponent to  $Kr$ , i.e., by letting  $w = 1$  and  $z = 0$ . It is then possible to select values of  $u$  and  $v$  to produce a best fit to the experimental data. Such calculations are lengthy, and it cannot be stated with certainty that the best values of these constants was found. The best fit obtained is shown by the open circles in Figure 5. For these points,  $u = 2.5$  and  $v = 7$ .

The final empirical expression for the underwater irradiance  $H_r$  produced by a uniform submerged point source at a distance  $r$  is

$$H_r = J \frac{e^{-ar}}{r^2} + J \frac{2.5(1 + 7e^{-Kr}) Ke^{-Kr}}{4\pi r} \quad (9)$$

#### 3.4 Applicability to Other Natural Waters

Equation (9), with its constants  $u = 2.5$  and  $v = 7$ , describes data taken in only one natural water. Its applicability to other waters is unknown. Inasmuch, however, as the first term is exact and the second term is founded upon an established mathematical model, there is at least foundation for the expectation that the general form of the expression will serve as a useful approximation relation for most natural waters and the hope that the constants  $u$  and  $v$  will be insensitive to the shape of the volume scattering function.

An important next step is, obviously, to test equations (7) and (9) by means of irradiance data collected in other types of natural waters.

SIO REFERENCE 60-57

MEASUREMENTS OF THE TRANSMISSION OF LIGHT FROM  
 AN UNDERWATER SOURCE HAVING VARIABLE BEAM-SPREAD

S. Q. Duntley

1. INTRODUCTION AND SUMMARY

Measurements of the transmission of monochromatic light from a submerged uniform point source have been reported.\* The spectral irradiance  $H_r$  at any distance  $r$  from the source was found to be represented by the semi-empirical equation

$$H_r = J \frac{e^{-\alpha r}}{r^2} + J \frac{u(1 + ve^{-Kr}) Ke^{-Kr}}{4\pi r} \quad (1)$$

where  $J$  is the spectral radiant intensity,  $\alpha$  is the attenuation coefficient for non-scattered light (monopath transmission),  $K$  is the attenuation coefficient for scattered light (multipath transmission) and the empirical constants  $u$  and  $v$  have the values  $u = 2.5$  and  $v = 7$  for the data from which the equation was evolved.

The present report describes underwater measurements of the transmission of light from a submerged source of variable beam-spread. Angular beam-widths down to  $20^\circ$  were used. It was found that the irradiance due to sources producing uniform circular light beams of

---

\* Duntley, S. Q., "Measurements of the Transmission of Light from an Underwater Point Source" Report No. 5-11, Bureau of Ships, Contract NObs-72039, October 1960.

total plane angular width  $\theta \geq 20^\circ$  can be represented by equation (1) if the empirical constants  $u_\theta$  and  $v_\theta$  are, respectively,

$$u_\theta = u_{2\pi} - \frac{3}{2} \log \frac{2\pi}{\theta} \quad (2)$$

and

$$v_\theta = v_{2\pi} \left( \frac{2\pi}{\theta} \right)^{1/2}, \quad (3)$$

where  $u_{2\pi} = 2.5$  and  $v_{2\pi} = 7$  for the data from which these equations were evolved.

An important implication of the foregoing equations is that, from the standpoint of efficiency, underwater lighting systems should employ narrow-beam sources to the maximum extent practicable, even at ranges so great that the monopath transmission is negligible.

The following sections of this report describe the experiments and present the data from which equations (2) and (3) and the foregoing conclusions have been evolved.

## 2. DESCRIPTION OF THE EXPERIMENT

### 2.1 Introduction

The irradiance data discussed in this report were obtained at the Visibility Laboratory's Diamond Island Field Station in Lake Winnepesaukee, New Hampshire where a unique combination of favorable experimental conditions permitted the work to be performed with simple apparatus and at low cost. A photoelectric radiance photometer was mounted at an underwater window of an anchored, floating barge which was specially constructed at the field station in 1948 for use in underwater research. A train of nine black-painted wooden rafts, each ten feet long, was attached to the barge in front of the photometer window, as shown in Figure 1. These rafts served to support the light source at selected distances from the photometer and also to eliminate specular reflection at the water surface. The measurements were made on a moonless night when no ambient light was detectable by the photometer.

### 2.2 The Underwater Light Source

A variable beam-spread light source was constructed by enclosing a 1000 watt incandescent "diving lamp" manufactured by the General Electric Company by a rectangular box as shown in Figure 2. The lamp, designed for underwater burning, had a spherical envelope three inches in diameter. It was sprayed with W. P. Fuller No. 7786 gloss white lacquer in order to produce a uniform translucent white

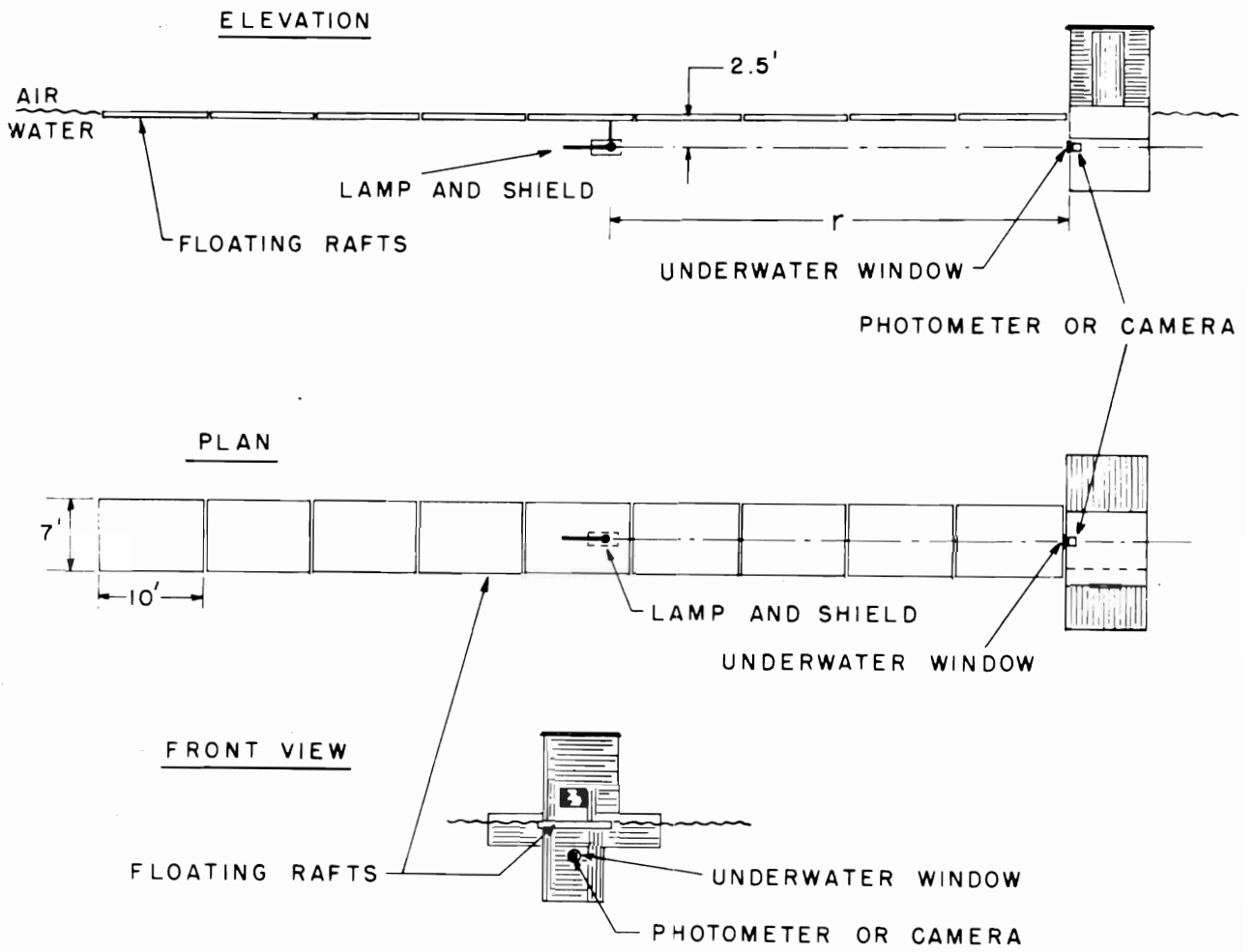


Figure 1



covering. After being painted, the lamp was found to produce the same radiant intensity in all directions to within  $\pm 7$  percent except toward the base, which was always away from the opening in the box (see Figure 2). The lamp was attached by its base to a length of hollow pipe through which the electric leads passed. The position of the lamp within the box could be adjusted by sliding the pipe through the supporting gland at the rear of the device, and the beam-spread produced by the system could thus be varied at will. The upper portion of Figure 2 indicates the lamp positions corresponding with various commonly used beam spreads. The indicated nominal values of the beam spread  $\theta$  are as measured from the center of the lamp. This geometry is illustrated by the lower portion of Figure 2, which shows that the source produced extreme rays with a spread of  $28^\circ$  when the nominal beam spread  $\theta$  was  $20^\circ$ .

Provision was made for mounting the lamp beneath any raft, i.e., at virtually any desired distance from the photometer window. The depth of the lamp was 30 inches; this depth corresponded with that of the center of the window in the barge.

The lamp was operated at rated current and voltage through a Sorenson 3000S regulator. Careful checks made with the irradiance photometer showed that the luminous output of the source was free from detectable warm-up effects, long-term, or short-term fluctuations.

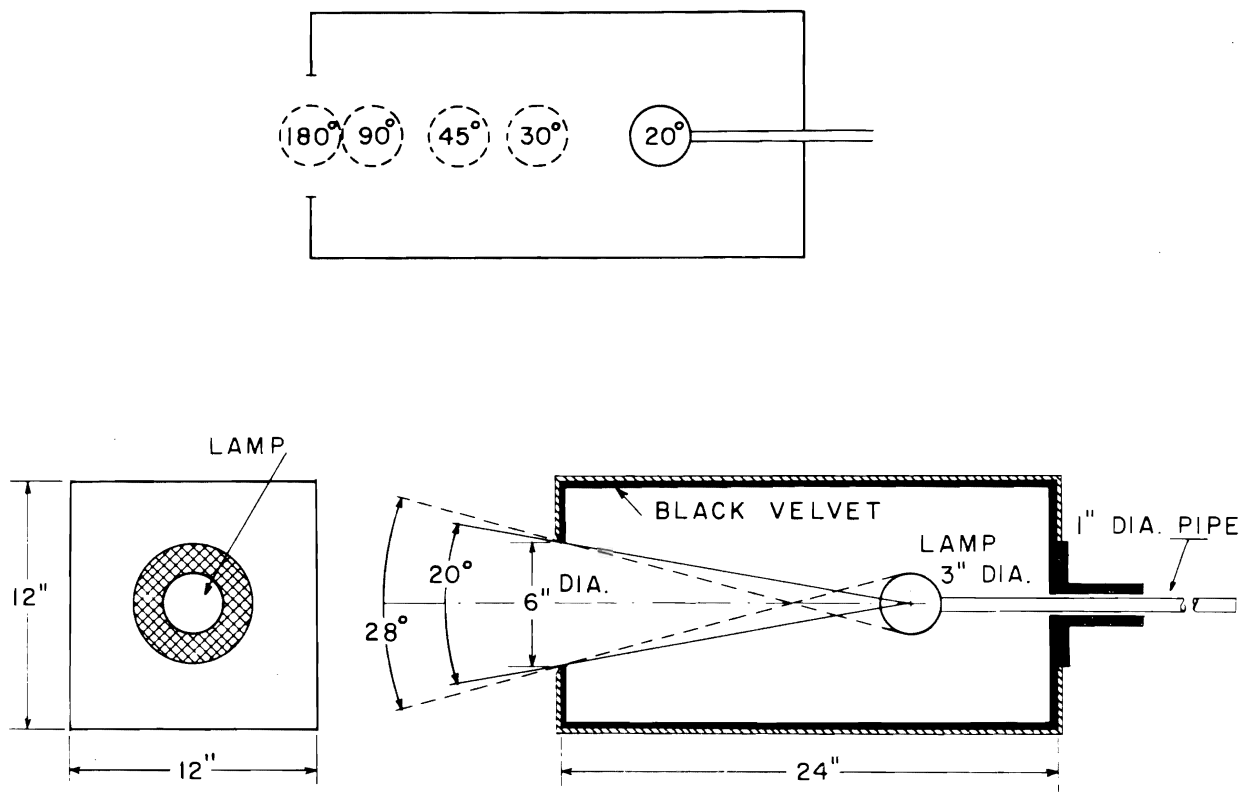


Figure 2

### 2.2.1 Minimization of Reflection Effects

An optically boundless, homogeneous body of water with no reflecting surfaces to affect the light-field produced by the submerged lamp is required for the experiment described by this report. This condition was approximated as closely as practical limitations permitted. The available barge had its observation window 2.5 feet beneath the water surface and only horizontal or near-horizontal viewing was possible. The lamp, therefore, was held at a depth of 2.5 feet. Reflection effects were minimized and, it is believed, adequately eliminated (1) by providing a "roof" of floating rafts to eliminate the air-water boundary and (2) by painting the under surfaces of these rafts and the side of the barge with matte black paint having a submerged reflectance of approximately 1.5 percent, a value chosen to match the measured reflectance function of the water. The visual impression gained by looking out through the barge window was of a highly uniform and symmetric light field with no evidence of specular glints or other unwanted reflected light.

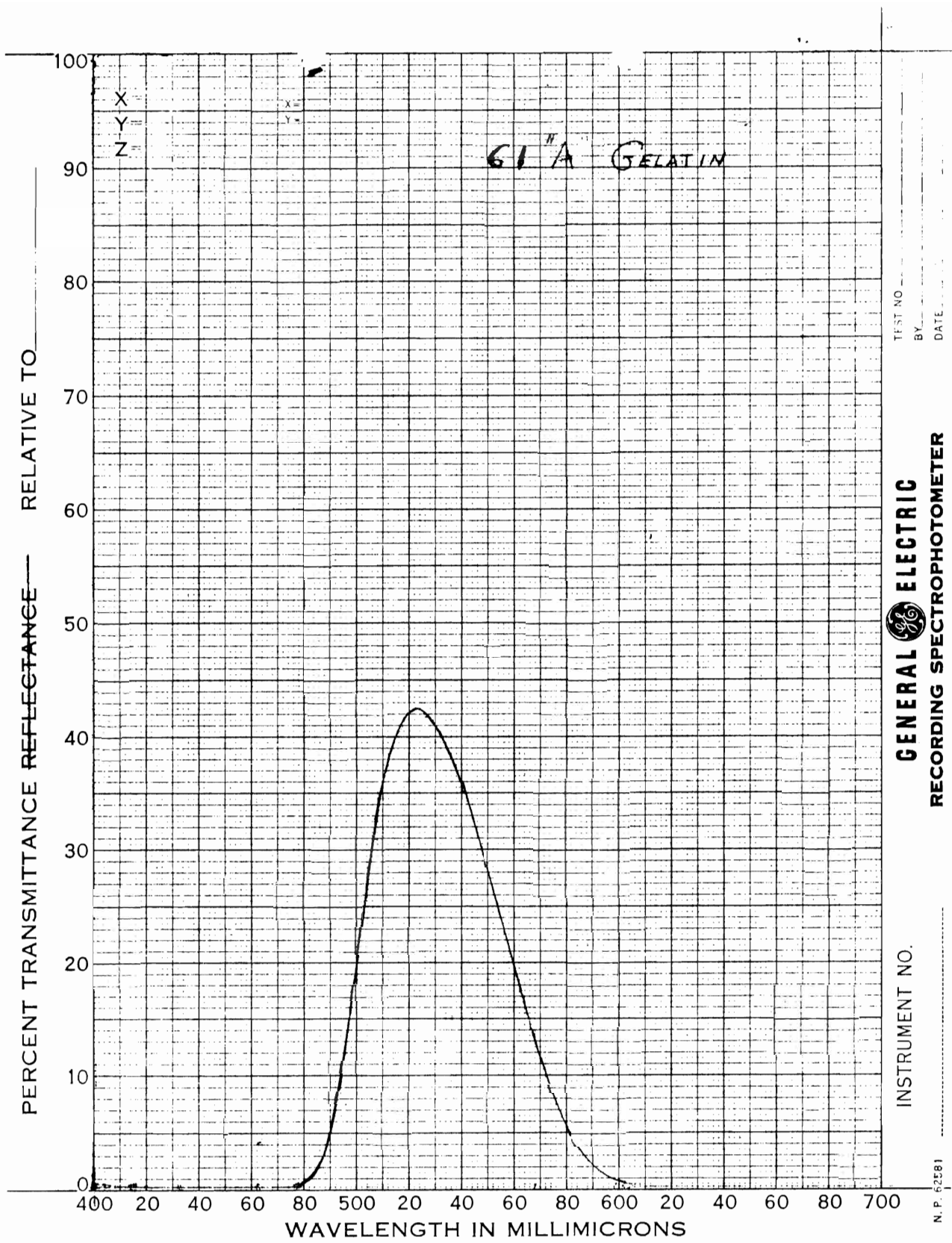
### 2.3 The Irradiance Photometer

The irradiance photometer consisted (1) of a sheet of translucent white plastic mounted in the water just outside the barge window and (2) a selected 931-A multiplier phototube in a light-tight metal housing placed just inside the barge window. An aperture in the housing admitted light from the rear surface of the white

plastic sheet to the phototube. Neutral filters, made from pieces of uniformly fogged photographic film, were inserted as necessary between the photocell housing and the window in order to keep the photoelectric readings on scale. The multiplier phototube was connected to a Sweet-type 4-cycle logarithmic photometer circuit which had been linearized to within  $\pm 0.02$  logarithmic units by means of a standard lamp and an inverse-square-law attenuator. A Brown strip-chart recording potentiometer was used to record the data. The strip-charts were read with a specially constructed rule embodying the detailed calibration data for the photometer. The reproducibility of the photometer and the stability of its calibration was such that the over-all photometric precision is believed to have been approximately  $\pm 1$  percent except at the lowest light levels where noise was appreciable.

#### 2.4 The Color Filter

A Wratten No. 61 gelatin filter was fastened to the surface of the 931-A multiplier phototube in order to limit the spectral response of the photometer to a narrow band in the green portion of the spectrum, as shown in Figure 3. This filter was chosen in the belief that the water exhibited minimum absorption at the wavelength interval it transmits.



TEST NO.  
BY  
DATE

**GENERAL ELECTRIC**  
RECORDING SPECTROPHOTOMETER

INSTRUMENT NO.

N. P. 62581

Figure 3

## 2.5 The Data

Photoelectric irradiance data were obtained with the source at 13', 23', 33', 43', 53', 63', and 73' from the photometer. At each of these distances the source was operated with beam spreads of 20°, 30°, 45°, 60°, 75°, 90°, 180°, and 360°. Unavoidable delays due to mechanical problems of several kinds, wind, rain squalls, and moonlight combined to prevent a complete run of this experiment from being made on any one of the few nights available for the work. Minor changes in the optical nature of the water occurred from night to night due, it is believed, to changes in the standing crop of organisms in the water caused primarily by variations in water temperature. The optical properties of the water were monitored by means of a hydrophotometer and a nephelometer and first order corrections were applied to the data with the intent of nullifying the small night-to-night changes. The resulting smoothed data are represented by the curves of irradiance  $H_r$  vs source distance  $r$  shown in Figure 4. Data points have been shown on the 360° curve in order to identify the source distances at which all of the data were taken. The 360° curve is the only one for which all points were obtained on a single night; it is, therefore, regarded as the most accurate of the data.

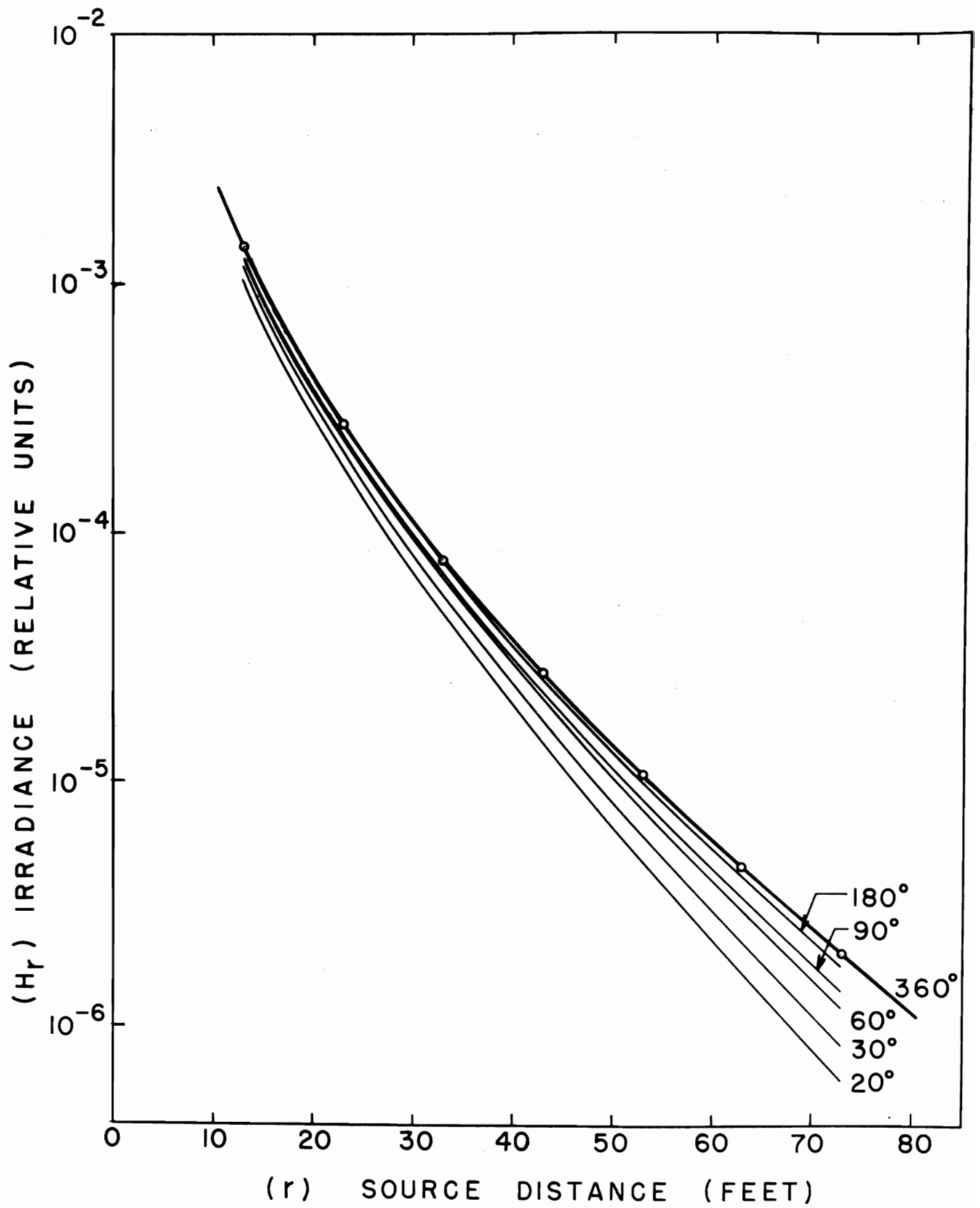


Figure 4

### 2.5.1 Efficiency

It is evident from Figure 4 that an increase in beam-spread from  $20^\circ$  to  $360^\circ$  produces only a minor increase in irradiance, particularly at small source distances. Even at 73 feet the increase in irradiance is only 5-fold. Since the radiant power (i.e., the total light) entering the water from the light source is linearly proportional to the solid angle of the beam, the 5-fold increase in irradiance at 73 feet results from a 132-fold increase in power output from the source. It is obvious, therefore, that increasing the beam-spread of the light source is a poor way to increase the irradiance on an underwater object. From the standpoint of efficiency, underwater lighting systems should employ narrow-beam sources to the maximum extent practicable, even at ranges so great that multipath (glow) transmission accounts for virtually all of the irradiance. A more quantitative discussion of this conclusion is given in Section 3.3 of this report.

### 2.5.2 Trends of the Data

The details of the curves shown in Figure 4 are better displayed by the cross-plot shown in Figure 5, which depicts the irradiance  $H_r$  at various source distances as a function of the beam-spread  $\theta$ . The circled points in this figure relate to the subject matter of Section 3.2 of this report and are of no relevance to the present discussion. The curves represent the same data shown in Figure 4.



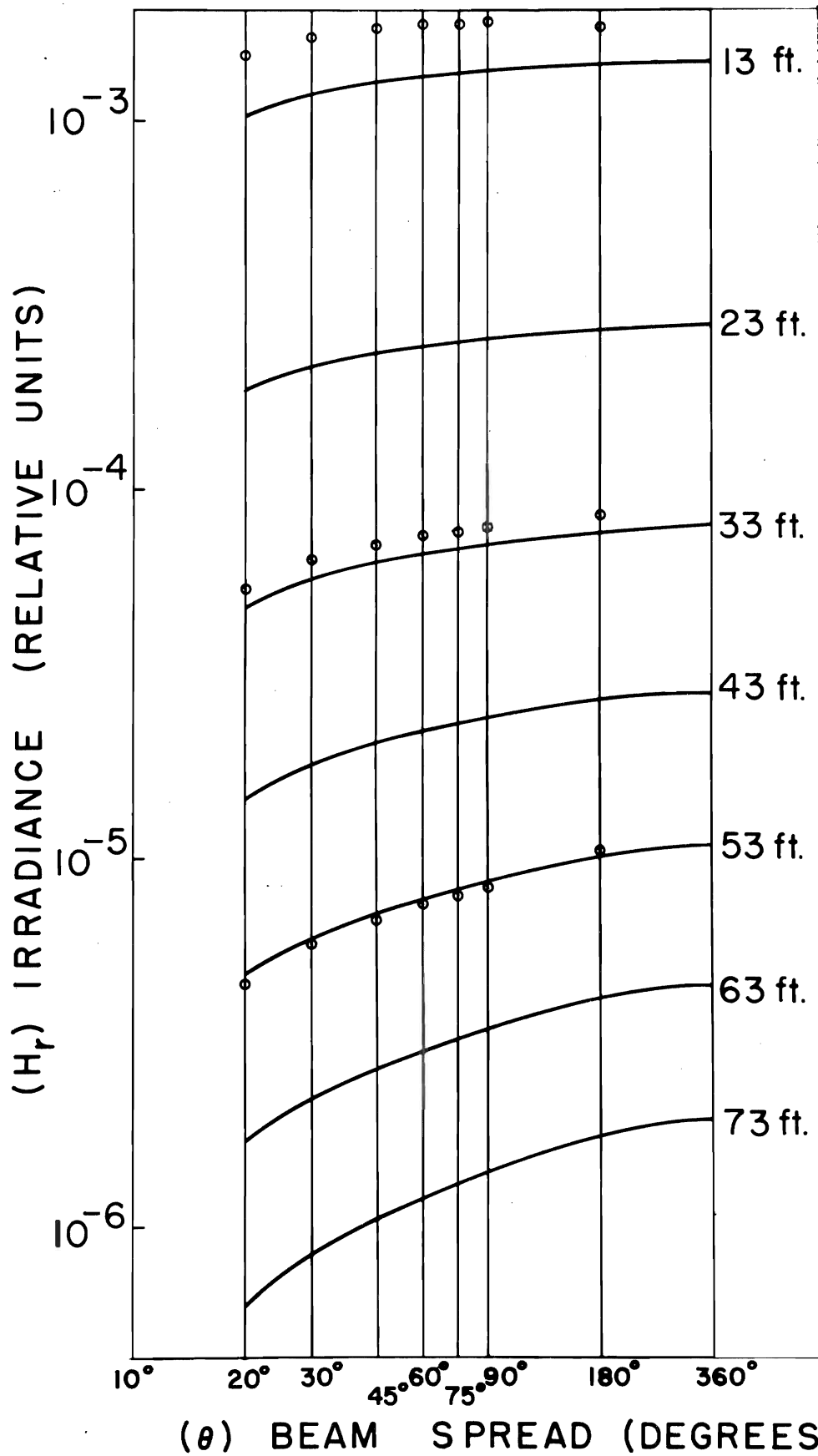
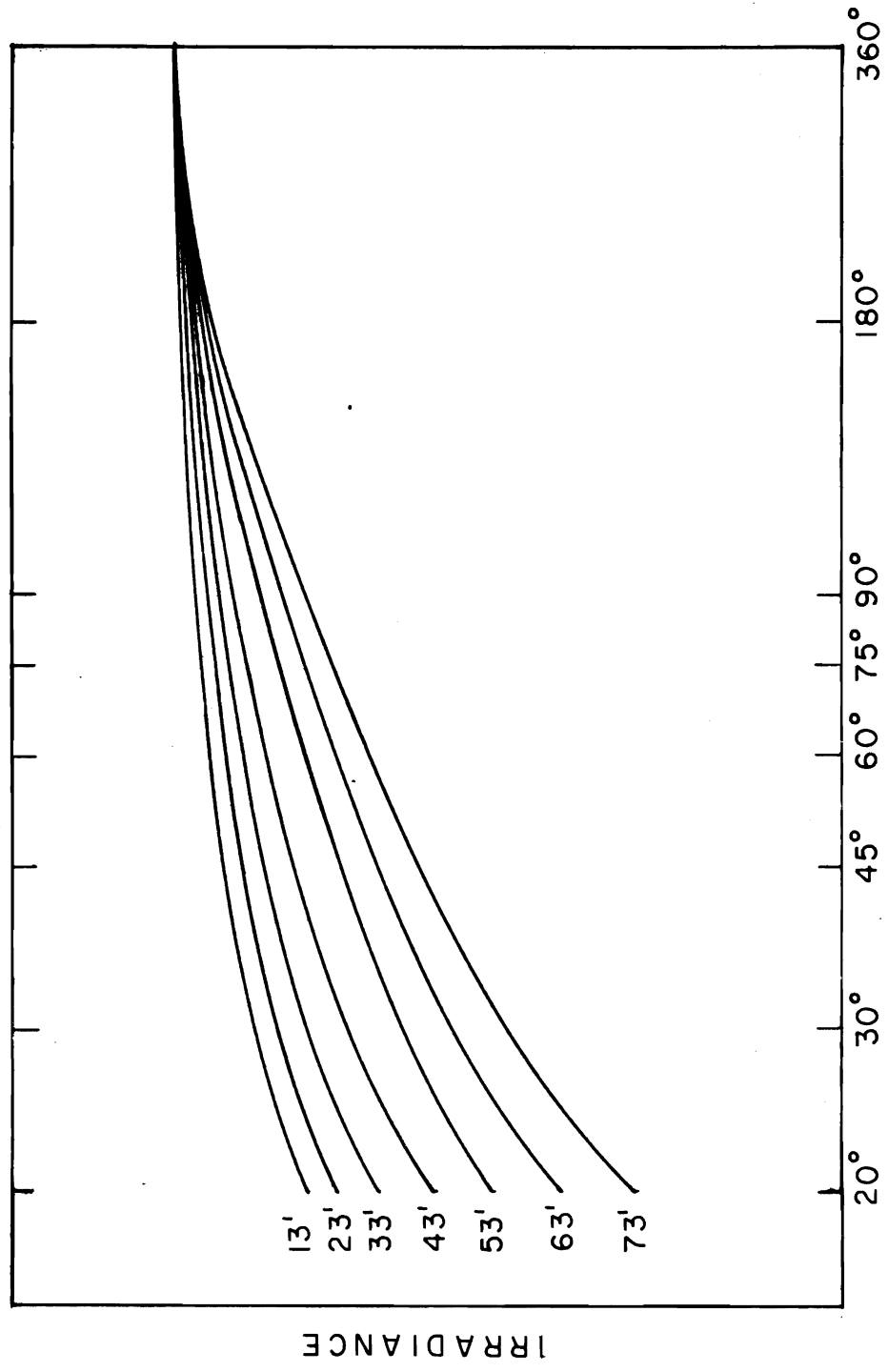


Figure 5  
APPENDIX H

It will be noted that there is a progressive change in curve shape such that the irradiance is more dependent upon beam spread at the longer distances. This progression is illustrated by Figure 6, wherein all of the curves in Figure 5 have been superimposed in such a way that they coincide at beam-spread  $360^{\circ}$ .

A primary goal of the research described by this report is the evolution of a useable empirical equation capable of specifying the irradiance produced by a distant underwater light source of restricted beam-spread in terms of measurable inherent or apparent optical properties of the water. Progress toward that goal is described in the following section.



(θ) BEAM SPREAD (DEGREES)

Figure 6

### 3. Empirical Relations

#### 3.1 Introduction

A rigorous treatment of the submerged point source has been given by Preisendorfer using his discrete-space method.<sup>1</sup> The resulting solution to this imposing problem in radiative transfer theory is iterative in character and application of it to any practical problem is a major task even for the largest electronic computers. A program for the IBM 7090 computer at Wright-Patterson Air Force Base is soon to be prepared by an Air Force contractor, but even after this advanced technique is available to predict the underwater radiance and irradiance distributions produced by any arbitrary underwater light source, a simple approximate empirical irradiance equation in closed form will be of use.

Such a relation for the special case of an unrestricted, uniform point source ( $\theta = 360^\circ$ ) has been reported.<sup>2</sup> The spectral irradiance  $H_r$  at any distance  $r$  from the source was found to be represented by the semi-empirical equation

$$H_r = J \frac{e^{-ar}}{r^2} + J \frac{u(1 + ve^{-Kr}) Ke^{-Kr}}{4\pi r} \quad (1)$$

---

<sup>1</sup> Preisendorfer, R. W., "Two Fundamental Methods of Solving Point-Source Problems in Discrete-space Radiative Transfer Theory," SIO Ref. No. 59-71, December 1959.

<sup>2</sup> Duntley, S. Q., "Measurements of the Transmission of Light from an Underwater Point Source," Contract NObs-72039, Report No. 5-11, October 1960.

The data described in Section 2 of this report provide the basis for an empirical extension of equation (1) to include the effect of restricted beam-spread  $\theta$ .

### 3.2 Effect of Beam Spread

The constants  $u$  and  $v$  in equation (1) were modified by a trial-and-error process until the equation fitted the data portrayed by Figures 4 and 5 of this report. At the conclusion of this lengthy task it was found that the required values of  $u$  and  $v$  varied in a systematic way with the beam-spread  $\theta$ . This is illustrated by figures 7 and 8, the plotted points on which represent values of  $u_{\theta}$  and  $v_{\theta}$  respectively required to make equation (1) represent the irradiance data. In each case a straight line representing a simple function of  $\theta$  has been drawn through the points. These functions are:

$$u_{\theta} = u_{2\pi} - \frac{3}{2} \log_{10} \frac{2\pi}{\theta} \quad (2)$$

and

$$v_{\theta} = v_{2\pi} \left( \frac{2\pi}{\theta} \right)^{1/2} \quad \text{respectively.} \quad (3)$$

In these equations  $u_{2\pi} = 2.5$  and  $v_{2\pi} = 7$  for figures 7 and 8.

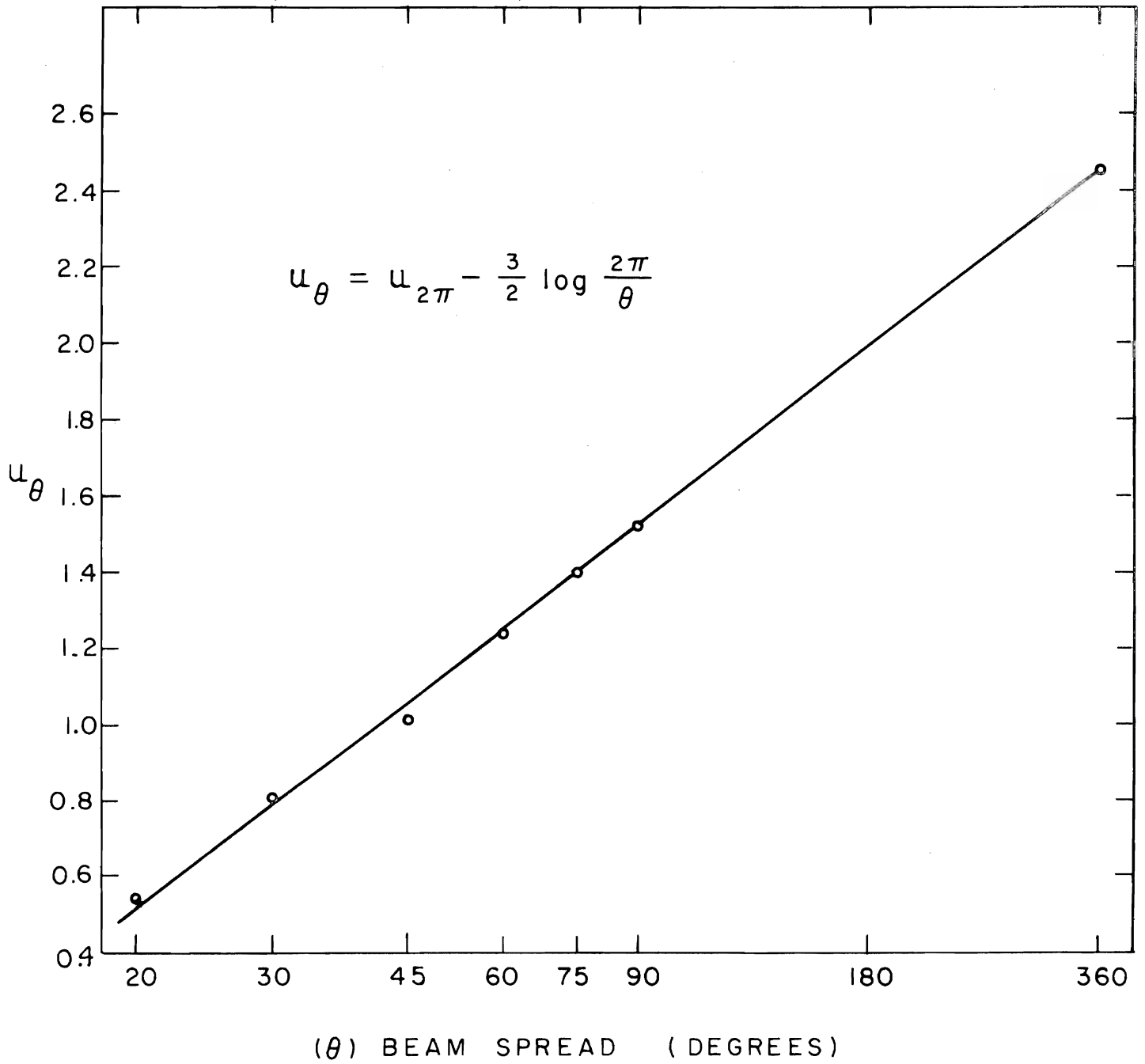


Figure 7  
APPENDIX H

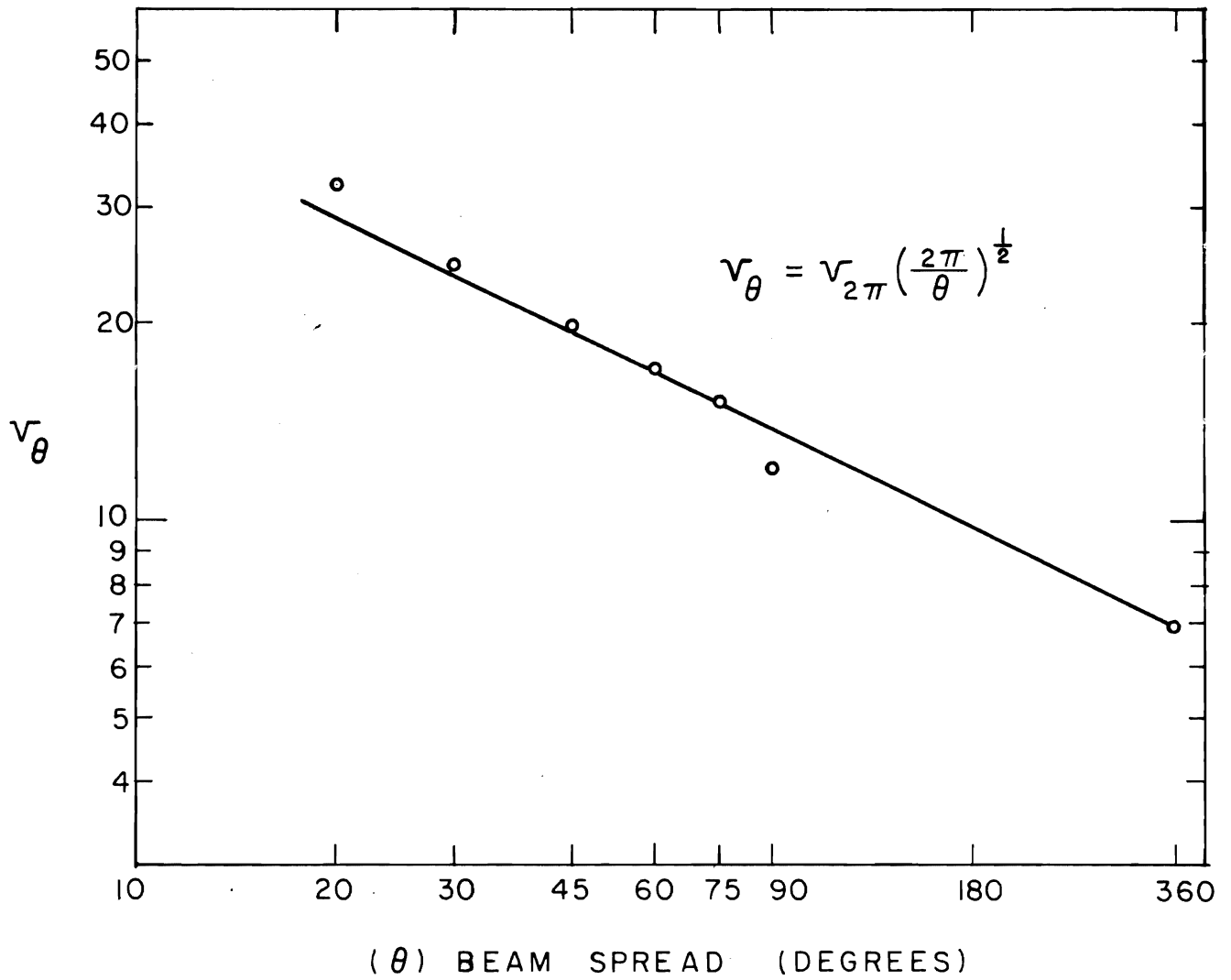


Figure 8

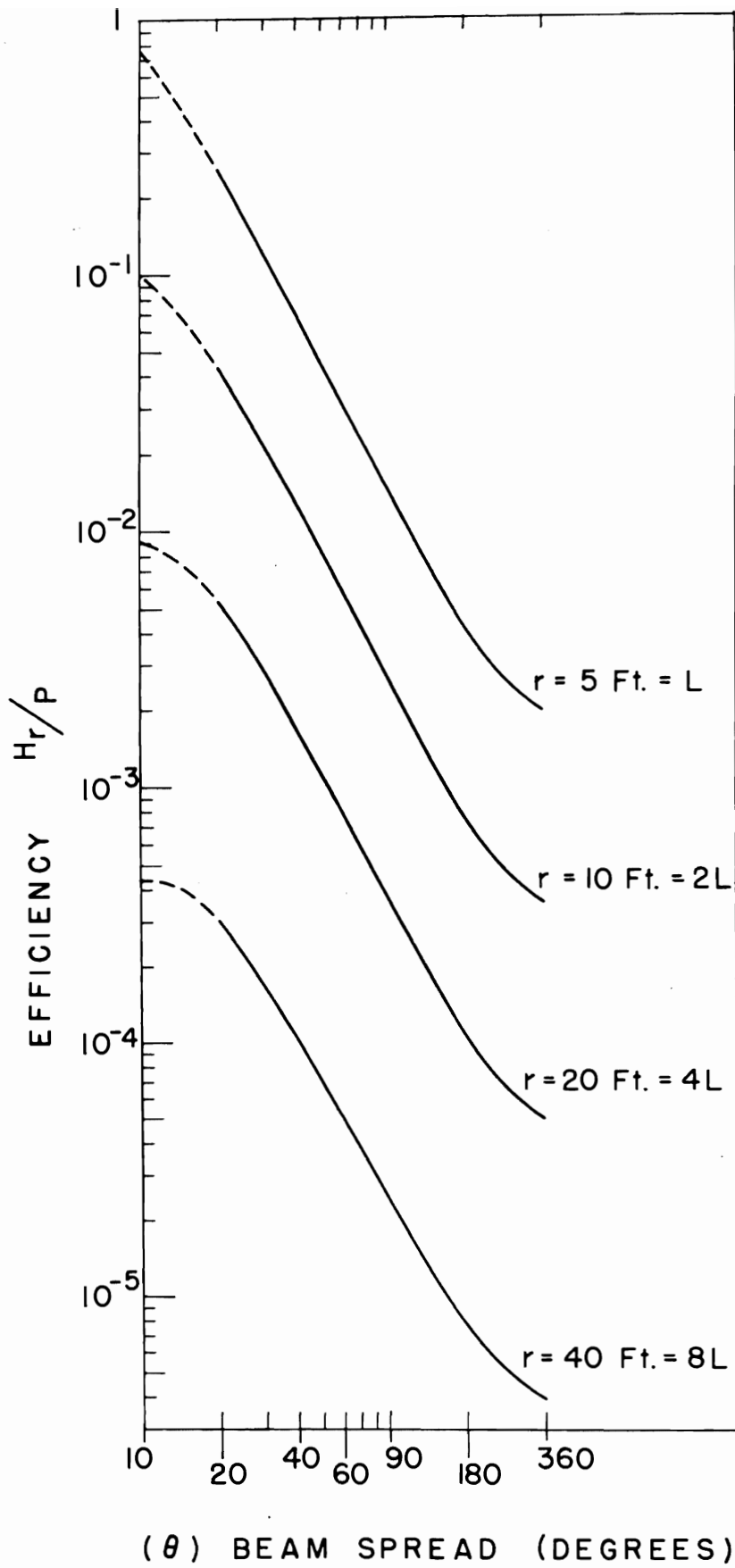


Figure 9



It is obvious from the form of equation (2) that negative values of  $u_\theta$  are possible when the beam-spread is small. Actually, these occur at  $\theta \leq 8$  degrees (approximately) and produce unrealistic implications. Equations (2) and (3) should not be trusted outside of the range of the data upon which they are based. Experiments with sources having smaller beam-spreads should provide the basis for better empirical functions than equations (2) and (3). Even the present data may suggest better functions or better-chosen constants for the present functions. It can only be said that equations (2) and (3) are the best that have been evolved thus far. It is believed that they enable the irradiance produced by sources having beam spreads of  $20^\circ$  or more to be calculated with sufficient accuracy for most practical purposes. The circles in Figure 5 represent the predictions of equation (1) when combined with equations (2) and (3); they illustrate that agreement is best at large distances from the source.

### 3.3 Efficiency

One measure of the geometrical efficiency of an underwater light source is the ratio of the monochromatic irradiance  $H_r$  produced at source-distance  $r$  to the total monochromatic power  $P$  radiated by the source. This is a function of  $r$  and  $\theta$ . In the special case of the uniform conical beam of spread  $\theta$  produced by the source considered in this report, the efficiency ratio  $H_r/P$  can be

expressed by means of equations (1), (2), and (3) by the relation

$$\frac{H_r}{P} = \frac{\frac{e^{-\alpha r}}{r^2} + \frac{(2.5 - \frac{3}{2} \log \frac{2\pi}{\theta})(1 + 7(\frac{2\pi}{\theta})^{1/2} e^{-Kr})Ke^{-Kr}}{4\pi r}}{2\pi(1 - \cos \theta/2)} \quad (4)$$

where  $\alpha = 0.200$  natural log-units per foot and  $K = 0.0570$  natural log-units per foot for the water in which the data depicted by Figures 4 and 5 were obtained.

Figure 9, a plot of equation (4), shows the geometrical efficiency ratio  $H_r/P$  as a function of beam spread  $\theta$  for four values of source-distance  $r$ , corresponding to 1, 2, 4, and 8 attenuation lengths or mean-free-photon-paths,  $1/\alpha$ . This plot demonstrates quantitatively that, from the standpoint of efficiency, underwater lighting systems should employ narrow-beam sources whenever practicable, even at ranges so great that the monopath transmission is negligible and the multipath (glow) transmission contributes virtually all of the irradiance.

### 3.4 Applicability to Other Natural Waters

Equations (1) through (4) with the constants given in this report describe data obtained in only one natural water. Their applicability to other waters is unknown. Inasmuch, however, as the first term of equation (1) is exact and the second term is founded upon a well established diffusion theory model, there is a basis for the expectation that the general form of the expressions will serve as a useful approximation relation for most natural waters and the hope that the constants other than  $\alpha$  and  $K$  will be insensitive to water type.

Important next steps are, obviously, to test equations (1) through (4) by means of irradiance data collected in other types of natural waters and to include sources having smaller beam-spreads.

DOCUMENT CONTROL DATA - R&D

(Security classification of title, body of abstract and indexing annotation must be entered when the overall report is classified)

1. ORIGINATING ACTIVITY (Corporate author) Visibility Laboratory University of California San Diego, California 92152		2a. REPORT SECURITY CLASSIFICATION UNCLASSIFIED	
		2b. GROUP	
3. REPORT TITLE UNDERWATER LIGHTING BY SUBMERGED LASERS and Incandescent Sources			
4. DESCRIPTIVE NOTES (Type of report and inclusive dates) Final Report			
5. AUTHOR(S) (Last name, first name, initial) Duntley, Seibert Q.			
6. REPORT DATE June 1971		7a. TOTAL NO. OF PAGES 275	7b. NO. OF REFS 12
8a. CONTRACT OR GRANT NO. N00014-69-A-0200-6013		9a. ORIGINATOR'S REPORT NUMBER(S) SIO Ref. 71-1	
b.			
c.		9b. OTHER REPORT NO(S) (Any other numbers that may be assigned this report)	
d.			
10. AVAILABILITY/LIMITATION NOTICES Distribution of this document is unlimited.			
11. SUPPLEMENTARY NOTES		12. SPONSORING MILITARY ACTIVITY Office of Naval Research Department of the Navy Washington, D. C. 20360	
13. ABSTRACT <p>Underwater lighting at virtually all distances (including long ranges) produced by submerged lasers (pulsed and continuous) was measured on-axis and at off-axis angles out to 90° in seven types of water. All of these data are summarized by a single closed form equation for engineering use. Computer studies using this equation have extrapolated the data to other types of water. The equation can predict the performance of submerged lasers operating at any wavelength. Methods for measuring the applicable optical constants of natural waters are described. Techniques for long-range underwater photography using conventional light sources are illustrated and supplemented by engineering equations.</p>			